

The University of Nottingham

UNITED KINGDOM • CHINA • MALAYSIA

Establishment of the human cardiac models using gene editing and reprogramming in Human Pluripotent Stem Cells to understand the putative functions of the G-protein coupled receptor kinase 5 polymorphism (GRK5-L41).

Submitted by: Minh Duc Hoang, BSc. MSc.

Thesis submitted to the University of Nottingham for the degree of

Doctor of Philosophy

School of Medicine

Department of Cancer and Stem Cell Biology

APRIL 2017

I would like to dedicate this thesis to my Mom, Mrs. Nguyen Thi Kim Chung, who spends her life to encourage and support my dream of becoming a scientist.

Vietnamese translation: Tôi giành tặng bản luận văn này cho mẹ của tôi, bà Nguyễn Thị Kim Chung, người đã hy sinh cả cuộc đời mình để động viên và giúp tôi hoàn thành ước mơ của mình là trở thành một nhà khoa học chân chính. Con cám ơn mẹ rất nhiều và con yêu mẹ lắm.

Declaration

I hereby declare that this thesis has been composed by myself and has not been submitted for any other degree previously. Acknowledgements of specific procedures not performed by myself and stated; otherwise, the work described is my own.

Minh Duc Hoang _____

Date:

Abstract

A nonsynonymous single polymorphism (SNP) in G protein-coupled receptor kinase 5 (GRK5) was discovered in 2008 that changes the amino acid at the position 41 from Glutamine (Q) into Leucine (L) (Liggett et al., 2008). The putative functions of the GRK5-L41 polymorphism were reported to be involved in faster desensitisation of both β_1 and β_2 adrenergic receptors *in vitro* and the cardiac protective functions by improving the survival rate of patients with heart failure conditions or transplantation *in vivo*. Nevertheless, the mechanisms underlying these processes are still poorly understood, which is the purpose of this thesis.

This thesis presents the establishment of the first human cardiac models of GRK5-L41 polymorphism using human pluripotent stem cells (hPSCs) and their derived cardiomyocytes (CMs). The thesis is distributed into four main themes, containing **(1)** the formulation of monolayer cardiac differentiation protocols; **(2)** the establishment of human induced pluripotent stem cells from lymphoblastoid cell lines bearing the *GRK5*-L41 sequence; **(3)** the development of footprint-free and shortcut CRISRP/Nickase approach that allowed generating the gene-edited human embryonic stem cells expressing *GRK5*-Q41, *GRK5*-Q/L41, and *GRK5*-L41; and **(4)** the evaluation of GRK5-L41 functions using cardiac functional analysis assays.

Relating to disease modelling and cardiovascular biomedical research, the ability to differentiate the hPSCs into CMs plays a critical role by providing an unlimited resource of human CMs for *in vitro* testing and experiments. Here, three main monolayer cardiac differentiation protocols, including E8-AB, mTeSR-AB, and mTeSR-CHIR, were described in details and proven to be highly consistent, efficient, robust, and reproducible. Additionally, these protocols have been ascertained to be effective in more than 27 hPSC lines routinely maintained in the lab regardless of the culture conditions (non-defined vs. defined culture conditions), cell types (human embryonic stem cells vs. human induced pluripotent stem cells), reprogramming methods, and somatic cell sources (in the case of induced pluripotent stem cells). Indeed, by using the E8-AB

protocol, more than $1x10^7$ CMs/line have been produced in this thesis, providing enough resource for functional assay analysis and mechanistic studies of GRK5-L41.

Furthermore, two independent approaches were made to create the human cardiac model of GRK5-L41 polymorphism, involving the establishment of *GRK5*-L41 bearing hiPSCs from lymphoblastoid cell lines, and simultaneously introducing the *GRK5*-L41 sequence to the HUES7 genome to create the Q/L41, and L41 expressing HUES7 lines. In general, four hPSC lines were successfully generated in this thesis, including hiPSC-GRK5-L41, hiPSC-GRK5-Q41, HUES7-GRK5-Q/L41, and HUES7-GRK5-L41. The H-Fib-hiPSC, cell lines generated from HUES7-derived fibroblast, was the additional line obtained after testing the effectiveness of episomal plasmid. All cell lines were able to differentiate into CMs at high purity, approximately 85%, and were used for the development of functional assays.

Four main functional experiments were developed focusing on the GRK5-related functions in the heart, consisting of contractility and hypertrophic response to catecholamine induction, especially during the chronic response. The effects of catecholamine, in this case, Isoprenaline (ISO), on the contractility of the CMs were measured by two assays, the CardioExcyte96 platform detecting the contraction rate and beating pattern in real-time, and the LANCE *Ultra* cAMP assay assessing the production of cAMP. These results indicated that extended culture of CMs in ISO (>30h) introduced the detrimental effects on the contractility and beating pattern of the CMs *in vitro*, generating the arrhythmias in GRK5-Q41 CMs. Interestingly, the GRK5-L41 CMs exhibited a high level of the beat rate in response to ISO and maintained it constantly during prolonged exposure to ISO similar to that of β-blocker treatments in GRK5-Q41 CMs. The Western Blot analysis of the cellular distribution of GRK5 spotted the localisation of GRK5 during ISO treatment for 72h. Further characterisation using immunofluorescence analysis of chronic exposure to ISO demonstrated the elevation of BNP level, a hypertrophic marker, indicating that ISO treatment duration (>30h) induced the hypertrophic response of hPSC-CMs *in vitro*.

Taken together, the findings within this thesis has been the first step in a discovery process of the cardiac protective functions of GRK5-L41 polymorphism during heart failure. Despite the presence of limitation and difficulty, it manages to provide sufficient information to explore further the interrelationship between nuclear accumulation of GRK5, hypertrophic response, and contractility regulation mediated by either GRK5-Q41 and GRK5-L41 in hPSC-CMs *in vitro*.

Acknowledgements

I would like to thank my supervisor, Professor Chris Denning for all his time, guidance, and support over the last three years of my Ph.D. He has been provided me great supports throughout the course, and this work would not be accomplished without his supervision and inspiration. I would also like to thank Prof. Chris Denning again for his sponsorship and the University of Nottingham for providing me the International Research Excellence Scholarship toward my research.

I would also like to express my gratitude to Dr. Vinoj Thomas George who trained, supported, and inspired me about the monolayer differentiation works. He is the first author of the monolayer cardiac differentiation establishing in our laboratory and his works shaped me as a scientist. Furthermore, I would like to thank Dr. Alexander Kondrashov for his excellent guidance in gene editing and molecular works. He has been supported me to evaluate the footprint-free and shortcut CRISPR/Cas strategy, and the reprogramming works.

Furthermore, I would like to acknowledge Dr. Spandan Kalra, Maria Barbadillo-Munoz, Jayson Bispham, Penny Howick, Ralph Hyde, Dr. Tony Melarangi, Katarzyna Lis-Slimak, Puspita Katili and Nguyen Vo who trained me in cell culture/molecular works and provided technical supports. Additionally, I would like to thank Dr. Maria Hortigon at the University of Glasgow for her inputs on CellOPTIQ data, and Dr. Arie O Verkerk at Amsterdam Medical Centre for this works on dynamic patch clamp.

Finally, I would like to thank my extended family (Nguyen, Hoang, Le, Vu) and friends, who mainly supported and encouraged me to complete this milestone of my life, particularly – my mother, brother, and sisters for providing me supports and allowing me to achieve my dream; Kim – for her patience; my “Lentonia” family – Ahmed, Yousuf, Mina, Spandan and Nirav; my “CBS” family – Divya, Pooja, Spandan, and Vinoj; and my lovely soulmate “M” for keeping me happy and joy during the course of my PhD.

A big thank to those always remind me that “You should never regret anything in life. If it’s good, it’s a beautiful memory. If it’s bad, it’s a forgettable experience”.

Abbreviation

Abbreviation	Description
AC	Adenylyl Cyclase
ANF	Atrial natriuretic factor
AP	Action potential
APA	Action potential amplitudes
APD	Action potential duration
APD_{20}	Action potential duration at 20% of repolarisation curve
APD_{50}	Action potential duration at 50% of repolarisation curve
APD_{90}	Action potential duration at 90% of repolarisation curve
AR	Adrenergic receptor
AT_1	Angiotensin II receptor type 1
BMP	Bone morphogenic protein
BNP	Brain natriuretic protein
Brachyury-T	Brachyury protein T
BSA	Bovine serum albumin
BSC	Biological safety cabinet
C59	WNT inhibitor
cAMP	Cyclic adenosine monophosphate
Cas9	CRISPR associated protein 9
CHIR	CHIR99021 WNT inhibitor
CMs	Cardiomyocytes
CRISPR	Clustered regulatory interspaced short palindromic repeat
cTNT	Cardiac troponin-T
CY3	Cyanin dye 3
DAG	1,2-diacylglycerol
DAPI	Di-amino pheyl-indole
DKK-1	Dickkopf-related protein 1
E8	Essential 8 medium
EB	Embryoid body
EBNA	Epstein-Barr virus nuclear antigen
ECM	Extracellular matrix
EOMES	Eomesodermin protein
ERK	Extracellular Receptor Kinase
ET_1	Endothelin 1 receptor
FBS	Fetal Bovine Serum
FGF	Fibroblast grow factor
GATA-4/5/6	Erythoid transcription factor
GPCR	G protein-coupled receptor
GRK	G protein receptor kinase
HAND-1	Heart and neural crest derivatives expressed 1
hESC	Human embryonic stem cell
hiPSC	Human induced pluripotent stem cell
hPSC	Human pluripotent stem cell

Abbreviation	Description
HUES7	Harvard university embryonic stem cell line 7
IP3	Inositol 3 phosphate
ISL-1	Islet 1 protein
KDR	Cardiac progenitor marker also known as Flk1
MDP	Maximal diastolic potential/ resting membrane potential
MEF	Mouse embryonic fibroblast
MEF-2C	Myocyte enhancer factor 2C
MESP-1	Mesoderm Posterior 1 transcription factor
MHC	Myosin heavy chain
MLC-2a/2v	Myosin light chain 2 atrial/ventricular
mTeSR	Modified TeSR medium
NANOG	Homeobox transcription factor
NKX2-5	NK 2 Homeobox 5
OCT4	Octamer binding transcription factor 4
PCR	Polymerase chain reaction
PFA	Paraformaldehyde
PLA	Proximity ligation assay
PLC	Phospholipase C
SD	Standard deviation
SEM	Standard error of the mean
SOX2	SRY (Sex Determining Region) – box 2
TALEN	Transcription activator-like effector nuclease
VECAM	Vascular Endothelial Cell Adhesion molecule
WB	Western blot
ZFN	Zinc-finger nuclease
α-ACT	α Actinin
α-AR	Alpha adrenergic receptor
β_1	Beta-1 adrenergic receptor
β_2	Beta-2 adrenergic receptor
β_3	Beta-3 adrenergic receptor

Contents

Declaration ..... **i**

Abstract ..... **ii**

Acknowledgements ..... **v**

Abbreviation ..... **vi**

Contents ..... **i**

List of Figures ..... **vii**

List of Tables ..... **xii**

Chapter 1 Introduction **1**

1.1 General Introduction 2

1.2 G protein-coupled receptors (GPCRs) 2

1.2.1 Overview of GPCR superfamily 2

1.2.2 Agonist-mediated activation of GPCR 4

1.2.3 G protein coupled receptor kinases (GRKs) and their roles in deactivation of GPCRs 7

1.2.4 GPCR functions in the heart 10

1.3 G protein coupled receptor kinase family 15

1.3.1 Members of GRK family 15

1.3.2 GRKs and their roles in heart failure conditions 17

1.3.3 Roles of GRK5 in cardiac biology and pathophysiology 22

1.3.4 GRK5 single nucleotide polymorphism (GRK5-L41) and its putative roles in cardiac physiology 24

1.4 Models for studying GRK functions 25

1.4.1 Mouse models for GRK studies 25

1.4.2 *In vitro* cellular models 28

1.4.3 Human pluripotent stem cell models 31

1.5 Cardiomyocyte differentiation process of hPSCs 31

1.5.1 Developmental cardiac differentiation: a fundamental lesson from cardiomyogenesis 31

1.5.2 The *in vitro* cardiac induction process 38

1.6 Establishment of human cardiac model using CRISPR/Cas technology 45

1.6.1 History of CRISPR 47
1.6.2 New classification system of CRISPR/Cas 49
1.6.3 Genome editing in hPSCs 52
1.7 Thesis rationale and objective 53

Chapter 2 Materials and Methods 55

2.1 Cell culture 56

2.1.1 Preparation of mouse embryonic fibroblast (MEF) conditioned medium (MEF-CM) 56
2.1.2 Feeder-free culture condition of hPSCs 58
2.1.3 Chemically defined culture conditions of hPSCs 59
2.1.4 Culture hPSCs in E8 medium 60
2.1.5 Establishment of hiPSCs using episomal reprogramming method 60
2.1.6 Pluripotency characterisation 64
2.1.7 Cardiac differentiation of hPSCs 66
2.1.8 Functional analysis of hPSC-CMs 69
2.1.9 Magnetic Activation Cell Sorting (MACS) 72
2.2 Molecular Biology 73

2.2.1 Extraction of genomic DNA 73
2.2.2 DNA gel extraction and purification process 73
2.2.3 Agarose gel electrophoresis 73
2.2.4 Total cellular RNA extraction and cDNA synthesis 74
2.2.5 Restriction enzyme digestion 74
2.2.6 Plasmid design, cloning procedure and plasmid transformation 75
2.2.7 Polymerase Chain Reaction (PCR) 75
2.2.8 qPCR analysis of gene expression 76
2.3 Statistical analysis 77

Chapter 3 Development of monolayer cardiac differentiation protocol to generate ventricular cardiomyocytes from hPSCs 78

3.1 Introduction 79

3.1.1 hPSC-CMs and their applications 79
3.1.2 hPSC culture conditions and their effects on cardiac differentiation 80

3.1.3 Variations of differentiation ability between hESCs and hiPSCs 84
3.1.4 2D monolayer cardiac differentiation procedure 86
3.1.5 The importance of Activin/Nodal and BMP signalling in cardiac differentiation of hPSCs 87
3.1.6 Chapter aims:..... 92
3.2 Results 93
3.2.1 Optimisation of cardiac induction process optimised for mTeSR culture condition 93
3.2.2 Problems with mTeSR culture conditions 96
3.2.3 Standardisation of the defined culture conditions of hPSCs 96
3.2.4 Cardiac induction process in E8-cultured hPSCs 99
3.2.5 Addition of precondition-step enhanced the cardiac differentiation in SP34 (Act, BMP4) protocol 101
3.2.6 Optimisation of CHIR99021 concentration and the establishment of mTeSR(CHIR) protocol..... 104
3.2.7 Establishment of cardiac differentiation protocols adapted for E8-cultured hPSCs 106
3.2.8 Investigation of protein kinetic expression during cardiac differentiation process..... 109
3.2.9 Investigation of BMP signalling activation during cardiac differentiation process..... 113
3.2.10 Analysis for the ventricular subtype formation *in vitro*..... 117
3.2.11 Electrophysiological analysis for hPSC-CMs using CellOPTIQ® 119
3.2.12 Non-invasive cell sorting of ventricular cardiomyocytes 121
3.3 Discussion..... 124
3.4 Chapter Conclusion 132

Chapter 4 Developing and implementing a strategy to produce GRK5 Q41L human induced pluripotent stem cells (hiPSCs) derived cardiomyocytes. 133

4.1 Introduction 134
4.1.1 Lymphoblastoid cell lines (LCLs) 135
4.1.2 Advantages of LCLs in biomedical research and disease modelling..... 136
4.1.3 Strategy for generation of *GRK5*-Q41 and *GRK5*-L41 bearing hiPSCs 139
4.1.4 Chapter Aims 141

4.2 Results 143

4.2.1 Genotypic confirmation of lymphoblastoid cell lines 143

4.2.2 Reprogramming lymphoblastoid cells using lentiviral approach 147

4.2.3 Establishment and characterisation of hiPSCs from HUES7-derived fibroblast (H-Fibs) using Episomal plasmids 149

4.2.4 Reprogramming of lymphoblastoid cell lines using Thomson's plasmid set 152

4.2.5 Reprogramming experiments using episomal reprogramming plasmids derived from Yamanaka's Lab 155

4.2.6 Pluripotency characterisation of newly established hiPSC-GRK5 from lymphoblastoid cell lines 158

4.2.7 Cardiac differentiation of hiPSC-GRK5-Q41 and hiPSC-GRK5-L41 160

4.3 Discussion 162

4.3.1 Lentiviral reprogramming of lymphoblastoid cell lines: an ineffective approach 162

4.3.2 The reprogramming ability of episomal plasmids 163

4.3.3 Defined episomal reprogramming methods 163

4.3.4 Episomal reprogramming of lymphoblastoid cell lines 165

4.3.5 Cardiac differentiation of lymphoblastoid-derived hiPSCs 168

4.3.6 Limitations of the method 169

4.4 Chapter conclusion 170

Chapter 5 Creating hPSC-derived CM model using Footprint-free and shortcut CRISPR/Cas approach 171

5.1 Introduction 172

5.1.1 Gene editing using programmable nuclease systems 174

5.1.2 Gene editing in hPSCs using sgRNA and Cas9 nuclease 176

5.1.3 Components required for an effective CRISPR/Cas9 gene editing 181

5.1.4 Seamless gene editing using CRISPR/Cas and the *piggyBac* transposon 188

5.1.5 Chapter Aims 190

5.2 Results 191

5.2.1 Identification of *GRK5* polymorphism at amino acid position 41 of hESC (HUES7) 191

5.2.2 Construction of sgRNA plasmids 192
5.2.3 Construction of the exogenous targeting plasmid to introduce *GRK5*-L41 into HUES7-GRK5-Q41 cell line 196
5.2.4 Establishment of the *GRK5*-L41 edited lines using Footprint-free and shortcut CRISPR/Cas approach 202
5.2.5 Characterisation of the HUES7-GRK5-L41 and HUES7-GRK5-Q/L41 214
5.2.6 Cardiac differentiation of the HUES7-GRK5-L41 and HUES7-GRK5-Q/L41 216
5.3 Discussion 217
5.3.1 Limitations of the conventional gene editing approach 217
5.3.2 The idea of “footprint free” and “shortcut” gene editing approach 219
5.4 Chapter conclusion 226

Chapter 6 Phenotypic Analysis of *GRK5*-L41 using hPSC-derived Cardiomyocyte Model 227

6.1 Introduction 228
6.1.1 Heart failure conditions 229
6.1.2 Molecular pathways occur during Heart failure 229
6.1.3 G-protein coupled receptor kinase 5 (GRK5) and its non-canonical functions during heart failure 238
6.1.4 Methods for measuring physiological responses of hPSC-derived CMs 239
6.1.5 Chapter aims: 245
6.2 Results 246
6.2.1 Quality control of hPSC-derived CMs 246
6.2.2 Gene expression profiles of adrenergic signalling pathways .. 248
6.2.3 Establishment of real-time analysis of beat rate and beating pattern from hPSC-CMs using CardioExcyte 96 platform 250
6.2.4 Measurement of intracellular cAMP production in response to ISO treatment using LANCE *Ultra* cAMP assay 260
6.2.5 Development of Western Blot assay to assess the cellular distribution of the GRK5 protein in hPSC-CMs 267
6.2.6 Establishment of hypertrophic assay using immunofluorescence analysis 271
6.3 Discussion 273

6.3.1 Development of real-time beat rate analysis of hPSC-CMs using CardioExcyte 96 platform 275
6.3.2 Determination of the cAMP production profiles from hPSC-CM using LANCE *Ultra* cAMP assay 280
6.3.3 Detection of cellular distribution of GRK5 using WB 282
6.3.4 Development of hypertrophic analysis assay 283
6.4 Chapter conclusion 283

Chapter 7 General Discussion 285

7.1 Monolayer cardiac differentiation – an essential tool requires for establishing human cardiac model using hPSCs 286
7.2 Establishment of hiPSC from lymphoblastoid cell lines 288
7.3 Development of footprint-free and shortcut gene editing strategy 289
7.4 Establishment of functional assays toward the putative functions of GRK5-L41 during heart failure condition 291
7.5 Limitations of the study 293
7.6 Final remark and Future work 295

Bibliography 297

Appendix 1 328

List of Figures

Figure 1.1: Summary of G-protein coupled receptor (GPCR).. 4

Figure 1.2: Summary of G protein coupled signal transduction pathways. 7

Figure 1.3: The activation and deaction of GPCR signalling pathway.. 9

Figure 1.4: Classification of GRK family. 16

Figure 1.5: Schematic depicts three arbitrary steps of GRK-mediated phosphorylation of β-ARs between GRK2 and GRK5 in heart. 19

Figure 1.6: Comparative structures of GRK2 and GRK5. 21

Figure 1.7: Non-canonical functions of GRK5 in the heart. 23

Figure 1.8: Overview of in vivo cardiovascular development during embryogenesis.. 35

Figure 1.9: In vitro cardiac differentiation of hPSCs. 39

Figure 3.1: Timeline of the development of cell culture for hPSC together with the evolution of cardiac differentiation process. 82

Figure 3.2: Summary of published cardiac induction monolayer protocols of hPSCs.. 85

Figure 3.3: In vitro cardiac differentiation of hPSC is regulated by either BMP/Nodal or WNT pathway.. 90

Figure 3.4: Examination the effects of growth factors, small molecules, and basal medium on cardiac differentiation capacity of hPSCs.. 95

Figure 3.5: Pluripotency characterisation of CP1, NCRM5, HUES7, and REBL-PAT-Sen cultured in E8 condition and passaged using CDS method. 98

Figure 3.6: Assess the viability of hPSCs after CDS dissociation using Cedex Automated cell counter. 99

Figure 3.7: The results in colour-coded grid indicates the variation of cardiac differentiation efficiency of the E8 cultured hPSCs across all tested conditions. 101

Figure 3.8: Improvement of cardiac induction process using preconditioning step. ... 103

Figure 3.9: Optimisation of CHIR concentrations.. 105

Figure 3.10: Establishment of three independent cardiac differentiation protocols, including E8-AB, mTeSR-AB, and mTeSR-CHIR. 107

Figure 3.11: Purification of CMs generated by E8-AB, mTeSR-AB, and mTeSR-CHIR methods. 108

Figure 3.12: Protein expression profiles during cardiac induction process. 109

Figure 3.13: Quantitative analysis of immunofluorescence images using Harmony High-content imaging and analysis software during time course analysis of stage-specific markers during cardiac induction process inducing by E8-AB, mTeSR-AB, and mTeSR-CHIR protocol. 111

Figure 3.14: Time course analysis of stage-specific markers during cardiac induction process triggered by using E8-AB, mTeSR-AB, and mTeSR-CHIR protocol in NCRM5..... 112

Figure 3.15: Mechanistic analysis of BMP pathways during cardiac induction process. ..... **Error! Bookmark not defined.**

Figure 3.16: Cardiac subtype analysis using FACS analysis of MLC-2v and MLC-2a population..... 118

Figure 3.17: Electrophysiological characterisation of cardiomyocytes. 120

Figure 3.18: Non-invasive procedure for isolation of ventricular cardiomyocyte subtype using Smart-flare and FACS sorting.. 123

Figure 4.1: Lymphoblast B cell generation during developmental process from pluripotent stem cells to mature blood cells (Barreto et al., 2014). 135

Figure 4.3: Overview of chapter's strategy. 142

Figure 4.4: Confirmation of GRK5 Q41L SNP in lymphoblastoid cell lines. 144

Figure 4.5: Confirmation of polymorphic variants of ADRB1 and ADRB2 in Lymp-GRK5-Q41 and Lymp-GRK5-L41. 147

Figure 4.6: Transduced lymphoblastoid cells using lentivirus on MEF feeder layer... 148

Figure 4.7: Episomal reprogramming of HUES7-derived fibroblasts (H-Fib) and pluripotency characterisation.. 150

Figure 4.8: Defined episomal reprogramming of lymphoblastoid cell lines. 153

Figure 4.9: Reprogramming of Lymp-GRK5-Q41 and Lymp-GRK5-L41 using episomal plasmid set derived from Thomson's Lab. 154

Figure 4.10: Reprogramming of lymphoblastoid cell lines (Lymp-GRK5-Q41 – A – and Lymp-GRK5-L41 – B) using episomal plasmid set derived from Yamanaka's Lab. 156

Figure 4.11: Pluripotency characterisation of hiPSC-GRK5-Q41 and hiPSC-GRK5-L41 lines. 159

Figure 4.12: The cardiac induction procedures of Lymphoblastoid-derived hiPSCs, including hiPSC-GRK5-Q41 and hiPSC-GRK5-L41 lines. 161

Figure 5.1: Overview of gene editing workflow from patient-derived samples to final clones. 173

Figure 5.2: Structure of ZFNs and TALENs. 175

Figure 5.3: Schematic of traditional gene editing workflow from in silico design of gRNA and targeting donor construct to selection and isolation of final clones. 180

Figure 5.4: Cas9 protein and its binding process to the target DNA sequence. (A) Cas9 and its mutant version used in CRISPR type II system. 182

Figure 5.5: Schematic describes detailed structure of Cas9-sgRNA complex use in gene editing. 184

Figure 5.6: Overview of strategies uses to generate sgRNA plasmids. 186

Figure 5.7: Comparison between Cre/loxP system and footprint-free piggyBac transposon system. 188

Figure 5.8: Identification of GRK5 sequence from HUES7.. 191

Figure 5.9: Identification of potential gRNA pairs. 194

Figure 5.10: Creation of the GRK5-L41 sequence from HUES7-GRK5-Q41 genomic DNA. 197

Figure 5.11: Establishment of the GRK5 targeting plasmid using Gibson Assembly..199

Figure 5.12: Diagnostic analysis of transformed bacteria after Gibson Assembly reaction. 201

Figure 5.13: The GRK5-L41 expression plasmid map for targeting the HUES7-GRK5-L41 using footprint-free and short-cut strategy. 202

Figure 5.14: The schematic illustrates the procedure of footprint-free and shortcut CRISPR/Nickase approach.. 204

Figure 5.15: Puromycin selection of positive clones for gene editing. 205

Figure 5.16: PCR-based screening strategy of intermediate clones. 207

Figure 5.17: PCR-based analysis of intermediated clones derived from Nickase-mediate (NG) and Cas9 (CG) conventional approach.. 209

Figure 5.18: PCR-based screening of transposon-excised clones. 211

Figure 5.19: DNA sequencing results of the final clones derived from Footprint-free and Shortcut gene editing approach.. 213

Figure 5.20: Characterisation of edited HUES7-GRK5-L41 and HUES7-GRK5-Q/L41 derived from footprint and shortcut method.. 215

Figure 5.21: Overview of the procedure for targeted modification using the piggyBac transposon system.. 219

Figure 5.22: Suggested procedure of footprint-free and shortcut gene editing strategy. 220

Figure 6.1: β-AR signalling pathways involved in Heart failure. 232

Figure 6.2: Signalling pathways involved in physiological (right panel) and pathological hypertrophy (left panel). 236

Figure 6.3: Schematic depicts the cellular signalling pathways triggered by GPCRs contributing to the development of Heart Failure. 237

Figure 6.4: Non-canonical signalling pathways of GRK5 during heart failure. 239

Figure 6.5: CardioExcyte 96 platform (Nanion). 241

Figure 6.6: Principle of the extracellular field potential (EFP) and impedance (IMP) mode obtained from CardioExcyte 96 platform. 243

Figure 6.7: Principle of LANCE Ultra cAMP assay. 244

Figure 6.8: Quality control of hPSC-CMs using immunofluorescence analysis and cell viability assay.. 247

Figure 6.9: q-PCR analysis of adrenergic gene expression profiles from hPSC-CMs. 249

Figure 6.10: Optimisation of CardioExcyte96 system. 252

Figure 6.11: The effects of ISO treatment on hPSC-CM beat rate.. 254

Figure 6.12: Evaluation the effects of β-blockers, including β_1-blocker (CGP20712 – CGP), β_2 blocker (ICI 118,551 – ICI), and Propranolol (Prop) on CMs during ISO treatment. 256

Figure 6.13: Validation the effects of prolonged exposure to ISO treatment (up to 48h) using CRISPR-edited lines.. 259

Figure 6.14: Experimental procedure for LANCE Ultra cAMP assay. 261

Figure 6.15: Optimisation of cell seeding density for LANCE Ultra cAMP assay.. 262

Figure 6.16: A cAMP standard curve generated from LANCE Ultra cAMP assay using the EnVision Multilabel Plate reader set in lamp mode. 263

Figure 6.17: cAMP production response curve of ISO treatment with/without β-AR antagonists, including CGP, ICI, and Propranolol.. 265

Figure 6.18: EC_{50} and E_{max} values of ISO concentration response curve with/without β-antagonist treatments (CGP, ICI, and Prop). 267

Figure 6.19: Optimisation of Western Blot analysis of GRK5 expression from hiPSC-CM-Q41 in response to ISO treatment (up to 72h). 269

Figure 6.20: Western Blot analysis of subcellular distribution of GRK5 during chronic exposure to ISO. 270

Figure 6.21: Analysis of intracellular GRK5 extracted from either cytoplasmic or nucleus of CMs during chronic ISO treatment. 271

Figure 6.22: Development of immunofluorescence analysis of BNP expression to assess the hypertrophic conditions in hPSC-CMs.. 273

Figure 6.23: Proposed cardiac response phases developed from the CardioExcyte 96 results. 278

List of Tables

Table 1.1: Summary of GPCR signalling pathways and their function in the human heart. 14

Table 1.2: Tissue distribution and cellular localisation of GRKs. (Adapted from Sato et al., 2015). 17

Table 1.3: Representative cellular models used to investigate GPCR functions. 29

Table 1.4: Comparison of different programmable nuclease platforms. 46

Table 2.1: MEF-culture medium used in the experiment. 57

Table 2.2: Cell dissociation solution (CDS) 59

Table 2.3: Culture medium used to maintain H-Fib and Lymphoblastoid cell lines. 61

Table 2.4: Composition of lymphoblastoid culture medium (LM) and reprogramming medium (RM). 63

Table 2.5: List of antibodies used for immunofluorescence analysis.. 65

Table 2.6: The list of antibodies used to analyse the CM purity and cardiac differentiation efficiency. 68

Table 2.7: List of antibodies used for flow cytometry analysis of hPSC-CMs. 69

Table 2.8: Buffers used in Western Blot 71

Table 2.9: Composition of the PCR reaction mixture used in this thesis. 76

Table 3.1: Summary of cell lines are currently available in our laboratory. 91

Table 3.2: Table summarises the original differentiation protocol (SP34 (ACT, BMP4)) and its variations, which are classified into Growth Factor Dependent and Small Molecule Dependent Protocols.. 93

Table 3.3: Details of hPSC lines used in the experiments. 94

Table 3.4: The results of flow cytometry analysis for α-Actinin from the experiment ($n \geq 3$). 95

Table 3.5: Scoring system based on the estimated percentage of beating areas in a well of 24-well plates after d12 post cardiac differentiation process. 100

Table 3.6: hPSC lines used to test the effects of precondition step on cardiac differentiation using SP34 (Act, BMP4) method. 102

Table 3.7: Summary of components present in chemically defined medium used in preconditioning step. 125

Table 3.8: Comparison of characteristic between adult-CMs and hPSC-CMs. 132

Table 4.1: Overview of methods for reprogramming somatic cells to hiPSCs.. 137

Table 4.2: Polymorphisms of human β_1 (ADRB1), β_2 (ADRB2), and GRK5. 145

Table 4.3: The list of primers used for amplify the DNA sequences spanning the polymorphisms of ADRB1, ADRB2, and GRK5. 146

Table 4.4: Summary of polymorphic variants of ADRB1, ADRB2, and GRK5 present in Lymp-GRK5-Q41, and Lymp-GRK5-L41. 146

Table 4.5: Karyotype results (30 spreads) of reprogrammed clones derived from Lymp-GRK5-Q41 and Lymp-GRK5-L41 using episomal reprogramming. 157

Table 4.6: Immunocytochemistry analysis for α-Actinin positive cells. 160

Table 4.7: Small molecules used to improve episomal reprogramming efficiency, their chemical structures, biological targets and functions. 165

Table 5.1: Summary of 36 On-target sgRNA Design Tools and seven posterior Genome editing analysis tools. 178

Table 5.2: Two-loops PCR reaction used to amplify Gibson Assembly fragments to construct GRK5 targeting plasmid. 198

Table 5.3: Components requires for footprint-free/shortcut CRISPR/Nickase and CRISPR/Cas9 approaches. 203

Table 5.4: Summary of the gene editing results. 212

Table 6.1: The EC_{50} values of ISO concentration curves in the presence of β-antagonists (CGP, ICI, and Prop) in hiPSC-derived CMs and gene edited HUES7-derived CMs. 264

Table 6.2: The E_{max} values of ISO concentration curves in the presence of β-antagonists (CGP, ICI, and Prop) in hiPSC-derived CMs and gene edited HUES7-derived CMs.. 266

Chapter 1 Introduction

1.1 General Introduction

Cardiovascular research and cardiac models have provided valuable knowledge about biological and pathophysiological conditions of the hearts, establishing new approaches and ideas toward the development of basic biological research, drug screening, cellular therapeutic, and regenerative medicine. This thesis focused on the development of a human cardiac model derived from human pluripotent stem cells (hPSCs) using advanced reprogramming technology and genome editing method to investigate the "gain-of-function" characteristics of the G-protein coupled receptor kinase 5 (GRK5) single polymorphism (GRK5-Q41L), especially its putative functions during heart failures.

The overall structure of this thesis is divided into four main themes, including **(1)** development of monolayer cardiac differentiation of hPSCs to generate functional cardiomyocytes (CMs) (chapter 3); **(2)** establishment of human induced pluripotent stem cells (hiPSCs) from lymphoblastoid cell lines bearing the GRK5 polymorphism of interest (GRK5-L41; chapter 4); **(3)** creation of the genetically modified human embryonic stem cell (Zhang et al.) lines expressing the targeted GRK5 polymorphism using the footprint-free and shortcut gene editing approach (chapter 5); and **(4)** formulation of functional assay set that could potentially be used to investigate the features of GRK5-L41 during normal and heart failure conditions (chapter 6).

The GRK5 is a downstream regulator of a complex G protein-coupled receptor (GPCR) network, which plays an essential role in maintaining cardiovascular functions, cardiac tissue homeostasis, and regulation of the heart responses during cardiac injuries or diseases (Kunapuli and Benovic, 1993; Lefkowitz, 2007). Therefore, it is important to discuss firstly about the GPCRs and their particular functions in the heart.

1.2 G protein-coupled receptors (GPCRs)

1.2.1 Overview of GPCR superfamily

To maintain its physiological homeostasis, the human body continuously circulates signals to organs, which receive and translate these stimuli into appropriate cellular

responses. Cellular communication is the principle of this homeostasis, which is also achieved by molecules, known as agonists. These molecules specifically bind to receptors and activate the downstream signalling transduction pathways. One of the major models of this agonist-receptor interactions is that of G-protein coupled receptors (GPCRs) (Lefkowitz, 2007).

The GPCRs are seven-transmembrane receptors, which function via their interaction with G-proteins inside the cells and form the largest protein superfamily in the mammalian system (Lefkowitz, 2007). They respond to a vast variety of extracellular signals such as photons, small molecules, peptides, and proteins to produce robust, diverse, and cell type specific responses including chemotaxis, neurotransmission, cell proliferation, differentiation, and communication (Katritch et al., 2013; Dolatshad et al., 2015). Therefore, this GPCR superfamily becomes a major target of therapeutic and pharmaceutical intervention (John P. Overington, 2006).

Although the exact size of this superfamily is unknown, human genome project identified nearly 800 human genes are encoded for GPCRs. This family includes α-adrenergic receptors (α-ARs), β-adrenergic receptors (β-ARs), rhodopsin, endothelin receptors, adenosine receptors, angiotensin receptors and others (Bjarnadottir et al., 2006; Li et al., 2002; Capote et al., 2015). The majority of GPCRs are membrane receptors, which are activated upon the binding of the agonist to the receptor triggering their conformational changes and activate heterotrimeric guanine-nucleotide binding regulatory proteins (or G proteins). The activated G-proteins bind to the receptors in the intracellular space and subsequently initiate downstream signal transduction pathways (Howard et al., 2002).

The GPCR signalling contains three main components, including the agonist-activated GPCR, the G-protein complex, and the downstream effectors, which initiate specific cellular responses depending on the extracellular signals received from the receptors (Figure 1.1). The signal transduction pathway is delivered via the receptor associated G-protein α-subunit, which is categorised into four major classes including $G\alpha_S$, $G\alpha_i$, $G\alpha_q$, and $G\alpha_{12/13}$ with each consisting of various subtypes, $G\beta$, and $G\gamma$ subunit.

To date, 16 Gα subunits have been identified, with 23 different isoforms. Moreover, 6 Gβ subunits and 12 γ subunits have also been revealed in the human genome (Figure 1) (Rockman et al., 2002; Dolatshad et al., 2015).

1.2.2 Agonist-mediated activation of GPCR

Binding to their agonist results in the stabilisation of the GPCR structure in its active conformation and stimulates heterotrimeric G-protein binding at the intracellular C-terminal domains of the receptor (Howard et al., 2002; Dorn et al., 2009). In fact, although

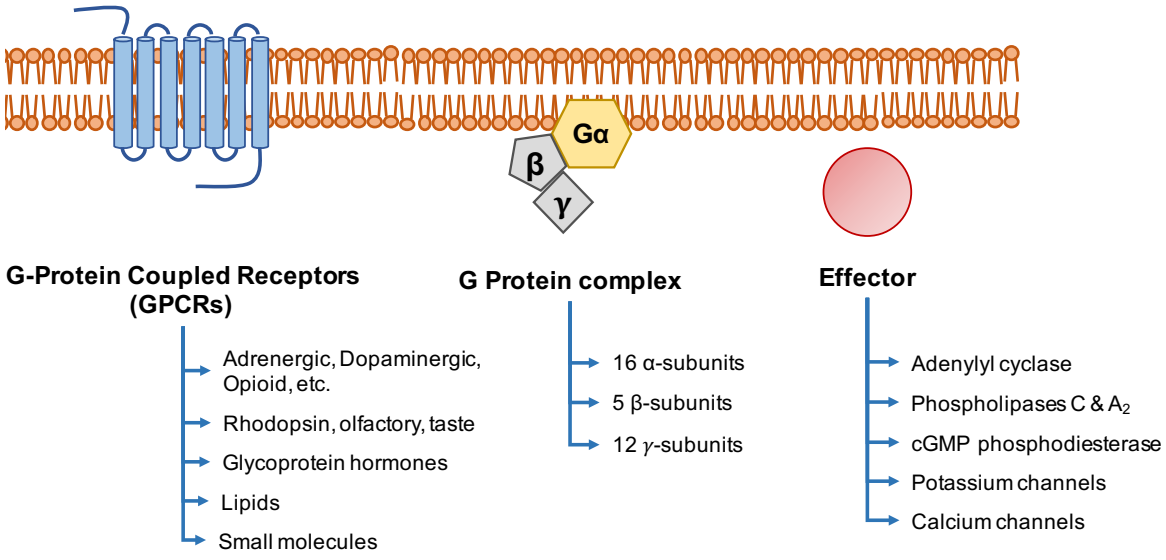


Figure 1.1: Summary of G-protein coupled receptor (GPCR). The principle components of GPCR signalling pathway are the seven-transmembrane-spanning receptor, a heterotrimeric G-protein complex, and a downstream effector. The GPCR is the largest receptor group found in our body, it consists of adrenergic receptors, dopaminergic receptors, Opioid receptors, etc. GPCRs can be activated by a vast variety of different molecules called agonists, including glycoprotein hormones, lipid, small molecules or photons. As its name implies, upon activation, GPCR associated with G-protein complex consists of Gα, Gβ, and Gγ subunit. The agonist-activated GPCRs lead to activation of many different downstream effectors, such as adenylyl cyclase, that involved in regulation of cellular activities.

the GPCR itself does not confer the catalytic activity, the downstream signalling pathways are mediated via the dissociation of G-protein complex into the Gα and Gβγ subunits. Subsequently, the disengaged G-protein subunits (both Gα and Gβγ) trigger the amplification and propagation of intracellular signals via specific effectors, including adenylyl cyclase (AC), phospholipases, or ion channels (Figure 1.1) (Li et al., 2002; Howard et al., 2002; Sato et al., 2015). Eventually, these activated effectors initiate second messenger molecules, which evoke cellular responses via different signalling

pathways. For instance, one of the important second messenger molecules is cyclic AMP (cAMP) produced by activation of β-adrenergic receptors (β-ARs) or inositol-1,4,5-triphosphate (IP_3) and diacylglycerol (DAG) generated by stimulation of α_1-ARs (Dorn, 2009).

Once dissociated from the GPCR, different G-protein complexes are involved in transmitting signals via their internal effector molecules that exist on cells, which, in turn, regulated various cellular responses. As shown in Figure 1.2A, stimulation of GPCR, particularly β_1- and β_2- ARs by catecholamines such as adrenaline or noradrenaline activates the canonical stimulatory $G\alpha_S$ signalling pathways that activate adenylyl cyclase (AC) effector molecules (Bers, 2008; Lymperopoulos and Negussie, 2013). In CMs, the activated AC results in an increased generation of cycle AMP (cAMP) and cAMP-dependent protein kinase (Tsai et al., 2015) whose primary functions are phosphorylation of multiple cellular proteins involving in cardiomyocyte contractility (Bers, 2008). Hence, the overall physiological effect of cardiac β-ARs activation is an increase in heart contractility (inotropic effect) and heart beat rate (chronotropic effect) (Capote et al., 2015).

In contrast, the activation of inhibitory $G\alpha_i$ protein via β_2- ARs signalling pathways by adenosine and muscarinic agonists results in a decrease of AC and inhibits cAMP production (Figure 1.2B) (Daaka et al., 1997). The $G\alpha_i$-regulated process is believed to be involved in cardiac protective function evoked by β_2- ARs to protect the heart during stress condition (Xiang and Kobilka, 2003; Lymperopoulos et al., 2013). Hence, $G\alpha_i$ activation produces the reversed effects to those elicited by $G\alpha_S$ signalling activation and results in a reduction of cardiomyocyte contractility and increase pro-apoptosis activities in ventricular CMs.

Additionally, the activation of α_1-ARs, angiotensin II type 1 receptors (AT_1), and endothelin-1 receptors (ET_1) by alpha-agonist, angiotensin II and endothelin-1, respectively, triggers the dissociation of $G\alpha_q$ proteins followed the initiation of inositol triphosphate (IP_3) pathway (Figure 1.2C) (Uchida, 1975; Ertan et al., 2010). Upon

activated, the pathways induce the accumulation of cytosolic IP_3 results in the stimulation of Ca^{2+} release by the sarcoplasmic reticulum in the CMs, thereby increases the inotropic activities during physiological hypertrophy (Cotecchia et al., 2015; Zalewska et al., 2014). Interestingly, most of the receptors coupled to $G\alpha_q$ proteins also associated with the $G_{12/13}$ protein (Worzfeld et al., 2008). It has been found that activation of $G_{12/13}$ coupled GPCRs causes activation of heterotrimeric $G_{12/13}$ protein which, in turn, associates with their regulator called Rho and stimulates their guanine nucleotide exchange factor (GEF activities) (Figure 1.2D) (Fukuhara et al., 2001). The regulator of G protein signalling is a class of protein that is involved in regulate the catalytic activities of G-protein, mostly as GTPase-activating proteins which could either accelerate G-protein inactivation or enhance its function (Siehler, 2009). The RhoGEF catalyses the nucleotide exchange of GDP for GTP, and upon activation by $G_{12/13}$ protein, RhoGEF translocates from cytosol to the plasma membrane to exhibit their activities involving in stabilisation of actin filament and increase contraction activities in CMs (Takashima et al., 2008).

While the activation of GPCR plays a significant role in the heart functions, so does the deactivation. When the balance of activation and deactivation process is impaired, imperative homeostasis becomes faulty, and if not corrected promptly, this signal could potentially become irreversibly detrimental to the body, leading to diseased states.

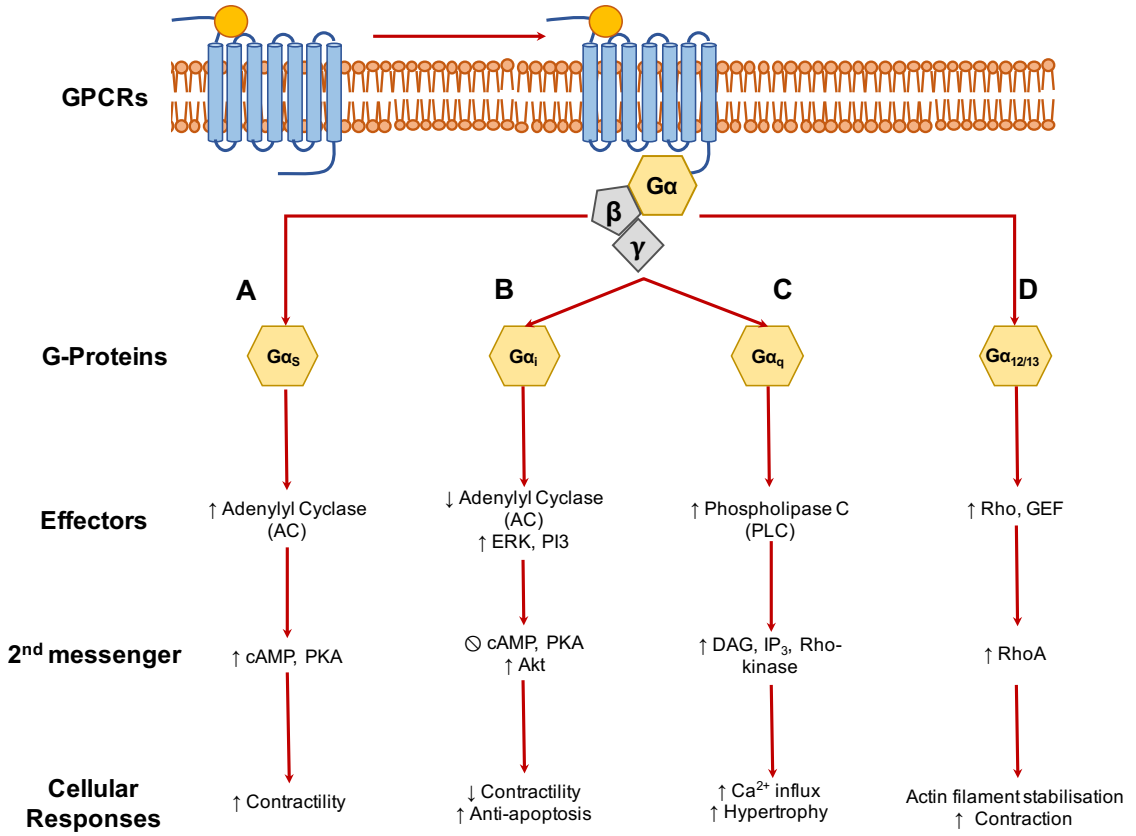


Figure 1.2: Summary of G protein coupled signal transduction pathways. Agonist-activated GPCRs triggers the recruitment of G-protein complex followed promoting their dissociation into Gα and Gβγ subunits. There are four primary classes of Gα proteins, including $G\alpha_S$ **(A)**, $G\alpha_i$ **(B)**, $G\alpha_q$ **(C)**, $G\alpha_{12/13}$ **(D)** found in the heart. Once dissociation from activated-GPCR, different Gα proteins involved in different signal transduction pathways that regulate cellular responses, including contractility, hypertrophy, actin filament stabilisation, etc. cAMP: cyclic AMP; PKA: cAMP dependent protein kinase; ERK: extracellular signal regulated kinases (ERK); PI3: phosphoinositide 3-kinase; Akt: protein kinase B; DAG: diacylglycerol; IP_3: inositol triphosphate; GEF: Guanin nucleotide exhange factor.

1.2.3 G protein coupled receptor kinases (GRKs) and their roles in deactivation of GPCRs

Deactivation of agonist-bound GPCRs is mainly accomplished by a group of protein kinases called G protein-coupled receptor kinases (GRKs) via a process called desensitisation – that is, the reducing of receptor responsiveness regardless of the persistent stimulation of the extracellular signals. The termination of GPCR signalling occurs in a two-step mechanism: **(1)** GRKs are recruited to the agonist-activated GPCRs where they phosphorylate the receptors in its active conformational form, resulting in the alteration of receptor conformational changes that promote the binding of β-arrestin; and **(2)** the β-arrestin-bound GPRCRs no longer bind to and activate G-proteins, which, in

turn, eliminate the signalling cascades (Dorn, 2009; Katritch et al., 2013; Lefkowitz, 2007).

Figure 1.3 illustrates a schematic of GPCR activation, signalling and desensitisation. In brief, at normal physiological condition (step 1), the GPCR is in inactivated confirmation or resting state. Upon agonist release and bind to the receptor, it causes the conformational changes in the receptor into stabilised active conformation and stimulates the dissociation of G-protein complex followed induction of downstream signalling through effector activation (step 2). The disengagement of $G\alpha$ and $G\beta\gamma$ subunits mobilises GRKs to phosphorylate at serine (Ser) and threonine (Thr) at the C-terminal domain of the receptor, a process which may vary depending on the GRK isoforms (step 3A). Phosphorylated GPCRs promote the recruitment and binding of β-arrestin to the receptors, leading to clathrin-induced endocytosis of the agonist-activated receptor inside the cells (step 3B) where the receptors are either degraded by protease activities or recycling back to the plasma membrane of the cells in its inactive conformation (step 4). Although the endocytosis reactivation or deactivation of agonist-bound GPCR is an important process that is involved in maintaining the body homeostasis which includes different proteins in a complex regulatory network, it is beyond the scope of this thesis and better reviewed in a previous study (Moore et al., 2007).

Another important mechanism for receptor desensitisation is the “downregulation” process, which refers to the total loss of receptors from the cells due to a decrease in receptor expression level and receptor synthesis. This process is controlled by either at mRNA level by destabilisation of receptor mRNA or protein level by degradation of internalised receptors. However, the downregulation of receptors requires longer times to operate (over hours) compares to termination the signals from its signal-transducing G-protein via receptor phosphorylation by GRK (seconds to minutes) (Bailey et al., 2008; Fisher et al., 2014).

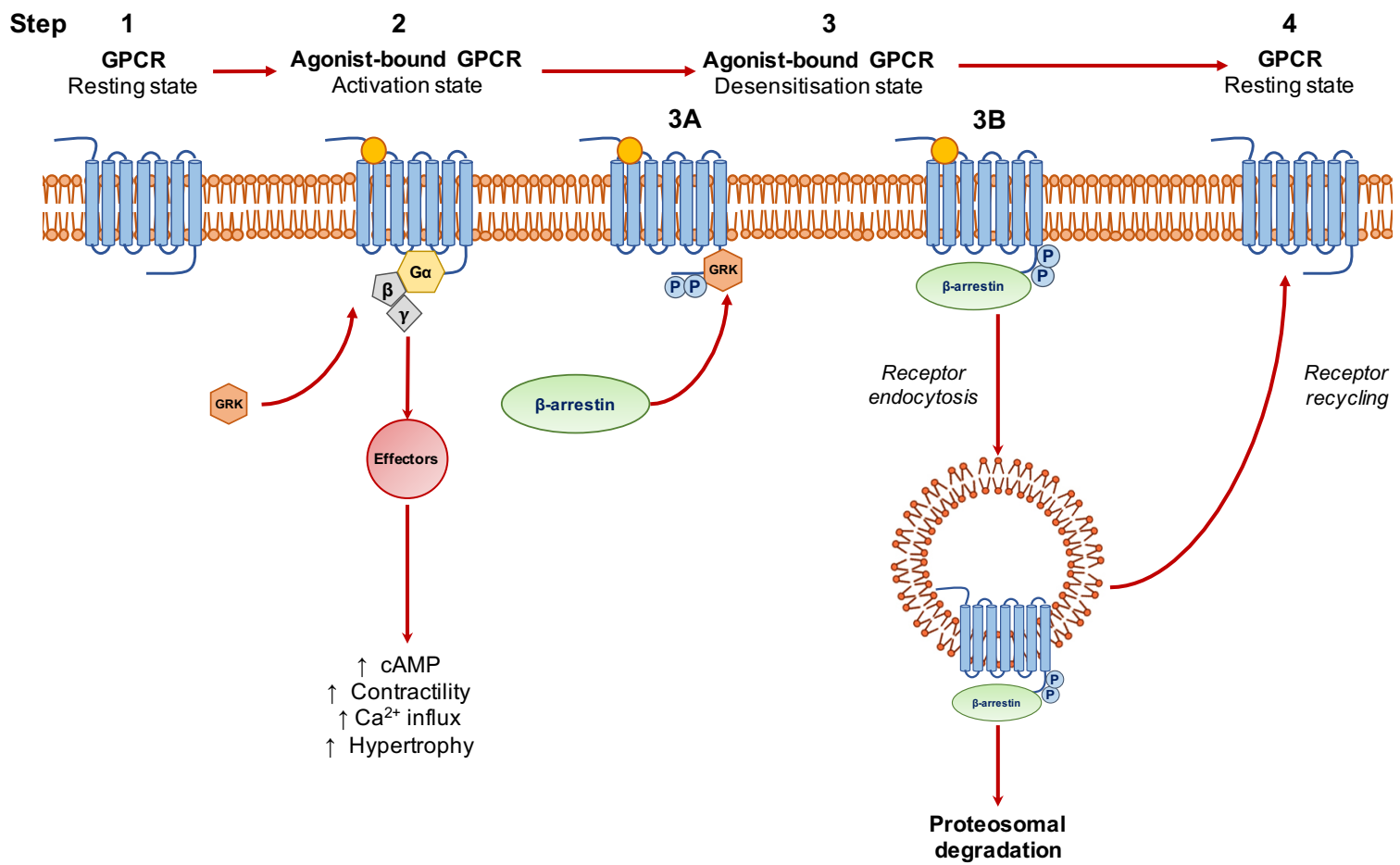


Figure 1.3: The activation and deaction of GPCR signalling pathway. At normal physiological condition, the GPCR is in its inactive or resting state (Step 1), and both the receptors and G-protein complex are not associated. Upon agonist stimulation, the receptors are activated by associate with G-protein complexes followed the induction of cellular response via effectors (Step 2). At the active receptor, dissociation of G-protein complex promotes the recruitment of GRKs which bind and phosphorylate the agonist-activated receptors leading to receptor conformational changes (Step 3A) and subsequent binding of cytosolic β-arrestin protein (Step 3B). The β-arrestin bound receptors are then subjected to clathrin-mediated endocytosis and either sorted for degradation by proteosomal activities in the endosome or recycling back to the plasma membrane of the cells in its inactive state (Step 4).

Taken together, it is important to summarise that GRK-mediated phosphorylation of agonist-bound GPCRs is a crucial for receptor desensitisation process, enhancing the receptor affinity for interaction with cytosolic protein (β-arrestin), which bind to the receptor and terminate further G-protein coupling. In the heart, especially in β-AR signalling pathways, this process prevents prolonged activation of $G\alpha_S$ signalling and the subsequent accumulation of adenylyl cyclase. Hence, increased GRK activities pushes the receptor equilibrium towards the inactive state, which, in turn, creates a condition of reduced receptor responsiveness to catecholamines. In the next section, the specific functions of GPCR including their canonical activities that appear to be critical for cardiovascular homeostasis will be discussed.

1.2.4 GPCR functions in the heart

The heart is one of the most vital organs in the entire human body. Its preeminent function is to pump blood, which carries all the essential materials involving in bodies functions and removing the waste products, by virtue of an orchestrated contraction – relaxation cycle of working CMs (Brade et al., 2013). In fact, a sophisticated GPCR network is involved in regulation of the heart functions.

In the normal heart condition, the sympathetic system is regulated by catecholamine through three central adrenergic systems, including α_1-AR family, α_2-AR family and β-AR family, each of the families consists of three subtypes (Bylund et al., 1994; Hieble et al., 1995; Lymperopoulos et al., 2012). Among them, β-AR family plays a vital role in control of the contractile machinery.

1.2.4.1 The β-adrenergic receptors

The human heart expresses three types of β-ARs, with the β_1-ARs being the predominant receptor (occupies up to 70-80% of total cardiac β-adrenergic receptor density), followed by β_2-ARs (comprises approximately 18-28% of total CMs β-ARs) and the rest is β_3-ARs (Brodde, 1993; Lymperopoulos and Negussie, 2013). Activation of β_1-

ARs and in a lesser extent, β_2-ARs, results in an increase cardiac contraction (positive inotropic effect), beating frequency (chronotropic effect), and the rate of relaxation (lusitropic effect) via stimulatory Gα proteins (Gα_S) signalling transduction pathways (Colucci et al., 1986; Dorn, 2007). Moreover, it is also involved in the acceleration of impulse conduction via the atrioventricular node and pacemaker activities from sinoatrial node (Capote et al., 2015). The functions of β_3-AR have remained unclear, but it was reported that β_3 receptors are inactive predominantly during normal conditions, and their stimulation seems to be involved in negative inotropic effects opposite to that of β_1 and β_2 receptors (Emorine et al., 1989; Garcia-Prieto et al., 2014).

The most important activities of β_1 and β_2 receptors upon activation by catecholamines are their inductions of increased physiological responses of the cardiac muscle cells. The epinephrine-bound β_1-ARs, and in lesser extend β_2 due to their physiological distribution of receptors on the surface of normal CMs, catalyses the nucleotide exchanges of GTP for GDP on the Gα subunit of the G-protein complex, resulting in the activation of Gα_S proteins. The Gα_S-regulated signalling pathway triggers the activation of downstream effector (AC), which converts ATP to the second messenger cAMP, which in turns promotes PKA activities. As mentioned above, PKA is a major cellular effector of cAMP and involved in phosphorylation of multiple substrates, including β-ARs themselves in the heart, and ultimately results in increased intracellular Ca^{2+} concentration, which is the master regulator of cardiomyocyte contraction machinery (Lohse et al., 2003).

The PKA-induce phosphorylation process targets the following cellular functions: **(1)** the cell membrane-located L-type calcium channels and the sarcoplasmic reticulum (Srivastava et al.) ryanodine receptors, both of these receptors regulate the release of Ca^{2+} from the compartmentalise reservoirs into the cytoplasm of the cells; **(2)** the PKA-phosphorylation of phospholamban, a negative modulator of sarcoplasmic/endoplasmic reticulum Ca^{2+}-ATPase, results in the deinhibit Ca^{2+}-ATPase activities followed the acceleration of Ca^{2+} reuptake by SR after contraction and increase SR Ca^{2+} stores

prepared for the next contraction sequence; **(3)** hyperpolarisation-activated cyclic nucleotide-gate channels, which generation the cation inward current (If) in the pacemaker cells; **(4)** cardiac troponin I and myosin-binding protein-C, which reduce myofilament sensitivities to Ca^{2+}, thereby enhance the relaxation of myofilament; and **(5)** the intracellular ion transport regulator (phospholemman protein), which tightly interacted with Na^{+}/K^{+}-ATPase and blocking its function, whose phosphorylation by PKA relieves the blocking function and stimulate the sodium pump enhancing cardiac muscle repolarisation and relexation (Bers, 2008; Ludwig et al., 1998; Sulakhe and Vo, 1995; Despa et al., 2005).

Interestingly, the signals and functions transduced via β_2 receptor in a substantially different manner compare to β_1 receptor due to its ability to associate with not only $G\alpha_S$ protein but also the inhibitory $G\alpha$ protein ($G\alpha_i$). Indeed, the $G\alpha$ protein switch ($G\alpha_S$ to $G\alpha_i$) in β_2-ARs occurs by the phosphorylation of the receptor by PKA, which allows the cells to activate the anti-apoptotic pathways, whereas persistent activation of β_1 via PKA engages in the pro-apoptotic process (Daaka et al., 1997). Therefore, these substantial differences between β_1 and β_2 receptors are ascribed to the signal of β_2 mediated by $G\alpha_i$ protein signalling pathway.

As far as β_3-ARs are concerned, their functions are mostly related to cardiac diseases and hypertrophy (Garcia-Prieto et al., 2014; Gauthier et al., 2011). Mice with the transgenic cardiac-specific expression of human β_3-ARs were protected from cardiac hypertrophy and fibrosis in response to hormonal stimulations. Most of these protective functions are mediated by $G\alpha_i$ protein and nitric oxide synthase (eNOS and nNOS) followed downstream cGMP/protein kinase G signalling (Gauthier et al., 1998). In addition to direct protection of cardiac myocytes from hypertrophic remodelling or post-ischaemic damage, β_3-ARs are also involved in the orchestration of paracrine signalling from CMs to surrounding cells and reciprocally, from endothelial cells to vascular and cardiac myocytes (Angelone et al., 2008). This regulation leads to the reduction of

interstitial fibrosis, increase neoangiogenesis as well as coronary vasodilatation, which is involved in the preservation of heart functions.

1.2.4.2 The α-adrenergic receptors

In contrast to β-ARs, the human CMs contain a relatively small number of α-ARs, with a ratio of β- to α-ARs of about 10:1 (Woodcock et al., 2008). In terms of α_1-ARs, their roles in the regulation of cardiac chronotropic effects are still a controversy, albeit the fact that their functions in cardiac hypertrophy and remodelling are well documented. The α_1-AR functions are translated by $G\alpha_q$ protein-dependent pathways that involve the activation of phospholipase C-beta (PLCβ) followed generation of IP_3 second messenger and DAG (Woodcock et al., 2008). IP_3 functions by binding to the receptors in the sarcoplasmic reticulum (Srivastava et al.) and triggers the release of Ca^{2+} from SR into cytoplasm of CMs, whereas DAG engages in activation of protein kinase C. Hence, increasing cytosolic Ca^{2+} concentration by α_1-ARs is similar to the activation of β_1 receptors, but due to the spatial restrictions imposed by signalling "compartmentalisation" within the CMs, α_1-ARs mediated increase Ca^{2+} concentration activates hypertrophy-promoting gene expression rather than cardiomyocyte contraction regulation as seen in β1 receptors (Lymperopoulos and Negussie, 2013).

Last but not least, the α_2-AR also orchestrates indirectly cardiac functions via sympathetic neuron innervating the heart as presynaptic inhibitory autoreceptors (Philipp et al., 2002). Its principal role is to control the outflow of catecholamine release mediated by $G\alpha_i$ protein coupling (Hein et al., 1999). Moreover, it was also reported that the α_2-AR inhibits the release of norepinephrine from cardiac sympathetic nerve and secretion of epinephrine from the adrenal medulla, thereby reducing the chronotropic and inotropic functions of the heart (Brede et al., 2003). Interestingly, a genetic mutation of the human α_2-AR (Del322-325) that compromises its ability to coupling with $G\alpha_i$ protein and thereby prohibit its capacity to control the sympathetic-inhibitory response is alone associated with increased heart failure risk in the African-American population (Ahles and Engelhardt, 2014).

Table 1.1: Summary of GPCR signalling pathways and their function in the human heart. α: α-adrenergic receptors (including α_1 and α_2 receptor); β: β-Adrenergic receptors (β_1, β_2, and β_3-ARs); AT_1: angiotensin II receptor subtype 1; ET_1: endothelin 1 receptor; cAMP: adenosine 3', 5' monophosphate; DAG: diacylglycerol; PKA: protein kinase AI PKC: protein kinase C; IP_3: intrositol – 1,4,5 – trisphosphate; M: muscarinic cholinergic receptor; MAPK: mitrogen-activated protein kinase; NOS: nitric oxide synthase.

Receptor	**β_1**	**β_2**	**β_3**	**α_1/AT_1/ET_1**	**α_2**	**M**
Primary G protein coupling	$G\alpha_S$	$G\alpha_S$/ $G\alpha_i$	$G\alpha_S$/ $G\alpha_i$/NOS	$G\alpha_q$	$G\alpha_i$	$G\alpha_i$
Endogenous agonist	Epinephrine, Norepinephrine	Epinephrine, Norepinephrine	Epinephrine, Norepinephrine	Epinephrine, Norepinephrine, Angiotensin II, Endothelin 1	Epinephrine, Norepinephrine	Acetylcholine
Primary effectors	Adenylyl Cyclase, L-type Ca^{2+} channel	Adenylyl Cyclase, L-type Ca^{2+} channel	Adenylyl Cyclase	phospholipase C-beta (PLCβ)	Adenylyl Cyclase	Adenylyl Cyclase, K^+ channel
Secondary messenger	↑ cAMP/PKA	$G\alpha_S$:↑ cAMP/PKA $G\alpha_i$: ↓ cAMP/PKA, MAPK	↑ cAMP/PKA	↑ IP_3/DAG, PKC, MAPK	↓ cAMP/PKA	↓ cAMP/PKA ↑ PI_3 kinase
Cellular functions	↑ contraction, beating frequency and regulate relaxation rate	$G\alpha_S$: Similar functions to β_1 $G\alpha_i$: cardiac protective functions	↑ relaxation, ↓ hypertrophy, protection from oxidative damage	↑ cardiac hypertrophy	↑ inhibition of catecholamine release from nerve, ↓ contraction and beat rate	↑ contraction, beating frequency and regulate relaxation rate

Thus far, this section has provided a brief summary of the literature relating to the functions of GPCRs in normal heart condition. It is clear that functional regulation of the heart activities is orchestrated by different GPCRs which associate with different Gα protein subtypes to evoke the various cardiac responses to sympathetic and adrenergic signals (Table 1.1). In the section that follows, the alteration of the GPCR network during heart failure and the crucial roles of GRKs during the process will be discussed.

1.3 G protein coupled receptor kinase family

1.3.1 Members of GRK family

The GRK family consists of seven members and is divided into three main subcategories based on their sequence similarity and gene structure analysis, including **(1)** retinal or rhodopsin kinases (comprising of GRK1 and GRK7), **(2)** β-AR kinases (consisting of GRK2 and GRK3), and **(3)** the GRK4 family (comprising of GRK4, GRK5 and GRK6) (Figure 1.4) (Sato et al., 2015). The GRK family acquires shared structural and functional hallmarks that are evolutionarily conserved among GRKs isolated from nematodes, insects, and mammals, indicating their biological significance (Cassill et al., 1991; Wilson et al., 1994; Pitcher et al., 1998).

Structurally, these protein kinases are composed of three essential regions: a centrally located ~500 to 520 amino acid catalytic domain, which performs a Ser/Thr kinase activities, flanked by large amino- and carboxyl-terminal regulatory domains. The amino-terminal domains of GRKs share a common structure, consisting of 25-residue proximal NH_2 terminal regions followed a regulator of G protein signalling (RGS) homology region. The carboxyl terminus is the most diverse component among GRK subfamilies in both length and structure manner. GRK1 and GRK7 have a short C-terminal sequences, which are approximately 60-90 residues (Chen et al., 2001). The GRK2 subfamily around 230 amino acid residues contains pleckstrin homology (PH) domain suggesting that these GRKs confer the ability to associate with anionic phospholipids and Gβγ subunits (Lymperopoulos et al., 2012). GRK4 and GRK6 have

palmitoylation sites, which have the covalent attachment of palmitic acid, as well as lipid binding capabilities, indicating that these kinases are typically membrane proteins (Dorn, 2009). The GKR5 kinase is also a membrane bound protein due to its phospholipid binding domain (residues 552 to 562). Interestingly, GRK5 is the only GRK has both nuclear localisation sequence (NLS) and nuclear export signal (NES) (Johnson et al., 2013).

Although most of the GRKs have been reported to ubiquitously express in human body, tissue-specific distribution of GRKs is also confirmed (Table 1.1). For instance, GRK1 subfamily was highly expressed in retina, especially in rod and cone photoreceptors, although both GRK1 and GRK7 presented in pinealocytes. Recently, GRK3 has been shown to be expressed in thyroid nodules, and its expression is up-

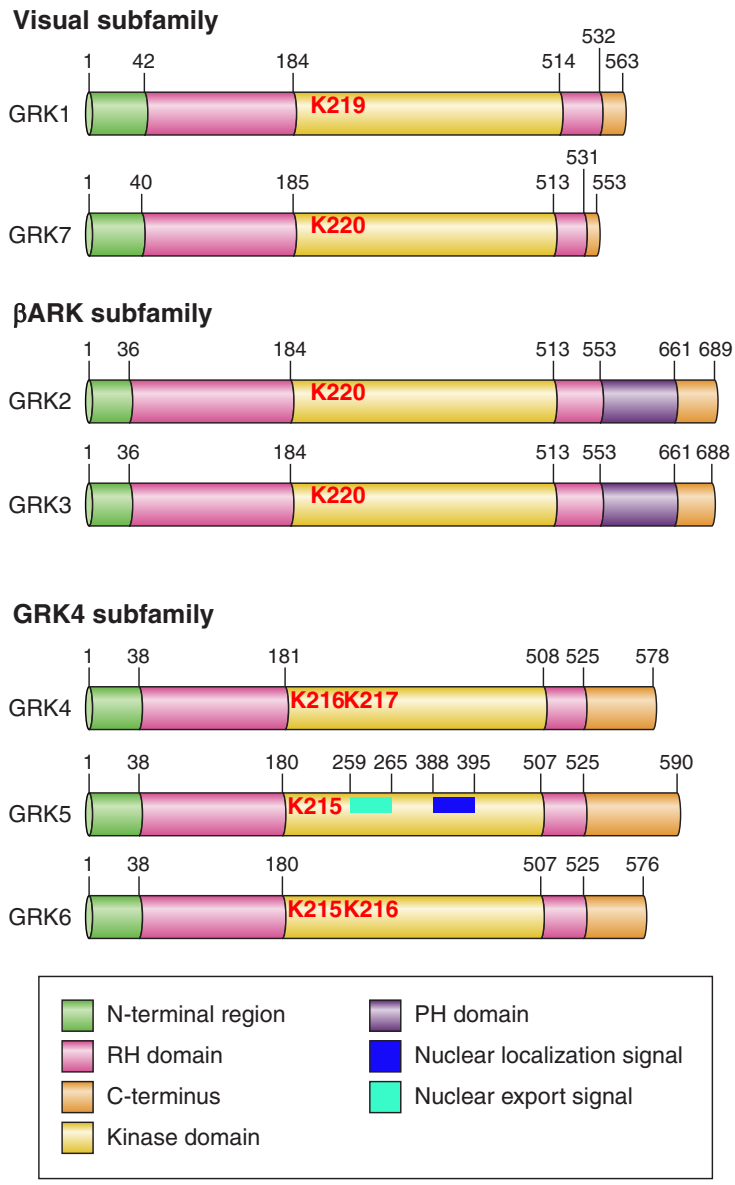


Figure 1.4: Classification of GRK family. All GRKs consist of three main important domains, including a N-terminal domain (Green), followed by an RH domains (Pink) interrupted by a kinase catalytic domain (Yellow) and a C-terminal regions (Orange). Number in red correspond to residues responsible for catalytic activities. Figure obtained from Sato *et al.,* 2015 (Sato et al., 2015).

regulated in hyper-functioning thyroid tissue. GRK4 is highly expressed in the testes as well as in proximal tubule cells in kidney and brain. Moreover, GRK2 and GRK5 are found to be expressed abundantly in the heart. Of notes, both GRK2 and GRK5 are the primary target of several GPCRs, including β-ARs and AT-1 receptors.

Table 1.2: Tissue distribution and cellular localisation of GRKs. (Adapted from Sato et al., 2015).

GRK	Tissue Specification	Cellular localisation	References
1	Retina > pineal	Cytoplasm but close to plasma membrane (outer rod segments)	(Chen et al., 1999; Shichi and Somers, 1978)
2	Leukocytes > brain > heart, lung, kidney, thyroid nodules	free protein in cytoplasm or associated with actin, actinin, and microtube > mitochondria	(Benovic et al., 1987; Fusco et al., 2012)
3	Brain > spleen > heart, lung, kidney, thyroid nodules	Cytoplasm > plasma membrane	(Benovic et al., 1986; Strasser et al., 1986)
4	Testis > brain, thyroid nodules	Different splice variants below: α, β, γ, and δ: Cytoplasm > plasma membrane >>> nucleus	(Yarfitz and Hurley, 1994)
5	Heart > Placenta, lung > skeletal muscle > brain, liver, pancreas > kidney, thyroid nodules	Plasma membrane > cytoplasm > nucleus	(Johnson et al., 2013; Kunapuli and Benovic, 1993)
6	Brain, skeletal muscle > pancreas > heart, lung, kidney, placenta > liver, thyroid nodules	Different splice variants below: A, B, C: Cytoplasm and closed to plasma membrane >>> nucleus D: exclusively in the nucleus	(Vatter et al., 2005)
7	Retina, particularly cones	Cytoplasm but close to plasma membrane (cone outer segments)	(Chen et al., 2001)

1.3.2 GRKs and their roles in heart failure conditions

The heart failure (HF) is the end point of many cardiovascular diseases, including myocardial infarction, hypertension, coronary artery disease, cardiomyopathies, congenital heart disease, and others. Several characteristics of HF are left ventricular dysfunction associated with a complex of symptoms that are related to inadequate perfusion of cardiac tissues, arrhythmias, hypertrophy, and pulmonary congestion (Towbin and Bowles, 2002). Under these conditions, activation of the sympathetic nervous system has a major role in readjusting circulatory homeostasis to scope with the

situation. In fact, one of the hallmarks of heart failure is the increased activation of sympathetic nervous system, resulting in the increase circulating catecholamine, which in turn evoke the activation of adrenergic signalling pathways (Lymperopoulos and Bathgate, 2013). In the human heart, these activities are translated by the activation of β-AR signalling transduction pathways. This augmentation in stimulus is believed to be involved directly in a compensatory mechanism that re-establishes cardiac performance and increases cardiac contractility as well as beating frequency (Esposito et al., 2002; Dorn, 2009). However, upon the extension of the condition, prolonged activation of sympathetic activities had adverse biological effects, which in turn facilitate the cardiovascular pathology. Studies about heart failure illustrated that increasing GRK activities in both heart and sympathetic nervous system enhanced further these pathological events. In the heart, GRK2 and GRK5 are the most abundant GRKs, which are directly involved in regulation of the adrenergic functions (Rockman et al., 2002; Thomas et al., 2004; van Meer et al., 2016).

As mentioned before, the chronotropic and inotropic activities of the heart are regulated by β_1- and β_2-ARs via $G\alpha_S$-mediated signalling pathways. However, chronic stimulation of β-ARs has been reported to induce opposing outcomes during heart failure; stimulation of β_1-, and β_2-ARs would lead to detrimental and cardioprotective effects, respectively. Hence, increasing β-AR activities results in an upregulation of GRK2 and GRK5 to turn off the β-AR signalling transduction. Continued activation of β_1-, and β_2-ARs on CMs during heart failure leads to the increase in their desensitisation regulated by GRK2 and GRK5 activities and chronically results in receptor downregulation and reduction of adrenergic signalling pathways (Penela et al., 2006). However, there are two distinct desensitisation mechanisms between these two GRKs due to their cellular distribution, cytosolic GRK2 vs. membrane bound GRK5 (Figure 1.5) (Pitcher et al., 1998).

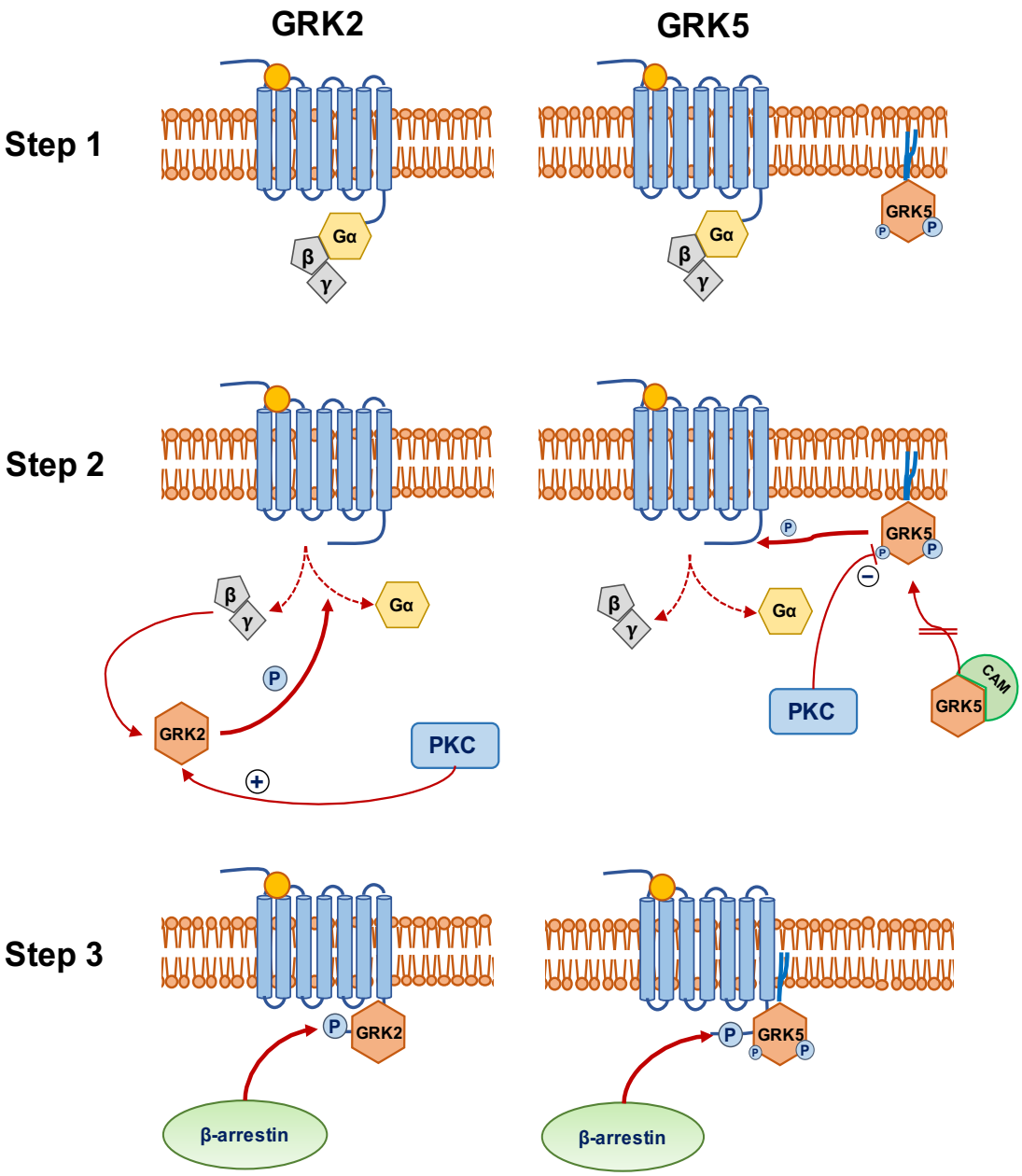


Figure 1.5: Schematic depicts three arbitrary steps of GRK-mediated phosphorylation of β-ARs between GRK2 and GRK5 in heart. Separate schemata illustrated for GRK2 (left panel) and GRK5 (right panel). **At step 1**: Agonist-bound β-AR triggers the binding of G-protein complex to the C-terminal domain of the receptors. At this step, GRK2 and GRK5 has not yet bound to receptors and still maintain at cytosolic and plasma membrane of the cells, respectively. GRK5 adheres to the membrane via interaction with phosphatidylinositol 4,5 biphosphate (PIP2) within the plasma membrane with its C-terminal domain. Phospholipid-bound GRK5 undergoes autophosphorylation (P) which is required for receptor-phosphorylating activities. In step 2: After associated with activated β-AR, the G-protein complex dissociates into Gα and Gβγ subunits and triggers the cellular response via effectors and second messengers, including PKC. The Gβγ subunits along with PKC facilitate the translocation of GRK2 from cytosolic to plasma membrane where GRK2 binds to the activated receptors. GRK5, on the other hand, associates with the activated receptor without the need of Gβγ subunits. In fact, GRK5 phosphorylation activities are inhibited by PKC. Also, the phospholipid binding by GRK5 is also interrupted by calcium/calmodulin (CAM). Step 3: the phosphorylation of agonist-bound β-AR by either GRK2 or GRK5 results in the recruitment of β-arrestin protein and consequently lead to the desensitisation of β-ARs. Figure is adapted from Pitcher et al., 1998.

To be more specific, upon dissociation of G-protein complex into Gα and Gβγ subunits from the agonist-bound β-ARs, the Gα subunit stimulate the effectors to produce second messengers, which in turn, activated protein kinase C (PKC), among other proteins. The activation of PCK together with Gβγ subunit facilitate the transportation of GRK2 from its local cytoplasmic position to plasma membrane of the CMs, where it binds to and phosphorylates the activated β-AR (Lobmeyer et al., 2011; Robinson and Pitcher, 2013). In contrast, the GRK5 is a membrane-bound protein that anchor itself into the membrane via interaction between its N-terminal domain and phosphatidylinositol 4,5 triphosphate (PIP2). It is important to emphasise that GRK5 phosphorylating function of β-AR depends on its auto-phosphorylation ability, which differs from that of GRK2 (Kunapuli and Benovic, 1993; Komolov et al., 2015). The cytoplasmic Calcium/calmodulin inhibit the binding of GRK5 to the plasma membrane of the CMs. While the PKC and Gβγ subunit facilitate GRK2 functions, the GRK5 does not require the assistant of Gβγ subunit (Dorn, 2009). Interestingly, the abolishment of GRK5 phosphorylation activities occurs when it is phosphorylated by PKC.

Hence, the two abundant GRKs in the heart have two distinct mechanisms in regulation and phosphorylation of the agonist-bound β-ARs to diminish catecholamine responsiveness by promoting receptor desensitisation and downregulation (Sato et al., 2015). Upregulation of GRK2 is postulated to contribute to the pathology of the heart failure by further reducing the adrenergic responsiveness, which in turn, prohibits the recovery of the heart. In terms of its chronotropic and inotropic functions results in the continuous firing of positive-feedback signal to sympathetic nervous systems which triggers the release of catecholamine. It was reported that GRK2 protein and its mRNA levels were increased significantly during heart failure which induced the GRK activities two to threefold (Ungerer et al., 1993). Overexpression of GRK2 and GRK5 in mouse model revealed that GRK modulatory functions have different specificities for β-AR and AT_1 receptor (Dzimiri et al., 2004; Koch et al., 1995). Mice overexpressing heart-specific GRK2 at approximately threefold endogenous levels demonstrated a diminishing effect

on responsiveness to isoprenaline treatment leading to the desensitisation of the receptors (Koch et al., 1995). Moreover, GRK2-overexpression was also reported to desensitise AT_1-mediated response to angiotensin II treatment. However, overexpression of GRK5 showed a similar effect on desensitising β-AR but had no effects on AT_1 receptor signalling, indicating the preferential GRK-receptor pairing in the heart (Dorn, 2009). Another difference between GRK2 and GRK5 is that members of the GRK2 subfamily do not have a nuclear localisation signal (NLS). The protein crystallisation study confirmed the NLS sequence of GRK5 (RKEKVKRE), which is located from amino acid 388 to 395 and mediates nuclear translocation as well as DNA binding functions of GRK5 (Komolov et al., 2015). Interestingly, GRK5 is unique among human GRKs in that it also possesses the nuclear exported signal (NES) sequence, which mediated the GRK5 nuclear export in a calcium-dependent manner. Also, the exportation of GRK5 via its NES is controlled by calcium/calmodulin (CAM) binding to the amino terminal CaM binding domain (Figure 1.6) (Sato et al., 2015).

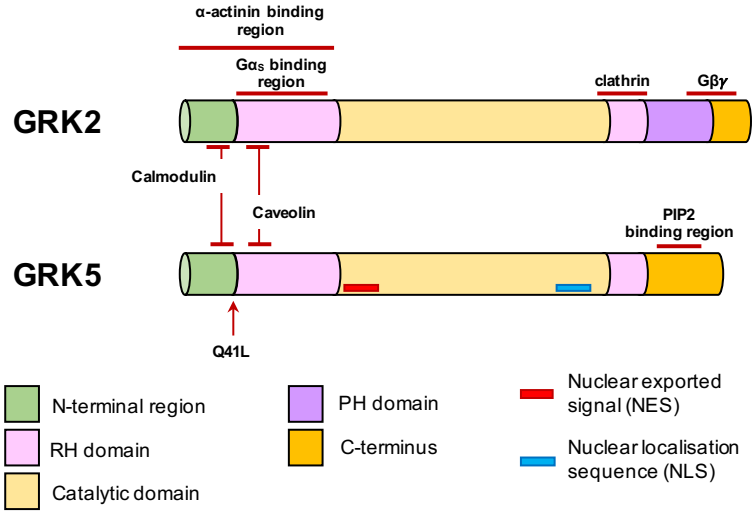


Figure 1.6: Comparative structures of GRK2 and GRK5. Both GRK2 and GRK5 share a common GRK structure, including N-terminal region, RH domain, a central catalytic domain, PH domain and C-terminal domain. The red line indicates the region of GRK specific binding. GRK2 structure has specific regions allocated for assiociated with α-actinin, $G\alpha_S$, clathrin, and Gβγ, which are not present in GRK5. GRK5 structure has PIP2 binding region, which associated with its membrane-bound ability. Both GRK2 and GRK5 structures contain the calmodulin and caveolin binding region, indicating that both GRKs could potentially associated with calmodulin and caveolin. The GRK5 has been found to confer the ability to localise to the nucleus via its nuclear localisation signal (NLS) sequence located in the catalytic domain, and also contains a nuclear export sequence (NES) within the centrally conserved kinase domain. Recently, a single nucleotide polymorphism was found in GRK5 (Q41L), which located close to calmodulin binding region of GRK5. (Figure is adapted from Dorn, 2009; Sato et al., 2015; Traynham et al., 2016).

1.3.3 Roles of GRK5 in cardiac biology and pathophysiology

In addition to GRK2, GRK5 is found to be highly expression in the human heart (Aguero et al., 2009; Dzimiri et al., 2004). In fact, the GRK5 expression level is highest in myocardium compared to that of other tissues and organs in human body (Kunapuli and Benovic, 1993). Interestingly, GRK5 is the most commonly found GRK in the transplanted hearts and has been suggested as a key factor that contributes to the development of cardiac hypertrophy and heart failure (Traynham et al., 2016). In dilated cardiomyopathy, GRK5 expression increased by 68% in left ventricular CMs and by 48% in volume-overload patients (Aguero et al., 2012). Studies from CMs isolated from patients experienced β-agonist infusion indicated the upregulation of GRK5 at both protein and mRNA level. CMs isolated from patients with β-blockage treatment showed a similar GRK5 expression level to that of the normal heart (Aguero et al., 2009). Last but not least, a comparative study of ischemic, dilated CMs and normal counterpart illustrated that expression levels of GRK5 inversely correlated with left ventricular end systolic and diastolic diameters (Monto et al., 2012).

The establishment of overexpression cardiac-specific GRK5 in transgenic mouse provided further information about its hypertrophic functions in the heart. These studies showed that overexpression GRK5 in transgenic mouse were intolerant to left-ventricular pressure-overload and the hypertrophic development as well as early progression of HF seen in the transgenic mice were attributed by the nuclear localisation of GRK5 within the CMs (Rockman et al., 1996a). Interestingly, it was demonstrated that accumulation of GRK5 in the nucleus mediated by $G\alpha_q$-dependent manners. Furthermore, GRK5 has been proven to act as a class II histone deacetylase (HDAC) kinase, phosphorylating HDAC5 resulting in its translocation from nucleus to cytoplasm of the cells, which in turn activated the MEF2 hypertrophic transcription factors (Figure 1.7) (Traynham et al., 2016; Sato et al., 2015). Importantly, to further confirm the attribution of GRK5 in hypertrophic and progression of heart failure, transgenic mice with GRK5 knock-out in both global and cardiac specific GRK5 illustrated a significant decrease in hypertrophic effects and improved functions after ventricular overload experiments.

Moreover, during the induction of pathological hypertrophy, GRK5 was also found to be able to interact with nuclear factor of activated T-cells (NFAT) pathway using NFAT-luciferase reporter mice (Hullmann et al., 2014). In this study, overexpression of GRK5 resulted in the increase of NFAT activity while GRK5 knock-out mice showed an opposite result (Hullmann et al., 2014). Further investigation using double transgenic mice with cardiac-specific GRK5 overexpression and deletion of NFAT resulted in the protective effects during early progression of heart failure.

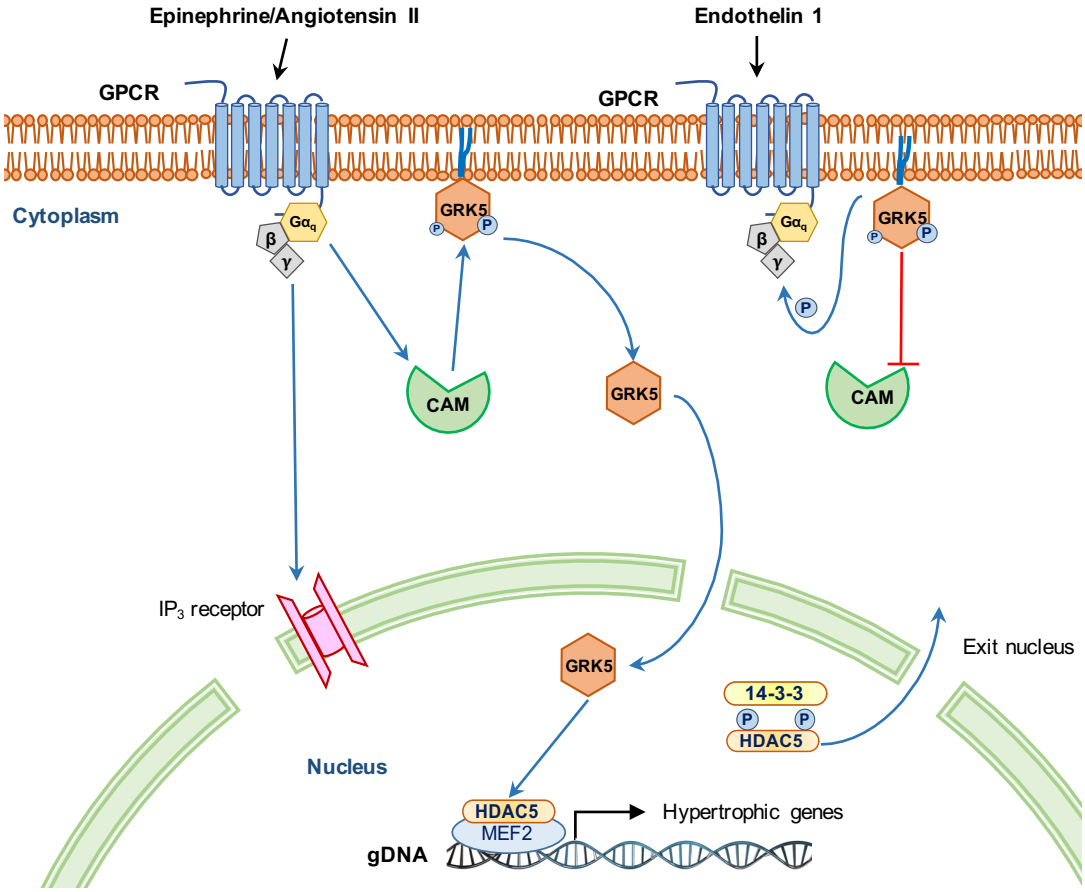


Figure 1.7: Non-canonical functions of GRK5 in the heart. Activation of catecholamine- or angiotensin II-mediated GPCR leads to the activation of $G\alpha_q$ signalling pathway, which promotes the activation of calmodulin. Calmodulin bind to membrane-bound GRK5 at N-terminus and release it from the plasma membrane and stimulate the nuclear translocation of the GRK5. Nuclear GRK5 associated with calmodulin stabilised the IP_3 receptor which involved in regulation of Ca release. The GRK5 proteins accumulated in the nucleus phosphorylate HDAC5 and promote its exportation from the nucleus and release the MEF2 from HDAC5 suppression, which, in turn, induces the expression of hypertrophic-related genes. On the other hand, endothelin-1 receptor activation results in its desensitisation mediated by GRK5, which prevent it from interaction with Calmodulin, thus preventing the accumulation of GRK5 inside the nucleus. Figure is adapted from Traynham et al., 2016 and Sato et al., 2015.

1.3.4 GRK5 single nucleotide polymorphism (GRK5-L41) and its putative roles in cardiac physiology

As introduced above, functional differences between myocardial GRK2 and GRK5 are distinct and the latter has been proven to be involved in the attribution of the development of heart failure and cardiac hypertrophy. Recently, a comprehensive SNP screening research was conducted to identify coding polymorphisms of both GRKs. No nonsynonymous (i.e. amino acid changing) polymorphisms were determined in GRK2, but there were four different variants were detected in GRK5 (Liggett et al., 2008). Among these four, a single nucleotide polymorphism that changes the amino acid substitution of glutamine (Q) to leucine (L) at position 41 of GRK5 protein was proven to have gain-of-function polymorphism by enhancing both β_1- and β_2-AR uncoupling during persistent agonist exposure (Liggett et al., 2008; Wang et al., 2008). Strikingly, this GRK5-L41 variant only occurs in approximately 40% African American cohort and 2% Caucasians carrying this gene (Liggett et al., 2008).

Studies in transgenic mice that expressed the human cardiac GRK5-L41 illustrated the enhancement in uncoupling rate of β-ARs in response to isoprenaline stimulation compared with GRK5-Q41 or non-transgenic littermate mice. Furthermore, this study also showed that GRK5-L41 conferred the ability to diminish β-AR signalling pathway similar to the β-blockade treatment. Clinical study on African American patients bearing GRK5-L41 demonstrated that they have prolonged survival and prolonged time for cardiac transplantation (Liggett et al., 2008). Moreover, a study size of 2,673 acute coronary syndrome patients showed improved outcomes from patients carrying GRK5-L41 (Cresci et al., 2012). Besides, detailed studies of patients with GRK5-L41 clarified the cardiac protective function in treated hypertensive patients with coronary artery disease, although antihypertensive treatment did not show any influence on blood pressure (Lobmeyer et al., 2011). Patients with the left ventricular apical ballooning syndrome also showed an increase prevalence of GRK5-L41 polymorphism (Spinelli et al., 2010). Overall, it is important to indicate that although this GRK5-L41 polymorphism might relate to the nuclear localisation events of GRK5 during pathological hypertrophy,

canonical GPRC phosphorylation and desensitisation, as well as non-canonical induction mediated by GRK5 activities might also be attributing factors to what has been observed in GRK5 polymorphism.

1.4 Models for studying GRK functions

1.4.1 Mouse models for GRK studies

Until recently, mouse models had proven to be a powerful tool to expand the knowledge about GPCR and GRK functions. Since the first mouse model was presented by Koch and colleagues in 1995 about the GRK1 knockout which resulted in the loss of light-dependent phosphorylation of rhodopsin receptor, various mouse models have been established to understand the complex structures and functions of GPCRs and their regulatory protein, GRKs (Koch et al., 1995). These studies, which utilised either transgenic and knockout mice, have both confirmed the predictions from earlier *in vitro* work and provided a fascinating insight of the interrelationship between GPCRs and GRKs.

1.4.1.1 Transgenic animals

Transgenic mice coupled with the use of cardiac-specific promoters has made it feasible to investigate the β-AR functions in both normal heart conditions and during heart failure conditions. Transgenic mice models created with ventricular overexpression of either β_1- or β_2-AR show significant different phenotypes, providing a principle difference between the two most important subtypes of GPCR in the heart, especially in CMs. A 5- to 15-fold increase in β_1 expression level promoted the development of dilated cardiomyopathy even in the early stage of development and was supported to the pathological phenotypes observed in chronic administration of catecholamines (Dorn, 2009; Pitcher et al., 1998). In contrast, upregulation of up to 200 times more β2-ARs than its endogenous level did not cause significant cardiac pathology in the transgenic mice, which were instead characterised by the improvement of cardiac functions in response

to biochemical compounds (Pitcher et al., 1998). However, overexpression of β2-ARs higher than 200-fold resulted in the rapid development of progressive cardiomyopathic phenotypes, which is consistent with the cardiotoxicity caused by exceeding β-AR activation (Du et al., 2000).

In terms of studying GRK functions, transgenic mice bearing cardiac-specific promoter – the murine alpha myosin heavy-chain – driven the expression of either GRK2 or a GRK2 antagonist, consisting of the C-terminal 195 amino acid residues of GRK2, illustrated the transportation inhibition of Gβγ subunits, the function similar to that of Gβγ sequestering protein *in vitro* (Koch et al., 1995). Furthermore, overexpressing GRK2 also demonstrated the depletion in left ventricular contraction stimulated by isoprenaline infusion, reduction of sarcolemma adenylyl cyclase activities, and diminishment of functional coupling of β-ARs in transgenic mice (Xiao et al., 1998). On the other hand, mice expressing the GRK2 inhibitor displayed increased cardiac contractility even without isoprenaline stimulation. Interestingly, transgenic mice which overexpressed cardiac-specific GRK5 showed faster desensitisation of β-ARs, as judged by isoprenaline infusion compare to normal non-transgenic littermate mice (Rockman et al., 1996b). The desensitisation effects observed in GRK5 overexpressing mice were even more impressed than that showed in GRK2 overexpressing mice; however, it is important to note that relative overexpression of GRK5 in the experiment was also much higher than that of GRK2 (Philipp et al., 2014).

One of the fascinating studies derived from transgenic mice models was the experiment with angiotensin II treatment. In this experiment, GRK5 overexpressing mice showed an increased contraction stimulated by angiotensin II treatment, whereas overexpressing GRK2 inhibited the effects of angiotensin II-stimulated contractility (Rockman et al., 1996a). Because angiotensin II activated AT_1 receptors which increase the intracellular Ca^{2+} concentration and subsequently activate calmodulin, it, in turn, inhibited the canonical function of GRK5 more than it does to GRK2 action. Hence, it explained the apparent GRK specificity occurs in the heart. From that fundamental

experiment, further study found that activation of calmodulin not only inhibited the canonical function of GRK5 but also promoted the nuclear translocation of GRK5 leading to its hypertrophic effects on CMs (Martini et al., 2008; Gold et al., 2012).

1.4.1.2 Knockout mice

Along with the transgenic approach, knockout models had also been proven to be a valuable tool to understand the principles of GPCRs and GRKs. During developmental process, it was reported that only global knockout of GRK2 is embryonically lethal (Jaber et al., 1996). This result is important to note as particularly significant because GRK2 was later found to be the predominant GRK to be expressed during embryogenesis (Sefton et al., 2000). Interestingly, cardiac-specific GRK2 knockout did not affect the embryonic development of transgenic mice. In fact, normal heart formation, cardiac function and gene expression were observed in cardiac-specific GRK2 knockout mice (Matkovich et al., 2006). Under isoprenaline treatments, these mice exhibited enhanced inotropic sensitivity, impaired lusitropic activity, and showed arrhythmias as well as irregular beating patterns during chronic treatment of catecholamines (Matkovich et al., 2006). While globally knockout of GRK5 was not embryonically lethal, double knock-out of both GRK5 and GRK6 resulted in the termination of embryonic development indicating that there is a compensatory mechanism between GRK5 and GRK6 during early development (Burkhalter et al., 2013).

Concerning cardiomyocyte functions, the role of β-ARs has been illustrated further by gene disruption experiments, where knockout of β_1-AR in mice results in embryonic lethality. Interestingly, when the mice were outbred, the developmental mortality was reduced (Rohrer, 1998). Although the survival mice exhibited normal resting heart rate and blood pressure, there was no contractility stimulation in response to β-agonist treatments. This result suggested that β1-AR is the predominant mediator of catecholamine-induced inotropic and chronotropic functions in the mouse heart (Rohrer, 1998). In contrast, knockout of β_2-AR in mice did not affect the survival rate of the

embryos; physiological consequences were observed only during the catecholamine challenges, or the stress of exercise, suggesting that a lack of β_2-ARs has little impact on cardiac functions (Rockman et al., 2002).

1.4.2 *In vitro* cellular models

Since the discovery of GRK2, *in vitro* cultured cells have been used as alternative tools for the demonstration of GPCR and GRK functions. Several approaches can be achieved using the models including **(1)** demonstration of specific GRPC functions via compound screening process; **(2)** evaluation of GRK actions in desensitisation of particular receptors; **(3)** investigation of GRK kinetics via desensitisation process; **(4)** defined GRK subcellular localisation; **(5)** screenings of assay that are involved in GPCR and GRK expression and activity; and **(6)** evaluation and identification of candidate receptor substrate (Table 1.4) (Wakefield et al., 2002; van Meer et al., 2016).

Moreover, the primary cells isolated from either healthy or patients with cardiovascular diseases can be used as *in vitro* models for disease modelling and GPCR functional analysing (Barajas-Martinez et al., 2013; Bogaard et al., 2009; Manders et al., 2014; Min et al., 2010). However, accessing patient samples with rare genotype, such as GRK5-L41 or the R16E27 haplotype of β_2-AR (less than 1% of population carrying the SNPs), can be a challenge (Liggett et al., 2008; Zee et al., 2005). Alternatively, immortalised cell lines (such as human epidermis carcinoma A431 and C6 glioma cells) and transformed cell lines (such as Chinese hamster ovary and HEK 293 – human embryonic kidney cells) can serve as an alternative method. However, these systems are similar to that of animal model in which the physiological and pathological responses of these lines might not similar to that of found in human, which also explained why the uses of *in vitro* models result in high rate of commercial drug rejection in pharmaceutical fields (John P. Overington, 2006). This obstacle led to the development of models derived from hPSCs, which can be cultured indefinitely *in vitro* and can differentiate into different cell types, including CMs (Burridge et al., 2015).

Table 1.3: Representative cellular models used to investigate GPCR functions.

Cell lines	Characteristics	Targeted GPCR and GRK	Methodology	Phenotype	Reference
Human A431	Human epidermis carcinoma	β_2-AR and GRK2	Permeabilised cell system	Observation of desensitisation of β_2-AR mediated by GRK2 using GRK2-selective inhibitor heparin.	(Pitcher et al., 1998)
		β_2-AR and GRK2	Permeabilised cell system	Observation of desensitisation of β_2-AR mediated by GRK2 using oligodeoxynucleotides to inhibit GRK2 synthesis.	(Pitcher et al., 1998)
		β_2-AR, GRK2, and GRK5	Permeabilised cell system	Rate of GRK-mediated phosphorylation and desensitisation was approximately 15s ($t_{1/2}$).	(Lorenz et al., 1991)
Rabbit cardiac myocytes	Primary cell line	β_2-AR, H_2-histamine receptor, and GRK2	GRK specific antibody	β_2-AR desensitisation was GRK2-dependent.	(Oppermann et al., 1996)
Rat neuronal cells	Dendrites of rat olfactory neuron	β_2-AR and GRK3	Permeabilised cell system	GRK3-mediated odorant receptor desensitisation was approximately 200ms ($t_{1/2}$).	(Roskams et al., 1993)
C6 cell line	Immortalised Glioma cells	β-ARs	Drug testing	Isoprenaline increased fast desensitisation of β-ARs and transient receptor sequestration.	(Garciahiguera and Mayor, 1992)
CHO	Chinese Hamster Ovary	Universal	Drug testing	Identification of ligand binding and induction specificity	(Martins et al., 2012)
Sf9 and Sf21	Insect cell lines	16 different human GPCRs	Baculovirus transfection and overexpression	Functional characterisation of 16 human GPCRs	(Akermoun et al., 2005)
HEK 293	Human embryonic kidney cells	Universal	Stable expression of human receptors	Identification of heterodimerisation process is involved in modulation of receptor function	(Jordan and Devi, 1999)
mESC	Mouse embryonic stem cells	Cannabinoid receptors (CB1 and CB2)	Using cannabinoid agonist treatment	CB1 and CB2 receptors are involved in maintenance and survival of mESC.	(Jiang et al., 2007)
		Chemokine receptor - CXCR4	RNA analysis and In situ hybridisation of embryonic body	Involved in stem cell maintenance and migration process	(Miller et al., 2008)
		AT_1 receptor	RNA analysis and Western Blot	Angiotensin II is involved in cardiac differentiation of mESC	(Wu et al., 2013)

Table 1.3: Continued

Cell lines	Characteristics	Targeted GPCR and GRK	Methodology	Phenotype	Reference
hESC	Human embryonic stem cells	G protein coupled Sphingosine 1 phosphate receptors (S1P); G protein-coupled lysophosphatidic acid receptor	qPCR analysis, immunocytochemistry and RNA analysis	Involved in stem cell maintenance and migration process	(Dottori et al., 2008; Wong et al., 2007)
hESC-CM	Human embryonic stem cell derived cardiomyocytes	β-ARs	mRNA analysis, genomic sequencing and functional assay	Identification of epigenetic regulation (phosphodiesterases 2A and 3A) is involved in regulation of β-AR during dilated cardiomyopathy	(Wu et al., 2015)

1.4.3 Human pluripotent stem cell models

Understanding the mechanism and functional differences of GRPCs and their regulators – GRKs – during physiological and pathophysiological conditions of the heart using human CMs can provide in-depth knowledge about disease state and pathological signalling underlying these conditions. As mentioned above, the GPCR family is a major target for therapeutic intervention and drug development as most cardiovascular physiological, and pathological processes are regulated through GPCRs (John P. Overington, 2006; Nguyen et al., 2016). However, due to its ethical issue, limited access to patient samples, and difficulties in culture *in vitro*, human primary CMs are not the best option for scientific research, disease modelling and drug development. Therefore, terminally differentiated cells, including CMs, derived from hPSCs provide a powerful tool to be employed as functional models for disease modelling, biomedical research, and high-throughput drug screening. Also, with the establishment of the "3R principle" – replace, refine, and reduce the use of animals in research testing (http://www.nc3rs.org.uk/) – the application of stem cell derived CMs in biomedical investigation and disease modelling becomes one of the method of choice (van Meer et al., 2016).

1.5 Cardiomyocyte differentiation process of hPSCs

1.5.1 Developmental cardiac differentiation: a fundamental lesson from cardiomyogenesis

During embryogenesis, the heart is one of the first organs to form and function in the human embryo. While developmental progression starts outside the embryonic disk, the heart finally retains in the chest cavity upon the embryos folding process (Rana et al., 2013). The formation of the heart originated from the bilateral heart fields that are established during gastrulation process and are divided into four specific processes including **(1)** cardiac mesodermal specification; **(2)** bilateral symmetry determination of the heart fields; **(3)** heart field arrangement; and **(4)** terminal cardiac differentiation (Figure 1.8) (Burridge et al., 2015; Paige et al., 2015).

1.5.1.1 Cardiac mesodermal specification

During gastrulation process, the formation of three germ layers starts in the pattern that the mesoderm layer sandwiched between ventral endoderm and dorsal ectoderm. The cardiogenic area is located in the anterior part of the embryonic disk, where mesoderm cells are occupied (Carnegie stage 8). The mesodermal structure is patterned into two distinct layers, the somatic outer layer and the splanchnic inner layer (Carnegie stage 9) and give rise to the formation of the myoepicardiac mantle, which later differentiates into epicardium and myocardium. The myocardial precursor cells express the T-box transcription factor T (*Brachyury-T*) and migrate from the posterior epiblast through the anterior portion of the primitive streak to form the anterolateral plate mesoderm that undergoes rapid migration toward the midline (Harvey, 2002).

This mesodermal induction process is tightly regulated by a complex growth factor network, in which, NODAL signalling pathway plays a central role. When the mesoderm induction starts, the germ layer from which the heart forms expresses high concentrations of NODAL. Soon after expressed, NODAL begins to diffuse to the surrounding extraembryonic ectoderm (ExEc), which is involved in the maintenance of BMP4 expression at high level. In terms of embryogenesis, BMP4 expression is considered as a secondary signal for mesoderm induction and specification. As the gastrulation proceeds, BMP4 signals from ExEc spread out and trigger the expression of WNT3 in the proximal epiblast. In mouse embryonic development, a signalling spot on the tip of the distal visceral endoderm migrates anteriorly and expression NODAL inhibitors (LEFTY1 and CER1) and a WNT inhibitor (DKK1), results in the restriction of NODAL and WNT signalling to the posterior epiblast, which later induces the mesodermal transcription factors including Brachyury-T – a specific mesodermal marker, T-box transcription factor Eomesodermin (EOMES), which, along with NODAL and growth factors (FGF4 and FGF8).

1.5.1.2 Determination of bilateral symmetry of the heart fields

Following the migration of posterior epiblast through the primitive streak toward the midline of the embryo, the population of cardiac progenitor cells then converge at the midline and rearrange into a crescent, with the peak of the crescent located at cranial area and the bottom of the crescent extending caudally. As the embryo folds, the two crescent branches met and fused to form a single heart tube at the end of the third gastrulation week (Carnegie stage 10). The morphology of the heart tube at this stage is similar to the inverted Y shape (from cranial to caudal position) and is segmented into the truncus arteriosus, bulbus cordis, primordial ventricle, primordial atrium, and sinus venosus. The heart starts to beat at day 22-23 of human embryonic development, forcing the cranial movement of blood from the sinus venosus.

During this process, a cascade of signalling pathways is activated and involved in cardiac specification and differentiation. The activation of EOMES transcription factor during mesodermal specification triggers the expression of the basic helix-loop-helix transcription factor mesoderm posterior 1 (Mesp1) (Costello et al., 2011; van den Ameele et al., 2012). *Mesp1* expression during gastrulation represents the first step of cardiogenesis, and it is considered as a specific marker of cardiovascular specification (Saga et al., 2000). Mesp1 function is to initiate the cardiac differentiation process *in vivo* by a multifaceted mechanism, in which it not only drives the expression of cardiac-specific transcription factors but also suppresses the expression of genes that regulate and maintain pluripotency stage (Bondue et al., 2008). As the mesodermal cells are committed to become cardiac precursors, they start to migrate away from the primitive steak to form the cardiac crescent, which in turn, leads to the downregulation of *Mesp1* and *Mesp2* expression (Bondue et al., 2008).

1.5.1.3 The heart field formation and chamber specification: from myocardial to immature cardiomyocytes

Soon after the heart tube is formed and functional, the elongation of the heart tube occurs and initiates a portion of the mid-streak mesoderm expressing *Mesp-1* undergoes

epithelial-to-mesenchymal transition and migrate bilaterally around the embryos from the primitive streak to the anterior side of the embryo to form the first and second heart fields (FHF and SHF, respectively). The FHF and SHF provide a regional differentiation pattern contributing to the formation of heart chambers. The FHF predominantly gives rise to the formation of the left ventricles, and in lesser extend the atria and conduction system, whereas the SHF forms the right ventricle, outflow tube, and atria.

During heart field formation and chamber specification, various cardiac specific factors are expressed exclusively in the atria or the ventricles, for example, the expression of the slow myosin heavy chain type 3 (MHC-3), which is directly involved in heart field formation process (Wang et al., 1998). In the FHF, the expression of MESP-1 resulted in the induction of DKK1 and other downstream WNT/β-catenin inhibitors, which, in turn, triggers the expression of NKX2.5 and TBX5 (David et al., 2008). Both of these transcription factors synergistically stimulate **(1)** MYOCD, whose primary function is driven the expression of FHF cardiac differentiation, and **(2)** activate connexin 40 (GJA5) as well as NPPA, which attribute to the specification of cardiac chambers and cardiac trabeculation in ventricles (Herrmann et al., 2012). Hence, the FHF specification can be identified by the expression of *Tbx5* and the first induction of *Nkx2.5*, which in turn induced the expression of subsequent genes involved in FHF specification.

While FHF cells start differentiation and proliferation during the formation of the linear heart tube, cells derived from the SHF maintain their undifferentiated myocardial progenitors. Within the SHF, MESP1 has a different target, which is *Foxh-1*. This gene is directly upstream of the homeodomain transcription factor *Islet-1* (*Isl1*) and *Mef-2c*. The latter is involved in gene expression regulation of NKX2.5, ISL-1, and GATA4 (Bondue et al., 2008). Also, both FOXH-1 and MEF-2C appear to initiate a SHF-specific cascade of signal transduction pathways involving in the expression of *HAND2*, *IRX-4*, *FGF-10*, *TBX-1* and *FGF8* (Dodou et al., 2004). In murine cardiogenesis, the basic helix-loop-helix transcription factors eHAND/HAND1 and dHAND/HAND2 were reported to be highly expressed in the primitive left and right ventricular chambers, respectively (Srivastava et al., 1997). Interestingly, the eHAND was suggested to act as a

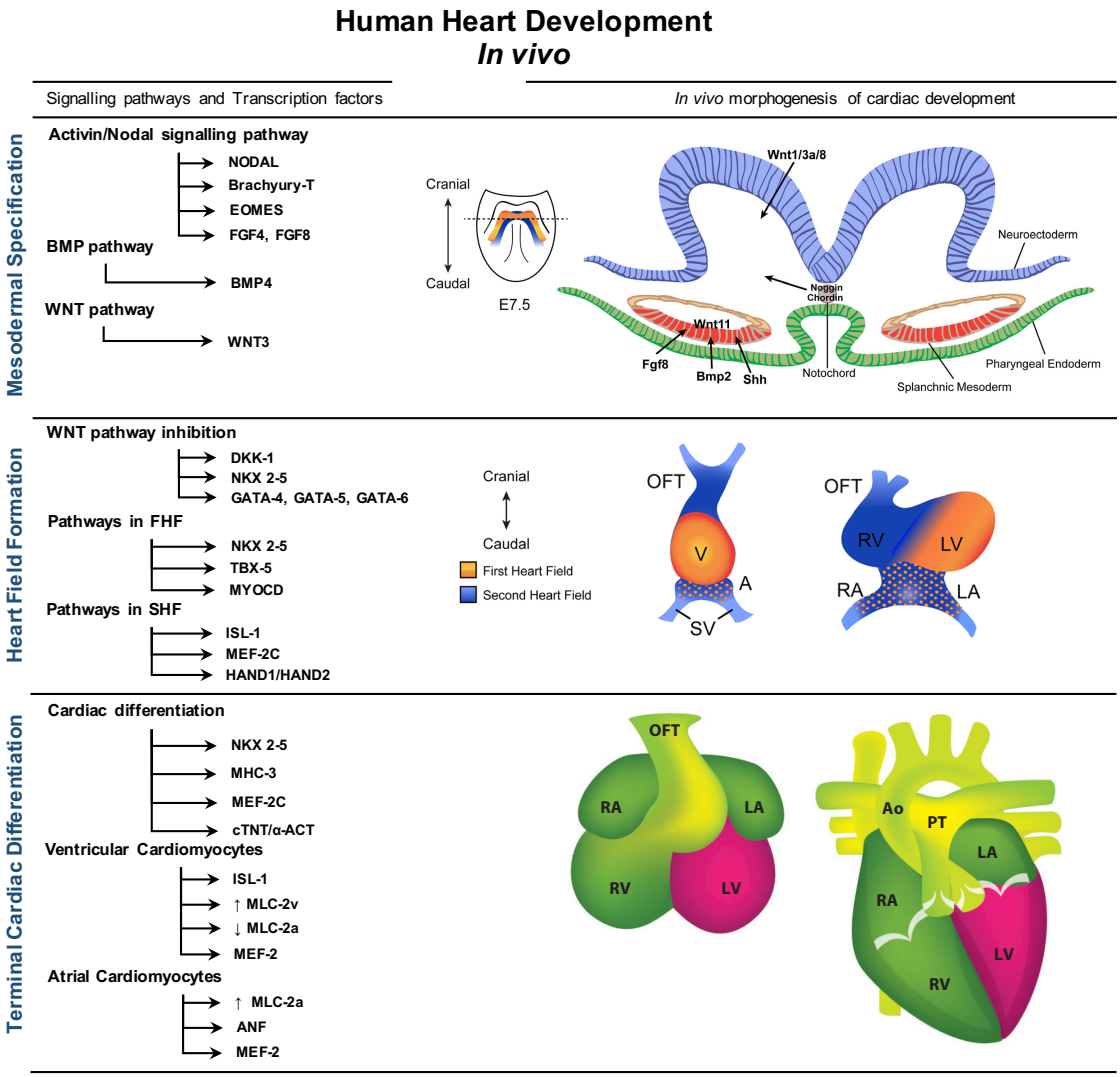


Figure 1.8: Overview of *in vivo* cardiovascular development during embryogenesis. The left panel depicts the *in vivo* signalling pathways and the key transcription factors expressed during cardiac development *in vivo*. The transcription factor expressions are divided based on cardiogenic steps during embryonic development. The right panel illustrates the major steps in cardiogenesis and the morphogenic of the heart during gastrulation. These steps are classified into four major phases, incuding (1) mesodermal specification, (2 + 3) symmetrical patterning and formation of the heart fields, and (4) chamber establishment and terminal differentiation of cardiomyocytes. ANF: atrial natriuretic factor; α-ACT: alpha-actinin; BMP: bone morphogenic protein; DKK1: dickkopf-1; FGF: fibroblast growth factor; MEF-2C: myocyte enhance factor 2C; MHC: slow myosin chain; NKX 2-5: NK2 homeobox 5; MLC-2a: myosin light chain 2a; MLC-2v: myosin light chain 2v; ISL-1: Islet-1; cTNT: cardiac troponin-T. Figure is adapted from Paige et al., 2015 and Burridge et al., 2015.

downstream regulator of NKX2.5 to control ventricular differentiation (Biben and Harvey, 1997). The maintenance of undifferentiated stage of SHF during proliferation of FHF is orchestrated by fibroblast growth factor, Hedgehog, and canonical Wnt/β-catenin signalling pathways. In mouse, conditional suppression of *Fgf8* resulted in the formation of hearts without a right ventricle and outflow tract, suggesting that Fgf8 is necessary for

SHF deployment and cardiac specification (Park et al., 2006). Moreover, it was also found that the activation of canonical Wnt/β-catenin signalling pathways is crucial for proliferation and differentiation of cells in SHF and also promotes the maintenance of multipotency of *Isl-1*$^{+}$ cardiac progenitor cells (Bu et al., 2009).

1.5.1.4 Terminal cardiomyocyte differentiation

Complete formation of the cardiac chambers divides the heart into highly specified areas with distinct functions, including working myocardium (atria vs. ventricles), the conduction system (sinoatrial node, atrioventricular node, the atrioventricular bundle, the left and right bundle branches and the Purkinje fibres (Van den Heuvel et al., 2014). The formation of working CMs occurs in two-steps process including the initial establishment of "primary" transcriptional program within the cardiac crescent and linear heart tubes followed by the development of "secondary" transcriptional program occurring in working CMs. This secondary wave of transcriptional activation results in the expression of genes that regulate terminally differentiated myocardium, including *ANF*, *Chisel* and *IRX5* expression, and upregulation of *SERCA-2a*, *MLC2v*, and *IRX4*.

1.5.1.5 Molecular regulation of ventricular and atrial cardiomyocytes

The establishment of cardiac chambers is the morphologic events accompanying by complicated signalling networks that mediate different heart fields to express cardiac-specific genes and to adopt different physiological properties. For example, the generation of the two-major working CMs, including ventricular and atrial CMs, requires the expression of two distinct isoforms of myosin light chain genes, including *MLC-2v* and *MLC-2a*, respectively. These two genes contribute to different contractile properties of the heart chambers, illustrating by an interesting experiment that replaced MLC-2v by MLC-2a in ventricular CMs of MLC-2v null mice, which led to the lack of sarcomeric structure of the CMs and lowered the contractility of the heart (Chen et al., 1999). Later, studies indicated the chamber-specific expression of Ca^{2+} cycling regulators which are

responsible for different contractile properties between atrial and ventricular CMs (Koss et al., 1995; Minamisawa et al., 2003).

The majority of studies about cardiac chamber specification were conducted in mouse models and indicated the ventricular signature gene is *MLC-2v*. The expression of *MLC-2v* is ventricular-restricted throughout the cardiac developmental process (Small and Krieg, 2004). Promoter analysis of *MLC-2v* in transgenic mice and human CMs revealed a small regulatory region for ventricular expression (28 bp segment) that are specific to the right ventricle, indicating that activation sequences for left ventricular were missing from this fragment. Moreover, further studies demonstrated that the right ventricular regulatory sequence contains an HF-1a site and an AT-rich region allowing transcription factors to bind both HF-1b and myocyte enhancing factor 2 (MEF-2) (Dodou et al., 2004).

In contrast to the ventricular-specific gene, it was found that *MLC-2a* expression was detected in the linear heart tube during cardiogenesis, and become restricted to atrial CMs later during embryonic development (Kubalak et al., 1994). Interestingly, *MCL-2a* expression was also found in left and right ventricle during early embryonic development and down-regulated independently at the later stage of cardiogenesis and subsequently lost from the ventricular CMs (Zammit et al., 2000; Devine et al., 2014). Further analysis of *MLC-2a* promoter sequence revealed that this gene contains the binding sites for several cardiac regulatory factors, including MEF-2, GATA-2, serum response factor (SRF), and retinoic acid response elements (RARE) (Small and Krieg, 2004). Although the precise mechanism that regulated the expression of *MLC-2a* during embryonic development is still remained unclear, it hypotheses that atrial expression of *MLC-2a* is achieved by the suppression of *MLC-2a* transcription in the ventricular CMs.

Therefore, due to the differences in biological and physiological functions of atrial and ventricular CMs, it is important to establish a cardiac differentiation method from hPSCs that might allow differentiating directly the hPSCs into CMs toward a particular chamber-specific subtype. Furthermore, it also provides a better understanding of the regulation of chamber-specific gene expression pattern which, in turn, allows scientists

to identify specific mechanisms involving in these processes as well as provide valuable knowledge for clinical applications in the diagnosis and treatment of congenital heart disease.

1.5.2 The *in vitro* cardiac induction process

As mentioned in the above section, multiple complex interactions between the highly-conserved gene regulatory networks orchestrate the cardiogenesis *in vivo*. The sequential activation of transcription factors that mediate the establishment of the cardiac mesodermal progenitors, and subsequently the determination of cardiac cell fate commitment is most likely controlled in hPSC in the same manner as it is in embryos. Evidence supporting this argument is the establishment of many successful protocols designed for cardiac differentiation of hPSC driven them from the pluripotent stage through the cardiogenesis process and eventually gives rise to the beating CMs (Burridge et al., 2012; Laflamme et al., 2007; Lian et al., 2012; Uosaki et al., 2011). All of these protocols apply the sequential inductions of cardiogenesis using growth factors that control precisely the series of gene expressions mimics *in vivo* developmental process (Figure 1.9). In fact, the most reproducible and efficient protocols involve stage-specific activation and inhibition of cardiac differentiation pathways in defined culture conditions, recapitulating the core steps of cardiogenesis in gastrulation process. In addition, cardiac differentiation is a delicate process, and the variability in each single step of the differentiation strategy need to be fully optimised to efficiently produce beating CMs with the highest purity (>80%) (Mummery et al., 2012).

Cardiac differentiation of hESCs was first observed by Itskovitz-Eldor's team when they formed hESCs into embryoid bodies (EBs) and differentiated them into three germ layers (Itskovitz-Eldor et al., 2000). Three years later, one of the first directed cardiac differentiation methods involved co-cultured hESCs with mouse visceral endoderm-like cells (END-2), which is relatively inefficient but has been claimed to generate mostly ~85% ventricular-like cardiomyocytes (Mummery et al., 2003). These two studies shed light into methods for improving cardiac differentiation efficiency, including removal of

fetal bovine serum (FBS), adding L-ascorbic acid (Passier et al., 2005), and elimination of insulin between d0 and d4 of differentiation (Freund et al., 2008). To date, three independent platforms for cardiac differentiation are established, including inductive co-culture, formation of the embryoid body (EB), and maintenance of hPSCs as monolayer method.

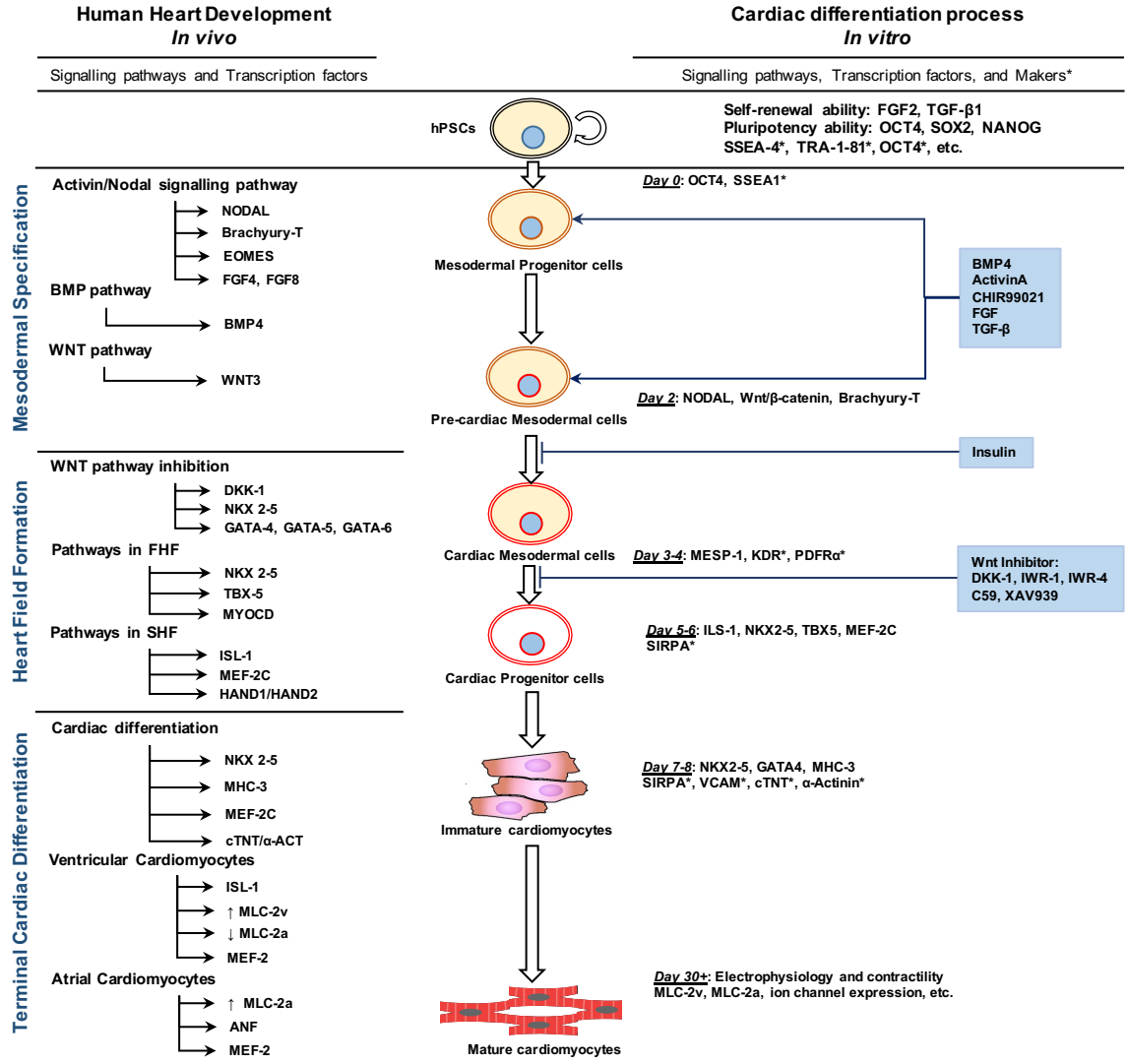


Figure 1.9: ***In vitro* cardiac differentiation of hPSCs.** The schematic illustrates the *in vitro* cardiac differentiation process (right panel) which mimic the developmental steps of cardiogenesis (Left panel). The same signalling pathways and transcription factors as shown in developmental process are applied to the right panel. Cardiac differentiation *in vitro* includes all major transitions from one cell fate to another and are activated by either BMP or WNT signalling pathways followed inhibition of WNT by using various WNT inhibitors, such as DKK-1, IWR-1, IWR-4, C59, XAV939, etc. Several stage-specific markers can be used to track the transition process, including SSEA-4, TRA-1-81, OCT4 (pluripotency stage); Brachyury-T (mesodermal induction); PDFRα, KDR, SIRPA, NKX2-5 (Cardiac precursor); and cTNT, SIRPA, VCAM, α-Actinin, etc. for early cardiomyocyte markers.

1.5.2.1 Cardiac differentiation using inductive coculture system

Generation of beating CMs from hESC using inductive co-culture system was first described by Mummery in 2003 using END-2 cells as a supportive layer for cardiac differentiation and was modified by Passier and colleagues to improve the efficiency of the method (Mummery et al., 2003; Passier et al., 2005). This approach utilised the inductive function of visceral endoderm layers to guide the cardiac differentiation of hESCs mimics the cardiogenic precursor formation mediated by signals release from endoderm layer adjacent to mesoderm *in vivo*. The initial step of this method is seeding hESCs as colonies on top of the END-2 cells, which was mitotically inactivated with mitomycin C. It took at least 12 days in co-culture to form beating areas with approximately 35% purity. However, only 1-2% CMs were obtained after dissociation process. Further optimisation revealed that removal of serum in either hESC culture condition or differentiation condition significantly reduced the efficiency of the protocol. In fact, elimination of both serum and Insulin, the essential component of the differentiation medium, resulted in a 10-fold increase in the number of beating colonies, and each beating colonies contained approximately 25% CMs (Passier et al., 2005). In addition to END-2 cell line, OP9-a stromal cell line has also been tested for induction of CM formation (Narazaki et al., 2008). Recently, an indirect co-culture method was described by using a commercially available cell culture insert which separated the neonatal CM population from mESC (Ou et al., 2013). Further modification of this method has also been reported using EB formation of mouse iPSC and coculture with neonatal CMs, and proven to be able to induce cardiac gene expression pattern and stimulate the proliferation of iPSC-derived CMs via activating FAK/JNK pathway (Ou et al., 2013).

Several advantages of the inductive co-culture system were reported, including the requirement of a small number of hESCs, simple procedure, generation of CMs in sufficient number and quality to detect quickly using immunocytochemistry staining (Mummery et al., 2012). However, the protocols required manual dissection of CMs, which is a labour-intensive process. Also, there is a risk of contamination of co-culture layers, which limits the utility of CMs in clinical application, biomedical application and

disease modelling. Besides, the protocol is not defined and required optimisation process to reduce lab-to-lab variation and generate an efficient, reproducible, and up-scalable protocol. Hence, it was suggested that this method was suitable for testing the ability of hPSCs to form cardiac mesoderm cells at an early stage of their derivation.

1.5.2.2 Cardiac differentiation via formation of embryoid bodies (EBs) method

Initially, the EB platform was designed to suspend mouse embryonic stem cell (mESC) colonies in the media to form spherical aggregates called EBs and differentiate them into three germ layers (Doetschman et al., 1985). Unlike embryonic development, these EBs were variable in size, structure, and composition, but under a specific condition, a portion of the EB exhibited spontaneously contracting regions (Burridge et al., 2012). From a set of comprehensive experiments, several parameters were identified and optimised for *in vitro* cardiac differentiation, including **(1)** number of suspension cells to form the EBs, **(2)** cardiac differentiation medium, **(3)** the mESC lines, and **(4)** culture duration with differentiation medium and the times of plating EB (Boheler et al., 2002). However, unlike mESCs, hESCs could not form the EBs effectively because they were unable to tolerate enzymatic digestion and isolation as single cells. Hence, in the first EB differentiation, collagenase IV was used to dissociate hESC colonies into small aggregates, each contained approximately 10 to 30 cells, which were allowed the cells to grow as suspension EBs in a non-adherent plastic culture dish (Kehat et al., 2001). The EBs were then transferred into 0.1% gelatine-coated plates for attachment and expansion, and beating areas were first observed from d4 to d7. Albeit low differentiation efficiency, the method had been used to differentiate successfully numerous of hPSC lines, including hiPSCs, and formed some spontaneously contracting outgrowths in the 5% to 15% range (Zwi et al., 2009).

In order to enhance the efficiency, several modifications and optimisations were applied, including addition of human recombinant BMP4 during d0 to d4, supplement of WNT3A during d0 to d2, and via small molecules inhibition of WNT signalling by IWR-1

during d4 to d6 (Takei et al., 2009; Tran et al., 2009; Ren et al., 2011). Similar to that of inductive co-culture system, serum- and Insulin-free differentiation media actively support EB cardiac differentiation, the efficiency of which can be enhanced by supplementing prostaglandin I2 and the MAP kinase inhibitor – SB203580 during d4 and d6 (Xu et al., 2008; Gaur et al., 2010). Studies in applications of growth factors and small molecules involving in cardiac differentiation revealed that WNT3A, granulocyte colony-stimulating factor (G-CSF), and L-ascorbic acid improve proliferation of cardiac progenitor cells, while Insulin-like growth factor 1 (IGF-1) and IGF-2 induced cardiomyocyte survival rate and expansion (Bu et al., 2009; Cao et al., 2012; McDevitt et al., 2005; Shimoji et al., 2010).

The potential problem of EB method is its heterogeneity in EB size, which can overcome using “force aggregation” technique developed in our lab (Burridge et al., 2007). In this method, a known number of hPSCs (usually ranging between 40.000 to 80.000 cells/well depending on cell line) was used to form an EB in a well of V-shaped 96-well plates from d0 to d2 followed by transferred the EBs to the U-shaped cell culture treated 96-well plates. The initial version of the method yielded approximately 23% beating EBs from four different hESCs provided the differentiation media needed to be supplemented with activin A and FGF2 (Burridge et al., 2007). The later refinement of the method, which used BMP4 and FGF2 as mesoderm inducer under hypoxia condition, increased the efficiency up to 94% of beating EBs in a wider range of hPSC lines (Burridge et al., 2011). Another modified version of the force aggregation technique using BMP4, activin A, WNT3A, SCF, and VEGFA for the first three days was also claimed to be able to enhance the differentiation efficiency (Elliott et al., 2011).

Although the suspension and force-aggregation EB methods have been proven to generate more than 70% CMs, these methods have potential problems of isolating CMs from EBs, heterogeneous population, require intensive optimisation, the risks of fibroblast outgrowth and still contained non-defined components. Hence, these drawbacks led to the development of monolayer differentiation methodology (Laflamme et al., 2007).

1.5.2.3 Monolayer cardiac differentiation process

The monolayer differentiation takes the advantage from a relatively uniform monolayer of cultured hPSCs without complex diffusional difficulties found in EB approach. As a result, the supplement of growth factors, small molecules, and other interventions will be distributed in a controllable and reproducible manner. Furthermore, the development of the chemically defined medium, such as mTeSR and E8, provides a standard culture condition to maintain the hPSCs in monolayer format, reduces significant batch-to-batch variations, and improves the quality of the cultured hPSCs (Chen et al., 2011). However, hPSCs grown in these media showed the difficulties in forming EBs, suggesting that cardiac differentiation performs in monolayer format could be a convenient alternative (Mummery et al., 2012). Moreover, the monolayer differentiation does not require different types of culture vessel for spinning or re-plating, which not only reduces the labour requirement but also reduces the use of laboratory culture supplies as well as cost effective.

In the first monolayer differentiation method, hPSCs were maintained in mouse embryonic fibroblast conditioned media (MEF-CM). Once the culture reached 80-90% confluence, the cells were dissociated enzymatically using Collagenase IV and seeded at high seeding density (100.000 cells/cm^2), then treated with high dose of activin A (100 ng/ml) followed by treatment with BMP4 for 4 days; critically, the media is not changed during these 4 days to allow the secreted factors from the monolayer to accumulate (Laflamme et al., 2007). The first sign of beating clusters can be observed after 12 days post-differentiation with the yield of approximately 30% cardiomyocytes. Although the yield and cardiomyocyte purity obtained from this method were not high, it provides a proof of principle for development and improvement of monolayer cardiac differentiation methodology.

Further refinement of the method involved the addition of WNT3A at d0 to d1 and DKK1 from d5 to d11 which improved the cardiac differentiation efficiency to approximately 60% (Paige et al., 2010). Additional improvements have also been reported by using Matrigel overlay one day before starting differentiation process to

enhance the epithelial-mesenchymal transitions, in conjunction with the elimination of Insulin and supplement of FGF2 from d1 to d5 followed by DKK1 from d5 do d7 (Uosaki et al., 2011). However, the use of DKK1 as Wnt inhibitor was inconsistent and less effective leading to the application of alternative Wnt antagonist by using the small molecules (IWR-1 or IWR-4) on d3 of differentiation process (Hudson et al., 2012).

In 2010, the core mechanism underlying the initiation of cardiogenesis was discovered in which the Activin/BMP4 differentiation is dependent upon the endogenous Wnt/β-catenin signalling pathway that stimulates the induction of cardiac differentiation and later needs to be inhibited after mesoderm specification to form cardiac mesodermal progenitor cells (Paige et al., 2010). Hence, suppressing this signalling at the early stage or stimulating its after mesoderm induction results in the significant reduction of cardiac differentiation efficiency. Interpretation of the role and timing of Wnt/β-catenin signalling pathway has led to the improvement of the monolayer differentiation protocol. In 2012, Lian and colleagues illustrated that stimulation of Wnt/β-catenin signalling using GSK3-inhibitor CHIR99021 on d0 followed suppressing the pathway using either chemical or by β-catenin shRNA expression led to the consistent generation of beating cardiomyocytes (Lian et al., 2012; Lian et al., 2013a). Furthermore, it was reported that Insulin, a component of B27 medium supplement, reduced the protocol efficiency if it was added during the first 5 days of differentiation. This result was supported by the fact that removal of Insulin from the differentiation medium resulted in a consistent increase of cardiac production (Lian et al., 2013b).

As far as the defined condition is concerned, recent works has focused on the development of chemically defined condition for cardiac differentiation to reduce the number of “unknown-function” compounds and understand further the effects of each component formulated the differentiation medium. In 2014, a simplified and defined cardiac differentiation protocol was introduced by using the chemically defined medium (CDM3), which contained only three components to replace the most commonly used RPMI 1640 + B27 supplement. In fact, this protocol is similar to Lian’s protocol in which hPSCs were first exposed to a GRK-inhibitor (CHIR99021) for two days and the Wnt/β-

catenin signalling was inhibited using Wnt-C59 inhibitor for the next two days (Burridge et al., 2014). The culture was then maintained in CDM3 medium until beating cardiomyocytes were observed on d8 of differentiation protocol. Importantly, this protocol has been proven to differentiate consistently 11 hiPSC lines and two hESCs with the cardiomyocyte purity more than 85%. However, it is important to note that in this protocol, the additional purification step using Lactate treatment in glucose-depleted RPMI medium to metabolically purify cardiomyocytes from fibroblast contamination (Burridge et al., 2014; Sharma et al., 2015).

To summarise this section, it is important to note that the mature version of each differentiation approaches illustrates the progressive sequential induction environment using growth factor, small molecules, and more importantly defined components of differentiation medium toward the enhancement of cardiac purity and protocol consistency. Eventually, cardiomyocytes derived from hPSCs can be used in a wide range of applications, including disease modelling, drug screening, biomedical application and gene therapy (Denning et al., 2016; van Meer et al., 2016).

1.6 Establishment of human cardiac model using CRISPR/Cas technology

The simplest meaning of genome editing (or genome engineering) takes advantage of the insertion, deletion or replacement of DNA at a particular site in the genome of an organism or cells (Urnov et al., 2010). It is usually accomplished *in vitro* using engineered nucleases to create the double strand breaks (DSBs) at the target sites, which can be later repaired via non-homologous end joining (NHEJ) or homology dependent repair (HDR) (Jasin and Rothstein, 2013). In the early development of gene editing field, several methods had been developed to be able to “site-specific” recognition of DNA sequences to induce DSBs, although the effectiveness and specificity were relatively low (Figure 1.12A). Thus, methods for introducing precise DNA breaks at the targeted sites where changes need to be added or replaced were considered as a powerful tool for targeted genomic engineering.

Table 1.4: Comparison of different programmable nuclease platforms.

	ZFNs	TALENs	CRISPRs
Components	Fok1 restriction nuclease fused with multiple Zinc finger peptides (each finger targets 3 bp of genomic DNA).	Non-specific nuclease fused to a DNA-binding domain specific to a genomic locus.	20nt crRNA linked with tracrRNA to form gRNA structure which is then associated with Cas9 endonuclease.
Nuclease activities	Induces DSBs in the target DNA locus	Induces DSBs in the target DNA locus	Induces DSBs in the target DNA locus (using wt Cas9) and single-strand breaks or DNA nicks (using Cas9 nickase)
Specificity	Moderate specificity; small number of positional mismatches tolerated.	High specificity; small number of positional mismatches tolerated.	High specificity; positional and multiple consecutive mismatches tolerated.
Off-target effects	High off-target effects	Low off-target effects	Low to none off-target effects bases on selection of unique crRNA sequences
Advantages	1. Small size: easy to delivery into the cells. 2. Cost and time effective synthesis 3. Successfully implemented in clinical trials of various diseases.	1. High specificity to the target DNA locus. 2. Can be used in combination with the catalytic domain of many enzymes	1. Highly specific and effective 2. DNA-binding domain is dependent from nuclease domain. 3. Cost effective and easy to generate 4. Less labour intensive 5. Can be used to specifically enhance or suppress gene expression with dead Cas9 (dCas9) protein, usually known as CRISPR interference (CRISPRi).
Disadvantages	1. High off-target effects 2. Difficult to design, might require substantial protein engineering	1. Highly sensitive to DNA methylation at the targeted reagion. 2. Time consuming and labour intensive. 3. Might require complex molecular cloning methods. 4. Large size might complicate delivery 5. Potentially induce DNA rearrangements	1. Large size might complicate delivery. 2. Specificity heavily depends on crRNA design and selection.
References	(Urnov et al., 2010; Carroll, 2011; Dreyer and Cathomen, 2012)	(Beurdeley et al., 2013; Kuhn and Wefers, 2014; Mahfouz et al., 2014)	(Doudna and Charpentier, 2014; Hsu et al., 2014; Kim et al., 2014)

To date, there are three main methodologies developed to actually introducing the DBS at site-specific location in the genome, including Zinc finger nucleases (ZFNs), transcription activator-like effector nucleases (TALENs) and Clustered Regulatory Interspaced Short Palindromic Repeat (CRISPR) method (Doudna and Charpentier, 2014). The Table 1.4 summaries the overall characteristics of each approach with pros and cons. Among these approaches, CRISPR technology becomes one of the fastest growing methodologies in the gene editing field due to its relatively easy to use, low start-up cost, high precision to modify targeted gene, less "off-target" effects, and less labour intensive compared to ZFNs or TALENs.

1.6.1 History of CRISPR

In parallel with genome editing field but in an entirely separate area of research, Japanese microbiologists identified a series of short repeat sequence in the *Escherichia coli* (*E. coli*), which was later classified as the Clustered Regulatory Interspaced Short Palindromic Repeat (CRISPR) system, although at that time its function remained a mystery to scientists (Ishino et al., 1987). Following this research, several studies reported their finding of CRISPR sequences presenting in archaea and bacteria and predicted its functions were related to DNA repair machinery or regulation of gene expression (Mojica et al., 2000; Makarova et al., 2002; Guy et al., 2004). A deeper understanding of the functions of CRISPR was derived from research which illustrated that CRISPR contains partial sequences found in plasmids and viruses (Bolotin et al., 2005; Mojica et al., 2005; Pourcel et al., 2005). The finding that revealed the transcription of CRISPR loci together with the discovery of CRISPR-associated gene (*cas*) encoding for the protein with putative endonuclease activities led to the hypothesis of CRISPR involved in an adaptive immunity in archaea and bacteria against viral infections (Tang et al., 2002; Jansen et al., 2002; Haft et al., 2005; Makarova et al., 2006). This hypothesis was proven by a series of experiments illustrating that infection of *Streptococcus thermophilus* with lytic phages resulted in the transcription of CRISPR sequences which acted as small CRISRP RNA (crRNA) guides resulting in disruption of the bacterial

phage DNA and protecting the bacteria against phage infection (Brouns et al., 2008; Marraffini and Sontheimer, 2008).

In nature, the adaptive immune system of bacteria can be described briefly in three stages: **(1)** acquisition of invading DNA: insertion of a short sequence of the invading DNA as a spacer sequence into the CRISPR array; **(2)** detection of invading DNA: transcription of CRISPR sequence generates precursor crRNA (pre-crRNA) that undergoes maturation by splicing into individual crRNA, each composed of a repeat portion and sequence derived from the invader (known as spacer); **(3)** degradation of the invading DNA: the crRNA together with the trans-activating RNA structure (trac-RNA) screens throughout the invading DNA sequence until the crRNA matches its complementary sequence via Watson-Crick base pairing leading to cleavage of exogenous sequence by Cas protein (Garneau et al., 2010; van der Oost et al., 2009). Using this basic principle of adaptive immunity, three original CRISRP-Cas systems were classified, including Type I, Type II, and Type III, each with its own specific mechanism to achieve the recognition of exogenous nucleic acid and initiation of DBSs by DNA cleavage.

Interestingly, more than one CRISPR type is often found in a single organism suggesting that these systems are potentially compatible and could share functional components (Makarova et al., 2011b; Wiedenheft et al., 2012). Furthermore, similar to other defence mechanism, the adaptive mechanism of CRISPR-Cas system evolves in the manner of an incessant arm race with mobile genetic elements (MGEs), providing the system with an extreme diversity in *cas* sequences and in the architecture of the CRISPR-*cas* loci, which provides a fundamental unit for the establishment of the innate immune system of prokaryotes (Makarova et al., 2011a; Makarova et al., 2013; van Houte et al., 2016). Owing to this diversity and the lack of universal *cas* genes, a new, broadest classification of CRISPR/Cas has been proposed, which bases on the combination of phylogenetic signature genes which is the repertoire of *cas* gene, sequence similar between Cas protein, and their loci organisation (i.e. locus

architecture). This new system categorises CRISPR/Cas into two main classes that are subdivided into six types and 19 subtypes (Makarova et al., 2015; Shmakov et al., 2015).

1.6.2 New classification system of CRISPR/Cas

One of the key features of the organisation and evolution of the CRISPR/Cas loci is their pronounced modularity, in which each module is responsible for the adaptation step. Moreover, it has been reported that the adaptation module is conserved among the diverse CRISPR/Cas system and *cas1* and *cas2* genes play an essential role in the adaptive acquisition of the spacer. Also, the effector module encodes genes that are involved in the maturation of the crRNAs as well as in the target recognition and cleavage. It has been showed that this module represents a greater level of versatility (Makarova et al., 2015). The fundamental difference between the two classes of CRISPR/Cas systems is the architecture of their effector modules, which composed of four to seven Cas protein subunits in Class 1 system, whereas Class 2's effector module contains a single multi-domain protein (Makarova et al., 2015).

1.6.2.1 Class 1 CRISPR/Cas

As mentioned above, Class 1 system is defined by the presence of a crRNA-Cas complex (or in the newly defined term, a crRNA-effector complex) which is involved in the maturation of the crRNAs and initiation of recognition and degradation of the invading DNA (usually in the form of MGEs). This class includes the original Type I, Type II, and the putative, newly discovered Type IV (Makarova et al., 2015). The standard feature of class 1 is the subunits of the effector complexes (in particular Cas5, Cas6, and Cas7 protein) which consist of the RNA-binding recognition motif (Herrmann et al.) domain (Makarova et al., 2011b). Although variation in number and diversity of *cas* gene have been identified, the distinguishing characteristic of Type I systems is their *cas3* gene encoding for Cas3 protein which contains an N-terminal HD phosphohydrolase domain and a C-terminal helicase domain (Makarova et al., 2006; Mulepati and Bailey, 2011). Type I systems are currently divided into seven subtypes, I-A to I-F and I-U

(uncharacterised mechanism), and each subtype has been characterised by its signature genes and distinct features of operon organisation (Makarova et al., 2011b). For example, *cas* genes in Type I-A and I-B are typically clustered in two or more operons, whereas most of the Type-I loci, each of the *cas* gene is encoded by a single gene (I-C, I-D, I-E, and I-F) (Vestergaard et al., 2014). In Type III system, the signature gene is *cas10*, which encodes a multi-domain protein containing a Palm domain (a variant of the RNA recognition motif – RRM) that is homologous to the core domain of numerous nucleic acid polymerase and cyclases. Two major variations were observed in Type III CRISPR system, which was later classified into Type III-A and Type III-B (Marraffini and Sontheimer, 2008; Hale et al., 2009). Subtype III-A has been found to contain *cas1*, *cas2*, and *cas6* genes in their adaptive modules, whereas subtype III-B does not have these genes and therefore its function depends on other CRISPR/Cas systems present in the same genome. Moreover, both III-A and III-B subtypes have been demonstrated to be transcribed and targeted invading RNA and DNA (Peng et al., 2015).

Recently, it has been reported that several bacterial genomes contain a putative, uncharacterised Type IV system, usually present on plasmids (Mohanraju et al., 2016). The loci architecture of Type IV is relatively similar to Type III-B as this system also lacks *cas1* and *cas2* gene in its adaptive modules. Furthermore, the effector modules of Type IV systems encode a partially degraded large subunit, Csf1, Cas5 and a single copy of Cas7, and in some cases, a putative small subunit. Interestingly, both effector and adaptive modules of this system are not often located next to a CRISPR array as seen in another CRISPR systems. In fact, the location of Type IV in a genome that has no detectable CRISRP array (Makarova et al., 2011a). Hence, the functions of Type IV might be similar to Type III-B systems, which use cRNAs from different CRIPRS arrays once these become available to initiate the targeting activities. To date, there are two variants of Type IV CRISPR/Cas systems have been isolated, one contains a DinG family helicase, and the other contains a small α-helical protein (White, 2009; Makarova et al., 2011a).

1.6.2.2 Class 2 CRISPR/Cas

In terms of genomic organisation, class 2 systems contain a single subunit of crRNA-effector modules and consist of Type II and Type V CRISPR/Cas systems. The Type V systems have just been established recently due to the discovery of a specific gene, namely *cpf1* (TIGRFAM reference TIGR04330), which was found in several bacterial genomes and one archaeal genome (Schunder et al., 2013; Zetsche et al., 2015). Cpf1 has been classified as a nuclease enzyme due to its ability to initiate a staggered DSBs via its RuvC-like nuclease domain homologous to the respective domain found in Cas9, and the TnpB protein of IS605 family transposons, together with the Zn finger of TnpB (Zetsche et al., 2015). However, Cpf1 does not have the HNH nuclease domain that is present in Cas9 protein and its genomic loci is encoded outside the CRISPR/Cas context in several genomes, and its high similarity with TnpB suggests that *cpf1* is recent recruitment from a transposable element (Zetsche et al., 2015).

Microbiological studies of CRISPR/Cas systems revealed the dramatic differences between Type II from other CRISPR types had been discussed so far, and by far it is the simplest regarding the number of genes. The signature gene for Type II is *cas9* encoding a multi-domain protein that combines the functions of the crRNA-Cas effector complex with target DNA cleavage. The adaptive module of the system contains *cas1* and *cas2*, and most type II loci also encode the trans-activated crRNA (namely tracRNA), which is complementary to the repeats present in the respective CRIPSR array.

The Cas9 protein is a large protein that confers the ability to cleavage the DNA via its Ruv-C and HNH nuclease domains and an Arg-rich cluster, most likely received from sequences of transposable elements and are not associated with CRISPR. Therefore, due to its sequence similarity between Cas9 and its homologues that are not involved in CRISPR functions, Type II signature could not be defined by only Cas9. In fact, the presence of *cas1* and *cas2* in vicinity of *cas9* genes has been considered as the hallmark of the system.

1.6.3 Genome editing in hPSCs

Understanding how CRISPR/Cas systems involved in bacterial defence system against virus infections led to the adaptation of the systems into genome editing of human cells in general and hPSCs, in particular. As mentioned above, CRISPR/Cas9 is by far the simplest system among the others in terms of genomic structure and transcription. Thereby, this system has been adapted and widely developed to facilitate a broad range of targeted genome applications. Indeed, the first milestone of genome editing using CRISPR/Cas9 system is established from the experiment that delivered a synthetic crRNA sequence capable of hybridizing to the targeted DNA, allow Cas9 to cleave at that region (Jinek et al., 2012). Following the experiment revealed that in order for Cas9 to target and subsequently cleave the designed site, a unique short (3-9 bp) sequence motif directly adjacent to the hybridized region is compulsorily required, namely the Proto-spacer Adjacent Motif (PAM). The second milestone is the work that combined the tracrRNA and crRNA to form a chimera structure called a single-guide RNA or gRNA, which allow researcher to abrogate the requirement of tracrRNA-mediated maturation (Jinek et al., 2012). The gRNA specific structure combines the targeting features of the crRNA with the dsRNA structure formed by the tracrRNA:crRNA complex, allowing this single gRNA to achieve the requirements of both small RNAs. This gRNA design and development allowed the applications of CRISPR/Cas9 not only restricted into prokaryotic but also expanded into the eukaryotic systems, by using the simplified components needed to induce the Cas9-mediated cleavage of the target gene. Later, the adaptation of Cas9 protein with human optimised codon is introduced further enhancing genome editing fields. These advances in development and adaptation of CRISPR/Cas9 shed light for multiple laboratories across the globe to port the Cas9 system into different experimental models. To date, this platform has been successfully used in bacterial cells, yeast, plants, nematodes, fruit flies, zebra-fish, rodents, and human cells (including human embryos, primary cell lines, immortalised cell lines, and hPSCs) (Dicarlo et al., 2013; Nekrasov et al., 2013; Yu et al., 2013; Hwang et al., 2013; Hou et al., 2013; Liang et al; 2015).

1.7 Thesis rationale and objective

The *GRK5*-L41 polymorphism has been reported as a "gain-of-function" mutation which occurs only in 40% African-American cohort and 2% Caucasian population. GRK5-L41 has been demonstrated to enhance β-ARs uncoupling during the persistent agonist exposure, which in turn, facilitate the desensitisation of β-ARs in mouse models (Liggett et al., 2008). In clinical studies with 375 prospectively followed African-American subject with heart failure condition, GRK5-L41 protected patients against heart failure, ischemia, death or cardiac transplantation. In general, the GRK5 polymorphism represents a potential mechanism in which genetic variability could associate with cardiac disease development and susceptibility. However, the mechanism underlying these putative cardiac protective functions of GRK5 still remains unclear. To date, no published article reported about using CRISPR/Cas9 system to create the human cardiac model to investigate the GPCR or GRK polymorphisms during normal and heart failure conditions.

Therefore, the aim of this study is to establish the first hPSC-derived CM model for testing assay strategies toward GRK5-L41 functions and establishment of potential mechanism underlying the cardiacprotective functions of GRK5-L41. To achieve this aim, the following targets were established, including:

1. Development and characterisation of monolayer cardiac differentiation protocol.
2. Identification of the effective reprogramming method to convert lymphoblastoid cell lines harbouring *GRK5*-Q41 and *GRK5*-L41 into pluripotent stage and characterisation of newly established hiPSC from lymphoblastoid cells.
3. Using CRISPR/Cas9 system to introduce *GRK5*-L41 into HUES7 genome to create and characterise the isogenic hESC lines.
4. Development of functional assays targets the GRK5 functions during normal condition and prolonged-exposure to isoprenaline treatment to identify the phenotypic differences between CMs expressing *GRK5*-Q41 and *GRK5*-L41.

Chapter 2 Materials and Methods

2.1 Cell culture

All cell culture experiments were conducted in Class II safety Cabinets. Cells were maintained at 37°C and 5% CO_2 in humidified environment [Heraeus HERAcell 150]. All culture reagents were purchased from Invitrogen and Thermo Fisher, and all chemicals and pharmaceutical drugs from Sigma, unless otherwise stated. All growth factors were kept at the temperature suggested by manufacturer manuscript and added freshly before use. All cell culture vessels were tissue culture-treated unless otherwise stated. List of companies and catalogues number used in the thesis is detailed in Appendix-I. Bright field images were taken using Nikon ECLIPSE RE2000-S inverted microscope. The immunofluorescence images were captured using Operetta confocal microscope (Perkin Elmer).

2.1.1 Preparation of mouse embryonic fibroblast (MEF) conditioned medium (MEF-CM)

2.1.1.1 Isolation of MEFs from mouse embryos

The pregnant CD1 mice were raised and took care in Biomedical Service Unit (BMSU) at Queen Medical Hospital (QMC). Mouse embryos were isolated on day 13.5 by cervical dissociation. All blood and embryos heads were removed before transferred to the cell culture suite. Isolated embryos were first treated with 0.25% trypsin-EDTA for 10 min before finely sliced using a scalpel followed transferred into the 250 ml pot containing up to 2 ml of trypsin per embryo. The mixture was then vortexed at max speed for 5 min and incubate at 37°C for 5 min. The step was repeated until the mixture become homogenous with minimal clumps.

To neutralise the enzymatic activities, MEF culture medium was added to the mixture at the ratio of 3 ml MEF-medium per embryo (Table 2.1). The cell suspension was then vigorously shaken and allowed to settle down at room temperature. After 20 min, the clumps and other cellular debris should settle down at the bottom of the pot leaving behind the homogenous cell suspension, which was then collected and transferred into 175 cm^2 tissue culture flasks (T175 flask), at the density of 2 embryos

per flask, in a total volume of 30 ml MEF medium, supplemented with penicillin and streptomycin and were incubated for 24h. The fresh MEF-CM supplemented with antibiotics were changed on the following day and were changed every three days until the culture reach 90% confluence. The confluent MEFs were then dissociated using 0.25% Trypsin-EDTA (3 min incubation followed centrifugation at 200g for 5 min) and cryopreserved using FBS containing 10% dimethyl sulfoxide (DMSO) in the cryotubes. These cryotubes were placed in the -80^{o}C freezer for 24h before transferred into liquid Nitrogen for long-term storage.

Table 2.1: MEF-culture medium used in the experiment. bFGF-2: beta fibroblast growth factor 2; DMEM: Dulbecco's Modified Eagle Medium; FBS: Foetal Bovine Serum; KSR: Knock-out serum replacement; NEAA: Non-essential Amino Acid.

Medium	Components	[Stock Conc]	[Working Conc]	Vol
BGK	DMEM-F12	N/A	1X	500 ml
	KSR	100%	15%	90 ml
	Glutamax	100x	1x	6 ml
	NEAA	100x	1x	6 ml
	β-mercaptoethanol	1 M	10 μM	60 μL
	bFGF-2	4 μg	8 ng/ml	N/A
MEF-Medium	DMEM	1X	1X	88 ml
	FBS	100%	10%	10 ml
	L-Glutamine	100x	10x	1 ml
	NEAA	100x	10x	1 ml

2.1.1.2 MEF culture condition

The cryopreserved MEFs at passage 0 (p0) were thawed at 37^{o}C in the water bath for 2 min followed diluting with MEF medium and centrifuged at 200g for 5 min. The pellet was then resuspended in 15 ml MEF medium and transferred to 75 cm^2 tissue culture flask (T75). The medium was changed every 2 consecutive days until the culture reached 90% confluence. The confluent culture was first wash with PBS and dissociated with 1.5 ml trypsin-EDTA (0.05%) for 3 min at 37^{o}C. The flask was tapped gently a few times to detach the cells from the culture surface followed enzymatic inactivation using 13.5 ml MEF medium. The cell suspension was collected and spin down at 200g for 5 min and re-seeded into the new T75 flasks at ratio 1 in 3 (1:3).

2.1.1.3 MEF-CM preparation

The MEFs at p2 were first dissociated as described in section 2.1.1.2 and re-seeded into the new T75 flasks at ratio 1:4. When the cells reached 80% confluences, usually on day 3, they were exposed to the MEF medium supplemented with 10 μg/ml mitomycin-c for 2.5 h. The mitomycin treated cells were then washed three times with PBS, dissociated and re-seeded into new T75 flasks at the density of 4.8 x 10^6 cells/T75 coated with 0.1% gelatine. On the following day, the mitomycin-treated MEFs were washed twice with PBS and the medium was replaced by 25 ml BGK medium (Table 2.1). After 24h, the MEF conditioned medium (MEF-CM) was collected and new BGK medium was added to the MEF flasks. The MEF-CM was collected every 24h for 7 days and can be stored at 4^{o}C overnight or at -20^{o}C for up to 6 months.

2.1.2 Feeder-free culture condition of hPSCs

The hPSCs were cultured in the feeder-free conditions by using MEF-CM supplemented with bFGF-2 (8 ng/ml) (MEF-CM-bFGF2). In brief, the hPSCs were first thaw from a cryotube in the water bath for 2 min followed resuspend in 9 ml of BGK medium. The cells were then pelleted down at 160g for 4 min and re-seeded into a Matrigel-coated 25 cm^2 (T25) culture treated flask in the MEF-CM-bFGF2 medium. The culture medium was changed every day until the cells reached 100% confluence. The compact culture was dissociated using 0.5 ml of 0.05% Trypsin-EDTA for 3 min at 37^{o}C followed enzymatic inactivation using 4.5 ml of the BGK medium. The cell suspension was transferred into a 30 ml universal tube and spun down at 160g for 4 min followed re-seed into a new Matrigel-coated T25 flask at required density. The hPSCs were passaged by trypsin maximum ten times and the culture was then terminated to prevent the accumulation of the abnormal karyotypes due to serial passages.

2.1.3 Chemically defined culture conditions of hPSCs

2.1.3.1 Culture of hPSCs in mTeSR medium

Transition procedure from MEF-CM to mTeSR condition: The MEF-CM cultured hPSCs were first seeded at a desired seeding density to achieve 80% confluence after 2 days in culture before starting transition process into mTeSR medium. When the confluence was achieved, the medium was switched from the MEF-CM-bFGF into mTeSR medium. After 24h in mTeSR, the cells were passaged using either Accutase or Cell Dissociation Solution (CDS) (Table 2.2) by adding 1 ml of CDS and incubated at 37^{o}C for 3 min. The dissociated cells were then resuspended with 9 ml of BGK for neutralising CDS and spun down at 160g for 4 min. The supernatant was removed and the pellet was resuspended with mTeSR medium and re-seeded into a new Matrigel-coated T25 flask at the ratio of 1:3. The medium was changed everyday with fresh mTeSR medium until reaching 80% confluence. The confluent mTeSR culture was dissociated as described above at the ratio 1:3 for the first three passages before splitting at higher ratio or for cryopreservation using FBS containing 10% DMSO. The mTeSR culture was routinely passaged for every 3 consecutive days.

Table 2.2: Cell dissociation solution (CDS)

Medium	Components	[Stock Conc]	[Working Conc]	Vol
Cell Dissociation Solution (CDS)	RPMI-1640	N/A	40 %	20 ml
	TryPLE select	1 X	20 %	10 ml
	CDB	1 X	40 %	20 ml

Growth and passage of hPSCs in mTeSR culture condition: A cryopreserved vial of the mTeSR cultured hPSCs was first thawed that 37^{o}C for 2 min in the water bath and then transferred to a 30 ml Universal tube followed adding drop-by-drop the BGK medium to prevent osmotic shock. The cell suspension was centrifuged at 160g for 4 min and the supernatant was aspirated carefully without interrupting the pellet, which was re-suspended with 5 ml of mTeSR culture medium and re-seeded into a ready-made Matrigel-coated T25 flask. The medium was changed every day until the cell reached 80% confluent. Once confluent, the culture was first washed with PBS followed 1 ml of

CDS for 3 min at 37°C. The CDS was neutralised by adding 9 ml of BGK medium and pelleted down at 160g for 4 min. The pellet was then re-suspended with the new mTeSR and re-seeded into the new Matrigel-coated T25 at desired density depending on the experiment.

2.1.4 Culture hPSCs in E8 medium

Transition procedure from either MEF-CM or mTeSR to E8 culture condition: To adapt to the new E8 culture condition, hPSCs maintained in either MEF-CM or mTeSR were cultured until reaching 60% followed switching into E8 culture medium. After 24h, the cells were washed one with PBS and dissociated using CDS method. After centrifugation at 160g for 4 min, the cell pellet was resuspended in E8 medium supplemented with HA-100 (100 ng/ml, E8-HA100) and transferred into the Matrigel-coated T25 flask at the ration 1:3. On the next day, the medium was changed back to the fresh E8 medium. To create the stable E8 culture lines after transition process, the cells were passaged as described for three passages post-transition at the ratio of 1:3. Once the culture was established, the E8 cultured cells were then cryopreserved in FBS containing 10% DMSO for long-term storage.

Growth and passage hPSCs in E8 medium: A cryopreserved E8 cells was first thawed at 37°C for 2 min followed transferred into 30 ml Universal tube and adding drop-wise the pre-warmed BGK to prevent osmotic shock. The cell suspension was centrifuged at 160g for 4 min and the supernatant was aspirated carefully without interrupting the pellet. The cell pellet was then mixed gently with 5 ml E8-HA100 medium and transferred into the Matrigel-coated T25 flask. The medium was changed everyday until the cell reached 80% confluent followed splitting using CDS method.

2.1.5 Establishment of hiPSCs using episomal reprogramming method

2.1.5.1 HUES7-derived fibroblast (H-Fib) culture condition

The H-Fib was previously generated by Dr. Elena Matsa and was cultured in the Fib medium (Table 2.3). A vial of cryopreserved H-Fib was thawed as similar to hPSCs

and cultured in the T75 flask. The medium was changed every three days until the culture reached 80% confluency followed Tripsinised passaged using 0.05% Trypsin and seeded at a 1:4 ratio.

Table 2.3: Culture medium used to maintain H-Fib and Lymphoblastoid cell lines.

Medium	Components	[Stock Conc]	[Working Conc]	Vol
Fib Medium	DMEM-F12	N/A	1X	500 ml
	FBS	100%	15%	90 ml
	Glutamax	100x	1x	6 ml
	NEAA	100x	1x	6 ml
	β-mercaptoethanol	1 M	10 μM	60 μL
Lymp Medium	RPMI 1640	1X	1X	84 ml
	FBS	100%	15%	15 ml
	L-Glutamine	100x	10x	1 ml

2.1.5.2 Human lymphoblastoid culture condition

A vial of cryopreserved human lymphoblastoid cells (Lymps) were obtained from Corriell Biorepository (https://catalog.coriell.org/1/Browse/Biorepositories) and maintained in Lymp-medium as shown in Table 2.3. The Lymps were cultured in the T25 flask standing upward containing 20 ml Lymp-medium as cell suspension culture. The medium was changed every 3 days by pipetting out 10 ml of the old medium and added the same amount back to the flask. When the culture reached 70% in density, i.e. formed large floating clusters and medium turned yellow in colour, the cells were dissociated mechanically by pipetting up and down to break the clumps and cell count was performed using the haemocytometer. The culture was centrifuged at 150g for 5 min followed adding appropriate amount of Lymp-medium to make a total of $1x10^6$ cells/ml. The cells were then re-inoculated into a new T25 flask containing 20 ml of Lymp-Medium at the cell seeding density of $2x10^4$ cell/ml for maintenance.

2.1.5.3 Reprogramming of H-Fib into hiPSCs using episomal reprogramming method

To reprogramming the H-Fib into pluripotent stage, the episomal plasmid sets derived from Thompson's Lab was used (Yu et al., 2009). The plasmid details were shown in Table 2.4. The H-Fib cells, between p10 and p20, were cultured in Matrigel-

coated T75 flask using Fib-Medium. When the cell reached 80% confluency, the were dissociated using 0.05% Trypsin-EDTA and seeded at $3x10^5$ cells/well of the Matrigel-coated 6-well plates. The medium was changed every 2 consecutive days until the culture reached 80% confluency followed the delivering the plasmid set using FuGENE HD Transfection Reagent (Promega, E2311). The ratio between transfection reagent and DNA was 6:1 ratio as suggested by the manufacture. Total 2 μg of DNA plasmid set were used in the experiment. The DNA/transfection reagent mixture was added drop-wise into the well and the cells were returned into the incubator. After 24h, the medium was replaced by the new Fib medium supplemented with 10 ng/ml bFGF-2 (Fib-bFGF medium). The Fib-bFGF medium was changed everyday until the reprogrammed colonies appeared. The appearance of colonies was tracked everyday. Once the colonies appeared, the culture were then dissociated and re-seeded into the Matrigel-coated 35 mm disks for manual dissection to collect monoclonal clones or the Matrigel-coated T25 flasks for Magnetic-activated cell sorting (MACS) column purification of TRA-1-81 positive cells for further expansion. The newly established H-Fib-hiPSCs were maintained in feeder-free culture conditions using MEF-CM supplemented with 8 ng/ml bFGF-2 and dissociated using trypsin as described previously.

2.1.5.4 Episomal Reprogramming of Lymphoblastoid cell lines

Two different episomal reprogramming plasmid sets were used in this thesis, including the Thomson's plasmid set and Yamanaka's plasmid set as described in Table 2.4. The Lymps were cultured in Lymp-medium until confluency and $2x10^6$ cells were collected on the day of the experiment followed centrifugation at 120g for 10 min. the cell pellet was then resuspended with 100 μL of Nucleofector Solution V containing appropriate amount of plasmids as shown in Table 2.4. The mixture was then transferred into the AMAXA electroporator cuvette and the plasmids were delivered into the cells using the programme X-005. After electroporation reaction completed, the cuvette was placed inside the incubator for 2 min following adding 400 μL of Lymp-medium and incubating 10 min in the incubator before transferred the cells into Matrigel-coated 6-well

plate containing 2 ml of Lymp medium. 12h-post electroporation, the medium was gently replaced by reprogramming medium (RM) as described in table 2.4. The cells were fed daily with fresh RM for 2 weeks.

Table 2.4: Composition of lymphoblastoid culture medium (LM) and reprogramming medium (RM).

Plasmid set	Plasmid name	Amount of plasmid DNA		Nucleofector Solution V	Electroporation Programme
		4 μg	*10 μg*		
Thompson's Lab	pEP4EO2SEN2L	1.33 μg	3.33 μg	100 μl	X-005
	pEP4EO2SET2K	1.33 μg	3.33 μg		
	pEP4EO2SEM2K	1.33 μg	3.33 μg		
Yamanaka's Lab	pCXLE-hOCT3/4	1.33 μg	3.33 μg	100 μl	
	pCXLE-hSK	1.33 μg	3.33 μg		
	pCXLE-hUL	1.33 μg	3.33 μg		
GFP control	pmaxGFP	4 μg	10 μg	100 μl	

Reprogramming medium		
Components	**Stock concentration**	**Working concentration**
DMEM-F12	N/A	N/A
NEAA	100x	1x
Glutamax	100x	1x
N-2	100x	1x
B27	50x	1x
β-mercaptoethoanol	1M	10 μM
bFGF-2	4μg/ml	100 ng/ml
PD0325901	5mg	0.5 μM
A-83-01	2mg	0.5 μM
CHIR99021	2mg	3 μM
HA-100	5mg	1 μM
LIF	10μg	1000 units/ml

The culture was monitored everyday to identify the formation of partially reprogrammed colonies. On d14 post-electroporation, the cultures were transitioned into mTeSR by replacing 50% of RM by mTeSR on d15, 75% of RM by mTeSR on d16, and the cultures were fed with mTeSR medium on d17 post-electroporation. The appearance of the hiPSC-like colonies was tracked everyday until d28. The hiPSC-like colonies were isolated by either manual dissection or MACS column purification.

2.1.6 Pluripotency characterisation

2.1.6.1 Growth curve

To generate the growth curve and calculate the population doubling time (PD) of hPSCs, the cells were seeded at 1.25x10^6 cells/T25 flask. The cells were dissociated accordingly based on the culture condition as described in section 2.1.2 and 2.1.3. The total cell number was recorded every split and repeated for 5 passages. The PD time was calculated using the equation below:

$$Cumulative\ Population\ Doubling\ Time\ (CPD) = \Sigma \frac{\log_{10}(\text{Fold increase in cell no. per passage})}{\log_{10} 2}$$

$$\text{Population Doubling time (hrs)} = \frac{(No.\ of\ days\ in\ culture)\times 24}{\text{CDP per passage}}$$

The accumulative PD was summed across the 5 passages to plot the growth curve relative to time in culture using linear regression best fit curve.

2.1.6.2 Immunofluorescence analysis of pluripotent-associated transcription factors

To conduct the immunofluorescence analysis of nuclear pluripotent-associated transcription factors, the hPSCs were cultured at 30,000 cells/cm^2 in a Matrigel-coated 96-well plates. When the culture reached 60% confluency, they were fixed using 4% Paraformaldehyde (PFA) for 12 min followed washing twice with PBS and stored at 4^{o}C in PBS for up to one week. On the day of experiment, the fixed cells were first penetrated using 0.05% Triton X-100 (diluted in PBS) for 15 min followed washing twice with PBS and Tween-20 at 0.01% (diluted in PBS). The cells were then incubated with 5% human serum (diluted in PBS) for at least 30 min before starting incubation with the primary antibody (OCT4, SOX2, and NANOG) for 1h and subsequence secondary antibody for 1h. The details of antibodies and their concentrations were demonstrated in Table 2.5. To count the number of cells, DAPI staining at 1:500 dilution was used to incubate the samples for 15 min followed washing three times with PBS. The immunofluorescence pictures were captured using the Operetta High-content imaging system (Perkin Elmer). and analysed using Harmony High-content imaging analysis software.

Table 2.5: List of antibodies used for immunofluorescence analysis. * Antibodies were made using 5% human serum diluted using PBS.

	Primary Antibody	Derived from	Dilutions	Secondary antibody	Dilutions
Pluripotency Markers	NANOG	Goat	1:200	Rabbit Anti-goat AlexaFluor 488	1:1250
	OCT4	Mouse	1:200	Goat Anti-mouse AlexaFluor 488	1:1250
	SOX2	Goat	1:200	Rabbit Anti-goat AlexaFluor 488	1:1250
	SSEA-4	PE-Conjugated	1:100	N/A	N/A
	SSEA-1	PE-Conjugated	1:100	N/A	N/A
	TRA-1-81	PE-Conjugated	1:100	N/A	N/A

2.1.6.3 Flow cytometry analysis of surface pluripotent markers

To analyse the surface pluripotency markers, including SSEA-4 and TRA-1-81, the hPSCs were harvested and fixed using 4% PFA as described above. The fixed cells were then incubated with PE-conjugated SSEA-1, SSEA-4, and TRA-1-81 (as shown in Table 2.5) antibodies for 20 min at 4^{o}C and subsequently analysed using Guava® easyCyte Benchtop Flow cytometer, Merck Millipore and the InCyte software was used to analyse the data.

2.1.6.4 Sample Preparation for Karyotype

To evaluate the karyotype of hPSCs after prolonged culture, the hPSCs were maintained in their culture condition for at least three passages before starting preparation for Karyotype analysis. To capture the maximum number of hPSCs in the metaphase, 1x10^{6} cells/T25 were seeded and cultured for 24h, which close to the doubling times, and incubated with 5 ml of culture medium containing 100 ng/ml of KaryoMAX® Colcemid™ for 30 min followed the collection of the culture medium in a 30 ml Universal tube. The adherent hPSCs were harvested using enzymatic dissociation according to their culture condition and pooled with the KaryoMAX medium. The cells were centrifuged at 160g for 4 min and the pellet was gently mixed by adding drop-wise 0.6% sodium citrate with vortex and incubated at room temperature (RT) for 20 min followed centrifuged at 300g for 5 min. The pellet was then fixed by adding drop-wise 10 ml of Methanol:Glacial acetic acid (5:1, vol/vol) for three times followed spinning down at 300g for 5 min and stored at -20^{o}C. The karyotype at 30 metaphase spreads and

karyogram analysis were performed by Mr Nigel Smith (Nottingham City Hospital, UK) in accordance with the International System for Human Cytogenetic Nomenclature International Guidelines (ISCN, 2005).

2.1.7 Cardiac differentiation of hPSCs

2.1.7.1 The original monolayer differentiation protocol or the SP34(Act, BMP4) protocol

The SP34(Act, BMP4) was originally designed for hPSCs in mTeSR culture condition. To initiate the cardiac differentiation process, the hPSCs were seeded at 40,000 cells/cm^2 in the Matrigel-coated T25 flask and maintained in mTeSR culture. The medium was changed every day until day 3 when the culture reached approximately 80% confluency and compaction. The compact and confluent culture was then exposed to StemPro34 medium supplemented with 10 ng/ml BMP4 and 8 ng/ml Activin-A (termed SP34-AB medium) for 48h. On d2, the medium was switched into RPMI medium containing B27 supplement (minus insulin) (termed RB27(-Ins) medium), 10 μM KY02111, and 10 μM XAV939 (termed KYX). On d4, the medium was changed into RPMI with B27 supplement (termed RB27 medium) and KYX, and the culture was maintained for 48h. From d6 onward, the culture was kept in RB27 medium. Beating cardiomyocyte was observed on d7 to d8, and synchronously beating monolayer appeared on d10 post-differentiation.

2.1.7.2 The E8-AB, and mTeSR-AB protocols

To adapt the original protocol for E8-cultured hPSCs, a preconditioning step was added to the SP34 (Act, BMP4) protocol, which was StemPro34 medium containing Matrigel (1:100 dilution) and BMP4 (1 ng/ml) for 12h to 18h before cardiac induction process. After the preconditioning step, the culture was then undergoing the SP34 (Act, BMP4) protocol as described in section 2.1.7.1. In the mTeSR-AB protocols, the mTeSR

was used to precondition the culture 12h to 18h before initiate the cardiac differentiation process using SP34 (Act, BMP4) protocol.

2.1.7.3 The mTeSR-CHIR protocol

In the mTeSR-CHIR protocol, the E8-cultured hPSCs were first seeded into the Matrigel-coated T25 followed medium changing every day for 2 days. On d2, the culture should reach 70% confluency followed the preconditioning step using mTeSR for 12h to 18h. After precondition using mTeSR, the culture was treated with StemPro34 containing 5 μM of CHIR99021 (CHIR) for 48h followed RB27(-Ins) containing KYX for another 48h. On d4, RB27 supplemented with KYX was used to maintain the cells and on d6, the culture was kept in RB27. The medium was changed every 2 consecutive days using RB27. Beating cardiomyocyte was observed on d7 to d8, and synchronously beating monolayer appeared on d10 post-differentiation.

2.1.7.4 Dissociation of monolayer CMs using CDS method

One day before dissociation, the culture was treated with 10% FBS in RB27 to enhance the survival rate of the CMs. The beating monolayer was then first washed one with PBS followed incubation with PBS for 4 min at 37^{o}C and 5% CO_2 in the incubator. Subsequently, the monolayer cardiomyocytes were treated with 3 ml of CDS for 6 min to 8 min at 37^{o}C followed gently tapping the flask to detach the cardiomyocytes. The dissociated cells were collected by adding 7 ml 10% FBS in RB27 and centrifuged at 300g for 4 min. The cell count, if desired, were carried out at this stage using Cedex Automated counting system. The pellet was then re-suspended in 10% FBS in RB27 and re-plated according to the experimental plan. Medium was changed 24h after dissociation and every 3 consecutive days thereafter.

2.1.7.5 Characterisation of hPSC-derived cardiomyocytes using immunofluorescence analysis

To identify the cardiac differentiation efficiency and CMs purity, the CDS-dissociated CMs were seeded into Matrigel-coated 96-well plate at 55,000 cells/well and maintained for at least 3 days before starting experiment. To stain the CMs using immunofluorescence technique, the CMs were fixed using 4% PFA for 10 min at RT. Cells were then washed three times with PBS followed permeabilize using 0.1% Triton X-100 (diluted in PBS) and washed two times with PBS and one time with 0.01% Tween 20 (diluted in PBS). The cells were then incubated with 5% human serum for at least 30 min and subsequently incubated with primary antibody (anti-human cardiac troponin T, cTNT, or α-actinin) as shown in Table 2.5 for 2h or overnight. On the next step, the cells were then washed three times with PBS and two times with 0.01 Tween 20 for 5 min before incubation with the appropriate secondary antibodies (Table 2.6) for 1h at RT protected from light. Cells were washed three times with PBS and two times with 0.01% Tween-20 followed adding DAPI for nucleus stain at 1:500 dilution for 15 min at RT. The final wash was carried out two times using PBS. The immunofluorescence pictures were captured using the Operetta High-content imaging system (Perkin Elmer) and analysed using Harmony High-content imaging analysis software.

Table 2.6: The list of antibodies used to analyse the CM purity and cardiac differentiation efficiency.
*All antibodies were made using 5% human serum diluted in PBS.

	Primary Antibody	Derived from	Dilutions	Secondary antibody	Dilutions
Cardiac Markers	cTNT	Rabbit	1:400	Goat Anti-Rabbit AlexaFluor 633	1:400
	α-Actinin	Mouse	1:800	Goat Anti-Mouse AlexFluor 488	1:1000

2.1.7.6 Time-course analysis of protein kinetics during cardiac differentiation process

To identified stage-specific markers expressed during the differentiation process, the hPSCs underwent either E8-AB, mTeSR-AB, and mTeSR-CHIR protocols were fixed using 4% PFA at different day interval including d0, d2, d4, d6, d8, d10, and d12 followed staining with the primary antibodies as listed in Table 2.7. The immunofluorescence

pictures were captured using the Operetta High-content imaging system (Perkin Elmer) and analysed using Harmony High-content imaging analysis software. The experiments were kindly performed by Dr. Vinoj T. George and Miss. Puspita Katili.

2.1.7.7 Flow cytometry analysis of CMs

The CMs were harvested using CDS method and fixed using 4% PFA for 15 min at RT. The fixed cells were then permeabilised using 0.1% Triton X-100 (diluted in PBS) for 30 min followed washing two times with PBS and one time with 0.01% Tween-20 for 5 min. The pellet was then centrifuged at 500g for 3 min and incubated with primary antibody for 2h or overnight. Once the incubation completed, the cells were washed two times with PBS and one time with 0.01% Tween-20 followed staining with appropriate secondary antibody for 2h. The cells were then centrifuged at 500g for 2 min and re-suspended in PBS followed running through a flow cytometer (FC500 Beckman Coulter). The list of antibodies was showed in Table 2.7

Table 2.7: List of antibodies used for flow cytometry analysis of hPSC-CMs.

	Primary Antibody	Derived from	Dilutions	Secondary antibody	Dilutions
Cardiac Markers	cTNT	Rabbit	1:800	Goat Anti-Rabbit AlexaFluor 633	1:800
	α-Actinin	Mouse	1:1000	Goat Anti-Mouse AlexFluor 488	1:1000
	MLC-2v	Rabbit	1:800	Goat Anti-Rabbit AlexaFluor 633	1:800
	MLC-2a	Mouse	1:800	Goat Anti-Mouse AlexFluor 488	1:1000

2.1.8 Functional analysis of hPSC-CMs

2.1.8.1 Measurement of beat rate and beating pattern of hPSC-CMs using CardioExcyte96 platform

The 96-well sensor plates of the CardioExcyte96 were coated with fibronectin at 1:100 dilution in PBS without Ca^{2+} and Mg^{2+} for 1.5 h inside the incubator. The CMs at d25 to d28 were dissociated using CDS method and seeded into the sensor plate at 60,000 cells/well. The plates were transferred into the incubator and cells were not touched or moved for 48h followed medium change before starting the experiment. The

CardioExcyte96 experiments were performed according to the manufacturer operation manuscript and analysed using CardioExcyte Control software.

2.1.8.2 Measurement of intracellular cAMP using LANCE Ultra cAMP assay

The intracellular cAMP production in hPSC-CMs was measured using the LANCE *Ultra* cAMP kit (Perkin Elmer) following the manufacturer's instruction. In brief, the CMs at d25 to d28 were seeded into the Matrigel-coated 384 well plate using the Fully Automated Tecan Evoware Liquid Handling (TEL) platform at 5,000 viable cells/well. The cells were maintained in the plate for at least seven days before starting the experiment. The medium was changed by TEL every 2 consecutive days. On the day of experiment, the cells were then treated with β-blocker, if desired, for 1 h prior to Isoprenaline (ISO) treatment in the incubator. After incubation completed, the medium was completely aspirated from the wells and 10 μL ISO at desired concentrations was added to the well and incubated for 1h. Tracer and U*Light*-anti-cAMP working solution were added and to the wells and incubated at 37°C and 5% CO_2 for 1h. The time-resolved fluorescence resonance energy transfer signal was determined using the EnVision Multilabel Plate Reader (Perkin Elmer). The cAMP levels were determined using a standard curve, and data were interporated using a comprehensive curve fitting (nonlinear regression) and Prism (GraphPad Software, Inc., San Diego, CA, http://www.graphpad.com). Each condition was used in triplicates, and the experiments were performed at least two times.

2.1.8.3 Western Blot analysis of cellular distribution of GRK5

The hPSC-CMs at d20 to d25 were dissociated using CDS method and seeded at $5x10^6$ cells/flask in Vitronectin (1:100 dilution)-coated T25 flask and maintained until d30 post-differentiation process. The CMs were then treated with 100 nM ISO and incubated for 24 h, 48 h, and 72 h. The cells were then collected by using scraper and centrifuged at 400g for 5 min followed washing twice with PBS. The cells were spun down at 400g

for 5 min, re-suspended gently in 400 μL of buffer A, and incubated for 15 min on ice followed adding 25 μL of 10% NP-40, vortexed for 10s, and incubate on ice for 3-5 min. The nuclei were collected by centrifuge at maximum speed for 90s. The supernatant containing the cytoplasmic fraction was collected to a new Eppendorf tube, aliquot and snap-frozen in liquid N_2 followed stored at -80°C. The collected nuclei were then re-suspended in 50 μL of ice-cold buffer C and vortex for 15 min in the cold room or at 4°C followed centrifugation at maximum speed for 15 min. The supernatant containing nuclear protein extract was then collected, aliquoted, snap-frozen in liquid N_2, and stored at -80°C. All centrifugation steps were conducted at 4°C.

Table 2.8: Buffers used in Western Blot

Buffer	Components	[Stock Conc]	[Working Conc]
Buffer A	Hepes pH 7.9	1 M	10 mM
	KCl	2 M	10 mM
	EDTA	0.5 M	0.1 mM
	EGTA	200 mM	0.1 mM
	DTT	1 M	1 mM
	Water	-	-
	Protease Inhibitor Cocktail	1 X	1:100 dilution
	Phosphatase Inhibitor Cocktail	1 X	1:100 dilution
Buffer B	NP40 Igepal	100%	10%
	Hepes pH 7.9	1 M	20 mM
Buffer C	NaCl	2 M	0.4 M
	EDTA	0.5 M	1 mM
	EGTA	200 mM	1 mM
	DTT	1 M	1 mM
	Protease Inhibitor Cocktail	1 X	1:100 dilution
	Phosphatase Inhibitor Cocktail	1 X	1:100 dilution
TBS (10X) Total Volume: 5 L, pH 7.4	NaCl	-	400 g
	KCl	-	10 g
	Tris	-	150 g
TBST	TBS	10 X	1X
	Tween-20	100%	0.1%

Western Blotting was performed for GRK5 using anti-human GRK5 antibody (1:1250, Abcam – ab64943) using NuPage system following the manufacturer instruction. The nitrocellulose membrane was blocked using 5% skimmed milk in TBST medium. The blots were stripped and then probed for Tubulin (1:5000, New England

biolabs, 2128P) and Lamin A/C (1:2000, New England Biolabs, 4777T) to normalise the protein loading and detect the cytoplasmic and nuclear fraction, respectively. The buffers used for Western Blot were described in Table 2.8.

2.1.8.4 Immunofluorescence analysis of hypertrophic response from hPSC-CMs

The hPSC-CMs at d20 to d25 post-cardiac differentiation were dissociated using CDS method and seeded at 55,000 cells/well of the 96-well plate coated with Vitronectin (1:100 dilution in PBS). The CMs were maintained for at least seven days before starting the experiment. On the day of experiment, different concentrations of hypertrophic drugs including Endolelin-1, Phenylephrine, and ISO were added to the cell culture medium and incubated for at least 15 h followed incubation with 10 μg/ml Brefeldin A (BFA, Sigma, B7651) for 3h. The cells were then fixed and followed the immunofluorescence process as described in section 2.1.7.5 using anti-human BNP antibody at 1:500 dilution.

2.1.9 Magnetic Activation Cell Sorting (MACS)

To isolate the newly established hiPSC, the MACS column purification was performed as previously described (Dick et al., 2011). To be more specific, once the reprogrammed colonies appeared and formed a distinct border from the surrounding culture, usually 2 weeks after transfection with the episomal plasmids, they were dissociated by Accutase treatment for 3 mins followed centrifuged at 200g for 5 min. The pellet was then washed in ice-cold column buffer containing Hanks Balanced Salt Solution (HBSS) with 2% FBS, adjusted pH to 7.4 using Sodium bicarbonate. After wash, the cells were then pelleted at 160g for 4 min and re-suspended with 200 μl of ice-cold column buffer containing TRA-1-81 PE-conjugated antibody (1:100 dilution). The cell suspension was incubated with the antibody at 4^{o}C for 20 min in the fridge. After incubation, the cells were washed with 5 ml of ice-cold column buffer and spun down. During the centrifugation process, the MS columns were placed in a MACS separator holding which attached to a MACS multistand. When the centrifugation completed, the

pellet was then re-suspended with 500 μl ice-cold column buffer and transferred to the MS column that allowed the cell suspension to drip through the column by gravity. The flow-through was collected and the column was washed three times with ice-cold column buffer. The trapped cells inside the column was collected by adding 1 ml of ice-cold column buffer and using the supplied plunger. The eluted cells were centrifuged at 160g for 4 min, re-suspended with appropriate culture medium and transferred to one well of the Matrigel-coated 6-well plate. The medium was changed every day until the culture reached 80% confluence.

2.2 Molecular Biology

2.2.1 Extraction of genomic DNA

Total cellular DNA of hPSCs was isolated using DNeasy Blood and Tissue kit (Qiagen) following the manufacturer's protocol. The DNA was eluted in 50 μl Molecular Graded water. The DNA concentration and purity were measure using NanoDrop DN100 spectrophotometer and stored at -20^{o}C until needed.

2.2.2 DNA gel extraction and purification process

The DNA amplicons generated from polymerase chain reaction (PCR) was purified using a PCR purification kit or was extracted from the agarose gel (1.5% v/v) using QIAquick Gel Extraction kit (Qiagen), according to the manufacture's guideline. DNA was eluted in 30 μl of Molecular graded water and measured using NanoDrop DN100 spectrophotometer and stored at -20^{o}C until needed.

2.2.3 Agarose gel electrophoresis

To perform the gel electrophoresis, Agarose in powder form was dissolved in TAE buffer (1X) containing 40 mM Tris Acetate and 1 mM EDTA by beating in the microwave for 20 min at 20% power. The medium was then cooling down at RT for 15 min and ethidium bromide (EthBr) was added at 0.4 μg/ml. The gel was formed by pouring the

Agarose into clean gel tray with combs and allowing the gel to solidify for 45 min. The gel was move into an electrophoresis tank containing TEA buffer (1X). Prior to loading into the gel, 2 μl of loading dye was added into 10 μl of sample. The gel was run at 85V for 90 min and was captured using Fujifilm LAS-1000CCD camera.

2.2.4 Total cellular RNA extraction and cDNA synthesis

Total RNA extraction process was performed according to the manufacture protocol of the Qiagen RNeasy Mini Kit. The RNA was eluted in 30 μl of RNase free water. The RNA negative sample (no cells) was used as a control to evaluate the RNA contamination during the extraction procedure. The extracted RNA was quantified using NanoDrop DN100 spectrophotometer and was stored at -80^{o}C until needed.

To convert RNA into cDNA for quantitative PCR (qPCR) and reverse transcriptase PCR (RT-PCR), the first strand cDNA synthesis kit (GE Healthcare) was used following the manufacture protocol. 350 ng RNA extraction was used to synthesis the cDNA template. The total reaction volume used was 20 μl. After the reaction completed, the samples were diluted by adding 80 μl of Molecular graded water to make up the total volume of 100 μl. All samples had their relative Reverse transcriptase negative control (RT-) and cDNA negative control. The product was kept at -20^{o}C until needed.

2.2.5 Restriction enzyme digestion

All the restriction enzyme digestions were performed under suggested buffers according to the manufacture's protocol. The reaction was prepared as shown in table 2.4. The digestion process was conducted at 37^{o}C for 3 hours. The control reaction comprised all reagents except the enzyme. In double digestion reaction where different buffers were required, sequential digestions were performed with DNA purification after each digest. The digested samples were analysed using gel electrophoresis and extracted using QIAquick gel extraction kit.

2.2.6 Plasmid design, cloning procedure and plasmid transformation

The genomic sequence of target genes was identified using GenomeBrowser and confirmed by PCR from the extracted gDNA. Specific PCR primers were designed using GenomeBrowser primer design tool. In order to perform plasmid transformation process, 50 μl of TOP10 competent cells were thawed on ice for 10 min and were mixed with 5 μl of plasmid DNA. The mixture was incubated on ice for 30 min followed 30s heat shock at 42^{o}C, in the water bath, and placed immediately on ice for 2 min. The cells were then re-suspended with 200 μl of SOC media and the culture was incubated in the shaking incubator at 37^{o}C for 1 hour.

Prior to the transformation process, the LB agar plates were prepared by melting LB agar in a microwave for 20 min at 20% power and allowed cooling down at RT for 15 min. Once the medium was cooling down about 50^{o}C, ampicillin (50 mg/ml) or kanamycin (25 mg/ml) was added depending on the antibiotic resistance gene of each transformed plasmid. About 15 ml of melted agar was poured into each 90 mm Peri-dish and the agar was left to solidify at RT for 30 min.

Once the incubation complete, the transformed bacteria were spread on the 90 mm LB agar plate using a sterile colony spreader and incubated inverted in the incubator at 37^{o}C overnight. On the following day, the number of bacterial colonies was recorded and the colonies were picked and culture in 5 ml of LB medium supplemented with ampicillin or kanamycin at 37^{o}C in a shaking incubator overnight. The plasmid DNA from bacteria was extracted and purified as described in section 2.2.1.

2.2.7 Polymerase Chain Reaction (PCR)

For normal PCR reaction, 2.5 μl of 10 μM each forward and reverse primers were used and DNA concentration (below 250 ng in total) was added to the master mix (Table 2.9). the total volume of each PCR reaction was 50 μl by topping up with Molecular grade water. The PCR was conducted using a thermal cycler with the following program: initial denaturation at 98^{o}C for 5 min (for Phusion polymerase) or 94^{o}C for 5 min (for Taq

polymerase), followed 25 to 33 repeated cycles of denaturation at 98°C (Phusion Polymerase) and 96°C (Taq Polymerase) for 30 sec, annealing at 64°C for 30 sec and extension at 72°C for 30 sec. The final extension step was carried out at 72°C for 10 mins. The samples were confirmed using gel electrophoresis and the remained samples were stored at -20°C until needed.

Table 2.9: Composition of the PCR reaction mixture used in this thesis. NOTE: restriction enzyme volume should not exceed 10% of total reaction volume and the total DNA used for PCR should not exceed 250ng.

Experiment	Components	Volume
Restriction Digestion	10x Restriction Enzyme Buffer	2.5 μl
	Enzymes	0.5 μl
	DNA	2 μl
	Water	Up to 25 μl
PCR (Phusion Polymerase)	Forward Primer (10 μM)	2.5 μl
	Reverse Primer (10 μM)	2.5 μl
	dNTP	1 μl
	5x Buffer	4 μl
	Phusion Polymerase	0.25 μl
	DNA (<250 ng)	2 μl
	dH_2O	Up to 20 μl
PCR (Taq Polymerase)	Forward Primer (10 μM)	2.5 μl
	Reverse Primer (10 μM)	2.5 μl
	dNTP	1 μl
	10x Buffer	2 μl
	Phusion Polymerase	0.5 μl
	DNA (<250 ng)	2 μl
	dH_2O	Up to 20 μl

2.2.8 qPCR analysis of gene expression

The RNA extraction and cDNA synthesis samples from the hPSC-CMs were performed as described in section 2.2.4. The qPCR reaction mixture contains 10 μl TaqMan® Fast Advanced Master Mix (2X), 1 μl Taqman Assay (20X), 7 μl Nuclease-free water, and 2 μl of cDNA template. The real-time PCR reaction was performed using 7500 Fast Real-time PCR template. Expression values were normalised to the average expression of *GAPDH*. Taqman assay IDs for *GAPDH*, *ADRB1*, *ADRB2*, GRK2 (*ADRK1*), and *GRK5* are Hs02786624_g1, Hs02330048_s1, Hs00240532_s1, Hs00176395_m1, and Hs00992173_m1

2.3 Statistical analysis

The statistical analysis in this thesis was conducted using two-way ANOVA, Prism (GraphPad Software, Inc., San Diego, CA, http://www.graphpad.com) unless otherwise stated. The two-way ANOVA was chosen to compare the mean differences between two independent groups (called factors) to understand the interaction between the two variables. All the data shown in this project are as mean ± s.e.m (n number) unless otherwise stated. The post-hoc tests were used as suggested by GraphPad Software including one of the following Turkey's test, Bonferroni, and Sidak. In this thesis, the experiments had three independent biological replicates unless otherwise stated. Each biological replicate had three technical replicates.

Chapter 3 Development of monolayer cardiac differentiation protocol to generate ventricular cardiomyocytes from hPSCs

3.1 Introduction

3.1.1 hPSC-CMs and their applications

Traditionally, the CMs derived from hPSCs are defined as the cardiac muscle cells generated from hPSCs and performed the spontaneous contractility *in vitro* (Mummery et al., 2003; Murry and Keller, 2008). However, this definition does not contain the purity of CMs after the differentiation process completed. Hence, in the scope of this thesis, the hPSC-CMs are re-defined as the population that contains more than 80% of cardiac muscle cells beating spontaneously *in vitro* without the need of the purification process.

The CM differentiation ability of hPSCs provides an opportunity for cardiovascular research and disease modelling. Firstly, the *in vitro* cardiogenesis enhances the knowledge about the human cardiac developmental process in ways not otherwise possible (Doetschman et al., 1985; Koss et al., 1995; Itskovitz-Eldor et al., 2000; Moorman and Christoffels, 2003; Stefanovic and Zaffran, 2017). Secondly, the hPSC-CMs emerge as an unlimited source of human CMs for testing pharmaceutical drugs, developing new cardioactive compounds, and more importantly, screening for potential cardiotoxicities, such as drug-induced QT prolongation, arrhythmias, and cardiac hypertrophy (Mitcheson et al., 2000; Hollenberg, 2011). Thirdly, the CMs generated from hiPSCs harbouring the patient-specific genotypes serve as an *in vitro* model to develop specific personal therapeutic approach and disease modelling, providing a powerful tool to understand rare genetic diseases and cardiac functions, especially during heart failure conditions (Takahashi and Yamanaka, 2006 2017; Galdos et al., 2017).

Since the first establishment of the three-dimensional embryoid bodies (EBs) by Itskovits-Eldor's team, three main platforms have been developed for CM differentiation, including the EB method, co-culture with END-2 cell lines, and 2D monolayer systems (Itskovitz-Eldor et al., 2000; Mummery et al., 2012). Although these early versions of the differentiation process generated low level of CM purity (below 30%), the CMs derived from these methods displayed many structural and functional features associated with the heart cells, including expression of cardiac markers, such as Troponin-T (cTNT), α-ACTININ (α-ACT), alpha/beta myosin heavy chain (α/β MHC), myosin light chains (MLC-

2a and MLC-2v), and the human cardiac surface marker (SIRPA) (Ma et al., 2011; Skelton et al., 2014; Sulakhe and Vo, 1995). Additionally, these CMs exhibit typical electrophysiology features as found in the human heart, and response to pharmacological compounds, including β-adrenergic inducer, hypertrophic treatment, and anticancer drugs, such as doxorubicin (Wu et al., 2015; Burridge et al., 2016).

Understanding the therapeutic and research potentials of hPSC-CMs, several studies have been conducted to improve the cardiac induction process. However, these studies replied on several conditions to optimise the efficiency, including culture conditions, reprogramming methods, and the application of growth factors and small molecules driven the cardiogenesis process *in vitro* (Batalov and Feinberg, 2015; Boheler et al., 2002; Murry and Keller, 2008; Mummery et al., 2012).

3.1.2 hPSC culture conditions and their effects on cardiac differentiation

From their first discovery in 1998 (Thomson et al., 1998), the culture of hESCs has evolved from undefined conditions, requiring co-culture with mouse embryonic fibroblast (MEF), to current defined conditions, as shown in Figure 3.1 (Chen et al., 2014a). Regardless of the culture conditions, the three key factors that influent the quality, robustness, and viability of hPSC for *in vitro* maintenance are extracellular matrix (ECM), growth medium, and passaging procedure (Chen et al., 2014b).

As mentioned previously, the original derivation and culture condition of hPSCs employed basal medium containing foetal bovine serum (FBS) and mouse embryonic fibroblast (MEF) feeder support (Thomson et al., 1998; Reubinoff et al., 2000; Xu et al., 2001). These culture conditions contained undefined components of animal origin, which became the problematic issue of the system due to two main reasons. First, unknown factors present in serum, ECMs such as Matrigel, or produced by MEF-feeder layers have been proven to be directly involved in the growth and differentiation of the stem cells by changing the hPSC morphology, and their growth rate during prolonged culture *in vitro* (Akopian et al., 2010). Second, these undefined components are prone to be significantly variable reducing the robustness of hPSC culture and introducing lab-to-lab

variation, which in turn, directly affects the hPSC behaviours and subsequent cardiac induction process.

Regarding cell dissociation techniques, three methods have been introduced and proven to be efficient to passaging the hPSCs, including the manual dissection, enzymatic dissociation, and non-enzymatic passaging process. The manual isolation was developed to dissect the colonies from the MEF layer and transferred into a new culture condition. The enzymatic dissociation utilises the effectiveness of protease such as trypsin, Accutase, or Collagenase to disrupt the attachment of stem cells to the ECMs in a quick, effective, and straightforward way. In the enzyme-free approach, EDTA dissociation buffer has been widely used, especially in E8 culture condition. EDTA is a general calcium and magnesium chelator that directly intervenes the calcium-dependent binding sites of the hPSCs to their ECMs, which in turn, gently releases the cells from the culture surface (Chen et al., 2011). Indeed, both enzymatic and EDTA approaches have been widely used to propagate the hPSCs *in vitro*, but the combination between these two methods has not been formulated properly. Reducing the enzyme concentration and supplementation with EDTA could provide the same effectiveness but reduce the hardness during the dissociation procedure, which in turn, increased the cell survival rate.

Hence, for these reasons listed above and their effects on propagation of hPSCs, it is important to eliminate the animal-derived components in the culture conditions to reduce the variations and inconsistencies in hPSC culture. Furthermore, it is also necessary to develop a standardized and defined conditions that allow culturing different hPSC lines in a robust way, reducing variation in cell growth and viability regardless of the origins of hPSCs.

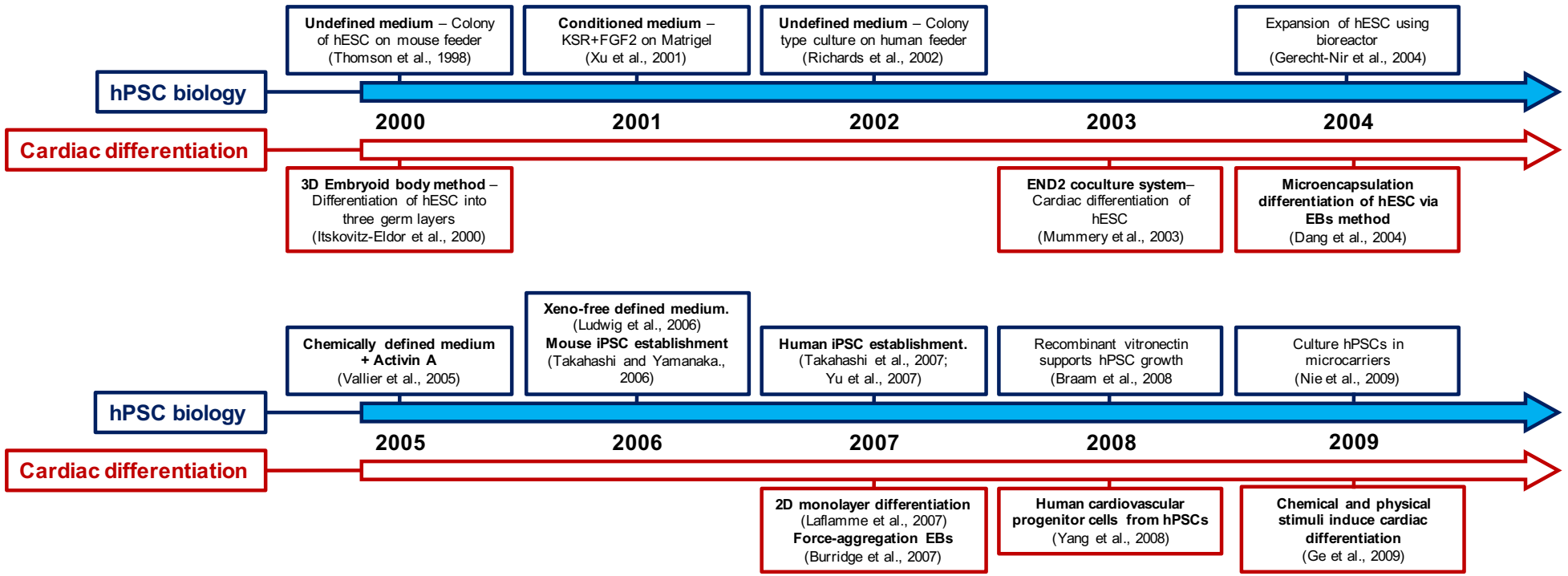


Figure 3.1: Timeline of the development of cell culture for hPSC together with the evolution of cardiac differentiation process. Adapted from Chen et al., 2014

References: (Thomson et al., 1998; Itskovitz-Eldor et al., 2000; Xu et al., 2001; Richards et al., 2002; Mummery et al., 2003; Gerecht-Nir and Itskovitz-Eldor, 2004; Dang et al., 2004; Vallier et al., 2005; Ludwig et al., 2006; Takahashi and Yamanaka, 2006; Nakagawa et al., 2008; Yu et al., 2007; Braam et al., 2008a; Yang et al., 2008; Nie et al., 2009; Ge et al., 2009).

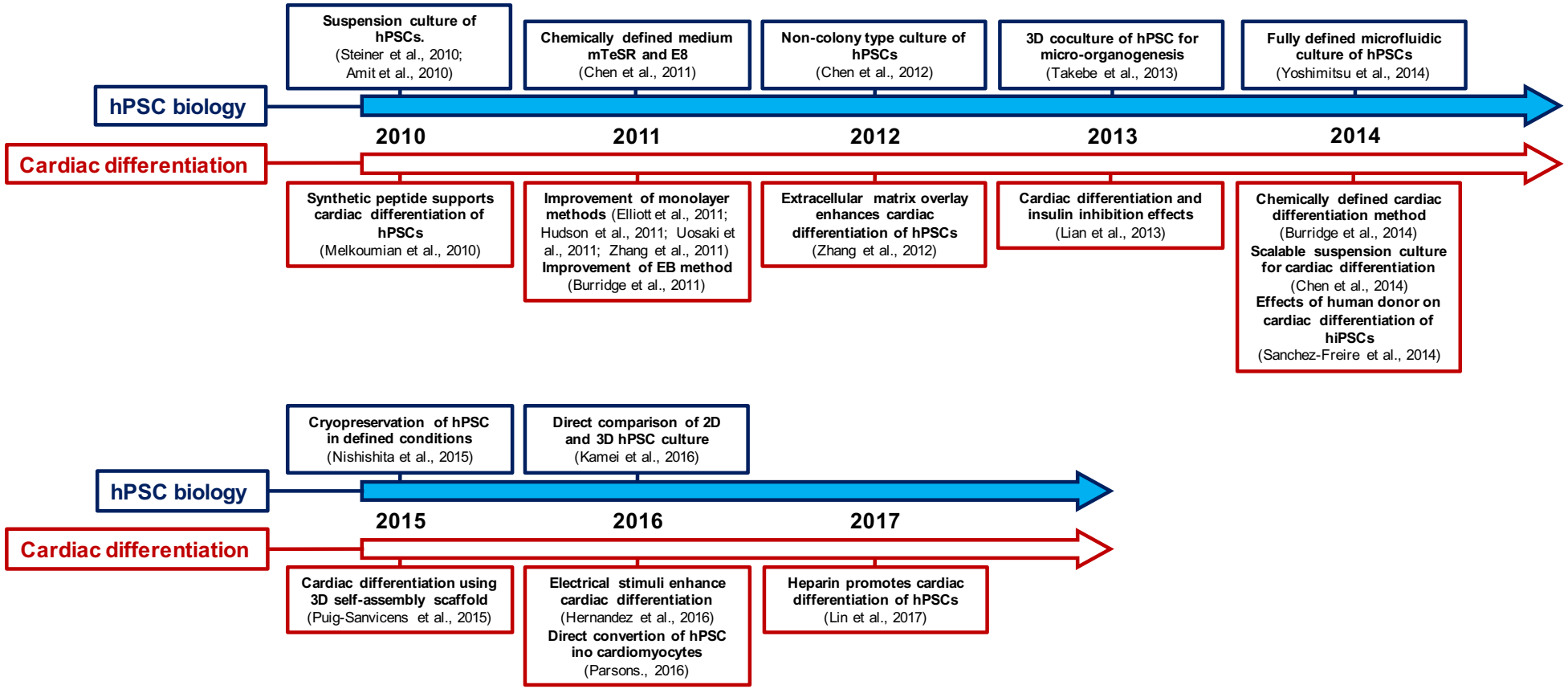


Figure 3.1 (Continued): Timeline of the development of cell culture for hPSC together with the evolution of cardiac differentiation process. Adapted from Chen et al., 2014

References: (Steiner et al., 2010; Amit et al., 2010; Melkoumian et al., 2010; Chen et al., 2011; Elliott et al., 2011; Hudson et al., 2012; Uosaki et al., 2011; Zhang et al., 2011; Burridge et al., 2011; Chen et al., 2012; Zhang et al., 2012; Takebe, 2013; Lian et al., 2013a; Yoshimitsu et al., 2014; Burridge et al., 2014; Chen et al., 2014b; Sanchez-Freire et al., 2014; Nishishita et al., 2015; Puig-Sanvicens et al., 2015; Hernandez et al., 2016; Parsons, 2016; Lin et al., 2017).

3.1.3 Variations of differentiation ability between hESCs and hiPSCs

Theoretically, the cardiac differentiation of hESCs and hiPSCs into CMs is no different as the process relies on the applications of growth factors and small molecules that are involved in the embryonic development of the heart *in vivo* (such as BMP4, Activin-A, TGF-β, Wnt, GSK3, etc.) and follow the same general differentiation timeline (Figure 3.2) (Mummery et al., 2012). Practically, the hiPSCs illustrate a line-to-line variations due to the effects of reprogramming methods and the sources of somatic cells used as starting materials (Ghosh et al., 2010; Lee et al., 2013; Takahashi and Yamanaka, 2016). Furthermore, majority of the published protocols illustrated the cardiac induction process in a narrow range of cell lines, which were usually specific cell lines using to optimise and develop those methods. Once other hPSC lines were used, most of these protocols either did not work completely, or at relatively low efficiency (Burridge et al., 2015; Mummery et al., 2012; Yester and Kuhn, 2017). In terms of disease-related hiPSC lines, differentiation process of these cell lines exhibited vast variations and difficulties due to the genetic background and its associated phenotypic behaviour. Therefore, there is a need for the cardiac differentiation procedure that is robust, efficient, reproducible, and up-scalable regardless of the cell types, reprogramming methods, and culture conditions.

Time line	hPSC line(s)	Medium	Substrate	Reprog	Differentiation procedure	Efficiency	Subtypes	References
2007	hESC: H7	MEF-CM	Matrigel	N/A	Act-A; BMP4; RPMI/B27	~30%	Ven, Atr	(Laflamme et al. 2007)
2011	hESC: H7	MEF-CM	Matrigel	N/A	BMP4 FGF2; Act-A; Noggin; DKK1+Rai/RA; DKK1; RPMI/B27	70%	Ven, Atr, Nod	(Zhang et al., 2011)
	hESC: KhES1; hiPSC: 201B6, 201B7, 253G1, 253G4	MEF-CM	Matrigel	Retro; Lenti	Act-A; BMP4 + FGF2; DKK1; RPMI/B27 (-Ins); RPMI/B27	60%	Ven, Atr	(Uosaki et al., 2011)
	Engineered hESC: H3, M1	MEF-CM	Matrigel	N/A	Act-A, BMP4, FGF2, VEGFA, SCF; LI-APEL; LI-PEL	40%	Ven, Atr	(Elliott et al. 2011)
2012	hESC: H9, H13, H14 hiPSC: IMR90C4	mTeSR1	Matrigel	Epi; Lenti	CHIR; IWP2; IWP4; RPMI/B27 (-Ins); RPMI/B27	85%	Ven, Atr	(Lian et al. 2012)
	hESC: H1, H9. hiPSC: DF6-9-9T, DF19-9-7T, DF19-9-11T, IMR90-C4	mTeSR1	Matrigel	Epi; Lenti	Matrigel; Act-A; BMP4 + FGF2; mTeSR1; RPMI/B27 (-Ins); RPMI/B27	75%	Atr	(Zhang et al. 2012)
2013	hESC: H1, H9 hiPSC: hAFDC-iPS-36	mTeSR1	Matrigel	Retro	CHIR, BMP4, Ascorbate; BMP4 + IWP1; CIM; RPMI/B27 (-Ins); RPMI/B27	80%	Ven, Atr	(Cao et al. 2013)
2014	hESC: H7, H9 hiPSC: 58FSDNC3, 64FSDNC1	E8	Matrigel, Laminin, Vitronectin	Sendai	CHIR; C59; CDM3	90%	Ven, Atr	(Burridge et al. 2014)
2015	hPSC: Line N/S	E8, mTeSR, MEF-CM	Matrigel	N/A	CHIR, BMP4, Act-A; XAV939; Cardiac Differentiation Medium	80%	Ven, Atr	(Van de Berg et al. 2015)

Figure 3.2: Summary of published cardiac induction monolayer protocols of hPSCs. Abbrevations: MEF-CM, mouse embryonic fibroblast conditioned medium; E8, Essential 8 medium; Reprog, Reprogramming methods; N/A, no applicable; Retro, retrovirus; Lenti, Lentivirus; Sendai, Sendai virus; Epi, Episomal plasmid, Act-A, Activin A; Ven, ventricular; Atr, Atrial; Nod, Nodal or pacemarker. (Denning et al., 2016)

3.1.4 2D monolayer cardiac differentiation procedure

Current methods designing for hPSC cardiac differentiation are classified into three main platforms, including **(1)** EB differentiation, **(2)** coculture with visceral endoderm-like stromal cells (END-2), and **(3)** 2D monolayer differentiation (reviewed in (Denning et al., 2016; Mummery et al., 2012). At the time of starting this thesis, although the first two techniques had been developed and optimised to achieve up to 70% differentiation efficiency, they contained several disadvantages such as inconsistent results between experiments In terms of number of EBs containing CMs, low yields (<1% CMs), difficulty in purification of CMs from coculture with END-2 cells, undefined and animal-derived components, and requirements of intensive optimisation process (Kawamura et al., 2012; Laflamme et al., 2007). Therefore, the 2D monolayer procedures emerged as an alternative approach that favours reproducibility in cardiac-specific differentiation. These methods were proven to enhance the uniform distribution of growth factors and small molecules and eliminate the diffusional berries found in EB method (Laflamme et al., 2007; Mummery et al., 2012). Additionally, the monolayer culture of hPSCs allows the system to be scalable to generate a large quantity of CMs in a single batch of the experiment (Batalov and Feinberg, 2015). It was also reported that monolayer method generates more mature CMs with relevant subtype specification (ventricular, atrial, or nodal cardiomyocytes) (Burridge et al., 2014).

However, in the beginning of the thesis, the monolayer cardiac differentiation was not well established and contained broad range of undefined components. Moreover, established protocols showed inconsistent results as well as difficulties in reproducing the process in different types of hPSCs, suggesting the needs of better version to overcome these obstacles. Therefore, a new cardiac induction procedure was established in our laboratory based on the 2D monolayer principle and designed particularly for the mTeSR-cultured hPSCs. At that time, the protocol was in its immature stage and still required optimisation to further improve the cardiac differentiation efficiency, consistency, and reproducibility.

3.1.5 The importance of Activin/Nodal and BMP signalling in cardiac differentiation of hPSCs

The cardiac differentiation procedures, in general, and the 2D monolayer methods, in particular, follow the step-wise approaches that replicate the key commitment stages found during embryonic development (Mummery et al., 2012). Studies in cardiac differentiation of hPSCs revealed that this process is tightly orchestrated by the optimal levels of Activin/Nodal and BMP signalling pathways, which control the cardiac differentiation process of hPSCs and play a vital role in defining the efficiency of the particular protocol (Kattman et al., 2011) (Figure 3.3A). During gastrulation, the cell fates in different germ layers are determined by the graded signalling activities. These gradients are established by inductive signalling centres such as the extraembryonic ectoderm (via BMP signalling pathway) and the posterior primitive streak (via WNT pathway) (Figure 3.3A) (Moorman and Christoffels, 2003; Murry and Keller, 2008).

3.1.5.1 Signalling involved in cardiac differentiation process

Cultured hPSCs present a unique system to study the putative mechanism underlying the effects of growth factor gradients during cardiac differentiation (Paige et al., 2010). Indeed, the initial stimulation of at least one of the major signalling pathways, notably BMP or WNT followed by WNT inhibition resulted in the formation of beating CMs. However, stimulation of BMP and WNT also leads to the establishment of non-cardiac fates such as hematopoietic, endothelial, or endodermal cells (Gertow et al., 2013; Kurian et al., 2013; Lalefar et al., 2016; Loh et al., 2014). Recently, through empirical optimisation, it has been reported that withdrawal of either BMP (by BMP4) or WNT (CHIR99021 [CHIR]) lead to a substantial divergence from conventional cardiac conditions, whereas removal of Activin A and FGF yielded an intermediated phenotype (Yamauchi et al., 2010). Further experiments adding BMP4 and withdrawal of either Activin A or FGF from d0 of differentiation was well tolerated and formed beating CMs (Takei et al., 2009). Hence, it was concluded that extrinsic activation of the BMP and

WNT cascades in the presence of Activin-A or FGF was the most essential for cardiac induction.

3.1.5.2 Establishment of the cardiac corridor

Remarkably, the definition of a “cardiac corridor” where the sum of BMP and WNT signal is conducive to specify cardiac mesoderm was reported (Figure 3.3B) (Rao et al., 2016). This cardiac corridor illustrated that the cardiac differentiation induction and subsequent formation of beating CMs were initiated not only with medium-BMP/medium-WNT, but also low-BMP/high-WNT or high-BMP/low-WNT conditions (Rao et al., 2016). Other concentration of BMP and WNT on either side of the corridor results in the formation of other cell fates, including under low-BMP/low-WNT conditions hPSCs differentiate into neuronal lineages, whereas exposure to high level of BMP results in the formation of lateral or ventral mesoderm signatures. Of note, the establishment of the endodermal signature was found to stand in between the cardiac corridor and the low concentration of BMP/WNT that induced the formation of neural fates (Rao et al., 2016).

3.1.5.3 Mesodermal induction process and cardiac differentiation

The mesodermal induction marks by the expression of Brachyury-T as a result of BMP and Nodal activation, which usually accomplished by the addition of BMP4 and Activin-A (Faial et al., 2015; Takei et al., 2009). Activin-A is used as a surrogate for NODAL as it activates the same receptors on hPSCs (van den Ameele et al., 2012). Using the Brachyury-T reporter line revealed that different concentrations of Activin-A induced different primitive streak sub-populations (Kattman et al., 2011). High level of Activin-A (100 ng/mL) primarily mediated the formation of the anterior streak and endoderm progenitors; whereas a high level of WNT in the presence of low level of Activin-A induced the establishment of primarily posterior streak and mesodermal progenitor cells (Parikh et al., 2015). Therefore, it is important to note that the initial concentrations of BMP4 and Activin-A are essential for induction of cardiac differentiation process in hPSCs.

In terms of WNT cascades, these pathways are highly conserved among species and are important for developmental process, especially during gastrulation (Birchmeier, 2007; Logan and Nusse, 2004). A seven-transmembrane receptor, called Frizzled (FZD), mediates the activation of WNT pathways, and its co-receptors the low-density lipoprotein receptor-related protein 5 and 6 (LRP5/6), following the initiation of intracellular signalling cascades including the glycogen synthase kinase – 3β (GSK-3β) and β-catenin (Lian et al., 2012; Tran et al., 2009). The GSK-3β play a central role in the regulation of WNT signalling pathways, as it phosphorylates β-catenin targeting it for proteasome degradation. Hence, inhibition of GSK-3β using small molecules such as SB216763, BIO, CHIR99021, etc. prevents the degradation of β-catenin, which in turn, increase WNT signalling activities (Lian et al., 2013a). However, GSK-3β inhibition is pleiotropic in its effects on the WNT signalling pathways, as it is also involved in other signalling pathways regulating various cellular process, including cellular proliferation, migration, glucose regulation, and apoptosis (Denham et al., 2012; Embi et al., 1980; Jope and Johnson, 2004; Woodgett, 1994). Hence, the uses of CHIR99021 in cardiac differentiation need to be considered carefully to not only enhance the protocol efficiency, but also reduce its effects on other pathways via controlling the concentration, duration, and application time-point during the cardiac induction process.

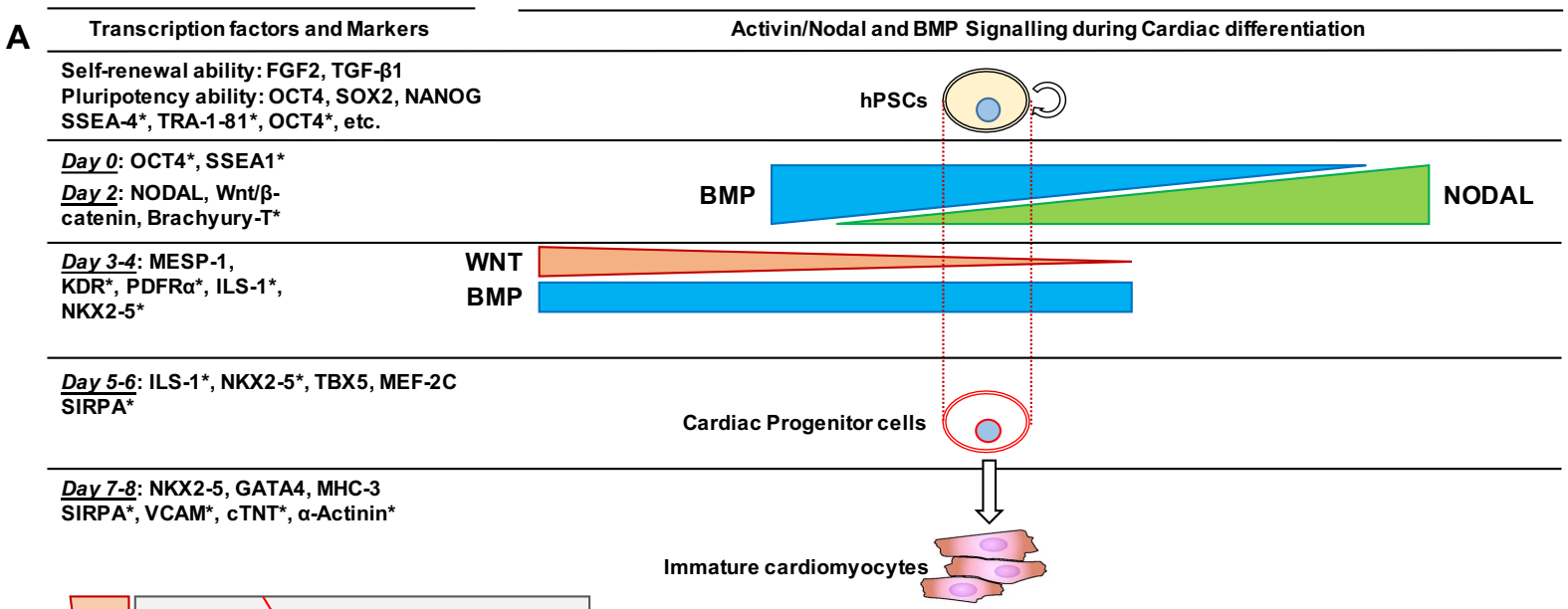


Figure 3.3: ***In vitro* cardiac differentiation of hPSC is regulated by either BMP/Nodal or WNT pathway. (A)** Illustration of *in vitro* differentiation process induced by BMP signalling pathways. *, stage-specific markers that can be used to detect the transformation of cellular stage during cardiac induction process. **(B)** The BMP/WNT-dependent patterning map for hPSCs. Cardiac induction is a function of the sum input of BMP and WNT pathway at the beginning of the differentiation. The Cardiac corridor illustrated the different combinations of BMP and WNT could contribute to the success of the protocol. Figure adapted from Rao *et al.,* 2016.

3.1.5.1 The needs of standard culture condition of hPSCs and cardiac differentiation protocol in our laboratory

Currently, our laboratory contains a wide variety of hPSC lines. A subset of 27 lines including are listed in Table 3.1, which include parental hESCs and hiPSCs produced by different methods and their genetically engineered progeny. Hence, with the currently published cardiac differentiation protocols, the intensive optimisation process is required to maximise the efficiency for all listed cell lines, increasing the workloads and related coast associated with the project. Therefore, standardisation of the culture condition to mTeSR and later E8 medium followed by the modifications of our established protocol were the main rationale of this chapter. Furthermore, it was important to identify the cardiac induction formulation that allowed minimal optimisation process to achieve high level of differentiation efficiency, consistency, robustness, and reproducibility.

Table 3.1: Summary of cell lines are currently available in our laboratory.

Types	Characteristics	Line	Reprogramming Method	Cell Source	Culture conditions
Control	Human embryonic stem cell	HUES7	Isolated	Harvard University	MEF-CM
		H9	Isolated	Harvard University	MEF-CM
	Human induced pluripotent stem cells	AT1	Lentivirus	Human adult teeth fibroblasts	MEF-CM
		ATwt	Retrovirus	Human fibroblasts	MEF-CM
		CBM1	Sendai virus	Human fibroblasts	E8
		NCRM5	Episomal (Rutgers)	Human fibroblasts	mTeSR
		NCRM1	Episomal (Rutgers)	Human fibroblasts	mTeSR
		REBL-Pat	Sendai virus	Human fibroblasts	E8
		Lymp-hiPSC	Episomal (Clonal)	Human lymphoblastoid cell line (Coriell)	mTeSR
Disease	CPVT	CP1	Sendai virus	Human fibroblasts	E8
	Long-QT 1	PHICR	Sendai virus	Human fibroblasts	E8
		ALPO	Sendai virus	Human fibroblasts	E8
		SADE	Sendai virus	Human fibroblasts	E8
	Long-QT 2	REBL	Sendai virus (Clonal)	Human fibroblasts	E8
	Duchenne muscular dystrophin	DMD4	Lentivirus	Human fibroblasts	MEF-CM
		DMD16	Lentivirus	Human fibroblasts	MEF-CM
		DMD19	Lentivirus	Human fibroblasts	MEF-CM
	Myotonic dystrophy (DM1)	DM1SJ1	Sendai virus	Human fibroblasts	E8
		DM1AR1	Sendai virus	Human fibroblasts	E8
	GRK SNP	Lymp-hiPSC-1	Episomal (Clonal)	Human lymphoblastoid cell line (Coriell)	mTeSR
CRISPR edited lines	Adrenergic receptor variants	Human embryonic stem cell (HUES7)	CRISPR/Cas9 edited (Monoclonal)	HUES7	MEF-CM, E8
	G-protein coupled receptor variants	Human embryonic stem cell (HUES7)	CRISPR/Nickase edited (Monoclonal)	HUES7	MEF-CM, E8
	Optogenetic reporter line	Human embryonic stem cell (HUES7)	CRISPR/Cas9 edited (Monoclonal)	HUES7	E8

3.1.6 Chapter aims:

The aim of this chapter is to establish the cardiac differentiation protocols, that are efficient, robust, and reproducible to generate hPSC-CMs. To achieve the goal, the following objectives were established, including:

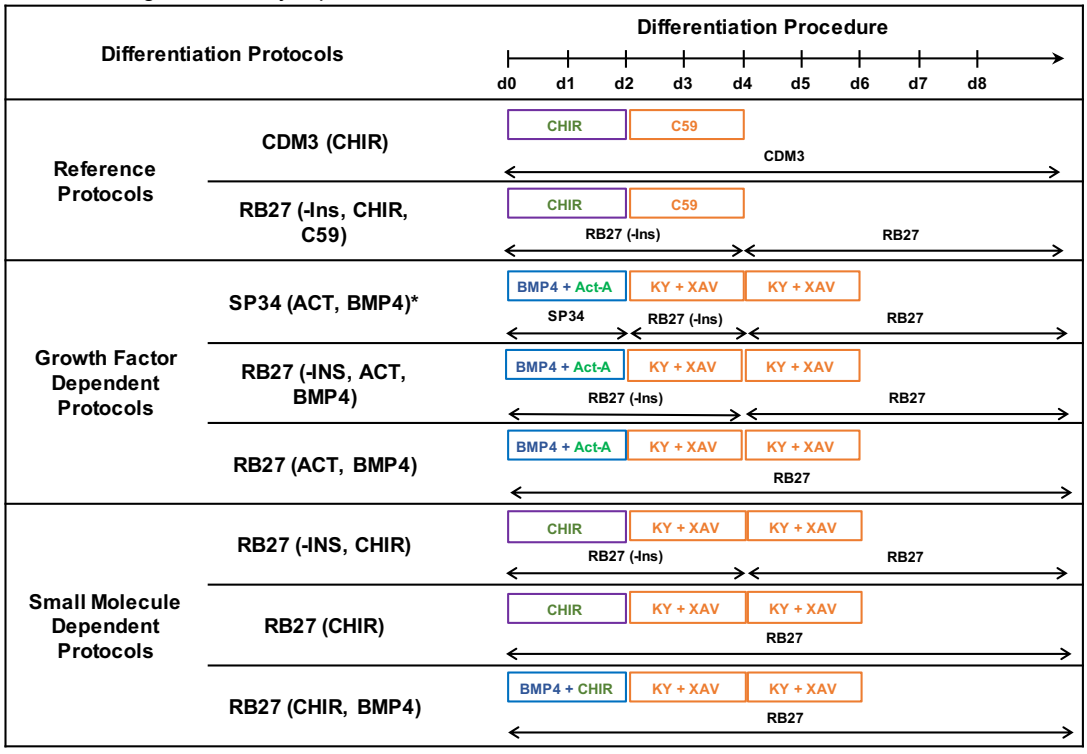
1. Optimising the culture condition in already established mTeSR hPSCs for CM differentiation.
2. Optimising the culture condition for hPSCs transitioned to E8 for CM differentiation potential.
3. Strategizing cardiac induction protocols for maximum efficiency by optimisation of cell seeding density, growth factors/small molecules concentration and using defined media.
4. Characterising differentiated CMs for their structural and functional properties.

3.2 Results

3.2.1 Optimisation of cardiac induction process optimised for mTeSR culture condition

Through empirical optimisation, our laboratory has previously developed a simple monolayer protocol for promoting cardiac induction of the mTeSR-cultured hPSCs, called the SP34 (ACT, BMP4) (Table 3.2). This procedure is based on a 2-days co-stimulation of mesoderm-inducing pathways using BMP4 (10 ng/mL) and Activin-A (Act-A - 8 ng/mL) in the StemPro34 (SP34) basal medium. In the second stage, the WNT signalling is blocked on days 2 – 6 using the small molecule inhibitors XAV939 (XAV) and KY02111 (KY). The insulin was subtracted from the differentiation medium from d2 to d4. The protocol routinely gave rise to monolayers of spontaneously beating CMs on day 7. From this platform, to investigate the effects of growth factors, small molecules, and basal media, four variants were made and classified into the growth factor dependent (GF) and small molecule dependent (SM) protocols (Table 3.2).

Table 3.2: Table summarises the original differentiation protocol (SP34 (ACT, BMP4)) and its variations, which are classified into Growth Factor Dependent and Small Molecule Dependent Protocols. The concentrations of growth factors and small molecules are as followed: Act-A (8 ng/mL), BMP4 (10 ng/mL), CHIR99021 (CHIR – 6 μM), KY02111 (KY – 10 μM), and XAV939 (XAV – 10 μM). * indicates the original monolayer protocol.



To be more specific, retrospectively, we sought to assess the contributions of the three components that are involved in mesodermal induction in more details, including growth factors (BMP4 + Act-A), small molecule (CHIR), and the base medium (SP34, RPMI supplemented with B27 without Insulin (RB27 (-Ins)), and RPMI supplemented with B27 (RB27)). The differentiation samples initiated with BMP4 and Act-A, and with CHIR were collected at d12 for flow cytometry analysis of α-Actinin positive cells. The recently published protocol (CDM3 (CHIR)) and its suggested variant (RB27 (-Ins, CHIR, C59) were used as reference methods to assess their effectiveness and reproducibility in mTeSR-cultured cell lines. Six hPSC lines were employed in the experiment (Table 3.3).

Table 3.3: Details of hPSC lines used in the experiments. hPSCs from passage 20 to 38 were cultured in mTeSR before starting experiment.

CELL LINE	REPROGRAMMING METHOD	CELL SOURCE	CULTURE CONDITIONS
HUES7	Isolated hESCs	Harvard University	mTeSR
AT1	Lentivirus	Human Adult Teeth Fibroblasts	mTeSR
DMD	Lentivirus	Human disease fibroblasts (Duchenne Muscular Dystrophy)	mTeSR
HUES7-Epi	Episomal	HUES7-derived fibroblasts	mTeSR
NCRM5	Episomal	Human Fibroblasts	mTeSR
RJB	Retrovirus	Human disease fibroblasts	mTeSR
REBL-PAT-Len	Lentivirus	Human Fibroblasts	mTeSR

Interestingly, the GF protocols showed consistent and high cardiac differentiation efficiencies compared to that of SM methods and the references across all tested cell lines (Figure 3.4). Indeed, the flow cytometry results indicated that the average differentiation efficiency obtained from GF protocols was approximately 78%, whereas it was 55% and 47% for SM and reference methods, respectively (Figure 3.4). A significant variation between the biological replicates was also observed in the SM protocols and the references. Additionally, the effects of the basal medium in the differentiation process were not apparent as there was no significant difference in purity of CMs between SP34, RB27 (-Ins), and RB27 medium in both GF and SM approaches. The only difference was

observed in DMD line, where RB27 (-Ins) showed a significantly high level of CMs compared to that of SP34 and RB27 in GF procedures (P<0.001, n=3, two-way ANOVA) (Figure 3.4). Moreover, the CDM3 (CHIR) protocol and its modified version exhibited a low efficiency in cardiac induction across all tested cell lines, indicating the inconsistency and low effectiveness of the protocols in mTeSR-cultured hPSCs. Taken together, in this experiment, the extrinsic activation using BMP4 and Act-A showed a consistent result in cardiac induction in all cell lines. The cardiac differentiation initiated by CHIR demonstrated a relatively low efficiency, and dramatic variations between different batches suggesting that the CHIR concentration needed to be optimised to achieve higher efficiency in cardiac induction.

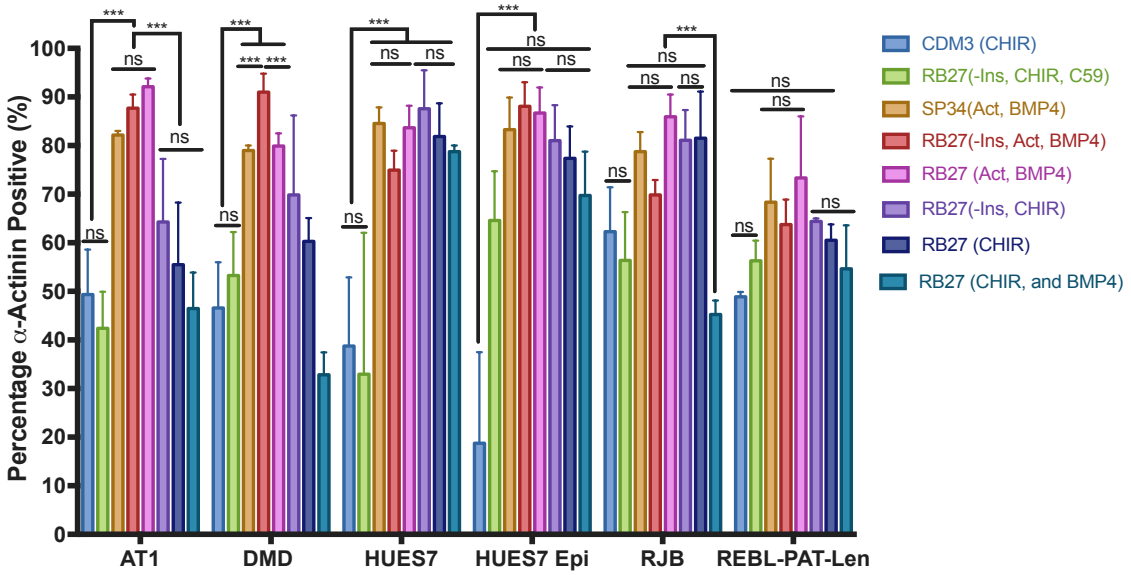


Figure 3.4: Examination the effects of growth factors, small molecules, and basal medium on cardiac differentiation capacity of hPSCs. In this experiment, six hPSC lines, from passage 20 to 38, were cultured in mTeSR. The hPSC cardiac induction protocols were conducted after three passages in mTeSR and could be classified into GF protocols, including SP34 (Act, BMP4), RB27 (-Ins, Act, BMP4) and RB27 (Act, BMP4), and the SM protocols, consisting of RB27 (-Ins, CHIR), RB27 (CHIR), and RB27 (CHIR, BMP4). The recently published protocols, the CDM3 (CHIR) and RB27 (-Ins, CHIR, C59), were used as reference protocol. (P<0.001, n ≥ 3 per sample, two-way ANOVA).

Table 3.4: The results of flow cytometry analysis for α-Actinin from the experiment (n ≥ 3).

Cell Lines	Reference Protocols		Growth Factors Dependent Protocols			Small Molecules Dependent Protocols		
	CDM3 (CHIR)	RB27 (-Ins, CHIR, C59)	SP34 (Act, BMP4)	RB27 (-Ins, Act, BMP4)	RB27 (Act, BMP4)	RB27 (-Ins, CHIR)	RB27 (CHIR)	RB27 (CHIR, BMP4)
AT1	49 ± 9	42 ± 8	82 ± 1	88 ± 3	92 ± 2	64 ± 13	56 ± 13	46 ± 7
DMD	47 ± 9	53 ± 9	79 ± 1	91 ± 4	80 ± 3	70 ± 16	60 ± 5	33 ± 5
HUES7	39 ± 14	33 ± 29	85 ± 3	75 ± 4	84 ± 5	88 ± 8	82 ± 7	79 ± 1
HUES7-Epi	19 ± 19	65 ± 10	83 ± 7	88 ± 5	87 ± 5	81 ± 7	77 ± 7	70 ± 9
RJB	62 ± 9	56 ± 10	79 ± 4	70 ± 3	86 ± 5	81 ± 6	82 ± 10	45 ± 3
REBL-PAT-Len	49 ± 1	56 ± 4	68 ± 9	64 ± 5	73 ± 13	64 ± 1	61 ± 3	55 ± 9

3.2.2 Problems with mTeSR culture conditions

Although the section above showed that hPSC differentiation could be achieved at high efficiency across multiple cell lines, the batch to batch variability of mTeSR impacted on cell viability and proliferation rates, hence the robustness of cardiomyocyte production. During this thesis, an alternative medium, E8, became routinely available. Whilst being cheaper than mTeSR, the simplified composition of E8 potentially meant less variation between batches. Therefore, the process to produce CMs from hiPSC moved from mTeSR to E8.

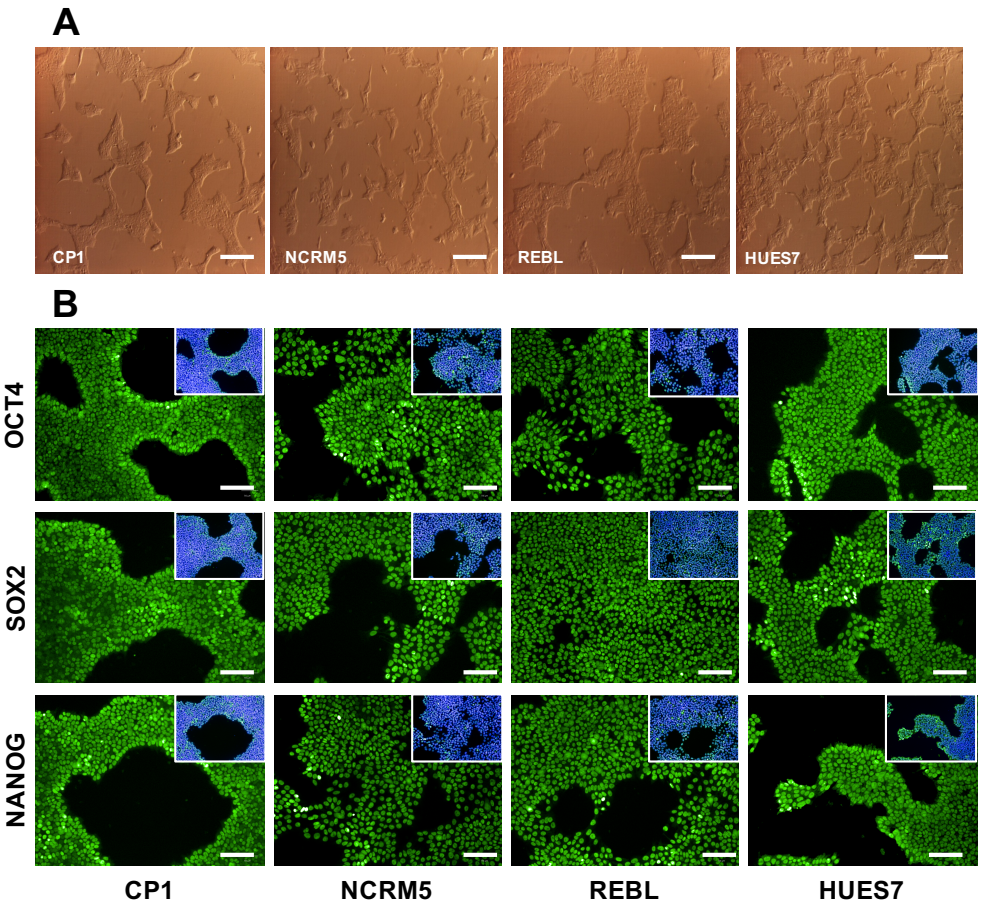
3.2.3 Standardisation of the defined culture conditions of hPSCs

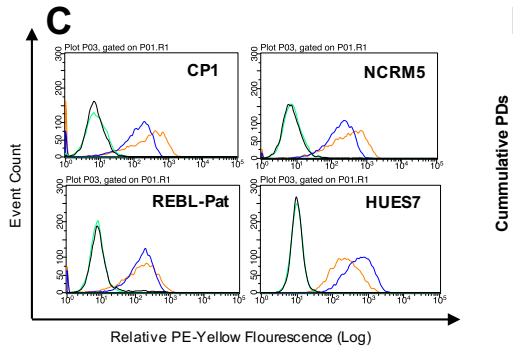
The list of 27 hPSC lines in Table 3.1 was specifically selected because of the diversity of culture condition used, varying with respect to medium (MEF-CM, mTeSR, and E8) and dissociation method (trypsin, Accutase, TrypLE, and EDTA). To provide a unified starting position for CM differentiation, there was a need to standardise the culture conditions. A method was adopted based on transitioning to E8 with passaging using a cell dissociation solution (CDS) method, containing 40% RPMI, 40% Cell dissociation buffer, and 20% trypsin or TrypLE Select. The CDS was formulated based on the combination of enzyme (TrypLE) and EDTA to achieve the same dissociation effectiveness and gentler to the cells. Furthermore, CDS was also be used to dissociated not only hPSCs but also differentiated CMs, providing as a universal dissociation method.

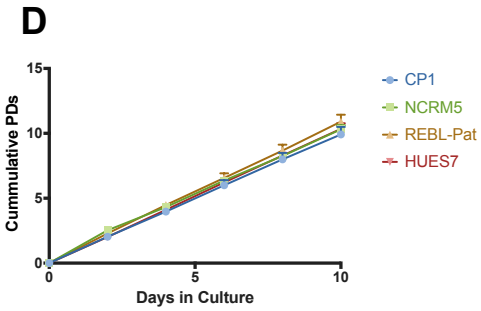
To implement this approach, four representative cell lines were selected. HUES7 was traditionally cultured in MEF-CM, NCRM5 in mTeSR, and both CP1 and REBL-PAT-Sen in E8. Each was transitioned to E8 and passaged using CDS for at least three passages. After this time, pluripotency characterisation was performed using immunocytochemistry to identify the expression of nuclear pluripotency markers (OCT4, SOX2, and NANOG), flow cytometry to detect the presence of surface pluripotency markers (SSEA-4 and TRA-1-81), growth curve, and karyotype (after 10 passages).

The results showed that all four cell lines maintained typical morphologies of pluripotency stem cells, including forming a defined border, prominent nucleus, and the high nucleus-to-cytoplasm ratio (Figure 3.5A). After six passages cultured in the E8 medium, CP1, HUES7, NCRM5, and REBL-PAT-Sen stained positive for the nuclear pluripotency markers, including OCT4, SOX2, and NANOG (Figure 3.5B). Furthermore, the flow cytometry in the lines showed the high level of SSEA-4 (between 88% to 95%) and TRA-1-81 (between 82% to 98%) presence on the surface of all tested cells and negative for SSEA-1 (<5%) – an early differentiation marker (Figure 3.5C). The proliferation rates of CP1, HUES7, NCRM5, and REBL-PAT-Sen, in terms of population doubling times, generated from growth curves were 24 ± 0.6 h, 23.1 ± 2.3 h, 23.74 ± 2.6 h, and 22.2 ± 1.6 h, respectively (mean ± SEM, n=3) (Figure 3.5D). These cells also maintained normal karyotypes after ten passages cultured in the E8 medium (Figure 3.5E). The results confirmed the established pluripotency in these culture conditions.

To evaluate the effects of CDS on the viability of hPSCs after dissociation, the CP1, HUES7, NCRM5, and REBL-PAT-Sen were subjected to viability counting using Cedex Automated cell counter. The Cedex counts the dissociated cells, after staining them with Trypan-Blue, based on the image of stained cells after sedimentation process in the counting chamber (Figure 3.6A). The viability of CDS-dissociated hPSCs was over 98% across all tested cell lines, with the aggregation rates of CP1, HUES7, NCRM5, and REBL-PAT-Sen were 21% ± 5%, 17.5% ± 2%, 26% ± 2%, and 31% ± 11%, respectively (mean ± SEM, n=3) (Figure 3.6B). Additional analysis of the aggregate size demonstrated the homogenous dissociation, suggesting that CDS effectively dissociated the cells into single cells with high viability rate (Figure 3.6C). In terms of the cell size, it is important to note that there is no significant difference between all tested cell lines, which was 14.3 ± 0.16 μm, 14.4 ± 0.22 μm, 14.3 ± 0.2 μm, and 14.5 ± 0.15 μm for CP1, HUES7, NCRM5, and REBL-PAT-Sen, respectively (all mean ± SEM, n>3, two-way ANOVA). Taken together, these data suggested the robustness in passage method under serum-free E8 conditions irrespective of their adaptation methods for each lines.







	CP1	NCRM5	REBL-Pat	HUES7
SSEA1	5% ± 0.1%	5% ± 0.4%	5% ± 0.5%	5% ± 0.8%
SSEA4	88.6% ± 2%	95%± 2.2%	91%± 3%	95%± 2.2%
TRA-1-81	82% ± 1.2%	94%± 1.6%	86% ± 2.3%	98% ± 1.4%

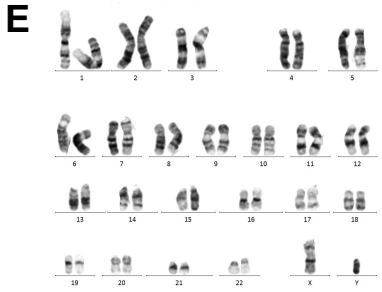


Figure 3.5: Pluripotency characterisation of CP1, NCRM5, HUES7, and REBL-PAT-Sen cultured in E8 condition and passaged using CDS method. (A) Bright field images illustrate the morphology of all four tested cell lines 24h after dissociation using CDS. **(B)** Immunocytochemistry images of OCT4, SOX2, and NANOG (green) illustrates the expression of these nuclear markers in tested lines. Small inserts showed the localisation of the markers and DAPI (Blue). **(C)** The flow cytometry histograms of surface pluripotency markers, including SSEA-4 (Blue line) and TRA-1-81 (Orange line) in CP1, HUES7, NCRM5, and REBL-Pat-Sen. The table showed the expression level of these markers (mean ± SEM, n=3). **(D)** Linear growth curves showing proliferation rates of all tested cell lines in E8 culture conditions. **(E)** Representative karyogram of HUES7 after 10 passages cultured in E8 and dissociated using CDS method.

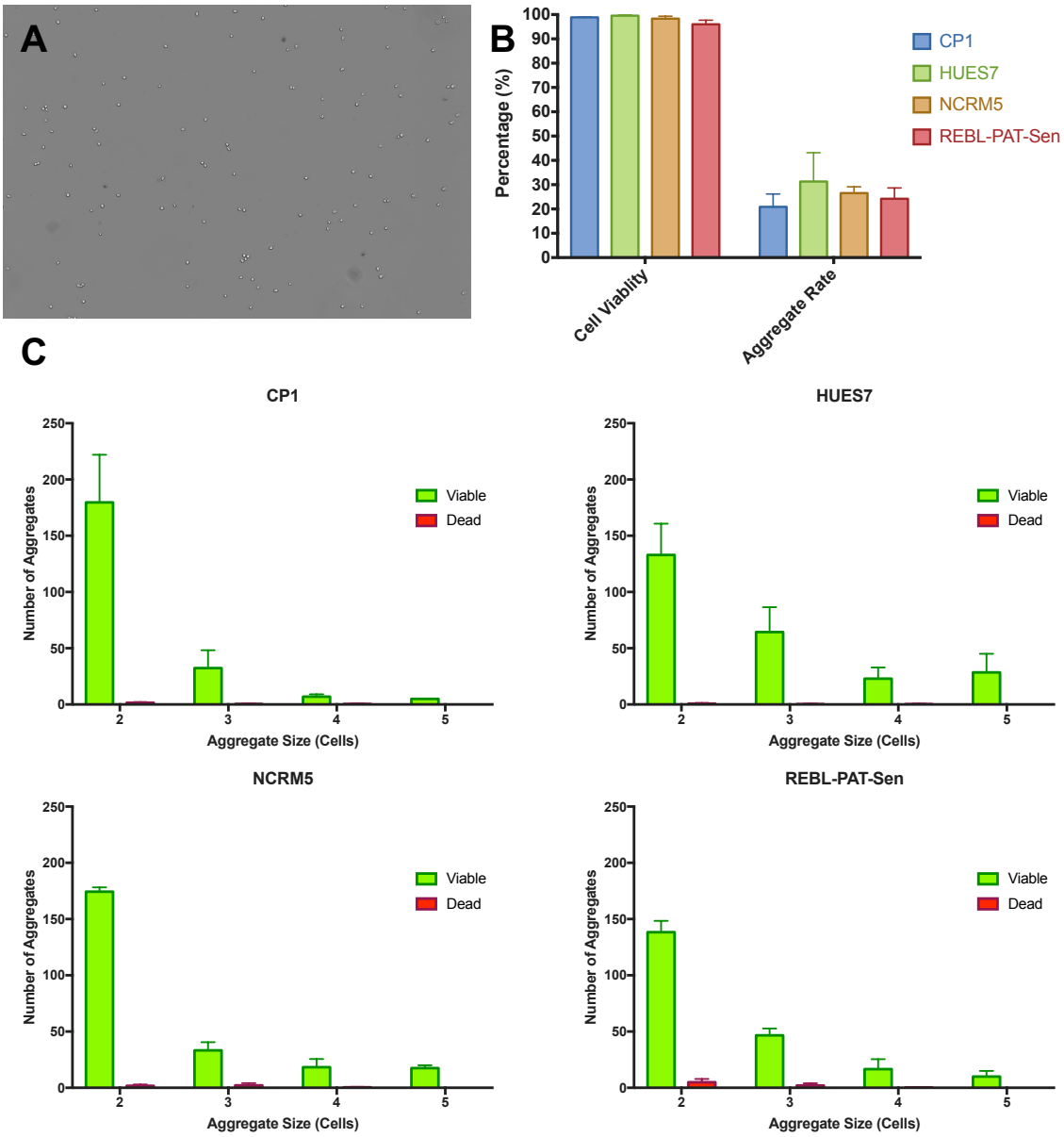


Figure 3.6: Assess the viability of hPSCs after CDS dissociation using Cedex Automated cell counter. **(A)** The representative image obtained from Cedex, which was processed and used to count the viable cells after Trypan-Blue staining. **(B)** The bar graph illustrates the cell viability and aggregation rate of CP1, HUES7, NCRM5, and REBL-PAT-Sen. **(C)** The analysis of aggregate size indicated the majority of the aggregate were 2 cells, indicating the efficiency of CDS in generating single cells.

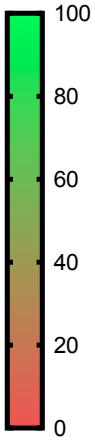
3.2.4 Cardiac induction process in E8-cultured hPSCs

The success of E8 culture condition encouraged us to initiate the cardiac differentiation process of E8-maintaining hPSCs. Six hPSC lines which had been used in the previous experiment in section 3.2.1, including AT1, CP1, DMD, HUES7, HUES7-Epi, and RJB, were cultured in E8 condition for at least five passages before starting cardiac induction process using the GF and SM protocols as described in Section 3.2.1.

However, the significant cell loss occurred during d0 to d2 of differentiation process resulted in the difficulty in collecting cells for Flow cytometry analysis. Hence, in order to assess the cardiac differentiation potential of hPSCs, the scoring system as shown in Table 3.5 was used.

The results indicated dramatic reduction in cardiac differentiation efficiency across all tested cell lines regardless of either GF, SM, or reference procedures. Successful differentiation with a low yield of CMs was obtained in HUES7 under SP34 (Act, BMP4) and RB27 (-Ins, CHIR) conditions. The latter also showed efficient induction of cardiac formation in CP1, although the number of CMs after differentiation was relatively low due to cell death between d0 to d2 of the process (Figure 3.7). The CDM3 (CHIR) condition did not work in all tested cell lines, and AT1 cells did not show any signs of beating in all tested condition (Figure 3.7). Taken together, it was indicated that the cardiac induction process of E8-cultured hPSCs was reduced because of significant cell loss between d0 to d2. Therefore, the subsequent optimisation focused on the mesodermal initiation step of the differentiation protocols to reduce the cell loss.

Table 3.5: Scoring system based on the estimated percentage of beating areas in a well of 24-well plates after d12 post cardiac differentiation process.

Score	Explanation	Colour coded
5	From 80% to 100% of culture area showed synchronously beating	
4	From 60% to 80% of culture area showed beating or beating clusters	
3	From 40% to 60% of culture area showed beating clusters.	
2	From 20% to 40% of culture area showed beating, preferably as clumps.	
1	Less than 20% of culture area showed beating.	
0	Not working.	

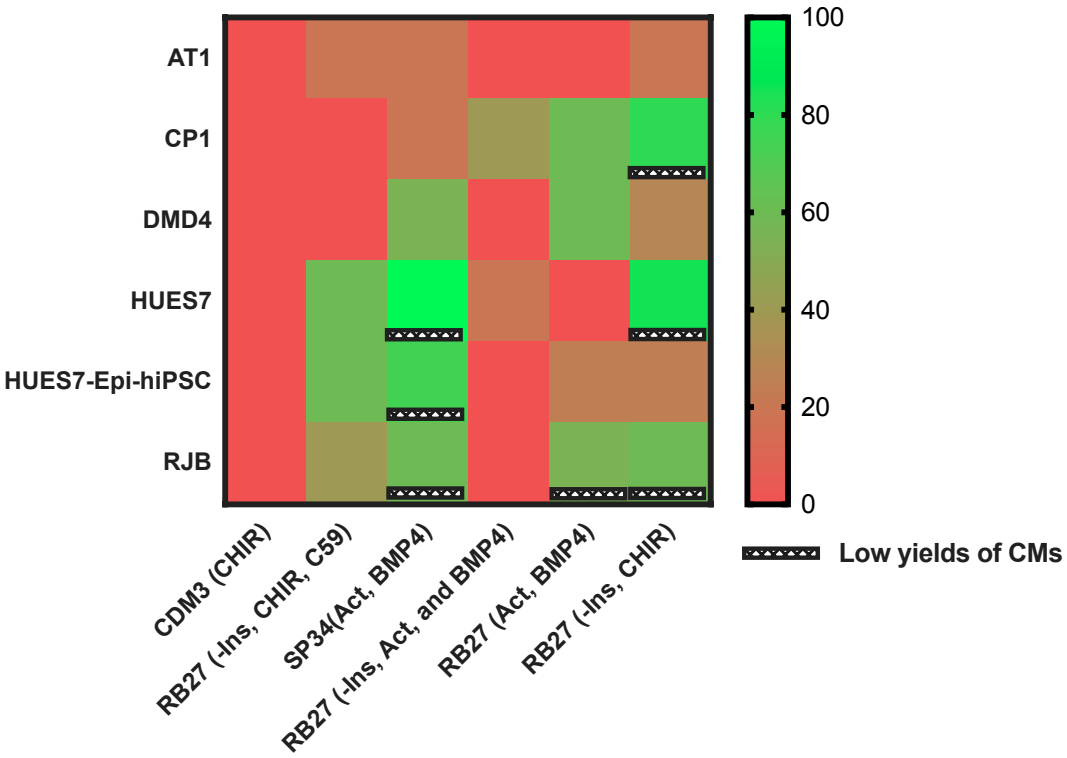


Figure 3.7: The results in colour-coded grid indicates the variation of cardiac differentiation efficiency of the E8 cultured hPSCs across all tested conditions. Significant cell loss observed during d0 to d2 after initiation of differentiation procedures resulted in the dramatic reduction in cardiac differentiation efficiency in all tested cell lines regardless of cardiac differentiation protocols (n=3).

3.2.5 Addition of precondition-step enhanced the cardiac differentiation in SP34 (Act, BMP4) protocol

Due to a significant cell loss during differentiation process of E8-cultured hPSCs especially between d0 to d2 post-differentiation, it was hypothesised that the culture condition needed to be enriched before starting differentiation process. Therefore, adapted from previously described protocol, an additional step, called precondition, was added to the original SP34 (Act, BMP4) protocol (Zhang et al., 2012). Nine randomly picked hPSC lines cultured in E8 medium were first seeded at different cell seeding density ranging from 40.000 cells/cm^2 to 90.000 cells/cm^2. These cells were cultured in the E8 medium for 48 h followed by the preconditioning step using SP34 supplemented with Matrigel (1:100 dilution) and BMP4 (1 ng/mL) for 24h. After precondition, the SP34

(Act, BMP4) method was used to induce cardiac induction process. The details of hPSCs employed in the experiment were shown in Table 3.6.

Table 3.6: hPSC lines used to test the effects of precondition step on cardiac differentiation using SP34 (Act, BMP4) method.

CHARACTERISATION	CELL LINE	ORIGINAL CULTURE	REPROGRAMMING METHOD	CELL SOURCE
HUMAN EMBRYONIC STEM CELLS	HUES7	MEF-CM	Isolated	Harvard University
HUMAN INDUCED PLURIPOTENT STEM CELLS	AT1	MEF-CM	Lentivirus	Human Adult Teeth Fibroblasts
	ATcamWT	MEF-CM	Retrovirus	Human Fibroblasts
	CP1	E8	Sendai Virus	Human disease Fibroblasts
	DMD4	mTeSR	Lentivirus	Human disease fibroblasts
	Hues7-Epi-hiPSC	mTeSR	Episomal	HUES7-derived fibroblasts
	NCRM5	mTeSR	Episomal	Human Fibroblasts
	REBL-PAT	MEF-CM	Lentivirus	Human Fibroblasts
	REBL-PAT-Sen	mTeSR	Sendai Virus	Human Fibroblasts
	RJB	MEF-CM	Retrovirus	Human disease fibroblasts

Interestingly, a dramatic morphology change was observed after 24h precondition, especially at 40.000 cells/cm^2. The culture converted from the stem cell morphology into a distinct perforated sheet of cells resembling the “Swiss cheese-like” morphology (i.e. monolayers with holes in between), possibly demonstrating the epithelial-to-mesenchymal transition (Figure 3.8A). Indeed, no cell death occurred during the differentiation process in all tested hPSC lines, suggesting that the preconditioning step enhances the viability of the E8-cultured cells. Furthermore, significant improvement in cardiac differentiation efficiency was also observed. All tested hPSC lines showed the synchronously beating monolayer on d7 post differentiation at either low cell seeding density (40.000 cells/cm^2 and 50.000 cells/cm^2), whereas high seeding density (80.000 cells/cm^2 and 90.000 cells/cm^2) worked effectively in the case of CP1, DMD4, HUES7-Epi-hiPSC (Figure 3.8B). Taken together, in this experiment, the preconditioning step was proven to be efficient in reducing the cell loss and improve the cardiac differentiation process in all tested conditions. Therefore, we focused our further attention on the

preconditioning step and apply it to other cardiac induction methods. The SP34 (Act, BMP4) protocol in combination with precondition step is now called E8-AB method.

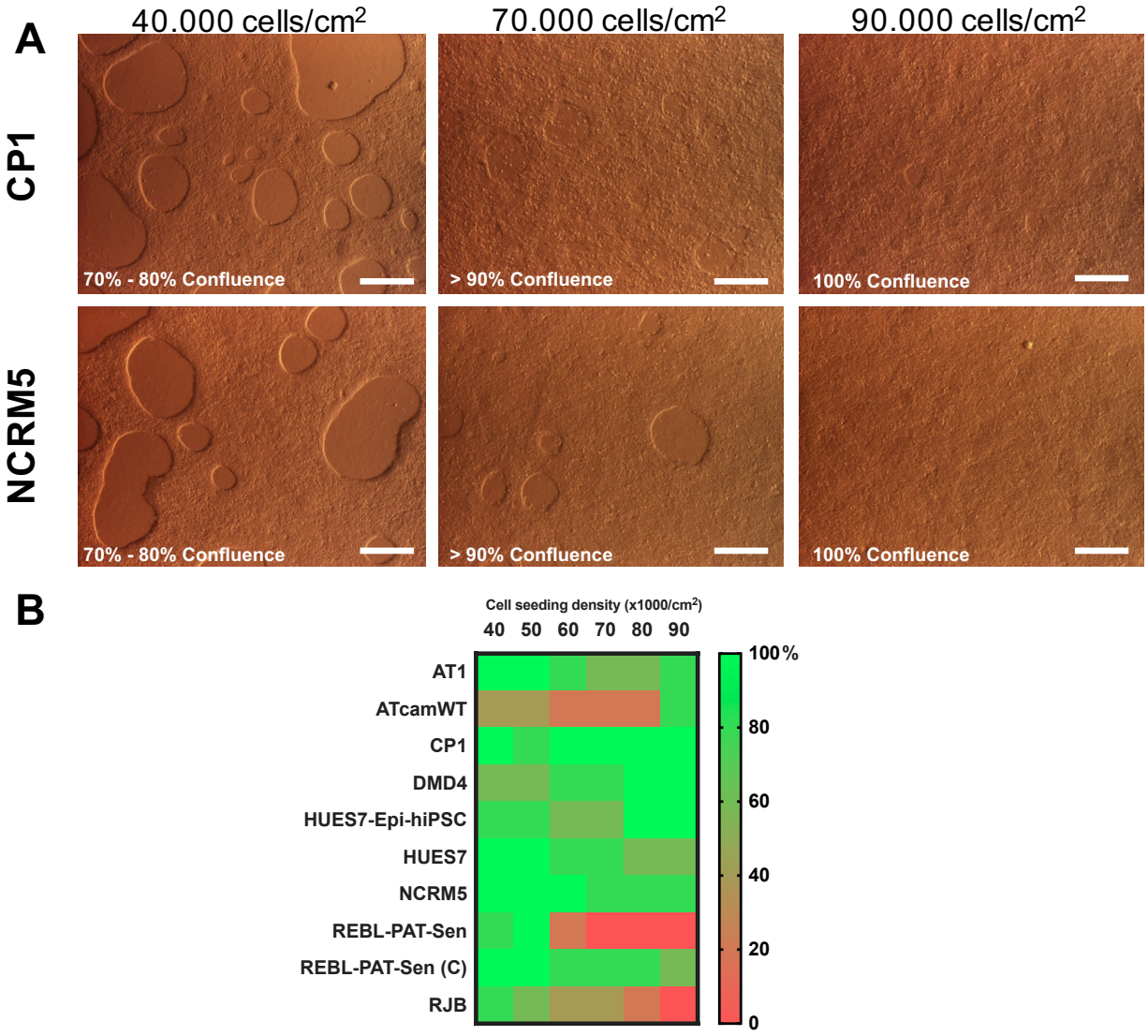


Figure 3.8: Improvement of cardiac induction process using preconditioning step. (A) Representative images illustrate the signature morphological change of E8-culture CP1 and NCRM5 cells at 40.000 cells/cm^2, 70.000 cells/cm^2, and 90.000 cells/cm^2 after 24 h incubation with SP34 supplemented with Matrigel (1:100 dilution) and BMP4 (1 ng/mL). **(B)** The results in colour-coded grid indicate the effectiveness of SP34 (Act, BMP4) in combination with preconditioning step using scoring system (n=3). *Scale bar*: 100 μM.

3.2.6 Optimisation of CHIR99021 concentration and the establishment of mTeSR(CHIR) protocol

The low efficiency and inconsistency of the protocols initiated by CHIR as shown in section 3.2.1 suggested that the CHIR concentration needed to be optimised to improve its effectiveness in the cardiac induction process. Hence, four different concentrations of CHIR were applied to assess the working range of the compound, including 4 μM, 6 μM, 8 μM, and 10 μM. The replacement of Act-A and BMP4 by CHIR in SP34 (Act, BMP4) in combination with the preconditioning step created the new method, namely SP34(CHIR) condition. Low CHIR concentrations at 4 μM and 6 μM were capable of inducing the cardiac differentiation in AT1, CP1, and HUES7, whereas 6 μM of CHIR produced beating clusters in ATcamWT, NCRM5, and REBL-PAT-Sen (C) (Figure 3.9A). High level of CHIR (8 μM and 10 μM) did not induce the cardiac differentiation process in tested hPSC lines, except HUES7-Epi-hiPSC and RJB, which showed few beating clusters (Figure 3.9A). In summary, these results indicated that CHIR effectiveness was cell line-dependence and the lower doses of CHIR (between 4 μM and 6 μM worked broadly across the majority of tested line.

Because the preconditioning step contains Matrigel, which is an undefined component, and with an aim to improve the consistency of the protocols, mTeSR was used to replace SP34 to precondition the culture before starting the differentiation process, using CHIR at 4 μM and 6 μM. The tested lines were AT1, ATcamWT, CP1, NCRM5, REBL-PAT-Sen, and REBL-PAT-Sen (C). The samples at d12 post differentiation were collected for flow cytometry analysis for cardiac Troponin-T (cTNT). The results confirmed that the protocol worked effectively, with the average differentiation efficiency of over 80%, except for REBL-PAT-Sen (Figure 3.9B). There was no significant difference between 4 μM and 6 μM CHIR in the cardiac induction process. Hence, the average concentration of CHIR, which was 5 μM, was chosen and the new protocol with mTeSR precondition step and CHIR at 5 μM adapted for E8 culture was established, hereinafter called the mTeSR-CHIR protocol.

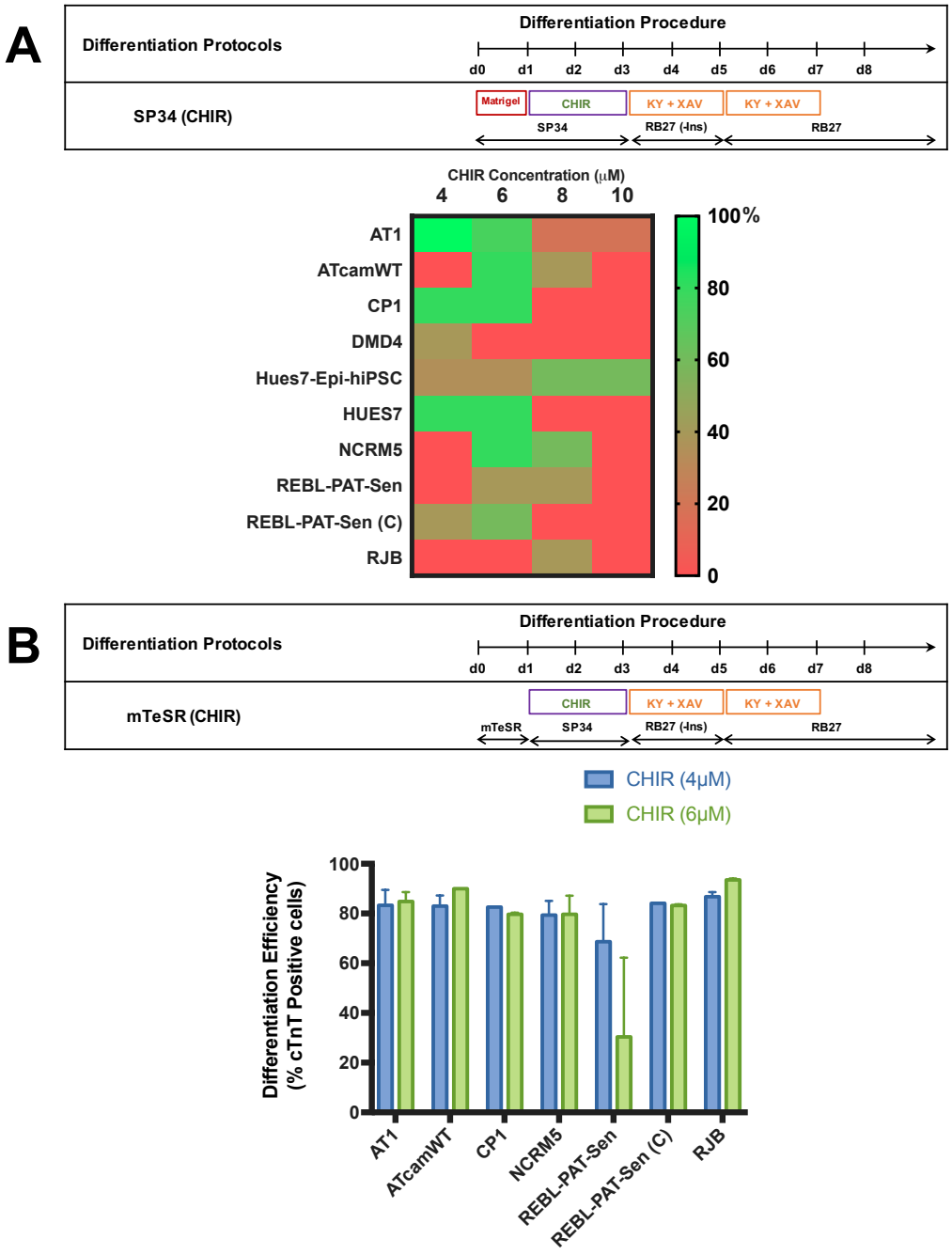


Figure 3.9: Optimisation of CHIR concentrations. (A) The cardiac induction efficiency of different CHIR concentrations in replacement of Act-A and BMP4 in SP34 (Act, BMP4) protocol in combination with precondition step using SP34 supplemented with Matrigel (1:100 dilution) and BMP4 (1 ng/mL) to establish the new protocol namely SP34(CHIR). The colour-coded grid illustrates that CHIR at 4 μM and 6 μM induced efficiently the cardiac differentiation process (n=3). **(B)** The top panel shows the mTeSR (CHIR) protocol. The bar chart demonstrates the flow cytometry analysis of cTNT positive cells obtained from d12 differentiated cells using mTeSR (CHIR) protocol at two CHIR concentration (4 μM and 6 μM). Of note, the concentration of KY and XAV was kept at 10 μM (n=3).

3.2.7 Establishment of cardiac differentiation protocols adapted for E8-cultured hPSCs

Developing the E8-AB and mTeSR-CHIR protocols suggested that an enrichment for cells in E8 defined media would be inductive to the differentiation processes. We therefore further evaluated a third protocol in which mTeSR replaced the preconditioning step (enrichment) before d0 differentiation (i.e. at day -1) of the E8-AB protocol, hereinafter the mTeSR-AB procedure. The details of these methods are summarised in Figure 3.10A. The representative pictures illustrate the morphological changes of the E8 cultured hPSCs during cardiac differentiation process are shown in Figure 3.10B. To reduce the scale of the experiment, the most commonly used hPSC lines in our laboratory were chosen for determination of cardiac differentiation efficiency of three newly established protocols, including AT1, CP1, NCRM5, HUES7, and REBL-PAT-Sen. The CDM3 (CHIR) protocol was used as the reference protocol for comparative purposes. The cell samples at d12 post cardiac differentiation were collected for both flow cytometry analysis for cTNT positive cells and immunocytochemistry analysis for cTNT and α-ACTININ positive cells.

We observed the differentiation efficiency ranging between 75% to 93% for all lines tested, as assessed by flow cytometry for cTNT (Figure 3.11A). Yields of greater than $2x10^5$ CMs/cm^2 was also obtained, and these CMs could be kept *in vitro* for over ten months. Additionally, the immunocytochemistry showed that over 90% of CMs had been achieved from E8-AB and mTeSR-AB, whereas the mTeSR-CHIR showed a significant reduction in CM purity after plating into new culture vessels (Figure 3.11B). The CDM3 (CHIR) protocol illustrated a variation in cardiac differentiation efficiency between batches across all tested cell lines, while the three protocols exhibited a consistency and robustness between different biological replicates.

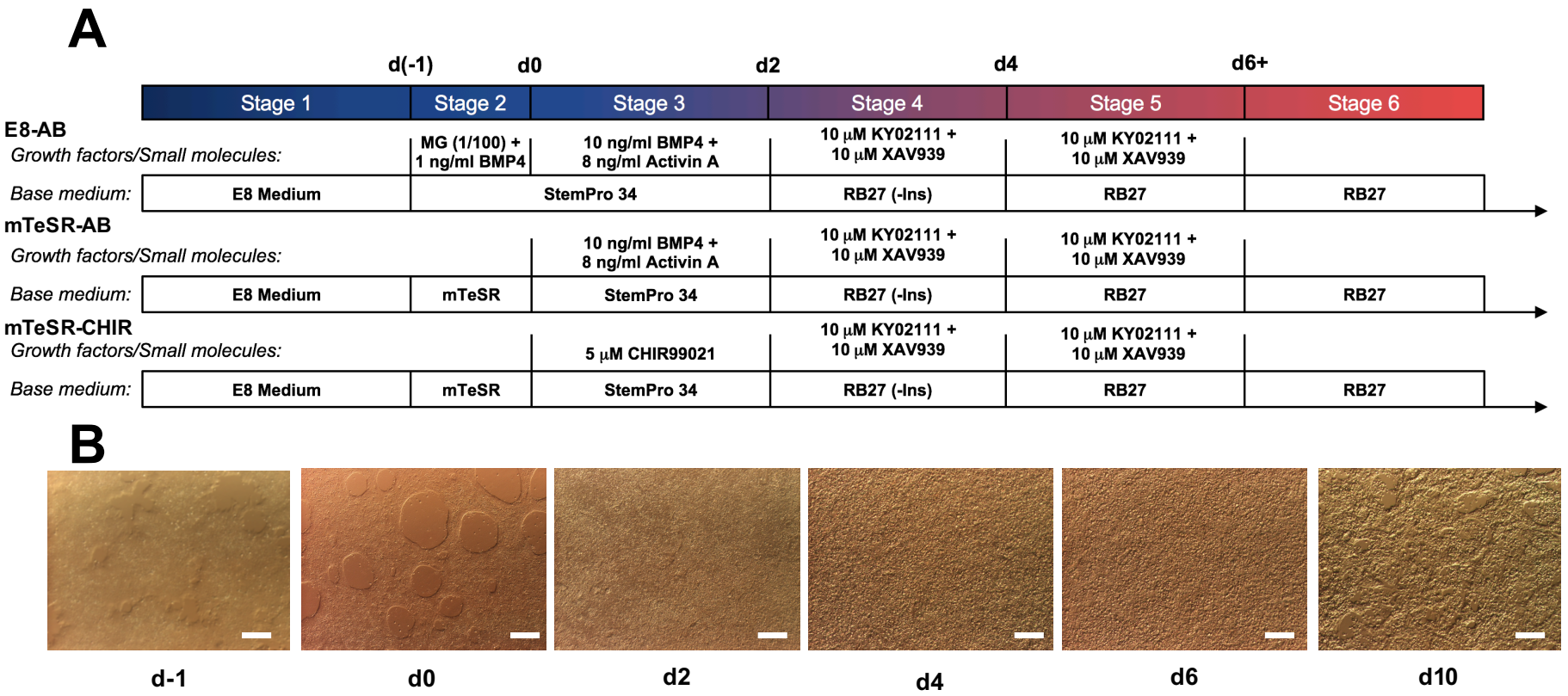


Figure 3.10: Establishment of three independent cardiac differentiation protocols, including E8-AB, mTeSR-AB, and mTeSR-CHIR. (A) The schematic depicts the procedures of the cardiac protocols including components and concentration of growth factors and small molecules driven the cardiac differentiation of E8-cultured hPSCs. **(B)** Representative pictures illustrate the morphological changes of hPSCs underwent cardiac differentiation procedure using E8-AB method. *Scale bar*: 100 μM.

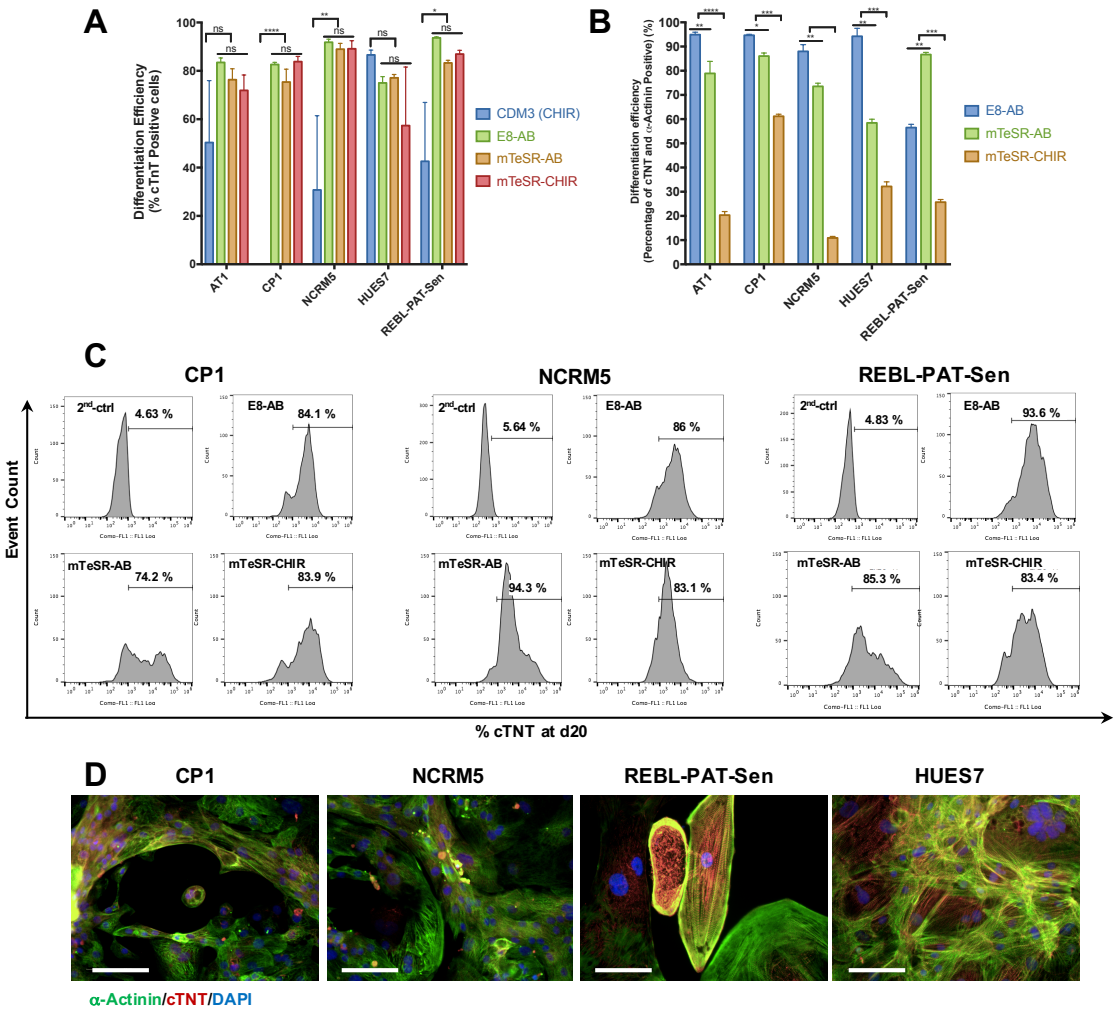


Figure 3.11: Purification of CMs generated by E8-AB, mTeSR-AB, and mTeSR-CHIR methods. (A) Percentage of cTNT$^+$ cells measured by flow cytometry on day 12 of differentiation. **(B)** Percentage of dual cTNT$^+$ and α-ACTININ$^+$ cells measured by immunocytochemistry of CMs on day 20 of differentiation. All hPSCs were cultured in E8 medium at least 5 passages before starting differentiation process, n = 3 independent biological replicates. Error bars, s.e.m. **(C)** Representative flow cytometry analysis of CMs obtained from CP1, NCRM5, and REBL-PAT-Sen underwent E8-AB, mTeSR-AB, and mTeSR-CHIR protocol. **(D)** Representative immunocytochemistry images of dual staining with cTNT and α-ACTININ antibody. *Scale bar:* 50 μm.

Overall, the results of this section indicated that the extrinsic activation of cardiac differentiation via growth factors or small molecules together with precondition step were efficient enough to induce the cardiac differentiation process of E8 cultured hPSCs. Furthermore, although the E8-AB, mTeSR-AB, and mTeSR-CHIR showed a relatively high level of CMs purity, the plating efficiency of the mTeSR-CHIR was lower compared to the other protocols, suggesting the requirement of subsequent purification.

3.2.8 Investigation of protein kinetic expression during cardiac differentiation process

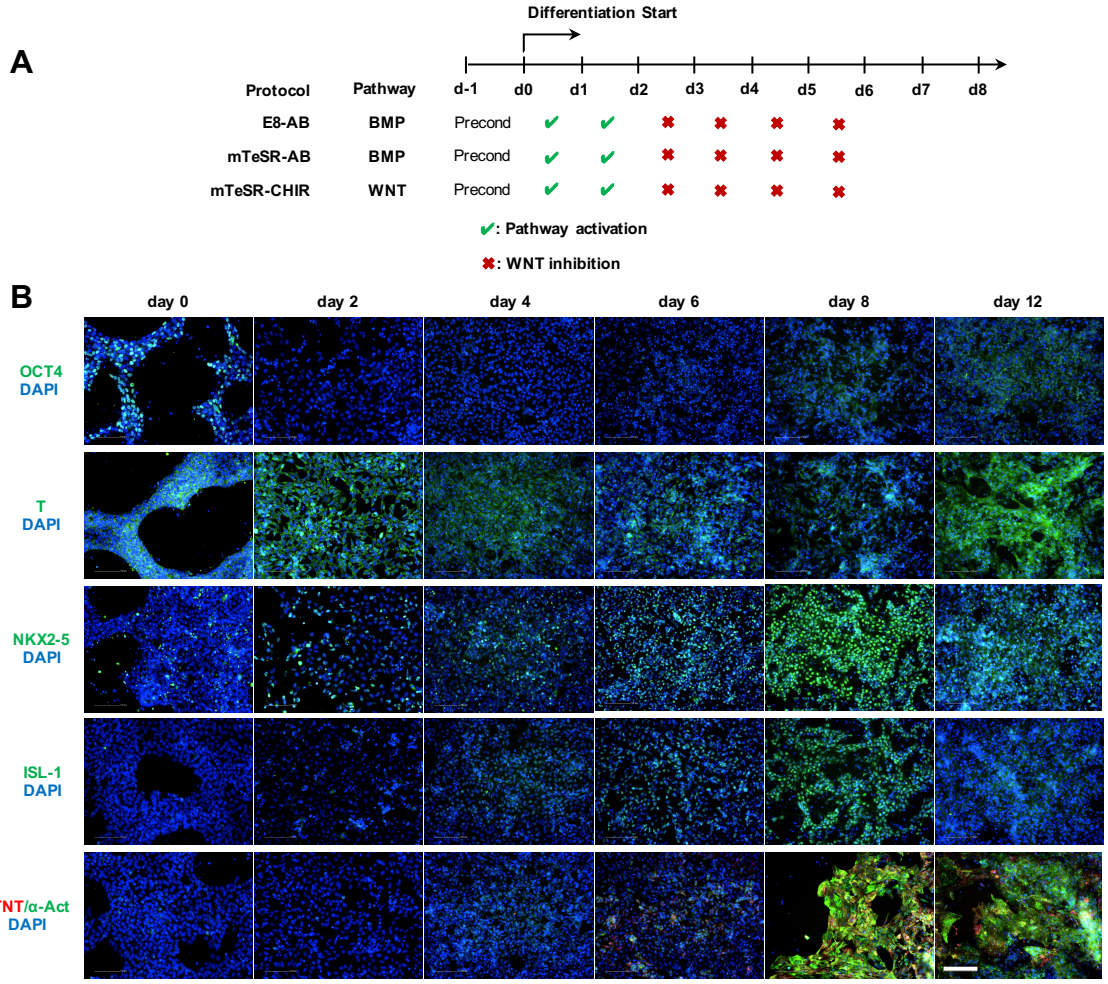


Figure 3.12: Protein expression profiles during cardiac induction process. (A) Illustration of hPSC induction protocols. Pathways are stimulated by growth factors (BMP4, Act-A) or small molecule (CHIR) and inhibited by KY and XAV as indicated. The stimulation of BMP signalling pathway is triggered by growth factors, whereas WNT pathway is induced by using CHIR99021(CHIR). **(B)** Representative time course immunofluorescence analysis of stage-specific markers during cardiac differentiation induced by E8-AB method in NCRM5 cell line. *Scale bar:* 100 μm.

The establishment of the growth factor dependent (E8-AB, and mTeSR-AB) and small molecule dependent (mTeSR-CHIR) protocols described in section 3.2.7 provided an opportunity to gain an insight into the cardiac induction process mediated by either BMP or WNT pathway using immunocytochemistry to detect the expression of stage-specific markers (Figure 3.12). In general, the preconditioning step followed by the mesoderm induction by either Act-A and BMP4 or CHIR resulted in the exit from pluripotency stage and expression of Brachyury-T by days 1-2. The appearance of putative cardiac precursor cell identity (NKX2-5 and ISL-1) was detected by days 4-8, and from d6 onward, induction of an early CM marker (cTNT and α-ACTININ) was

observed (Figure 3.12B). Of note, the expression of Brachyury-T was found specifically in the nucleus of the cells from d0 to d6, while from d8 onward, non-specific binding of the antibody was found in the cytoplasm of the cells, suggesting that the detectable window of Brachyury-T during cardiac differentiation process using the particular antibody was from d0 to d6.

Subsequently, we investigated the contribution of the two signalling pathways in more details in three cell lines, including CP1, NCRM5, and REBL-PAT-Sen (Figure 3.13). Differentiation time course samples initiated with E8-AB, mTeSR-AB, and mTeSR-CHIR were fixed at different time points as shown in Figure 3.12B. Immunofluorescence analysis revealed that precondition using either SP34 or mTeSR significantly reduced the expression of OCT4 on d0 followed by complete suppression from d2 onward (Figure 3.13A). Interestingly, the BMP activation on d0 lead to a strong increase in Brachury-T level, which reached a peak on d4. Indeed, the activation of Brachyury-T resulted in the inductive expression of cardiac progenitor markers (NKX2-5 and ISL-1), which was at higher level in E8-AB and mTeSR-AB compared to that of mTeSR-CHIR protocol (Figure 3.13 C-D). Significant low level and variations of NKX2.5 level was observed in mTeSR-CHIR protocol between d4 to d6, suggesting that CHIR-induced samples virtually fluctuated in cardiac differentiation process. Analysis for cTNT and α-ACTININ further confirmed the effectiveness of E8-AB and mTeSR-AB protocols in the generation of high purity CMs compared to that of mTeSR-CHIR conditions.

Taken together, the experiment illustrated that extrinsic activation of BMP and WNT signalling pathways induced different protein expression patterns which played essential roles in cardiac induction process of hPSCs. Furthermore, the growth factor dependent protocols resulted in higher induction of Brachyury-T followed by the expression of NKX2-5 and ISL-1 compared to that of CHIR-mediated protocol. Figure 3.14 represented the comparative immunofluorescence images of three protocols in NCRM5 captured by the confocal microscope.

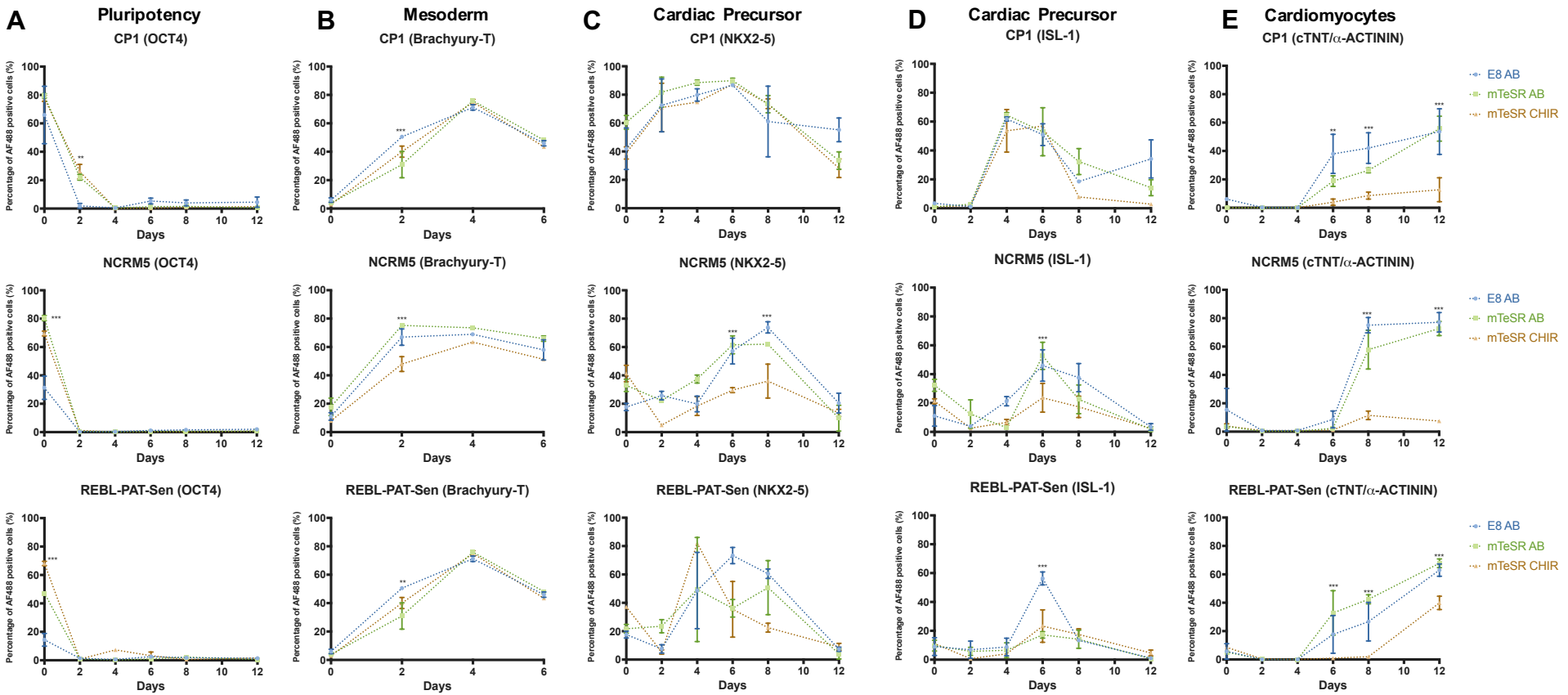


Figure 3.13: Quantitative analysis of immunofluorescence images using Harmony High-content imaging and analysis software during time course analysis of stage-specific markers during cardiac induction process inducing by E8-AB, mTeSR-AB, and mTeSR-CHIR protocol. Three hPSC lines, including CP1(top), NCRM5 (middle), and REBL-PAT-Sen (bottom), were used to test the cardiac induction by three established protocols for immunofluorescence analysis of **(A)** pluripotency marker (OCT5), **(B)** Mesodermal marker (Brachyury-T), **(C-D)** Cardiac Precursor markers (NKX2-5 and ISL-1), and **(E)** cardiomyocyte early marker (cTNT and α-Actinin). (** P<0.01, ***P<0.001, n=3, two-way ANOVA, Error bar: s.e.m.)**.**

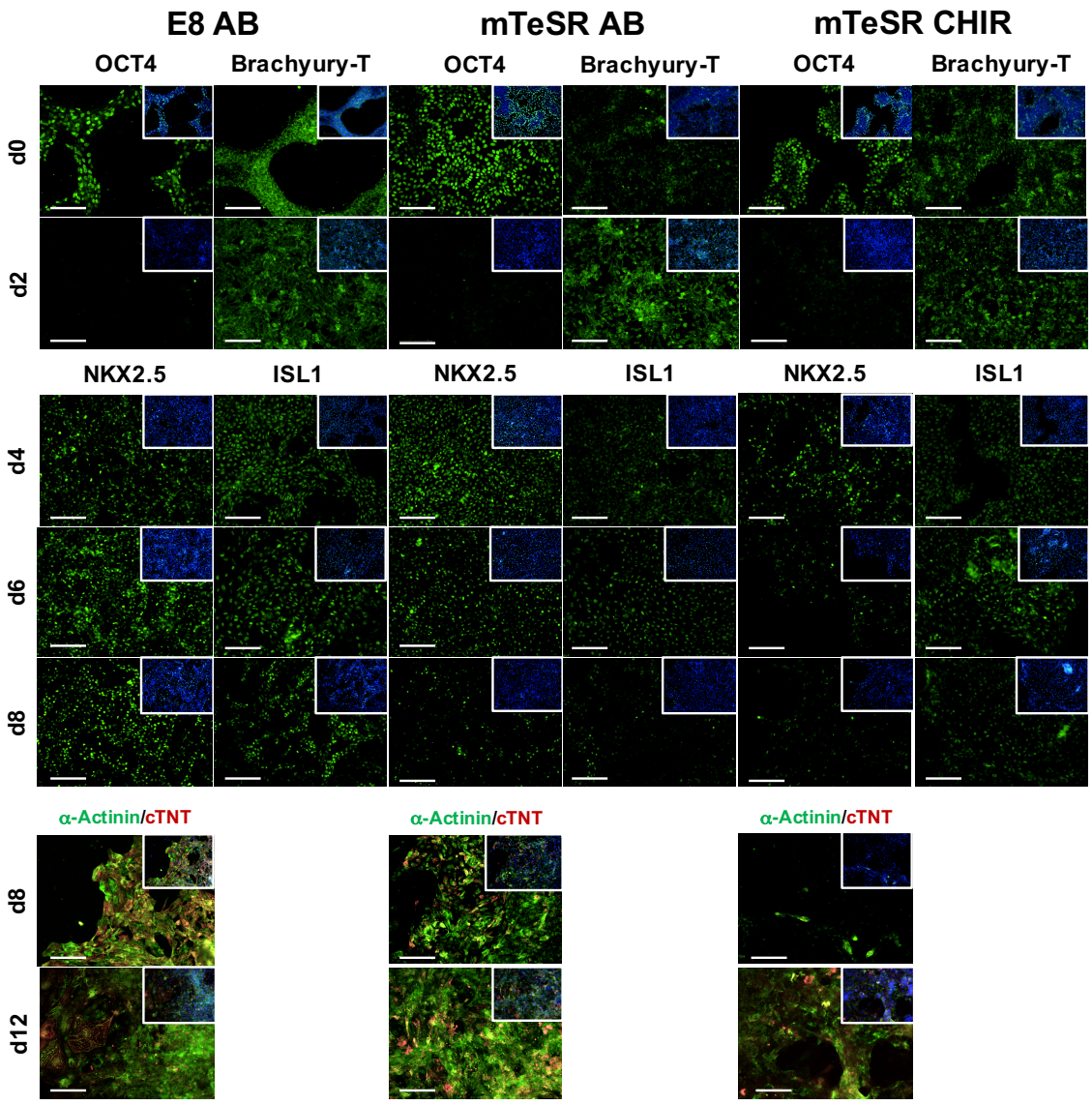


Figure 3.14: Time course analysis of stage-specific markers during cardiac induction process triggered by using E8-AB, mTeSR-AB, and mTeSR-CHIR protocol in NCRM5. The representative fluorescence images of NCRM5 derived CMs illustrate the expression of stage-specific markers during cardiac induction mediated by E8-AB, mTeSR-AB, and mTeSR-CHIR protocol. The expression of pluripotent-associated transcription factor (OCT4) was repressed after the first two days of differentiation protocols followed the expression of Brachyury-T, indicating the mesodermal formation. From d4 to d8, the cardiac regulatory transcription factors, including NKX2-5 and ISL-1, were expressed and induced the formation of terminally differentiated cardiomyocytes. *Scale bar:* 100 μm.

3.2.9 Investigation of BMP signalling activation during cardiac differentiation process

The initiation of either BMP or WNT pathways presents a necessary, but not sufficient, condition for cardiac differentiation, because inhibition of WNT is the additional requirement for a successful cardiac differentiation process. In our protocols, KY02111 and XAV939 are the common WNT inhibitors across all three established methods regardless of the difference in mesodermal induction factors (growth factors vs. small molecules). Both KY and XAV were proven to be efficient in inducing the cardiac differentiation process of hPSCs by acting as WNT-inhibitor, and the former was shown to be involved in the ventricular specification process. Hence, the uses of KY and XAV in our protocols were to inhibit the WNT pathways as well as driven the CMs toward ventricular subtype.

To identify the mechanism underlying the activation of BMP and WNT followed by WNT inhibitor, we sought to exploit the major cardiac regulatory signalling cascade, the BMP pathway, using Proximity Ligation Assay (PLA). Four main reported transcription factor (TF) candidates in BMP signalling, including phosphorylated Smad 1/5/8 (pSmad1/5/8), Smad4, ATF2, and TCF7, and ventricular TFs, IRX4 and NKX2-5, were targeted for PLA analysis for their potential interaction during cardiac induction process, especially during d2 to d6 of differentiation procedure. To this end, the time course analysis for the interaction of pSmad1/5/8 with Smad4, pSmad1/5/8 with ATF2, pSmad1/5/8 with TCF7, and IRX4 with NKX2-5 was generated during days 0-6, when pathways were generally activated towards linage specification, as illustrated in Figure 3.15. It was found that regulation of BMP pathway via interaction between pSmad1/5/8 and Smad4 occurred at d6 of differentiation processes regulated by mesodermal activation via BMP pathway (in E8-AB, and mTeSR-AB protocol) but not in WNT activation protocol (mTeSR-CHIR) (Figure 3.16). The interaction of pSmad1/5/8 with ATF2 and TCF2 was detected from d2 and maintained until d6 of differentiation process in only E8-AB condition. Of note, detection of pSmad1/5/8 and TCF7 was also observed at d6 in REBL-PAT-Sen samples underwent mTeSR-AB and mTeSR-CHIR condition but

at a lower level compared to that of the E8-AB method. The interaction of IRX4 and NKX2-5, indicating the induction of ventricular specification, was observed only at d6 of differentiation process in all three protocols, in which the highest level of interaction was detected in E8-AB protocol (Figure 3.16).

Taken together, the PLA results confirmed the targeted association between pSmad1/5/8 to Smad4, ATF2, and TCF7 between d2 to d6 post-differentiation, suggesting that pSmad1/5/8 is involved in both regulation of BMP pathways and subtype specification process. Furthermore, the couplings were observed clearly in the E8-AB and mTeSR-AB, but not in mTeSR-CHIR protocol, indicating that the cardiac induction via growth factors specifically induce the expression and association of pSmad1/5/8 to its target TFs that are directly involved in ventricular formation process. Indeed, this observation was further supported by the interaction of ventricular TFs, NKX2-5 and IRX on d6 of E8-AB and mTeSR-AB process

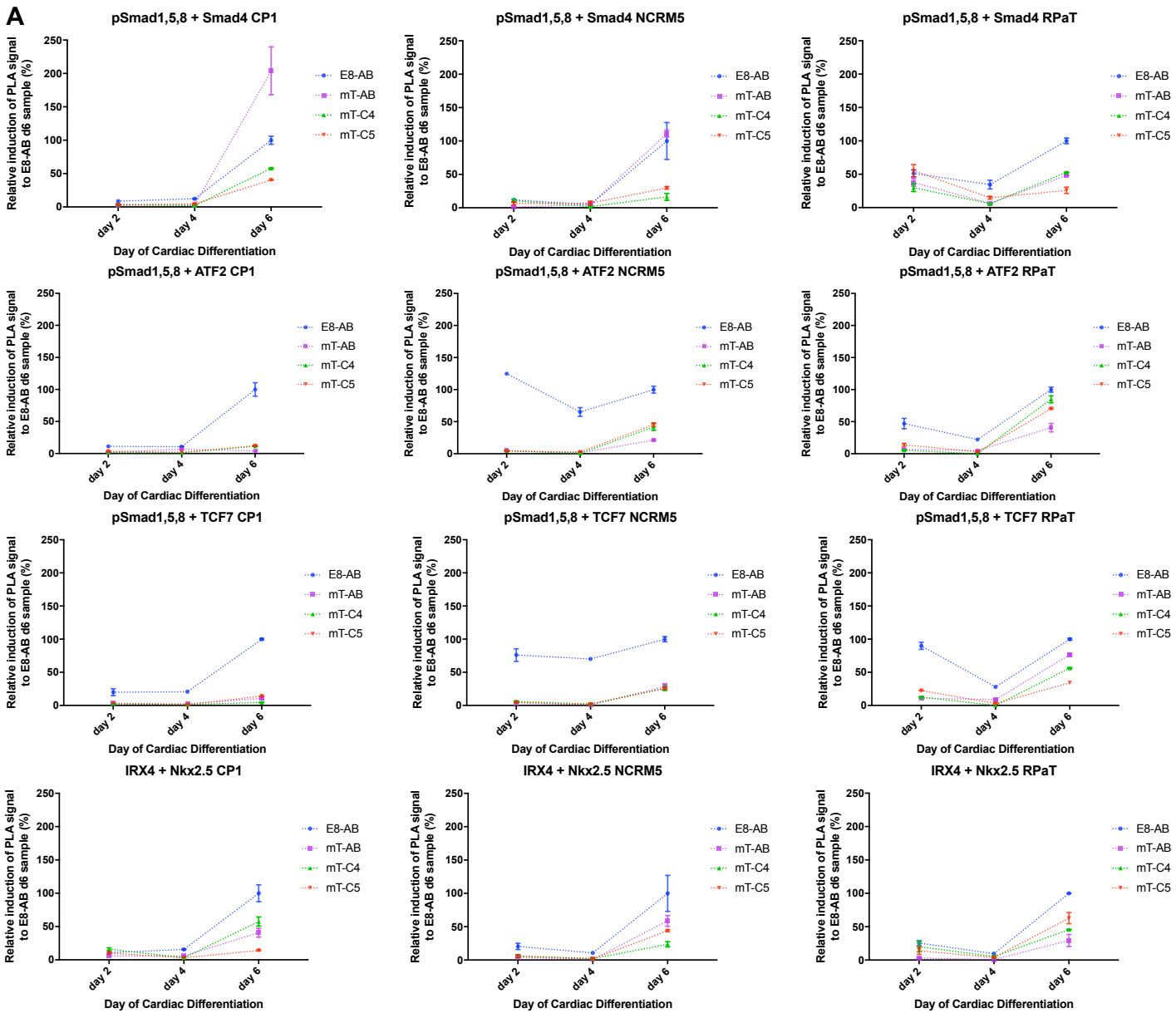


Figure 3.15: Mechanistic analysis of BMP pathways during cardiac induction process. (A) The results obtained from PLA assay analysing the interaction between pSmad1/5/8 with Smad4, pSmad1/5/8 with ATF2, pSmad1/5/8 with TCF7, and IRX4 with NKX2-5 under three independent procotols, including E8-AB, mTeSR-AB, and mTeSR-CHIR (with two CHIR concentrations: 4 μM (C4) and 5 μM (C5). Two concentrations of CHIR were used due to the batch-to-batch variation of the protocols which could results in the generation of inconsistent results. (n=3, error bar: s.e.m.). **(B)** The heat-maps illustrate the interactions converted from **A** in three cell lines, including CP1, NCRM5, and REBL-PAT-Sen (RPat). **(C)** Representative images of PLA assay detecting the interaction between pSmad1/5/8 and Smad4 at d6 in NCRM5. *Scale bar:* 100 μm.

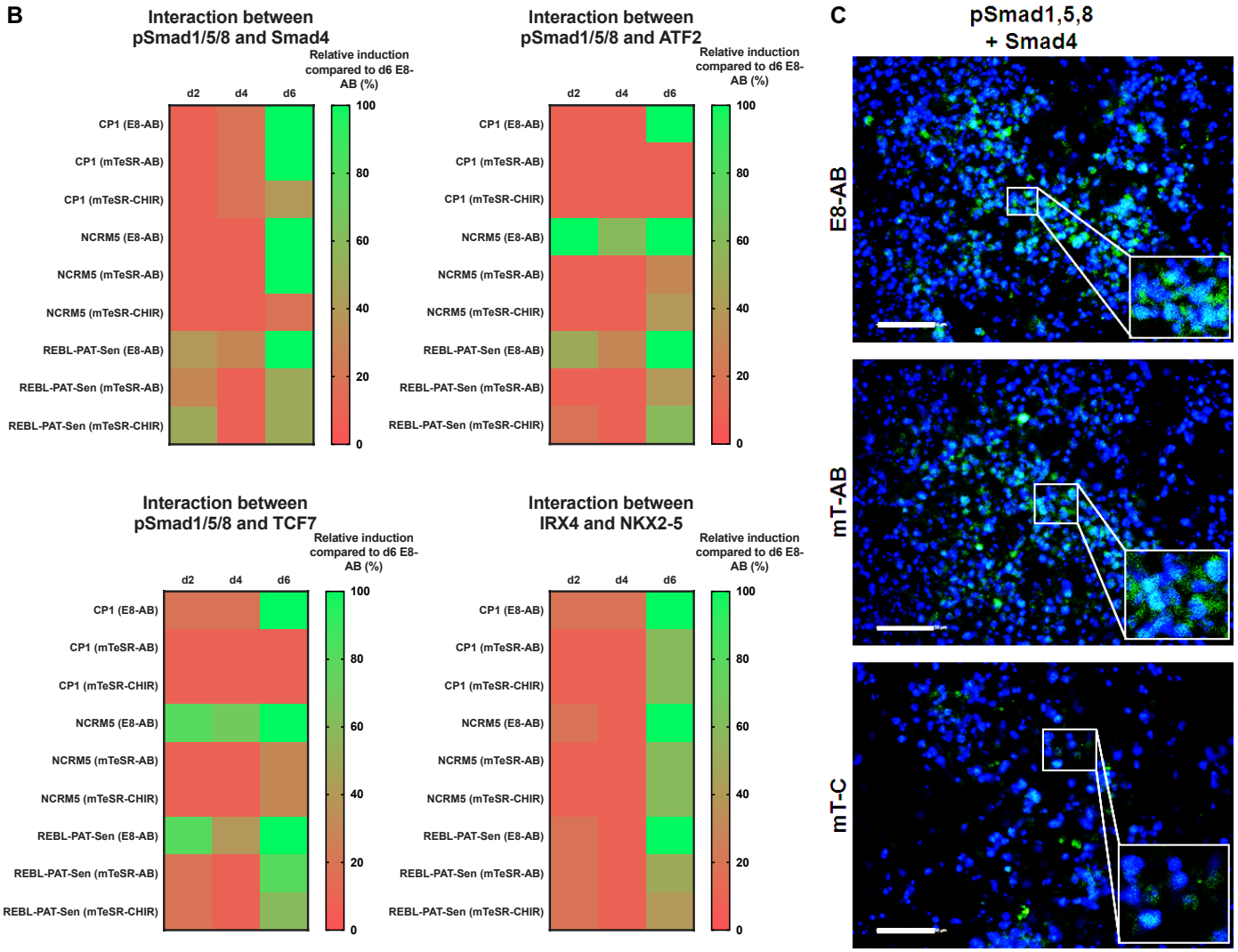


Figure 3.15 (Continue): Mechanistic analysis of BMP pathways during cardiac induction process. (B) The heat-maps illustrate the interactions converted from **A** in three cell lines, including CP1, NCRM5, and REBL-PAT-Sen (RPat). **(C)** Representative images of PLA assay detecting the interaction between pSmad1/5/8 and Smad4 at d6 in NCRM5. *Scale bar:* 100 μm.

3.2.10 Analysis for the ventricular subtype formation *in vitro*

The PLA results suggested the interaction of TFs was involved directly in the ventricular specification process posed a question about the formation of ventricular CMs from our protocols. Accordingly, we repeated the cardiac differentiation in CP1, NCRM5, and REBL-PAT-Sen using E8-AB, mTeSR-AB, and mTeSR-CHIR protocol. CMs were collected at d15, d30, and d60 of differentiation procedure for FACS analysis for subtype-specific markers, MLC-2v and MLC-2a (Figure 3.16A).

The results at d15 indicated approximately 40% of the CM population expressed ventricular marker (MLC-2v), 30% CMs expressed atrial marker (MLC-2a), and 30% CMs expressed both markers (2a+2v) in all three cell lines (Figure 3.16B). Similar patterns were observed at d30 with a slight increase in MLC-2v expressing CMs together with a proportional decrease in MLC-2a and 2a+2v population. Strikingly, on d60, the majority of CM population expressed MLC-2v, whereas a significant reduction in 2a+2v population was observed, indicating the switch in MLC-2v expression during prolonged culture of CM *in vitro* (Figure 3.16B). Of note, the E8-AB protocol induced the highest MLC-2v population followed by mTeSR-AB protocol across all tested cell lines, which showed an average of 80% and 70% CM expressing MLC-2v, respectively, indicating the formation of ventricular CMs. The mTeSR-CHIR condition generated approximately 60% ventricular CMs at d60 post-differentiation.

In summary, these data showed that the MLC-2v population was established at low proportion at an early stage of differentiation process and increased proportionally during prolonged culture *in vitro* due to the reduction of the 2a+2v population. Variation in MLC-2a population was also observed during extended culture *in vitro*, although the MCL-2a population was relatively small (<20%) after d30 onwards in all tested conditions and hPSCs (Figure 3.16B).

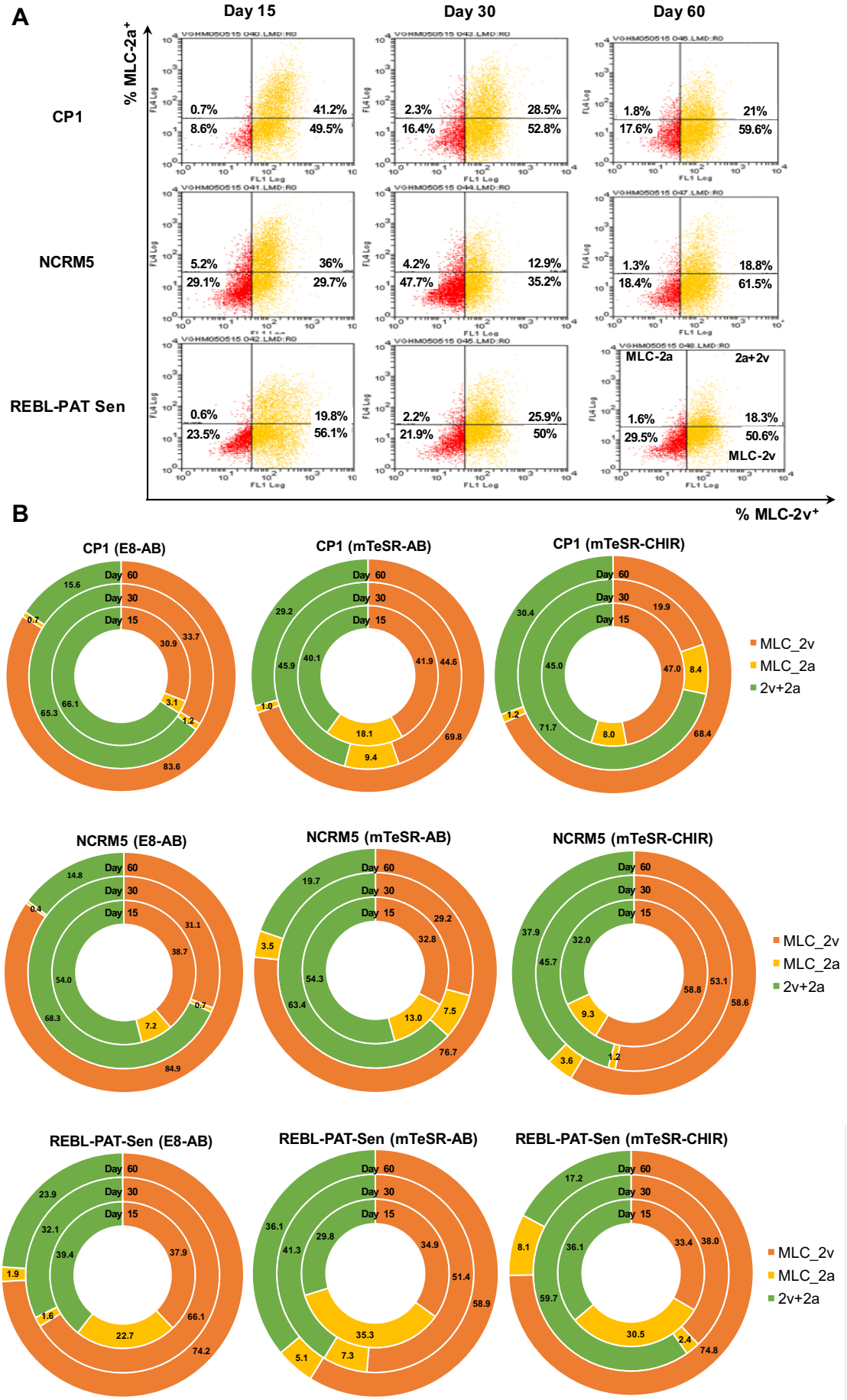


Figure 3.16: Cardiac subtype analysis using FACS analysis of MLC-2v and MLC-2a population. (A) Representative FACS data obtained from CP1, NCRM5, and REBL-PAT-Sen underwent three differentiation protocols, including E8-AB, mTeSR-AB, and mTeSR-CHIR. Samples were collected at d15,

d30, and d60 of differentiation for FACS analysis (n=3). **(B)** The pie charts depict the increase in MLC-2v expressing CMs during prolong culture *in vitro*.

3.2.11 Electrophysiological analysis for hPSC-CMs using CellOPTIQ®

Identification of MLC-2v positive CMs using flow cytometry encouraged us to further characterise the ventricular CMs in terms of electrophysiological functions using CellOPTIQ® system, kindly performed by Dr. Maria Hortigon at the University of Glasgow. The result demonstrated that at days 30-40, CMs derived from E8-AB and mTeSR-AB condition had a ventricular-like action potential, whereas CMs derived from mTeSR-CHIR protocol had an atrial-like action potential (Figure 3.17A). Analysis for action potential duration measured (APD) at 90% repolarisation (APD_{90}) from these CMs indicated that CMs derived from all three tested hPSC lines that underwent E8-AB, and mTeSR-AB protocols had the APD_{90} value higher than 350 ms, suggesting the ventricular subtypes. Interestingly, the mTeSR-CHIR protocol produced different results between tested lines. While CP1 and REBL-PAT-Sen (Rpat) showed an APD_{90} represented of atrial CMs, NCRM5-derived CMs demonstrated a ventricular APD_{90} value. To appreciate the differences, the shape factor (or RO index)

$$\mathrm{APD_{Ratio}(RO\ index)} = \frac{\mathrm{APD_{30}} - \mathrm{APD_{40}}}{\mathrm{APD_{70}} - \mathrm{APD_{80}}}$$

was calculated as it has been reported that the RO index can be used to discriminate ventricular and atrial cardiomyocytes: as in Ma *et al.,* (2011), an action potential is considered ventricular subtype if the RO index > 1.5 and atrial cardiomyocyte if RO index < 1.5. Calculated RO values further confirmed that CMs derived from E8-AB and mTeSR-AB had RO>1.5, suggesting ventricular subtypes, whereas mTeSR-CHIR produced CMs had RO<1.5, confirming the atrial-like CMs (Figure 3.17C). Additionally, the spontaneous cycle length of CMs derived from all three protocols ranged between 1 to 1.5 s, and there was no significant difference detected, suggesting the robustness in performance across the monolayer independent of the protocols (Figure 3.17D).

In conclusion, the data illustrated the generation of ventricular CMs from E8-AB and mTeSR-AB protocols, whereas the mTeSR-CHIR protocols generated mixture of both atrial and ventricular CMs.

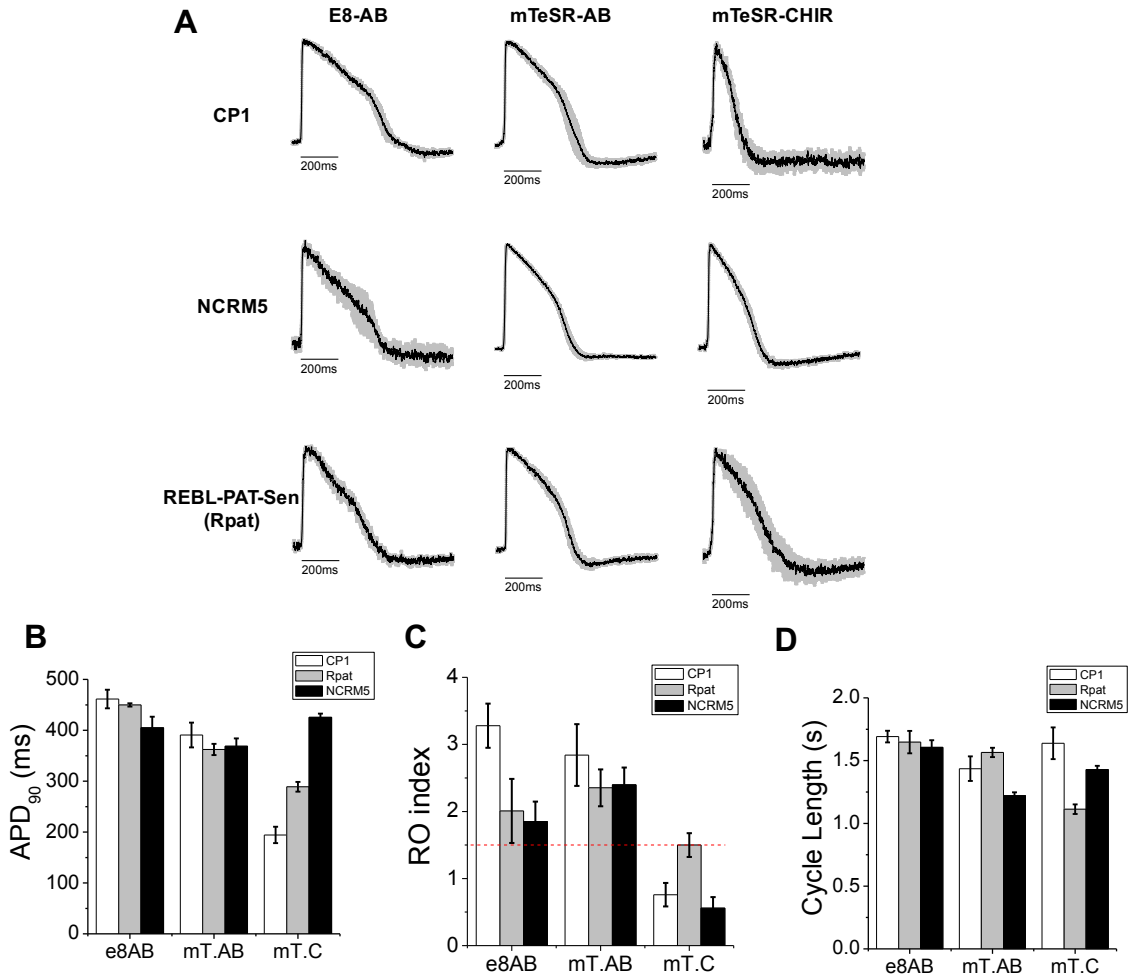


Figure 3.17: Electrophysiological characterisation of cardiomyocytes. (A) Representative action potential recording using CellOPTIQ® platform of cardiomyocyte subtypes produced from d30 to d40 (n=3). **(B-D)** Voltage recording obtained from CellOPTIQ® of differentiation cells derived from either E8-AB (e8AB), mTeSR-AB (mT.AB), and mTeSR-CHIR (mT.C) protocols demonstrating action potential duration at 90% repolarisation (ADP_{90}), the RO index, and cycle length (n=3, error: SEM).

3.2.12 Non-invasive cell sorting of ventricular cardiomyocytes

Although our protocols contained dominantly ventricular CMs, it was important to investigate the phenotypic functions of purer ventricular population. To isolate the ventricular CMs, the non-invasive method called Smart-Flare was used. The Smart-Flare technology is based on the gold particles coated with the target RNA sequence labelled with fluorescence probe, which allows the detection of the complementary binding of the host mRNA to the target RNA sequence and releases the probe for detection. Because the gold particles are uptake into the cells via endocytosis and release after 48h, it allows developing the non-invasive cell sorting using FACS. Hence, the gold particles coated with specific MLC-2v mRNA sequence were ordered and delivered into NCRM5-derived CMs generated from E8-AB method followed by FACS sorting of positive cells (Figure 3.18A). The CDM3(CHIR) protocol was also applied as a control for immunofluorescence analysis before cell sorting (Figure 3.18B). The scramble control contains the gold particles coated with non-specific RNA sequence and used as the negative control for the experiment. After 24h, the MLC-2v-Cy3 probes could be detected using the standard fluorescence microscope in E8-AB differentiation procedure (Figure 3.18B). The result showed the high level of signals obtained from the E8-AB protocol, but not CDM3(CHIR) protocol, suggesting that the E8-AB protocol generated ventricular CMs and the MCL-2v probe was highly specific. This encouraging result allowed us to initiate FACS sorting the Cy3-positive population, which showed approximately around 70% to 80% in CMs at d60 post-differentiation, which agreed to previous data on ventricular subtype specification using PLA, flow cytometry, and electrophysiological anlaysis (Figure 3.18C). The sorted cells were then collected for electrophysiological analysis using dynamic patch clamping method, kindly performed by Dr. Arie O Verkerk at Amsterdam Medical Centre.

Patch-clamp analysis demonstrated that Smart-flare sorted CMs ($MLC2v^+$) at d60 had a ventricular characteristic with a low average maximum diastolic potential (MDP) of -83.4 ± 0.5 mV, whereas the scramble CMs (Smart-flare control using non-specific RNA capture strand) and the flow-through population ($MLC2v^-$ population) had the MDP of -

82.7 ± 0.6 mV and -81.3 ± 0.7 mV (mean ± SEM, n=24 for scramble cells, n=14 for $MLC2v^+$ sorted cells, and n=5 for $MLC2v^-$ population). In terms of action potential amplitude (APA), all tested CMs showed a relatively similar APA value, which was approximately 120 mV (Figure 3.18 D). Interestingly, the maximum rate of depolarisation or maximal upstroke velocity (V_{max}) of $MLC2^+$ CMs is relatively fast, which was 248.3 ± 22.4 V/s, whereas slower rate was obtained in Scramble sample (235.3 ± 21.6 V/s), and $MLC2v^-$ CMs (229.4 ± 25.4 V/s) (mean ± SEM, n number as mentioned above). Furthermore, the $MLC2v^+$ also showed a longer AP duration at 20%, 50%, and 90% repolarisation (ADP_{20}, ADP_{50}, and ADP_{90}, respectively) compared to that of Scramble and $MLC2v^-$ population, suggesting that $MLC2^+$ cells repolarised earlier and faster. Of note, the Scramble population showed a medium range of ADP_{20}, ADP_{50}, and ADP_{90}, which was 65.2 ± 8.8 ms, 158.6 ± 18.6 ms, and 214.7 ± 17.4 ms, respectively, indicating a heterogeneous phenotype, with ventricular-like cells being the dominant phenotypes. In contrast, the $MLC2v^-$ population demonstrated the ADP_{20}, ADP_{50}, and ADP_{90} values of 41.8 ± 7.5 ms, 123.1 ± 17.8, and 165.6 ± 19.6 ms, suggesting the dominant phenotype was atrial-like CMs (Figure 3.18D).

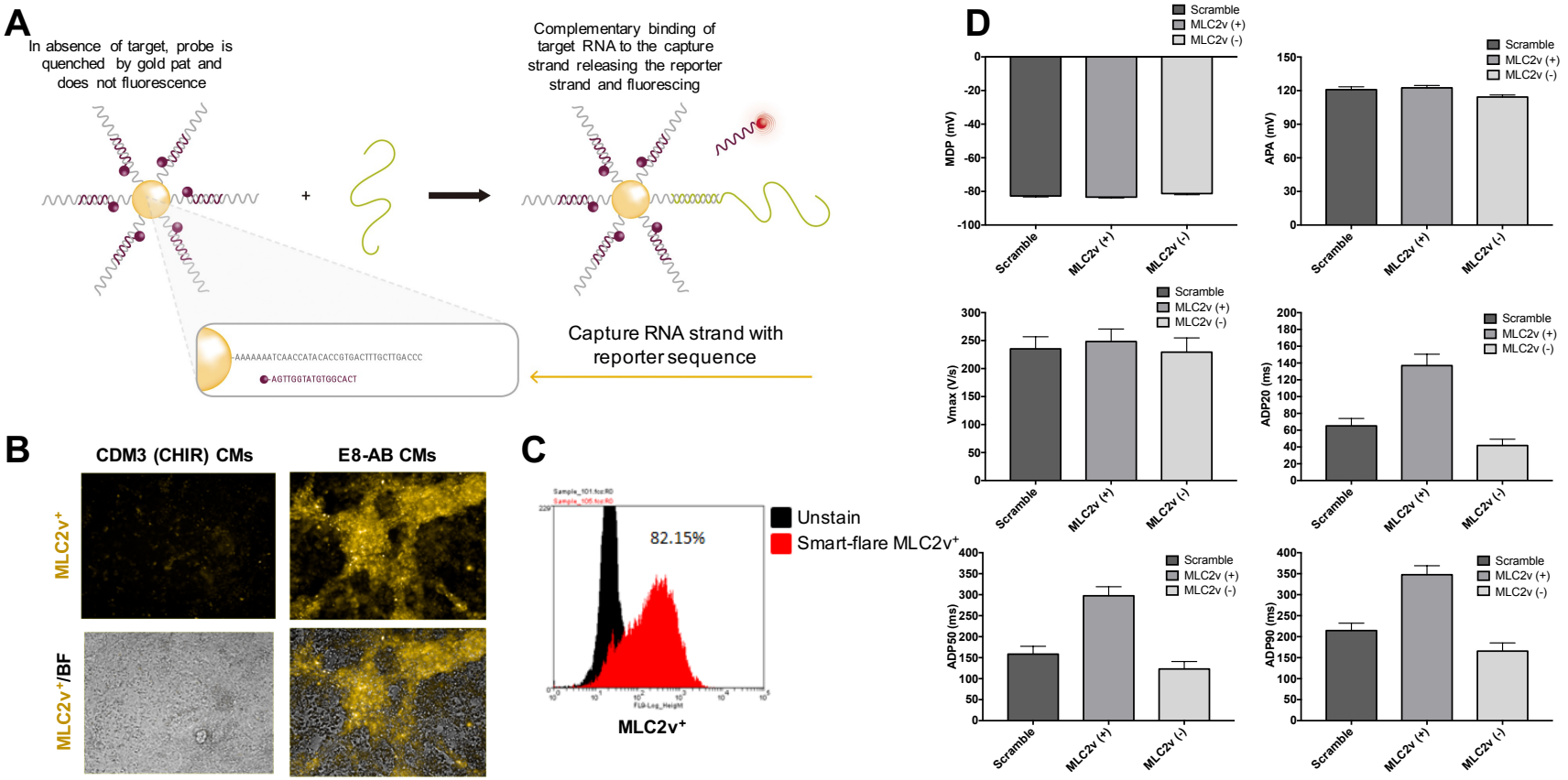


Figure 3.18: Non-invasive procedure for isolation of ventricular cardiomyocyte subtype using Smart-flare and FACS sorting. (A) The schematic (adapted from Merck Millipore website) depicts the mechanism of Smart-flare technology, which based on the detection of fluorescence probe by complementary binding of target RNA to the capture RNA stands attached on the gold particle surface. **(B)** Representative images of MLC2v$^+$ cells in 24h post Smart-flare treatment. Upon entering the cells via endocytosis, the binding of MLC2v mRNA to the specific RNA capture sequence released the reporter sequence (Cy3), allow the detection of yellow fluorescence using normal fluorescence microscope. **(C)** Representative FACS analysis of Cy3-positive population, indicating the MLC2v$^+$ population. **(D)** Patch clamp analysis of CMs derived from Scramble, MLC2v$^+$ sorted cells, and MLC2v$^-$ population demonstrating Maximum diastolic potential (MPD), action potential amplitude (APA), maximum upstroke velocity (V_{max}), and action potential duration at 20%, 50%, and 90% repolarisation (ADP_{20}, ADP_{50}, and ADP_{90}, respectively).

3.3 Discussion

This chapter reports a set of cardiac differentiation protocols that are robust, efficient, and reproducible in producing cardiomyocytes from diverse hPSCs regardless of their culture condition, reprogramming method, and somatic cell source (in the case of hiPSCs). The set contains three independent protocols with an optimal condition of well-orchestrated extrinsic induction of mesoderm via activation of BMP pathway (in E8-AB, and mTeSR-AB protocol) or WNT signalling (mTeSR-CHIR protocol) followed by WNT inhibition using the combination of two small molecules, KY02111 and XAV939. These three protocols can be classified into the growth factor-dependent protocols, including E8-AB and mTeSR-AB method, and small molecule-dependent process (mTeSR-CHIR). As their name implies, the growth factor protocols using BMP4 and Activin-A as the major mesoderm induction, whereas in the small molecule protocol, CHIR99021 was used to induce mesodermal formation via activation of WNT pathway. Our results indicated that efficient cardiac induction regardless of mesodermal induction factors (growth factors vs. small molecules) requires certain concentrations, especially in the case of CHIR99021, as well as the precise timing of chemical applications.

We found that the efficiency, robustness, and consistency of cardiac induction procedures were significantly improved by preconditioning the E8-cultured hPSCs with either StemPro34 supplemented with Matrigel and 1 ng/mL BMP4 (SP34-MT-BMP4) or using the mTeSR medium. Matrigel overlay for 48h was reported previously in hPSC cultured in mTeSR medium to improve the cardiac differentiation efficiency by promoting an epithelial-to-mesenchymal transition in cell phenotypes (Zhang et al., 2011). In our study, we observed a dramatic morphological change after precondition using SP34-MT-BMP4, demonstrating the epithelial-to-mesenchymal transition process. However, we also found that the duration of precondition, between 12h to 16h, strongly supported the cardiac differentiation process, whereas longer incubation times resulted in the reduction of cardiomyocyte induction efficiency. In fact, the same effects were observed when mTeSR was used as precondition medium, indicating that enrichment of culture conditions before starting cardiac differentiation of E8-culture hPSC plays a crucial role

in enhancing the differentiation process. The E8 medium is the most simplified hPSC culture medium containing only eight components, including insulin, selenium, transferrin, L-ascorbic acid, FGF2, and TGFβ in DMEM/F12 with pH adjusted with $NaHCO_3$ (Chen et al., 2011). This simplified medium contains significantly less amount of nutrients compared to that of the mTeSR medium, which had 18 components required for the healthy growth and expansion of hPSCs (Table 3.7) (Ludwig et al., 2006; Sun et al., 2009). Furthermore, in preconditioning step, the direct comparison between mTeSR and StemPro34 in the maintenance of hPSCs was conducted and confirmed the major roles of nutrients together with growth factors involving in the quality of hPSC culture (Akopian et al., 2010). To be more specific, cross comparison between mTeSR and SP34 medium indicated several common components that are missed from E8 medium, including albumin, L-glutamine, non-essential amino acid, trace elements, and β-mercaptoethanol. Hence, the putative effects of preconditioning step could be derived from these additional components and it was important to investigate further contributions of each components in enhancing the cardiac differentiation process of E8-cultured hPSCs.

Table 3.7: Summary of components present in chemically defined medium used in preconditioning step. HRG: meuregulin-1, LR^3-IGF: Long R Insulin-like growth factor, FGF2: Fibroblast growth factor 2, TGF-β: Transforming growth factor-β, GABA: γ-aminobutyric acid, LiCl: Lithium chloride.

Medium components	E8 (Chen et al., 2011)	mTeSR (Ludwig et al., 2006)	StemPro34 (Wang et al., 2007)
Activin-A			✔
Albumin		✔	✔
Ascorbic acid	✔	✔	✔
DMEM/F12	✔	✔	✔
FGF2	✔	✔	✔
GABA		✔	
HRG1β			✔
Insulin	✔	✔	
L-glutamine		✔	✔
LiCl		✔	
LR^3-IGF			✔
$NaHCO_3$	✔	✔	✔
Non-essential amino acids		✔	✔
Pipecolic acid		✔	
Selenium	✔	✔	
TGF-β	✔	✔	
Thiamine, Glutathione		✔	
Trace elements		✔	✔
Transferrin	✔	✔	✔
β-mercaptoethanol		✔	✔

Furthermore, in our protocols, medium without insulin was used from d2 to d4 of cardiac induction process as previously reported due to its detrimental effects on the cardiac specification of early mesoderm (Lian et al., 2012; Lian et al., 2013b). It was reported previously that withdrawal of insulin in the first two days of differentiation introduced additional stress to the cells resulting in the reduction of the efficiency and consistency of the protocols (Kadari et al., 2015). This observation was similar to our results obtained from RB27(-Ins) protocols, in which, insulin withdrawal from days 0-4, exhibited a low level of cardiac differentiation efficiency. Additionally, two basal media were used in cardiac differentiation process, including StemPro34 and RPMI with B27 supplement (RB27), and both had proven to be effective in supporting cardiac induction process. However, in our experience, StemPro34 medium maintained the protocol consistency across all tested cell lines, whereas RB27, in some cases, showed inconsistent results and variations between experiments.

In light of our data, the cardiac differentiation process is orchestrated by two steps mediated by combined either BMP/WNT activation followed by WNT inhibition. Our analysis revealed that activation of BMP via growth factors induces different patterns of both protein expression and signalling cascade compared to that of WNT induction via small molecules. The data indicated that activation of BMP and WNT cascades converges on rapidly repressing the pluripotency-associated marker OCT4, which has also been negatively correlated with Brachyury-T expression. Interestingly, the protein kinetic analysis demonstrated the higher suppression of pluripotency happened in E8-AB, especially during the preconditioned step, whereas mTeSR-AB and mTeSR-CHIR showed the reduction in OCT4 protein after two days in the differentiation process. Of note, activation of BMP pathway induced stronger expression of Brachyury-T protein on d2 compared to that of WNT pathway. This data is supported by the previous study, which showed that activation of BMP pathway by using BMP4 and Act-A destabilised pluripotent-associated genes, such as *SOX2* and in lesser extent *OCT4* at mRNA level within hours via activation of Smad1 (Wang et al., 2012; Rao et al., 2016). Indeed, Smad1 has been illustrated to confer the ability to facilitate the miRNA maturation,

including an SOX2-targeting miRNA (Camilo et al., 2010). Moreover, it was suggested that BMP activation directly initiates mesodermal induction via posttranscriptional mechanism enhancing rapid reduction of pluripotency-associated transcription factors, which in turn, elevated mesodermal transcription factors, including Brachyury-T – a specific mesodermal marker (Rao et al., 2016). In contrast, activation of WNT downregulated the pluripotency-associated transcription factors with a delay via the mediation of the WNT-specific induction of T-box transcription factor Eomesodermin – EOMES. In fact, activation of EOMES is involved in the later stage of mesodermal induction and formation of cardiac mesodermal precursors (Costello et al., 2011). In conclusion, these data suggested that activation of BMP/WNT pathway promotes the mesodermal induction in different timeline manner, in which, BMP4 and Act-A inducing the mesodermal induction in a matter of hours whereas WNT activation by CHIR induced the formation of later stage mesoderm. Additionally, our data also showed that single-factor-based protocols that rely either on BMP (E8-AB, and mTeSR-AB) or WNT (mTeSR-CHIR) activation could effectively induce cardiac differentiation process across a broad range of hPSCs. It also appears that combined BMP activation and its antagonizing Activin signalling at precise doses of BMP4 and Act-A not only enhances but also stabilises the mesodermal induction process via activation of WNT pathway as seen in the cardiac developmental process (Loh et al., 2014; Murry and Keller, 2008). The variation in the consistency of mTeSR-CHIR protocol observed in our study can also be explained by the fact that WNT activation at a lower level was counterproductive for mesoderm induction (Mehta et al., 2014). This observation also in line with the previous report suggesting the WNT signalling strength at low level might account for segregating diverse endo and neuro lineages (Rao et al., 2016).

In fact, activation of BMP/WNT signalling presents a necessary condition for cardiomyocyte differentiation, but not a sufficient one (Murry and Keller, 2008). To achieve a successful cardiac differentiation, the subsequent step is to inhibit the WNT signalling pathways, which regulated the mesodermal inducted cells toward cardiac lineage (Mummery et al., 2012; Yester and Kuhn, 2017; Zwi et al., 2009). In this thesis,

XAV939 and KY02111 were used to inhibit WNT signalling pathway for four days (from d2 to d6 of cardiac induction process). By using the WNT reporter line, it was proven that XAV939 has a strong WNT inhibitory effects by stimulating β-catenin degradation via inhibition of tankyrase-1 and tankyrase-2 (Huang et al., 2009). XAV939 has been used in other published protocols (Kadari et al., 2015; van den Berg et al., 2015). The small molecule, KY02111, was reported to promote cardiac differentiation and acts as WNT inhibitor in hPSC. The effective window of KY02111 was suggested between days 3-8 as treatment during the mesoderm induction stage resulted in suppression of cardiac differentiation (Minami et al., 2012). In our study, KY02111 promoted cardiac induction when it was used together with XAV939 from days 2-6. Furthermore, it was also proven that CMs derived from KY02111 exhibit the ventricular subtypes, although the molecular pathway underline this effect is remained unclear (Minami et al., 2012). Our data indicated that combined inhibitory effects of XAV939 and KY02111 (KYX) improved the expression of Brachyury-T proteins until days four post cardiac differentiation process. Furthermore, the cardiac precursor markers, including NKX2-5 and ISL-1, were also enhanced after KYX was applied from d2 of the differentiation process, further confirming the proposed role of KYX in inhibitory WNT and induction of cardiac progenitor formation.

Furthermore, the data in this section highlighted the potential mechanism underlying the cardiac induction protocols, especially the BMP pathways. After blocking the mesodermal induction, BMP is involved in regulation of cardiac differentiation by up-regulating cardiac transcription factors, like NKX2-5 and GATA4 in a Smad1 dependent manner (Faial et al., 2015). BMP signalling pathway, especially BMP4 cascade, has a critical role in the terminal differentiation of cardiomyocyte progenitors into cardiomyocytes (Morrell et al., 2016; Noseda et al., 2011). Activation of BMP pathway during mesodermal cardiac formation resulted in the phosphorylation of Smad1/5/8 (pSmad1/5/8), a downstream effector of BMP pathway, which often form complexes with Smad4 for nuclear translocation and initiation of cardiac-regulator genes, including *NKX2-5*, *MEF-2c* and *ISL-1* (Furtado et al., 2008; Pereira et al., 2012). In light of our reported results, the interaction between pSmad1/5/8 and Smad4 has detected in growth

factor dependent protocols at d6 of the process using PLA assay. These results are consistent with the protein kinetic analysis using immunofluorescence, which illustrated an increase in NKX2-5 protein from d4 and reached a peak at d6 in E8-AB, and mTeSR-AB protocols. A low signal level of pSmad1/5/8 and Smad4 interaction was seen in the mTeSR-CHIR protocol, which might explain the variation in NKX2-5 protein expression during cardiac induction of hPSCs. Induction of the cardiac transcription factors by BMP also resulted in the induction of other cardiac-specific genes, including *ISL-1*. Interestingly, it was reported that BMP cascade also induces the transcription of the activating transcription factor-2 (ATF2), which stimulate the β-MHC expression in terminal cardiac differentiation (Monzen et al., 2001). This observation was in agreement with our data, which indicated the interaction of the pSmad1/5/8 and ATF2 in E8-AB protocol at d6 of the differentiation process, suggesting that ATF2 is also the target of pSmad1/5/8. Hence, it was concluded that the BMP activation via Act-A and BMP4 triggered the association of pSmad1/5/8 with its targeted transcription factors, including Smad4, ATF2, and TCF7, which were directly participated in the cardiac precursor formation and ventricular subtype specification process.

A recently published paper reported that activation of WNT signalling pathway by CHIR99021 followed by the small molecules (C59) acting as WNT inhibitor effectively induced cardiomyocytes in the chemically defined medium (CDM3), which contained only three components, including Ascorbic acid, human albumin, and RPMI basal medium (the CDM3-CHIR) (Burridge et al., 2014). However, this protocol was inconsistent and generated relatively low level of CM purity in this thesis. Additionally, the CDM3-CHIR protocol requires the optimisation of CHIR concentration in all tested cell lines to achieve a high level of cardiac differentiation efficiency. Using the RPMI medium with the B27 supplement as the alternative differentiation medium improved the consistency and efficiency of the CDM3-CHIR protocol, which is consistent with the suggestion from the original paper (Burridge et al., 2014). The inconsistency and low purification of CDM3-CHIR derived cardiomyocyte was later reported by the same group, which the differentiation efficiency was between 50% to 60%, and additional purification

step was added using Glucose starvation process (Sharma et al., 2015). This observation was strongly supported our data. Furthermore, it was also mentioned that the cardiomyocytes generated from CDM3-CHIR were predominantly MLC2a positive during d20 to d30 post-differentiation, and the predominant population of MLC2v positive (approximately 52%) was observed from d40 cardiomyocytes (Burridge et al., 2014). However, the study did not analyse the dual population (MLC2v+2a), which potentially misled the results.

In our protocols, all three cardiac induction procedures generated mainly MLC2v positive CMs, approximately 45% at d15 differentiation and the proportion of MLC2v population increase up to 83% at d60, suggesting that our protocols produced ventricular CMs. This result was in line with the previously study, which also generated ventricular CMs by using KY02111 and XAV939 as WNT inhibitor and it was proven that KY02111 itself or in combination with other small molecules might be able to induce the generation of the MLC2v positive population (Minami et al., 2012). CMs derived from hPSCs were immature and similar to human foetal cardiomyocytes because of the presence of the MLC2v/2a double-positive population with disorganised sarcomeres and low level of HERG channel responses (Mummery et al., 2012). Indeed, our data confirmed the presence of the 2v+2a population after cardiac induction process, which was approximately 30% to 40% at days 15 of cardiac differentiation procedure. Strikingly, we observed the proportional reduction of the 2v+2a population and the increase of MLC2v population during *in vitro* culture, illustrating the ventricular specification and maturation process similar to previously described (Kamakura et al., 2013). Our observation was strongly supported the previous study which showed that ventricular cardiomyocytes could be derived from either MLC2v positive and MLC2v/2a dual positive population, whereas atrial cardiomyocytes derived mainly from the MLC2a positive population (Franco et al., 1998). This phenomenon was similar to that of described during cardiac developmental process *in vivo* (Franco et al., 1998). These ventricular CMs not only exhibited the expression of MLC2v marker but also demonstrated the electrophysiological response representing the ventricular subtypes. Additionally, these

ventricular CMs can also be isolated and purified using the non-invasive method followed by FACS sorting of the positive cells.

The methods developed in this chapter produced dominant ventricular cardiomyocytes, which could be used in functional analysis and disease modelling. Large numbers of CMs can be generated from our protocols, as it was demonstrated that the E8-AB protocol, for example, produced approximately $5x10^6$ CMs from $8x10^5$ hPSCs seeded initially in one Matrigel-coated T25 flask. Although there is room for further improvement and investigation, our cardiac induction methods may provide a robust, efficient, reproducible, and practical procedure for cell-based study of cardiac diseases *in vitro.*

However, in this chapter, the immaturity of hPSC-CMs has yet accessed because maturation process of hPSC-CM requires complicated procedures and is not included in the scope of this thesis. In fact, it is known that hPSC-CMs display immature phenotype, usually known as foetal-like CMs, and each improvement made to hPSC-CM maturity further increase utility and functionality. Several approaches have been developed to improve the maturity of hPSC-CMs, including mechanical/electrical stimuli, soluble factors, genetic manipulation, topography, stiffness, substrate ligands, etc (Denning et al., 2016). Structurally, hPSC-CMs are round or multi-angular cells with a single nucleus without any alignment of sacomeric structure. In fact, they have unstructured and disorganised sarcomeres, an aspect ratio of 2 or 3:1 and no T-tubules. By using electron microscope, only Z-discs and I-bands can be observed. In contrast, the adult CMs are highly organised, large rod-shaped poly-nucleated cells with sarcomeres of 2.2 μm and show longitudinal alignment. Furthermore, they also illustrate an aspect ratio of 5 to 9.5:1 and prominent T-tubules and sacomeric structure with Z-discs, and I-, H-, A-, and M-bands (Table 3.8).

Table 3.8: Comparison of characteristic between adult-CMs and hPSC-CMs (Denning et al., 2016).

		Adult-CM	hPSC-CM
Structure	Structure	Rod-shaped	Round or polygonal
	Alignment	Longitudinally aligned	Chaotically organised
	Nucleation	~30% cells bi- or poly-nuclear	Very limited bi-nucleation
	Sarcomere organisation	Highly organised	Disorganised
	Aspect ratio	5–9.5:1	2–3:1
	Banding	Z-discs, I-, H-, A- and M-bands	Mainly Z-discs and I-bands
	Sarcomere length	2.2 μm	1.6 μm
	Sarcoplasmic reticulum	Well developed	Mixed response: caffeine, Thapsigargin & ryanodine
SR	SR proteins	e.g. CSQ, PLN, RYR2, SERCA/ATP2A2	Expression lower than adult
	T-Tubules	Yes	No
Expr.	Gene expression	MYH7 (β-MHC) > MYH6 (αMHC)	MYH6 (αMHC) > MYH7 (βMHC)
		TNNI3 (cTnI) > TNNI1 (foetal ssTnI)	TNNI1 (foetal ssTnI) > TNNI3 (cTnI)
		MYL2 (MLC2v) > MYL7 (MLC2a)	MYL2:MYL7 ratio not determined
		Titin isoform N2B predominates	Titin isoform N2BA predominates
		ADRA1A (α-adrenoceptor) expressed	ADRA1A (α-adrenoceptor) not expressed
Energy & force	Metabolism	Mainly fatty acids	Glucose and lactate but can use fatty acids
	Energy production	Mainly oxidative phosphorylation	Mainly oxidative phosphorylation
	Mitochondria	Throughout cell; occupies 20–40% of cell volume	Near nuclei; numbers increase during differentiation
	Beating	Quiescent	Many cells spontaneous
	Force	40 to 80 mN/mm^2 (muscle strips)	0.08–4 mN/mm^2 (3D constructs)
		~μN range (single cells)	~200 nN (single cells)
	Capacitance	150 pF	20–50 pF
	Resting mem potential	−80 to −90 mV	−20 to −60 mV
Conduct^n	Upstroke velocity	150–350 V/s	10–50 V/s
	Conduction velocity	60 cm/s	10–20 cm/s
	Location of gap junctions	Intercalated discs	Circumference of cells
Ion channel density (pA/pF)	I_{Na}	−196	−100 to −244
	I_{CaL}	−4.3 to −10.2	−2.2 to −10
	I_{to}	2.3 to 10.6	2.5 to 13.7
	I_{Ks}	0.18 to 0.58	Most publications 0.3 to 0.7
	I_{Kr}	0.5	0.4 to 0.8
	I_{K1}	−12	0 to −3.4
	I_{NCX}	2.5 to 3	3.6 to 7.9 (inward mode)
Ca^{2+} kinetics	APD90	260 ms	300–700 ms
	Cycle Length	0.8–1 s	0.8–2 s
	T-rise	2.5 ms	3.5-10 ms
	Triangulation	45 ms	45-120 ms

3.4 Chapter Conclusion

Taken together, this chapter represented a set of cardiac induction procedures that is efficient, robust, reproducible, and consistent, including E8-AB, mTeSR-AB, and mTeSR-CHIR. The mechanisms found in this chapter provided information toward the potential molecular signalling pathways underlying the cardiac differentiation procedure mediated by either BMP or WNT pathways. Furthermore, our results also demonstrated that the induction and inhibition of WNT pathway together with BMP cascade play a central role in regulating the cardiac differentiation process of hPSCs, and CMs generated from different protocols are slightly different regarding cardiac subtypes, and electrophysiological characteristics. Therefore, it is important to choose the appropriate cardiac differentiation protocol producing the cardiomyocyte subtypes that are required for pharmaceutical analysis for drug or molecular studies of a particular gene of interest. Additionally, the cardiac differentiation protocols described in this chapter provided an essential tool to produce CMs at high purity for the next chapters and contributed to the success of establishment of the human cardiac model of GRK5 polymorphism of interest, the GRK5-L41.

Chapter 4 Developing and implementing a strategy to produce GRK5 Q41L human induced pluripotent stem cells (hiPSCs) derived cardiomyocytes.

4.1 Introduction

The advancement in hiPSC technology together with the improvement in CM differentiation implements the new way to establish the human cardiac model that capture the rare genotype to analyse their effects on the functionality of CMs. Since the original breakthrough papers from Shinya Yamanaka's laboratory reported the ability to convert the somatic cell lines into pluripotent stage using OSKM factors, several projects have been established to generate large bank of hiPSC lines across the globe, including the large scale banking schemes that have an ambitious of creating hiPSC lines from 7000 healthy or diseased skin biopsy donors using non-integrating reprogramming methodology, including Sendai-virus, Episomal and mRNA protocol (Takahashi and Yamanaka, 2006; Soares et al., 2014). Indeed, it has been proven that reprogramming procedure using non-integrating approaches converts the somatic cell lines to the pluripotent stage without alliterating their inherited genomic information (Takahashi and Yamanaka, 2016).

Several sources of somatic cells have been utilised to generate hiPSC, including fibroblasts, adult peripheral blood cells, mononuclear cells, exfoliated renal epithelial cells, and keratinocytes (Aasen et al., 2008; Okita et al., 2011; Loh et al., 2009; Zhou et al., 2012; Rajesh et al., 2011). Among them, the blood-derived somatic cells emerge as an easy access and non-invasive cell sources for hiPSC and biomedical research, as the B-cells, for example, can be easily isolated from patient blood test samples. The lymphoblast B-cells are the immature cells that can develop into mature lymphocytes and contain full inherited genetic information of the patient (Barreto et al., 2014) (Figure 4.1). It has been reported that extracted lymphoblast B-cells from as little as 0.5 mL blood is enough to transform them into lymphoblastoid cell lines using Epstein-Barr virus, which in turn, provide an unlimited proliferative source of cells for reprogramming (Rajesh et al., 2011).

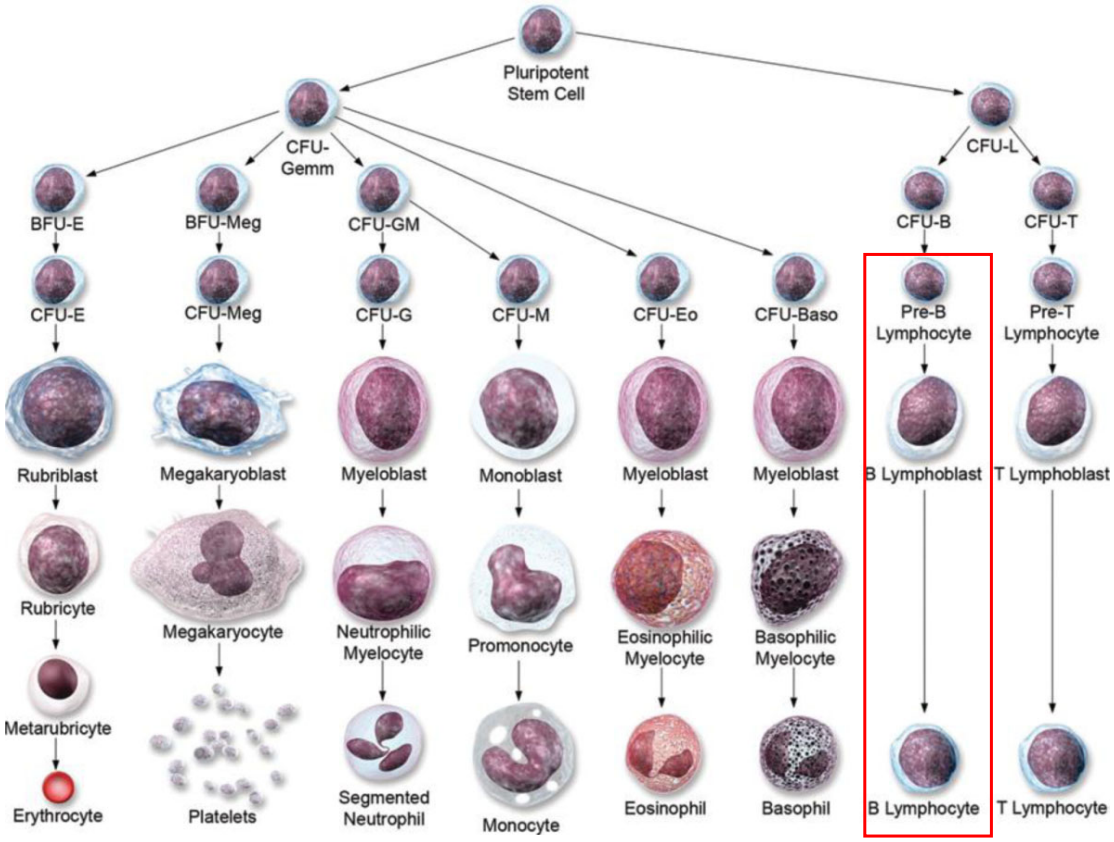


Figure 4.1: Lymphoblast B cell generation during developmental process from pluripotent stem cells to mature blood cells (Barreto et al., 2014). The red box indicates the developmental pathway that give rise to B-lymphoblast cells.

4.1.1 Lymphoblastoid cell lines (LCLs)

The ability to generate lymphoblastoid cell lines (LCLs) from lymphoblast B cells is one of the major contributions of biomedical research, which provides long lasting supply of somatic cells with matching genotypes as seen in patients. To establish LCLs, peripheral blood lymphocytes are infected with Epstein Barr virus (EBV) and have been proven to be able to immortalise human lymphoblast B cells (at resting stage) and convert them into proliferating B cell population (Neitzel, 1986). The technical procedures used to generate LCLs have not changed in the last three decades, which involved the delivery of EBV genes including Epstein Barr virus nuclear antigen (EBNA), and Simian virus 40 (SV40) large T antigen in the form of free EBV particles into the lymphoblast cells (Figure 4.2). The EBV particles gains entry to B lymphocytes via their CD21 cell surface molecules. Once inside the cells, the EBV remains in the episomal form which imparts least genetic changes and only a few viral genes are expressed causing minimal

change in the host genome (Amoli et al., 2008; Sie et al., 2009). Furthermore, it has been proven that the EBV episomal plasmids were lossed completely during reprogramming and the proliferation of newly established hiPSCs, eliminating the effects of viral plasmid expression in the host genome (Rajesh et al., 2011; Kumar et al., 2016).

4.1.2 Advantages of LCLs in biomedical research and disease modelling

There are several advantages of using LCLs in research and hiPSC reprogramming. It is relatively cost effective to generate and maintain LCL as compared to animal models owing to features like accelerated growth, minimal nutrient requirement, and ease of culture condition (Sie et al., 2009). In fact, it was reported that the reagent costs involved per sample were approximately £5 (Amoli et al., 2008). Moreover, the immortality feature of LCLs is the significant advantage for the use of this cell line in medical research and hiPSC technology as these cells confer the ability to grow indefinitely in culture. In terms of hiPSC reprogramming, LCLs exhibit added conveniences, including being easy to obtaining starting material (lymphocytes) in handy non-invasive way (blood test). Also, because a biological feature of LCL culture is suspension culture, these cells can be dissociated and re-plated easily by pipetting and transferring into new culture condition. As far as the accumulation of abnormal karyotype is concerned, the LCLs have been proven to maintain their chromosomal stability up to high population doublings in contrast to other transformed cell lines (Neitzel, 1986; Amoli et al., 2008; Hussain and Mulherkar, 2012). Lastly, due to its high proliferation rate and high purity, LCL culture can be increased in biomass easily and eliminated the risks of contamination from other cell lines, such as fibroblasts.

Interestingly, there is a globally genotyped cell bank that transforms human lymphoblast B cells obtained from blood test samples into LCLs and cryopreserves them for long term storage, called Coriell Biorepository in the USA (https://catalog.coriell.org). A screening survey of the Coriell database identified the LCLs bearing the GRK5-L41 polymorphism of interest, providing an excellent opportunity to gain an access to these cell lines as a reprogramming source to achieve the aim of the thesis.

Table 4.1: Overview of methods for reprogramming somatic cells to hiPSCs. OSKM is the common combinations of four key transcription factors required for reprogramming of somatic cells, including OCT4 (O), SOX2 (S), KLF-4 (K), and c-MYC/L-MYC (M); LIN28 (L); Valporic Acid (VPA); CHIR99021(CHIR); Pluripotin /SC1; Clustered regulatory interspaced short palindromic repeat sequence (CRISPR) interference – CRISPRi. Table was adapted from (Gonzalez et al., 2011; Robinton and Daley, 2012; Takahashi and Yamanaka, 2016).

Reprogramming Methods		Cell types	Factors	Efficiency (%)	Advantages	Disadvantages
Integrative	Retroviral	Fibroblasts, neural stem cells, liver cells, blood cells, and adipose cells	OSKM, OSK, OSK+VPA	0.001 – 1	Transgene-free and vector-free; average efficiency.	Randomly integrate into host genome; slow reprogramming process; incomplete silencing of transduced genes.
	Lentiviral	Fibroblasts	OSLN, OSKM	0.1 – 1.1	Transgene-free and vector-free; average efficiency; transduces both dividing and non-dividing cells	Randomly integrate into host genome
	Inducible lentiviral	Fibroblasts, blood cells, and melanocytes	OSKM or OSKMN	0.1 – 2	Average efficiency; allows controlled expression.	Randomly integrate into host genome; transactivator expression is required.
	LoxP-flanked lentiviral	Fibroblasts	OSKM	0.1	Average efficiency; excisable.	Potential risk of genomic integration; labour intensive screening of excised clones; *loxP* sites remained in the genome
	Transposon	Fibroblasts	OSKM	0.1 – 1	Average efficiency; excisable.	Potential risk of genomic integration; negative selection strongly advised and labour-intensive.
Non-integrative	Adenoviral	Fibroblasts and liver cells	OSKM	0.001	No genomic integration	Slow and inefficient
	Sendai Virus	Fibroblasts	OSKM	1	No genomic integration	Sequence-sensitive RNA replicase
	Episomal Plasmid	Fibroblasts and blood cells	OSKM, OSLN, OSKM + small molecules	0.1 – 2	No genomic integration, defined medium	Slow and inefficient
	Plasmids	Fibroblast	OSKM	0.001	Average efficiency	Potential risk of genome integration; low efficiency
	piggyBac Transposon	Fibroblasts	OSKM	0.1 – 1	Average efficiency; excisable.	Labour intensive and slow
DNA-free	Synthetic mRNA	Fibroblast	OSKM or OSKML+VPA	1 – 4.4	No genomic integration; bypasses innate antiviral responses; increase reprogramming speed; controllable and high efficiency	Difficulty in delivery mRNA; potential risks of reverse transcription and integration into host genome.

Reprogramming Methods		Cell types	Factors	Efficiency (%)	Advantages	Disadvantages
	microRNA	Adipose stromal cells and dermal fibroblasts	miR-200c, miR-302s, miR-369s, or miR-138	0.1	No genomic integration, faster reprogramming kinetics, no requirements of exogenous transcription factors.	Relatively low efficiency compare to other methods; difficulty in preparation of miRNA.
	Protein	Fibroblasts	OS	0.001	No genomic integration; faster reprogramming kinetics; direct delivery of reprogramming factors; average efficiency.	Protein preparation is labour intensive; difficulty in delivery; extremely low efficiency
Chemical induction	Small molecules	Fibroblasts	VPA, CHIR, PD0325901, A83-01, SC1	0.001	No genomic integration; transgene-free and vector-free; defined components	Extremely low efficiency; potential toxicity; activate wide range of molecular signalling pathways.
Modified gene editing	CRISPRi	HEK	O	NA	Overexpression of pluripotency factor (OCT4) using p300 chromatin regulator; No genomic integration; transgene free and viral-free.	No reports yet about reprogramming efficiency and generation of hiPSCs from this approach.

4.1.3 Strategy for generation of *GRK5*-Q41 and *GRK5*-L41 bearing hiPSCs

4.1.3.1 Reprogramming methods

Since the first establishment of the hiPSC line, a large contribution regarding the technology improvements and the potential clinical translations of hiPSCs significantly accelerated the maturation of the hiPSC fields and resulted in the first autologous transplantation of hiPSC-derived retinal cells in human (Mandai et al., 2017). However, in terms of the applications of hiPSCs in medical research and disease modelling, the first-generation methods of hiPSC using unfavourable approaches, such as retrovirus, and lentivirus becomes the primary limitations of the usability, especially in studying genetic modification and molecular mechanisms underlying inherited diseases in human (Table 4.1) (Picanco-Castro et al., 2010; Dick et al., 2011; Ohnuki et al., 2014). Indeed, the major drawback of these methods is the random integration of the OSKM factors into the host genome due to the nature of these viral delivery systems might compromise the gene expression machinery and regulation of the hiPSCs and result in incomplete silencing of the transgenes (Takahashi and Yamanaka, 2016).

A major milestone in the field is the establishment of integration-free reprogramming methods, that allow converting the somatic cell lines to the pluripotent stages without the needs of transgene integration in the host genome, including adenovirus (Stadtfeld et al., 2008), episomal plasmid (Yu et al., 2009; Okita et al., 2011), *piggyBac* transposon (Yusa et al., 2009; Woltjen et al., 2009), Sendai virus (Fusaki et al., 2009), synthetic mRNA (Warren et al., 2010), recombinant proteins (Kim et al., 2009), and small molecules (Hou et al., 2013). Recently, episomal plasmids and Sendai viruses emerge as the most widely use methods for inducing the reprogramming process due to their simple to perform, efficient, consistent, and cost-effective, especially the episomal approach (Takahashi and Yamanaka, 2016). Additionally, since 2009, the xeno-free and serum-free defined culture medium have been introduced and proven to be effective in maintaining hPSCs *in vitro*, providing an opportunity for the generation of hiPSC lines in a defined culture condition.

4.1.3.2 Episomal reprogramming approach

As an alternative to integration-defective viruses, the transient transfection of episomal plasmid emerges as a method of choice to convert somatic cell lines into pluripotency state. The advantages of the method lie in the fact that it is relatively simple to implement into the lab, requires only standard molecular biology experience, and reduces the time-consuming production of viral particles (Gonzalez et al., 2011). Despite the biological safety concern, episomal vectors had been proven as a non-integration method which reduced the potential risk of carcinogenesis significantly due to potential activation of the oncogenes such as *KLF4* and *c-MYC,* or insertional mutagenesis (Jia et al., 2010). However, in the first generation of episomal plasmid, the potential problem was its non-replicating functions leading to low transfection efficiency and multiple transfections of the target cells being required (Okita et al., 2011). This observation could be explained by the fact that transfection efficiency of large polycistronic plasmids was low, and they could also potentially trigger the transgene silencing mechanism of the host cells, especially in mammalian systems (Gonzalez et al., 2009).

The limitation was overcome by using the Epstein-Barr virus (EBV) reprogramming technology, which utilised the EBV-encoded nuclear antigen-1 (EBNA-1) *trans*-acting element and EBV-encoded oriP *cis*-acting element to enable plasmids to persist by dividing within human cells as multiple episomal copies (Hung et al., 2001). The high transfection efficiency of episomal plasmid derived from the nuclear import signal of oriP/EBNA-1 and retention of vector DNA. Unlike the traditional system, the oriP/EBNA-1 allowed the system to be replicated within the host cells by anchoring itself to the host chromatin. It displayed a natural loss at the rate of 5% per cell cycle due to defect in vector synthesis and partitioning, allowing the removal of episomal vectors from the hiPSCs without any additional manipulation (Yu et al., 2009; Okita et al., 2011).

Since the first establishment of hiPSCs, many thousands of hiPSC lines have been created all over the globe; and the criteria for determination of hiPSCs have also been described (Denning et al., 2016). According to the International Stem Cell Initiative Consortium, a set of minimal criteria was defined to determine the pluripotent features

of newly established hiPSCs, and to ensure the availability of high-quality hiPSC lines (Akopian et al., 2010). These include: **(1)** hiPSC-like morphology (growth as colonies with defined borders, prominent nuclei and high nuclear-cytoplasmic ratio); **(2)** ability to prolonged culture *in-vitro*, usually known as self-renewal capacity; **(3)** expression of nuclear pluripotency markers, including OCT4, SOX2, NANOG; **(4)** presence of surface pluripotency markers, including SSEA4, TRA-1-81, and low expression of differentiated marker, SSEA1; **(5)** ability to differentiate into all three germ layers *in vitro* and teratoma formation *in vivo;* and **(6)** silencing or loss of exogenous reprogramming factors. Additionally, toward the aim of the study, any hiPSC lines created need to be successfully differentiated into cardiomyocytes at high differentiation efficiency compatible with the high efficiency cardiac induction protocols developed in Chapter 3.

4.1.4 Chapter Aims

The aims of this chapter were to identify appropriate LCLs that contain polymorphic variants at amino acid position 41 of the GRK5 peptide (L41 or Q41), and use episomal reprogramming to generate hiPSCs. Subsequently, the aim was to provide a resource for cardiomyocytes, in order to give mechanistic insights into the putative functions of the GRK5 polymorphism (GRK5-L41) of interest. Hence, to achieve the aim, several objectives were established, including:

1. Confirmation of the *GRK5* polymorphism presents in the lymphoblastoid cell lines obtained from Coriell Cell Bank.
2. Establishment of episomal reprogramming platform using HUES7-derived fibroblasts (H-Fib) as testing cell source.
3. Establishment and characterisation of hiPSC lines derived from lymphoblastoid cells using episomal reprogramming approach.
4. Differentiation of newly established hiPSC lines into cardiomyocyte using monolayer differentiation method described in Chapter 3.
5. Cardiomyocyte characterisation using immunocytochemistry and flow cytometry.

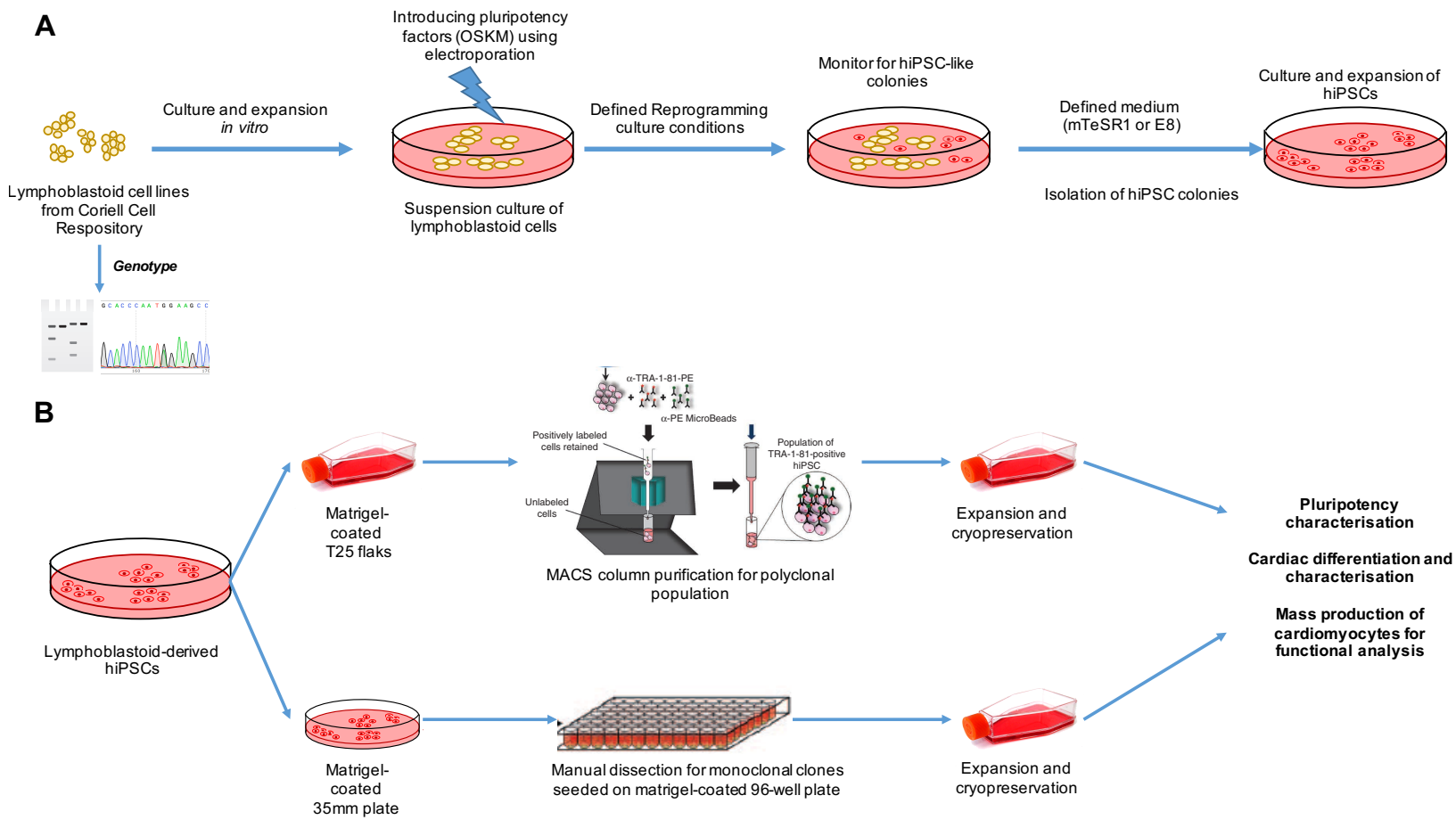


Figure 4.2: Overview of chapter's strategy. (A) The schematic shows an overview of this chapter, in which, the aims were to reprogram lymphoblastoid cells obtained from Coriell Biorepository using episomal reprogramming approach. Before conducting the reprogramming experiment, lymphoblastoid cells were genotyped to confirm the *GRK5* variants (Q41 or L41) and *ADRB2* SNP at amino acid position 16 and 27. The episomal plasmids containing OSKM factors were introduced into the lymphoblastoid cells using electroporation. **(B)** Strategy for generation of polyclonal hiPSCs and monoclonal hiPSCs. hiPSC-like colonies from the pool were either re-plated on Matrigel-coated T25 flaks or 35 mm culture plates, for MACS column purification of polyclonal population or manual dissection for monoclonal clones, respectively. These clones were further expanded and cryopreserved from p2 to p10, followed by pluripotency characterisation, cardiac differentiation and cardiomyocyte characterisation.

4.2 Results

4.2.1 Genotypic confirmation of lymphoblastoid cell lines

The available resource of lymphoblastoid cell lines harbouring the *GRK5* polymorphism of interest (GRK5-L41) encouraged us to start obtained seven lines from the Coriell Biorepository and validated the genotypes before starting further experiments. Although the cell lines obtained from Coriell have been confirmed by sequencing and provided from Coriell database, other researchers in the lab had identified the genotyping errors in cells ordered from this supplier. Therefore, the first task was to verify the genotypes from four cell lines received from Coriell, including the GRK5-L41 variants (termed Lymp-GRK5-L41, and Lymp-GRK5-L41a), and GRK5-Q41 (called Lymp-GRK5-Q41, and Lymp-GRK5-Q41a).

4.2.1.1 Verification of GRK5 variants

To confirm the *GRK5* sequence, the SNP-specific primer pairs, including GRK5-Q and GRK5-L, were designed to amplify either *GRK5* Q41 (C**A**G, at the nucleic acid position 122) or *GRK5* L41 (C**T**G, at the nucleic acid position 122) sequence, respectively. To accurately detect the target GRK5's SNP, the forward primer of both GRK5-Q and GRK5-L contain the SNP-specific sequence, Q41 (Cg**A**) and L (Cg**T**), respectively, at the end of the primer together with the guanine (G, illustrated as g) instead of Cytosine (C) (Figure 4.4A). The combination of g**A** and g**T** at the end of the primer allows a firm anchor to the template if the SNP sequence matches followed a successful PCR amplification. If the SNP sequence is not correct, the primer has one end not complementarily bind to the template, which, in turn, prevent the PCR amplification to occur. Based on this principle, the results indicated that the *GRK5*-Q primer pair amplified the 223 bp product successfully from DNA samples derived from Lymp-GRK5-Q41 and Lymp-GRK5-Q41a but not in the GRK5-L41 lymphoblastoid lines, while the *GRK5*-L primer pair only generated the 223 bp band from Lymp-GRK5-L41 and Lymp-GRK5-L41a (Figure 4.4B&C).

A

Genes	Primer Name	SNP recognition	Strand	Sequence (5' to 3')	Amplicon size (bp)
GRK5	***GRK5*-Q**	Q41	Fwd	CTGAAGTTCCCTCACA TTAG Cg**A**	223
			Rev	GCAAAAAGGTCAGCCTGGAG	223
	***GRK5*-L**	L41	Fwd	CTGAAGTTCCCTCACA TTAG Cg**T**	223
			Rev	GCAAAAAGGTCAGCCTGGAG	223

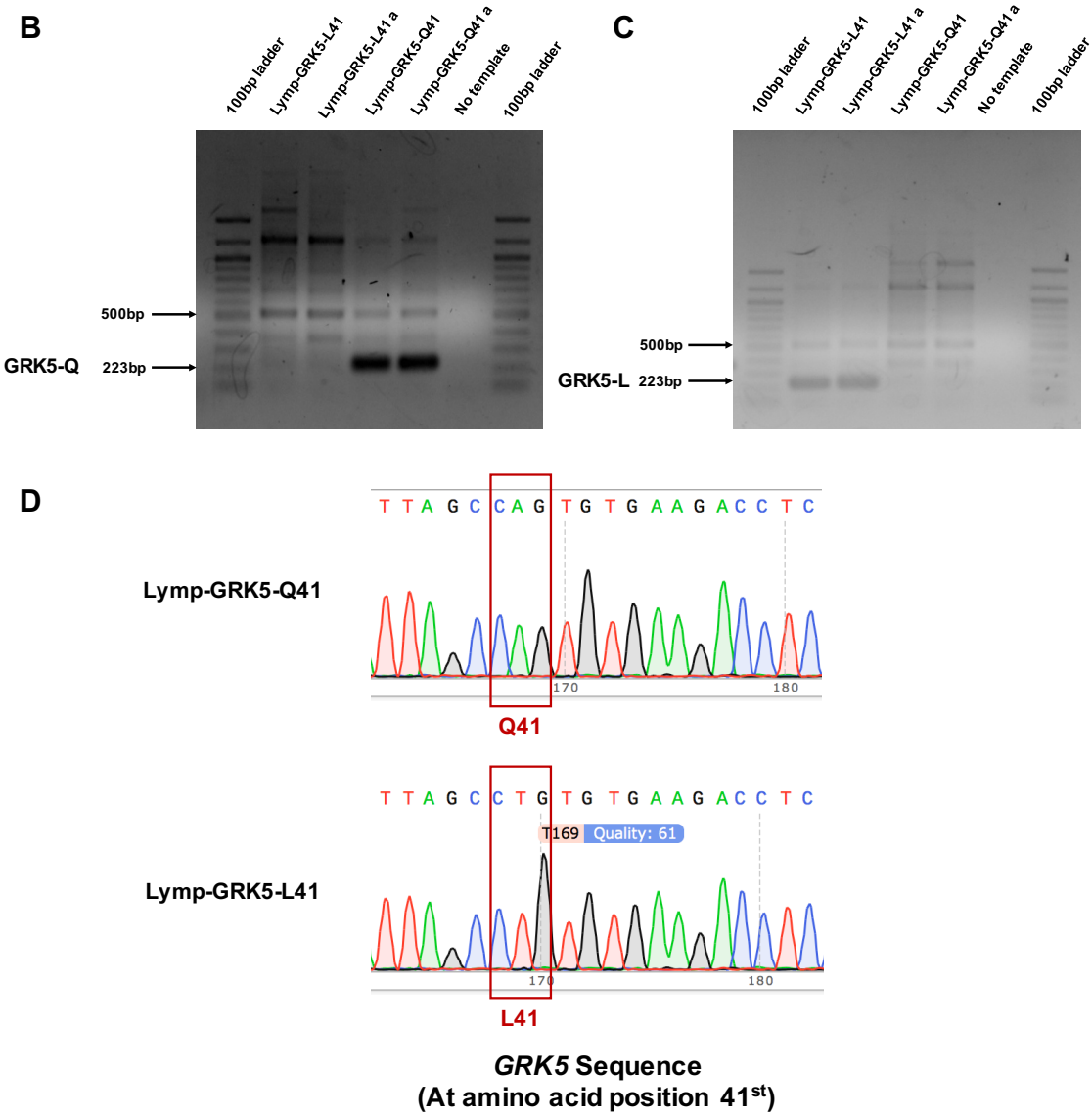


Figure 4.3: Confirmation of *GRK5* Q41L SNP in lymphoblastoid cell lines. (A) The *GRK5* SNP was confirmed using two SNP specific primer pairs, which recognised either *GRK5* Q41 (C**A**G variant) or *GRK5* L41 (C**T**G variant). **(B)** Gel analysis of PCR products amplified using *GRK5* Q41 primer pairs showed a 223 bp band from genomic DNA extracted from only two of the four lymphoblastoid cell lines (Lymp-GRK5-Q41 and Lymp-GRK5-Q41 a). **(C)** Gel analysis of PCR product amplified using *GRK5* L41 primer pairs showed a band at 223bp from genomic DNA extracted from the other two lymphoblastoid cell lines (Lymp-GRK5-L41 and Lymp-GRK5-L41 a). **(D)** Sequencing results of *GRK5* at nucleic acid position 122 confirmed the presence of *GRK5* L41 (C**T**G) and *GRK5* Q41 (C**A**G) in Lymp-GRK5-L41 and Lymp-GRK5-Q41, respectively. The red box indicates the codon triplet encoding for amino acid at position 41 of GRK5.

To strengthen the results, amplicons obtained from each cell lines were sent for DNA sequencing using the PCR primers spanning the amino acid position 41 of *GRK5*. Predictably, the sequencing data confirmed that the nucleotide position 122 in *GRK5* obtained from Lymp-GRK5-Q41 and Lymp-GRK5-Q41a was C**A**G, and from Lymp-GRK5-L41 and Lymp-GRK5-L41a was C**T**G (Figure 4.4D). Hence, these results illustrated that the SNP-specific primer pairs were efficient to detect the presence of the GRK5-L41 polymorphism in the lymphoblastoid cell lines and confirmed the *GRK5* sequence of all tested lymphoblastoid cell lines was correct as shown in Coriell database. Therefore, two lines were selected for further experiments, including Lymp-GRK5-Q41 and Lymp-GRK5-L41.

4.2.1.2 Verification of adrenergic receptor variants

The canonical functions of GRK5 in cardiac muscle are involved in the desensitisation of catecholamine-mediated adrenergic receptors, especially β_1 (ADRB1) and β_1 (*ADRB2*). Indeed, the β_1 receptors are the most important receptors in the heart, which regulate acutely minute-by-minute cardiac output in response to neuronal stimulation. The two most relevant SNPs found in *ADRB1* are the 49(S/Q) variant and the 389(R/G) variant. The major functions of β_2 are involved in promoting vasodilation and cardiac protective functions during heart failure, and two SNPs were also reported to play a significant role in the regulation of β_2 functions including 16(G/R) and 27(E/Q) (Table 4.2). Hence, it is important to identify these particular SNPs in the lymphoblastoid cells.

Table 4.2: Polymorphisms of human β_1 (*ADRB1*), β_2 (*ADRB2*), and *GRK5*. Abbreviation: NS, nonsynonymous; Ref, reference; Var, Variant; AA, Amino acid

Gene Name	dbSNP	SNP type	Allele Variability (Ref/Var)Position	AA Variability (Ref/Var)Codon	Reference
ADRB1	rs1801252	Coding NS	(A/G) 145	(S/G) 49	Levin et al., 2002
	rs1801253	Coding NS	(G/C) 1165	(G/R) 389	Rathz et al., 2002
ADRB2	rs1042713	Coding NS	(G/A) 46	(G/R) 16	Green et al., 1994
	rs1042714	Coding NS	(G/C) 79	(E/Q) 27	Turki et al., 1995

Gene Name	dbSNP	SNP type	Allele Variability (Ref/Var)Position	AA Variability (Ref/Var)Codon	Reference
GRK5	rs2230345	Coding NS	(A/T) 122	(Q/T) 41	Liggett et al., 2008

Table 4.3: The list of primers used for amplify the DNA sequences spanning the polymorphisms of *ADRB1*, *ADRB2*, and *GRK5*.

Targeted Gene	Polymorphism (Codon)	Strand	Sequence (5' to 3')
ADRB1	49	Fwd	CCGGGCTTCTGGGGTGTTCC
		Rev	GGCGAGGTGATGGCGAGGTAGC
	389	Fwd	CGCTCTGCTGGCTGCCCTTCTTCC
		Rev	TGGGCTTCGAGTTCACCTGCTATC
ADRB2	16 and 27	Fwd	GCTGAGTGTGCAGGACGAGT
		Rev	ATGGCAAAGTAGCGATCCAC
GRK5	41	Fwd	AGCGCAAAGGGAAAAGCAAG
		Rev	ACTGACATCCCCAGCAAGTG

To accomplish the task, the PCR primers spanning the above-mentioned polymorphisms of β_1, β_2, and GRK5 were designed as described in Table 4.3. The amplicons from the PCR reaction were then sent for DNA sequencing. The results indicated that the Lymp-GRK5-Q41 harbours wild-type *ADRB1* at amino acid position 49 and 398, whereas Lymp-GRK5-L41 possesses heterozygous alleles at these positions (Figure 4.5A). Additionally, both cell lines have similar *ADRB2*'s SNP sequences, which are heterozygous R/G at position 16 and Q at position 27 (Figure 4.5B). The details of adrenergic polymorphisms present in both cell lines were shown in Table 4.4.

Table 4.4: Summary of polymorphic variants of *ADRB1*, *ADRB2*, and *GRK5* present in Lymp-GRK5-Q41, and Lymp-GRK5-L41.

Gene	*ADRB1*		*ADRB2*		*GRK5*
Codon	**49**	**398**	**16**	**27**	**41**
Lymp-GRK5-Q41	**S**49	**G**389	**R/G**16	**Q**27	**Q**41
Lymp-GRK5-L41	**S/G**49	**G/R**389	**R/G**16	**Q**27	**L**41

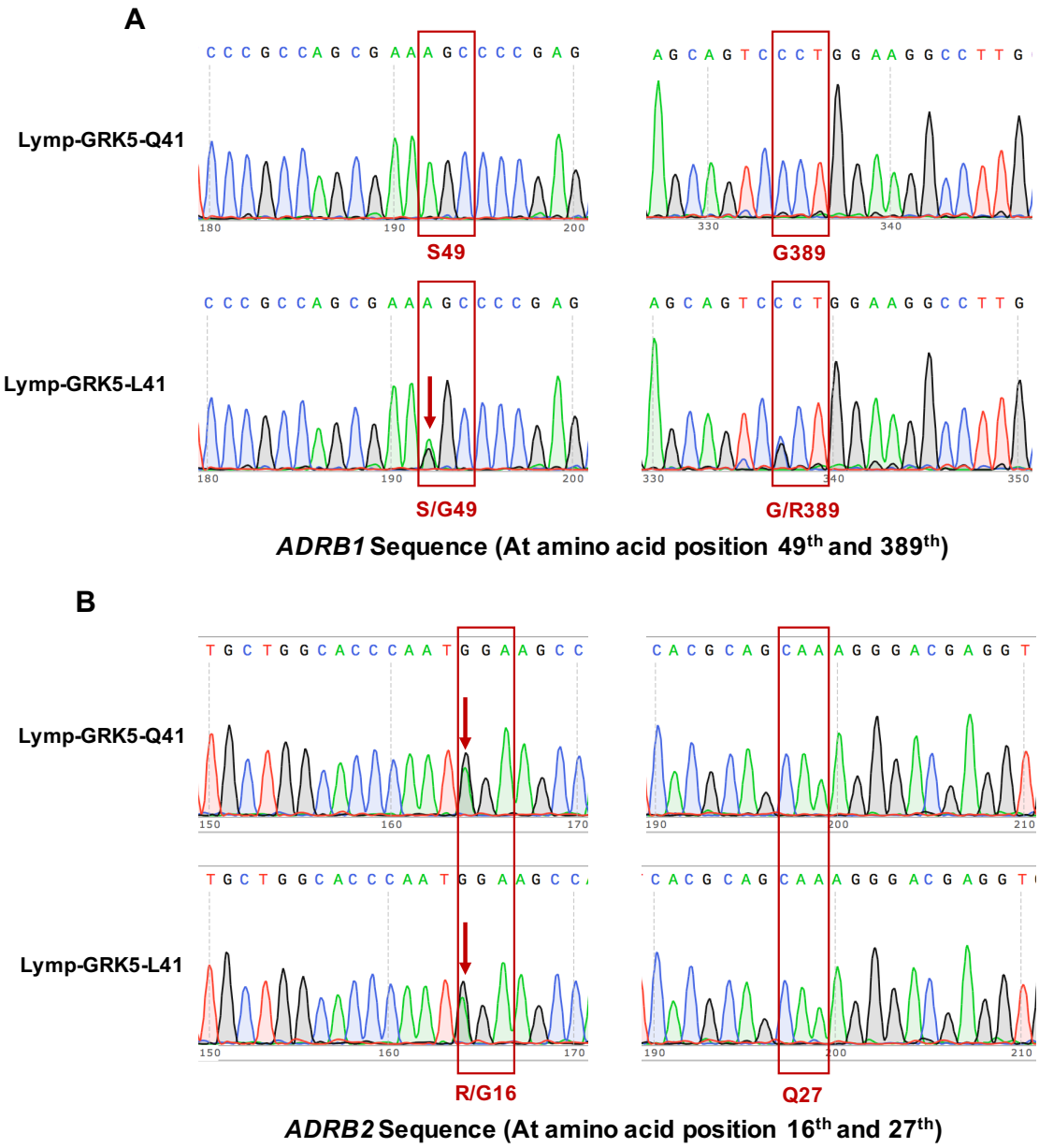


Figure 4.4: Confirmation of polymorphic variants of *ADRB1* and *ADRB2* in Lymp-GRK5-Q41 and Lymp-GRK5-L41. (A) The chromatograms from DNA sequencing results indicate the presence of wild-type sequence of *ADRB1* at both amino acid position 49 and 389 in Lymp-GRK5-Q41, whereas heterozygous variants at these positions were seen in Lymp-GRK5-L41. **(B)** The chromatograms illustrate the *ADRB2* polymorphism sequence at position 16 and 27, both cell lines have heterozygous R/G at the position 16 and homozygous Q at amino acid 27.

4.2.2 Reprogramming lymphoblastoid cells using lentiviral approach

As previously reported, a novel lentivirus reprogramming protocol was developed in our lab (Dick et al., 2011). The method was optimised for adherent culture, especially for human fibroblasts. Our initial attempts on reprogramming lymphoblastoid cells utilized

this lentiviral approach (courtesy of Dr. Tony Melarangi). However, they were unsuccessful, possibly because the lymphoblastoid cells were grown as suspension cultures, in which the surface-to-volume ratio of the cells was too low for an efficient binding during the reprogramming procedure that was optimised for adherent cultures.

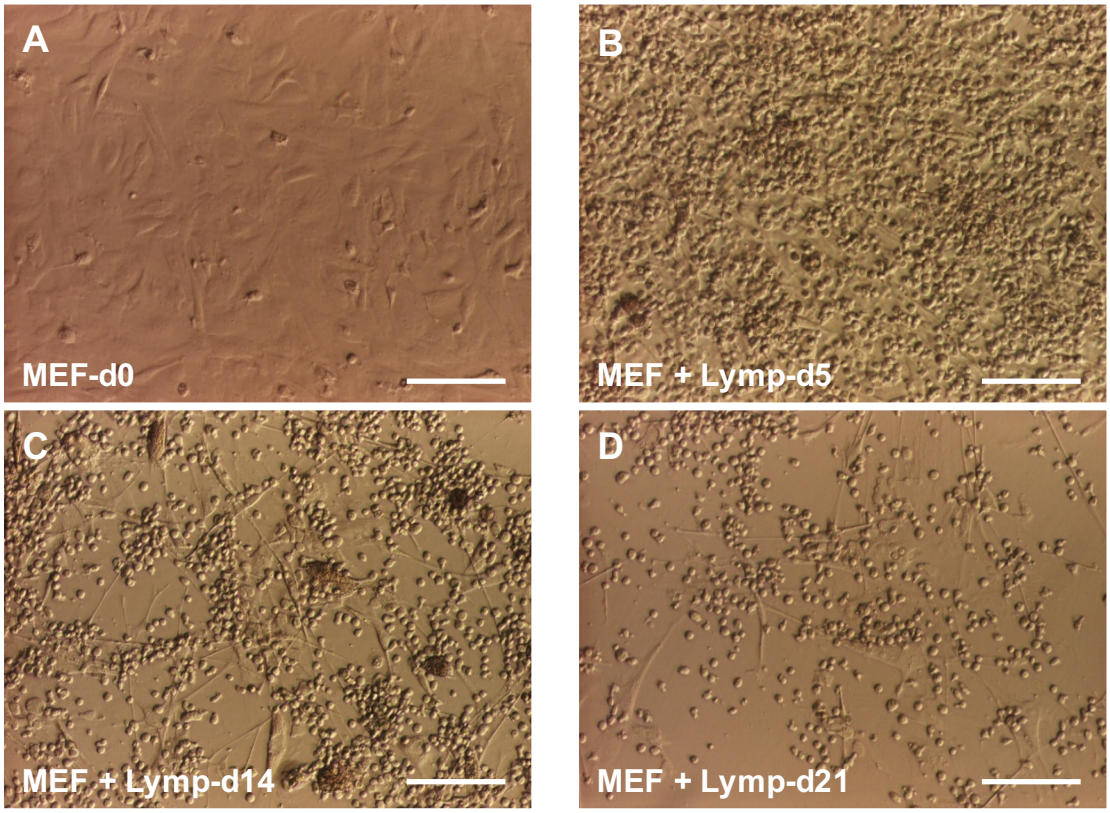


Figure 4.5: Transduced lymphoblastoid cells using lentivirus on MEF feeder layer. (A) Elongated and spindle morphology of MEF on d0 before co-culture with transduced lymphoblastoid cells. **(B)** Representative bright field image of transduced lymphoblastoid cells (rounded morphology) seeded on MEF-feeder layer 5-day post-transduction. **(C)** A bright field image illustrates the reduction in cell density of MEF after 14-day post-transduction. **(D)** After 21 days, significant reduction in cell density of MEF was observed, no sign of partially reprogrammed colonies appeared. Scale bar: 100μm.

To overcome these problems of poor transduction efficiencies, lymphoblast cultures were centrifuged with lentivirus-conjugated particles, followed by seeding these cells onto an MEF-feeder layer. However, it was observed that the transduced lymphoblastoid cells started to adhere and kill the MEF-feeder (Figure 4.6). Two weeks post-transduction, the density of the MEF-feeder reduced dramatically (Figure 4.6C); and after three weeks, an entire layer of the MEF-feeder was destroyed leaving behind only lymphoblastoid cell lines (Figure 4.6D). No sign of partially reprogramming colonies was

observed. These results showed that the lentiviral reprogramming approach was not suitable for reprogramming lymphoblastoid cell lines (Figure 4.6D).

4.2.3 Establishment and characterisation of hiPSCs from HUES7-derived fibroblast (H-Fibs) using Episomal plasmids

4.2.3.1 Evaluation of episomal reprogramming method

Although episomal plasmid approach had been widely used to generate hiPSCs from somatic cell lines, it was important to evaluate the reprogramming efficiency of the episomal plasmids and adapt the procedure to our lab standard. Therefore, the HUES7-derived fibroblast line (H-Fibs), previously generated in the lab, was used to evaluate the episomal plasmid sets derived from Thomson's Lab. The plasmid set containing three independent vectors were first delivered to the fibroblasts using FuGENE HD transfection reagent. The transfection efficiency measured using GFP plasmid showed only 8% ± 0.6% (mean ± SEM, n=2) (Figure 4.7A). Surprisingly, albeit the poor delivery efficient, the transfected H-Fibs began to change their morphologies from d6 post-transfection followed the appearance of partially reprogrammed colonies (Figure 4.7B). By d15, hiPSC-like colonies started to emerge with defined border and eventually gave rise to the formation of hiPSC from d25 to d30 (Figure 4.6B).

To isolate the hiPSCs from the non-reprogrammed cells and partially reprogrammed population, MACS column purification was applied using a late surface pluripotency marker (TRA-1-81 PE-conjugated antibody) as described previously (Dick et al., 2011). Under magnetic fields, the TRA-1-81 positive cells were collected by treating the cells with Anti-PE magnetic beads, which were eventually trapped in the column. The purified cells were eluted using a syringe and then maintained in MEF-CM media, supplemented with 10 ng/ml of bFGF to support their pluripotent nature. These H-Fib-hiPSC cells displayed typical hiPSC morphologies such as growing as colonies with defined border, large nuclei, high nucleus-to-cytoplasm ratio and able to proliferate *in vitro*.

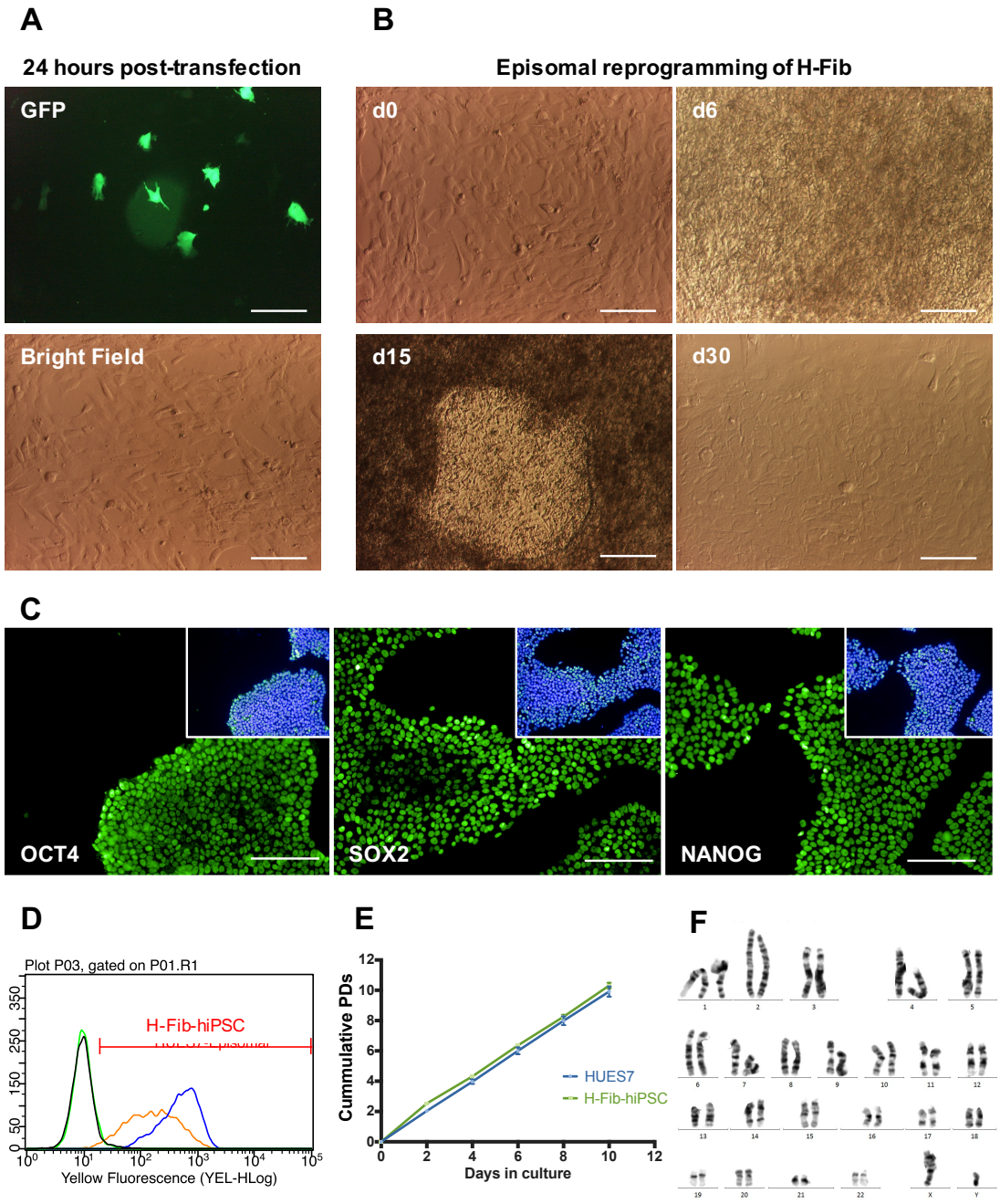


Figure 4.6: Episomal reprogramming of HUES7-derived fibroblasts (H-Fib) and pluripotency characterisation. (A) Transfection efficiency of H-Fib with GFP plasmid using FuGene HD transfection reagent, only 8% ± 0.6% (Mean ± SEM, n=2) of the cell population expressed GFP. **(B)** Representative bright field images of H-Fib during episomal reprogramming procedure at d0, d6, d15 and d30 post-transfection. Morphological changes were observed on d6, partially reprogrammed colonies appear on d15 and H-Fib-hiPSC line was established on d30 after MACS column purification. **(C)** Representative images of H-Fib-hiPSC colonies after immunostaining for the nuclear pluripotency markers OCT4, SOX2, and NANOG. The merged images additionally include a DAPI staining confirming the localisation of these markers in the nuclei of the cells. Scale bar: 100μm. **(D)** Flow cytometry analysis of surface pluripotency markers – SSEA4 (95% ± 0.8%, mean ± SEM, n=3, Blue) and TRA-1-81 (96% ± 0.4%, mean ± SEM, n=3, Orange) confirmed the expression of these markers in H-Fib-hiPSC. Differentiation marker (SSEA1) and unstained samples were used as negative control. **(E)** Growth curves for HUES7 and H-Fib-hiPSC illustrate the population doubling (PD) time of 23.8 ± 4.6 hours and 24.8 ± 4 hours, respectively (both mean ± SEM, n=3). **(F)** Representative karyogram of a metaphase spread (n=30) for H-Fib-hiPSC at passage 30, illustrating a normal 46 XY karyotype.

4.2.3.2 Pluripotency characterisation of the hiPSC obtained from H-Fibs (the H-Fib-hiPSC)

A successful isolation of the hiPSCs derived from H-Fib allowed performing the pluripotency check to confirm the stemness of these newly generated hiPSCs, termed the H-Fibs-hiPSC. To evaluate the pluripotency characteristics of the stem cell lines, a set of assays was performed, including growth curve, immunostaining of pluripotent-associated transcription factors (OCT4, SOX2, and NANOG), flow cytometry analysis for surface markers (SSEA-4, and TRA-1-81), and karyotype analysis after prolonged culture *in vitro* (from p15 to p25).

The immunostaining results showed that the H-Fib-hiPSC expressed all pluripotency transcription factors, and these transcription factors were localised in the nuclei of the cells (Figure 4.7C). Furthermore, the flow cytometry results confirmed that 96% ± 3% and 98% ± 2% of the population were highly expressing TRA-1-81 and SSEA4 respectively (both mean ± SEM, n=3). The results were negative for differentiation marker SSEA1 (<5%) (Figure 4.7D). To estimate the growth rate of the H-Fib-hiPSC, a growth curve was calculated during five serial passages as described previously (Denning et al., 2006). The results showed that there was no significant difference in terms of population doubling time between HUES7 and H-Fib-hiPSC (24.8 ± 4 hours and 23.8 ± 4.6 hours, respectively, both mean ± SEM, n=3, $P<0.05$, One-way ANOVA test) (Figure 4.6E). On karyotype analysis for 30 metaphase spreads using G-banding, H-Fib-hiPSC exhibited ordinary 46 XY karyotype between passages 15 to 30 similar to the parental line (HUES7), confirming that these cells maintained normal karyotype during *in vitro* culture. This result ruled out any possibility of gross chromosomal abnormalities (Figure 4.6F).

These results illustrated that H-Fib, as a readily reprogrammable source of cells, could be successfully converted using episomal reprogramming plasmid set to hiPSCs with demonstrated pluripotent characteristics. This data provided a promising evidence of this technology's viability, and that it was worth to be explored further for more

challenging cell types like EBV-immortalised patient-derived adult lymphoblastoid cells in suspension culture.

4.2.4 Reprogramming of lymphoblastoid cell lines using Thomson's plasmid set

The establishment of H-Fibs-hiPSCs using episomal approach provided substantial evidence about the efficiency of the protocol, allowed us to start the process in lymphoblastoid cell lines. However, the electroporation was used to deliver the vectors into the cells as it has been proven to be more effective in suspension culture (Rajesh et al., 2011). Hence, the AMAXA electroporation system using Lonza Nucleo Kit V and programme X-005 was employed. The results showed that 67% ± 2% and 58% ± 3% of Lymp-GRK5-Q41 and Lymp-GRK5-L41 were GFP positive, respectively, indicating the high efficiency of the electroporation procedure (both mean ± SEM, n=2) (Figure 4.7B). Following the established protocol (Rajesh et al., 2011), the process was summarised in Figure 4.8. Of note, a modification in the protocol was made that two concentrations of episomal plasmid set were applied including 4 μM and 10 μM.

A day after electroporation, the lymphoblastoid lines maintained as suspension culture, and no sign of adherent cells was observed (Figure 4.9 a-f). Of note, cell death was observed as single floating cells in culture after 24h post-electroporation followed significant cell loss on d5 (Figure 4.9 g-h). The medium was changed to RM, and floating clumps of the lymphoblastoid cell and culture debris were removed proportionally during the medium change. After days 14, a majority of lymphoblastoid cells disappeared in the culture, and a few partially reprogramming colonies emerged but showed no sign of proliferation (Figure 4.9 k-n). Both concentrations of the plasmid set illustrated the same results, indicating that the combination of episomal plasmid set with small molecule cocktail was not efficient enough to convert lymphoblastoid cells into the pluripotent stage. Therefore, after days 14 cultured in RM, the cultures were terminated as the cells did not proliferate further, and their morphologies did not change from d5 to d14, suggesting that these partially reprogrammed cells would not develop into hiPSC.

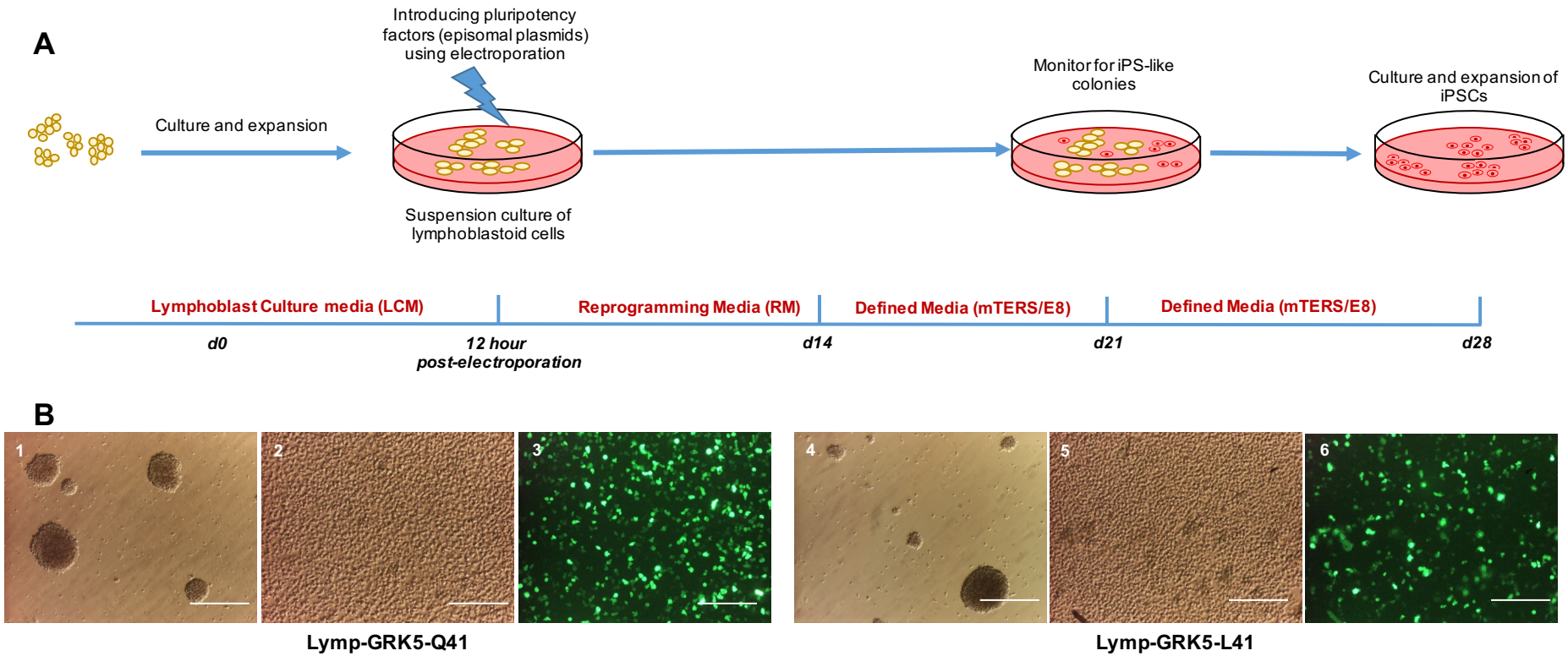


Figure 4.7: Defined episomal reprogramming of lymphoblastoid cell lines. (A) The schematic diagram shows the major points and related media used during the reprogramming process. On d0, $1x10^6$ lymphoblastoid cells were electroporated with episomal reprogramming plasmids, seeded in 35mm Matrigel-coated culture dishes and maintained in lymphoblast culture media (LCM) for 12 hours before switching to reprogramming media (RM). From d14 onward, media was switched from RM to mTeSR1 and the culture was screened every day to monitor the appearance of hiPSC-liked colonies. **(B)** Representative images of lymphoblastoid cell lines: Lymp-GRK5-Q41 and Lymp-GRK5-L41 grew as suspension culture (B1 and B4, respectively). Optimisation of Amaxa electroporation system using Nucleofector Kit V (Lonza) to introduce GFP plasmid to Lymp-GRK5-Q41 and Lymp-GRK5-L41 cell lines. Both Lymp-GRK5-Q41 (67% ± 2%, mean ± SEM, n=2; bright field and GFP images – B2 and B3, respectively) and Lymp-GRK5-L41 (58% ± 3%, mean ± SEM, n=2; bright field and GFP images - B5 and B6, respectively) showed the highest electroporation efficiency when programme X-005 was used. Scale bar: 100 μm.

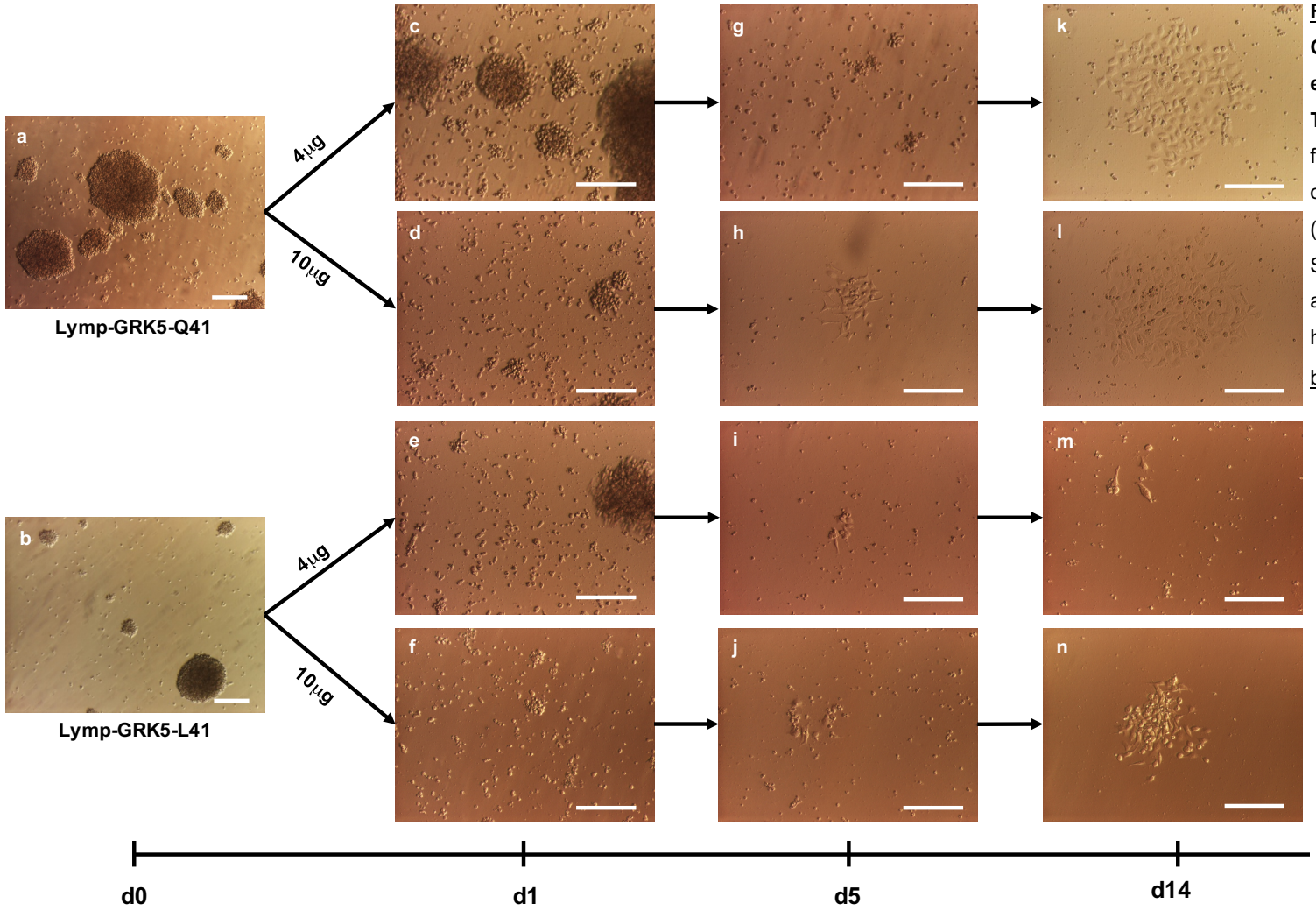


Figure 4.8: Reprogramming of Lymp-GRK5-Q41 and Lymp-GRK5-L41 using episomal plasmid set derived from Thomson's Lab. Representative bright field images of lymphoblastoid cell lines on d1 (**c,d,e,f**), d5 (**g,h,i,j**) and d14 (**k,l,m,n**) during reprogramming process. Significant cell loss was observed from d5 and culture was terminated on d14. No hiPSC-like cells were observed. Scale bar: 100 μm.

As the attempt to reprogram lymphoblastoid cells using Thomson's plasmid set was not successful, it led to the investigation of other approaches. An alternative episomal plasmid set derived from Yamanaka's Lab was identified as a possible replacement for the Thomson's plasmid set. The reprogramming experiments were repeated with Yamanaka's episomal reprogramming plasmids, and a small modification was made to the RM, in which LIF was removed because it was reported that LIF was not required for human reprogramming process (Yu et al., 2011).

4.2.5 Reprogramming experiments using episomal reprogramming plasmids derived from Yamanaka's Lab

The reprogramming procedure was repeated using the alternative Yamanaka's plasmid set, and the same electroporation set up showed a relatively similar efficiency, approximately 65% observed in both concentrations of the plasmids (4 μg and 10 μg). 24h after electroporation, the cells were maintained as single cell suspension with no sign of cell death (Figure 4.10, A1-3, B1-3). Interestingly, significant morphological transformations of both cell lines were detected in both tested plasmid concentrations. The cells switched from suspension culture and had rounded morphology, began to attach to the culture surface and displayed spindle and elongated morphology (Figure 4.10, A4-5, B4-5). These cells proliferated rapidly and changed into fibroblast-like cells forming large colonies, suggesting that the partially reprogramming process occurred from d5 to d14. These results provided the basis for proceeding to the next step of the protocol, where the medium was then switched to chemically defined media (mTeSR).

After three days in mTeSR1 medium (d18 post-electroporation), due to high proliferation rate of the partially reprogrammed cells, the cultures were split into two independent culture platforms: T25-Matrigel coated flasks for MACS column purification generating polyclonal clones, and 35mm-Matrigel coated plates for manual dissection of single clones to establish clonal hiPSCs. On d20 post-electroporation, hiPSC-like colonies started to appear (Figure 4.9, A8-9, B8-9).

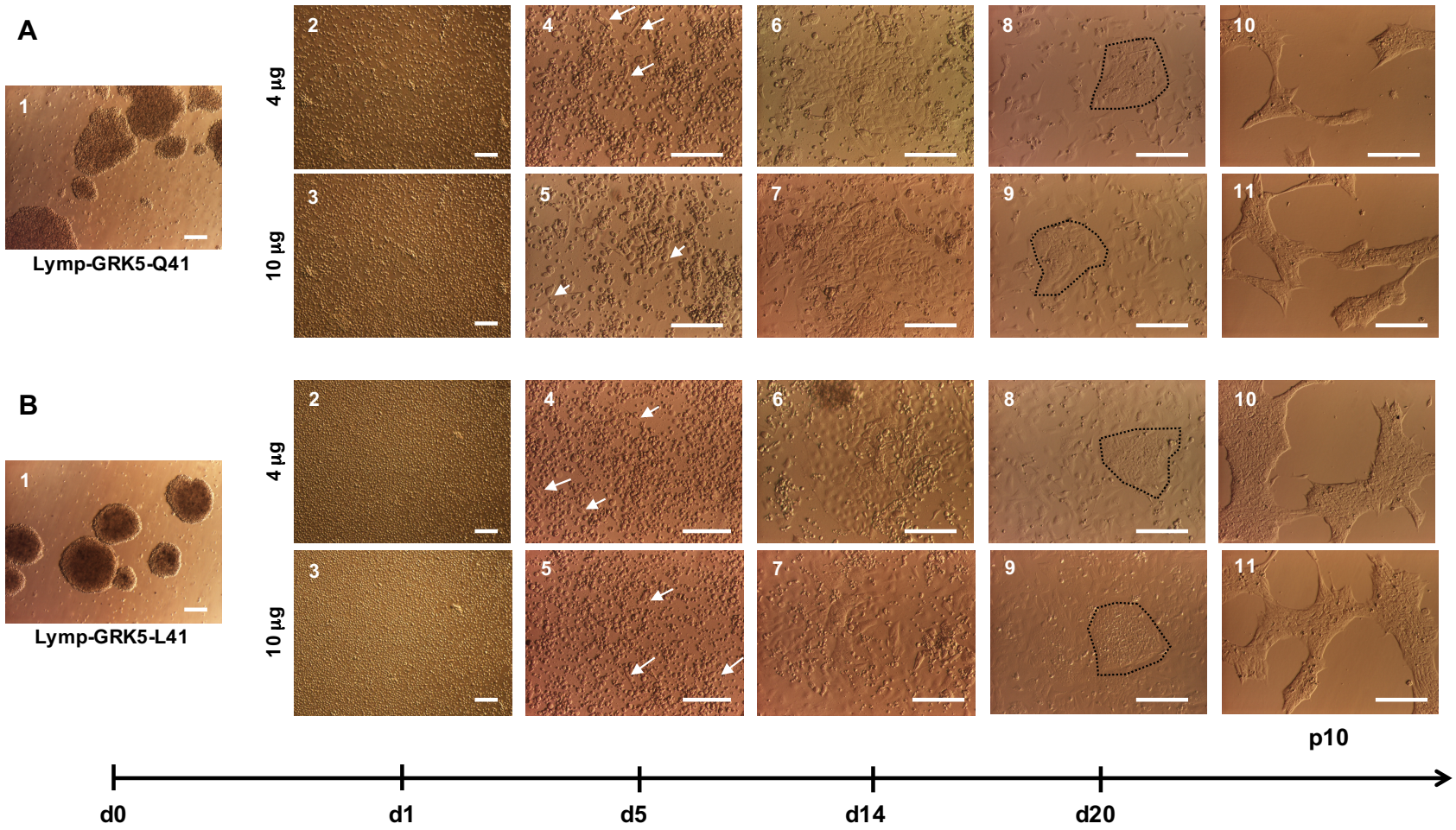


Figure 4.9: Reprogramming of lymphoblastoid cell lines (Lymp-GRK5-Q41 – A – and Lymp-GRK5-L41 – B) using episomal plasmid set derived from Yamanaka's Lab. Representative bright field images of Lymphoblastoid cells before starting reprogramming (1), on d1 post electroporation (2&3), on d5 (4&5), d14 (6&7), d20 (8&9) and at passage 10 (10 & 11). Significant morphology changes were observed on d5 where lymphoblastoid transformed into fibroblast-like cells (indicated by white arrow in 4&5). hiPSC-like colonies started to emerge on d20 (region marked in back dotted line in figure 8&9). Scale bar: 100 µm.

Both polyclonal and clonal colonies from Lymp-GRK5-Q41, Lymp-GRK5-L41 lines showed a hiPSC-like morphology and cultures began to stabilise after two weeks maintained in mTeSR1 medium (Figure 4.9, p10). All the polyclonal cells derived from MACS column purification were harvested and cryopreserved for long-term storage; while the manually picked hiPSCs was expanded for further characterisations.

From the manual dissection group, 24 clones from Lymp-GRK5-L41 and four clones from Lymp-GRK5-Q41 were successfully maintained and cryopreserved. A low number of clones was retrieved from Lymp-GRK5-Q41 due to the over-confluence of the culture (>90%) at the day of isolation, which resulted in a significant reduction in cell survival rate. This result illustrated the importance of splitting at the correct density (from 70% to 80% confluency) during the reprogramming process. Clones from both cell lines showed typical hiPSC morphology as defined earlier (Figure 4.10, A9-11, B9-11). At passage 15, four clones from each line were taken for karyotyping; and only the clones with correct karyotype were maintained and expanded until passage 20 where the pluripotency characterisation process started. The karyotype analysis revealed that only one Lymp-GRK5-Q41 clone had normal karyotype (Clone 4) whereas Clone 1, 2 and 3 had abnormal karyotype where additional chromosome 1 was observed. Three normal karyotype clones were retrieved from Lymp-GRK5-L41, including clone 2, 3, and 4 (Table 4.5). From the karyotype results, hiPSCs derived from Lymp-GRK5-Q41 (Clone 4) and Lymp-GRK5-L41 (Clone 3) were selected for further experiments and hereinafter called hiPSC-GRK5-Q41 and hiPSC-GRK5-L41, respectively.

Table 4.5: Karyotype results (30 spreads) of reprogrammed clones derived from Lymp-GRK5-Q41 and Lymp-GRK5-L41 using episomal reprogramming.

Reprogrammed cell line at p15	Clone 1	Clone 2	Clone 3	Clone 4
Lymp-GRK5-Q41	46,XX[18] 47,XX,+1[8] 48,XX,+1,+1[1] 46,XX,+1,-9[1] 45,XX,+1,-?10,-?11[1] 45,XX,-16[1]	46,XX[27] 47,XX,+1[1] 47,XX,+7[1] 45,XX,-19[1]	46,XX[27] 47,XX,+9[1] 45,XX,-5[1] 45,XX,-21[1]	46,XX[30]
Lymp-GRK5-L41	46,XX[27] 45,XX,-14[2] 45,XX,inv(4)(p15q12)[1]	46,XX[30] 45,XX,-5[1] 45,XX,-12[1] 45,XX,-21[1] 45,X,-X[1]	46,XX[30]	46,XX[25] 45,XX,-7[2] 45,XX,-8[1] 45,XX,-12[1] 45,XX,-22[1]

4.2.6 Pluripotency characterisation of newly established hiPSC-GRK5 from lymphoblastoid cell lines

The monoclonal hiPSC lines carrying normal karyotype as mentioned in section 4.2.5 were cultured and expanded in mTeSR until reaching p20 before starting pluripotency characterisation process. The immunofluorescence analysis for nuclear pluripotency transcription factors expressed in hiPSC-GRK5-Q41 and hiPSC-GRK5-L41 showed a high level of induction, including OCT4 (98% ± 2% and 99% ± 1%, respectively), NANOG (97% ± 3% and 99% ± 1%) and SOX2 (99% ± 1% and 98% ± 2%,) (percentage of cells reported as mean percentage ± SEM, n=3) (Figure 4.11A). Expression of all these factors was centralised in the nucleus of the cells. The flow cytometry analysis for surface pluripotency markers confirmed that hiPSC-GRK5-Q41 and hiPSC-GRK5-L41 expressed a high level of SSEA-4 and TRA-1-81, and negative for differentiation marker SSEA-4 (below 5%) (Figure 4.11B). Additionally, the growth curve and population doubling times of these cell lines were also established, indicating that both hiPSC-GRK5-Q41 and hiPSC-GRK5-L41 had normal growth rate, which was 22.8 ± 1.3 hours and 23.6 ± 1.2 hours, respectively, and similar to that of HUES7 and H-Fib-hiPSC (both mean ± SEM, n=3) (Figure 4.11C). The karyotype analysis of 30 metaphase spreads by G-banding method confirmed that both of the newly established hiPSC lines maintained the normal karyotype after prolonged maintenance *in vitro*, from passage 20 to 30 in mTeSR culture condition (Figure 4.11).

As mentioned in Chapter 3, section 3.2.2 and 3.2.3, about the problems of mTeSR culture condition and standardisation of defined culture condition in the lab using E8 medium, the two hiPSCs were transitioned into E8 culture conditions. Both of the lines showed normal growth rates in E8 medium, 25.4 hour ± 2 hours and 24.3 ± 1.4 hours for hiPSC-GRK5-Q41 and hiPSC-GRK5-L41 respectively (both mean ± SEM, n=3). These cells maintained normal expression of pluripotency markers, including OCT4, SOX2, NANOG, SSEA4 and TRA-1-81, as well as showing normal karyotype after transition and ten passages culture in the E8 medium.

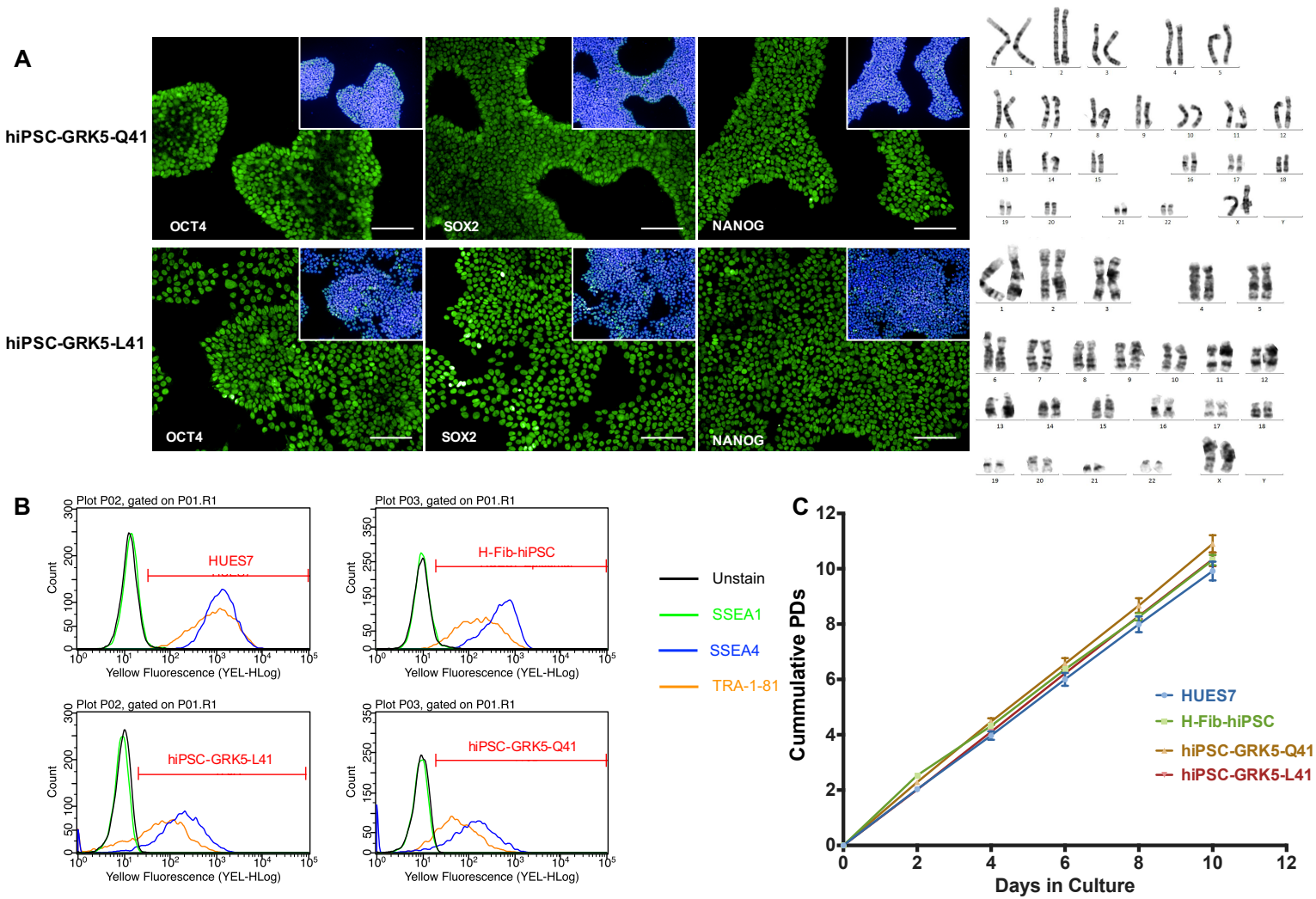


Figure 4.10: Pluripotency characterisation of hiPSC-GRK5-Q41 and hiPSC-GRK5-L41 lines. (A) Representative of immunostaining images of OCT4, SOX2, and NANOG. The merged images additionally include DAPI staining confirming the localised of these markers in the nucleus of the cells. Scale bar: 100 μm. Representative of a metaphase spread (n=30) for hiPSC-GRK5-Q41 and hiPSC-GRK5-L41 at passage 25, illustrating a normal 46 XX karyotype. **(B)** Growth curves for HUES7, H-Fib-hiPSC, hiPSC-GRK5-Q41 and hiPSC-GRK5-L41 show the PD time of 23.8 ± 4.6 hours, 24.8 ± 4 hours, 24.3 ± 1.4 hours, and 23.6 ± 1.2 hours, respectively (both mean ± SEM, n=3). **(C)** Flow cytometry analysis of surface pluripotency markers of hiPSC-GRK5-Q41 and hiPSC-GRK5-Q41 shows SSEA4 positive (93.5% ± 3.5% and 95.7% ± 2.1%, respectively, both mean ± SEM, n=3), and TRA-1-81 (80% ± 4.8% and 68.5% ± 2%, respectively, both mean ± SEM, n=3) and negative for SSEA1 (less than 5%).

4.2.7 Cardiac differentiation of hiPSC-GRK5-Q41 and hiPSC-GRK5-L41

To assess the differentiation ability of the newly established hiPSCs, especially the cardiac induction process, the E8-AB monolayer differentiation protocols were used to generate the CMs from hiPSC-GRK5-Q41 and hiPSC-GRK5-L41. The protocol was described in Chapter 3 and summarised in Figure 4.12A. Of note, before switching to E8 culture condition, the cardiac optimisation of mTeSR-cultured hiPSC-GRK5-Q41 and hiPSC-GRK5-L41 using SP34 (Act, BMP4) protocol was also conducted, which showed a relatively low cardiac differentiation efficiency (below 40%) regardless of the cell seeding density (Table 4.6).

Table 4.6: Immunocytochemistry analysis for α-Actinin positive cells. Both lines were cultured in mTeSR and seeded at different seeding density for differentiation optimisation (mean ± SEM, n=3).

	60.000 cells/cm^2	**80.000 cells/cm^2**	**100.000 cells/cm^2**
hiPSC-GRK5-Q41	38% ± 2%	32% ± 5%	28% ± 1.5%
hiPSC-GRK5-L41	39.5% ± 2.5%	36% ± 2.5%	31.4% ± 2%

Although the E8-AB protocol had been optimised to be efficient, robust, reproducible, and consistent in cardiac induction process of hPSCs, it was important to optimise the cell seeding density to achieve highest differentiation efficiency. Hence, the Lymp-GRK5-Q41 and Lymp-GRK5-L41 were seeded at three different densities, including 1x10^6 cells/T25 (40,000 cells/cm^2), 1.5x10^6 cells/T25 (60,000 cells/cm^2) and 2x10^6 cells/T25 (80,000 cells/cm^2). Flow cytometry analysis for α-Actinin positive cells revealed that both hiPSC-CM-Q41 and hiPSC-CM-L41 gave a highest cardiac differentiation efficiency at 40,000 cells/ cm^2, which were 89.3% ± 2.2% and 89% ± 2%, respectively (mean ± SEM, n=3) (Figure 4.12B). To validate the results, the E8-AB derived CMs at d12 post-differentiation were dissociated and plated in the 96-well plate for immunostaining of α-Actinin followed analysis using Harmony high content imaging analysis software. The results confirmed that 92% ± 1.5% of cells derived from Lymp-GRK5-Q41 and 94% ± 2% from Lymp-GRK5-L41 after underwent E8-AB differentiation protocol, were positively stained with α-Actinin (all mean ± SEM, n=3) (Figure 4.11E).

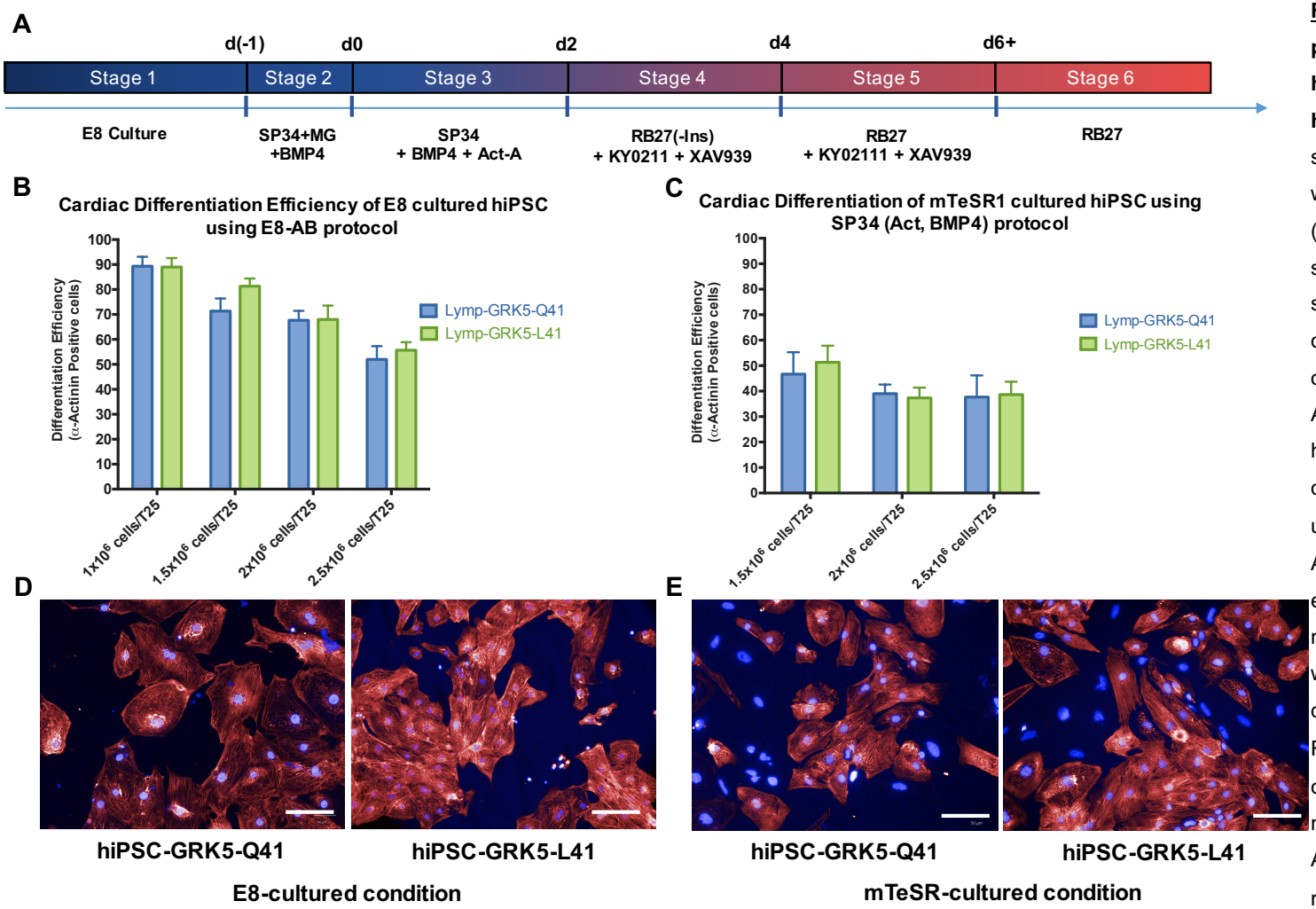


Figure 4.11: The cardiac induction procedures of Lymphoblastoid-derived hiPSCs, including hiPSC-GRK5-Q41 and hiPSC-GRK5-L41 lines. (A) The schematic depicts the E8-AB protocol, which is the modification version of SP34 (Act, BMP4) with additional preconditioning step from d-1 to d0 using SP34 supplemented with Matrigel (MG, 1:100 dilution), and BMP4 (1 ng/ml). **(B)** The optimisation of cell seeding density for E8-AB protocol conducted in newly established hiPSC lines cultured in E8 medium. The differentiation efficiency was assessed using immunocytochemistry to detect α-Actinin positive cells. **(C)** Similar experiment conducting in hiPSC cultured in mTeSR and SP34 (Act, BMP4) protocol was used to induce the cardiac differentiation process. **(D-E)** Representative images of α-Actinin positive cells obtained from E8-derived and mTeSR-maintained hiPSCs underwent E8-AB and SP34 (Act, BMP4) protocol, respectively. *Scale bar:* 100 μm.

4.3 Discussion

4.3.1 Lentiviral reprogramming of lymphoblastoid cell lines: an ineffective approach

The first attempt to convert lymphoblastoid cells into pluripotency state in our lab focused on using the lentivirus approach, which was developed and optimised previously for adherent culture (Dick et al., 2011). In this system, three major components were contributing to the success of the method, including virus production process, the streptavidin superparamagnetic beats, and the supportive roles of MEF layers. In terms of virus production, it was shown that low DNA concentration, an addition of sodium pyruvate, and multiple harvesting steps facilitated successful virus production and improved approximately 100-fold viral production compared to other approaches. To further enhance the effectiveness of viral transduction, the lentivirus-conjugated streptavidin superparamagnetic particles were employed and had been proven to increase significantly (up to 60-fold) the transduction efficiency (Dick et al., 2011).

Although these optimised conditions had been proven to work well in patient-derived fibroblast cells, it was ineffective in reprogramming lymphoblastoid cell line. First, the lymphoblastoid cells grow as suspension culture, preferably as clumps, which significantly reduce the surface area to volume ratio for the binding of the lentiviral particles. Several solutions had been suggested including culturing lymphoblastoid cells with lentiviral particles in spinning flasks or centrifuging the culture with the particles followed by seeding onto MEF-feeder layers. Both approaches did not show any improvement in viral attachment to the surface of the lymphoblastoid cells. Second, the immunological features of these lymphoblastoid cells prevented them from being co-cultured with any other cell types, especially MEF. Upon seeding onto MEF, lymphoblastoid cells were activated and started to kill the MEF feeder. Hence, in our study, it was illustrated that lentivirus reprogramming was not competent to amend lymphoblastoid cells into pluripotency state due to the unsuccessful delivery of viral vectors.

4.3.2 The reprogramming ability of episomal plasmids

Our results illustrated that the episomal plasmids from Thomson's lab were effective in converting H-Fib into pluripotency state with all the characteristics required to be classified as hiPSCs, including stem cell morphology (polygonal shape, high nucleus to cytoplasm ratio, prominent nuclei, and defined border), expression of pluripotency markers (OCT4, SOX2, NANOG, TRA-1-81 and SSEE4), high proliferation rate, and ability to maintain normal karyotype during prolonged culture *in vitro*. This observation was similar to that of previously described and supported the efficiency of the plasmid set in the reprogramming of fibroblasts and adherent cells into hiPSCs (Buchholz et al., 2009; Maehr et al., 2009; Yu et al., 2009).

In their report, Rajesh showed that by using the episomal plasmid set derived from Thomson's lab, hiPSC lines were generated with the reprogramming efficiency ranging from 2% to 23%, which was higher than the average efficiency of viral reprogramming of differentiated B-cells (Hanna et al., 2008), but lower than that of episomal reprogramming of human fibroblasts or human cord blood (Yu et al., 2011; Okita et al., 2013). In our study, although the transfection efficiency was only 8%, polyclonal H-Fib-hiPSCs were obtained after days 25 post-transfection suggesting that the reprogramming ability of the episomal vectors was high. Furthermore, the episomal reprogramming procedure of H-Fib did not require co-culturing transfected cells with MEF feeder layer. Alternatively, the MEF-conditioned medium supplemented with 10 ng/ml bFGF was used to maintain the transfected cells and supported the cells during the reprogramming process. Taken together, two essential requirements for reprogramming of lymphoblastoid cells were met, including high reprogramming efficiency of episomal plasmids and elimination of MEF-feeder layers. Hence, these observations provided the basis to initiate the reprogramming process of more challenging cell types like the lymphoblastoid cells.

4.3.3 Defined episomal reprogramming methods

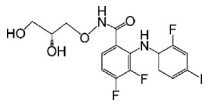
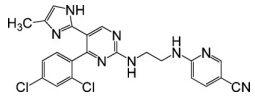
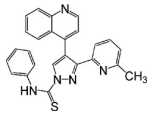
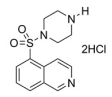
During the successful establishment of H-Fib hiPSCs, there was a significant finding on the role of the MEF feeder during reprogramming, and the possibility of

eliminating or replacing the feeder layer with better alternatives. Alternative options, such as medium conditioned from MEF, could support the pluripotency features of hiPSCs well in the presence of bFGF (Braam et al., 2008b). As the supportive feeder cells secrete growth factors into the culture, they can facilitate hiPSC survival, proliferation, and inhibition of spontaneous differentiation. However, the use of MEF-CM has been limited by the fact that it contains a broad range of undefined component and batch-to-batch variation contributing to the inconsistency of the system (Ludwig et al., 2006; Chen et al., 2011). Additionally, the establishment of chemically defined culture conditions for hPSCs provides a reliable and consistent culture system (Chen et al., 2011). More recently, a rapid development of recombinant protein technologies and biochemical productions introduced the use of small molecules as a compelling alternative to replace the MEF feeder, and MEF-conditioned medium. Moreover, the small molecules can target a wider range of molecular pathways involving in the regulation of cell fate, cell cycle, cellular proliferation, and apoptosis (Hou et al., 2013; Li and Ding, 2010).

Hence to further enhance the reprogramming efficiency of lymphoblastoid cell lines, after electroporation, the cells were maintained in the defined reprogramming medium (RM) supplemented with small molecules (Yu et al., 2011; Rajesh et al., 2011). The RM contained the cocktail of small molecules, which were directly involved in reprogramming process, including PD0325901, CHIR99021, A83-01, HA-100, and LIF. As reported, PD0325901 was used as MEK/ERK inhibitor that inhibited the activation and downstream signalling pathways regulated by MEK, which in turn, increased the expression of OCT4 (Ying et al., 2008). It was also published that TGF-β signalling inhibitors (CHIR99021 – GSK3β inhibitor – and A83-01 – a TGF-β/Activin/Nodal receptor inhibitor) together with MEK inhibitor PD0325901 resulted in >100 folds increase in viral reprogramming efficiency (Ying et al., 2008; Yu et al., 2011). Besides, CHIR99021 was reported to be involved directly in the reprogramming process by inhibiting GSK3β and boosting the expression level of SOX2 (Li and Ding, 2010). The small molecule, A83-01, was proven to be able to replace KLF4 (Li et al., 2009). To improve the survival rate of cells after electroporation, an isoform of ROCK inhibitor called HA-100 was used as a

protein kinase inhibitor, including PKA, PKC, and PKG. It was illustrated that HA-100 significantly enhanced single cell survival and supported high cloning efficiency during the reprogramming process and it had been widely used to improve the survival rate of peripheral blood-derived cell lines (Table 4.5) (Yu et al., 2011). Taken together, the combination of small molecules and the use of defined culture medium has shown to be effective in supporting the reprogramming process of lymphoblastoid cell lines in this thesis.

Table 4.7: Small molecules used to improve episomal reprogramming efficiency, their chemical structures, biological targets and functions. (Table obtained from Yu et al., 2011).

Name	Chemical Structure	Targets	Functions
PD0325901		Selective MEK/ERK signalling pathways	• Allows reprogramming and maintenance of mouse ES cells without LIF. • Increase reprogramming efficiency of human somatic cells. • Increase OCT4 expression.
CHIR99021		GSK3 inhibitor and WNT activator	• Maintain pluripotency of mESCs. • Supports hESCs self-renewal ability. • Generate hiPSCs from human somatic cells and lymphoblastoid cells.
A83-01		Selective TGF-β Inhibitor	• Support hiPSC self-renewal in combination with PD0325901 and CHIR99021. • Inhibits TGF signalling pathway. • Increase KLF4 expression level.
HA-100		ROCK-inhibitor, Protein Kinases Inhibitors	• Improves single cell survival • Supports high cloning efficiency • Increase human fibroblast reprogramming in combination with PD0325901 and CHIR99021

4.3.4 Episomal reprogramming of lymphoblastoid cell lines

Amongst the experimental evidence obtained from reprogramming lymphoblastoid cell lines using episomal plasmids, contrary to previously reported results (in Rajesh et al., 2011), Thomson's plasmid set did not show positive outcomes when used to convert lymphoblastoid cell lines into the hiPSC state, as described in Section 3.5. These results, however, are consistent with another research, in which hiPSCs could not be derived using existing episomal non-integrating protocols (Barrett et al., 2014). In our study, the switch to Yamanaka's plasmid set provided astonishing results, when partially reprogrammed colonies derived from lymphoblastoid cells were successfully transformed five days post-electroporation with significantly lower cell loss. Furthermore, hiPSCs were shown to establish in only 28 days after electroporation.

Possible explanations for these observations can be traced back to the differences between these two episomal plasmid sets. The Thomson plasmid set is the first human episomal reprogramming plasmid that delivered a combination of pluripotency transcription factors, including OCT4, SOX2, NANOG, KLF4, c-MYC, LIN28 with Simian virus 40 (SV40) into the cells. Yamanaka's plasmid set, on the other hand, was originally designed to reprogram mouse fibroblast and later modified to convert human fibroblast cells. This set contained four key pluripotency factors, including OCT3/4, SOX2, KLF4 and L-MYC (hereafter called OSKM factors) in combination with LIN28, and shRNA p53 inhibitor. The two plasmid sets have four common factors, which are OCT3/4, SOX2, KLF4, and LIN28. However, they are different in the presence of c-MYC in one, and L-MYC as well as shRNA p53 inhibitor in the other. A further look into the biological functions of the *MYC* and the *p53* genes can lead us to several proposed hypothetic explanations for the results obtained in this chapter.

The use of *MYC* as one of the original reprogramming factors is due to its ability to facilitate the somatic cell lines to proliferate indefinitely, which mimics the self-renewal ability of hESCs (Yu et al., 2011). Indeed, the *MYC* is well known as an oncogene promoting the cellular proliferation and cell cycle regulation. Interestingly, two different members of the *MYC* family were used in the two plasmid sets. The Thomson plasmid set contained *c-MYC* whereas *L-MYC* was found in Yamanaka plasmid set. Of note, the oncogenic transformation activities of *L-MYC* (encoded by *MYCL-1* gene) have been proven to be much lower than other members of the MYC family, indicating that it is safer to reprogram somatic cells into hiPSCs using Yamanaka plasmid set, especially for clinical applications.

Although expression of *MYC* is required for reprogramming, overexpression of *MYC* might trigger the apoptosis pathway (Okada and Mak, 2004). It was found that *MYC* binds to genomic loci with methylated H3K4, which is a hallmark of the chromatin remodelling process. In activated B-lymphocyte cells, expression of *MYC* leads to the redistribution of RNA polymerase from promoters into gene bodies; which in turn, amplifying the gene transcription machinery through the pause release, particularly in

genes related to metabolism, proliferation, and apoptosis (Nie et al., 2012). Overexpression of *MYC* might also introduce undesirable effects on the apoptosis pathway, especially when apoptosis genes are switched on, which eventually trigger cell death (Takahashi and Yamanaka, 2016). The *L-MYC* overexpression produced resistance to the apoptotic pathways induced by toxic drug whereas *c-MYC* increased the sensitivities of the cells (Nesbit et al., 1998). Hence, it is possible that overexpression of *c-MYC* during lymphoblastoid reprogramming can lead to major cell death. This result is consistent with the observations in Section 3.5, where a massive cell loss happened two days after electroporation in experiments using Thomson's plasmid set but not in those using Yamanaka's plasmid set.

Furthermore, it is evident that regulation of cell cycles during reprogramming transition states plays an important role in the success of any reprogramming method. One of the most important cell cycle regulators is the tumour suppressor *p53* gene, which was previously proven to have an inhibitory effect on hiPSC generation (Takashi and Yamanaka; 2016). Several studies showed that inactivation of *p53* led to a sharp increase in reprogramming efficiency in both mice and human (Ebrahimi, 2015). Further investigations revealed that *p53* is involved in DNA damage and cellular senescence which occurs frequently and rapidly during reprogramming process (Kawamura et al., 2009; Li et al., 2009; Marion et al., 2009). In addition, *p53* and its protein activities are highly expressed and regulated in immune cells, especially lymphocytes. Severe DNA damage occurs in lymphocytes, switching the cells to the *p53*-mediate apoptosis responses (Strasser et al., 1994; Gasser and Raulet, 2006). Therefore, temporary inhibition of *p53* expression can be crucial for reprogramming of lymphoblastoid cell lines, protecting them from *p53*-mediated apoptosis during genotoxic stress throughout the reprogramming process (Rasmussen et al., 2014). Additionally, it was reported that suppression of *p53* enhanced the reprogramming efficiency by preventing apoptosis-regulated *p53*. Others showed that inhibition of *p53* led to an increase in the expression level of Rem2 GTPase, whose main function is to maintain the survival of hESCs (Edel et al., 2010). We can thus conclude that the combination of OSKM reprogramming

factors and shRNA *p53* inhibitor enhanced the effectiveness of the episomal method by preventing cell loss and preserving genetic integrity (Barrett et al., 2014).

4.3.5 Cardiac differentiation of lymphoblastoid-derived hiPSCs

To develop a cardiac model to study the specific protective functions of *GRK5* SNP, there is a need of high-purity cardiomyocytes. The existing methods for hiPSC cardiac differentiation are feasible. However, they require complicated optimisation processes and involve the use of undefined medium components that hinder further interpretation of the molecular mechanisms of cardiomyogenesis. The effectiveness of cardiac differentiation protocol depends heavily on the cell types (hESC vs. hiPSC), the culture conditions (non-defined culture vs. chemically defined culture), the reprogramming methods, the somatic cell source, and the patient-related genotypes (Burridge et al., 2014). In this study, by using the monolayer differentiation protocol, the optimisation process is reduced to only one factor, which is cell seeding density (i.e. reaching 80% confluence on the day of differentiation). The results demonstrated that cell seeding at 40.000 cells/cm^2 was optimal for E8 cultured Lymp-hiPSCs to achieve up to 95% cardiac differentiation efficiency. This result is consistent with a previous study by Burridge et al., 2014. Furthermore, another major point to note from this study was that preconditioning the culture with StemPro34 supplemented with BMP4 and Matrigel was essential for cardiac differentiation of lymphoblastoid-derived hiPSCs. Without the preconditioning step, relatively low differentiation efficiency was obtained, ranging only from 35% to 51%. This observation also correlated well with a previous study which used the matrix sandwich protocol to differentiate human peripheral blood mononuclear-derived hiPSCs into cardiomyocytes (Riedel et al., 2014; Zhang et al., 2012). In addition, it was demonstrated in our study that overlaying the mTeSR culture hiPSCs with Matrigel enhanced the cardiac differentiation notably to 65%-95%. These cardiomyocytes displayed similar electrophysiological properties and pharmacological responses to those derived from other somatic cells. Finally, counting the number of cardiomyocytes

using Cedex automated platform showed that approximately $6.5x10^6$ cardiomyocytes were generated from a single T25 flask, yielding 7 cardiomyocytes/input hiPCS.

4.3.6 Limitations of the method

The establishment of the lymphoblastoid-derived hiPSCs followed cardiac differentiation presented in this chapter indicated the potential application of the hiPSC-derived CMs as a model to investigate the putative functions of GRK5-L41 polymorphism *in vitro*. However, our genotypic analysis revealed that the hiPSC-GRK5-L41 harbours different *ADRB1* polymorphisms compared to that of hiPSC-GRK5-Q41, which introduce the differences in functions of adrenergic receptors in response to catecholamines *in vitro*. The variation in adrenergic signalling pathways detected in this chapter was not the only difference between the genetic background of these two lines, indicating the limitation of the hiPSC models and the important of the isogenic models in biomedical research. Furthermore, because EBNA-1 is required for the establishment of latent EBV infection and long-term maintenance of the lymphoblastoid cell lines, and is the only protein requires for the existence of the EBV in host cells. Furthermore, the EBNA-2 protein was also encoded in the episomal plasmid set. Hence, it is important to examine the presence of these proteins at both mRNA and protein levels to confirm the transgene-free in hiPSCs. However, due to the time constraint, the analysis was unable to conduct. Alternatively, the lymphoblastoid-derived hiPSCs in this thesis were maintained until passage 25 before starting expanding for cardiac differentiation, as it was proven that the EBNA-1 and EBNA-2 were completely lost after passage 25 (Barrett et al., 2014; Okita et al., 2011; Rajesh et al., 2011).

4.4 Chapter conclusion

In summary, the results from this chapter suggest that episomal reprogramming vectors derived from Yamanaka's lab are viable for the conversion of lymphoblastoid cell lines into the pluripotency state. These cells met all the necessary requirements of pluripotency characteristics and were able to be differentiated into cardiomyocytes using monolayer differentiation with high purity and elevated yield. The cardiomyocytes generated here will be utilised as a valuable cell source for further characterisation and investigation of *GRK5* phenotypes.

Chapter 5 Creating hPSC-derived CM model using Footprint-free and shortcut CRISPR/Cas approach

5.1 Introduction

The previous chapter described the establishment of hiPSCs from lymphoblastoid cell lines bearing *GRK5*-Q41 and *GRK5*-L41 using episomal reprogramming method. This approach is consistent with the use of hiPSCs in disease modelling, with other examples including restoration of Dystrophin function in hiPSCs derived from patients with Duchenne muscular dystrophy (Young et al., 2016), investigation of Brugada syndrome – a cardiac disorder associated with characteristic electrocardiogram (Liang et al., 2016), and evaluation of doxorubicin cardiotoxicity in hiPSC-CMs (Burridge et al., 2015). However, the limitation of human cardiac model using hiPSC-CMs is the variations in the genetic background of these cell lines, resulting in the misinterpretation of the effects of the target genes or proteins of interest under tested conditions *in vitro*. To overcome the problems, gene editing technology is used to either correct the mutation of interest or introducing the mutation to the target loci or knockout the particular gene in the same cell line and assess the effects of these modifications using functional assays. Nevertheless, this approach is time-consuming, which requires the verification and characterisation of the newly established hiPSC lines before starting gene editing process. The estimated timeline need to complete the process is approximately 18 months (Figure 5.1).

Toward the aim of this thesis, the alternative approach would be **(1)** edit the hiPSC GRK5-L41 to make a parallel isogenic GRK5-Q41 in the same genetic background, and vice versa (i.e. GRK5-Q41 to L41); **(2)** produce an isogenic set of Q41, Q/L41, and L41 into a single hPSC line with a consistent genetic background. Here, option **(2)** was followed. This was because it could be initiated in parallel to the work in Chapter 4 (hiPSCs from GRK5-L41 and GRK5-Q41) and this could be completed within the length of the PhD.

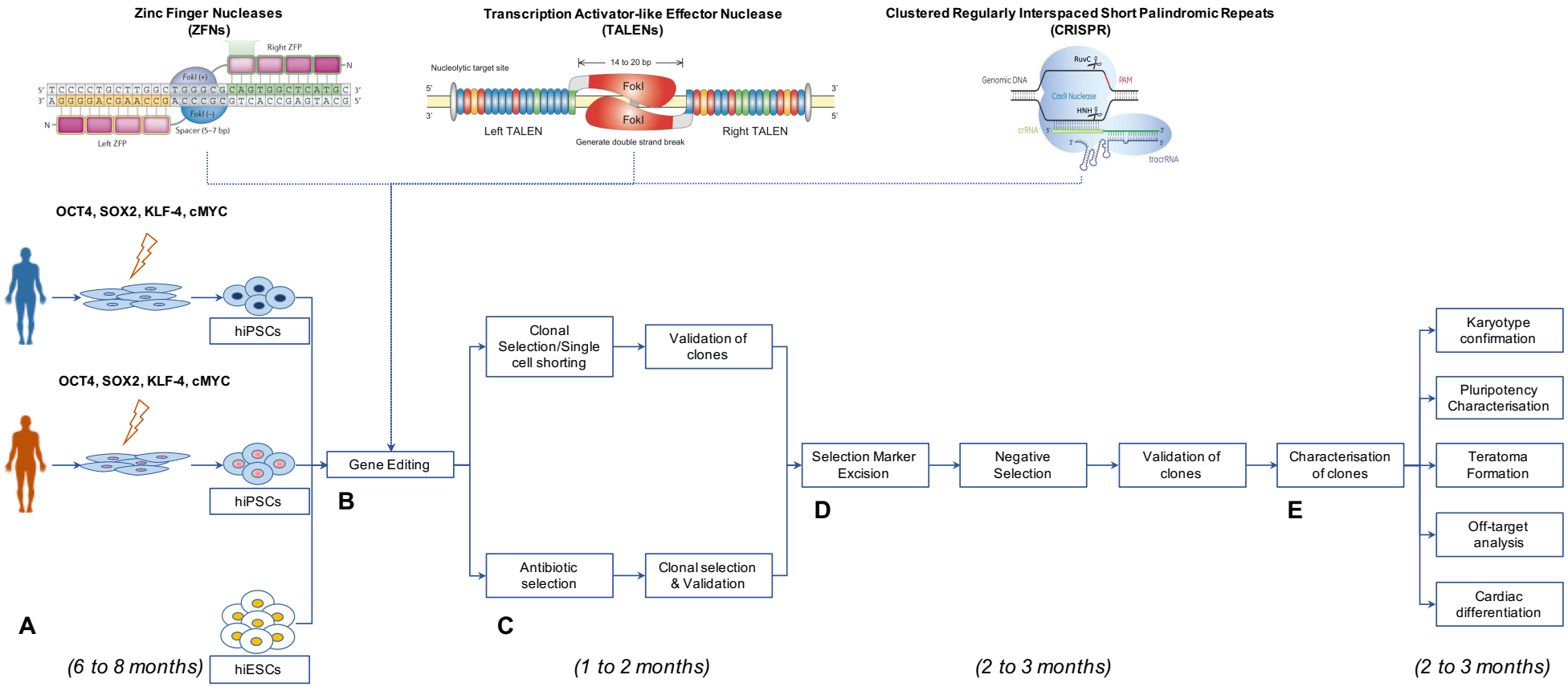


Figure 5.1: Overview of gene editing workflow from patient-derived samples to final clones. (A) To perform gene editing, the established hESCs or hiPSCs are required. The process of reprogramming human somatic cells into hiPSCs requires 6-8 month to complete the characterisation of the new hiPSCs. **(B-C)** Once the quality of hPSCs is confirmed, different gene editing approaches could be conducted, including ZFNs, TALENs, or CRISPR/Cas9. This is followed by the first round of clonal selection by either FACS or antibiotic selection if the antibiotic selection cassette was used. **(D)** Once an antibiotic selection cassette is used, it is essential to excise so as not to interfere with normal gene expression leading to the second rounds of negative selection and clonal isolation of final clones. **(E)** Finally, the engineered clone cell lines need to be fully validated and characterised. Diagram was modified from Parekh et al., 2017.

5.1.1 Gene editing using programmable nuclease systems

Gene editing is the advanced techniques that can remove, replace, or insert DNA at a particular locus in the genome of an organism. This process based on the cellular repair machinery triggered by the double-stranded breaks (DSBs) in the DNA (Muellener et al., 1989; Rouet et al., 1994; Bibikova et al., 2003; Jasin and Rothstein, 2013). In mammalian cells, the DSBs can be repaired by two mechanisms: the non-homologous end joining (NHEJ) and the homology-directed repair (HDR) (Bibikova et al., 2001; Bibikova et al., 2003). The former often results in the nucleotide loss or insertion at the end of the DSBs allowing the efficient constructions of knockout alleles through the induction of frame-shift mutation or early formation of the stop codon. By contrast, the latter usually occurs by homologous recombination from the intact DNA strands or the sister chromosomes. It can be used for precise genetic modifications such as codon/nucleotide replacements, or insertion of reporter genes by recombination with exogenous targeting vectors acting as the repair template for DNA repair machinery (Choulika et al., 1995).

Recently, genome engineering studies have discovered programmable nuclease systems that confer the ability to target and perform genome editing at specific gene (i.e. modifications of the host genome at a precise, predetermined locus) by producing DSBs. These systems include Zinc-finger nucleases (ZFNs), Transcription Activator-like Effector Nucleases (TALENs) and the most recently Clustered Regularly Interspaced Short Palindromic Repeat (CRISPRs). These three types of nucleases share a primary principle: they cleave the host chromosomal DNA in the site-specific manner, which in turn, induces the cellular repair mechanisms and targeted genome modification. However, each of the platforms has its unique features.

The ZFN is the first custom-engineered, site-specific endonuclease successfully used for genome editing in hPSCs (Hockemeyer et al., 2009; Zou et al., 2009). It composes of several tandem Zinc-finger DNA-binding domains associated with the endonuclease FokI domain. To recognise and bind to the DNA, ZFN system has its array consisting of three to six zinc-finger DNA-binding domain (ZFDBD) (Urnov et al., 2005).

The specificity of the system bases on the ZFDBD, each recognise and bind to a particular nucleotide triplet. The activation of FokI nucleases requires the homodimerisation of the ZFNs, adding another level of complication to the system (Urnov et al., 2005) (Figure 5.2A).

Soon after the discovery of the ZFNs, the TALEN system was found from the plant pathogen *Xanthomonas* (Boch et al., 2009). Similar to ZFNs, the DNA cleavage ability of TALENs derives from the non-specific FokI nuclease domain fused with a customised transcription activator-like effector (TALE) DNA-binding domain. The TALE is composed of the array of 33 to 35 amino acid repeats, each of which recognises a single base-pair in the major groove. The specificity of the system is determined by the two amino acids at positions 12 and 13, which are called repeat variable bi-residues. TALENs have been used to generate hPSC reporter line, homozygous knockout of genes, and mutation modifications, including introduction or repair (Ding et al., 2013; Hendriks et al., 2016) (Figure 5.2B).

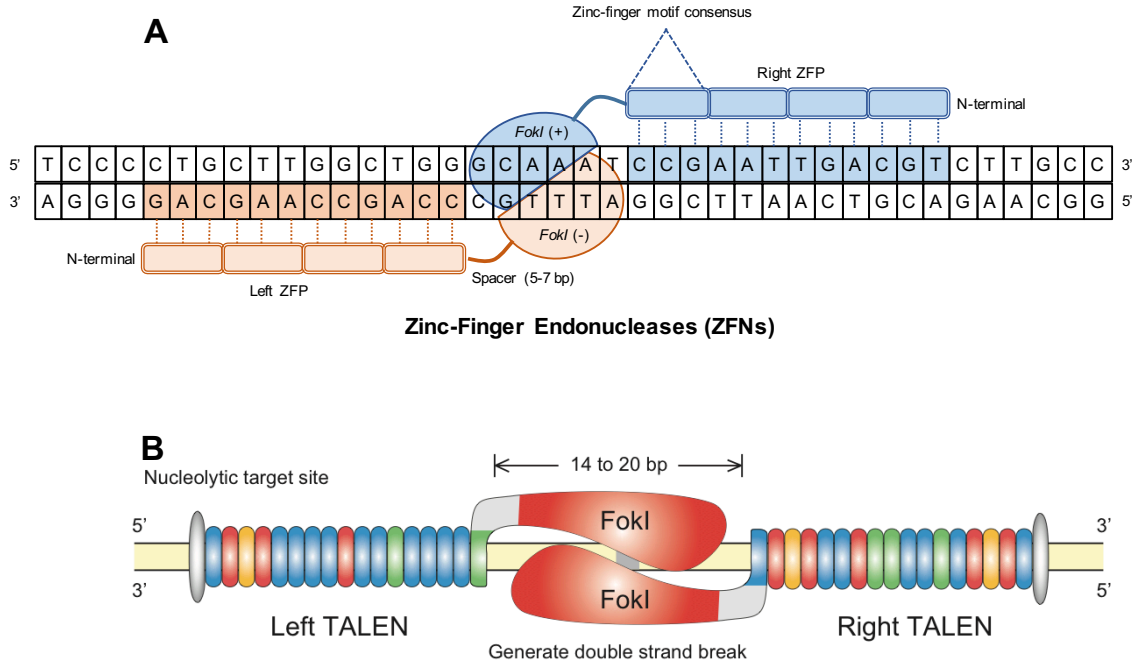


Figure 5.2: Structure of ZFNs and TALENs. (A) A schematic diagram illustrates a zinc-finger endonuclease (ZFNs) pair, each is composed of a zinc-finger protein (ZFP) at the amino terminus and the FokI nuclease domain at the C-terminus. **(B)** A schematic representation of a transcription activator-like effector nuclease (TALEN) pair is shown. Each TALEN is comprised of transcription activator-like effectors (TALEs) at the amino terminus and the *FokI* nuclease domain at the C-terminus. Each TALE repeat is consisted of 33-35 amino acid forming the recognition unit, each recognises a single base pair via the amino acid at positions 12 and 13. Adapted from (Kim and Kim, 2014).

Recently, the RNA-guided engineering nucleases, called the CRISPR platform, have been developed for performing gene editing in hPSCs (Cong et al., 2013; Shalem et al., 2014; Ran et al., 2013b). The CRISPR were derived from the adaptive immunity of bacteria and archaea against invading of phage or plasmids. The CRISPR systems consist of two classes, which are discussed in Chapter 1, section 1.11. Among various types of CRISPRs, type II CRISPR system is the most well studied and used for genome editing in hPSCs (Cong et al., 2013; Ran et al., 2013b; Kim et al., 2014). In this system, the CRISPR regions are transcribed as pre-CRISPR-RNA, which later is processed to give rise to target-specific CRISPR-RNA (crRNA). An invariable target-independent *trans*-activating crRNA (tracrRNA) structure is encoded in the same locus with crRNA and plays a significant role in the processing of the crRNA as well as target recognition. The association of crRNA and tracrRNA forms a unique cr-tracrRNA structure, which is a compulsory requirement for CRISPR-associated protein 9 (Cas9) to form an active DNA endonuclease. The complex between cr-tracrRNA and Cas9 protein is usually known as dualRNA-Cas9 complex (Jinek et al., 2012; Mali et al., 2013). To utilise the system for programmable genomic engineering, the crRNA and tracrRNA can be linked to form a single-chain guide RNA (sgRNA), which simplifies the components of the CRISPR/Cas9 system (Mali et al., 2013).

5.1.2 Gene editing in hPSCs using sgRNA and Cas9 nuclease

The CRISPR/Cas9 system has a crucial advantage over ZFNs and TALENs due to its simple design and preparation. This system requires three main components, including the gRNA plasmid, the targeting plasmid and the plasmid encoding the Cas9 protein. The gRNA plasmid is easily prepared by cloning 20-bp sequence-specific of the target locus in a vector that encodes the sgRNA scaffold (Mali et al., 2013). Several studies combined the gRNA plasmid with the Cas9 expression plasmid to form a single plasmid to reduce the number of delivering plasmid (Ran et al., 2013b; Chen et al., 2013). To avoid using plasmid approach, the recombinant Cas9 protein can also be generated without the need of complicated protein engineering (Kim et al., 2014). Furthermore, the

new approach has been developed without the need of plasmids: annealing of two complementary oligonucleotides followed *in vitro* transcription to generate crRNA and tracrRNA. In combination with Cas9 protein, the *in vitro* transcription of cr- and tracrRNA was proven to be mediated efficiently gene editing in hPSCs (Kim et al., 2014).

Conventionally, to introduce a particular modification in the specific gene of hPSCs, the first step is to verify the genetic information of the target gene present in the host cells via PCR and DNA sequencing. Once the DNA sequence is confirmed, custom made sgRNA targeting the DNA sequence of interest is designed *in silico* using the CRISPR Design tool (Table 5.1). The sgRNA can be ordered as a single oligonucleotide and cloned into an expression plasmid bearing the sgRNA scaffold, specially designed for CRISPR/Cas9 system (Mali et al., 2013). The sgRNA vector can be constructed as single expression plasmid or in combination with Cas9 to form a sgRNA-Cas9 expression plasmid (pSpCas9 plasmid) (Ran et al., 2013b). The sgRNA plasmid, the Cas9 plasmid and the exogenous repair templates for facilitating the HDR process are then delivered into the hPSCs via electroporation or chemical transfection. Depending on the selection cassettes incorporated in the construct, different screening strategies can be employed. The positive clones can be sorted using Fluorescence Activated Cell Sorting (FACS) if the selection construct contains fluorescence expression, such as GFP, RFP, etc. This approach is usually applied to create the reporter lines or visualisation of genomic loci in living human cells (Chen et al., 2013; Den Hartogh and Passier, 2016; Wu et al., 2016). Alternatively, the positive clones can be isolated using antibiotic treatment if the antibiotic resistant genes are incorporated into the selection cassette. This methodology has been widely used in genome editing due to its effectiveness in selection of the positive clones, easy to perform, not require cell sorting and less time-consuming (Ran et al., 2013a; Yusa, 2013; Xia et al., 2014; Cao et al., 2013).

Table 5.1: Summary of 36 On-target sgRNA Design Tools and seven posterior Genome editing analysis tools. Table was modified from Chuai et al., 2017 (Chuai et al., 2017). The tools in red were used in this thesis.

Tool Name	Searching Type	Website	Off-target analysis	Platforms
sgRNAcas9	Alignment based	http://www.biootools.com/	Yes	Perl script/offline/ command-line
Jack Lin's CRISPR/Cas9 gRNA finder	Alignment based	http://spot.colorado.edu/~slin/cas9.html	No	Web/online/graphic interface
GT-Scan	Alignment based	http://gt-scan.braembl.org.au/gt-scan/	Yes	Web/online/graphic interface
CRISPRdirect	Alignment based	http://crispr.dbcls.jp/	Yes	Web/online/graphic interface
CRISPR RNA configurator	Alignment based	http://dharmacon.gelifesciences.com/ch/gene-editing/crispr-rna-configurator/	No	Web/online/graphic interface
CRISPRseek	Alignment based	http://www.bioconductor.org/	Yes	R package/offline/ command-line
CCTop	Alignment based	http://crispr.cos.uni-heidelberg.de/	Yes	Web/online/graphic interface
Cas-OFFinder	Alignment based	http://casoffinder.snu.ac.kr/	Yes	C++/offline/ command-line
SSFinder	Alignment based	https://code.google.com/p/ssfinder/	No	Python script/offline/ command-line
CasFinder	Alignment based	http://arep.med.harvard.edu/CasFinder/	Yes	Python script/offline/ command-line
CRISPR-P	Alignment based	http://cbi.hzau.edu.cn/crispr/	Yes	Web/online/graphic interface
CRISPRer	Alignment based	http://jstacs.de/index.php/CRISPRer	No	Web/online/graphic interface
CRISPRTarget	Alignment based	http://bioanalysis.otago.ac.nz/CRISPRTarget		Web/online/graphic interface
CRISPRfinder	Alignment based	http://crispr.u-psud.fr/Server/	No	Web/online/graphic interface
flyCRISPR	Alignment based	http://tools.flycrispr.molbio.wisc.edu/targetFinder/	Yes	Web/online/graphic interface
CRISPR gRNA Design Tool	Alignment based	https://www.dna20.com/eCommerce/cas9/input	No	Web/online/graphic interface
WGE	Alignment based	http://www.sanger.ac.uk/htgt/wge/	Yes	Web/online/graphic interface
COD (Cas9 Online Designer)	Alignment based	http://cas9.wicp.net/	Yes	Web/online/graphic interface
CRISPOR	Alignment based	http://crispor.tefor.net/crispor.cgi	Yes	Web/online/graphic interface
Protospacer Workbench	Hypothesis driven	www.protospacer.com	Yes	Mac OS X/offline/ graphic interface
E-CRISP	Hypothesis driven	http://www.e-crisp.org/E-CRISP/index.html	Yes	Web/online/graphic interface
CRISPR	Hypothesis driven	http://crispr.mit.edu/	Yes	Web/online/graphic interface
CRISPR-ERA	Hypothesis driven	http://CRISPR-ERA.stanford.edu	Yes	Web/online/graphic interface
CHOPCHOP	Hypothesis driven	https://chopchop.rc.fas.harvard.edu/	Yes	Web/online/graphic interface
Cas9 design	Hypothesis driven	http://cas9.cbi.pku.edu.cn/	No	Web/online/graphic interface
EuPaGDT	Hypothesis driven	http://grna.ctegd.uga.edu/index.html	Yes	Web/online/graphic interface
CROP-IT	Hypothesis driven	http://cheetah.bioch.virginia.edu/AdliLab/CROP-IT/homepage.html	Yes	Web/online/graphic interface
Cas-designer	Hypothesis driven	http://www.rgenome.net/cas-designer/	Yes	Web/online/graphic interface
sgRNA Designer	Learning based	http://www.broadinstitute.org/rnai/public/analysis-tools/sgrna-design	No	Web/online/graphic interface
SSC	Learning based	http://crispr.dfci.harvard.edu/SSC/	No	Web/online/graphic interface
SgRNA Scorer	Learning based	http://crispr.med.harvard.edu/sgRNAScorer	Yes	Web/online/graphic interface
CRISPR Multi-targeter	Learning based	http://www.multicrispr.net/	Yes	Web/online/graphic interface
CRISPRscan	Learning based	http://www.crisprscan.org/	Yes	Web/online/graphic interface

Tool Name	Searching Type	Website	Off-target analysis	Platforms
WU-CRISPR	Learning based	http://crispr.wustl.edu/	Yes	Web/online/graphic interface
CRISPR Library Designer	Learning based	https://github.com/boutroslab/cld	Yes	Web/online/graphic interface
CRISPR-GA	Posterior experimental analysis	http://crispr-ga.net		Web/online/graphic interface
Microhomology Predictor	Posterior experimental analysis	http://www.rgenome.net/mich-calculator/		Web/online/graphic interface
caRpools	Posterior experimental analysis	http://github.com/boutroslab/caRpools		R package/offline/ command-line
MAGeCK	Posterior experimental analysis	http://liulab.dfci.harvard.edu/Mageck		Python script/offline/ command-line
CRISPResso	Posterior experimental analysis	http://crispresso.rocks/		Web/online/graphic interface
MAGeCK-VISPR	Posterior experimental analysis	https://bitbucket.org/liulab/mageck-vispr/		Web/online/graphic interface
CrispRVariants	Posterior experimental analysis	https://github.com/markrobinsonuzh/CrispRV-ariants		R package/offline/ command-line

Although the utilisation of selection cassette reduces the workloads significantly and enhances the effectiveness of positive clone isolation, the side effects of selection cassette expression and its epigenetic modulation once the gene engineering completed raising the important concerns (Hsu et al., 2014; Hotta and Yamanaka, 2015). Thus, to prevent the potential influences from its expression, selection cassette can be removed from the host genome. This approach has been developed and adapted to the mammalian system years ago, and several methods have been proven to be useful including the Cre recombinase, Cre-Lox system, FLP-FRT, etc., (Nagy A, 2000; Turan et al., 2011). However, removal of drug selection markers from Cre/*loxP* or Flp/*FRT* system often leave behind a single *loxP* or *FRT* site, usually known as “footprint” (Yusa et al., 2009; Turan et al., 2011). Although the selection cassette is typically inserted into an intron of the target gene to minimise its effects on the gene expression machinery of the host cells, these footprints could potentially influence the RNA splicing process and expression of the target genes (Sander and Joung, 2014; Hsu et al., 2014). The summary of general editing step is described in Figure 5.1 and Figure 5.3.

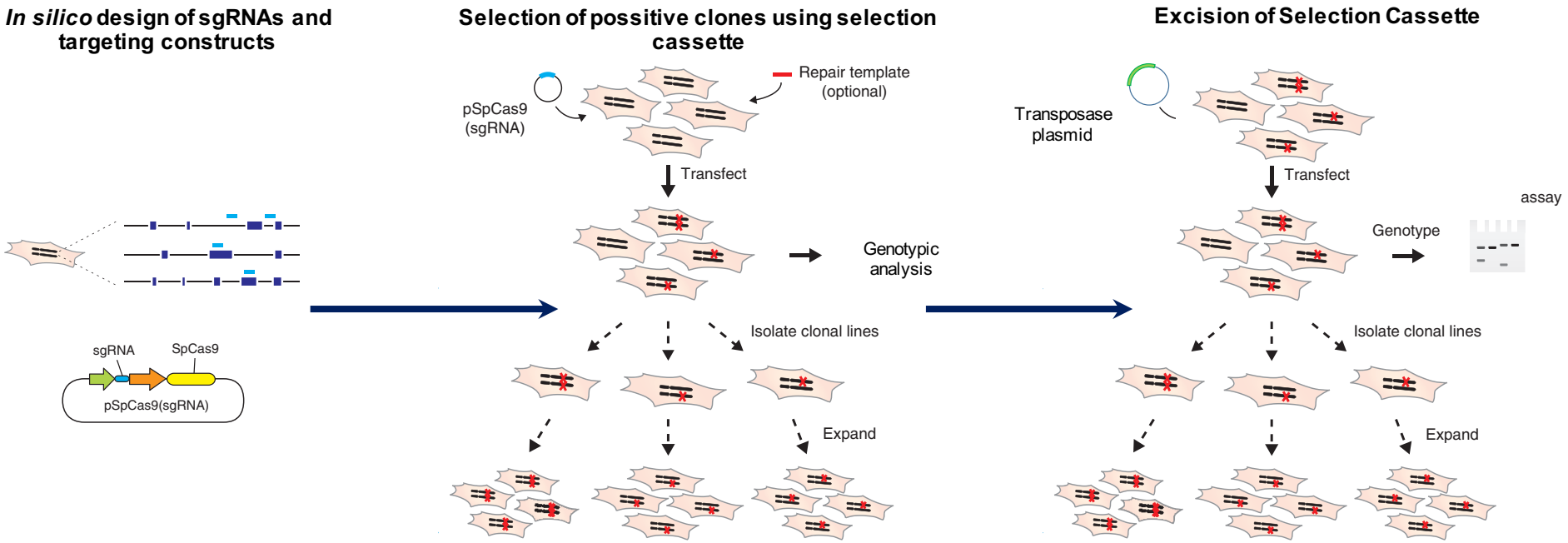


Figure 5.3: Schematic of traditional gene editing workflow from *in silico* design of gRNA and targeting donor construct to selection and isolation of final clones. The gene editing begins with the verification of the target gene followed the *in silico* design and construction of sgRNA plasmid (light blue bar), which can be incorporated with Cas9 expression gene to form a single plasmid (the pSpCas9 plasmid). The pSpCas9 plasmid containing sgRNA and Cas9 in combination with the exogenous repair template (red bar) are then introduced into the cells using electroporation or transfection reagent. The positive cells can be isolated based on the selection cassettes (sorting using FACS or antibiotic selection if the antibiotic resistance gene is used). If the cells were selected by using antibiotic resistance, the selection cassette need to be removed from the cells to prevent potential effects on host gene expression. Upon excision, second round of negative selection and clonal expansion was required to isolate the final clones. The total time required for entire process might take at least 3 to 6 months. Diagram is modified from Ran et al., 2013.

5.1.3 Components required for an effective CRISPR/Cas9 gene editing

5.1.3.1 CRISPR associated protein 9 (Cas9) endonuclease

The Cas9 is exclusively associated with the type II CRISPR locus and acts as a signature protein of the type II system. The Cas9 protein family is characterised by two nuclease domain structures, including RuvC and HNH. To adapt the nuclease activities of Cas9, its human-codon optimised version was generated specifically for the mammalian system (Mali et al., 2013). The wild type (WT) Cas9 carries both nuclease domains which, in turn, creates DSB at the target locus. The mutant Cas9 was also constructed where the mutation was created at either RuvC domain by modifying aspartate-to-alanine (D10A) or HNH domain by changing histidine-to-alanine (H84A). The mutant Cas9 has the ability to create single stranded break or a nick at the targeting loci by catalytically inactivating the RuvC or HNH nuclease domains, and hence given the name “Nickase” (Gasiunas et al., 2012; Jinek et al., 2012; Sapranauskas et al., 2011) (Figure 5.4). As the DNA single-stranded break are repaired via the high fidelity base excision repair (BER) pathways, the Cas9 Nickase can be used for more specific NHEJ or HR approach (Figure 5.4A).

To perform its endonuclease function, the Cas9-sgRNA complex requires the identification of the target DNA, which occurs in a stepwise process involving not only the base-pairing between sgRNA and the target DNA sequence but also the recognition of a short sequence motif, usually known as the protospacer-adjacent motif (PAM) (Figure 5.4B). The PAM, which is NGG or NAG, is located on the non-complementary strand of the DNA and is required for Cas9 to recognise and stabilise its binding to the predetermined DNA sequence. Therefore, the targetable sequences of the CRISPR/Cas9 system are 5’-X_{20}NGG-3’ or 5’-X_{20}NAG-3’, where X_{20} corresponds to the 20 bp of the crRNA sequence of the sgRNA. It was proposed that the binding of the Cas9-sgRNA complex to the DNA sequence of interest starts with the pairing of a small seed region of the sgRNA triggers after PAM recognition and subsequent DNA

unwinding (Figure 5.4B). The cleavage occurs when the seed sequence complementary to the target DNA and extensive the pairing to the rest of the sgRNA sequence.

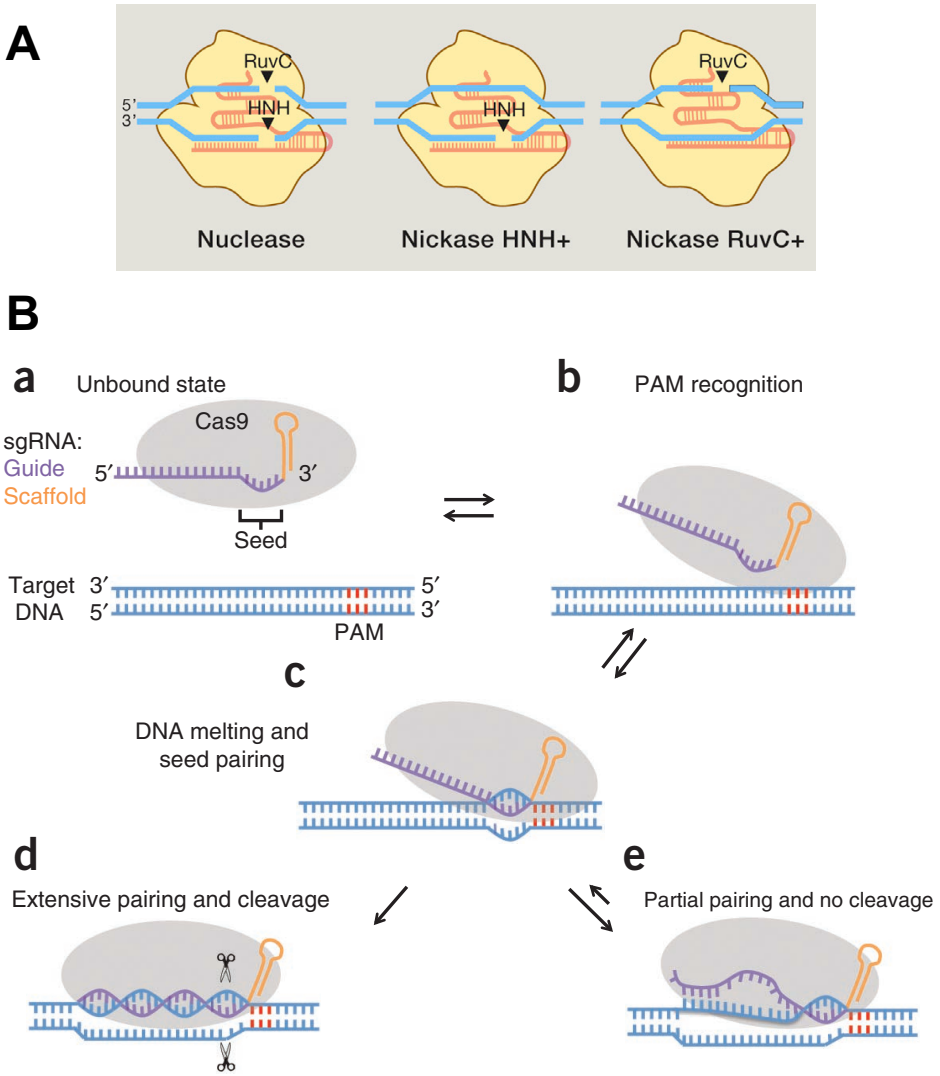


Figure 5.4: Cas9 protein and its binding process to the target DNA sequence. (A) Cas9 and its mutant version used in CRISPR type II system. The Cas9 nuclease initiates the DSB via its RuvC and HNH nuclease domains; each of which nicks a DNA strand to generate blunt end DSBs. Either catalytic domain of Cas9 can be mutated to inactivate the nuclease function leading to the generation of Nickase mutants that can generate single-strand DNA breaks. **(B) The binding process of Cas9-sgRNA complex.** (a) The Cas9 always associates with the sgRNA scaffolds in its unbound state. (b-c) Recognition of the Cas9-sgRNA complex starts by the identification of the PAM site (red) which allow the seed pairing. If the seed pairing can be propagated to PAM-distal regions, the Cas9 nuclease domains are locked to the target DNA and initiate cleavage (d), if not there is no cleavage and Cas9 remains bound to the target (e). Figures are adapted from {Hsu et al., 2014; Wu et al., 2014)

5.1.3.2 Single guide RNA (sgRNA)

Because gene editing results in permanent alteration of the host genome, the targeting specificity of the CRISPR/Cas method is a major concern, especially for clinical

application and biomedical therapeutic approach (Tsai and Joung, 2016). As above-mentioned, the specificity of the system is based on the Cas9 target recognition, dictates by the Watson-Crick base-pairing interactions of the Cas9-sgRNA complex with its targeting sequence (Figure 5.5 A). The sgRNA recognition sequence was 20 nucleotides upstream from the PAM; and the seed sequence of the sgRNA, which is the first 8-12 PAM-proximal sgRNA sequence determines the specificity of Cas9 protein (Jinek et al., 2012) (Figure 5.5B & C). Later, it was collectively demonstrated that Cas9 could potentially tolerate the mismatches throughout the guide sequence. However, it heavily depends on the number, position, and distribution of the mismatches (Hsu et al., 2014; Pattanayak et al., 2013).

Because gene editing results in permanent alteration of the host genome, the targeting specificity of the CRISPR/Cas method is a major concern, especially for clinical application and biomedical therapeutic approach (Tsai and Joung, 2016). As above-mentioned, the specificity of the system is based on the Cas9 target recognition, dictates by the Watson-Crick base-pairing interactions of the Cas9-sgRNA complex with its targeting sequence (Figure 5.8 A). The sgRNA recognition sequence was 20 nucleotides upstream from the PAM; and the seed sequence of the sgRNA, which is the first 8-12 PAM-proximal sgRNA sequence determines the specificity of Cas9 protein (Jinek et al., 2012) (Figure 5.5B & C). Later, it was collectively demonstrated that Cas9 could potentially tolerate the mismatches throughout the guide sequence. However, it heavily depends on the number, position, and distribution of the mismatches (Hsu et al., 2014; Pattanayak et al., 2013).

The gRNA plasmid consists of three main principal components: **(1)** a sgRNA sequence, **(2)** a sgRNA scaffold, and **(3)** an expression plasmid backbone (Cong et al., 2013; Jinek et al., 2012; Mali et al., 2013). Three primary methods have been developed to synthesise the sgRNA plasmids, including the ligation-free approach, the sgRNA oligos method, the ligation of sgRNA sequence into the pU6 expression vector using restriction enzyme, and the generation of sgRNA plasmid using Gibson Assembly (Cho et al., 2013; Mali et al., 2013; Shao et al., 2014) (Figure 5.6). In the ligation-free

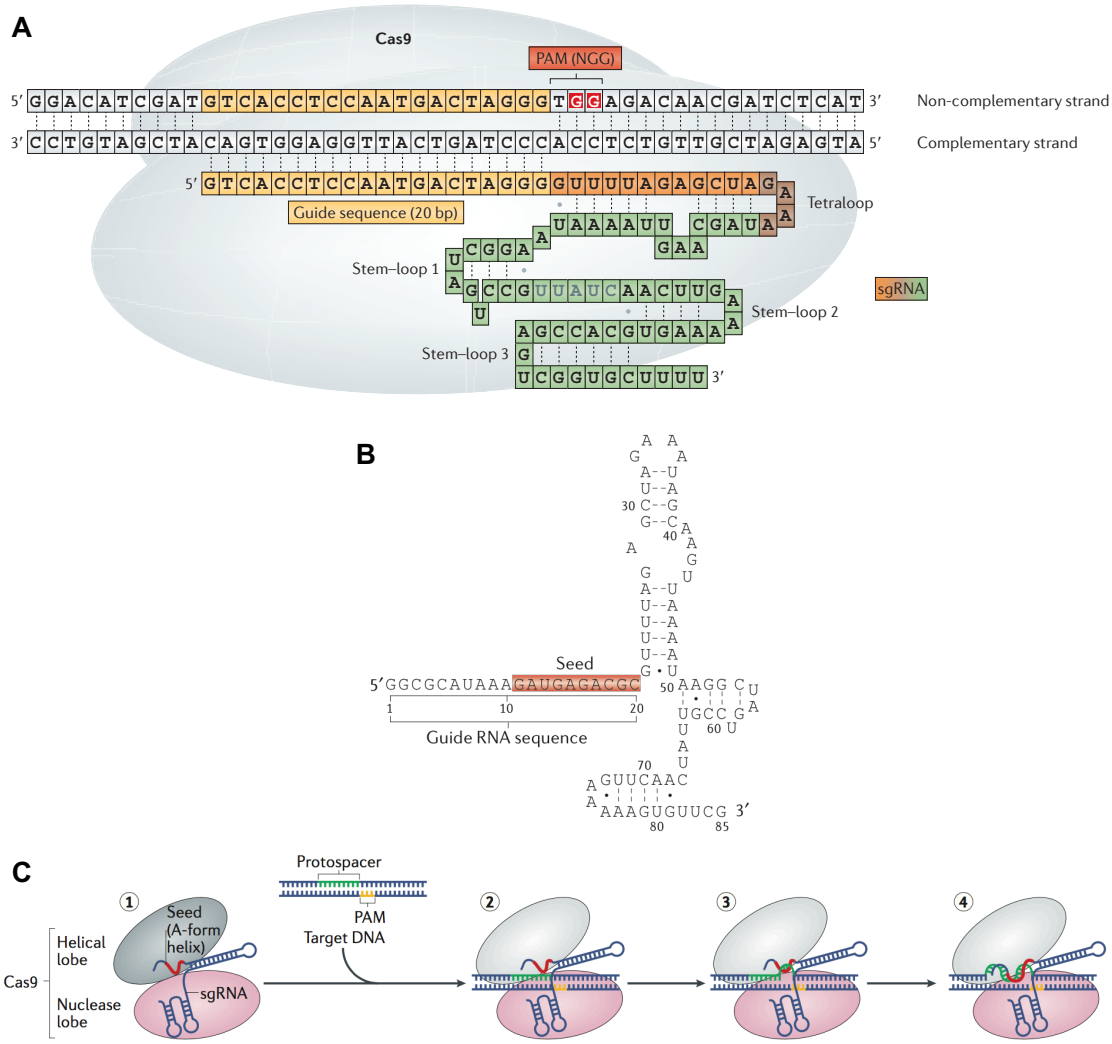


Figure 5.5: Schematic describes detailed structure of Cas9-sgRNA complex use in gene editing. (A) The specific structure of Cas9 forms the complex with sgRNA scaffold, which consists of the guide sequence (20 bp) integrated in the scaffold providing the tetraloop to connect the crRNA and the tracrRNA. **(B)** Structure of the sgRNA in detail with the stem loop sgRNA scaffold and the guide RNA sequence, the specificity of the system based on the seed sequence (the first 8 to 12 bp distance from PAM site, coding red) of sgRNA. **(C)** The diagram illustrates the binding process of the Cas9-sgRNA complex to the target DNA in stepwise manner, including **(1)** the formation of the Cas9-sgRNA complex in unbound stage, **(2)** The complex recognises firstly PAM site from the target DNA, **(3-4)** the recognition of PAM followed the complementary process of the seed sequence to the target DNA locks the Cas9-sgRNA complex to the intended DNA locus following the extension binding via Watson and Crick base pairing process of the remaining sgRNA, allowing the Cas9 to initiate cleavage at the target DNA sequence and create the DSBs. Figure is adapted from (Kim et al., 2014; Gorski et al., 2017).

approach, the 60 bp targeting oligos, containing a promoter, a sgRNA sequence and a sgRNA scaffold structure are synthesised, followed by a PCR to produce the sgRNA template (Shao et al., 2014) (Figure 5.6A). The sgRNA oligos method requires the complementary binding of the two oligos consisting of a promoter, a sgRNA coding sequence, and a gRNA scaffold (Cho et al., 2013). The third strategy involves the 20 nt

targeting sequence of the sgRNA together with 40 bp of the U6 promoter regions and 40bp of the sgRNA scaffold being synthesised as two oligos, followed hybridisation of the two oligos and ligated on the vector (pU6-AflII) using Gibson Assembly (Mali et al., 2013) (Figure 5.6B). The expression of the sgRNA scaffold is driven by the U6 polymerase III promoter, which allows the transcription of the non-coding RNA using polymerase III. The derivatives from the last method were also introduced by using PCR amplification of the sgRNA plasmids or using restriction enzymes (*NotI* and *Bam*HI) to insert the target sequence to the sgRNA plasmid (Norris et al., 2015) (Figure 5.6C&D).

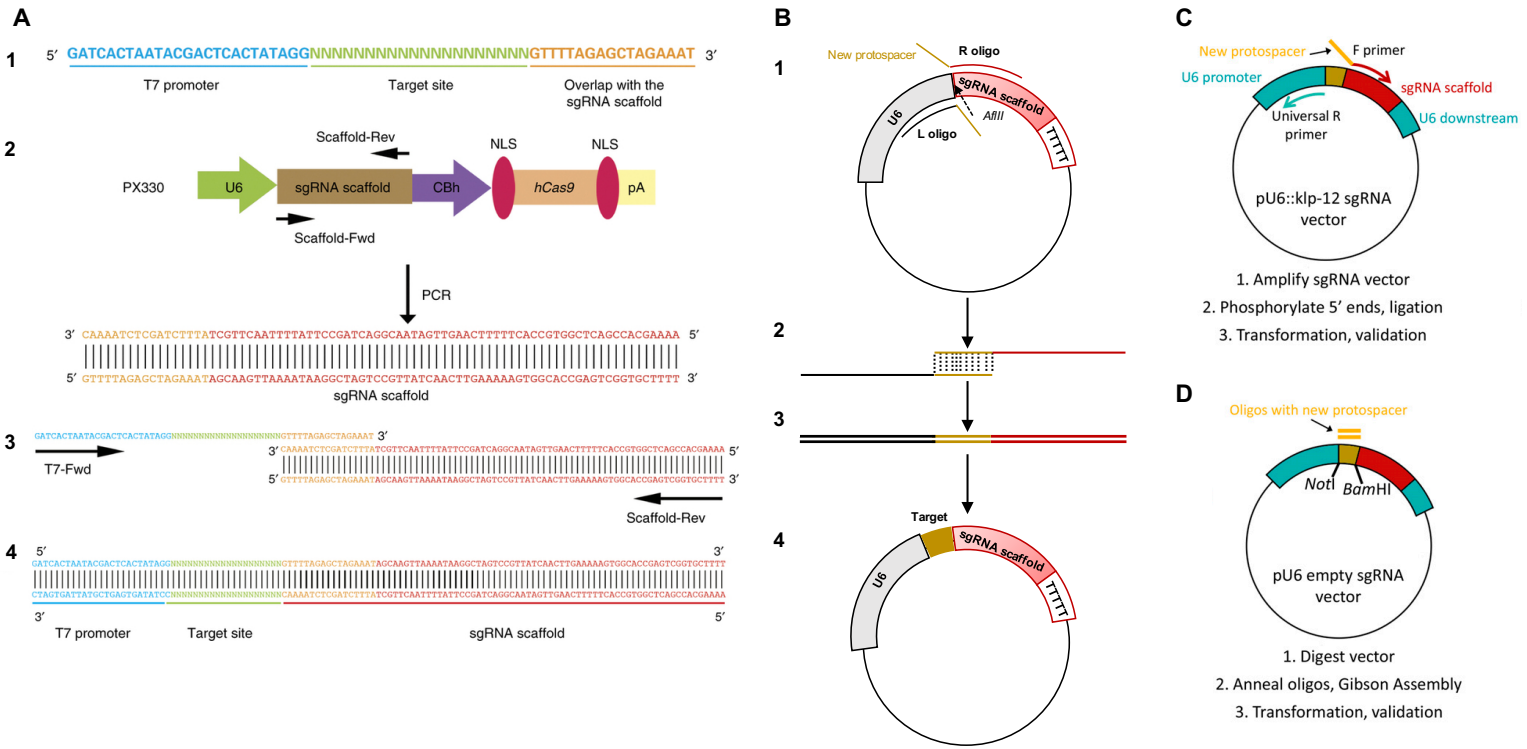


Figure 5.6: Overview of strategies uses to generate sgRNA plasmids. (A) The ligation free method consists of **(1)** synthesis of an oligo containing the T7 promoter, the target sequence, and the sgRNA scaffold, **(2)** DNA template preparation using the PX330 plasmid, **(3)** amplification of the DNA template via overlapping PCR using ssDNA oligos and sgRNA scaffold from **(2)**, **(4)** purification of the DNA template of sgRNA for *in vitro* transcription. **(B)** The universal sgRNA plasmid is generated by Mali and colleague which contains the *AflII* restriction site between the U6 promoter and the sgRNA scaffold, **(1)** the two oligos containing the new protospacer (or target sequence) and 40 bp of U6 promoter (Left oligo) or 40 bp of sgRNA scaffold (Right ologo) are hybridisation to form a target DNA template **(2-3)**, followed ligation to the *AflII* digested sgRNA plasmids using Gibson Assembly. **(C)** The sgRNA vectors are alternatively generated from an existing sgRNA plasmid using a universal reverse primer (green curved arrow) and a protospacer-specific forward primer (yellow and red curved arrow) to PCR amplify the entire plasmid, followed by 5' phosphorylation, ligation, and transformation. **(D)** The sgRNA plasmids can be constructed using cloning strategy where an empty protospacer sgRNA vector backbone is digested using *Not*I and *Bam*HI restriction enzymes, followed by insertion by Gibson assembly of annealed oligonucleotide carrying a new protospacer. Figures are adapted from {Norris et al., 2015; Shao et al., 2014).

5.1.3.3 Exogenous donor plasmid

To initiate the HDR-mediated gene editing, a donor plasmid carrying homology arms complementary to the targeting sequence is required. The DNA template comprises the left and right homology arms and an intervening DNA sequence that contains the DNA insert of interest or the selection cassette. Contradictory to the previous study which suggested the homology arms can be kept short without affecting the HDR-mediated gene editing efficiency (Bottcher et al., 2014; Gratz et al., 2014), other studies demonstrated that the targeting efficiency increases with the increase in length of the homology arms (Hasty et al., 1991; Beumer et al., 2013; Merkle and Schupbach, 2015; Hendriks et al., 2016). In several studies, it has been reported that HDR-mediated gene editing efficiency is improved when using homology arms of 400 bp or longer (Voit et al., 2014; Merkle and Schupbach, 2015). Also, sequence divergence between the two homology arms of the donor template and the chromosomal locus should be less than 2% to avoid the decrease in HDR-mediated editing efficiency (Elliott et al., 1998). Hence, the particular sequence of the homology regions spanning the locus in each cell line needs to be known before starting the construction of donor plasmid (Hendriks et al., 2016). Another significant aspect of designing donor template is the location of the mutation of interest (up- or downstream of the DSB). The distance between the mutation and DSB is called “conversion tract”. This conversion tract should be as short as possible. It should not be longer than 100 bp beyond which the HDR-mediated editing efficiency decreases significantly (Yang et al., 2013).

5.1.4 Seamless gene editing using CRISPR/Cas and the *piggyBac* transposon

As mentioned above, the excision process of selection cassette creates the "scar" in the host genome, which could potentially influence the expression of the gene of interest. Hence, it is important to investigate the technique that could generate the footprint-free gene editing which allows modifying the target gene without introducing any "scar" after excision of the selection cassette. In fact, this idea of "footprint-free" has been established and developed by Kosuke Yusa and his colleagues in 2009 in the experiment that used the *piggyBac* (PB) transposon system to create the transgene-free iPSCs (Yusa et al., 2009) (Figure 5.7). Later, this system was incorporated in ZFNs platform to generate the first "footprint-free" gene editing in hPSCs (Yusa, 2013) followed its application in TALENs (Sun and Zhao, 2014), and CRISPR/Cas platform (Xie et al., 2014; Wang et al., 2017).

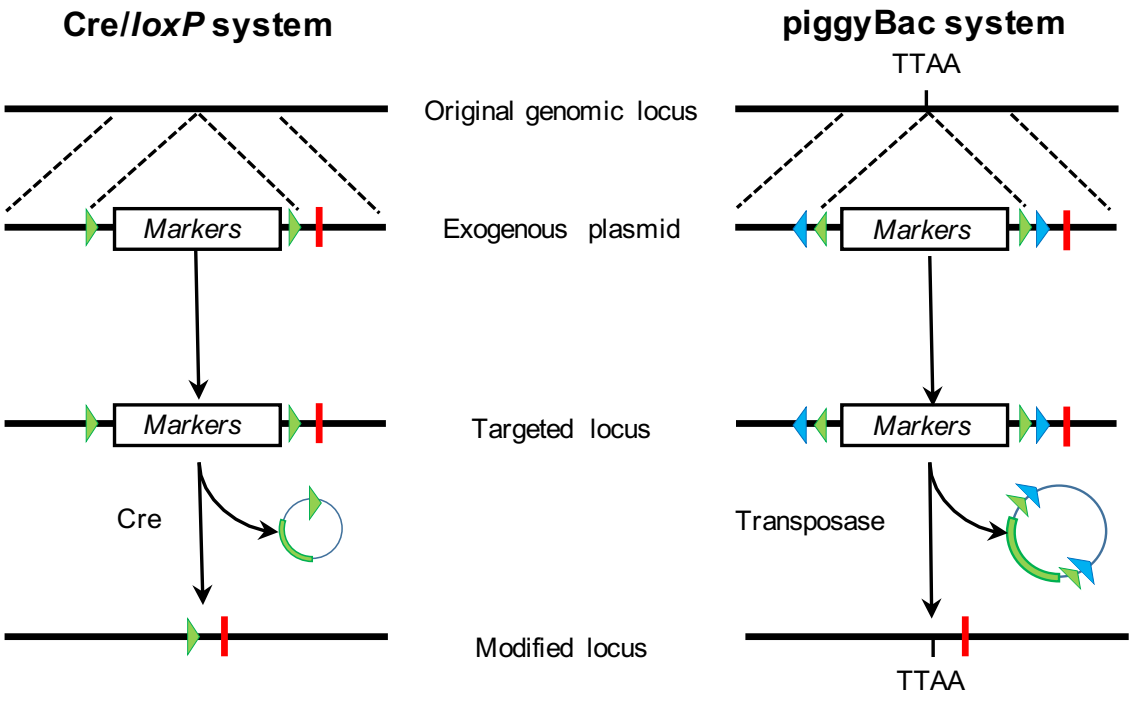


Figure 5.7: Comparison between Cre/*loxP* system and footprint-free piggyBac transposon system. The left panel illustrates the Cre/*loxP* system which leaves one *loxP* sequence (green triangle) and the intended modification (red bar) after marker excision. The right panel shows the *piggyBac* transposon system which carrying a selection cassette (markers) inserted into a genomic integration site (TTAA). The intended modification (red bar) is present in one of the two homology arms flanking the *piggyBac* sequence of the targeting construct. The excision of the selection cassette is induced by transposase results in the removal of the cassette while the genomic sequence remains the same. (adapted from Yusa et al., 2013)

The PB transposon system was derived from the moth DNA transposon and has been adapted to enhance the efficiency in mammalian cells (Yusa et al., 2009). The PB transposon can carry and remove up to 10 kb DNA fragment without affecting the transposase ability. The unique feature of the PB transposon over other systems is its requirement of the presence of TTAA integration site, which later can be repaired back to the original sequence (TTAA) upon excision. This feature allows the removal of the transposon containing the selection cassette from the host genome without changing any nucleotide sequence. Furthermore, the appearance level of TTAA sites in the mammalian genomes is theoretically high, approximately 246 bp distance between sites. Of note, the presence of TTAA site in the GC content of protein-coding regions (exons) is greater than that of the rest of the genome (Yusa et al., 2009; Li et al., 2013). It is, therefore, possible that the appearing frequency of TTAA site in particular loci is less than expected. In this case, TTAA sites can be created manually near the targeted modification site by single-nucleotide substitutions in the way that it only changes the nucleotide sequence but not the amino acid sequence of the targeted protein based on the codon triplet coding table.

To utilise the PB transposon in genome editing, the two components of the PB are required, including a DNA element flanked by transposon-specific terminal inverted repeats and a transposase that catalyse the excision process of PB. The nature of PB transposon is integrated into a TTAA site and restores this original TTAA upon excision, and it leaves no “footprint” behind. Also, approximately 50% of the excision events are not associated with re-integration back into the host genome, and hence the transposon can be permanently removed.

5.1.5 Chapter Aims

The ultimate goal of the chapter is to establish an isogenic cellular model of *GRK5* variants from hESC using the newly developed "short-cut" strategy. The gene-edited *GRK5* lines will also be isogenic to the parental HUES7 line and can be utilised for creating the research model in future. The aim was achieved by completing the following objectives:

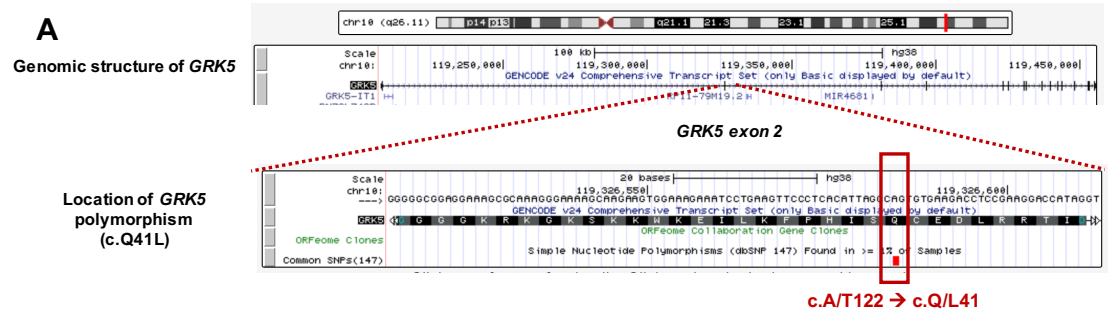
1. Confirmation of *GRK5* polymorphism at amino acid position 41 presence in HUES7.
2. Designing gRNAs and PB targeting constructs.
3. Generation of gRNA and targeting constructs using Gibson Assembly.
4. Conduction of gene editing experiments using the footprint-free and shortcut approach and compare it to the conventional footprint-free method.
5. Identification and characterisation of *GRK5* variants upon gene editing.
6. Pluripotency characterisation and optimisation of cardiac differentiation process of positive clones.

5.2 Results

5.2.1 Identification of *GRK5* polymorphism at amino acid position 41 of hESC (HUES7)

To verify the *GRK5* variant of HUES7 cell lines, five primer pairs were designed based on the *GRK5* reference sequence obtained from Genome Browser (RefSeq: NM_005308). The *GRK5* gene consists of 16 exons and locates at chromosome number 10 of the human genome (HumanGRCh38/hg38), and the polymorphism of interest (c.Q41L) is found in Exon 2 of the GRK5 (Figure 5.8A). The details of each primer pair are shown in Figure 5.8B.

A

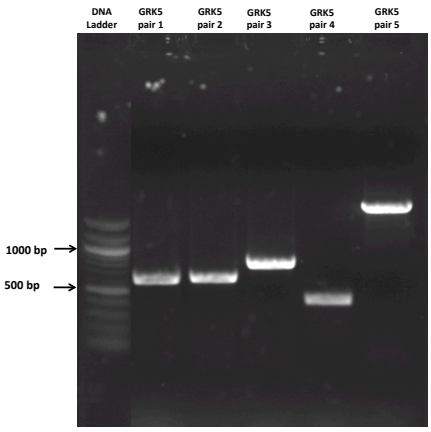


B

Primers used to verify *GRK5* sequence of HUES7

GRK5		Primer sequence	Product Size (bp)
Pair 1	*Forward*	AGCGCAAAGGGAAAAGCAAG	630
	Reverse	ACTGACATCCCCAGCAAGTG	
Pair 2	*Forward*	TTCCACTTGCTGGGGATGTC	638
	Reverse	GGCACAGATGGCCTCCTATC	
Pair 3	*Forward*	ACGTGCTCAGTACTCGTGTG	793
	Reverse	GCCTTAATGCACAAACGGCT	
Pair 4	*Forward*	TCCCCAGTTCTGTGCCTACT	420
	Reverse	CACCCTTACAGTGGCGCTTA	
Pair 5	*Forward*	ACGTGCTCAGTACTCGTGTG	1890
	Reverse	GGCACAGATGGCCTCCTATC	

C



D

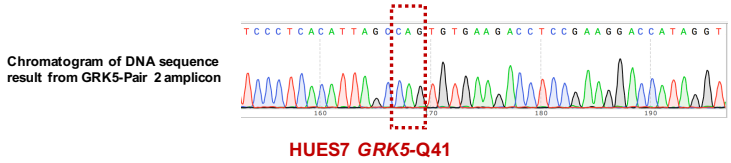


Figure 5.8: Identification of *GRK5* sequence from HUES7. (A) Reference *GRK5* sequence (NM_005308) obtained from Genome Browser (http://genome.ucsc.edu). Exon 2 of *GRK5* contains the *GRK5* polymorphism where Adenine at nucleic acid positions 142 changes into Thymine (T); which alters the codon triplet encoding for Glutamine (Q) into Leucine (L) at amino acid positions 41 (c.A122T → c.Q41L). **(B)** The table represents the primer pairs used to verify the *GRK5* sequence of HUES7 **(C)** Gel electrophoresis demonstrated the correct band size of the PCR products derived from GRK5-P1, GRK5-P2, GRK5-P3, GRK5-P4 and GRK5-P5 primers. **(D)** The chromatogram of extracted band from GRK5-P2 confirmed that HUES7 possesses the wild-type (WT) GRK5-Q41.

The results obtained from PCR analysis and gel electrophoresis indicated the correct band sizes from Pair 1, Pair 2, Pair 3, Pair 4, and Pair 5 at approximately 630 bp, 640 bp, 800 bp, 420 bp, and 1900 bp, respectively (Figure 5.8C). The DNA sequence obtained from PCR-Pair 2 amplicons detected that the nucleic acid positions 122 is Adenine (A), which is in the codon triplet encoding for Glutamine (Q) at amino acid positions 41, verifying that HUES7 possesses the wild-type (WT) *GRK5*-Q41 and hereinafter is called HUES7-GRK5-Q41 (Figure 5.8D).

5.2.2 Construction of sgRNA plasmids

5.2.2.1 Design of sgRNA target sequence for footprint-free approach

Identification of TTAA site: the confirmation of *GRK5* variant existing in HUES7 provided sufficient information to proceed the next step of *in silico* design of the sgRNA target sequence. To produce the footprint-free edited line, the utilisation of PB transposon system together with CRISPR/Cas9 was applied in this thesis. The key of this system is the combination of the PB transposon element carrying the Puromycin resistance and thymidine kinase selection cassette (PuroΔtk) with CRISPR/Cas9 approach. Therefore, it is important to identify the nearest PB integration site (TTAA) distance to the GRK5-Q41 position. Using SnapGene Viewer to screen the 2 kb *GRK5* reference sequence resulted in the identification of the TTAA site which was 93 bp downstream from the polymorphism of interest.

Identification of sgRNA target sequence: To identify the specific target sequence for sgRNA, the CRISPR design tool, called WGE from Sanger Institute (http://www.sanger.ac.uk/htgt/wge/) was used. The intended modification sequence was *GRK5* exon 2 with the target coverage of 1 kb up- and downstream of the GRK5-Q41 position. To select the best sgRNA target sequence, several criteria were set, including **(1)** the number of off-targets should be less than two for those sgRNA sequences possess the two to three mismatch in their seed sequence, **(2)** the number of combined off-target sites of the two gRNAs (Nickase approach) should be less than two, **(3)** the

target sequence need to cover the identified TTAA sites to prevent the Cas9 initiate cleavage on the targeting construct, **(4)** the distance between two sgRNAs should be between 0 to 30 bp (Len et al., 2014), and **(5)** the Cas9-mediated cleavage site should be close to the GRK5-Q41 position to achieve higher gene editing efficiency via HDR mechanism (Inui et al., 2014). Based on these criteria, four sgRNA pairs were selected, and among them, sgRNA pair 2 and sgRNA pair 4 are chosen because these pairs have a closer cleavage site to the GRK5-Q4 position than that of Pair 1 and Pair 3 (Figure 5.9A). Both sgRNA pair 2 and pair 4 contain the identified TTAA site for PB transposon system have the least off-targets between all four pairs (Figure 5.9B). Indeed, the combination of sgRNA pair 2 for Nickase approach show no off-target effect, indicating that pair 2 is the best sgRNA pair can be used to target *GRK5* sequence of the HUES7.

5.2.2.2 Construction of the sgRNA plasmids

Upon the identification of the sgRNA Pair 2 after completion of the *in silico* design, the construction of the sgRNA plasmids was conducted using the pU6-*AflII* approach as described in section 5.1.3.2 (Mali et al., 2013). The results of bacterial transformation after Gibson Assembly reaction followed the DNA sequence using M13F and M13R primer pair showed that 60% of the picked bacterial clones had successful integration of the target gRNA sequence, 20% of the clones were relegation of the plasmid backbone and 20% of clones illustrated the unclean sequence. In terms of DNA sequencing results of sgRNA pair 2 showed a clean chromatogram indicating the correct orientation of the gRNA after being cloned into the constructs, which further ensured that the gRNA 2a construct was successfully generated and ready for use. Similar results for gRNA 2b, gRNA 4a, and gRNA 4b were also observed (Figure 5.9C).

A



B

Table summarises the sgRNA pair selected from WGE - a CRISPR Design Tool from Sanger Institute

		WGE ID	Target sequence	Location (chromosome numer: location)	Strand	Off-targets (no. of mismatch : no. of off target)	Combined Off-targets
sgRNA pair 1	gRNA 1a	1075072171	CCGCCAAGCCGTTTGTGCATTAA	10:119326660-119326682	-	0:1, 1:0, 2:0, 3:6, 4:42	18
	gRNA 1b	1075072178	GCCAAGCTGTCTGTGCAGTGAGG	10:119326699-119326721	+	0:1, 1:1, 2:2, 3:35, 4:470	
sgRNA pair 2	gRNA 2a	1075072174	CCGTTTGTGCATTAAGGCAAATG	10:119326668-119326690	-	0:1, 1:0, 2:0, 3:19, 4:193	0
	gRNA 2b	1075072180	GTGAGGCAAATGCCAATCAGTGG	10:119326716-119326738	+	0:1, 1:0, 2:0, 3:7, 4:125	
sgRNA pair 3	gRNA 3a	1075072173	CCAAGCCGTTTGTGCATTAAGGC	10:119326663-119326685	-	0:1, 1:0, 2:0, 3:4, 4:35	4
	gRNA 3b	1075072180	GTGAGGCAAATGCCAATCAGTGG	10:119326716-119326738	+	0:1, 1:0, 2:0, 3:7, 4:125	
sgRNA pair 4	gRNA 4a	1075072169	CCTGGGGGCTGTGCGGGGAGTGA	10:119326625-119326647	-	0:1, 1:0, 2:3, 3:22, 4:316	4
	gRNA 4b	1075072172	GCCAAGCCGTTTGTGCATTAAGG	10:119326662-119326684	+	0:1, 1:0, 2:0, 3:7, 4:32	

Figure 5.9: Identification of potential gRNA pairs. (A) Position of selected sgRNA pairs, including sgRNA pair 2 (Grey arrows) and sgRNA pair 4 (Purple arrows) according to WGE – a CRISPR Design Tool from Sanger Institute. **(B)** Details of four gRNA pair selected from the gRNA reservior suggested from the WGE website. Each pair has its own WGE ID number for later access and information retrieval. Each sgRNA pair has at least one gRNA has the target sequence overlapping the identified TTAA site (red) to prevent the cleavage of the targeting construct. The off-targets are defined by compare the target sequence bearing number of mismatch (first digit) to the human genome database to identify number of potential matching sequence (second digit) (for example, 2:3 means that if there are two mismatches occur randomly in any positions of the target sequence, there would be three potential off-target sites found in the human genome). In Nickase approach, when two sgRNAs are used, the combined off-targets between the two sgRNA are calculated and presented in the table.

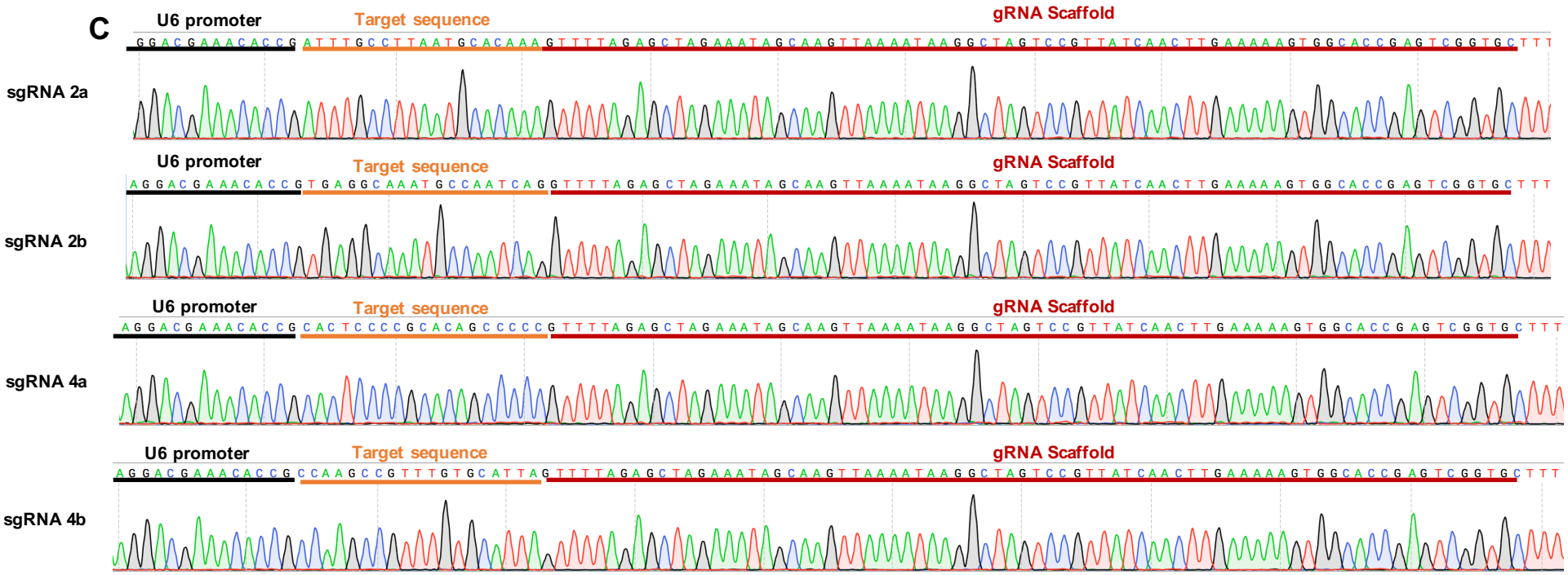
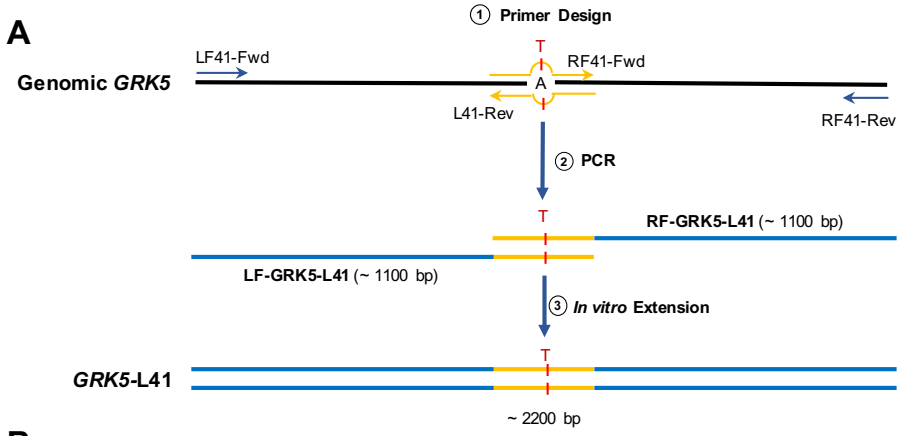


Figure 5.9 (Continued): (C) The DNA sequences of the picked bacterial clones from each sgRNA, including sgRNA 2a, sgRNA 2b, sgRNA 4a, and sgRNA 4b, showed a correct orientation and clean sequence of the U6 promoter (Black), target sequence (Orange) and gRNA scaffold (Red), indicating the successful constructions of the gRNA plasmids.

5.2.3 Construction of the exogenous targeting plasmid to introduce *GRK5*-L41 into HUES7-GRK5-Q41 cell line

5.2.3.1 Introducing of the GRK5 polymorphism sequence

To create the *GRK5*-L41 sequence, the SNP introducing PCR was used with the genomic template obtained from the HUES7-GRK5-Q41 cell line (Kondrashov et al., 2012). The principle of this technique is shown in Figure 5.10A. Two separate sets of PCR primer were designed, including GRK5-L41-a and GRK5-L41-b (Figure 5.10B). In brief, each primer set consists of two primer pairs, the left flank (LF41) and right flank (R41) primer pair. The LF41-Rev and the RF41-Fwd primer are complementary, and both contain T at the nucleic acid positions 122 to create the *GRK5*-L41 polymorphic sequence. The LF41 primer pair amplifies the LF-GRL5-L41 fragment, which is approximately 1100 bp upstream from the GRK5-Q41 position, whereas the RF41 primer pair generated the RF-GRK-L41 fragment, which is about 1100 bp downstream from the SNP. The amplifications of genomic DNA from HUES7-GRK5-Q41 using LF41 and RF41 primer pairs were conducted separately, and the two amplicons (the LF-GRK5-L41 and RF-GRK5-L41) from each PCR reaction were then ligated and extended *in vitro* to form an approximately 2200 bp *GRK5*-L41 sequence. As demonstrated in Figure 5.10C, both GRK5-L41-a and GRK5-L41-b primer sets have successfully generated the bands at expected sizes. After ligation and extension using Phusion Polymerase, correct bands at 2200 bp were observed in both sets suggesting that the SNP introducing PCR reaction was successfully (Figure 5.10D). The DNA sequence results from GRK5-L41-b set confirmed the presence of *GRK5*-L41 sequence from amplicon, which showed a clear chromatogram of T at nucleic acid position 122 (Figure 5.10E).



B

Primer Set	Primer Pair	Primer Sequence	Product Size (bp)
GRK5-L41 a	LF41-Fwd a	TAAGCGCCACTGTAAGGGTG	1024
	LF41-Rev a	GGTCTTCACACAGGCTAATG	
	RF41-Fwd a	CATTAGCCTGTGTGAAGACC	1196
	RF41-Rev a	GATAGGAGGCCATCTGTGCC	
GRK5-L41 b	LF41-Fwd b	TAAGCGCCACTGTAAGGGTG	1018
	LF41-Rev b	CACACAGGCTAATGTGAGGG	
	RF41-Fwd b	CCCTCACATTAGCCTGTGTG	1202
	RF41-Rev b	GATAGGAGGCCATCTGTGCC	

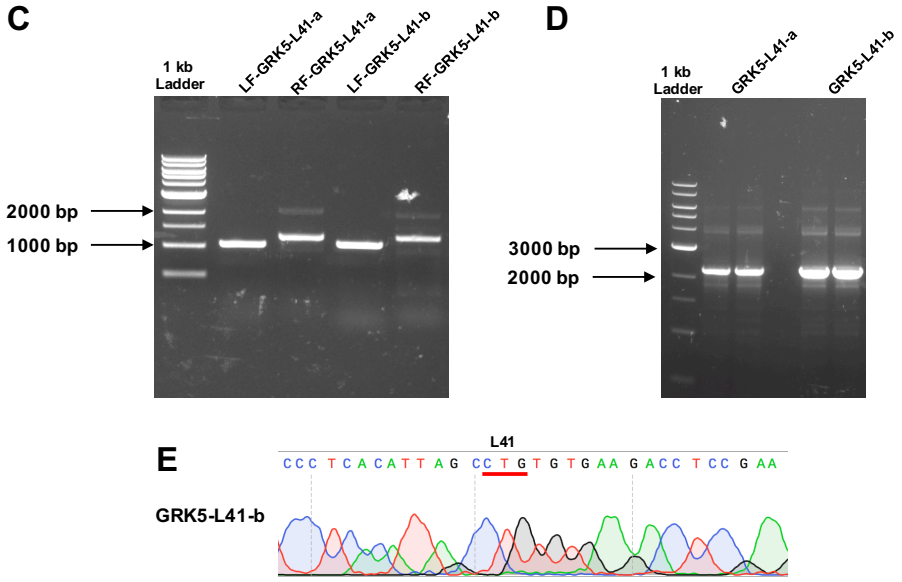


Figure 5.10: Creation of the *GRK5*-L41 sequence from HUES7-GRK5-Q41 genomic DNA. (A) The diagram illustrates the principle of the SNP introducing PCR reaction. **(1)** The primers were designed so that the L41-Rev and R41-Fwd were complementary and contained T at nucleic acid position 122. **(2)** The separated PCR reaction to create the LF-GRK5-L41 fragment and the RF-GRK5-L41 fragment, both are approximately 1100 bp. **(3)** *In vitro* ligation and extension of the two fragments create the *GRK5*-L41 fragment, which is approximately 2200 bp. **(B)** The table show the details of the two primer sets used in the experiment. **(C)** Gel electrophoresis results indicated the successful amplification using the GRK5-L41-a and GRK5-L41-b to create LF-GRK5-L41 and RF-GRK5-L41 at a correct band size. **(D)** Gel electrophoresis result demonstrated the successful ligation and extension of the LF-GRK5-L41 and RF-GRK5-L41 fragments to form the 2200 bp *GRK5*-L41 sequence. **(E)** The chromatogram obtained from the GRK5-L41-b product confirmed the presence of T at the nucleic acid position 122 which is in codon triplet encoded for L at the amino acid 41 of GRK5 protein.

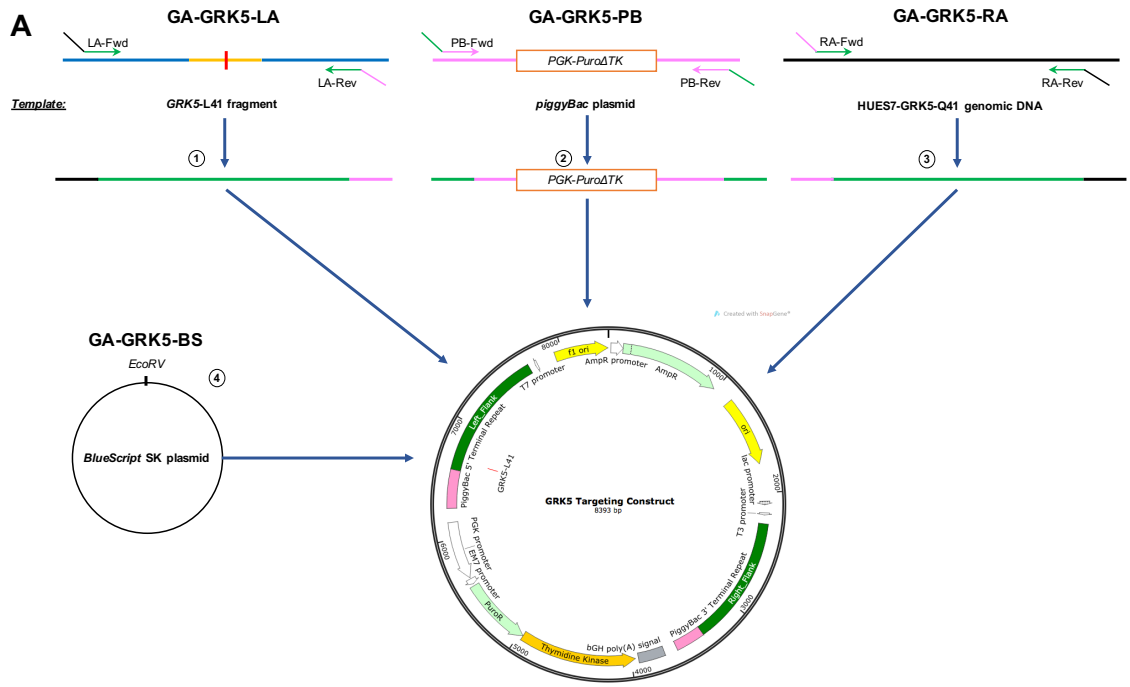
5.2.3.2 Construction of the GRK5 targeting vector

Generation of the targeting vector using Gibson Assembly: The *GRK5* targeting construct was generated using Gibson Assembly that joined three independent PCR-amplified fragments, including **(1)** left-flank homology arm (GA-GRK5-LA), **(2)** the *piggyBac* transposon element (GA-GRK5-PB), and **(3)** right-flank homology arm (GA-GRK5-RA) with the BlueScript SK plasmid backbone digested with *EcoR*V restriction enzyme (GA-GRK5-BS) (Figure 5.11A). Multiple primer sets were designed to amplify the fragments required for Gibson Assembly reaction in the way that they contain 40 bp overlapping sequence at each end of the assembly (Figure 5.11B). Because each primer length is 40 bp which consists only 20 to 25 bp complementary sequence to the DNA template, two loops PCR reaction was conducted to improve the PCR efficiency and specificity (Table 5.2).

Table 5.2: Two-loops PCR reaction used to amplify Gibson Assembly fragments to construct *GRK5* targeting plasmid.

Step	Temperature	Time
Initial Denaturation	98°C	30s
Loop 1 (3 Cycles)	98°C	15s
	56°C	15s
	72°C	3 mins 20s
Loop 2 (30 Cycles)	98°C	30s
	61°C	15s
	72°C	3 mins 20s
Final Extension	72°C	4 minutes
Hold	4°C	-

The PCR results indicated the successful amplification of both GA-GRK5-LA and GA-GRK5-RA fragment, which showed the corrected band sizes at approximately 1100 bp (Figure 5.11C). However, the double bands at 3100 bp and 3500 bp were observed in GA-GRK5-PB fragments, suggesting that the PCR reaction amplified the non-specific regions of the *ADRB2-piggyBac* plasmid. To increase the specificity of the reaction, the annealing temperature of Loop-1 was reduced from 56°C to 48°C, and the result still showed double bands suggesting that the problems were not from the PCR reaction itself but either the templates or the PCR primers (Figure 5.11C, 1st PCR reaction).



B

	Primer Pair	Primer sequence	Product Size (bp)
GA-GRK5-LA	LA-Fwd	GGTCGACGGTATCGATAAGCTTGATTAAGCGCCACTGTAAGGGTGGAGAG	1156
	LA-Rev	ACGCAGACTATCTTTCTAGGGTTAATGCACAAACGGCTTGGCGGATCACC	
GA-GRK5-PB	PB-Fwd	GGTGATCCGCCAAGCCGTTTGTGCATTAACCCTAGAAAGATAGTCTGCGT	3286
	PB-Rev	CAGCTTGGCGGCTCACCCATTTGCCTTAACCCTAGAAAGATAATCATATT	
GA-GRK5-RA	RA-Fwd	CAATATGATTATCTTTCTAGGGTTAAGGCAAATGGGTGAGCCGCCAAGCTG	1146
	RA-Rev	AGTGGATCCCCCGGGCTGCAGGAATTCGATGGCACAGATGGCCTCCTATC	

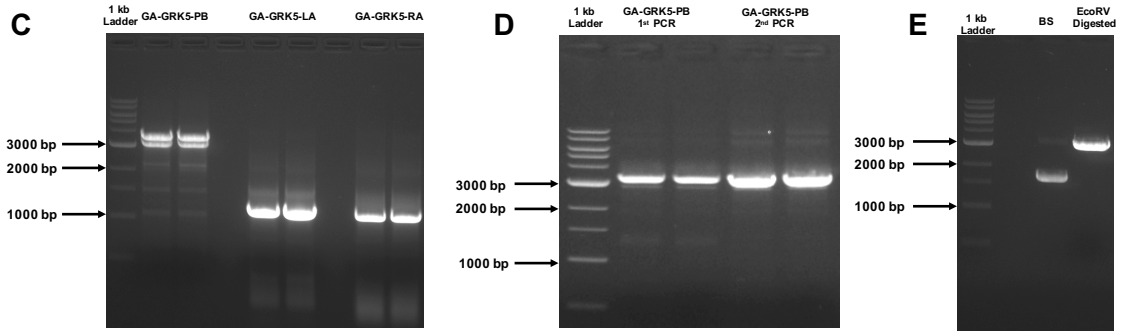


Figure 5.11: Establishment of the *GRK5* targeting plasmid using Gibson Assembly. (A) The Gibson Assembly reaction required four fragments, including **(1)** left-flank homology arm containing the *GRK5*-L41 sequence, which was amplified from the *GRK5*-L41 fragment (GA-GRK5-LA), **(2)** the *piggyBac* fragment, which was amplified from the *piggyBac* plasmid, **(3)** right-flank homology arm, which was amplified from the HUES7-GRK5-Q41 genomic DNA (GA-GRK5-RA), and **(4)** BlueScript SK (BS) plasmid backbone, which was digested using *EcoR*V. **(B)** Primers used to amplify the Gibson Assembly components. **(C)** Gel electrophoresis result confirmed the successful amplification of the GA-GRK5-LA and GA-GRK5-RA, although the GA-GRK-PB showed non-specific amplification as double bands were observed at 3100 bp and 3500 bp. **(D)** The 1st PCR reaction with the decrease of annealing temperature in Loop 1 of the PCR reaction (from 56°C to 48°C) showed a non-specific amplification of GA-GRK5-PB fragment. The 2nd PCR reaction, in which the original *piggyBac* plasmid was used, indicated the successful generation of the GA-GRK5-PB. **(E)** Overnight *EcoR*V digestion of the BlueScipt Plasmid.

To test this hypothesis, the original *piggyBac* plasmid obtained from AddGenes was used as a new template. Surprisingly, when the new *piggyBac* template was used, a distinct band was obtained from the reaction at the expected band size of 3200 bp (Figure 5.11D, 2nd PCR reaction). The plasmid backbone was prepared by digestion of the BlueScript SK plasmid using *EcoR*V restriction enzyme overnight. The result indicated that a complete digestion of the plasmid was obtained as a single band at approximately 3000 bp was observed and compared to the non-digested plasmid as a control (Figure 5.11E).

Transformation of Gibson Assembly products: The Gibson Assembly products were cloned into One-Shot TOP10 E. Coli competent cells. 19 clones were isolated for plasmid extraction process followed by enzyme digestion with *Hind*III, which produced two fragments at 1500 bp and 7000 bp approximately. The clones showing these two bands were sent for DNA sequencing to validate. Interestingly, 12 clones out of 19 showed double bands after *Hind*III digestion, illustrating that our Gibson Assembly worked at high efficiency (63%) (Figure 5.12A). To further confirm the correct sequence of these positive clones, the DNA samples were sent for sequencing using M13 Fwd, M13 Rev, PB Fwd and PB Rev primers provided by SourceBiosciences and Dr. Alexander Kondrashov (Figure 5.12B). Five regions were screened for mismatch sequence including the overlapping sequence between **(1)** BlueScript SK plasmid and the Left-flank homology arm, **(2)** the GRK5-L41 sequence, **(3)** Left-flank homology arm and 5' PB terminal repeat, **(4)** 3' PB terminal repeat and Right-flank homology arm, and **(5)** the Right-flank homology arm and the BlueScript SK vector (Figure 5.12C). The results confirmed that only two clones (clone 17 and clone 19) had a correct sequence without any mismatches, providing two *GRK5* targeting plasmids which could be used for the next targeting step. From this result, the targeting plasmid from clone 19 was taken further for the main gene editing experiment (Figure 5.13).

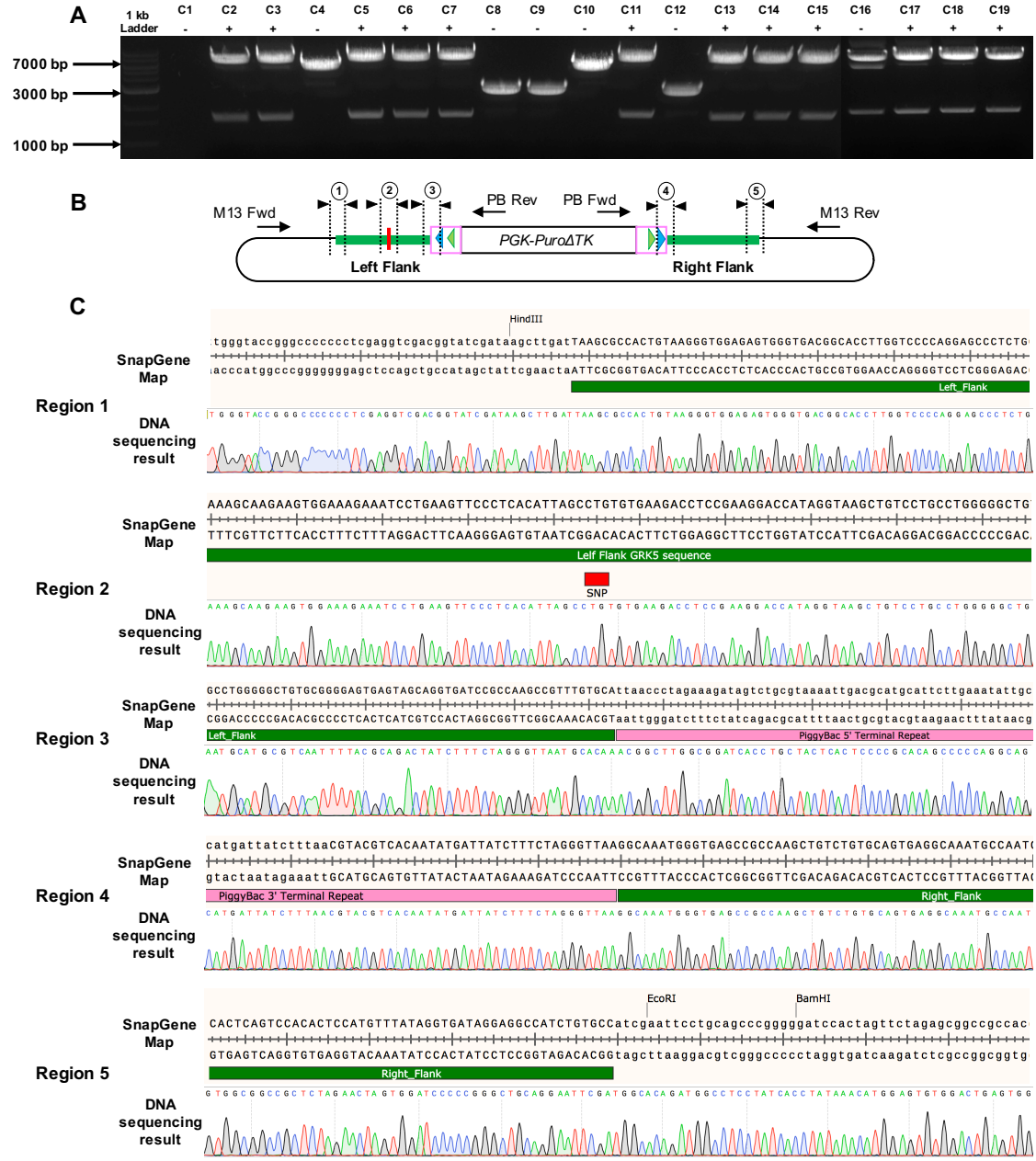


Figure 5.12: Diagnostic analysis of transformed bacteria after Gibson Assembly reaction. **(A)** Dianostic digestion of potential targeting construct using HindIII restriction enzyme, which cut the successfully assembled plasmid into two specific pieces at appoximately 1.5 kb and 7.3 kb (+: positive clone, -: negative clone). **(B)** Schematic of the targeting plasmid and primers used in DNA sequence (back arrows), including M13 Fwd, M13 Rev, PB Fwd, and PB Rev. 5 regions were screened for mismatch, the region border indicated by the dotted lines and back triangles. The *GRK5*-L41 polymorphism is located at the left-flank of the plasmid, indicated as red line. **(C)** Detail screening of each regions. The SnapGene Map shows a 100 bp sequence between **(1)** BlueScript SK plasmid and Left-flank (LF) homology arm, **(2)** the GRK5-L41 sequence, **(3)** LF and 5' PB terminal repeat, **(4)** 3' PB terminal repeat and Right-flank (RF) homology arms, and **(5)** RF and the BlueScript Vector backbone.

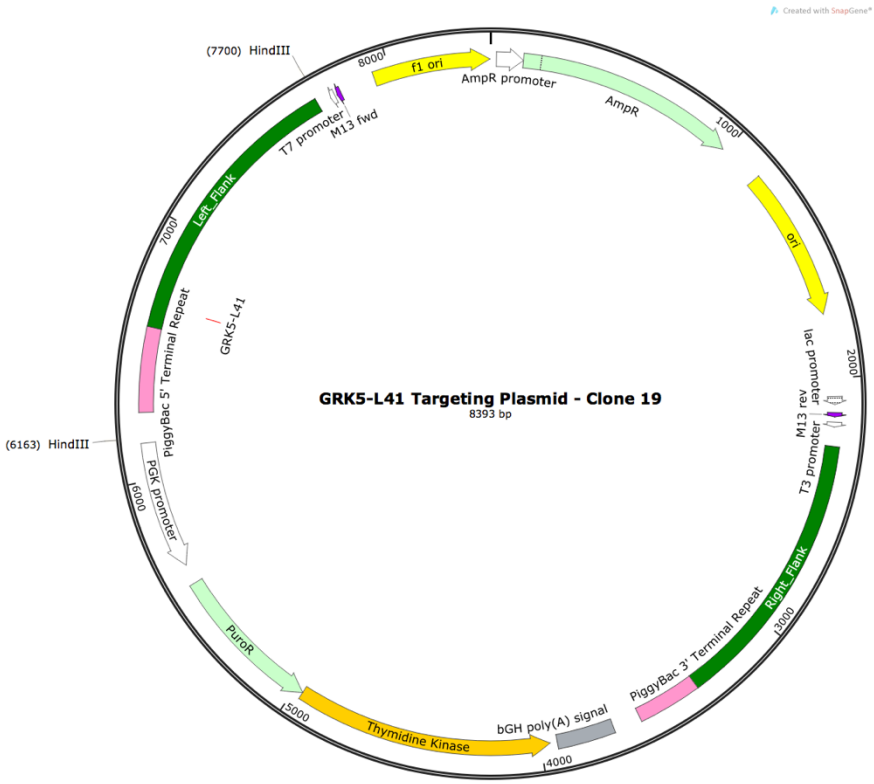


Figure 5.13: The GRK5-L41 expression plasmid map for targeting the HUES7-GRK5-L41 using footprint-free and short-cut strategy. The donor plasmid GRK5-L41 for introducing the GRK5-L41 to HUES7-GRK5-Q41 via HDR-mediated pathway. The expression plasmid comprises the Left flank homology arm (GRK5-LF, Green box) carrying the GRK5-L41 at exon 2 of *GRK5*, the GRK5-PB cassette containing the 5' PB terminal repeat (Pink box), PuroR, TK and PB 3' terminal repeat (Pink box), and the Right flank homology arm (GRK5-RF, Green). The expression of PuroR and Thymidine Kinase was driven by PGK promoter.

5.2.4 Establishment of the *GRK5*-L41 edited lines using Footprint-free and shortcut CRISPR/Cas approach

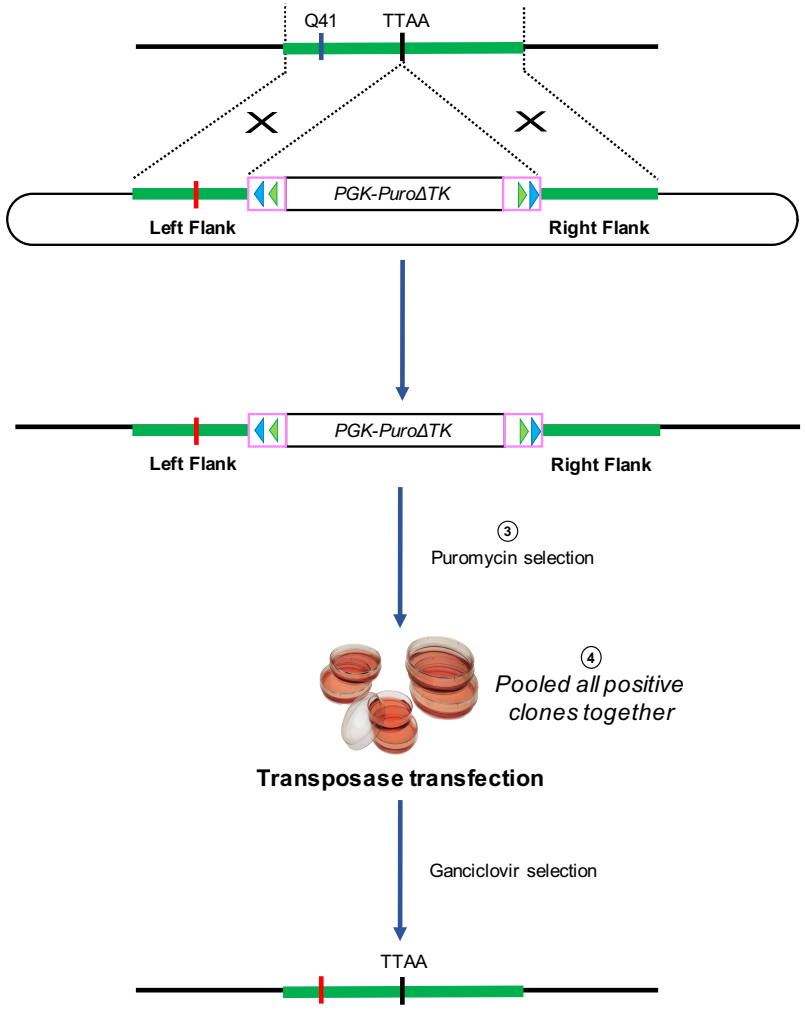
In the following stage of the process, we investigated the feasibility of using the footprint-free and shortcut gene editing approach to create the *GRK5*-L41 gene-edited cell lines via the HDR-mediated pathway. The Figure 5.14 illustrates the proposed short-cut protocol for gene editing using CRISRP/Nickase approach. The comparison between the shortcut and original CRISPR/Cas method was also demonstrated. The components required for each approach is described in Table 5.3. To ensure the specificity and efficiency of the CRISPR system, several controls were used, including **(1)** gRNA control, which contains only gRNA plasmid backbone without target sequence to ensure that the backbone itself could not form the Cas-sgRNA complex, **(2)** the gRNA negative control,

which contains *GRK5* targeting vector, Cas9 expression plasmid, and GFP, to ensure that without sgRNA, CRISPR system will not mediate any DSBs, **(3)** GFP control, to measure the transfection efficiency, and **(4)** Untreated control.

Table 5.3: Components requires for footprint-free/shortcut CRISPR/Nickase and CRISPR/Cas9 approaches.

Editing method	Transfected plasmids	Amount of plasmid (μg)	Total plasmid DNA (μg)	Transfection reagent
Footprint-free and shortcut strategy	GRK5-L41 plasmid	1.1	3.3	FuGENE HD
	gRNA 2a	0.5		
	gRNA 2b	0.5		
	Nickase	1.1		
Conventional Cas9	GRK5-L41 plasmid	1.1	3.3	FuGENE HD
	gRNA 2a	1.1		
	Cas9	1.1		
gRNA control	gRNA plasmid backbone	3.3	3.3	FuGENE HD
gRNA Negative control	GRK5-L41 plasmid	1.1	3.3	FuGENE HD
	Cas9	1.1		
	GFP	1.1		
GFP control	GFP	3.3	3.3	FuGENE HD
Untreated Control	NA	NA	NA	NA

It was observed that Puromycin treatment induced dramatic effects across all tested condition after 24h incubation, where significant cell death was detected (Figure 5.15, d1). After two days in treatment with Puromycin, a majority of cells were lost during the medium change in all conditions, except the untreated control, which showed approximately 40% cell population still attached on the surface of the culture plate (Figure 5.15, d2). On d8 post-transfection, no sign of viable cells was detected in all control condition, indicating that all components of CRISPR, including sgRNA, Nickase/Cas9 expression plasmid, and *GRK5* targeting vectors are essential to induce the gene editing process. Interestingly, colonies started to appear after five days in Puromycin treatment, and on day eight visible colonies could be observed in both footprint-free/short-cut approach and the conventional Cas9 method (Figure 5.15, d8).



	Time requires	Estimated PDs
Original *GRK5*-Q41 allele		
① *GRK5* Targeting Plasmid (in a circular form)	2 weeks	6 PDs
② Targeted *GRK5* allele	2 week	9 PDs
	3 week	11 PDs
⑤ Targeted *GRK5* allele (After PB excision)	2 weeks	9 PDs
Total:	**9 weeks**	**35 PDs**

Figure 5.14: The schematic illustrates the procedure of footprint-free and shortcut CRISPR/Nickase approach. (1) *In silico* design of *GRK5* targeting plasmid and sgRNA. **(2)** Deliver *GRK5* targeting plasmid, sgRNA pair, and Nickase expression plasmid into HUES7-GRK5-Q41 using FuGENE HD transfection reagent. **(3)** 24-post transfection, the cells were cultured with Puromycin for one week. **(4)** Puro-positive clones were then harvest and subjected for transposase transfection followed by incubation with Ganciclovir. **(5)** Colonies were collected using manual dissection and characterisation was conducted. Total time requires for completing the procedure is 9 weeks, and the expected PDs of hPSC is approximately 35 PD times.

At d8, colonies from Cas9 method were harvested and transferred into Matrigel-coated 96 well plate using manual dissection, whereas colonies from footprint-free/short-cut strategy were harvested and cultured in Matrigel-coated 35 mm culture dishes followed by transfection with Transposase expression plasmid.

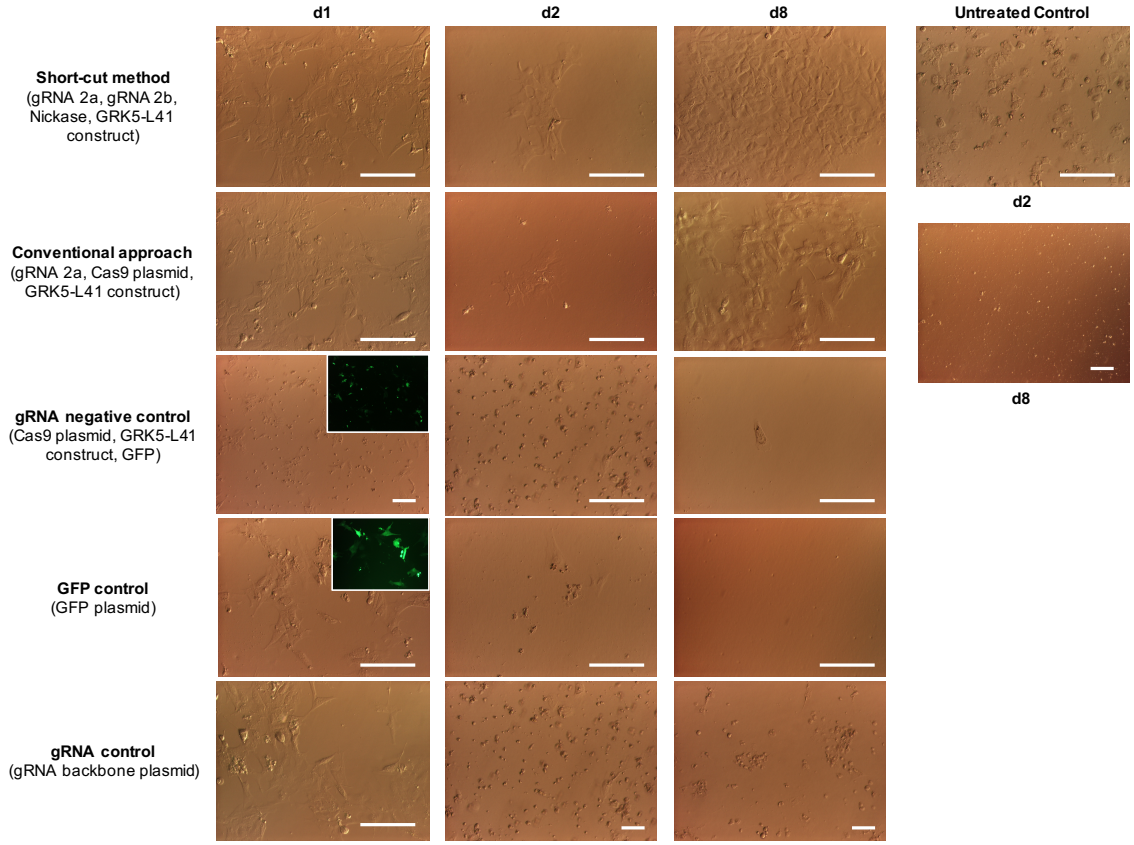
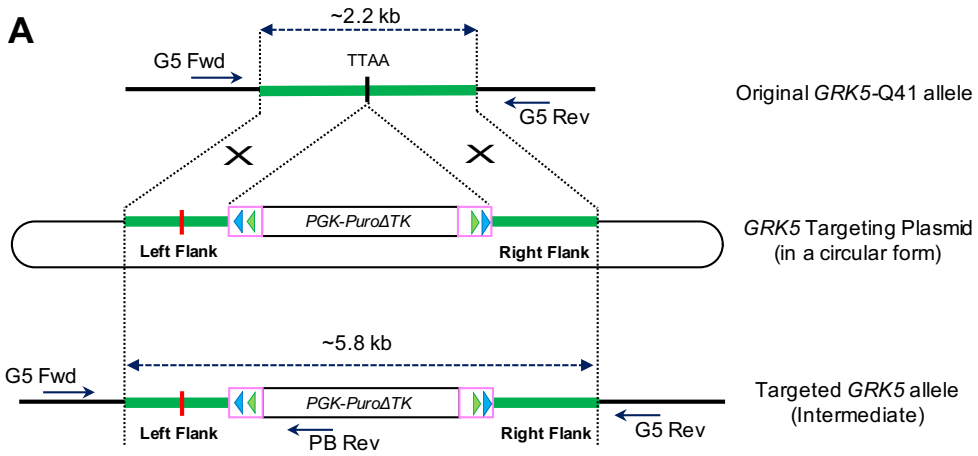


Figure 5.15: Puromycin selection of positive clones for gene editing. Bright field images of HUES7-GRL5-Q41 after undergoing different transfection conditions, including shortcut approach, conventional editing method, gRNA negative control, GFP control and gRNA control. One day after adding Puromycin at 1 μg/ml, significant cell death was observed in all conditions (d1). On d2, more cell death was observed in control condition, but the untreated control still had approximately 40% confluent. Small colonies started to emerge from both shortcut and conventional method. On d8, no sign of living cells was detected from the controls but colonies started to expanded and reached 60% confluent in both shortcut and conventional editing condition. *Scale bar*: 100 μm.

5.2.4.1 Genotypic analysis of intermediated clones derived Footprint-free/Shortcut procedure (Nickase-mediated editing) and conventional CRISPR/Cas9 approach

To analysis the clones obtained from the gene editing experiments, a PCR-based screening of targeted clones was developed using two primer sets, including Left flank analysis (LF) and GRK5 analysis primer pair (Figure 5.16A). The former was designed to amplify the specific sequence spanning from outside of the left-flank (LF) homologous arm to the 5' PB terminal repeat. The latter contained primers that located outside left and right homology arms to amplify the sequence covered the entire targeted locus (Figure 5.16A and B). Several possible results could be obtained from the two primer sets as showed in Figure 5.16C and D. In terms of intermediate clones (after Puromycin selection), if a clean band at approximately 1.5 kb was observed in LF analysis primer pairs, it would mean that the PB transposon was successfully integrated into both alleles, whereas a 2.5 kb PCR product appeared in GRK5 analysis primer pair indicated the unsuccessful integration of the PB transposon element or random combination occurred. When both LF analysis and GRK5 analysis products were observed, it confirmed that the PB transposon was inserted into one allele (heterozygous clones).

A

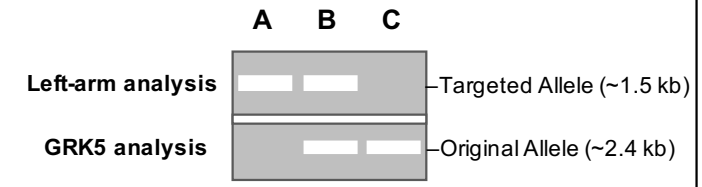


B

	Primer Pair	Primer sequence	Extension time	Product size (bp)
Left Flank analysis	G5 Fwd	CAGAGCAAGGTGGAGGACAG	90 s	1446
	PB Rev	CCTGGGGCTGTAGCTTACTG		
GRK5 analysis	G5 Fwd	CAGAGCAAGGTGGAGGACAG	120 s	2442
	G5 Rev	GATAGGAGGCCATCTGTGCC		

Note: In term of GRK5 analysis primer pair, the extension time is set at 120 s, which allows the amplification of the excision allele only. To amplify the targeted *GRK5* allelle (intermediate stage), the extension time need to be set at 330 s.

C

	Left Arm Analysis	Both Left and Right Arm (GRK5 analysis)
Primer Combination	G5 Fwd and PB Rev	G5 Fwd and G5 Rev
Original Allele	-	G5 Fwd and G5 Rev
Targeted Allele (Intermediate)	G5 Fwd and PB Rev	G5 Fwd and G5 Rev
Band Pattern		

D

Band Pattern	Edited clones	Possible Genotype
A	Intermediate	Both allele targeted (Homozygous); PB transposon element is successfully integrated in both alleles.
B	Intermediate	One allele targeted (Heterozygous); one allele targeted and small indel on the other allele.
C	Intermediate	Non-targeted alleles; one non-targeted and a small indel on the other allele. Both have random integrations.

Figure 5.16: PCR-based screening strategy of intermediate clones. (A) A diagram illustrates the gene targeting and primer design for genotypic analysis of edited clones. The arrows represent primers used in genotyping. The red bar indicates the modified nucleotide (*GRK5*-L41). **(B)** The details of primer pairs used to genotypic analysis of targeted clones. **(C)** PCR-based genotyping of alleles. The Left flank and GRK5 analysis is analysed in a separated PCR reaction. **(D)** Possible genotypes predict from the band pattern obtained from **C**.

Because of the Footprint-free and Shortcut approach using Nickase instead of Cas9 as the core endonuclease, it is important to compare the gene editing efficiency mediated by the two enzymes. To complete the task, 38 intermediate clones from Footprint-free and Shortcut procedure (NG clones) were manually picked before combining the remaining Puro-positive clones together for transposase transfection. In CRISPR/Cas9 approach, 22 intermediate clones (CG clones) were collected for genotypic analysis and the remaining culture was terminated due to intensive workloads required for maintenance of these clones. To confirm the specificity of the LF-analysis and GRK5 analysis primer pairs, the genomic DNA obtained from HUES7-GRK5-Q41 was used. Expectedly, the LF-analysis primer pair did not amplify any product, whereas the GRK5 analysis set generated a band at approximately 2.4 kb, confirming the specificity of these two primer sets (Figure 5.17A).

In terms of Nickase-mediated gene editing (Footprint-free and shortcut approach), the PCR-based screening strategy as described above identified 18 heterozygous NG clones, eight homozygous clones, and eight non-targeted clones, accounting for 47%, 21% and 21% of the total analysed clones, respectively (Figure 5.17A and C). This result was slightly different from that of Cas9-mediated gene editing, which showed 59% of the analysed clones were heterozygous, 9% was homozygous, and 18% was non-targeted clones (Figure 5.17B and D). Both Nickase- and Cas9-mediated editing techniques had 11%, and 13% of total analysed clones illustrating an unclear result from PCR screening, which might be the technical problems occurred during harvesting and DNA extraction of a vast number of isolated clones.

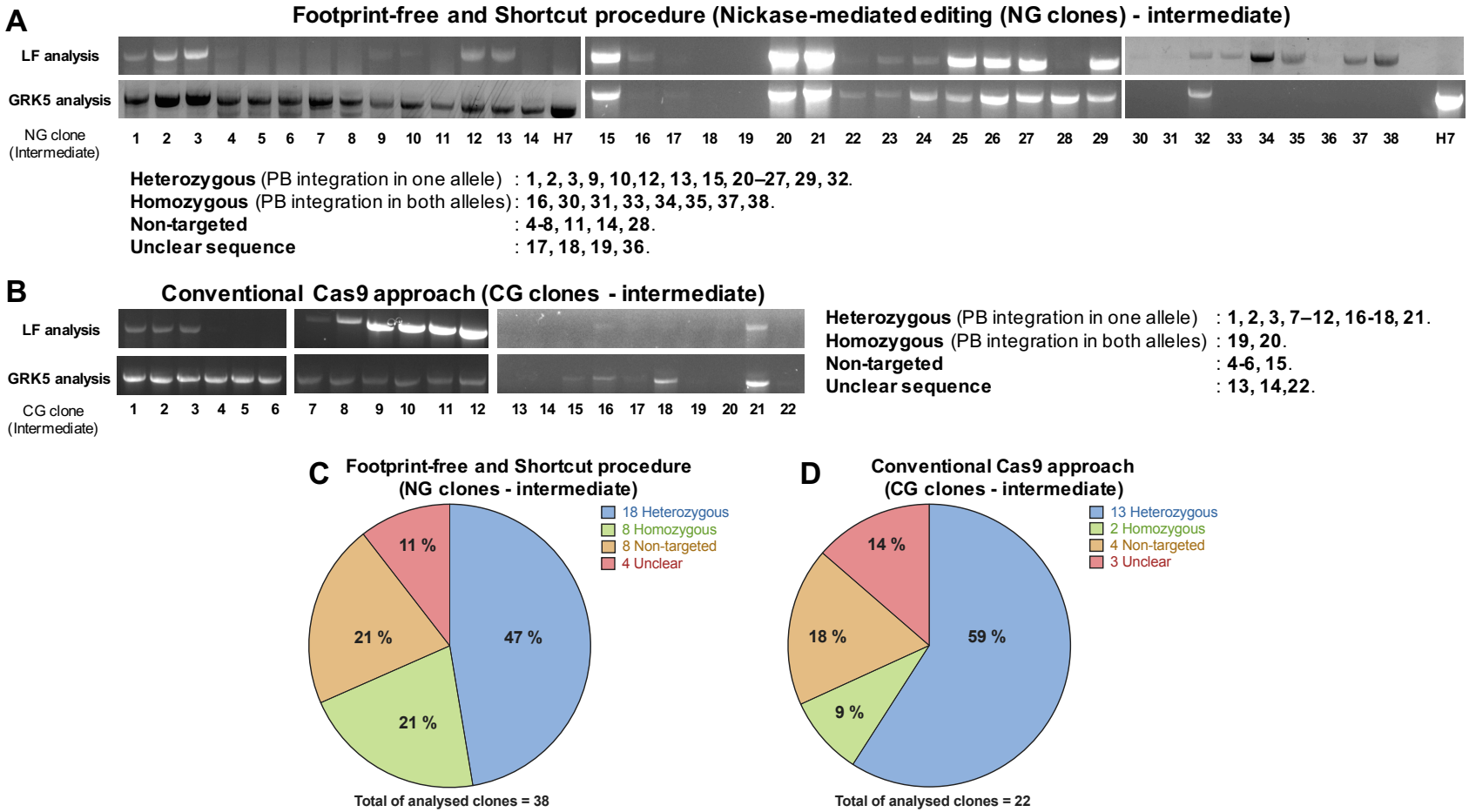
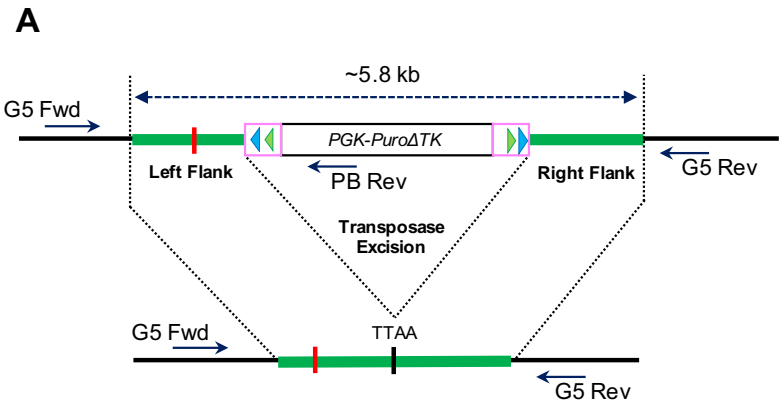


Figure 5.17: PCR-based analysis of intermediated clones derived from Nickase-mediate (NG) and Cas9 (CG) conventional approach. (A) The agarose gel analysis illustrates the results obtained from genotyping of Nickase-mediated (NG) clones. The HUES7-GRK5-Q41 (H7) sample was used as the control to confirm the specificity of both LF-analysis and GRK5 analysis primer set. **(B)** The genotyping results of the clones derived from conventional CRISPR/Cas9 method (CG clones). **(C and D)** The pie charts display the percentage of heterozygous, homozygous, non-targeted and unclear results from the NG and CG clones, respectively.

5.2.4.2 Genotyping analysis of final clones generated from Footprint-free and Shortcut strategy

After ten days in Ganciclovir treatment, 30 clones from Footprint-free and Shortcut approach (SG clone) were manually picked and expanded in culture. The first 15 clones that were able to be transferred into the Matrigel-coated 6-well plate were subjected for PCR-based screening diagnostic using the LF-analysis and GRK5 analysis primer pair as mentioned above (Figure 5.18A). The amplicons generated from GRK5 analysis primer pair were collected and sent for DNA sequence to confirm the genomic sequence of the clones at the *GRK5*-L41 position and the TTAA integration sites. The remaining clones were harvested and cryopreserved as a backup plan.

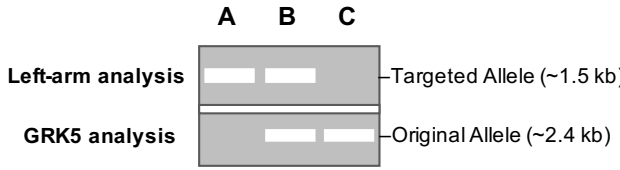
Depending on the band pattern from the two primer sets, different genotypic possibilities of the clones are predicted (Figure 5.18B). The analysis results indicated that ten SG clones out were successfully removed the PB transposon from both alleles (Figure 5.18C). The remaining five clones showed bands derived from both LF-analysis and GRK5 analysis primer sets indicated that the PB transposon was completely excised from one allele, whereas it re-integrated in the other alleles (Figure 5.18C). From the PCR-screening results, 67% of the clones are homozygous excision of PB in both alleles, and only 33% of the clones had PB transposon removal from one allele (Figure 5.18D).



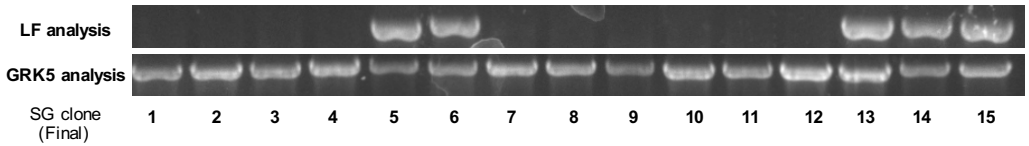
Targeted *GRK5* allele (Intermediate)

Targeted *GRK5* allele (Final - After PB excision)

B

	Left Arm Analysis	Both Left and Right Arm (GRK5 analysis)
Primer Combination	G5 Fwd and PB Rev	G5 Fwd and G5 Rev
Intermediate clones	G5 Fwd and PB Rev	G5 Fwd and G5 Rev
Final clones (after excision)	G5 Fwd and PB Rev	G5 Fwd and G5 Rev
Band Pattern		
Predicted genotypes	**A**: PB transposon remaining at both alleles (Unsuccessful excision) **B**: Transposon removed from both alleles, but at least one transposon re-integrated (Heterozygous excision). **C**: Transposon removed from both alleles and no-reintegration (Homozygous excision).	

C



Heterozygous (PB excision in one allele) : 5, 6, 13, 14, 15.
Homozygous (PB excision in both alleles) : 1-4, 7-12.

D

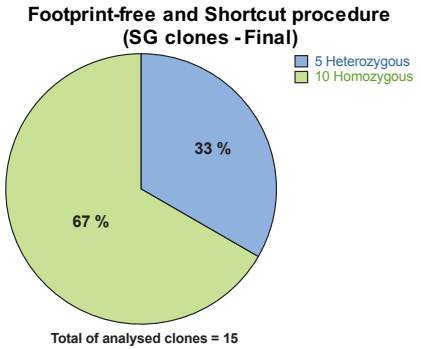


Figure 5.18: PCR-based screening of transposon-excised clones. (A) Schematic of PB selection cassette excision and primer design. Arrows presents the primers. The LF-analysis and GRK5 analysis primers were used, which amplified amplicons at ~1.5 kb and 2.4 kb, respectively. The red bar demonstrates the position of the *GRK5*-L41 polymorphism. **(B)** The possible band patterns and predicted genotypes from the PCR samples. **(C)** The PCR results of the final clones obtained from Footprint-free and Shortcut gene editing approach. **(D)** The pie chart illustrates the percentage of heterozygous excision and homozygous excision of the PB analysed from the PCR result (C).

The DNA sequencing results indicated that all 15 clones showed a sign of genetic modification at the genomic level around the targeted locus (*GRK5*-Q41), accounting for 100% gene editing efficiency (Table 5.4). Furthermore, the data indicated that two clones had the replacement of *GRK5*-Q41 by *GRK5*-L41 in both alleles, and the SG08 clone appeared to have intact sequence at the PB integrated site (TTAA) and no other mismatch sequence when compared to the original HUES7-GRK5-Q41 genomic sequence (Figure 5.19). Seven heterozygous clones were identified, which have the modification occurred in one allele (GRK5-Q/L41). Further analysis of the DNA sequence identified the clone number 12 (SG12) bearing the clean *GRK5*-Q/L41 sequence, a complete formation of the integration site (TTAA) after transposon excision, and no mismatch sequence compared to that of HUES7-GRK5-Q41 genomic DNA (Figure 5.19). Of note, the mismatch sequence usually occurred around the cleavage site of the Nickase and at the integration site after PB transposon excision (Figure 5.19, clone number: SG01, SG02, and SG03). Hence, depending on the DNA sequence results, the homozygous SG08 and the heterozygous SG12 clones were selected for further expansion and characterisation; and hereinafter they were called HUES7-GRK-L41 and HUES7-GRK5-Q/L41, respectively.

Table 5.4: Summary of the gene editing results. Table represents the gene editing efficiencies, percentage of homozygous (L41) and heterozygous (Q/L41) clones established by using Footprint-free and Shortcut procedure or the conventional CRISPR/Cas9 method.

Editing method	Transfected plasmids	Distance b/w nicks (bp)	Isolated clones	Number of clones analyzed	Number of positive clones	Editing Efficiency (%)	*GRK5* variants	Percentage
Footprint-free and shortcut strategy	GRK5-L41 plasmid	55	Intermediate	38	26	68.4 %	L41	21 %
	gRNA 2a						Q/L41	47 %
	gRNA 2b		Final (After PB excision)	15	15	100 %	L41	13 %
	Nickase						Q/L41	47 %
Conventional Cas9	GRK5-L41 plasmid	-	Intermediate clones	22	15	68.1%	L41	9 %
	gRNA 2a							
	Cas9						Q/L41	59 %
	-							

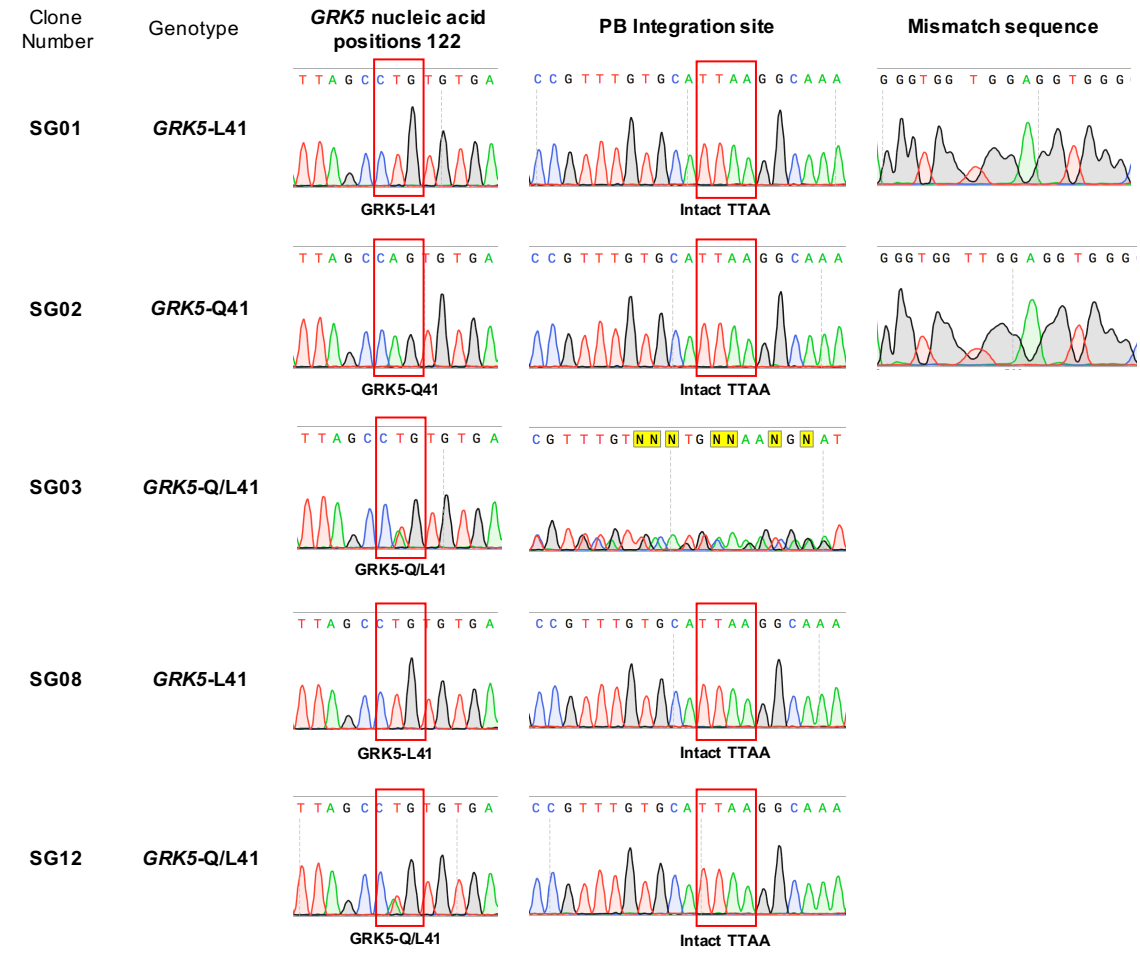


Figure 5.19: DNA sequencing results of the final clones derived from Footprint-free and Shortcut gene editing approach. A genetic modification of the *GRK5*-Q41 locus is shown here. The chromatograms represent different genotypes obtained after PB transposon excision. The TTAA sequence should be observed at the transposon excision site. Modified nucleotides at the nucleic acid positions 122 of the *GRK5* should be detected. Depending on the DNA sequencing results, four main genetic modifications were observed, including **(1)** *GRK5*-L41 + mismatch (SG01): successful modification at the intended locus in both alleles, intact TTAA site, but clones showed the mismatch sequence near the cleavage site of Nickase, **(2)** *GRK5*-Q41 + mismatch (SG02): no modification was detected at the target site, intact TTAA and mismatch occurred close to the Nickase cleavage site, **(3)** *GRK5*-Q/L41 (SG03): the targeted modification happened in one allele but the TTAA site was interrupted after PB transposon excision, **(4)** *GRK5*-L41 (SG08): successful modification of the *GRK5*-L41 in both alleles, intact TTAA integration site, and no mismatch sequence was found, and **(5)** *GRK5*-Q/L41 (SG12): successfully introduced the *GRK5*-L41 sequence in one allele of the cells, intact TTAA site, and no mismatch sequence was found.

5.2.5 Characterisation of the HUES7-GRK5-L41 and HUES7-GRK5-Q/L41

After the clones HUES7-GRK5-L41 and HUES7-GRK5-L/Q41 were successfully edited, it was important to determine whether these clones could maintain the pluripotent characteristic and normal karyotype after the two rounds of selection and clonal isolation. These two clones were first cultured in the MEF-CM-bFGF medium as described in Section 2.1.3 and cryopreserved to create the cell bank. The lines were then transitioned into E8 culture medium as described in Section 2.1.4. and maintained in the E8 culture for at least three passages before starting characterisation. In E8 culture condition, the clones displayed high nuclear-cytoplasmic ratio, prominent nuclei, and maintained a polygonal shape similar to the parental HUES7-GRK5-Q41 line (Figure 5.20A). The population doubling times of HUES7-GRK5-L41 and HUES7-GRK5-L/Q41 were 21.7 ± 0.9 hours and 22.7 ± 1.4 hours, respectively, which were calculated over five passages (Figure 5.20B). To confirm the pluripotency, both cell lines were harvested and stained for pluripotency markers, including NANOG, OCT4, and SOX2. Immunocytochemistry results confirmed that both cell lines expressed all tested pluripotency markers, concentrated in the nucleus of the cells (Figure 5.20C). Chromosomal abnormalities were ruled out by analysing 30 metaphase spreads, which illustrated the normal karyotype obtained from both cell lines (Figure 5.20D).

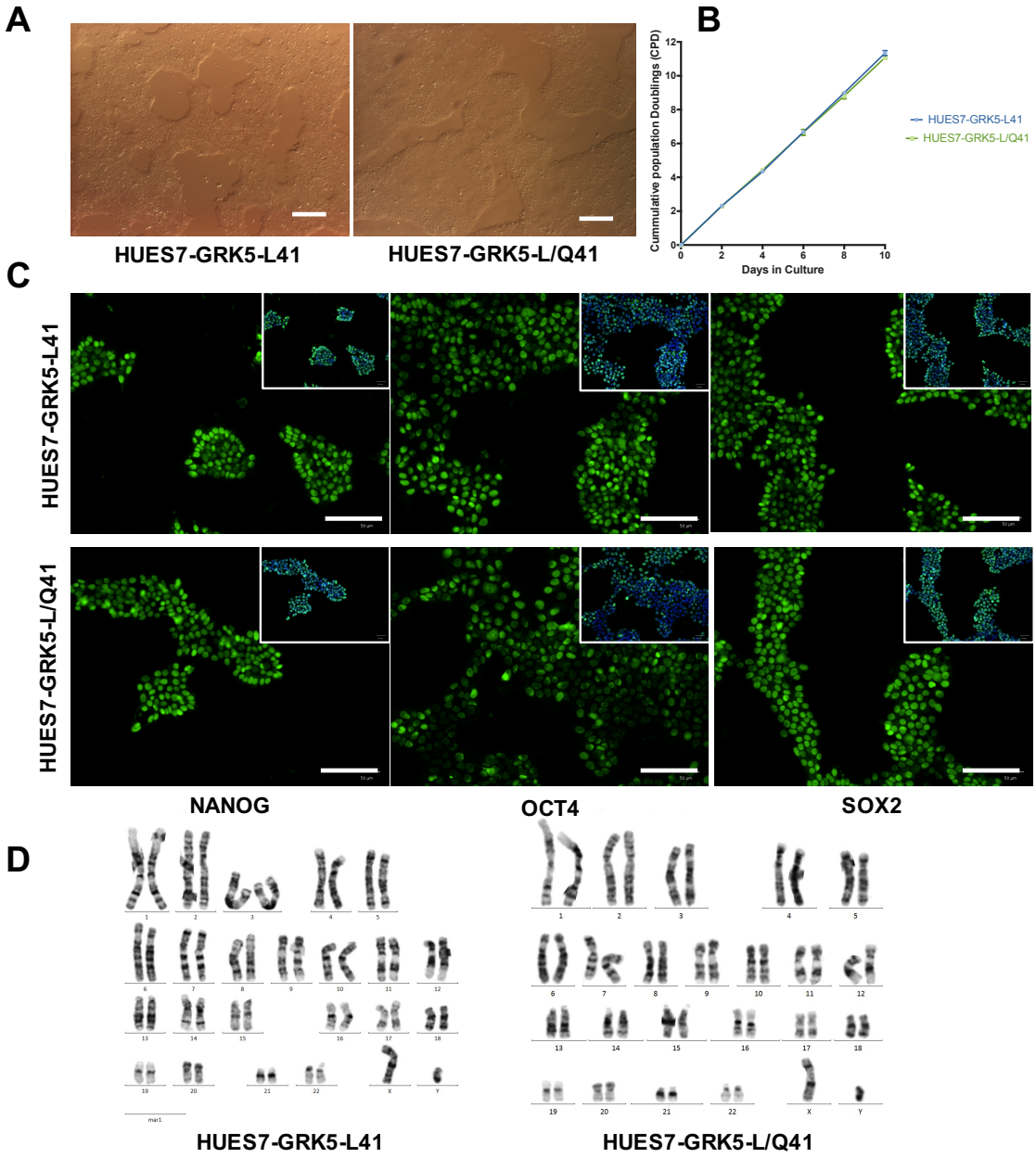


Figure 5.20: Characterisation of edited HUES7-GRK5-L41 and HUES7-GRK5-Q/L41 derived from footprint and shortcut method. (A) Bright-field images of both cell lines at passage 35 in E8 culture condition. **(B)** Growth curve of HUES7-GRK5-L41 and HUES7-GRK5-L/Q41 over 5 passages in E8 (between passage 32 to 37) demonstrated PD of 21.7 ± 0.7 and 22.7 ± 1.4 hours. **(C)** Representative immunocytochemistry images of pluripotency markers, including NANOG, OCT4, and SOX2, confirming these cells expressed high nuclear pluripotency markers. **(D)** Representative karyograms of a metaphase spread of HUES7-GRK5-L41 and HUES7-GRK5-L/Q41 depicting a normal 46, XY karyotype at passage 37.

5.2.6 Cardiac differentiation of the HUES7-GRK5-L41 and HUES7-GRK5-Q/L41

Regarding the cardiac differentiation ability of newly established gene editing lines, HUES7-GRK5-L41, and HUES7-GRK5-L/Q41, the monolayer cardiac differentiation as described in Chapter 3 was used to differentiate these cell lines into cardiac lineage. Both of the clones were cultured at least five passages after the E8 transition to render cells genetic and growth stability before starting differentiation. The optimised cell seeding density of both HUES7-GRK5-L41 and HUES7-GRK5-L/Q41 was 40.000 cells/cm^2. Established HUES7-GRK5-L41 and HUES7-GRK5-L/Q41 were successfully differentiated into cardiomyocytes, with beating monolayer observed on day 8 of the cardiac differentiation process. Cardiomyocyte purity was confirmed using flow cytometry with a cardiac-specific marker, cardiac troponin T (cTNT). The results showed that 85% ± 3% and 88% ± 5% of the population derived from HUES7-GRK5-L41 and HUES7-GRK5-L/Q41, respectively, were cTNT positive cells (mean ± SEM, n=3). This result indicated that high purity of cardiomyocytes could be generated from both of edited lines.

5.3 Discussion

The *GRK5*-L41 has been reported to have cardiac protective functions during heart failure. This *GRK5* polymorphism bears a single mutation which changes a nucleotide at position 122 of *GRK5* from A to T (c.A122T), leading to the alteration of the codon triplet encoding for Q into L at position 41 of GRK5 protein (c.Q41L) (Ligget et al., 2008). To date, a human cardiac model has yet been established to investigate the "gain-of-function" *GRK5*-L41 polymorphism. Hence, this chapter demonstrates the new approach that using the latest advance in genome editing (CRISPR/Cas technology) to introduce the *GRK5*-L41 polymorphism into the hESC line (HUES7) and create isogenic lines followed cardiac differentiation to provide an unlimited source of human cardiomyocytes harbouring the *GRK5*-L41 genotype.

To accomplish the task, we developed a Footprint-free and shortcut gene editing procedure which uses CRISPR/Nickase and *piggyBac* transposon containing puroΔtk selection cassette as a core of the technique. Furthermore, the high effectiveness of the CRISPR system together with the high transfection efficiency allows us to skip the first round of the clonal selection and expansion after Puromycin treatment. The Puro-positive clones were harvested, combined and expanded followed transfection of transposase expression vector to remove the PB element. The Ganciclovir treatment directly eliminated the clones which still possessed the selection cassettes. The final clones were then manually dissected and characterised using a simple PCR-based screening strategy. This chapter demonstrated that the Footprint-free and Shortcut strategy significantly reduced the time required for generating the final clone into two months, which in turn, lowered the PDs time of the hESCs into 56 PDs time lessened the potential risks of abnormal karyotypes, mutation accumulations, and reduction in cardiac differentiation ability.

5.3.1 Limitations of the conventional gene editing approach

Besides the technical limitations of the gene editing itself, for example the difficulty in design (ZFNs, TALENs), labour intensive (ZFNs), expensive cost (ZFNs, TALENs)

and off-target effects (ZFNs, TALENs, and CRISPRs), the time consuming is one of the great challenges, especially for genome editing of hPSCs. Originally, the PB transposon incorporation with ZFNs was developed to induce the footprint-free editing in hPSCs, which requires approximately 16 weeks to complete the procedure (Yusa, 2013). Recently, efficient and footprint-free hPSC genome editing by the consolidation of PB transposon and CRISPR/Cas9 technology has been established, which requires 14 weeks to generate the final edited clones (Wang et al., 2017).

Figure 5.21 summarises the current gene editing process using CRISPR/Cas9 system incorporation with PB transposon technology. Indeed, the total time required to complete the procedure is approximately 16 weeks. Assuming that the hPSC growth rate is similar to the average growth rate of hESC lines (HUES7), which has the population doubling (PD) time around 21 hours (Denning et al., 2016). To accomplish the gene editing process, the hPSCs undergo approximately 46 PD times, excluding cardiac differentiation optimisation process. Also, it is important to note that during the gene editing process, the hPSCs proliferate slowly from single cells into the fully packed colonies and undergo serial passages. Indeed, the effects of serial passages on hPSCs have been well characterised by the accumulation of genetic abnormalities and epigenetic instability which result in the formation of aberrant karyotypes and compromise the differentiation ability of the hPSCs (Mitalipova et al., 2005; Allegrucci and Young, 2007; Takahashi and Yamanaka, 2016). Hence, it is important to reduce the time required for gene editing to eliminate the potential threats of serial passages and prolonged cultures of stem cells *in vitro*.

Upon investigation of the gene editing procedure, it is noted that the first drug selection step is comprised of the full characterisation of the colonies after isolation, including clonal expansion, PCR-base verification, DNA sequence, karyotype, and cryopreservation of targeted clones. All of these steps are not only time-consuming but also labour-intensive due to the high number of clones to be isolated and maintained. Also, this process took at least 11 weeks to complete and resulted in the accumulation of approximately 20 times of PDs from the hPSCs. Moreover, in our experience,

cryopreservation of clones could strongly affect the expression of the resistance cassette after thawing.

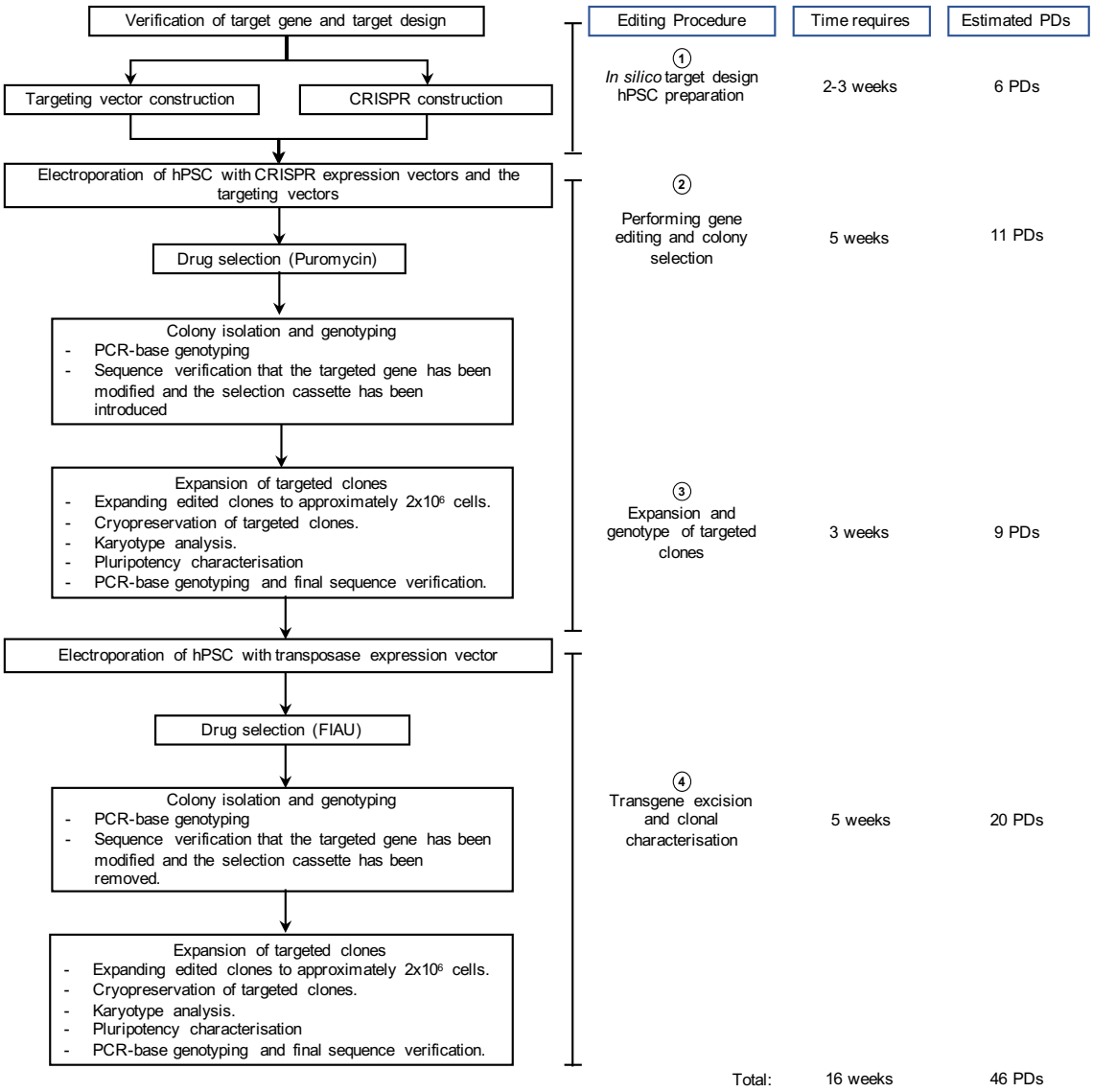


Figure 5.21: Overview of the procedure for targeted modification using the *piggyBac* transposon system. The schematic on the left illustrates the detail procedure, which is summarised in four main steps, including **(1)** *In silico* design modification of the target sites and preparation of the hPSCs, **(2)** starting gene editing experiments by delivered the CRISPRs components into the hPSCs using electroporation or transfection, **(3)** Clonal selection and expansion using Puromycin followed the genotypic analysis of the targeted clones, **(4)** electroporation of transposase expression plasmid to remove the selection cassette and clonal characterisation. The estimated time requires to complete the procedure is approximately 16 weeks, and the hPSCs undergo 46 population doubling (PD) times. Timeline is adapted from Yusa., 2011.

5.3.2 The idea of "footprint free" and "shortcut" gene editing approach

Detailed analysis of the gene targeting procedure using *piggyBac* transposon system and CRISPR/Cas9 technology indicates that there are two around of clonal expansion and fully characterisation of drug-selected clones in the process. However,

the first round of selection where clones are picked based on Puromycin selection results in the addition of passages and labour intensive due to a high number of clones needed to be isolated and maintained followed cryopreservation of targeted clones. Corrected clones from this first round are then subjected to the second round of clonal selection to remove the drug resistant cassette using transposase, which adding the same amount of PD time as well as labour and time require to finish the process. Hence, assuming that the targeting efficiency is high enough due to the effectiveness of the CRISPR/Cas technology and the optimisation of transfection method, it is possible that the first round of clonal expansion and characterisation can be skipped (Figure 5.22).

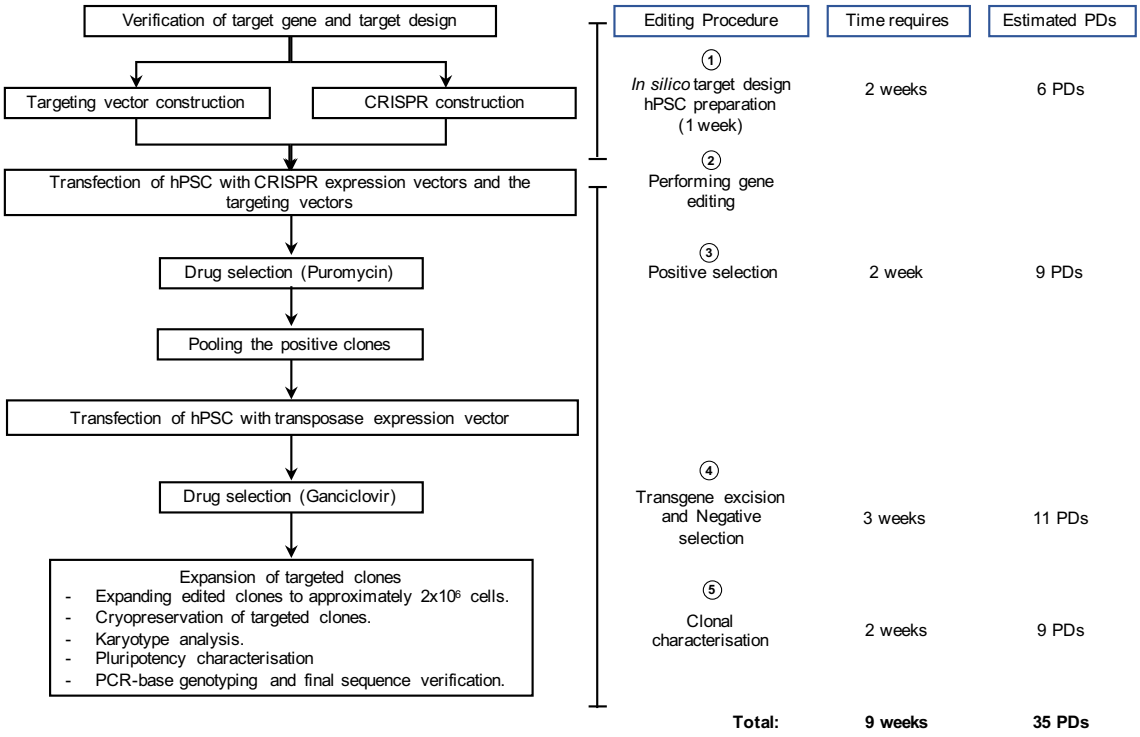


Figure 5.22: Suggested procedure of footprint-free and shortcut gene editing strategy. The diagram describes the procedure that could potentially reduce significantly the time requires to generate the footprint-free gene edited hPSCs after cassette excision. The procedure is consisted of five main steps: **(1)** *In silico* design of target modification and gene editing constructs, the hPSCs at early passage are cultured one week before starting gene editing experiment (enough time to allow the stable growth after cryopreservation), **(2)** Once all components requires for CRISPR/Cas are prepared (sgRNA plasmids, Cas9 plasmids, and targeting vectors), gene editing is performed followed treatment with puromycin for one weeks to positively select the clones **(3)**, the Puromycin-positive clones are then pooled together and subjected to transfection with transposase expression plasmid, **(4)** the resulting clones are then underwent negative selection using Ganciclovir treatment. The final clones are expanded and fully characterised to confirm and verify the modification at the target locus. This strategy reduces significantly the time required for gene editing to 9 weeks, which in turn, decrease the PDs of the hPSCs to 35 PDs, excluding the times require for cardiac differentiation optimisation.

The idea of Footprint-free genome editing using *piggyBac* transposon is firstly derived from Kosuke Yusa, who incorporated the *piggyBac* system with ZFNs platform to correct a mutation causing α-1 antitrypsin deficiency in patient-derived hPSCs (Yusa, 2013). The approach required two rounds of genetic manipulation together with clonal isolation and expansion to achieve homozygote modification. The entire process takes approximately four months to complete (Yusa, 2013). Following this work, PB transposon was then incorporated into different genome editing platforms, including TALENs and CRISPR/Cas to amend the gene mutation causing β-thalassemia in patient-specific iPSC (Sun and Zhao, 2014; Xie et al., 2014). Recently, the *piggyBac* transposon system incorporation with CRISPR/Cas9 platform has been used to create the Doxycycline (Dox) inducible cell lines which allow performing genome editing by the only transfection of CRISPR/Cas components under Dox treatment. The Dox-inducible transposon is later can be excised to generate Footprint-free edited cell lines (Wang et al., 2017). The advantage of this method is that establishment of a Dox-inducible clonal line just needs to perform once to generate the common parental line, which later can be used to target different gene and reduces the gene editing time significantly to 7 weeks (Wang et al., 2017). Although this approach provides a new strategy that could shorten the gene editing times, the edited lines derived from the parental lines, in fact, are undergone the entire editing process, which takes 14 weeks (112 PD times). Also, the gene editing is restricted in the genotype of the parental line, which in turn, limits the downstream applications. One might argue that several parental lines could be generated depending on the research purposes, but the time requires to create the parental lines, and final edited lines might be equal to the time generate the edited lines using normal CRISPR/Cas9 and *piggyBac* transposon procedure.

In terms of gene editing field, three major systems for specific DNA cleavage to promote homologous recombination have been described, including zinc-finger nuclease (ZFNs), transcription activator-like effector nucleases (TALENs) and CRISPR/Cas nuclease (Urnov et al., 2005; Wood et al., 2011; Jinek et al., 2012). The ZFNs requires a complicated system to design and costly to generate. TALENTs can be

made within a short time using an established protocol; but it is expensive, labour intensive and requires multiple pairs to test their cleavage efficiency. Moreover, TALENT's activities are heavily depending on the DNA methylation and histone modification of the target genes, and are hampered by chromatin inactivation (Miller et al., 2007; Wood et al., 2011). In contrast, the CRISPR/Cas system is not limited by these obstacles and is easily produced. In this system, the sgRNA contains 20 nucleotides of the homologous sequence to the target gene; and it can be generated by simple cloning onto the gRNA plasmid (Jinek et al., 2012; Mali et al., 2013; Cong et al., 2013).

To introduce the *GRK5*-L41 into HUES7-GRK5-Q41 (Zhang et al.), we constructed the GRK5-L41 targeting plasmid to provide an exogenous sequence containing 2 kb homology arms carrying the *GRK5*-L41 sequence generated by using specific SNP introducing PCR in the Left-flank homology arm (1 kb) and the Right-flank homology arm bearing 1kb sequence downstream the PB integrated site (TTAA). The donor plasmid also contains a *piggyBac* transposon, which is a mobile element that can be removed efficiently in human stem cells (Yusa, 2015). Also, the PB transposon carries a bi-functional fusion protein called puroΔtk driven by PGK promoter, the highly-activated promoter in mammalian systems, including hPSCs (Yusa, 2013; Wang et al., 2017). This fusion protein construct forms the specific selection cassette providing the advantage for the system. In this construct, puro (puromycin N-acetyltransferase) is used for positive selection of the clones after the first round of clonal selection. After transposase transfection, Δtk (a truncated version of herpes simplex virus type 1 Thymidine kinase) is used for negative selection that allows selecting the clones, which do not harbour the PB selection cassette under Ganciclovir treatment (Yusa et al., 2009; Sun and Zhao, 2014). In fact, most of the papers using the PB transposon in gene editing used 1-(2-deoxy-2-fluoro-β-D-arabinofuranose)-5-iodouracil (called Fialuridine or FIAU) as a thymidine analogue because FIAU can be used at a relatively low concentration (0.2 μM) compared to Ganciclovir (2 μM) and had claimed to have no associated with genomic instability (Yusa, 2013). However, FIAU is far more expensive compared to Ganciclovir.

Using PB transposon element containing puroΔtk selection cassette allows isolating the edited clones that are seamlessly removed the PB transposon, which differ from the conventional *Cre/loxP* and FRT system that leaves 34 bp footprint upon excision of the insert (Hockemeyer et al., 2009; Zou et al., 2009).

In our study, by analysing the intermediate clones of the footprint-free and shortcut method, the homologous recombination rate mediated by Nickase was 68.4%, which is higher that of previously reported in ZFNs (Yusa, 2013), TALENs (Sun and Zhao, 2014) and CRISPR/Cas9 platform (Xie et al., 2014). Eight out of 38 intermediate clones had recombination occurring in both alleles (Homozygous clones); and 18 out of 38 clones had PB integration in single allele (Heterozygous clones), accounting for 21% and 47%, respectively. There is no significant different between Nickase- and Cas9-mediated editing at the intermediate stage, as our Cas9 results indicated 68% of homologous recombination rate. However, the rate of PB integration in both alleles (bi-allelic modification) in Nickase-mediated approach is higher than that of Cas9 protocol, which was 21% and 9% rate, respectively. This result is in line with other studies confirming that Nickase mediated gene editing creates higher rate of bi-allelic targeting compare to that of Cas9 and reduces significantly the off-target effects (Eggenschwiler et al., 2016; Hsu et al., 2014; Mikami et al., 2016; Shen et al., 2014). Furthermore, the Footprint-free and Shortcut approach is proven to have higher excision efficiency, which 100% analysed clones show the excision of the PB transposon in at least one allele after Ganciclovir selection, compared to previously reported study (Xie et al., 2014). Among them, 67% of selected clones showed a successful excision of the PB transposon in both of the alleles. The DNA sequencing confirmed 13.3% homozygous edited *GRK5*-L41 and 46.6% heterozygous edited *GRK5*-Q/L41. These solid results demonstrated the efficiency of the presented editing strategy. The effectiveness can be explained by the fact that longer homologous arms were used in our study (2 kb in total) compared to the earlier study by Xie and colleagues, which used 500 bp homologous arms (Xie et al., 2014). This speculation is firm supported by other reports which stated that longer

homology arms increased the HDR-mediated recombination of gene editing (Hasty et al., 1991; Beumer et al., 2013; Merkle et al., 2015; Hendriks et al., 2016).

Although the PB transposon showed an effective way to create "footprint-free" GRK5-L41 edited clones, the conventional PB method required two rounds of clonal selection and expansion, which increased significantly the passage number of hESC leading to the potential karyotypic abnormalities and compromised severely differentiation efficiency of hESCs due to serial passages (Mitalipova et al., 2005; Allegrucci and Young, 2007). Therefore, a shorter editing process is needed to prevent these problems. This chapter has proven that under high editing efficiency, it was possible to eliminate the first round of clonal expansion and genotypic analysis of intermediate clones. The Puro-positive clones can be directly pooled together and subjected to transposon transfection, and Ganciclovir selection subsequently. This workflow created a new footprint-free, shortcut gene targeting method, which shortened the time required for editing notably, from 4 months to 8 weeks, without affecting the editing efficiency. Furthermore, the shortcut editing approach also reduced the PD times significantly, protecting the hPSCs from mutation accumulation and genomic instability.

One of the main concerns of genome engineering is the off-target effect, which is the term defining the potential modifications that occur in different loci apart from the intended gene. So far, deep DNA sequence is the best method for screening the off-target effects of CRISPR/Cas9, although several alternative methods have been developed including Southern Blot, off-target PCR analysis, GUIDE-seq method, etc. (Tsai et al., 2015; Hsu et al., 2014). Furthermore, it has been reported the design of sgRNA plays a significant role in the prevention of off-target effects (Doench et al., 2014). In our project, the design of sgRNA was conducted using the Online CRISPR tool called WGE from Sanger Institute, which provides an easy access and precise prediction of gRNA design and off-target effects (Hodgkins et al., 2015). Additionally, the sgRNA chosen from the tool are followed a set of rules to not only minimise the off-target effects but also support the scenarios established by Footprint-free approach, including **(1)** two sgRNA need to be used for Nickase approach, **(2)** at least one gRNA of the pair need to

cover the identified TTAA site, **(3)** distance between the two sgRNA should be between 5 to 26 bp (Len et al., 2014), **(4)** the off-target analysis from WGE of the sgRNA pair need to be less than 2, and **(5)** the nuclease cutting site need to be close to the *GRK5*-Q41 position to achieve higher gene editing efficiency (Inui et al., 2014). By following these criteria, the sgRNA pair chosen in this study has shown no off-target effects using Nickase approach, confirming by both WGE Tool and MIT CRISPR/Cas design tool (http://crispr.mit.edu). Also, CRISPR/Nickase approach has been demonstrated to lower the incident of off-targets and increase the homologous recombinant efficiency (Cong et al., 2013; Ran et al., 2013a; Shen et al., 2014).

Although the GRK5-L41 was successfully integrated into HUES7-GRK5-Q41 using the footprint-free, shortcut method, the functional analysis of the cardiomyocytes derived from these cell lines was hindered by the fact that these cardiomyocytes expressed embryonic and foetal characteristics (Mummery et al., 2012; Burridge et al., 2014). Investigation of a switch to mature cardiomyocytes has been the subject of intense research. Nevertheless, in this chapter, functional analysis of the cardiomyocytes has not been conducted. Hence, we were not able to conclude about the effects of GRK5-L41 in cardiac protective function.

The combination of CRISPR/Nickase, piggyBac element, and shortcut method achieved the site-specific modification in the *GRK5* locus without any footprint. This approach provides a novel method for editing other cardiac-related gene in the future. Other hurdles such as the functional analysis of cardiomyocytes derived from these edited clones still call for further solutions. The phenotypic analysis will be shown in the next chapter; where cardiomyocyte characterisation, functional analysis, cardiotoxicity and other assays will be presented. The study will move toward the aim to prove the cardioprotective effects of GRK5-L41, especially during prolonged exposure to Isoprenaline and hypertrophic drugs mimicking the heart failure conditions.

5.4 Chapter conclusion

From this study, it can be concluded that the combination of cleaving the *GRK5* gene using CRISPR/Nickase, the use of piggyBac transposon and elimination of the first round of clonal genotypic verification has efficiently introduced GRK5-L41 and converted homozygous GRK5-Q41 to either GRK5-L41 or GRK5-L/Q41 from the parental cell line – HUES7-GRK5-Q41. As a result, the two edited lines harbouring the GRK5-L41 were successfully generated, namely HUES7-GRK5-L41 and HUES7-GRK5-L/Q41. The footprint-free, shortcut gene-editing strategy reported here provides an important method for reduction of times require for gene editing, reduces passage number of hESC, and increased the editing efficiency.

Chapter 6 Phenotypic Analysis of *GRK5*-L41 using hPSC-derived Cardiomyocyte Model

6.1 Introduction

The putative role of the *GRK5*-L41 polymorphism has been described from transfected cell models, from transgenic mouse models expressing human *GRK5*-Q41 or *GRK5*-L41 variant, and from clinical studies (Liggett et al., 2008; Komolov et al., 2015). In transfected cell models, co-transfection of *GRK5*-L41 with either β_1-AR or β_2-AR expression plasmids demonstrated the faster desensitisation rate of both β_1 and β_2 adrenergic receptors mediated by GRK5-L41 protein compared to that of GRK5-Q41 (Liggett et al., 2008; Wang et al., 2008). Transgenic mice were established expression GRK5-Q41 and GRK5-L41 under α-myosin heavy chain (α-MHC) promoter and were used to study the role of these polymorphisms in the context of heart failure condition, which was provoked by prolonged infusion of isoprenaline (ISO) over six days (Rockman et al., 1996a). In these circumstances, the GRK5-Q41 expressing mice developed a hypertrophic ventricular end diastolic dimension indicative of a dilated cardiomyopathy under ISO infusion. However, when the β-blocker, Propranolol, was added into the daily drinking water, the mice were completely protected from ISO treatment, with no sign of cardiomyopathy being observed. In contrast, the GRK5-L41 mice showed a small increase in left ventricular end-diastolic dimension and β-blocker treatment did not show any effects during ISO infusion (Liggett et al., 2008).

Clinical studies of 375 African-American individuals with heart failure condition confirmed that GRK5-L41 and GRK5-Q/L41 patients had prolonged survival rate during heart failure and cardiac transplantation compared to that of the GRK5-Q41 cohort (Liggett et al., 2008). Furthermore, research conducted in 2,673 patients with acute coronary syndrome indicated the improved outcomes from the African-American group harbouring *GRK5*-L41 variant (Cresci et al., 2012). Other investigation of coronary artery disease confirmed that the GRK5-L41 patients showed a significant improve in survival rate, especially during hypertensive treatment (Lobmeyer et al., 2011). Taken together, these data illustrated the improved outcomes from patients carrying *GRK5*-L41 polymorphism, although the mechanism is still poorly understood.

6.1.1 Heart failure conditions

The heart failure is classified into two categories, including diastolic and systolic heart failure (Chatterjee and Massie, 2007). The former condition is associated with concentric cardiac hypertrophy which is involved in a thickening of the ventricular wall and results in impaired filling (Grossman et al., 1975). The latter is related to the eccentric hypertrophy, a dilation of the ventricles that mainly affects the pumping capacity of the heart (Gerdes et al., 1992). Both conditions eventually lead to the reduction of cardiac output, increased risks of cardiac arrest, and insufficient supply of the circulating blood to the rest of the body. Besides, heart failure creates the catastrophic effects on the cardiovascular homeostasis in a multi-scale phenomenon (Campbell and McCulloch, 2011). On the molecular level, heart failure is initiated by the response of the cardiomyocyte to the vast range of neuronal inductive signals trying to regulate the heart functions via adrenergic signalling pathways. These molecular pathways are involved mainly in heart contractile machinery, monitor the activities of ion channels, control the addition or removal of sarcomeres, the smallest functional units of a heart muscle cell (i.e. cardiomyocytes) (Dorn, 2009; Kainuma et al., 2015). On the cellular level, these alterations in contractile functions and cytoskeletal ultrastructure result in the development of a chronic thickening or lengthening of the cardiomyocytes indicative of hypertrophic symptoms. On the whole organ level, the hypertrophic effects on muscle contraction and structures result in chronic ventricular remodelling and dilation (Zucker, 2017).

6.1.2 Molecular pathways occur during Heart failure

6.1.2.1 Adrenergic signalling pathways and their functions in regulation of the heart contractility

The heart failure is marked by a perpetual interaction between underlying myocardial dysfunction and the compensatory neuronal hormonal mechanism that are activated to maintain cardiac outputs and the heart functions (Dorn, 2009). Upon cardiac injuries or stress, a vast range of different growth factors and neuronal hormones are

released in the circulation system. Among them, the adrenergic (or sympathetic) nervous system (ANS) plays a vital role in maintaining the cardiac homeostasis and function (Lehnart, 2013) (Figure 6.1).

The direct targets of neuronal hormones, mainly catecholamines (epinephrine and norepinephrine), released during cardiac injuries are β-ARs, especially β_1 and β_2 receptors (Brodde, 1993; Lefkowitz, 2007). The catecholamine-activated β-ARs result in the induction of $G\alpha_S$-mediated pathways via its effector molecules Adenylyl Cyclase (AC) followed the increase of the cellular cAMP (Dorn, 2009). The principal target of cAMP is the protein kinase A (Tsai et al.), which functions in phosphorylation of several proteins involving essentially in cardiomyocyte functions, such as L-type calcium channels, phospholamban, cardiac troponin I, ryanodine receptors, myosin binding protein – C (MyBP-C) and protein phosphatase inhibitor-1 (Gerhardstein et al., 1999; Simmerman and Jones, 1998; Zhang et al., 2002; Zhao et al., 1994). This particular pathway modulates the cardiomyocyte contractility via increase Ca^{2+} influx (L-type channel), increasing Ca^{2+} reuptake from sarcoplasmic reticulum (phospholamban/sarcoplasmic reticulum calcium ATPase – SERCA) and myofilament Ca^{2+} sensitivities (troponin I, and MyBP-C), which in turn, increase the cardiac output to compensate the progressive loss of cardiac functions (Lohse et al., 2003). This process is usually known as an acute compensation process (Figure 6.1, step 3).

However, during heart failure development, the acute response of the heart that increases its contractility functions introduces further compromising and deteriorating effects, and leads to the enhance of ANS activities and high level of catecholamine in the blood stream (Lymperopoulos and Negussie, 2013). Chronic exposure to the high concentration of catecholamines induces further pathological damages to the heart, including continued progressive deterioration in cardiomyocyte structure and function leading to cardiac decompensation and progressively worsened function and the inability to sustain daily life activities (Dorn, 2009; Schluter, 2001). Persistent activation of β_1-ARs triggers the activation of the pro-apoptotic process in cardiomyocytes (Bisognano et al., 2000; Geng et al., 1999). It is important to note that activation of the β_2-ARs followed the

association of $G\alpha_i$-mediated pathways has been reported to have the cardiac protective function by reducing the cellular cAMP accumulation and increase the anti-apoptotic effects via activation of Akt kinase and p38 MAP kinase (Zhu et al., 2001).

To prohibit the detrimental effects of perpetual induction by catecholamine, the human body has the protective mechanism which directly involves the reduction of β-AR activities (Lefkowitz et al., 1992). This process is known as the desensitisation inducing by the phosphorylation of the β-ARs by either PKA and PKC or GRK2 and GRK5. The desensitisation process mediated by PKA via $G\alpha_S$ pathway and PKC activated by $G\beta\gamma$ directly alters the receptor conformational changes impairing the interaction between the receptor with its associated G-proteins (Hausdorff et al., 1990; Pitcher et al., 1992). This machinery is called heterologous desensitisation or non-specific desensitisation, because this procedure desensitises both activated and inactivated β-ARs present on the plasma membrane of the cells (Pitcher et al., 1992; Pierce et al., 2002). On the other hand, the GRK-mediated desensitisation is usually described as the “agonist-specific” downregulation of the β-ARs, because the GRKs only phosphorylate the agonist-bound receptors triggering its internalisation followed either degradation of the receptors or recycling the receptor back to the plasma membrane of the cells in its inactive stage (Figure 6.1, step 4) (Pierce et al., 2002; Lefkowitz, 2007; Najafi et al., 2016).

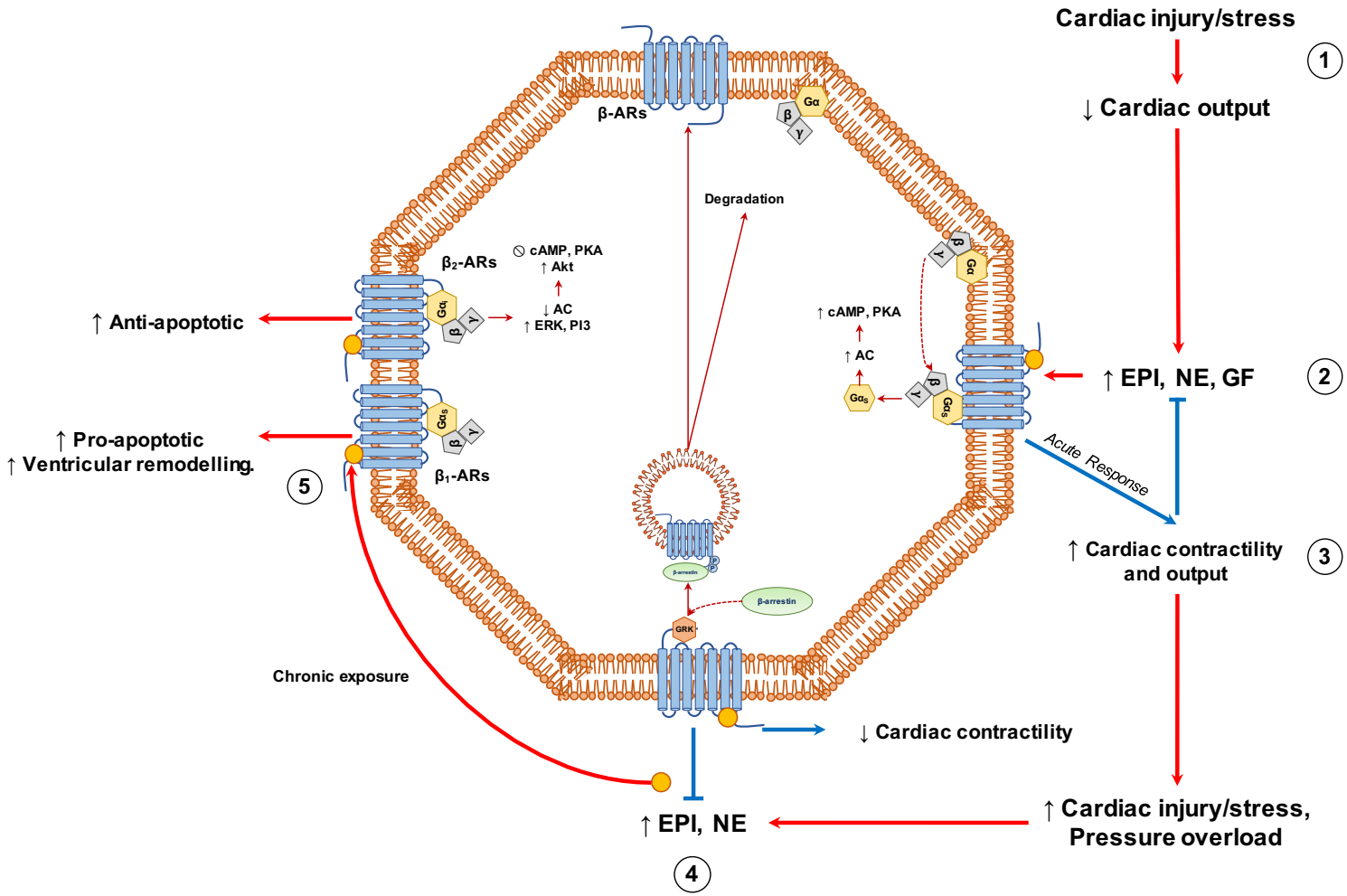


Figure 6.1: β-AR signalling pathways involved in Heart failure. (1) The results of the cardiac injury/stress are the reduction of the cardiac output, which in turn, triggers the release of Catecholamines (Epinephrine and Norepinephrine, namely EPI and NE, respectively) and growth factors (GF) into the bloodstream. **(2)** The direct targets of EPI and NE are the β-ARs, which induce the dissociation of $G\alpha_S$-mediated transduction pathway followed increase cellular cAMP production. **(3)** The agonist-activation of β-ARs increase the cardiac contractility and cardiac output to compensate the loss of cardiac function during acute response. However, this activation results in further detrimental effects in the system. **(4)** Consistent induction by catecholamines trigger the cardiac protective mechanisms called desensitisation of the β-ARs mediated by GRK followed the internalisation of the activated receptor. The internalised receptors can be either degraded or recycle back to the plasma membrane of the cells in its inactivate stage. **(5)** Chronic exposure to catecholamines induces the pro-apoptotic signalling pathways and increases ventricular remodelling via β_1-ARs. Of note, a cardiac protective function has been reported by activation of $G\alpha_i$-mediated pathway through β_2-ARs.

6.1.2.2 Adrenergic signalling pathways and hypertrophic during heart failure

In response to an increased workload caused either by physiological or pathological stimulation, the mammalian heart undergoes the growth process namely hypertrophy, a Greek word for “increased growth” (Maillet et al., 2013). A majority of hypertrophic response occur in cardiomyocytes, the primary contracting cells of the heart occupying 85% of its mass (Bernardo et al., 2010). As mentioned before in chapter 3, cardiomyocytes are the terminally differentiated cells that have a limited capacity of turnover throughout life. Therefore, although the cardiac mass can increase by either proliferation of cardiac fibroblasts and to a lesser extent, the proliferation of cardiac progenitor cells, the mass increase in response to physiological needs mainly occurs via the hypertrophy of individual cardiomyocytes (Heineke and Molkentin, 2006; Dorn, 2007).

The physiological hypertrophy regulates the heart growth from birth to early adulthood, the growth of maternal heart during pregnancy, and the cardiac growth in well-conditioned athletes as a result of extreme and/or repetitive exercises (Dorn, 2007). It is typically characterised by a mild increase by 10-20% in the total heart mass normalised to the body weight (Nishimura et al., 1980; Sugishita et al., 1983). In fact, the physiological hypertrophy is often known as reactive hypertrophy, that is, hypertrophy that occurs in response to an extrinsic increase in cardiac workload, providing the mechanical advantages to the heart function (Dorn, 2007). Importantly, cardiac function is preserved during physiological cardiac hypertrophy. At the molecular level, physiological hypertrophy is triggered by intermittent signals of growth factors, including Triiodothyronine (T3), vascular endothelial growth factor B (VEGFB), insulin and insulin-like growth factor 1 (IGF1) and among them, IGF-1 is the major stimuli for both physiological hypertrophy and normal developmental growth of the heart (Bellomo et al., 2000; Bry et al., 2010; Karpanen et al., 2008). These growth hormones activate their specific membrane-localised tyrosine kinase receptors (VEGF receptor 1, IGF1 receptor, and Insulin receptor) and nuclear receptors (thyroid hormone receptor) followed initiation

of downstream cellular signalling cascades specific to physiological hypertrophy. These signalling pathways appear to be directly involved in the PI3K/Akt pathway followed the induction of mTOR, which directly regulate the protein synthesis process (Figure 6.2, right panel).

In contrast, the enlargement of the heart induced by hypertensive stress, myocardial injury, excessive neuronal hormonal activation, genetic mutations in genes encoding sarcomeric proteins, diabetic and metabolic cardiomyopathy, viral and bacterial myocarditis, valvular insufficiency and congenital heart defects, is associated with cardiac dysfunction and is classified as pathological hypertrophy (Shimizu and Minamino, 2016). During the early stage of heart failure condition, the cardiac function is maintained in the pressure overload-induced hypertrophy and is described as an adaptive phase. However, persistent induction from catecholamine and pressure overload promotes the transition from the adaptive to maladaptive phase, which is characterised by the reduced ejection fraction, ventricular dilation, cardiomyocyte death, and fibrotic remodelling (Heineke and Molkentin, 2006). During heart failure, the elevated level of Angiotensin II, endothelin 1 and catecholamines triggers the activation of Angiotensin II type 1 receptor (AT_1), endothelin 1 receptor (ET_1) and adrenergic receptors followed the induction of the $G\alpha_q$ signalling cascade. The $G\alpha_q$ pathway activates phospholipase C (PLC), which catalyses the synthesis of inositol-1,4,5-triphosphate and DAG resulting in an increase of cytosolic Ca^{2+} (Dorn, 2007; Hullmann et al., 2014). The elevation of Ca^{2+} concentration then activates calcium/calmodulin-dependent protein kinase (CaMK) or calcineurin, which dephosphorylates nuclear factor of activated T cells (NFAT) transcription factors. NFAT forms complexes with GATA4 or myocyte enhancer factor-2 (MEF-2) to transactivate the transcription of hypertrophic target genes involving in the maladaptive process (Figure 6.2, right panel) (Hullmann et al., 2014).

Taken together, the molecular pathways were involved in heart failure are presented in Figure 6.3. These mechanisms in the early stage of heart failure participate

in compensation process that attempts to improve the cardiac function, which shows adverse effects on the system and worsen the situation.

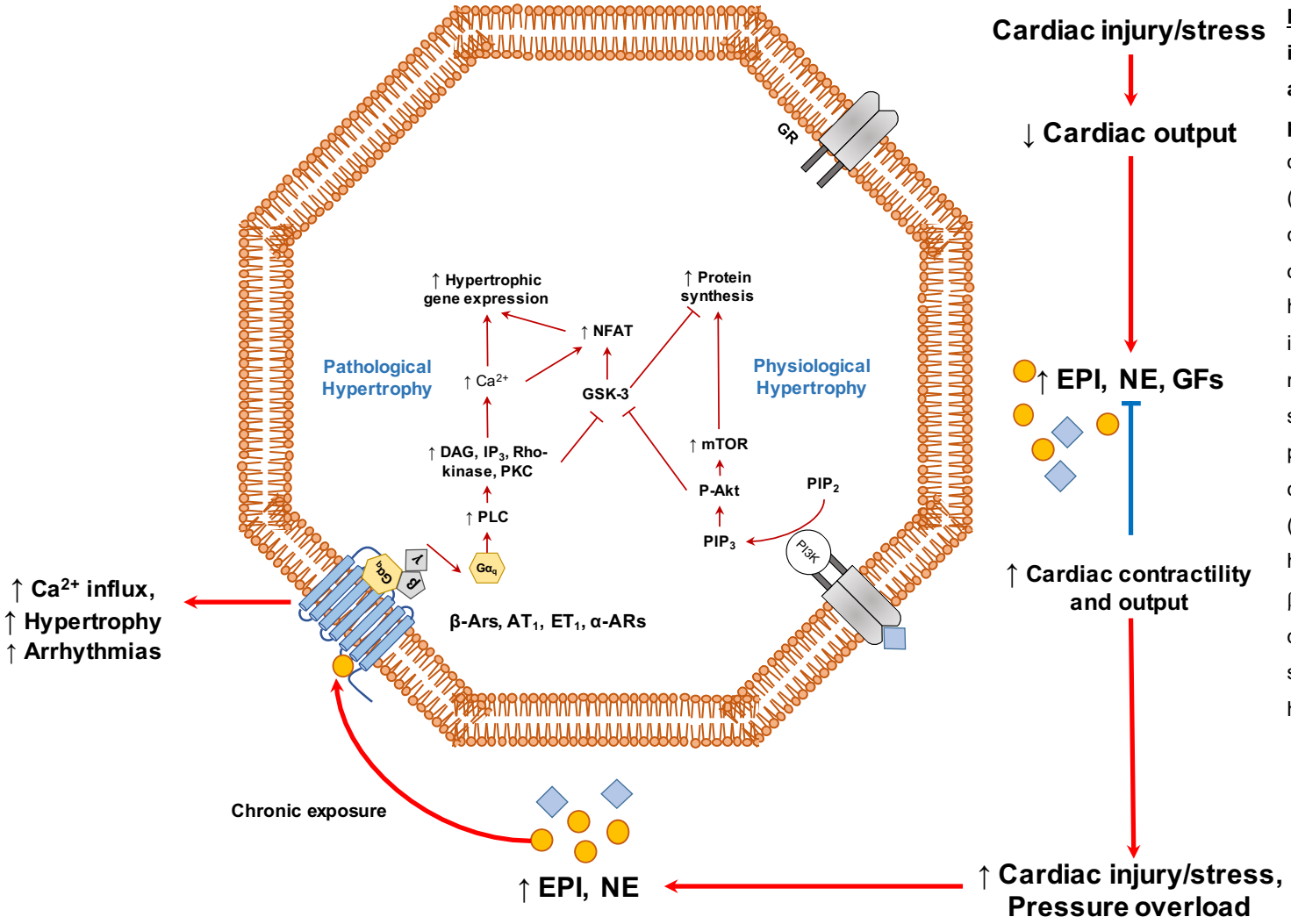


Figure 6.2: Signalling pathways involved in physiological (right panel) and pathological hypertrophy (left panel). Cardiac injury triggers the release of wide range of neuronal hormones (orange sphere) and growth factors (blue cube). To compensate the potential needs of cardiac activities, physiological hypertrophy is initiated by the activation of insulin-like growth factor 1 receptor (IGF-1 receptor), which increase the protein synthesis via PI3K/Akt signalling pathways. Prolonged exposure to catecholamines and hypertrophic inducer (Angiotensin II, endothelin 1, etc.) during heart failures results in the stimulation of β-ARs, AT_1, ET_1, α-ARs, etc. which directly regulate a molecular and cell signalling toward pathological hypertrophic conditions.

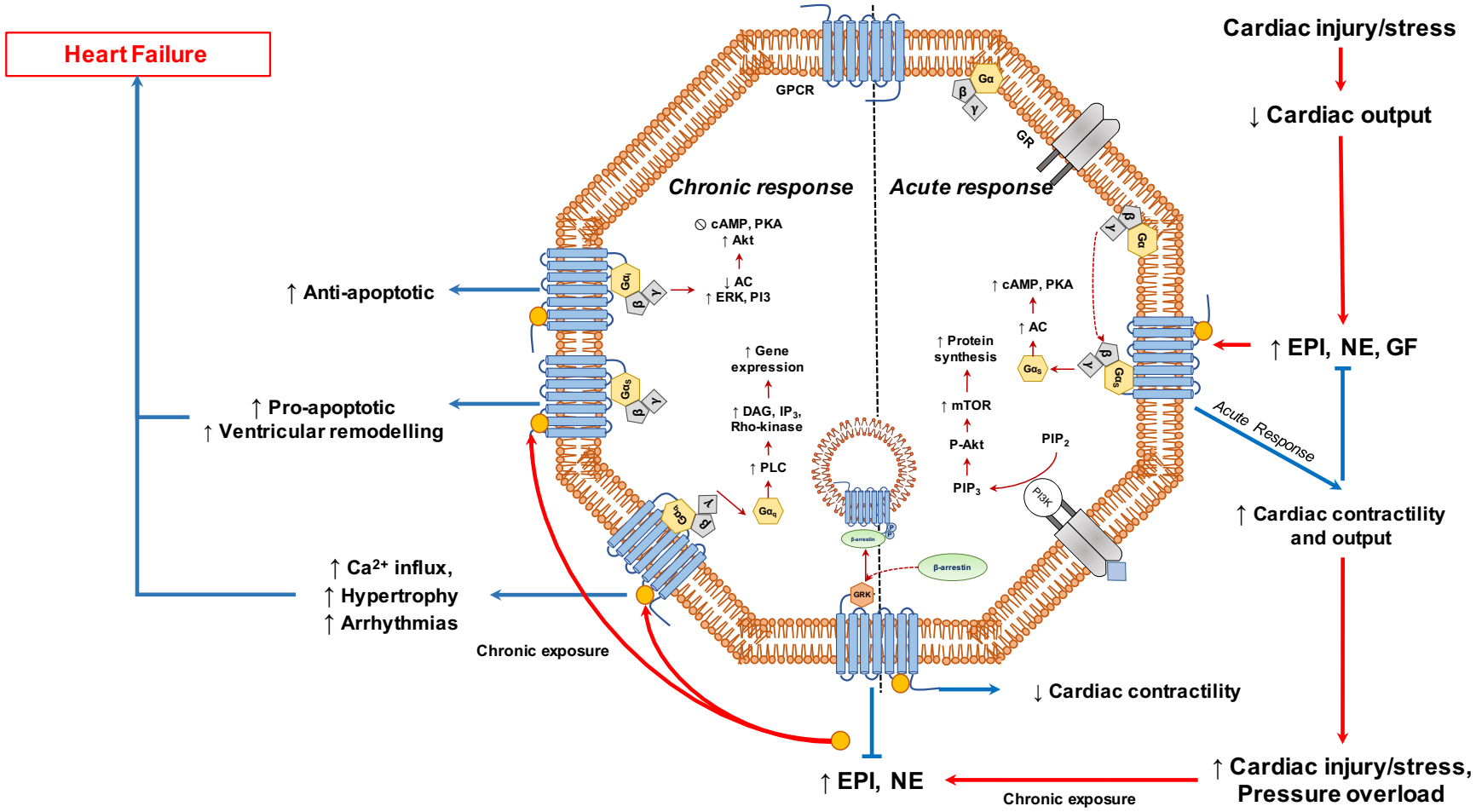


Figure 6.3: Schematic depicts the cellular signalling pathways triggered by GPCRs contributing to the development of Heart Failure. Two distinct phases of heart failure have been described including acute response (happens in second to few hours), and chronic response (initiates in hours to days). The catastrophic effects of GPCRs on cardiomyocyte physiology and function during heart failure include the development of arrhythmias, hypertrophy, ventricular remodelling, and cardiomyocyte death.

6.1.3 G-protein coupled receptor kinase 5 (GRK5) and its non-canonical functions during heart failure

As a brief summary of section 1.4.3, the non-canonical functions of GRK5 are involved in its nucleus activities that mediated via the $G\alpha_q$-dependent pathway. Upon the increase of cytosolic Ca^{2+} level during heart failure, the activation of calcium/calmodulin-dependent protein kinase (CaMK) mediates two major pathological pathways. The first pathway is involved in phosphorylation of NFAT, which forms a complex with the cofactors GATA-4 or MEF-2 for activation of hypertrophic genes (Dorn, 2007). The second pathway includes the interaction with membrane-bound GRK5 and initiates the translocation of GRK5 into the nucleus of the cells where GRK5 phosphorylates Histone Deacetylate 5 (HDAC5) and acts as a class II HDAC kinase (Hullmann et al., 2014). The GRK5-mediated phosphorylation of HDAC5 stimulates its export from the nucleus, which in turn, release its suppression of *MEF2* gene. The process of releasing MEF2 from HDAC modulators has been well-known as one of the pathological hypertrophic pathways in cardiomyocytes (Figure 6.4). This study was crucial to implement the new function of GRK5 beside its canonical role, which leads to pathological hypertrophic effects of GRK5. Recently, intensive studies about nuclear translocalisation of GRK5 revealed that GRK5 could potentially transport into the nucleus of cardiomyocytes in a manner that depends on calmodulin binding to the N-terminus of GRK5 following the activation of specific $G\alpha_q$-coupled receptors (Hullmann et al., 2014). In fact, GRK5 does not participlate in desensitisation process of catecholamines, and angiotensin II-mediated activation of AT_1 receptors (Jaffre et al., 2008). It was demonstrated that activation of AT_1 receptors during the persistent level of catecholamines and hypertrophic stimulus results in the nuclear translocation of GRK5 in a CaMK-dependent manner. Surprisingly, stimulation of Endothelin-1 receptor (ET_1), which is desensitised by GRK5, did not trigger the nuclear localisation of GRK5 because the desensitisation process prevents the interaction between GRK5 and CaMK. Therefore, it was concluded that the nucleus translocation activity of GRK5 distinctively happens when GRK5 is not

actively engaged with a membrane-bound activated GPCRs (Mailet et al., 2013; Sato et al., 2015).

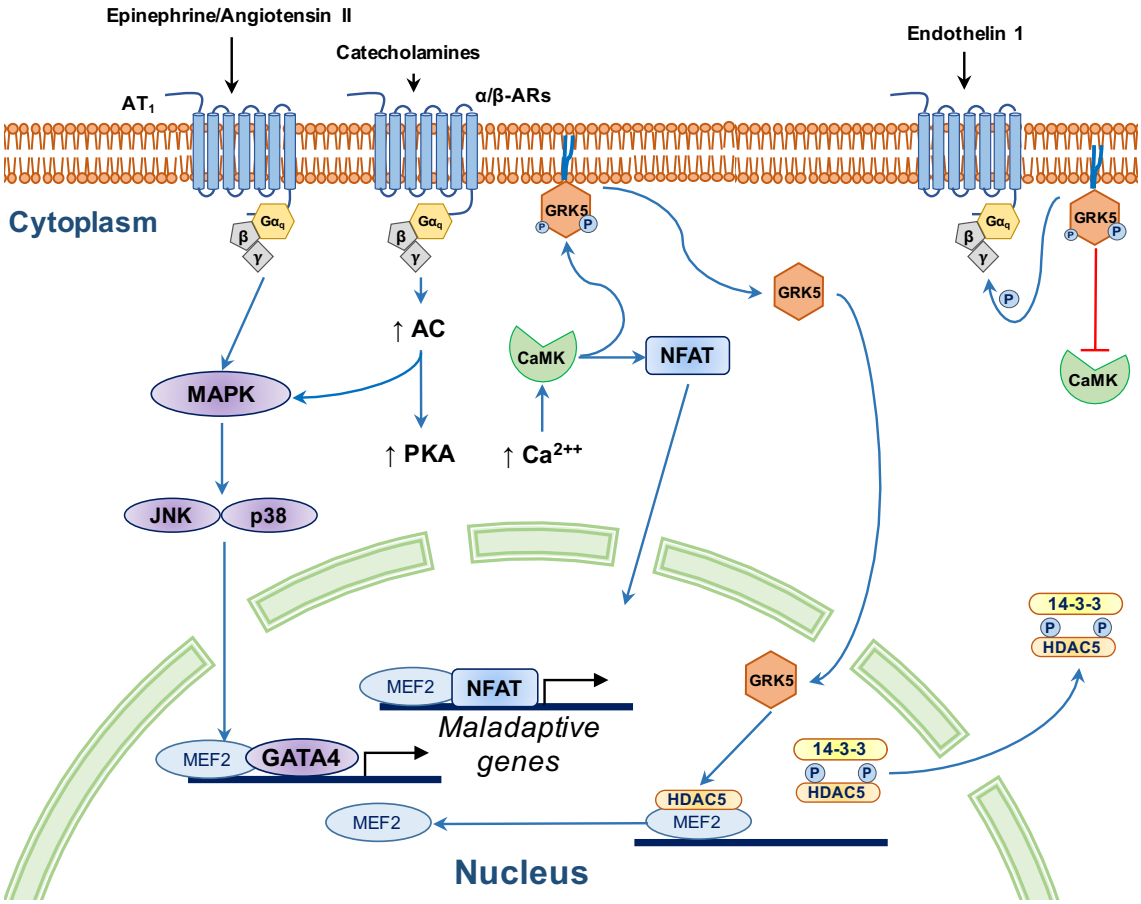


Figure 6.4: Non-canonical signalling pathways of GRK5 during heart failure. The schematic illustrates the involvement of GRK5 in pathological hypertrophic process, which initiates by the induction of cytosolic Ca^{2++} level followed the association between calcium/calmodulin dependent protein kinase (CaMK) with membrane-bound GRK5. The CaMK trigger the release of GRK5 from the membrane and translocate into the nucleus of cardiomyocytes where it phosphorylates Histone Deacetylate 5 (HDAC5). The phosphorylation process of HDAC5 stimulates its export from the nucleus and release its suppression effects on *MEF2*, which are directly involved in expression of maladaptive genes related to pathological hypertrophy. Figure is modified and adapted from Sato *et al.*, 2015.

6.1.4 Methods for measuring physiological responses of hPSC-derived CMs

6.1.4.1 Direct measurement of catecholamines effects on cardiomyocytes contracting machinery

During the early phase of heart failure, increase beat rate in response to catecholamine in the circulation is the initial reaction of the heart to compensate for the loss of reduction in cardiac output. This phenomenon can be translated *in vitro* by the

catecholamine treatment, such as isoprenaline, and measurement of the cardiomyocyte beat rate and beating pattern can be detected. On the late phase of the heart failure, one of the end results is arrhythmias which are common and potentially life-threatening due to prolonged exposure to circulating catecholamine in the blood (Laverty et al., 2011). In the same manner, persistent stimulation of sympathetic nervous system modulates the human potassium channel (Gherghiceanu et al.), which in turn, creates arrhythmias during heart failure (Mitcheson et al., 2000; Thomas et al., 2004). The hERG-dependent current I_{Kr} has also been found to regulate human cardiac repolarisation phase, and its inhibition is a common cause of severe ventricular arrhythmias, including "Torsades-des-Pointes" (TdP) arrhythmias (Boulagnon et al., 2009). Several methods have been developed to detect the hERG channel activities, and cardiac contracting functions, including patch clamp of hERG, multi-electrode assays (MEA) and impedance measurement. Recently, due to its simplicity and easy to perform, the impedance measurement using electrode-embedded sensor plate emerges as a method of choice for detecting beat rate and beating pattern of hPSC-CM (Jonsson et al., 2011; Doerr et al., 2015).

Recently, the introduction of xCelligence real-time cell analyser Cardio system and CardioExcyte 96 provide more access to detailed information of cardiac contractility with a temporal resolution (i.e. an ability to follow the change in beat rate of CMs) of 12.9 ms and 1 ms, respectively (Jonsson et al., 2011; Obergrussberger et al., 2016). Both of these systems consist of 96-well sensor plate where the measurement of the cultured beating CMs take place, the central analyser or detector (for measurement of the electrical signals), and a computer for storage, analysis, and display of the data (Figure 6.5A). The sensor plate was designed in the way that it could support the attachment and maintenance of beating CMs for up to 2 weeks and directly measure the beat rate of CMs in real time. Also, it allows monitoring the immediate effects of drug treatment directly (Figure 6.5B). Importantly, the measurement of beat rate is made from intact cells beating synchronously in a monolayer.

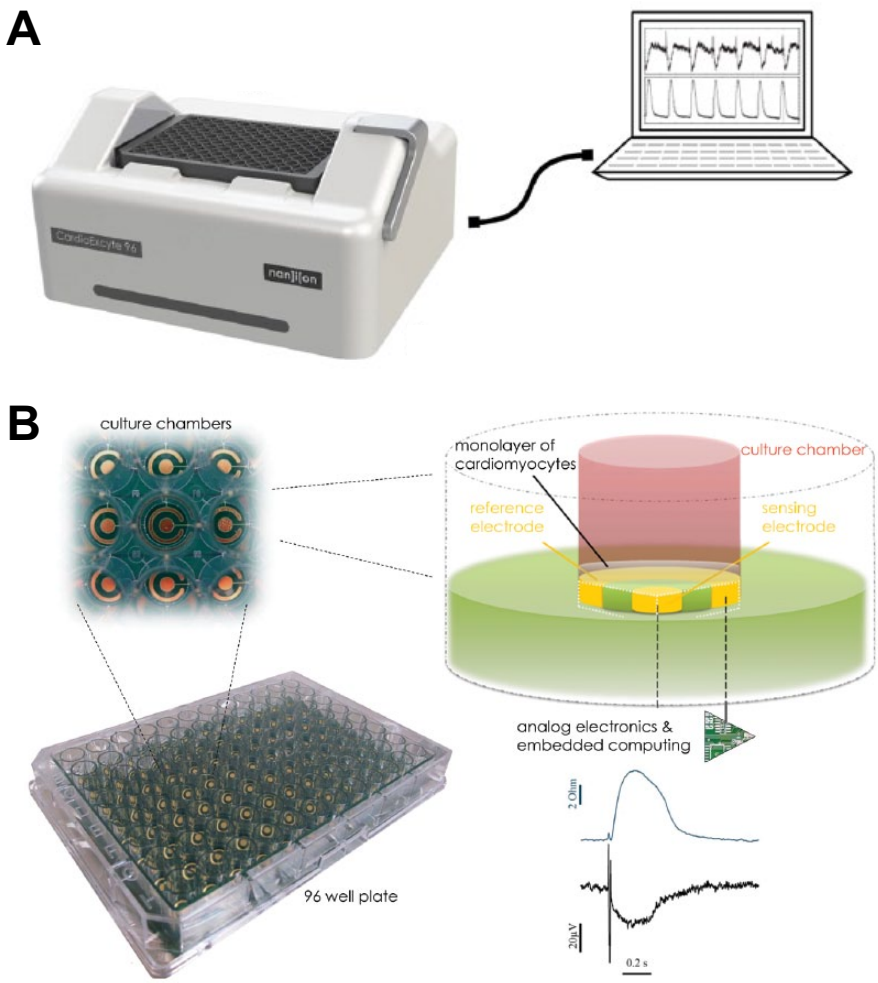


Figure 6.5: CardioExcyte 96 platform (Nanion). (A) The CardioExcyte 96 with recording function contains all electronic system and places inside incubator. **(B)** Details of CardioExcyte 96 sensor plate**.** Each well of the sensor plate is a single recording unit containing culture area on top of two specific gold-coated rings (the reference electrode forming the outside ring and the sensing electrode forming the inside circle. Monolayer cardiomyocytes growth on top of both reference and sensing electrode and generate the overlay of an impedance (top) and extracellular field potential (bottom) trace. The data were obtained by the CardioExcyte 96 in the combined mode. (Adapted from Doerr et al., 2015).

6.1.4.2 CardioExcyte 96 systems and its principle of impedance detection

The CardioExcyte 96 confers the ability to detect, record and analyse cardiomyocyte contraction in real-time based on a fixed-frequency impedance calculation with an outstanding fast sampling rate of 1 ms (Doerr et al., 2015). It acquires the data every step of the experiment (high-resolution impedance) and transferred into connected computer. The impedance measurement depends on the planar gold

electrodes that detect the changes in adhesion and morphology of the adherent cardiomyocytes (Figure 6.5B) (Doerr et al., 2015). The quality of attachment, the number of healthy cardiomyocytes and the cell seeding density, together, contribute to the steady components of the impedance signal. On the other hand, the spontaneous and synchronise contraction of the cells provide information about the working conditions of the cardiomyocytes. Therefore, the impedance recording function of CardioExcyte 96 is a powerful tool for detection of any drug-induced modulations directly involving in contractile activities of cardiomyocytes as well as the quality of the cells.

To initiate impedance detection, the machine imposes a small excitation voltage between the sensing and reference electrode followed by picking up the resulting current release from the culture. The details of how the excitation voltage is release and its origin are described in Figure 6.6 (Doerr et al., 2015; Obergrussberger et al., 2016). In order to detect high-resolution signals and reduce the background noise EFP signals, it is important to have the full (100% confluence) and non-disrupted monolayer of cardiomyocytes seeded in each well of the CardioExcyte 96 sensor plate, so that the cleft between the electrode and the cells is separated at minimum distance created by a high sealing resistance (Doerr et al., 2015; Obergrussberger et al., 2016). By synchronise their beating rate, the cardiomyocytes released ions which accumulate in the cleft and thereby changing its potential referred to the surrounding medium, which is set to a zero potential by the reference electrode. Once the monolayer of cardiomyocytes starts to synchronise the beat rate, the charge builds up in the cleft is release through the seal resistance created by the monolayer, but because of its relatively high value, a voltage can be detected and recorded by the sensing electrode below the beating layer and the reference electrode directly conducting the medium (Doerr et al., 2015; Obergrussberger et al., 2016). The signal is amplified by the relatively large surface area of the sensing electrode, which was designed as single-electrode surface especially adapted to well-connected and synchronise beating cardiomyocytes. The large electrode with its integrating characteristics accumulates the total extracellular signals from a

greater number of cells and provides the data representative to an EFP signal of the cells in the respective well.

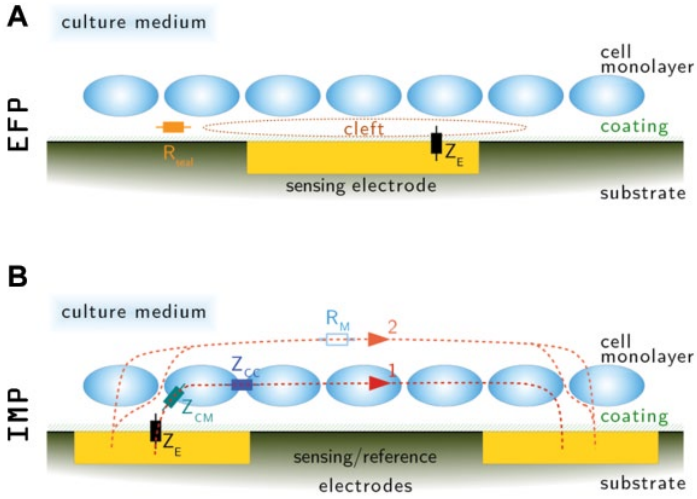


Figure 6.6: Principle of the extracellular field potential (EFP) and impedance (IMP) mode obtained from CardioExcyte 96 platform. Once the cardiomyocytes formed a monolayer covered the surface of the sensor, it formed a resistive sealing (R_{Seal}) between active sensor area and the surrounding electrolyte, which is directly connected to the reference electrode. In EFP mode **(A)**, the model parameter (Z_E) was measured and represented the electrode-electrolyte transfer impedance. In IMP mode **(B)**, the Z_{CM} and Z_{CC} are models for transmembrane impedance between either the extra- and intracellular space or two adjacent cells. The resistive behaviour of the medium (R_M) was recorded. Picture obtained from Doerr et al., 2015.

6.1.4.3 Detection of cellular cAMP production using LANCE Ultra cAMP assay (Perkin Elmer)

The increase in cardiac beat rate due to catecholamine-activated β-ARs is mediated by $G\alpha_S$ cascade, which stimulates the AC effector inducing the elevation of cAMP production. Hence, the measurement of intracellular cAMP provides information about the effect of catecholamine (in our case, Isoprenaline) on GPCR-mediated adenylate cyclase activation or inhibition. The LANCE *Ultra* cAMP assay principle bases on the time-resolved fluorescent resonance energy transfer (TR-FRET) immunoassay (Figure 6.7). The assay consists of two major components, the U*Light*™-anti-cAMP and Eu-cAMP tracer. When a cAMP antibody is bound to the europium (Eu) chelate-labelled cAMP tracer, light pulse at 320 or 340 nm excites the Eu chelate molecule of the tracer. The energy emitted by the excitation of Eu chelate is transferred by FRET to U*Light* molecules linked to the cAMP antibody, which in turn emit light at 665 nm. Residual

energy release from Eu chelate will produce light at 615 nm. Hence, the assay is based on the competition between the intracellular cAMP and the Eu-labelled cAMP for binding sites on cAMP-specific antibody labelled with U*Light*.

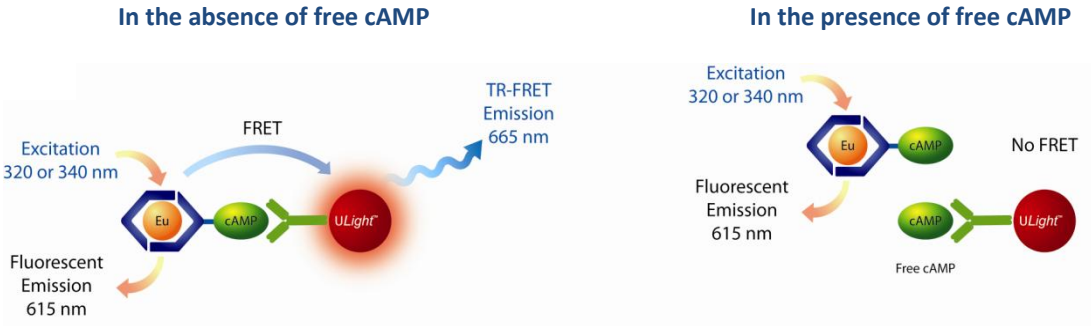


Figure 6.7: Principle of LANCE *Ultra* cAMP assay. The assay based on time-resolved fluorescence resonance energy transfer (TR-FRET) immunoassay to measure cAMP produced upon the activation of β-AR by catecholamine. Picture is obtained from the LANCE *Ultra* cAMP manuscript.

6.1.4.4 Assays for detection of cardiac hypertrophy

One of the first studies compared the cardiac gene expression profile between physiological and pathological hypertrophy identified the specific set of genes that were upregulated specifically during pathological hypertrophy, including atrial natriuretic peptide (ANP), brain natriuretic peptide (BNP), angiotensin-converting enzyme, myosin light chain-2, or α and β-myosin heavy chain (Maytin and Colucci, 2002; Iemitsu et al., 2001; Ramirez et al., 1997; Swynghedauw, 1999). Among these genes, BNP has been considered as classical biomarkers for pathological hypertrophy and detection of BNP expression in response to a particular compound treatment to investigate its hypertrophic effects on cardiomyocytes has been considered as a method of choice (Carlson et al., 2013; Dorn, 2007; Shimizu and Minamino, 2016). Hence, development of the immunocytochemistry that allows detecting the expression of BNP under certain treatments in combination with high content imaging system could provide an effective way to measure the hypertrophic development *in vitro*. Recently, a workflow for staining of BNP protein in hPSC-derived CMs has been introduced from Cellular Dynamic (https://cellulardynamics.com) which allows indentifying the expression of BNP using

Flow cytometry. This workflow can also be adapted for immunocytochemistry and using the high-content imaging system to quantify the expression of the BNP.

6.1.5 Chapter aims:

To establish a set of functional analysis assays towards the identification of the cardiac protective mechanism of *GRK5*-L41, the hiPSC-CMs (L41 vs Q41), and gene-edited HUES7-CMs (L41 vs Q/L41 vs Q41) were evaluated by:

1. Investigating the expression of β-AR signalling pathways in hiPSC-CM using qPCR analysis over a differentiation timecourse from undifferentiated (d0) to terminal differentiated CMs (d66).
2. Developing the real-time measurement of the beat rate and beating pattern of hPSC-CM in response to Isoprenaline (ISO) using CardioExcyte 96 system.
3. Investigating the cellular production of cAMP during ISO treatment using LANCE *Ultra* cAMP assay.
4. Identifying the nuclear localisation of GRK5-L41 during chronic exposure of ISO (72 hours) using Western Blot analysis.
5. Establishing the hypertrophic assay associated with viability assay to distinguish the physiological hypertrophy and pathological hypertrophy in hiPSC-CM.

6.2 Results

6.2.1 Quality control of hPSC-derived CMs

In terms of phenotypic analysis and assay development for CM functional evaluation, the quality of CMs plays a critical role because the high purity of CMs (>80%) with high viability after dissociation of CMs (>80%) allow forming a monolayer of synchronously beating CMs, reducing the overgrowth of non-cardiomyocyte cells, and obtaining the results that are representative of CM functions. Therefore, before starting the experiments described in this chapter, the monolayer differentiation, E8-AB protocol, as previously established in Chapter 3, was used to induce cardiac formation from hiPSC-GRK5-Q41, hiPSC-GRK5-L41, HUES7-GRK5-Q41, HUES7-GRK5-L41, and HUES7-GRK5-Q/L41. The CMs derived from these cell lines were called, hiPSC-CM-Q41, hiPSC-CM-L41, HUES7-CM-Q41, HUES7-CM-L41, and HUES7-CM-Q/L41, respectively. These CMs were dissociated on d12 to d16 post-differentiation followed the quality control assays, including immunofluorescences to detect the cTNT-positive population, and cell viability using Cedex Automated counting system.

As shown in Figure 6.8A, the majority of the hPSC-CMs utilised for the assays had the purification of CMs of approximately 80% to 90% (n>3). The CDS method was used to dissociated CMs with a viability rate ranging from 85% to 95% across all cell lines (n>3) (Figure 6.8B). The CMs after dissociation had the average size of 13.5 μm and the aggregation rate after dissociation was approximately 40% (Figure 6.8C&D). Further analysis of the aggregate size revealed that majority of the aggregates were formed from two to three cells suggesting that the CDS method is efficient in dissociating monolayer CMs at high viability and low level of clumps (Figure 6.8E).

Taken together, this section illustrated the quality control procedure conducted in this chapter to ensure that the hPSC-CMs generated from the E8-AB protocol were at high purity (>80%) and high viability (>80%) before using for functional analysis. Therefore, from this section onward, all CMs employed in the assay development were of this standard.

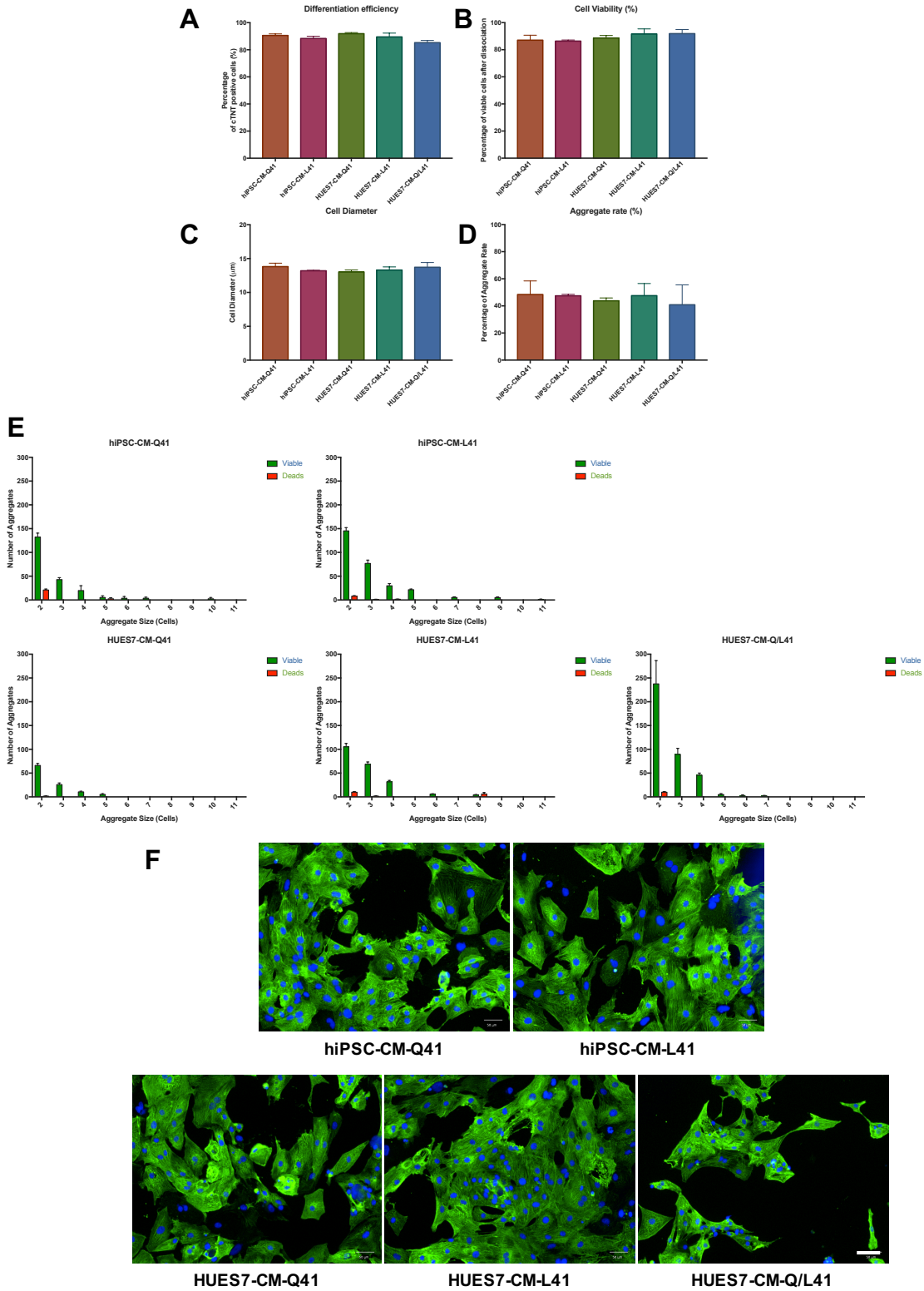


Figure 6.8: Quality control of hPSC-CMs using immunofluorescence analysis and cell viability assay. The CMs from d12 to d16 post-differentiation were dissociated using CDS methods and subjected for assessing **(A)** purity control using immunofluorescence detecting cTNT-positive cells, and **(B)** cell viability using Trypan Blue via Cedex automated counting system. Additional details obtained from the Cedex system were cell size **(C)**, aggregate rate **(D)**, and the aggregate size **(E)**. The representative figures from immunofluorescence illustrate the high purity of CMs after dissociation. *Scale bar:* 50 µm.

6.2.2 Gene expression profiles of adrenergic signalling pathways

As previously mentioned, the hPSC-CMs exhibit the foetal-like characteristics, which are similar to that of human foetal cardiomyocytes (Snir et al., 2003; Robertson et al., 2013). Therefore, it was first important to define the expression dynamics of β-adrenergic signalling genes to determine when subsequent assays should be conducted. The CMs derived from each of cell lines as mentioned earlier together with the commercial human ventricular sample, total heart sample (Total HH), and HUES7-derived fibroblast sample (Fib) were collected at different day intervals from d0 (undifferentiated hPSCs) to d66 post-differentiation for RNA extraction. The Q-PCR analysis was then performed for β_1 (*ADRB1*), β_2 (*ADRB2*), GRK2 (*ARDK1*), and GRK5 (*GRK5*) gene. The result revealed that the *ADRB1* and *ADRB2* were upregulated in CMs after 20 days cultured *in vitro* (Figure 6.9). The expressions of both adrenergic receptor genes were stabilised after d30 at the level that was closed to that of ventricular CMs and total HH samples. Interestingly, the expression of *GRK2* was slightly reduced in CMs compared to that of hPSCs, whereas *GRK5* showed a significant increase from days 20 and started to stabilise at d30 post-differentiation (Figure 6.9). These results illustrated that GRK5 expression was upregulated in CMs whereas GRK2 level maintained at the level that was similar to that of pluripotency stage. Additionally, relatively low expressions of *ADRB1*, *ADRB2*, *GRK2*, and *GRK5* were detected in Fibroblast sample suggested that the expression of adrenergic-related genes was higher in CMs compared to that of Fib samples, eliminating the possibility of false induction of gene expression from the non-cardiomyocyte population.

Overall, these results indicated that the expression of genes encoding for adrenergic signalling components in hPSC-CMs stabilised at or after d30 post-cardiac differentiation. This observation suggested that development and investigation of functional assays in hPSC-CMs, especially those focused on adrenergic signalling pathways, should be conducted in CMs culture at least 30 days *in vitro* to obtain the accurate responses.

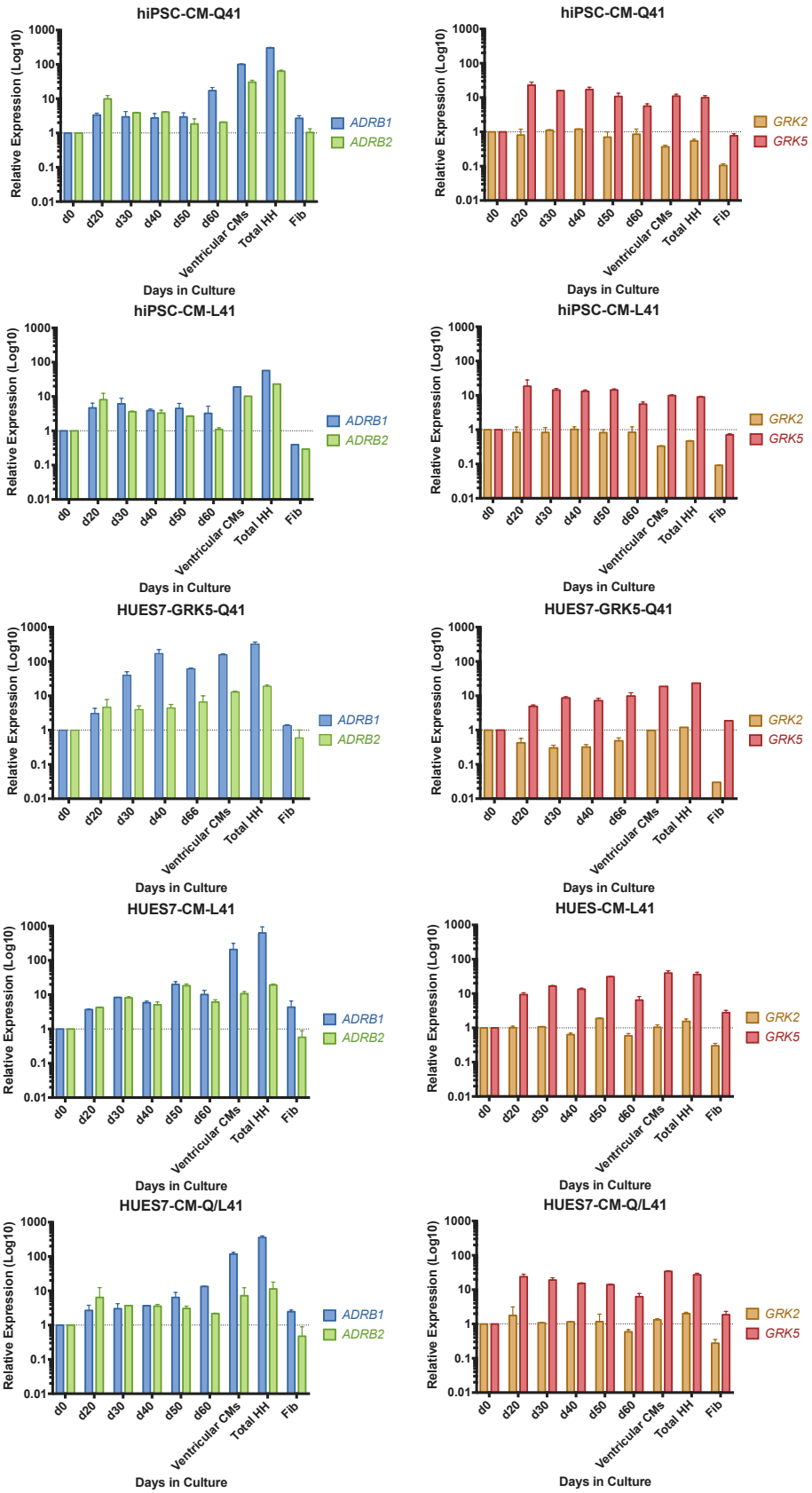


Figure 6.9: q-PCR analysis of adrenergic gene expression profiles from hPSC-CMs. The left panel demonstrates the Q-PCR results analysed the expression of *ADRB1* and *ADRB2* in hPSC-CMs, commercial ventricular CM sample, total human heart sample (total HH), and HUES7-derived Fibroblast sample (Fib). The right panel illustrates the results analysed the expression of *GRK2* and *GRK5*, the downstream regulators of adrenergic signalling pathways and the two GRKs abundantly expressed in human heart. (Error: SEM, n=2).

6.2.3 Establishment of real-time analysis of beat rate and beating pattern from hPSC-CMs using CardioExcyte 96 platform

In the human heart, the most apparent function of CMs is their ability to response to catecholamines presence in the bloodstream, which immediately increases the CM's beat rate, which in turn, elevates the output of the heart. This particular function could be detected *in vitro* via application of adrenergic inductive drugs, such as Isoprenaline (ISO) followed the measurement of CM's beating frequency. Recently, the development of the CardioExcyte 96 platform provides a reliable screening platform that specifically designs to detect the contractility of hPSC-CMs *in vitro* using impedance technology (Doerr et al., 2015). To generate consistent and accurate results, several requirements need to be met, including CM purity, cell seeding density, surface coating substrate, culture time, and medium changing method.

6.2.3.1 Technical optimisation of CardioExcyte 96 system

Before seeding the CMs into the CardioExcyte sensor plates, the hPSC-CMs derived from E8-AB differentiation protocols were subjected to Quality control (QC) assays as described in section 6.3.1. Only CMs from the differentiation batches that had the cardiac differentiation efficiency higher than 85% and the viability rate after dissociation over 80% were used for the experiments. To identify the cell seeding density that allows the formation of complete monolayer, the HUES7-CM-Q41 was seeded in the CardioExcyte 96 sensor plate at densities ranging from 20,000 cells/well to 80,000 cells/well coated with either Matrigel (1:100 dilution in cold DMEM medium), vitronectin, and fibronectin. The results indicated that signals were detected from CMs seeded at 60,000 cells/well and 80,000 cells/well, illustrating the steady beat rate after 2 days post-dissociation, while CMs seeded at below 40,000 cells/well showed an inconsistent beat rate. Fibronectin and Vitronectin coated wells appeared to have consistency beat rate, and the base impedance rises from about 600 Ω to 800 Ω reaching a stable level after 48h, according to the increasing adherence of the CMs. The results indicated that the seeding density of 60,000 cells/well in either Fibronectin or Vitronectin produced the

consistent attachment and beating results. Indeed, because fibronectin is cheaper than Vitronectin, it is selected as the main coating substrate for further experiments.

Before starting the compound screening tests, it was essential to examine the ability to detect the induction in the beat rate of CMs in response to ISO treatment. Therefore, the hiPSC-CM-L41 were first seeded into the sensor plate at 60,000 cells/well in Fibronectin-coated sensor plate followed ISO treatment at 100 nM. The basal beat rate of hiPSC-CM-L41 before the ISO treatment was measured at 83 $\pm$ 3 beats per minutes (bpm) (n=5, technical replicates). The 100 nM ISO was added after two hours measurement of the basal rate and the increase in contraction rate was detected after 2 hours, which was 124 $\pm$ 2 bpm or 140% relatively to the basal beat rate. This result confirmed that the ISO-induced contractility of hPSC-CMs could be detected using CardioExcyte 96 platform (Figure 6.10A). However, after 28h maintaining in ISO, the CMs started to reduce the beat rate back to basal level. Repeating the experiments in other lines also generated a similar result, suggesting that the effects of ISO could not be maintained for longer than 24h (Figure 6.10A). Furthermore, it was found that isoprenaline (in the form of Isoprenaline hydrochloride) was dissolved in our laboratory using H_2O, which significantly reduced its effects during long-term culture *in vitro*. In fact, ISO needs to be prepared in 4 mM HCl and stored at -20^{o}C within two weeks due to its instability and prone to be oxidised in culture condition (Nayak et al., 1986; Weil et al., 2006).

Based on these reports, the ISO was freshly prepared in 4 mM HCl to make a stock solution and to maintain the effects of ISO, the second dose of ISO was added into the experiment after 24h post-ISO-treatment. To minimise the effects of medium changing, the CM culture medium (RPMI + B27 supplement) was pre-warmed in the same incubator where the CardioExcyte96 platform was kept so that the medium temperature was not fluctuated dramatically for using to prepare the ISO treatment. The results illustrated a significant increase in beat rate observed after 4h incubation with ISO, which was 4-fold higher than that of previous experiment (Figure 6.10B). Except for a drop in the beat rate of CMs observed at 23h which was due to a technical problem during

preparation for medium changing, the CMs maintained a relatively high contractility rate up to 48h incubation with 100 nM ISO.

In general, these results confirmed that **(1)** the CardioExcyte96 platform could detect the ISO-mediated induction of hPSC-CM contraction rate in real-time, **(2)** the CMs need to be high purity (>85%) with high viability (>80%) after dissociation, **(3)** the optimal seeding density was 60,000 cells/well in Fibronectin coated sensor plate to achieve a consistent readout, **(4)** ISO needs to be prepared in 4 mM HCl to enhance its stability, and **(5)** multiple doses of ISO need to be added to the medium to maintain its effects during long-term culture *in vitro* (>24h). Therefore, we focused our further experiments using these conditions mentioned above.

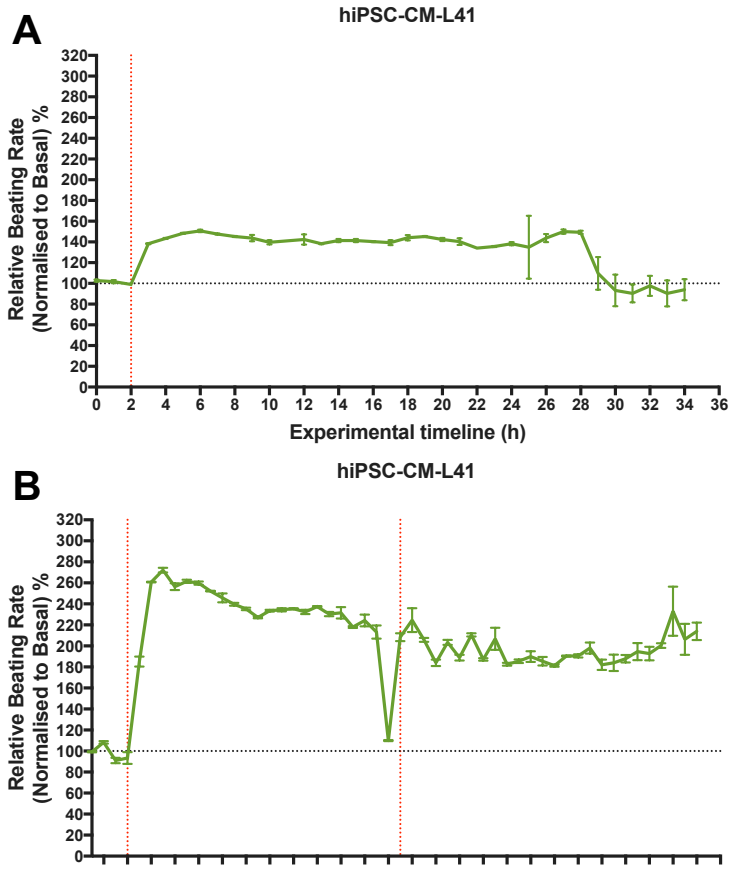


Figure 6.10: Optimisation of CardioExcyte96 system. (A) The recorded beat rate obtained from hiPSC-CM-L41 underwent ISO treatment for 34h. In this experiment, ISO was prepared in H_2O. **(B)** The results obtained from hiPSC-CM-L41 underwent ISO treatment for 48h under optimal conditions. The ISO was prepared in 4 mM HCl to make 10 mM ISO stock, which was kept in -20^{o}C for maximal two weeks, and the second dose of ISO was added after 24h to maintain the its effects during prolonged culture *in vitro*. (Error bar: SEM, n=1).

6.2.3.2 Evaluation the effects of ISO treatment on hiPSC-CMs

The establishment of optimal conditions to generate consistent results from CardioExcyte96 system encouraged us to initiate the functional assay to evaluate the effects of ISO treatment on hiPSC-CM-Q41 and hiPSC-CM-L41. Two ISO concentrations were used in the experiments including 100 nM and 1 μM. The basal beat rate was measured four hours prior to the ISO treatment, which showed that hiPSC-CM-Q41 and hiPSC-CM-L41 had the contraction rate at 80 ± 3 bpm and 55 ± 2 bpm (mean ± SEM, n=2). For comparative purposes, the increase in beat rate was normalised to basal to generate the relative beat rate. At both concentrations, an immediate response from both cell lines was observed, indicating the effectiveness of ISO in inducing the contractility of the CMs.

At 100 nM ISO treatment, the hiPSC-CM-L41 reached a maximum beat rate after 4h, 272% ≈ 2.2%-fold increase, which was higher than that of hiPSC-CM-Q41, 208% ± 0.7% (mean ± SEM, n=2). In the first 24h, both cell lines maintained their contraction at relatively high level, in which, the GRK5-L41 expressing CMs showed a steady decrease while the GRK5-Q41 counterpart experienced a drop after 10h incubation followed a constant beating frequency (Figure 6.11A). A slight increase was observed in both cell lines after the second addition of ISO, although the peak was relatively lower than that of the first peak after the initial ISO treatment. Interestingly, while the hiPSC-CM-L41 maintained the high contraction level until the end of the experiment, dramatic fluctuation in beat rate was observed in hiPSC-CM-Q41 after 30h incubation with 100 nM ISO, with a beat rate ranging from 238% ± 10.7%-fold to 40% ± 2.5% compared to the basal level (Figure 6.12A).

Similar results were also obtained from 1 μM ISO dose (Figure 6.12B). Indeed, both hiPSC-CM-Q41 and hiPSC-CM-L41 showed a relatively similar maximal beat rate after 2h incubation with ISO, which was 286% ± 6% and 281% ± 3.6%, respectively (mean ± SEM, n = 2). In the first 24h, both cell lines exhibited a relatively high beating frequency until 36h when a dramatic drop was observed in hiPSC-CM-Q41 followed

fluctuating beating pattern similar to that of 100 nM ISO. At the end of the experiment, the hiPSC-CM-L41 maintained its beat rate at 194% ± 11.8%, while hiPSC-CM-Q41 was at 65% ± 11%. Therefore, it was observed that although hiPSC-CM-L41 showed a fluctuated beating pattern after 32h incubation with ISO, its beat rate still maintained at a relatively high level until the end of the experiment. However, in the case of hiPSC-CM-Q41, the fluctuating pattern was observed followed a significant drop in beat rate below the basal level, which was similar to the beating pattern seen in arrhythmic CMs (Doerr et al., 2015; Jonsson et al., 2011).

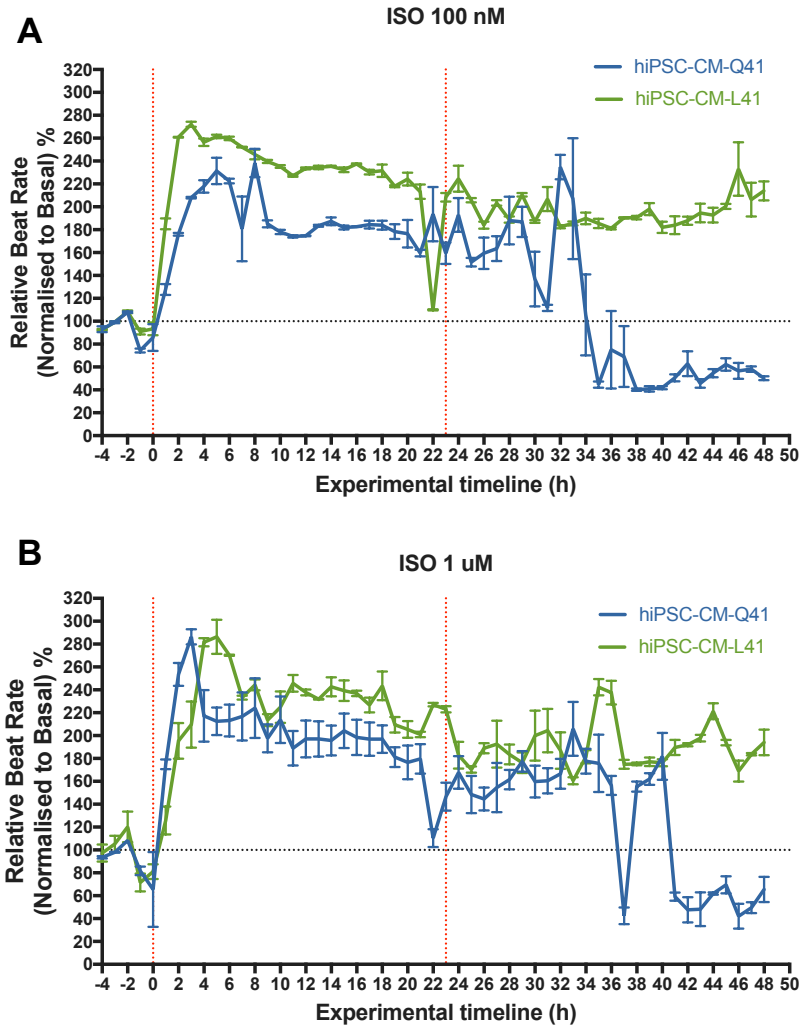


Figure 6.11: The effects of ISO treatment on hPSC-CM beat rate. The hiPSC-CM-Q41 and hiPSC-CM-L41 were subjected for ISO treatment at 100 nM **(A)** and 1 μM **(B)** for 48h *in vitro*. The basal beat rate was measured in the first four hours prior to ISO treatment. The second dose of ISO was added after 24h incubation *in vitro* to maintain its effects throughout the experiment. The red line indicated the time when ISO was added into the culture. (Error bar: SEM, n=2).

Taken together, these data revealed that there was no different between the two cell lines in the first 24h incubation with ISO (at both 100 nM and 1 μM dose). A significant difference between GRK5-L41 expressing CMs and its counterpart was observed after 32h to 36h incubation, when the arrhythmic beating pattern was observed in hiPSC-CM-Q41 but not in hiPSC-CM-L41 (Figure 6.11A&B) ($P<0.01$, n=2, two-way ANOVA).

6.2.3.3 Investigation the effects of β-blockers on contractility machinery of hiPSC-CMs

The chronotropic effects of ISO on CMs are mediated via β-adrenergic receptors, especially β_1 and β_2. Therefore, it was important to investigate the effects of different β receptors in response to ISO by using β-blockers, including β_1 blockade (CGP20112 – CGP), β_2 blocker (ICI 118,551 – ICI), and non-selective β-blocker (Propranolol – Prop). To maximise their effects, the β-blockers were added one hour before the treatment followed 100 nM ISO with either 100 nM CGP, 100 nM ICI, or 200 nM Prop. Accordingly, the CardioExcyte96 was used to measure the beat rate and beating pattern of these CMs for up to 48h.

The data illustrated a significant reduction in contraction rate of CMs underwent β-blocker treatment, indicating that the β-blockers inhibited the contractility machinery of the CMs. To be more specific, blocking either β_1 or β_2 of hiPSC-CM-Q41 resulted in an approximately 20% reduction in maximal beat rate after 4h incubation with ISO (Figure 6.12A). Interestingly, hiPSC-CM-L41 showed a high level of β_2 activities compared to that of β_1 indicating by an approximately 40% reduction in the maximal beat rate when β_1 blocker was used, whereas more than 110% reduction in the maximal rate when β_2 blocker was applied (Figure 6.12B). Completely block the adrenergic pathways using Prop resulted in an approximately 150% reduction in beat rate observed in both cell lines, indicating that β-ARs play a major role in orchestrating the ISO-mediated contractility of CMs.

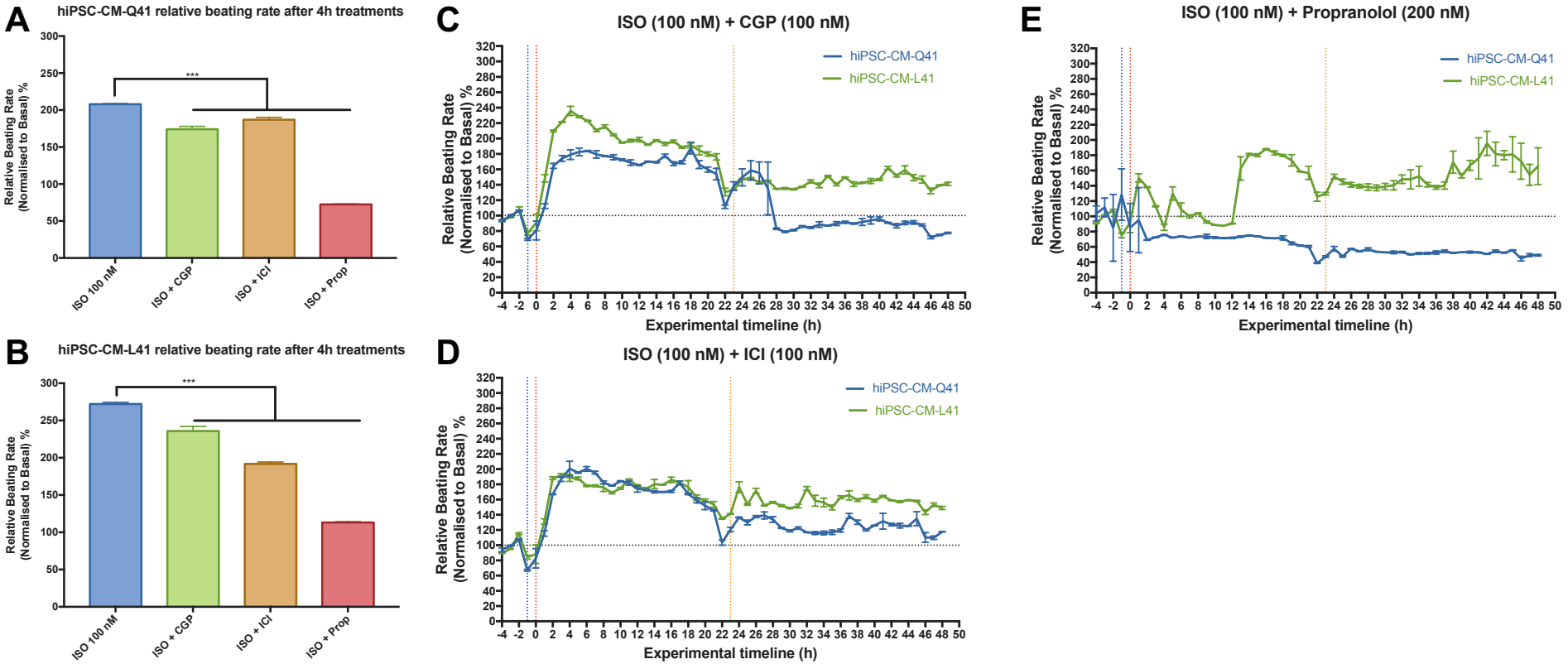


Figure 6.12: Evaluation the effects of β-blockers, including β_1-blocker (CGP20712 – CGP), β_2 blocker (ICI 118,551 – ICI), and Propranolol (Prop) on CMs during ISO treatment. **(A, B)** The bar charts illustrate the inhibitory effects of β-blockers on the maximal beat rate of hiPSC-CMs after 4h incubation with 100 nM ISO. **(C, D, E)** The line charts demonstrate beating pattern of hiPSC-CM-Q41 (blue line) and hiPSC-CM-L41 (Green line) after CGP, ICI, and Prop treatment together with ISO. The blockers were added 2 hours prior to the treatment, and were added together with ISO to maximise their effects. The dotted blue line indicates the time when blockers were added, the dotted line indicates the first ISO + blocker added, and the dotted orange line illustrates the second dose of ISO and blocker. (Error bar: SEM, n=2).

Furthermore, our results also demonstrated that blocking either β_1 or β_2 could not eliminate the effects of ISO treatment entirely. Indeed, both hiPSC-CM-Q41 and hiPSC-CM-L41 elevated their beat rate immediately after ISO treatment and reached a peak at 182% ± 4.9% and 228.2% ± 1.2%, respective, in the case of CGP treatment (Figure 6.12C), and at 200% ± 10% and 188% ± 2%, respectively, when ICI was used (Figure 6.12D) (mean ± SEM, n=2). Both cell lines showed a gradual reduction in their contraction rate in the first 24h. Strikingly, there was no dramatic fluctuation, and arrhythmic beating pattern was observed in both cell lines until the end of the experiment, suggesting that β-blockers protected the CMs from prolonged effects of ISO *in vitro*. Of note, while the hiPSC-CM-Q41 reduced their beat rate close to the basal level after 30h incubation with ISO and remained at the level until the end of the experiment, the hiPSC-CM-L41 maintained the relatively high beat rate at both ISO concentrations (Figure 6.12C&D). Additionally, blocking the entire β adrenergic system using Prop completed block the effects of ISO in the first 12h post-ISO treatment. However, the induction of beat rate in hiPSC-CM-L41 was observed at 12h followed maintaining at a relatively high level until the end of the experiment. Interestingly, Prop significantly reduced the beat rate of hiPSC-CM-Q41 and completely block the ISO effects throughout the experiment (Figure 6.12E).

The data from this section illustrated the effects of β-blockers on the beat rate and beating pattern of hiPSC-CMs. Indeed, our CMs showed a high activity level of β_2-ARs compared to that of β_1-ARs. Furthermore, the β-blockers showed the cardioprotective effects by preventing the arrhythmic patterns in both cell lines during prolonged exposure to ISO treatment (up to 48h).

6.2.3.4 Validation the effects of prolonged exposure to ISO in vitro using CRISPR-edited HUES7 lines (HUES7-CM-Q41 and HUES7-CM-L41)

The exciting results obtained from the hiPSC-CM illustrated the phenotypic difference between GRK5-L41 and GRK5-Q41 expressing CMs during prolonged exposure to ISO treatment. To validate the results, we repeated the experiment using the CMs generated from the CRISPR-edited lines, including HUES7-CM-Q41 and HUES7-CM-L41. Furthermore, the time required for measuring the basal beat rate was also reduced from 4h to 2h to shorten the experiment duration.

Retrospectively, we sought to assess the responsiveness of these lines to ISO treatment with the two concentrations, including 100 nM and 1 μM. Both lines showed the immediate response to ISO treatment, although 1 μM of ISO induced stronger contraction level from both lines compared to that of 100 nM (Figure 6.13A&B). Additionally, at 100 nM ISO, both HUES7-CM-Q41 and HUES7-CM-L41 lines reached a maximal beat rate after 2h post-ISO treatment at 163% ± 0.6% and 171% ± 10.4%, respectively followed the reduction in the basal rate after 8h treatment (mean ± SEM, n=2) (Figure 6.13A). A second ISO dose increased the beat rate of HUES7-CM-L41 but not that of HUES7-CM-Q41. Interestingly, the HUES7-CM-Q41 started to show the irregular beating pattern after 38h incubation with ISO followed the significant drop in the beat rate at the end of the experiment, whereas the HUES7-CM-L41 maintained a slightly high level of beat rate (around 120% at the end of the experiment). A significant difference in ISO-induce responses between the two tested cell lines was observed at 1 μM ISO treatment. The HUES7-CM-L41 reached a peak at 336% ± 1.2% after 4h post-treatment, while the HUES7-CM-Q41 achieved the maximal beat rate at 220% ± 3.4% after 2h incubation with ISO (Figure 6.13B). Intriguingly, while the former gradually reduced the beat rate toward basal level, no contractility signal was detected from the later, suggesting the potential ISO-induced cardiotoxicity effect.

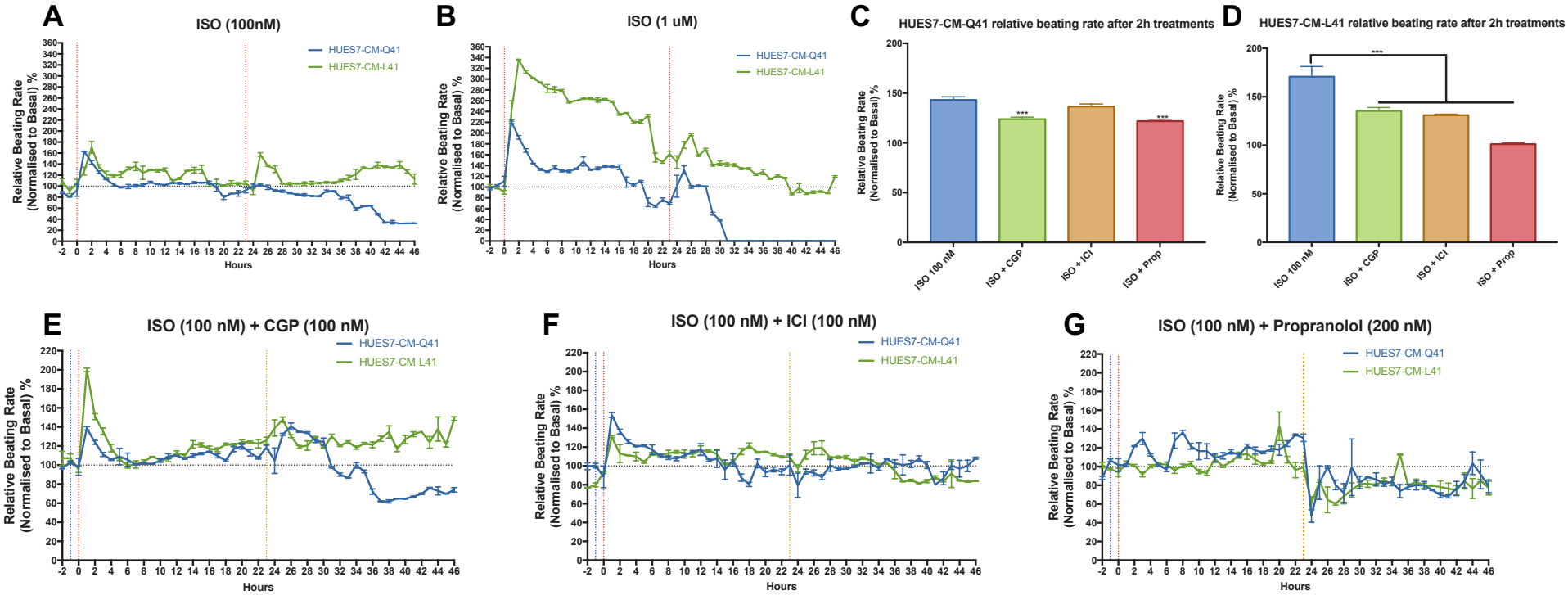


Figure 6.13: Validation the effects of prolonged exposure to ISO treatment (up to 48h) using CRISPR-edited lines. The CMs generated from the two edited lines, HUES7-CM-Q41 and HUES7-CM-L41 were used to validate the effects of ISO treatment with/without β-blockers, including CGP, ICI, and Prop. **(A,B)** The line charts illustrate the effects of ISO at 100 nM and 1 μM on CMs up to 48h, respectively. **(C,D)** The inhibitory effects of β-blockers on the maximal beat rate of HUES7-CM-Q41 and HUES7-CM-L41, respectively, during 100 nM ISO treatment. **(E,F,G)** The real-time beating pattern of HUES7-CM-Q41 and HUES7-CM-L41 during ISO treatment together with CGP **(E)**, ICI **(F)**, and Prop **(G)**. (Error bar: SEM, n=2, P<0.001, two-way ANOVA). The blue line indicated the time when blocker was added, the red dotted line indicated the addition of ISO into the culture, and the orange line indicated the addition of both ISO and blocker.

Further investigation on the effects of β-blockers illustrated the inhibitory effects on the maximal beat rate in both hiPSC-CM-Q41 and hiPSC-CM-L41. While the former demonstrated the relatively high level of β_1 activities, the β_2 seemed to be the dominant player in the latter (Figure 6.13C&D). Similar to the previous experiments conducted in hiPSC-CMs, the β-blockers illustrated the cardiac protective effects against extended cultured with ISO treatment, up to 48h.

In general, the data confirmed that extended culture of hPSC-CMs in ISO at either 100 nM or 1 μM created the irregular beating pattern in GRK5-Q41 expressing CMs, which was similar to the arrhythmic patterns and in some cases, the CMs completely stopped contracting illustrated the cardiotoxicity mediated by extended ISO treatment. Additionally, our data also showed that GRK5-L41 expressing CMs represented a high level of beat rate that maintained at a steady level until the end of the experiment, indicating that extended ISO treatment up to 48h did not introduce detrimental effects on the contractility functions of these CMs. The similar effects were observed in GRK5-Q41 under β-blocker treatments. However, it is unable to draw the conclusion that the GRK5-L41 variant is the main cause of the protective effects, which are similar to that of β-blockers. Therefore, further experiments need to be conducted to confirm the roles of GRK5-L41 involving the cardiac protective functions against the effects of prolonged exposure to ISO *in vitro* (up to 48h).

6.2.4 Measurement of intracellular cAMP production in response to ISO treatment using LANCE *Ultra* cAMP assay

The detection of ISO-induced contractility in hPSC-CM provided sufficient information about the responsiveness of adrenergic systems in hPSC-CMs. As previously mentioned, the CM's contraction is tightly orchestrated by β-adrenergic signalling pathways, especially via $G\alpha_S$-mediated cascade, which directly participates in the regulation of secondary messenger, cAMP via induction of Adenylyl Cyclase (AC). The generation of intracellular cAMP in response to catecholamine induction is one of

the most important second messengers mediating diverse physiological responses of the heart, especially the contractility machinery (Dorn, 2009; Lefkowitz, 2007). Therefore, it was important to investigate the production of intracellular cAMP mediated by ISO treatment. To accomplish the task, the LANCE *Ultra* cAMP assay was used, and the procedure was described in Figure 6.14.

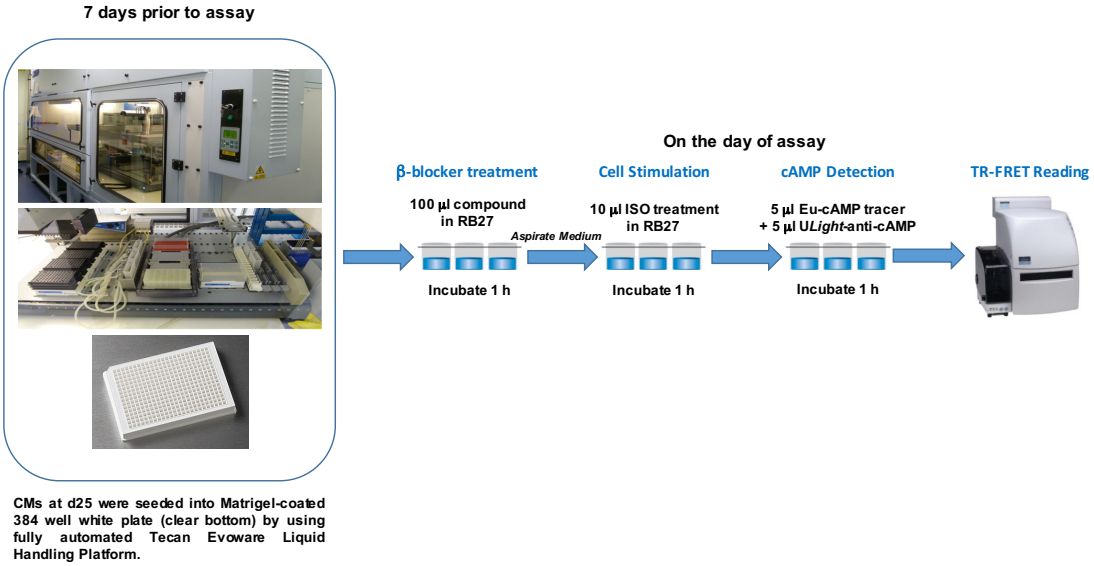


Figure 6.14: Experimental procedure for LANCE Ultra cAMP assay. CMs were maintained until d25 of differentiation and seeded one week before the assay using fully automated Tecan Evoware Liquid Handling Platform (TEL). The CMs maintaining medium (RPMI supplemented with B27 supplement – RB27) was changed every 3 days using TEL. On the days of assay, CMs were incubated 1 h with β-blockers (CGP, ICI, or Prop – depending on experimental plan) before adding ISO treatment (in half-log dilution). After 1 h incubation with ISO, 5 µl Eu-cAMP tracer and 5 µl ULight-anti-cAMP and incubate for 1h followed by reading of TR-FRET signal using EnVision Plate-reader set in lamp mode.

6.2.4.1 Optimisation of cell seeding density

Identification of the optimal cell seeding density is a crucial step of LANCE *Ultra* cAMP assay establishment. Uneven seeding or too low or too high density directly reduces the test window, introduces variability within the assay and does not reflect the cAMP production of the cells. Too low cell seeding density decreases the maximal signal, whereas too high density increases the minimal signal (i.e. the background noise) due to the increase in basal cAMP levels. Moreover, development of a cAMP assay outside the dynamic assay range would wrongly report the cAMP profiles of the CMs.

To determine the optimum cell seeding density, hiPSC-CM-Q41 were seeded at varying density, including 1000 cells/well, 2500 cells/well, 5000 cells/well and 10.000 cells/well of the Matrigel-coated 384 well plate. A Forskolin dose-response curves were generated in half-log dilution. The cAMP production from Forskolin in different cell seeding density was then used to compare with a cAMP standard curve. The assay was read using EnVision Plate-reader.

The results showed that the optimal cell seeding density was 5.000 cells/well because at this cell density, the highest assay window (indicating by the ratio between maximum and minimum TR-FRET readout –S/B – Figure 6.15A) was obtained while staying within the IC_{10} and IC_{90} dynamic range of the cAMP standard curve (Figure 6.15B and C). Of note, although the assay window at 1000 cells/well was already acceptable, its maximum and minimum cAMP signals were outside the detectable range of the cAMP standard curve. Therefore, it was not considered as an optimal cell seeding density for the cAMP assay.

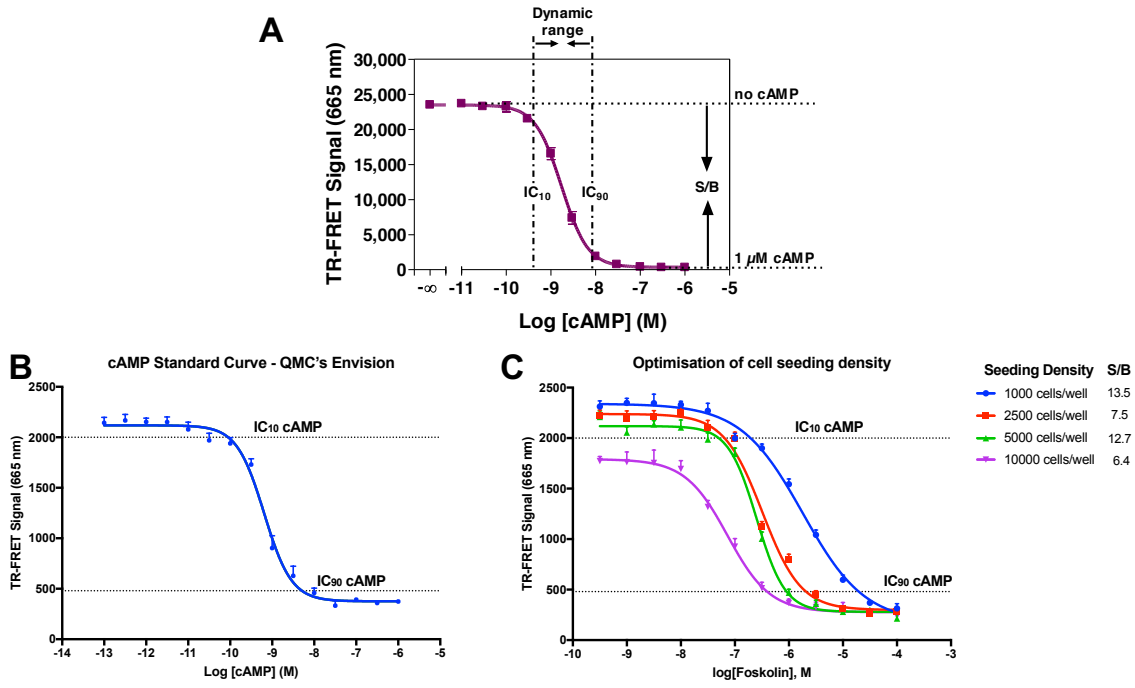


Figure 6.15: Optimisation of cell seeding density for LANCE *Ultra* cAMP assay. (A) Representative standard curve (obtained from LANCE Ultra cAMP assay protocol - showed the signal-to-background (S/B) ratio was of 70, with a 1.5 log dynamic range (IC_{90} – IC_{10} values). **(B)** cAMP standard curve generated LANCE *Ultra* cAMP kit. **(C)** Cell seeding densities and Forskolin cross-titration. TR-FRET signal was measured with the EnVision Plate reader set in lamp mode. (Error bar: SEM, n=1, 5 technical replicates).

Additionally, we also found out that the cAMP assay was relatively sensitive and the signal from the EnVision Plate reader obtained in the experiment was relatively low compared to the reported results in the assay manual. Further investigation revealed that the EnVision Plate Reader that was used in the experiments was faulty due to the problem in its filter system which only generated low readout but also introduced large variations between reads. By using the new EnVision Plate reader in the lab, the problem was solved, in which, the readout from the new system ranging from 2000 counts to 20.000 counts, which was similar to that of described in the manual handbook. Therefore, the subsequence cAMP assays were conducted using the new system in our lab, and each experiment was carried out alongside with the cAMP standard curve for assay quality control. The cAMP standard curve from the new system was demonstrated in Figure 6.16.

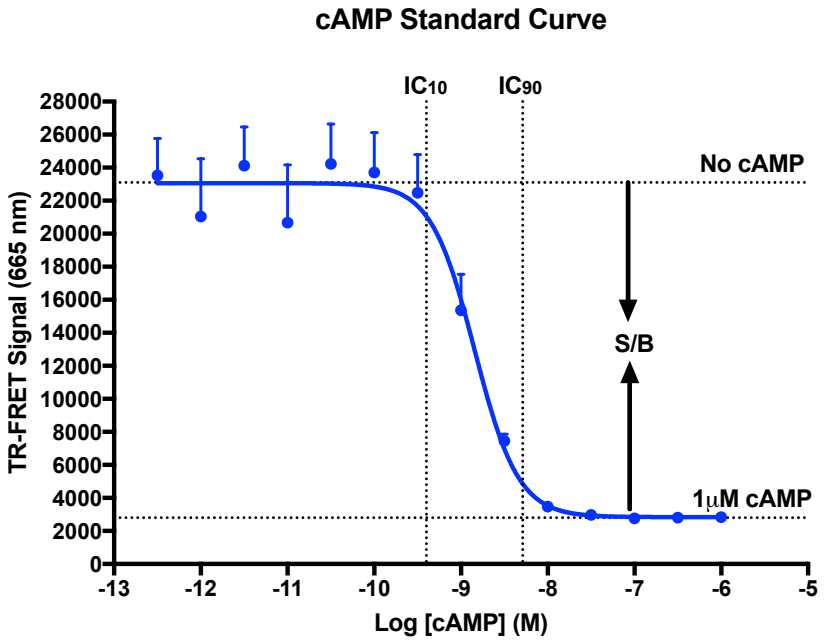


Figure 6.16: A cAMP standard curve generated from LANCE Ultra cAMP assay using the EnVision Multilabel Plate reader set in lamp mode. The standard curve was generated using the GraphPad Prism with a sigmoidal dose response curve. The results showed a S/B ratio was of 10.97 with 1.5 log dynamic range (indicated by IC_{10} – IC_{90} value) and the sensitivity of the assay was 1.43 nM (IC_{50} value). (Error bar: SEM, n=3).

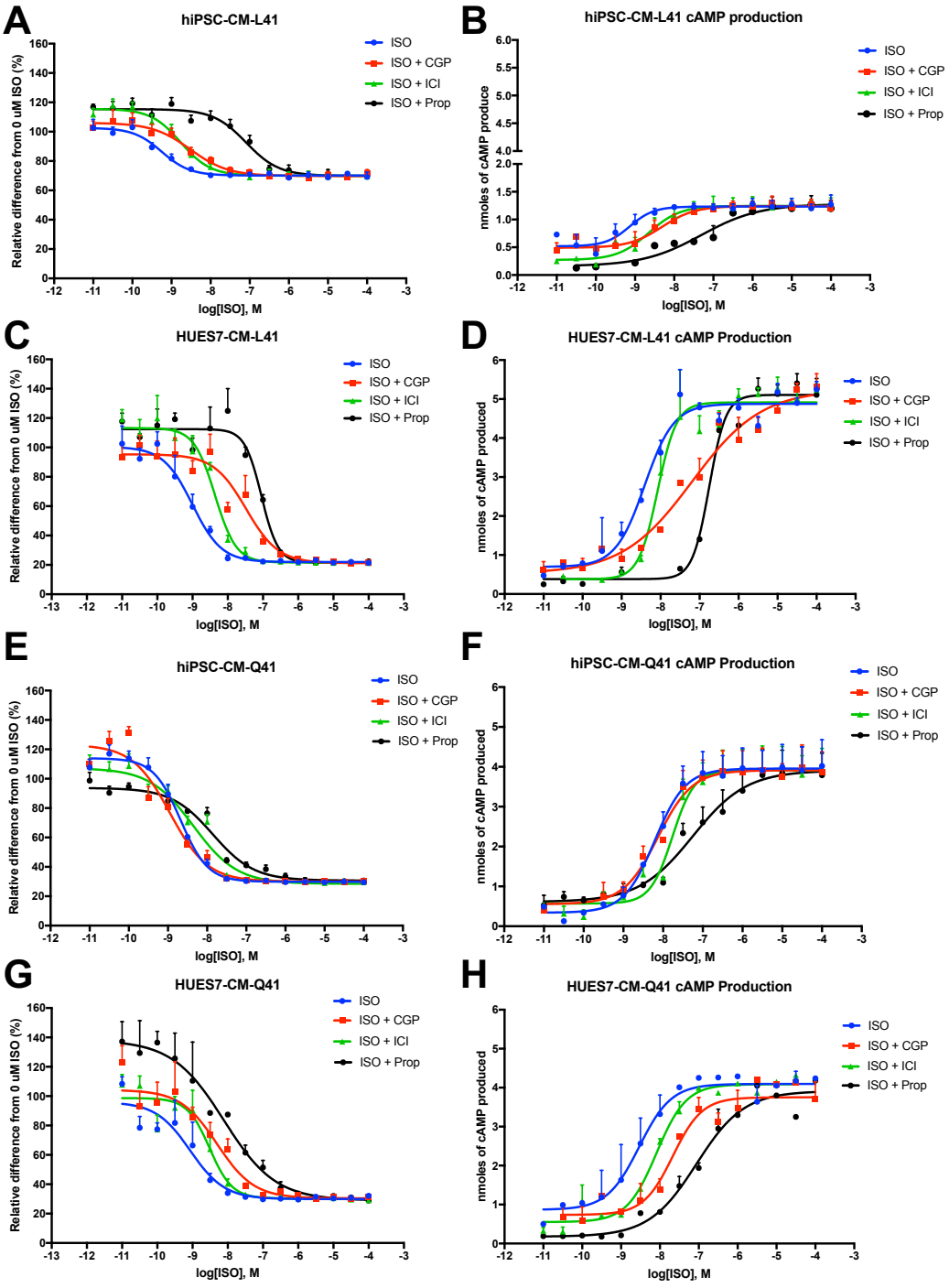
6.2.4.2 Measurement of intracellular cAMP in response to ISO treatment

To gain an insight of intracellular cAMP production in CMs in response to ISO treatment, the hiPSC-CM-Q41, hiPSC-CM-L41, HUES7-CM-Q41, and HUES7-CM-L41 were first seeded into the Matrigel-coated 384 well plate using automated Tecan Evoware Liquid Handling Platform (TEL), kindly supported by Dr. Ralph Hyde. The CMs were maintained at 37^{o}C for seven days before the assay, and the medium was changed every two consecutive days. The dose response curve of ISO with/without β-blockers, including CGP, ICI, and Prop was applied to the culture for 1h followed the cAMP measurement using the LANCE *Ultra* cAMP assay as described in Figure 6.14.

The results indicated that the dose-response curve of ISO treatment could be created in all tested cell lines, confirming that the assay worked properly under optimised conditions. The EC_{50} values generated from the assay were at nM scales, ranging from 0.5 nM to 2 nM, depending on cell lines (Figure 6.17A, C, E, G and Table 6.1). By using the standard curve, the amount of intracellular cAMP generated from all tested cell lines were ranging from 0.5 nM to 5.5 nM, which was at approximately 0.1 fmol/cell to 1.1 fmol/cell (Figure 6.17B, D, F, and H). Interestingly, although the β-blockers did not alter the maximal rate of ISO-response curve and maximal cAMP production, their inhibitory effects were illustrated by the right-shift of the ISO dose-response curve in the manner characteristic of classic competitive antagonism. Indeed, the β-blocker treatments reduced the responsiveness of the CMs by increasing its ability to withstand a higher level of ISO dose illustrating by the higher ISO EC_{50} and E_{max} values (Table 6.1 and 6.2).

Table 6.1: The EC_{50} values of ISO concentration curves in the presence of β-antagonists (CGP, ICI, and Prop) in hiPSC-derived CMs and gene edited HUES7-derived CMs. Values are mean ± SEM, n=3.

EC_{50} (nM)	ISO	ISO + CGP	ISO + ICI	ISO + Prop
hiPSC-CM-Q41	1.92 ± 0.59	1.22 ± 0.27	4.46 ± 1.47	11.88 ± 7.2
hiPSC-CM-L41	0.56 ± 0.006	3.14 ± 0.01	1.83 ± 0.11	94.96 ± 14.145
HUES7-CM-Q41	1.29 ± 0.722	7.86 ±2.78	3.04 ± 0.19	6.31 ± 0.96
HUES7-CM-L41	0.742 ± 0.526	28.28 ± 18.155	4.08 ± 0.036	87.86 ± 6.32



<u>Figure 6.17</u>: cAMP production response curve of ISO treatment with/without β-AR antagonists, including CGP, ICI, and Propranolol. Concentration-response curves of ISO using TR-FRET normalised signal plotted against the logarithmic values of ISO concentration (left panel) and its re-plotted in terms of cAMP data (right-panel) by interpolating from a cAMP standard curve run in parallel on CMs at d30 of differentiation were shown. Pretreatment with β-blockers right-shifted the ISO-stimuated concentration response curves of hiPSC-CM-Q41 **(Yang et al.)**, hiPSC-CM-L41 **(C-D)**, HUES7-CM-Q41 **(E-F)**, and HUES7-CM-L41 (**G-H)**.

Table 6.2: The E_{max} values of ISO concentration curves in the presence of β-antagonists (CGP, ICI, and Prop) in hiPSC-derived CMs and gene edited HUES7-derived CMs. Values are mean ± SEM, n=3.

EC_{max} (μM)	ISO	ISO + CGP	ISO + ICI	ISO + Prop
hiPSC-CM-Q41	12.7 ± 2.43	12.24 ± 0.63	73.49 ± 1.05	238.12 ± 9.26
hiPSC-CM-L41	3.677 ± 0.337	36.7 ± 4.8	11.72 ± 1.12	519.19 ± 84.02
HUES7-CM-Q41	7.38 ± 2.76	46.03 ± 12.525	15.69 ± 1.05	360.93 ± 38.95
HUES7-CM-L41	6.45 ± 1.01	216.58 ± 60.33	20.4 ± 4.2	295.51 ± 2.74

Interestingly, the cAMP assay confirmed that the hPSC-CMs had higher β_1 activities compared to that of β_2. In all tested lines, except the hiPSC-CM-Q41, blocking β_2 receptors using ICI resulted in lower EC_{50} values of ISO compared to that of β_1 blocker (CGP). This result indicated that when β_2 was the only adrenergic receptors responsible for ISO chronotropic effects, a higher dose of ISO was required to trigger 50% response from CMs compared to that of β_1 alone, which in turn, illustrated that β_1 plays a dominant role during the acute response of CMs to ISO treatment. However, there was no significant difference between GRK5-Q41 and GRK5-L41 expressing CMs in ISO EC_{50} values with and without β-blocker treatments, suggesting that the functions of GRK5-Q41 and GRK5-L41 during acute response of CMs to ISO treatment were similar ($P<0.001$, n=3, two-way ANOVA) (Figure 6.18A&B). Interestingly, complete blocking of adrenergic receptors using Prop significant increased the EC_{50} and E_{max} values up to 20 nM to 100 nM and 200 μM to 500 μM, respectively, depending on cell lines (Table 6.1&6.2) (Figure 6.18). Of note, there was a significant difference in EC_{50} values between GRK5-Q41 and GRK5-L41 expression CMs when Prop was used, suggesting that completely block adrenergic receptors require much higher ISO concentration to triggered the response from GRK5-L41 CMs (Figure 6.18).

Taken together, the data in this section illustrated that the ISO dose-response curves could be generated from the cAMP assay providing the information about the sensitivities of hPSC-CM to ISO treatment. Indeed, our results demonstrated that there was no significant difference between GRK5-Q41 and GRK5-L41 CMs in response to 1h ISO treatment at 100 nM. Indeed, during acute chronotropic responses of hPSC-CMs, the β_1-ARs play a dominant role in regulating the contractility of CMs followed β_2.

Furthermore, it is important to note that the significant difference between the two GRK5 variants was detected when β adrenergic signalling pathway was completely blocked by Prop treatment. Therefore, to identify the distinct functions between GRK5-Q41 and GRK5-L41 phenotype in hPSC-CMs, chronic exposure to ISO need to be considered, which also mimics the observation during heart failure condition *in vivo*.

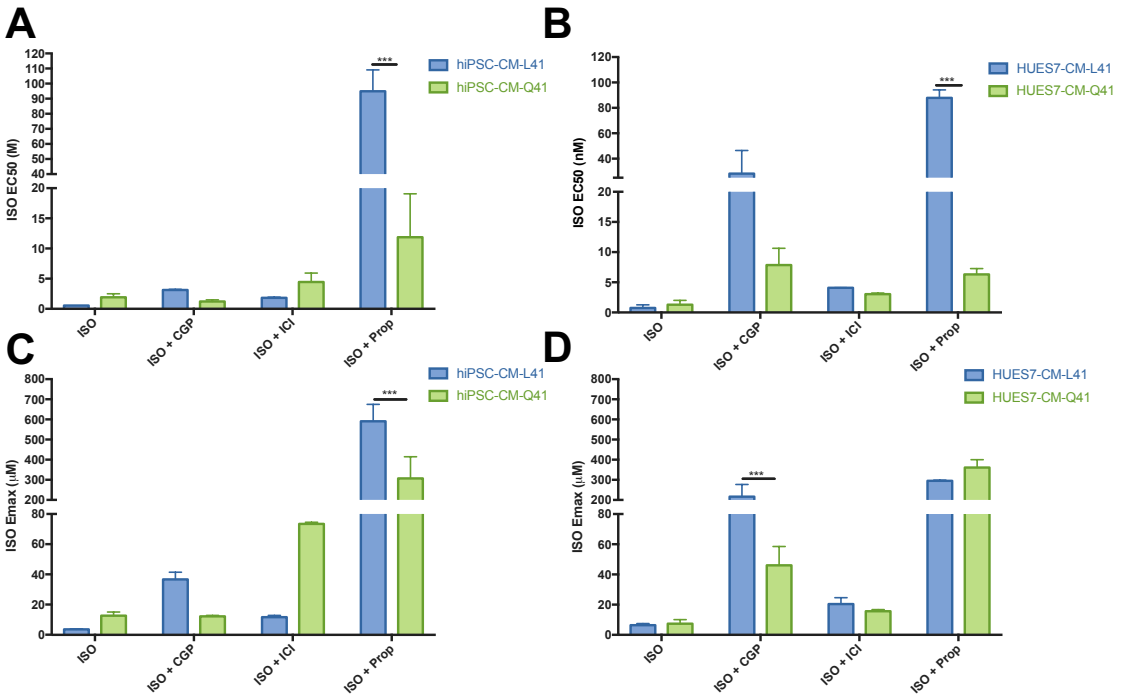


Figure 6.18: EC_{50} and E_{max} values of ISO concentration response curve with/without β-antagonist treatments (CGP, ICI, and Prop). (A-B) The EC_{50} values of hiPSC-derived CMs and gene edited HUES7-derived CMs in response to ISO treatment. Values are shown as ISO concentration (nM). **(C-D)** E_{max} values calculated from the ISO concentration response curves. Values are shown as ISO concentration (μM). All values were calculated as mean ± SEM, n=3, P<0.001, two-way ANOVA.

6.2.5 Development of Western Blot assay to assess the cellular distribution of the GRK5 protein in hPSC-CMs

During heart failure, the chronic exposure to high level of catecholamines introduced the detrimental effects on CM functionalities and physiologies, especially the development of pathological hypertrophy which later resulted in the disruption of sarcomeric structure and contractility machinery followed apoptotic effects on CMs (Dorn., 2007; Bernardo et al., 2010). Recently, the non-canonical functions of GRK5 were reported to be involved in the development of pathological hypertrophy via its

accumulation in the nucleus of CMs (Hullmann et al., 2014). Therefore, it is important to investigate the distribution of GRK5 protein during chronic exposure to ISO *in vitro* using Western Blot analysis.

6.2.5.1 Optimisation of Western Blot condition

The anti-human GRK5 antibody from Santa Cruz Biotechnology (sc-565) was first used at 1:1000 dilution suggested by the manufacturer protocol to detect the presence of GRK5 in hiPSC-CM-Q41 samples. Two protein concentrations, including 10 μg to 15 μg, of cytoplasmic and nucleus extraction were used for WB analysis. To block the non-specific binding of the primary antibody, the 5% BSA solution in blocking buffer was used. The result indicated the non-specific binding of the primary antibody which led to the formation of smear bands in all samples, although there were strong bands at approximately 68 kDa (Figure 6.19A). This result suggested that the primary antibody is not highly specific for detection of GRK5 and the blocking solution was not sufficient enough to prevent non-specific binding during the blocking process.

The same nitrocellulose membrane was stripped using the ReBlot Plus Stripping solution (Merck Millipore), and another anti-human GRK5 antibody from Abcam (ab64943) was used. Additionally, 5% skimmed milk was used as a blocking buffer in replacement of 5% BSA medium. Interestingly, this combination significantly improved the specificity of the WB. A clear band was observed at approximately 68 kDa, suggesting the right band of GRK5 protein (Figure 6.19B). Of note, stronger bands were found in the CM samples underwent 48h and 72h treatment with ISO (in both cytoplasmic and protein fractions) (Figure 6.23B).

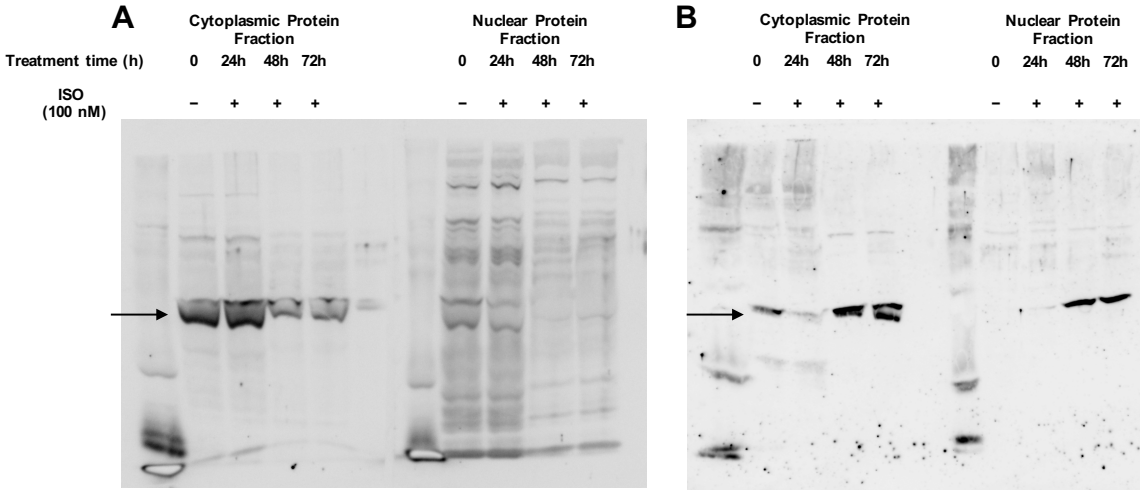


Figure 6.19: Optimisation of Western Blot analysis of GRK5 expression from hiPSC-CM-Q41 in response to ISO treatment (up to 72h). 15 μg of cytoplasmic and nuclear proteins from hiPSC-CM-Q41 during treatment with ISO for 24h, 48h, and 72h were subjected for Western blot analysis using anti-human GRK5 from Santa Cruz Biotechnology (sc-565) **(A)** and Abcam (ab64943) **(B). (A)** Membrane was blocked using 5% BSA overnight resulted in non-specific binding of antibody. **(B)** Membrane was blocked using 5% skimmed milk and GRK5 from Abcam increased the specificity of Western Blot analysis and reduced non-specific binding of the antibody. The back-arrows indicated the potential GRK5 bands at 68 kDa.

6.2.5.2 Detection of cellular distribution of GRK5 in hPSC-CMs

Cellular distribution of GRK5 during ISO treatment was successfully detected using WB analysis of the cytoplasmic protein fraction and the nucleus fraction extracted from $5x10^6$ CMs underwent 100 nM ISO treatment for 24h, 48h, and 72h. The result illustrated different patterns between cytoplasmic GRK5 and nucleus GRK5 during prolonged exposure to ISO (Figure 6.24). The densitometry analysis of the WB bands showed that the cytoplasmic GRK5 extracted from hiPSC-CM-L41 increased upon ISO incubation (0h: 48%, 24h: 96%, 48h: 109%, and 72h: 142%, n=1). A similar result was seen from cytoplasmic GRK5 isolated from hiPSC-CM-Q41 (Figure 6.25A). In contrast, the nuclear GRK5 extracted from the same cell line indicated the decrease in GRK5 protein during ISO treatment (0h: 179%, 24h: 164%, 48h: 20%, and 72h: 19%, n=1), while hiPSC-CM-Q41 illustrated an elevated level of nucleus GRK5 (Figure 6.25B).

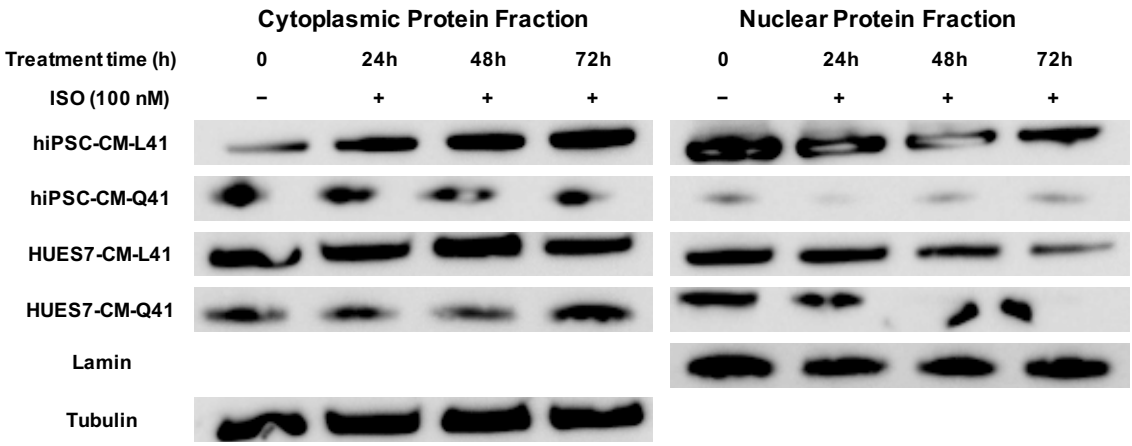


Figure 6.20: Western Blot analysis of subcellular distribution of GRK5 during chronic exposure to ISO. 15 μg of proteins extracted from either cytoplasmic fraction or nuclear fraction lysed from CMs exposure to 100 nM of ISO in 0h, 24h, 48h, and 72h were subjected to Western Blot analysis using anti-GRK5 antibody. The cytoplasmic protein fraction was confirmed using anti-Tubulin antibody whereas the nuclear fraction was confirmed using Lamin antibody.

In terms of gene-edited derived CMs, the densitometry analysis indicated a slight induction in cytoplasmic GRK5 obtained from HUES7-CM-Q41, while the HUES7-CM-L41 showed no change in cytoplasmic GRK5 level upon ISO treatment (Figure 6.25C). Interestingly, a reduction in nucleus GRK5 was seen in HUES7-CM-L41, which was 108% at 0h and reduced to 42% after 72h incubation with ISO (Figure 6.25D). The reverse trend was found in the case of HUES7-CM-Q41, which showed a gradual increase in its nucleus GRK5 fraction.

Taken together, these results illustrated the ability to detect the cytoplasmic and nucleus fractions of GRK5 protein in hPSC-CM in response to ISO treatment *in vitro*. Although the difference in the cellular distribution of GRK5-Q41 and GRK5-L41 was detected using Western Blot analysis, it is impossible to draw any conclusion because of lacking biological replication. Therefore, it is important to repeat the experiments to achieve the concrete data to firmly validate this data set. Of note, if the observations were accurate, it would be possible to hypothesise that the cardioprotective effects of GRK5-L41 protein were derived from its ability to be exported outside the nucleus, preventing the development of the pathological hypertrophic condition.

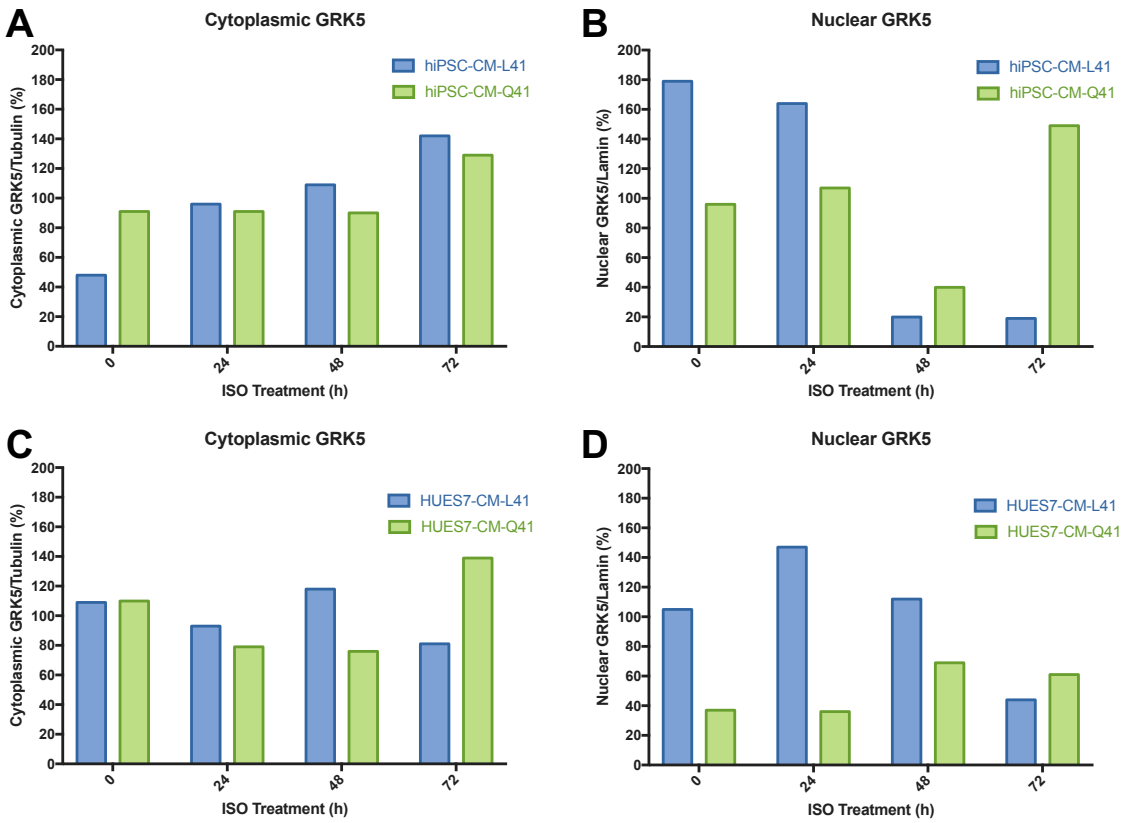


Figure 6.21: Analysis of intracellular GRK5 extracted from either cytoplasmic or nucleus of CMs during chronic ISO treatment. The results were obtained from densitometry analysis of Western Blot experiments. The values are the relative difference between cytoplasmic GRK5 and Tubulin or nuclear GRK and Lamin. (n=1).

6.2.6 Establishment of hypertrophic assay using immunofluorescence analysis

During heart failure, the development of pathological hypertrophy is one of the leading causes of cardiomyocyte dysfunction and ventricular remodelling, especially during the chronic response to high level of catecholamines (Dorn., 2007). Recently, it was found that a specific peptide, called the brain natriuretic peptide (BNP), was specifically expressed during pathological hypertrophic conditions, providing a specific marker of this condition (Heineke et al., 2006; Carlson et al., 2015). Therefore, detection of BNP expression using immunofluorescence approach is a valuable tool to assess the hypertrophic condition in hPSC-CMs. To evaluate the conditions that could potentially trigger hypertrophic responses from hPSC-CMs, several hypertrophic compounds,

including phenylephrine (PE) and Endothelin-1 as well as ISO was used in this experiment.

Our data indicated a low-level expression of BNP protein in the control sample (Figure 6.22). Interestingly, the CMs underwent prolonged exposure to ISO (96h) showed a relatively high level of BNP expression compared to that of the control sample, suggesting that the assay worked properly and allowed the detection of both low and high level of BNP presented in hPSC-CMs. Treatments with either 1 μM PE or 100 nM Endothelin-1 resulted in the expression of BNP protein as shown in Figure 6.22. Importantly, the detrimental effects on cardiomyocyte viability and physiology were observed when the CMs underwent 100 nM ISO with 1 μM PE treatment for 24h, indicating the cardiotoxic conditions causing the death of CMs *in vitro*. Additionally, incubation of CMs with Endothelin-1 and ISO at 100 nM resulted in a significant induction of BNP after 24h treatment, which was much higher compared to that of ISO or Endothelin-1 treatment alone, suggesting that this condition could be potentially used for further investigation of the hypertrophic condition in hPSC-CMs.

However, it is important to develop the pipeline to analyse the expression level and fluorescence intensity of BNP under these particular conditions to generate quantitative results from immunofluorescence assay, which could later be used to cross comparison between GRK5-Q41 and GRK5-L41 CMs.

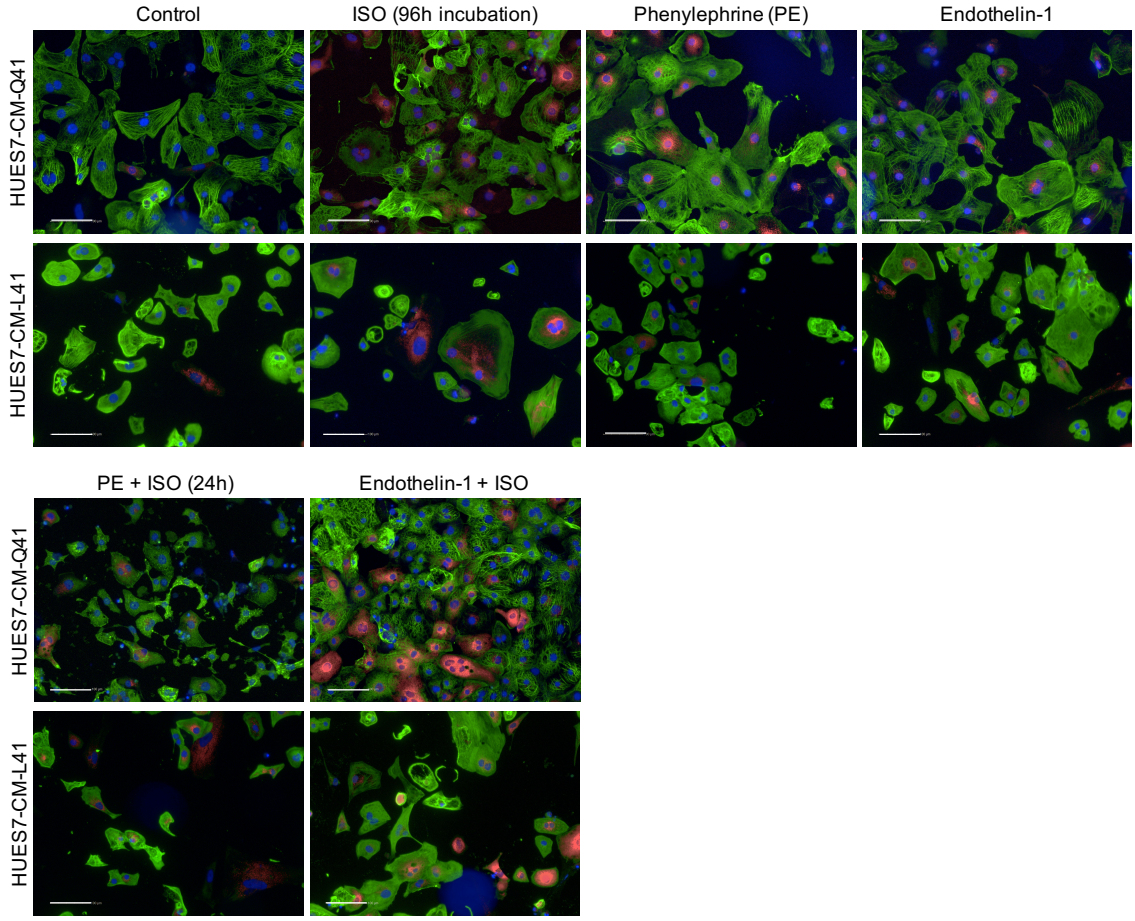


Figure 6.22: Development of immunofluorescence analysis of BNP expression to assess the hypertrophic conditions in hPSC-CMs. The HUES7-CM-Q41 and HUES7-CM-L41 was treated with either ISO for 96h, Phenylephrine (PE – 1 μM), Endothelin-1 (100 nM), PE + ISO, and Endothelin-1 + ISO. *Scale bar*: 100 μM.

6.3 Discussion

A primary function of GRKs is the uncoupling of agonist-activated GPCR from extracellular induction signals, leading to the reduction in cellular desensitisation of the receptors (i.e. decrease in receptor responsiveness) and a time-dependent loss of ligand-promoted function at organ level (Lefkowitz et al., 1992; Kim et al., 2005). In the human heart, especially during heart failure, elevation of GRK2 and GRK5 expression and marked desensitisation of β-ARs represent an endogenous mechanism that protects the heart against chronic circulation of high-level catecholamine in the blood stream (Dorn, 2009; Lefkowitz, 2007). Recently, cardiomyocytes derived from hPSCs emerge as an alternative model that could be used to investigate the human cardiac functions *in vitro*, although they possess certain limitations, especially the immature phenotypes

(Denning et al., 2016). In this chapter, we investigate the phenotypic functions of CMs derived from either lymphoblastoid reprogrammed hiPSCs and gene-edited HUES7 stem cells toward analysis of adrenergic signalling pathways and GRK5 functions *in vitro*.

The β_1 and β_2 ARs have been found to be expressed in isolated single human left ventricular CMs (del Monte et al., 1993), where the ratio between β_1 and β_2 is around 80%/20% at normal condition (Brodde, 1993; Engelhardt et al., 1996). *GRK5* was also found to be highly expressed in human CMs (Kunapuli and Benovic, 1993; Lefkowitz, 2007). It has been reported that the fetal CMs response to catecholamine induction via both β_1 and β_2 ARs, whereas in adult CMs, β_1 ARs plays a dominant role (Lefkowitz, 2007). In our study, gene expression analysis of adrenergic signalling components illustrated that *in vitro* culture of CMs increases and stabilises the expression of genes that are involved directly in adrenergic signalling pathways, including *ADRB1, ADRB2, GRK2,* and *GRK5.* Furthermore, the expression of *ADRB2* has been found to be highly expressed during the early stage of CMs post differentiation process, and prolonged culture *in vitro* stabilises the expression of *ADRB2* and induces the expression of *ADRB1*. This result is consistent with the previous study which also demonstrated the dominant expression of *ADRB2* in hPSC-CMs and elevation of *ADRB1* during *in vitro* culture up to 60 days post cardiac differentiation process (Wu et al., 2015). Our results also confirmed that adrenergic signalling pathways from hPSC-CMs started to be expressed at high level and stabilised from d30 post-differentiation, consistent with previously described (Wu et al., 2015). Keep this in mind; one needs to be sceptical in annotating any pharmacological results obtained from hPSC-derived CMs, especially with compounds target adrenergic signalling pathways. Interestingly, a detailed observation was found in mouse, and human cardiac progenitor cells where β2-AR expression was dominant, while cardiac commitment lead to the acquisition of β1-AR expression and establishment of a similar pattern of β1/β2 AR expression regulation in cardiac progenitor and cardiac progenitor-derived CMs (Khan et al., 2013). Hence in our

study, it is compulsory to maintain CMs until d30 of differentiation to allow the adrenergic system to stabilise before starting any functional analysis and drug testing experiment.

6.3.1 Development of real-time beat rate analysis of hPSC-CMs using CardioExcyte 96 platform

The immediate effect of catecholamines observed in vivo is regulation of heart contractile functions, which increases the beat rate to enhance the workload compensating for the loss caused by either exercise or cardiac injury. Hence, it is important to assess the chronotropic induction of ISO treatment and analyse the beating pattern of hPSC-CMs in response to different ISO doses. By using CardioExcyte 96 system, the beat rate of CMs can be monitored directly in real-time. The results indicated that under the optimised conditions, the beating frequency of CM monolayer could be stably recorded over several days. Additionally, the system was able to detect small changes in beating frequency as a result of added testing compounds. Furthermore, irregular beating pattern or complete disappearance of beating on drug addition indicated arrhythmias and cardiotoxicity could be observed.

Base on the beating pattern of CMs during ISO treatment, our results demonstrated five distinct phases of CM contractility, including **(1)** Phase 1 or induction phase: where the CMs response to ISO treatment by increasing their beat rate to maximum usually within 2-4 h; **(2)** Phase 2 or acute response phase: where the CMs maintain their beat rate at high level upon the treatment; **(3)** Phase 3 – or second induction phase: in this phase, a second boost of ISO treatment was applied to ensure the chronotropic activities of ISO maintain the same throughout the experiment, which induced the beat rate of CMs to a second peak, which was always smaller than the first induction peak in Phase 1 ; **(4)** Phase 4 – or adaptation phase: the treatment duration in this phase is from 26h to 34h. It was observed that the beat rate of CMs started to either maintain at high beat rate or gradually reduce toward basal level; and **(5)** Phase 5 or chronic response phase: CMs at this stage have been exposed to the treatment for more than 35h and irregular beating patterns started to appear (Figure 6.27A).

Intriguingly, regardless of their origin (hiPSC-CMs or genetically modified HUES7-CMs), CMs under ISO treatment showed the same phases as described above. No significant difference between *GRK5*-L41 and *GRK5*-Q41 phenotype was observed during the acute response phase, except the relative beat rate of *GRK5*-L41 was higher than *GRK5*-Q41, especially in hiPSC-CMs (Figure 6.27B). Both *GRK5*-Q41 and *GRK5*-L41 expressing CMs illustrated a reduction of the beat rate after 4 h incubation toward basal level indicating no clear distinction between the two genotypes in this phase (Figure 6.27B). In phase 3, second ISO induction increased the beat rate of *GRK5*-L41 bearing CMs to a second peak which was lower than that of the first peak, whereas the *GRK5*-Q41 started to have different pattern during this period. This phenomenon can be explained by the fact that the ISO-activated β-ARs were desensitised by GRKs and began to internalise inside the cells, which in turn, not only reduced the responsiveness of the receptors to ISO but also decrease the receptor density on the surface of the cells (Moore et al., 2007). Therefore, second ISO addition allowed the remaining surface receptors to be activated and triggered the second wave of signalling cascade resulting in a second peak of the beat rate but is relatively lower to that of the first peak. A clear distinction between *GRK5*-L41 and *GRK5*-Q41 phenotype was observed at Phase 4 and Phase 5 of the treatment. In Phase 4, the GRK5-L41 group showed a rapid decrease in beat rate and started to stabilise whereas, in GRK5-Q41 group, CMs showed irregular beating patterns where in hiPSC-CM-Q41, the beat rate increased and stayed at high level where as in HUES7-CM-Q41, the contraction was dropped dramatically until undetectable after 32h in the experiment. At phase 5, the GRK5-L41 group declined the contractility toward basal level without any fluctuations in the records, whereas the GRK5-Q41 showed irregular beating and complete disappearance of contraction, indicating arrhythmias and potential cardiotoxicity.

In fact, the endogenous catecholamines level in the early stage of heart failure is increased acutely to provide a “short-term” adaptation process in response to stressful conditions, which is usually known as the *fight-to-fly response* (Bers and Despa, 2009). In the same manner, the exogenous administration of catecholamines is life-saving in

clinical situations with reduced cardiac output and hypotension (Hollenberg, 2011). In contrast to these short-term benefits, prolonged secretion of catecholamines introduce detrimental effects on the heart due to its cardiotoxicity, as marked in chronic HF, stress-induced cardiomyopathy or Takostubo syndrome, and during long-term treatment with high dose of exogenous catecholamines. These phenomena strongly supported our observation where chronic exposure to ISO-induced arrhythmias and cardiotoxicity in cardiomyocytes *in vitro* in our model. Furthermore, the cardiotoxicity of catecholamine at high doses was described more than half a century ago as an infarct-like injury (Rona et al., 1959). Sustain administration of isoprenaline in other models, such as rats, induces cardiomyocyte apoptosis, hypertrophy and cardiac dysfunction with reproducibly and dose-dependently manner associated with the full molecular features of chronic heart failure (Stanton et al., 1969; El-Armouche and Eschenhagen, 2009). In terms of *in vitro* models using hPSC-derived cardiomyocytes, numerous studies illustrated the acute effects of ISO treatment on contractility of CMs using cell impedance (Jonsson et al., 2011), multi-electrode array (Tanaka et al., 2009), whole cell voltage clamp (Moretti et al., 2010), and optical force transducer (Zhang et al., 2009). However, all of these studies focused on the acute response of CMs to wide range of ISO concentration (fom nM to μM scale) but not chronic response of CMs (Eder et al., 2016).

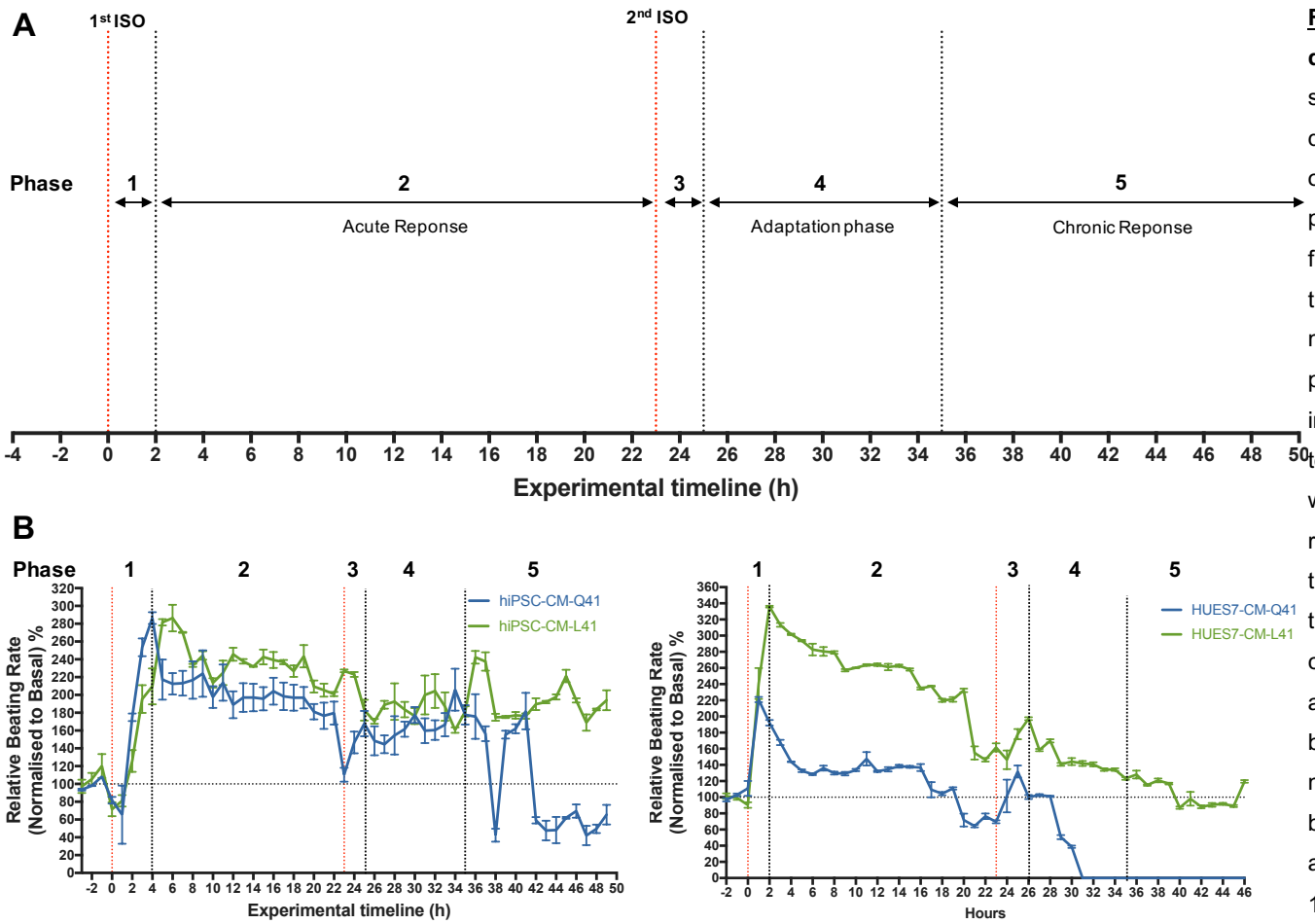


Figure 6.23: Proposed cardiac response phases developed from the CardioExcyte 96 results. (A) The schematic depicts different response phases of CMs during chronic exposure to ISO treatment (50h). Based on the results obtained from CardioExcyte 96, five primary phases were proposed, including **phase 1**: the first induction of ISO, usually in the first 2h of ISO treatment, in this phase, CMs increased the beat rate to maximal level; **phase 2**: the acute response phases, the period between 2 and 23h after the first ISO induction, in this phase, CMs started to reduce the contraction rate toward basal level; **phase 3**: second ISO addition, in which some lines showed a second peak in their beat rate in response to the second ISO addition; **phase 4**: the adaptation phases, the time between 25h to 35h, in this phase, the CMs tried to adapt to the long-term culture in ISO; and **phase 5**: chronic response phase, after 35h treatment with ISO, in this phase, the distinct beating patterns were observed where *GRK5*-L41 maintained the beat rate at high level but *GRK5*-Q41 bearing CMs illustrated irregular beating pattern and arrhythmic effects. **(B)** Demonstration of CMs treated at 1 μM for 50h illustrated different phases in their responses to ISO treatment, similar patterns were observed in both hiPSC-CMs and gene-edited HUES7-CMs.

In summary, the CardioExcyte 96 experiments illustrated two distinct beating patterns after 32h incubation with ISO at 100 nM and 1 μM. The *GRK5*-L41 bearing CMs demonstrated a reduction in beat rate toward basal level with no irregular beating pattern observed. On the other hand, the CMs harbour *GRK5*-Q41 genotype showed dramatic fluctuation in beat rate and arrhythmic beating pattern after 32h culture with ISO. The application of β-blockers, including β_1-blocker (CGP), β_2-blocker (ICI), and non-selective β-blocker (Prop) prevented the development of irregular beating pattern in *GRK5*-Q41 expressing CMs especially during chronic response phase, indicating the cardiac protective function similar to the description of β-blockers (Bristow, 1997; Woo et al., 2015). Moreover, the β-blocker effects during chronic response to ISO were comparable to that of phenotype results detected from *GRK5*-L41 expressing CMs, which was also supported by previous study proving that *GRK5*-L41 exhibited the cardiac protective function that mimics pharmacological β-blockages (Liggett et al., 2008; Wang et al., 2008; Kurnik et al., 2009). Although the results indicated that *GRK5*-L41 bearing CMs could maintain the high beat rate and regular beating pattern during prolonged exposure to ISO (up to 50h), it was insufficient information to conclude that the *GRK5*-L41 genotype is the main causes of this functions, as in the heart, both GRK2 and GRK5 have been found to be highly expressed during normal and severe heart failure condition (Philipp et al., 2014; Capote et al., 2015). Furthermore, it has been reported that by using commercial hiPSC-derived CMs, cells from different batches did not respond equally with changes in beating patterns, especially the beating irregularity after compound addition showed an inconsistency in results. Hence, it was suggested that the number of biological replicates needs to be higher than three to have a representative picture about the responses to ISO (Jonsson et al., 2011).

6.3.2 Determination of the cAMP production profiles from hPSC-CM using LANCE *Ultra* cAMP assay

The ability to detect the changes in beat rate in response to ISO during acute and chronic condition using CardioExcyte 96 platform shed light into the investigation of cAMP production. Because the contraction machinery of CMs is driven by the secreted catecholamines via adrenergic signalling pathways, which translate their functions via $G\alpha_S$-mediated cascade (Pitcher et al., 1998; Lefkowitz, 2007). The activation of the pathway triggers the formation of cellular cAMP from ATP catalysed by Adenylyl Cyclase (AC). Hence, detection and measurement of cAMP production in response to ISO treatment was considered as an important phenotypic assay that could validate the functional activities of our models.

In this chapter, the intracellular increases in cAMP detected by LANCE Ultra cAMP assay were used as the primary measurement of β-AR activation in response to ISO. It is important to note that although a total cellular increase in cAMP production is not always crucial for β-AR signalling, that transient increases in total cAMP play essential roles in initiating downstream signalling cascades (Cooper, 2005). Furthermore, in this study, we detected robust increases of cAMP production, which mostly correlated with induction of CM contraction in response to ISO treatment. We found that 1h incubation of CMs with ISO (100 nM) did not show any difference in cAMP production between GRK5-L41 and GRK5-Q41 group. In terms of β-blocker treatments, differences emerged when Prop was used, suggesting that ultimately block adrenergic signalling pathways by Prop required higher ISO treatment to activated cAMP production in GRK5-L41 expressing CMs. Our results revealed that both hiPSC-CM-L41 and HUES7-CM-L41 showed a significantly high EC_{50} of ISO (94.96 ± 14.145 nM and 87.86 ± 6.32 nM, respectively) compared to that of hiPSC-CM-Q41 and HUES7-CM-Q41 (11.88 ± 7.2 nM and 6.31 ± 0.96 nM, respectively).

Taken together, two main observations from cAMP assay were detected, including **(1)** there was no significant difference between GRK5-L41 and GRK5-Q41 in cAMP

production during acute exposure to ISO, **(2)** blocking the β-AR signalling pathways using Prop (200 nM) require a significantly high dose of ISO in order to induced the cAMP production in GRK5-L41 expressing CMs but not GRK5-Q41 counterpart. From these results, we concluded that there was no different between *GRK5*-L41 and *GRK5*-Q41 during acute response of CMs to ISO treatment, which was also supported the previous studies indicating that no significant difference between the two genotypes was detected during early responses of CMs to ISO treatment in mouse model (Liggett et al., 2008; Johnson et al., 2013). Besides, the results from Prop treatment indicated that complete blocking β-adrenergic signalling potentially induces *GRK5*-L41 to participate in other signalling pathways that allow CMs to withstand relatively high ISO concentration compared to that of *GRK5*-Q41 bearing CMs. This conclusion could be explained by the fact that high level of catecholamines could potentially trigger other pathways, including angiotensin II, and endothelin-1 receptors, which have been reported as a target of GRK5 during chronic heart failure conditions (Kim et al., 2005; Dorn, 2009; Gold et al., 2012). Moreover, it was further found that by using experiments conducted in neonatal cardiomyocytes, Simpson and colleagues observed that the alpha-adrenergic receptors (α1-ARs) which are involved in cardiac hypertrophy process could potentially activate by ISO in a concentration-dependent manner. Further research also demonstrated that at high concentration (more than 10 μM), ISO acts as the biased agonist of the α1-ARs (Copik et al., 2015).

Even though differences were found in cAMP production have been observed, the results need to be interpreted carefully until further experiments are completed to verify the results. Some of these experiments include blocking AT_1 and ET_1 receptors in the presence or absence of Prop, inhibition of GRK5 activities, and investigate the effects of chronic exposure to ISO on cAMP (See General Discussion, Chapter 7).

6.3.3 Detection of cellular distribution of GRK5 using WB

The successful optimisation of WB to detect the presence of GRK5 in cytoplasmic and nucleus of ISO-treated CMs is one of the main results in this project. It is important because the localisation of GRK5 during the chronic response to catecholamine and its pathological functions have been proven to be not related to *GRK5*-L41 (Liggett et al., 2008). This result is contrasted to our finding that potential shift between the nuclear fraction and cytoplasmic fraction of GRK5-L41 protein was observed and occurred in response to ISO treatment up to 72h. Also, the GRK5 ratios (cytoplasmic/nucleus) of hiPSC-CM-L41 at 0h, 24h, 48h, and 72h treatment with 100 nM ISO were 3.6, 1.8, 0.2, and 0.15, respectively, indicating the reduction in nucleus fraction and the cytoplasmic/nucleus switch. However, because the WB experiment was conducted only one time, it is not enough information to draw any conclusion from it. Contracted result between hiPSC-CMs and HUES7-CMs in the same experiment illustrated the need for increase the number of repeats to firmly verify the results.

Previously, the nuclear localisation of GRK5 in cardiac myocytes has been characterised as its non-canonical activity and played a critical role in pathological hypertrophy. Localisation of GRK5 in transgenic mice overexpressed cardiac specific GRK5 showed an increase in cardiac hypertrophy after pressure overload and chronic exposure to ISO infusion. Hence, we hypothesise that the GRK5-L41 is involved in the mechanism that blocks the accumulation of GRK5 in the nucleus which in turn protect the cardiomyocytes from pathological hypertrophy during chronic exposure to catecholamine. Further experiments also need to be conducted in order to confirm the hypothesis, including using beta-adrenergic antagonists to show the reverse effects on normal GRK5-Q41 expressing CMs, using GRK5 inhibitor to block its activities and investigate whether the translocation still happens or not, and further tracking GRK5 localisation using gene editing also a feasible option (see General discussion, chapter 7).

6.3.4 Development of hypertrophic analysis assay

As mentioned above, during the chronic condition of heart failure, pathological hypertrophy is one of the main pathways directly contribute to the development of a failing heart. Numerous reports revealed the links between GRK5 activities and hypertrophic conditions in the patient with heart failure condition (Dorn., 2007; Gold et al., 2012; Johnson et al., 2013). Furthermore, catecholamines, angiotensin II, phenylephrine (PE), and endothelin-1 directly regulate CM functions towards hypertrophy, apoptosis, extracellular matrix disarrangement, and fibrosis (Packer., 1992; Dorn., 2007). Therefore, development of hypertrophic assays for hPSC-CM provides a valuable functional assay to investigate the differences between *GRK5* genotypes in our models. The preliminary results from immunostaining of BNP protein illustrated the possible identification of hypertrophic marker in hPSC-CMs. It would be better to develop a quantitative analysis using the high-content confocal platform, such as Operetta system from Perkin Elmer, to generate the exact number of cells with the fluorescent intensity of BNP expression under tested conditions. Furthermore, the hypertrophic assay would be more powerful in combination with cell viability experiment using either WST-1, Caspase-3, or Annexin-V assay to identify the pathological conditions induced by catecholamines and hypertrophic inducers. This result would be beneficial to distinguish the effects of *GRK5*-L41 and *GRK5*-Q41 phenotypes during chronic and pathological conditions directly contribute to cardiac contraction machinery and hypertrophic response of the CMs.

6.4 Chapter conclusion

In summary, this chapter described the process of functional assay development to investigate the cardiac protective functions of *GRK5*-L41 using hPSC-CMs. Although the number of cardiomyopathy models using patient-derived hiPSC-CMs with known mutations continues to establish, the non-genetic cardiomyopathy models are a deficiency and more challenge. Thus far, to the best of our knowledge, there was no report about the non-genetic model for hypertrophic analysis using hPSC-CM models.

Hence, the efforts illustrated in this chapter indicated the several approaches that could be used to further investigate the hPSC-CM model toward functional analysis, including detection of real-time beat rate and beating pattern using CardioExcyte 96 platform, formation of cAMP production profile using LANCE *Ultra* cAMP assay, detection of cellular distribution of GRK5 in response to ISO treatment via Western Blot analysis, and construction of hypertrophic analysis assay using immunocytochemistry to identify the presence of pathological hypertrophic marker, BNP.

Chapter 7 General Discussion

Thus far, this study illustrated the process of establishing the human cardiac model using hPSC to investigate the cardiac protective functions of GRK5-L41 polymorphism. Working toward the aims, several experimental results have been described including **(1)** establishment of monolayer cardiac differentiation procedures that are efficient, robust, reproducible, and consistent; **(2)** generation of hiPSC lines bearing the GRK5-Q41 and GRK5-L41 polymorphism from lymphoblastoid cells using defined episomal reprogramming method; **(3)** development of "footprint-free and short-cut" gene editing method to create the GRK5-L41 and GRK5-Q/L41 variants in the hESC line; and **(4)** establishment of functional assays toward the putative functions of GRK5-L41 *in vitro.*

7.1 Monolayer cardiac differentiation – an essential tool requires for establishing human cardiac model using hPSCs

One of the key results of this thesis is the establishment of the three monolayer differentiation protocols adapted for E8-culture conditions, including the E8-AB, mTeSR-AB, and mTeSR-CHIR method. From repeatedly differentiating 12 hPSC lines over a range of more than 30 passages, these protocols have been proven to be efficient, reproducible, robust, and consistent across all tested cell lines. A preconditioning step was added to the cardiac induction procedures which increased the efficiency of the differentiation process dramatically, and enhanced the robustness as well as consistency, preventing the variation between cell lines and differentiation batches.

Additionally, our analysis revealed the importance of mesodermal initiation by either BMP pathway via growth factors (BMP4 and Activin-A) or WNT pathway via small molecules (CHIR). Precise concentrations of BMP4 and Activin-A used in E8-AB, and mTeSR-AB protocol have been proven to be highly efficient in inducing mesodermal formation from hPSCs. The precondition followed growth factor additions was shown to rapidly repress the pluripotent-associated transcription factor (OCT4), and induced the expression of mesoderm marker, Brachyury-T, during the first two days of the protocol. To inhibit the WNT pathway, KY02111, and XAV939, the two WNT inhibitors, were used and proven to be efficient to drive the hPSCs into cardiac lineage by increase the

expression of cardiac regulatory genes, such as *NKX2-5* and *ISL-1*. This observation is consistent with earlier studies and followed the cardiac developmental process *in vivo* (Mummery et al., 2012; Rao et al., 2016).

In contrast, although the WNT inductive molecule, CHIR, was also efficient to initiate the mesodermal formation, variations in protein expression were detected throughout the differentiation process using the mTeSR-CHIR protocol. In fact, the concentration of CHIR contributed a significant role in the success of cardiac induction process, as a high level of CHIR resulted in significant cell death during the first two days of the procedure, whereas the too low level of CHIR led to the unsuccessful differentiation. Indeed, the level of CHIR has been previously reported to be involved in the cardiac differentiation process, in which, high level of CHIR was a mandatory requirement for cardiac differentiation whereas, at the low level, CHIR induced the formation of endoderm and neuro-related linages (Rao et al., 2016). Furthermore, the concentration of CHIR was reported to be cell line-dependent, and extensive optimisation is required to achieve a high purity of CMs (Burridge et al., 2014; Kadari et al., 2015; Berg et al., 2015).

Furthermore, our data also demonstrated the distinct pathways that induced by the BMP-mediated protocols (E8-AB, and mTeSR-AB), and allowed the interaction between phosphorylated Smad1/5/8 (pSmad1/5/8) and Smad4 during cardiac lineage formation. The interaction between pSmad1/5/8 and Smad4 was previously reported to be involved in the induction of cardiac-specific transcription factor NKX2-5 (Furtado et al., 2008; Takei et al., 2009). The induction of NKX2-5 follow by the ISL-1 was observed in both E8-AB and mTeSR-AB from d4 to d8 of cardiac differentiation process, which was in the same timeline when the interaction between pSmad1/5/8 and Smad4 was detected using PLA and was similar to earlier studies (Christoffels et al., 2004; den Hartogh et al., 2016).

Also, our data highlight the impact of the cardiac subtype verification process, which needs to be conducted after d30 post cardiac differentiation to analyse accurately the cardiac subtypes using immunofluorescence and flow cytometry analysis of subtype markers, including MLC-2v and MLC-2a. Notably, our result illustrated the proportional

changes in MLC-2v$^+$ population during prolonged culture *in vitro*, in which, an increase in the MLC-2v$^+$ population was observed, and an equivalent reduction in MLC-2a + MLC-2v population was also detected. These results were also supported by the electrophysiological analysis of cardiac subtype using CellOPTIQ® platform. Also, our data was in line with the previously study, which also found that using both KY02111 and XAV939 as WNT inhibitor driven the cardiac differentiation toward the establishment of ventricular subtype (Minami et al., 2012).

7.2 Establishment of hiPSC from lymphoblastoid cell lines

The advancement in hiPSC technology together with the improvement in CM differentiation implements the new way to establish the human cardiac model that capture the rare genotype to analyse their effects on the functionality of CMs. Since the original breakthrough papers from Shinya Yamanaka's laboratory reported the ability to convert the somatic cell lines into pluripotent stage using OSKM factors, several projects have been established to generate large bank of hiPSC lines across the globe, including the large scale banking schemes that have an ambitious of creating hiPSC lines from 7000 normal or diseased skin biopsy donors using non-integrating reprogramming methodology, including Sendai-virus, Episomal and mRNA protocol (Takahashi and Yamanaka, 2006; Soares et al., 2014). Indeed, it has been proven that reprogramming procedure using non-integrating approaches converts the somatic cell lines to the pluripotent stage without alliterating their inherited genomic information (Takahashi and Yamanaka, 2016).

Several sources of somatic cells have been utilised to generate hiPSC, including fibroblasts, adult peripheral blood cells, mononuclear cells, exfoliated renal epithelial cells, and keratinocytes (Aasen et al., 2008; Okita et al., 2011; Loh et al., 2009; Zhou et al., 2012; Rajesh et al., 2011). Among them, the blood-derived somatic cells emerge as an easy access and non-invasive cell sources for hiPSC and biomedical research, as the B-cells, for example, can be easily isolated from patient blood test samples. The lymphoblast B-cells are the immature cells that can develop into mature lymphocytes

and contain full inherited genetic information of the patient (Barreto et al., 2014) (Figure 1.10). It has been reported that extracted lymphoblast B-cells from as little as 0.5 mL blood is enough to transform them into lymphoblastoid cell lines using Epstein-Barr virus, which in turn, provide an unlimited proliferative source of cells for reprogramming (Rajesh et al., 2011).

The data represented in this thesis described the episomal reprogramming method for converting lymphoblastoid cell lines into hiPSC under defined culture conditions (mTeSR medium) using Yamanaka's plasmid set. In contrast to the previous study, our data indicated that the episomal plasmid set derived from Thomson's lab was not sufficient enough to induce the reprogramming process in lymphoblastoid cell lines (Rajesh et al., 2011; Choi et al., 2011). Extensive characterisation was performed on the hiPSC lines derived from lymphoblastoid cell lines harbouring either *GRK5*-Q41 or *GRK5*-L41 variant. Both hiPSC lines expressed pluripotent-associated transcription factors and surface markers, including OCT4, SOX2, NANOG, SSEA-4, and TRA-1-81. Moreover, these cells maintained normal karyotype over 30 passages in culture using mTeSR medium and E8 condition. Furthermore, these cell lines can be differentiated into cardiomyocyte efficiently using the E8-AB method.

7.3 Development of footprint-free and shortcut gene editing strategy

It has been well-known that cardiotoxicity of particular treatment could not be detected accurately in animal models, immortalised cancer cells, or cultured cells expressing selected cardiac specific genes due to the differences between their biological and physiological responses from that of the human heart (John P. Overington, 2006; Laverty et al., 2011). For instance, in mouse, the heart rates are almost ten times faster than in humans and ion channels, most importantly the potassium (K_v7.1) and hERG channels, are expressed in different pattern compare to human (Redfern et al., 2004). As a result, it is important to have a human cardiac model which can generate results that are reprehensive to what happens in the heart, especially during the chronic response to catecholamine treatment. However, the adult primary human CMs are non-

proliferative, difficult to obtain, and impossible to extract in mass. Therefore, creating the gene-edited hPSC lines provides a powerful model to explore further the mechanism underlying several cardiac disease conditions and cardiac protective functions, including the GRK5-L41 polymorphism.

The chapter 5 in this thesis demonstrated the establishment of the new footprint-free and short-cut CRISPR approach, which reduced the editing time to 8 weeks and was proven to be an efficient way to generate genetically modified hPSCs. The procedure utilised the *piggyBac* construct with homologous genomic sequences on each side of the selection cassette allowed positive selection of homologous recombination events that introduced the GRK5-L41 polymorphism to the HUES7 genome followed the negative isolation of *piggyBac*-free clones after excision step. The final clones were footprint free due to the nature of *piggyBac* transposon which reformed the TTAA site after excision. The combination of CRISPR/Nickase and the *piggyBac* system achieved the site-specific modification in *GRK5* locus while preserving the genome integrity as well as reduce the off-target effects, which was similar to earlier studies (Eggenschwiler et al., 2016; Shen et al., 2014). Furthermore, our results also illustrated a high level of bi-allelic modification compared to that of conventional Cas9 approach and were consistent with the previous report, which was proven that CRISPR/Nickase improved the bi-allelic modification (Eggenschwiler et al., 2016).

While our strategy provides a viable tool for bi-allelic modification of single nucleotide polymorphism, the single stranded oligonucleotide (ssODN) is also the option that was proven to be efficient to create bi-allelic targeting in hPSCs (Kim et al., 2014). The application of ssODN in CRISPR/Cas technology is elegant and innovative, but it also comes with numerous drawbacks. In fact, the rate of accurate modification and incorporation of ssODN is relatively low, which results in the requirement of intensive screening of positive clones. For instance, it was reported that to identify the HDR clones using bar-coding PCR-amplicon from single iPSC colonies, an intensive bioinformatic analysis was required (Paquet et al., 2016). Furthermore, although it was demonstrated that inactivation of the PAM in ssODN donor improved the HDR efficiency by blocking

the Cas9 from re-binding to the corrected genomic DNA, the increasing distance from the targeted position also reduced significantly the homologous recombination (Paquet et al., 2016). Moreover, silent PAM mutations might not be feasible in many genomic loci, where such favourable conditions are not available, for example in the case of *ADRB2* loci. In such cases, our approach with long flanking arm plasmid donors provides a suitable alternative, because the chance of homozygous recombination increases in a linear manner along with the length of the homology arm closer to the targeted editing site in hPSCs (Kan et al., 2014). Additionally, the ssODN approach is suitable for introducing point mutation or short modification of the target DNA, it is not applicable to be used for larger DNA fragments or corrected a large fragment of gene, for example in the case of Dystrophin gene in Duchenne muscular dystrophy patient cells (Popplewell et al., 2013).

7.4 Establishment of functional assays toward the putative functions of GRK5-L41 during heart failure condition

The experimental designs and assay developments represented in chapter 6 of this thesis allowed us to detect the beat rate, beating pattern, cAMP production, intracellular distribution of GRK5, and hypertrophic stage of hPSC-CMs. These assays were developed to analyse the two main responses of CMs which have been proven to be associated with GRK5 functions *in vivo*, including the contractility machinery via β-adrenergic signalling pathways and the hypertrophic responses.

The beat rate and beating pattern of hPSC-CMs were measured using the CardioExcyte96 platform based on the impedance recording technology (Doerr et al., 2015). This platform provides a high throughput analysis of CM contractility behaviours in response to drug treatment in real time. Indeed, our results indicated the arrhythmic effects of ISO treatment during 48h incubation *in vitro*. The distinct responses between GRK5-L41 and GRK5-Q41 CMs were also observed, suggested that this platform is sensitive and efficient enough to detect changes in cellular contractility, and interestingly, identified the detrimental effects of prolonged exposure to ISO on CMs *in vitro* and

cardiac protective functions of β-blockers against the ISO treatment. Additionally, based on the β-blocker results, our data demonstrated the dominant roles of β_1 in hiPSC-CM-Q41 whereas hiPSC-CM-L41 showed a high level of β_2 activities. This observation did not relate to the effects of GRK5 variant, but in fact, indicating the immaturity stage of the hPSC-CMs, which was intensively reported previously (Eschenhagen et al., 2015; Mummery et al., 2012; Sharma et al., 2017). The results from CardioExcyte96 were strongly supported by analysis of cAMP production in response to ISO treatment using LANCE *Ultra* cAMP assay. The results confirmed that there was no significant different between GRK5-L41 and GRK5-Q41 CMs during acute response to ISO treatment, which suggested that further assays need to be targeted the chronic response stage of ISO treatment (>48h).

The time-course tracking of cellular distribution of GRK5 in CMs treated with ISO for up to 72h using Western Blot revealed the potential route to investigate the mechanism underlying its cardiac protective effects. The preliminary data indicated the different in cellular distribution of GRK5-L41 and GRK5-Q41 protein in hPSC-CMs underwent ISO treatment, which was contradicted by the previously study (Liggett et al., 2008). However, the data from our study was not strong enough to draw the solid conclusion due to lack of biological replicates.

In terms of hypertrophic analysis, the immunofluorescence assay allowed detecting the presence of pathological hypertrophic marker, BNP, under ISO and hypertrophic inducing compounds, such as Endothelin-1 and PE. Our observation and strategy was similar to previously described study, which also demonstrated the successful detection of hypertrophic phenotypes using immunofluorescence assay (Sara S. Nunes, 2016). Our results illustrated the induction of hypertrophy after short-term treatment (15h-24h) with Endothelin-1 and PE, which was similar to other groups that used similar agents to induce hypertrophy in hPSC-CM monolayers (Aggarwal et al., 2014; Carlson et al., 2013). It was reported that short-term treatment of hiPSC-CMs with endothelin-1 induced cell hypertrophy and reactivated foetal genes, including skeletal muscle α-actin (*ACTA1*), myosin heavy chain β (*MYH7*), *NPPA*, and significant

upregulate BNP secretion (Carlson et al., 2013). In a similar experiment, hiPSC-CMs treated with PE had been illustrated and characterised by increased cell size and volume associated with increase sarcomeric organisation and cytoskeletal assembly (Foldes et al., 2011). Interestingly, our results also indicated an increase in BMP secretion after 96h incubation with ISO at 100 nM, suggesting that prolonged ISO treatment induced hypertrophic response from hPSC-CMs. Also, there are two distinct types of hypertrophy, including physiological hypertrophy, which has been proven to provide functional and ultrastructure advantages in human engineered cardiac tissues, and pathological hypertrophy, which was associated with activation of apoptosis genes, disruption of sarcomeric structure, and compromising the contractility of the CMs (Bernardo et al., 2010; Schaaf et al., 2011; Tulloch et al., 2011). Furthermore, our data illustrated the hypertrophic induction by elevation of BNP secretion in hPSC-CMs after 96h ISO treatment at 100 nM. The results were in line with the previous studies, which found the increase in hypertrophic response by prolonged treatment with ISO in cellular models and intensive infusion (up to 7 days) of catecholamines in mouse models (Esposito et al., 2002; Tanaka et al., 2014; Tashiro et al., 1990).

Taken together, our results demonstrated the impaired contractile function of hPSC-CM during prolonged ISO treatment, which illustrated the distinct responses between GRK5-L41 and GRK5-Q41 CMs. The former maintained a high level of beat rate and regular beating pattern after 48h treatment with either 100 nM and 1 μM ISO, whereas the same condition introduced the detrimental effects on the contractility of the later. In light of the results, observation of BNP upregulation in hPSC-CMs treated with 100 nM ISO suggested that these cells exhibited the hypertrophic phenotype *in vitro*.

7.5 Limitations of the study

The cardiac induction procedures described in this thesis have been proven to be highly efficient, robust, reproducible, and consistent, but there is still space for improvement. For instance, these methods have a problem in the up-scaling process. The largest culture vessel tested was the T75 flask, which showed the decent amount of

high purity cardiomyocytes, up to $15x10^6$ CMs/flask, although batch to batch variation was also observed. The protocols showed the inconsistent when larger culture flasks were used, and only the cells closed to the neck of the culture vessel illustrated a successful cardiac differentiation suggesting the potential problems in ventilation and distribution of nutrients as well as growth factors across the culture surface.

Although our results demonstrated the activation of the BMP signalling pathways activated throughout the differentiation process, the data can only be used as the guideline for further investigation about the specific downstream effectors associated with a successful cardiac induction process. Thus far, these key mechanisms remain to be determined. Although the preconditioning step using either SP34 supplemented with Matrigel and BMP4 or mTeSR was proven to improve the effectiveness of the protocols, especially for E8 cultured hPSCs, the cell confluence and compaction on the day of precondition were proven to be essential as it was observed that the cell confluency needs to be between 60% to 80% to achieve the highest cardiac differentiation efficiency, beyond the range results in a significant reduction of the success rate. However, the reason behind this observation is still poorly understood.

Additionally, the hPSC-CMs were reported to have the characteristics similar to the foetal human cardiomyocytes, and they are not identical to the mature CMs found in human adult heart (Robertson et al., 2013; Yang et al., 2014; Zhang et al., 2015). These immature features of the hPSC-CMs represent a critical limitation for drug testing and the use of the hPSC-CM model in the investigation of the cardiotoxicity. Several parameters illustrate the differences between hPSC-CMs and adult CMs including **(1)** the hPSC-CMs are smaller in size and length-to-width ratio (7:1) compared to adult CM (Gerdes et al., 1992); **(2)** the morphology of hPSC-CMs is flat-spread cells whereas its adult counterpart illustrates the classical rod-shape geometry ; **(3)** the immature hPSC-CMs do not display complete sarcomeric organisation as seen in adult CMs including formation of organised array, presence of t-tubules, and other ion channels, which are essential for coordinated contraction in large CMs (Gherghiceanu et al., 2011; Lieu et al., 2009). Therefore, although our data indicated the expression profiles of adrenergic

signalling pathways throughout differentiation process up to days 66 and identified the stabilisation of the system after d30 post-cardiac differentiation, it is important to note that these hPSC-CMs still exhibited the immature phenotypes.

In terms of episomal reprogramming procedure, the major limitation was the incomplete analysis to detect the presence of EBNA-1 and EBNA-2 in our hiPSCs after culture until passage 20. Although numerous of reports has been proven the loss of episomal plasmid during prolonged culture *in vitro* of episomal reprogrammed hiPSCs, it is important to conduct the EBNA analysis experiment to confirm the loss of episomal plasmids.

7.6 Final remark and Future work

Thus far, this thesis presents the human cardiac models produced to investigate how peptide position 41 homozygote and heterozygote polymorphic variants of GRK5 influence the phenotypes, drug responses, and molecular pathways of CMs. Two independent approaches were developed, including **(1)** the generation of hiPSC lines harbouring GRK5-L41 and GRK5-Q41 variant from the lymphoblastoid cell lines using episomal reprogramming method, and **(2)** the establishment of genetically modified hESCs carrying the GRK5-Q41, GRK5-Q/L41, and GRK5-L41 using the footprint-free and short-cut CRISPR/Nickase approach. In this thesis, three monolayer cardiac differentiation protocols, including E8-AB, mTeSR-AB, and mTeSR-CHIR, and a total of five hPSC lines were produced, including three hiPSC lines (H-Fib-hiPSC, hiPSC-GRK5-Q41, and hiPSC-GRK5-L41) and two gene-edited hESC lines (HUES7-GRK5-Q/L41, and HUES7-GRK5-L41). Each of these hPSC lines was differentiated successfully into CMs using E8-AB method to give purities exceeding 90%, thereby providing an unlimited resource for cellular and functional analysis. A set of functional analysis assays was also established including measurement of CM's beat rate and beating pattern using the CardioExcyte96 platform, analysis of intracellular cAMP production using LANCE *Ultra* cAMP assay, detection of intracellular distribution of GRK5 using Western Blot, and high throughput analysis of hypertrophic phenotype in hPSC-CMs.

Taken together, our data demonstrated the distinct responses of GRK5-L41 and GRK5-Q41 CMs during chronic exposure to ISO treatment, where the GRK5-L41 CMs exhibited the results similar to that of β-blocker treatment in rescued the GRK5-Q41 from arrhythmic effects after 32h incubation with ISO *in vitro*. Additionally, the prolonged exposure to ISO treatment was also proven to be associated with the development of hypertrophy in our hPSC-CM model, suggesting the interlink between irregular beating patterns observed in hPSC-CMs and the hypertrophic responses during extended culture in ISO (>48h). Preliminary data from the project indicated the potential cardiac protective functions of GRK5-L41 might derive from its ability to **(1)** faster desensitisation of adrenergic receptors during acute response to catecholamine, and **(2)** export outside the nucleus during chronic response of CMs to catecholamine treatment, which, in turn, reduce the pathological effects of GRK5 in triggering the hypertrophic pathways.

Working toward the hypothesis, several future experiments need to be conducted, including:

1. Performing the cAMP accumulation assay using LANCE *Ultra* cAMP kit to determine the desensitisation rate of β-ARs mediated by GRK5-Q41 and GRK5-L41.
2. Completing the biological replicates of Western Blot analysis of GRK5 cellular distribution during prolonged culture in ISO.
3. Identification of hypertrophic inductive conditions using immunofluorescence analysis of BNP positive cells and cardiotoxicity assay to identify the percentage of viable cells in different conditions.
4. Performing the measurement of contraction force analysis using CellOPTIQ® platform to distinguish the pathological and physiological hypertrophic condition, which in turn, allow appraising the effects of the nuclear accumulation of GRK5 on triggering these conditions.

Bibliography

Uncategorized References

AASEN, T., RAYA, A., BARRERO, M. J., GARRETA, E., CONSIGLIO, A., GONZALEZ, F., VASSENA, R., BILIC, J., PEKARIK, V., TISCORNIA, G., EDEL, M., BOUE, S. & BELMONTE, J. C. I. 2008. Efficient and rapid generation of induced pluripotent stem cells from human keratinocytes. *Nature Biotechnology,* 26**,** 1276-1284.

AGGARWAL, P., TURNER, A., MATTER, A., KATTMAN, S. J., STODDARD, A., LORIER, R., SWANSON, B. J., ARNETT, D. K. & BROECKEL, U. 2014. RNA Expression Profiling of Human iPSC-Derived Cardiomyocytes in a Cardiac Hypertrophy Model. *Plos One,* 9.

AGUERO, J., ALMENAR, L., D'OCON, P., OLIVER, E., MONTO, F., RUEDA, J., VICENTE, D., MARTINEZ-DOLZ, L. & SALVADOR, A. 2009. Myocardial and Peripheral Lymphocytic Transcriptomic Dissociation of beta-adrenoceptors and G Protein-coupled Receptor Kinases in Heart Transplantation. *Journal of Heart and Lung Transplantation,* 28**,** 1166-1171.

AGUERO, J., ALMENAR, L., MONTO, F., OLIVER, E., SANCHEZ-LAZARO, I., VICENTE, D., MARTINEZ-DOLZ, L., D'OCON, P., RUEDA, J. & SALVADOR, A. 2012. Myocardial G Protein Receptor-Coupled Kinase Expression Correlates With Functional Parameters and Clinical Severity in Advanced Heart Failure. *Journal of Cardiac Failure,* 18**,** 53-61.

AHLES, A. & ENGELHARDT, S. 2014. Polymorphic Variants of Adrenoceptors: Pharmacology, Physiology, and Role in Diseases. *Pharmacological Reviews,* 66**,** 598-637.

AKERMOUN, M., KOGLIN, M., ZVALOVA-IOOSS, D., FOLSCHWEILLER, N., DOWELL, S. J. & GEARING, K. L. 2005. Characterization of 16 human G protein-coupled receptors expressed in baculovirus-infected insect cells. *Protein Expression and Purification,* 44**,** 65-74.

AKOPIAN, V., ANDREWS, P. W., BEIL, S., BENVENISTY, N., BREHM, J., CHRISTIE, M., FORD, A., FOX, V., GOKHALE, P. J., HEALY, L., HOLM, F., HOVATTA, O., KNOWLES, B. B., LUDWIG, T. E., MCKAY, R. D. G., MIYAZAKI, T., NAKATSUJI, N., OH, S. K. W., PERA, M. F., ROSSANT, J., STACEY, G. N., SUEMORI, H. & CONSORTIU, I. S. C. I. 2010. Comparison of defined culture systems for feeder cell free propagation of human embryonic stem cells. *In Vitro Cellular & Developmental Biology-Animal,* 46**,** 247-258.

ALLEGRUCCI, C. & YOUNG, L. E. 2007. Differences between human embryonic stem cell lines. *Human Reproduction Update,* 13**,** 103-120.

AMIT, M., CHEBATH, J., MARGULETS, V., LAEVSKY, I., MIROPOLSKY, Y., SHARIKI, K., PERI, M., BLAIS, I., SLUTSKY, G., REVEL, M. & ITSKOVITZ-ELDOR, J. 2010. Suspension culture of undifferentiated human embryonic and induced pluripotent stem cells. *Stem Cell Rev,* 6**,** 248-59.

AMOLI, M. M., CARTHY, D., PLATT, H. & OLLIER, W. E. R. 2008. EBV immortalization of human B lymphocytes separated from small volumes of cryo-preserved whole blood. *International Journal of Epidemiology,* 37**,** 41-45.

ANGELONE, T., FILICE, E., QUINTIERI, A. M., IMBROGNO, S., RECCHIA, A., PULERA, E., MANNARINO, C., PELLEGRINO, D. & CERRA, M. C. 2008. beta(3)-Adrenoceptors modulate left ventricular relaxation in the rat heart via the NO-cGMP-PKG pathway. *Acta Physiologica,* 193**,** 229-239.

BAILEY, C., HENDERSON, G. & KELLY, E. 2008. Functional selectivity in GPCR desensitization. *Fundamental & Clinical Pharmacology,* 22**,** 7-7.

BARAJAS-MARTINEZ, H., HU, D., GOODROW, R. J., JR., JOYCE, F. & ANTZELEVITCH, C. 2013. Electrophysiologic characteristics and pharmacologic

response of human cardiomyocytes isolated from a patient with hypertrophic cardiomyopathy. *Pacing Clin Electrophysiol,* 36**,** 1512-5.

BARRETO, J. N., MCCULLOUGH, K. B., ICE, L. L. & SMITH, J. A. 2014. Antineoplastic agents and the associated myelosuppressive effects: a review. *J Pharm Pract,* 27**,** 440-6.

BARRETT, R., ORNELAS, L., YEAGER, N., MANDEFRO, B., SAHABIAN, A., LENAEUS, L., TARGAN, S. R., SVENDSEN, C. N. & SAREEN, D. 2014. Reliable Generation of Induced Pluripotent Stem Cells From Human Lymphoblastoid Cell Lines. *Stem Cells Translational Medicine,* 3**,** 1429-1434.

BATALOV, I. & FEINBERG, A. W. 2015. Differentiation of Cardiomyocytes from Human Pluripotent Stem Cells Using Monolayer Culture. *Biomark Insights,* 10**,** 71-6.

BELLOMO, D., HEADRICK, J. P., SILINS, G. U., PATERSON, C. A., THOMAS, P. S., GARTSIDE, M., MOULD, A., CAHILL, M. M., TONKS, I. D., GRIMMOND, S. M., TOWNSON, S., WELLS, C., LITTLE, M., CUMMINGS, M. C., HAYWARD, N. K. & KAY, G. F. 2000. Mice lacking the vascular endothelial growth factor-B gene (Vegfb) have smaller hearts, dysfunctional coronary vasculature, and impaired recovery from cardiac ischemia. *Circulation Research,* 86**,** E29-E35.

BENOVIC, J. L., KUHN, H., I, W., CODINA, J., CARON, M. G. & LEFKOWITZ, R. J. 1987. Functional Desensitization of the Isolated Beta-Adrenergic-Receptor by the Beta-Adrenergic-Receptor Kinase - Potential Role of an Analog of the Retinal Protein Arrestin (48-Kda Protein). *Proceedings of the National Academy of Sciences of the United States of America,* 84**,** 8879-8882.

BENOVIC, J. L., STRASSER, R. H., CARON, M. G. & LEFKOWITZ, R. J. 1986. Beta-Adrenergic-Receptor Kinase - Identification of a Novel Protein-Kinase That Phosphorylates the Agonist-Occupied Form of the Receptor. *Proceedings of the National Academy of Sciences of the United States of America,* 83**,** 2797-2801.

BERG, C. W. V. D., ELLIOTT, D. A., BRAAM, S. R., MUMMERY, C. L. & DAVIS, R. P. 2015. Differentiation of Human Pluripotent Stem Cells to Cardiomyocytes Under Defined Conditions. Methods in Molecular Biology.

BERNARDO, B. C., WEEKS, K. L., PRETORIUS, L. & MCMULLEN, J. R. 2010. Molecular distinction between physiological and pathological cardiac hypertrophy: Experimental findings and therapeutic strategies. *Pharmacology & Therapeutics,* 128**,** 191-227.

BERS, D. M. 2008. Calcium cycling and signaling in cardiac myocytes. *Annual Review of Physiology,* 70**,** 23-49.

BERS, D. M. & DESPA, S. 2009. Na/K-ATPase-An Integral Player in the Adrenergic Fight-or-Flight Response. *Trends in Cardiovascular Medicine,* 19**,** 111-118.

BEUMER, K. J., TRAUTMAN, J. K., CHRISTIAN, M., DAHLEM, T. J., LAKE, C. M., HAWLEY, R. S., GRUNWALD, D. J., VOYTAS, D. F. & CARROLL, D. 2013. Comparing Zinc Finger Nucleases and Transcription Activator-Like Effector Nucleases for Gene Targeting in Drosophila. *G3-Genes Genomes Genetics,* 3**,** 1717-1725.

BEURDELEY, M., BIETZ, F., LI, J., THOMAS, S., STODDARD, T., JUILLERAT, A., ZHANG, F., VOYTAS, D. F., DUCHATEAU, P. & SILVA, G. H. 2013. Compact designer TALENs for efficient genome engineering. *Nat Commun,* 4**,** 1762.

BIBEN, C. & HARVEY, R. P. 1997. Homeodomain factor Nkx2-5 controls left/right asymmetric expression of bHLH gene eHand during murine heart development. *Genes & Development,* 11**,** 1357-1369.

BIBIKOVA, M., BEUMER, K., TRAUTMAN, J. K. & CARROLL, D. 2003. Enhancing gene targeting with designed zinc finger nucleases. *Science,* 300**,** 764-764.

BIBIKOVA, M., CARROLL, D., SEGAL, D. J., TRAUTMAN, J. K., SMITH, J., KIM, Y. G. & CHANDRASEGARAN, S. 2001. Stimulation of homologous recombination through targeted cleavage by chimeric nucleases. *Molecular and Cellular Biology,* 21**,** 289-297.

BIRCHMEIER, W. 2007. The Wnt/beta-catenin signaling pathway in development and disease. *Pathology Research and Practice,* 203**,** 341-341.

BISOGNANO, J. D., WEINBERGER, H. D., BOHLMEYER, T. J., PENDE, A., RAYNOLDS, M. V., SASTRAVAHA, A., RODEN, R., ASANO, K., BLAXALL, B. C., WU, S. C., COMMUNAL, C., SINGH, K., COLUCCI, W., BRISTOW, M. R. & PORT, J. D. 2000. Myocardial-directed overexpression of the human beta(1)-adrenergic receptor in transgenic mice. *Journal of Molecular and Cellular Cardiology,* 32**,** 817-830.

BJARNADOTTIR, T. K., GLORIAM, D. E., HELLSTRAND, S. H., KRISTIANSSON, H., FREDRIKSSON, R. & SCHIOTH, H. B. 2006. Comprehensive repertoire and phylogenetic analysis of the G protein-coupled receptors in human and mouse. *Genomics,* 88**,** 263-273.

BOCH, J., SCHOLZE, H., SCHORNACK, S., LANDGRAF, A., HAHN, S., KAY, S., LAHAYE, T., NICKSTADT, A. & BONAS, U. 2009. Breaking the Code of DNA Binding Specificity of TAL-Type III Effectors. *Science,* 326**,** 1509-1512.

BOGAARD, H. J., ABE, K., NOORDEGRAAF, A. V. & VOELKEL, N. F. 2009. The Right Ventricle Under Pressure Cellular and Molecular Mechanisms of Right-Heart Failure in Pulmonary Hypertension. *Chest,* 135**,** 794-804.

BOHELER, K. R., CZYZ, J., TWEEDIE, D., YANG, H. T., ANISIMOV, S. V. & WOBUS, A. M. 2002. Differentiation of pluripotent embryonic stem cells into cardiomyocytes. *Circulation Research,* 91**,** 189-201.

BOLOTIN, A., OUINQUIS, B., SOROKIN, A. & EHRLICH, S. D. 2005. Clustered regularly interspaced short palindrome repeats (CRISPRs) have spacers of extrachromosomal origin. *Microbiology-Sgm,* 151**,** 2551-2561.

BONDUE, A., LAPOUGE, G., PAULISSEN, C., SEMERARO, C., LACOVINO, M., KYBA, M. & BLANPAIN, C. 2008. Mesp1 acts as a master regulator of multipotent cardiovascular progenitor specification. *Cell Stem Cell,* 3**,** 69-84.

BOTTCHER, R., HOLLMANN, M., MERK, K., NITSCHKO, V., OBERMAIER, C., PHILIPPOU-MASSIER, J., WIELAND, I., GAUL, U. & FORSTEMANN, K. 2014. Efficient chromosomal gene modification with CRISPR/cas9 and PCR-based homologous recombination donors in cultured Drosophila cells. *Nucleic Acids Research,* 42.

BOULAGNON, C., LAMIABLE, D. & FORNES, P. 2009. Drug-induced QT Prolongation and Sudden Cardiac Death: A Case Report and Review of the Literature. *Drug Safety,* 32**,** 987-987.

BRAAM, S. R., DENNING, C., MATSA, E., YOUNG, L. E., PASSIER, R. & MUMMERY, C. L. 2008a. Feeder-free culture of human embryonic stem cells in conditioned medium for efficient genetic modification. *Nature Protocols,* 3**,** 1435-1443.

BRAAM, S. R., ZEINSTRA, L., LITJENS, S., WARD-VAN OOSTWAARD, D., VAN DEN BRINK, S., VAN LAAKE, L., LEBRIN, F., KATS, P., HOCHSTENBACH, R., PASSIER, R., SONNENBERG, A. & MUMMERY, C. L. 2008b. Recombinant vitronectin is a functionally defined substrate that supports human embryonic stem cell self-renewal via alpha V beta 5 integrin. *Stem Cells,* 26**,** 2257-2265.

BRADE, T., PANE, L. S., MORETTI, A., CHIEN, K. R. & LAUGWITZ, K. L. 2013. Embryonic Heart Progenitors and Cardiogenesis. *Cold Spring Harbor Perspectives in Medicine,* 3.

BREDE, M., NAGY, G., PHILIPP, M., SORENSEN, J. B., LOHSE, M. J. & HEIN, L. 2003. Differential control of adrenal and sympathetic catecholamine release by alpha(2)-adrenoceptor subtypes. *Molecular Endocrinology,* 17**,** 1640-1646.

BRISTOW, M. R. 1997. Mechanism of action of beta-blocking agents in heart failure. *American Journal of Cardiology,* 80**,** L26-L40.

BRODDE, O. E. 1993. Beta-Adrenoceptors in Cardiac Disease. *Pharmacology & Therapeutics,* 60**,** 405-430.

BROUNS, S. J. J., JORE, M. M., LUNDGREN, M., WESTRA, E. R., SLIJKHUIS, R. J. H., SNIJDERS, A. P. L., DICKMAN, M. J., MAKAROVA, K. S., KOONIN, E. V. & VAN DER OOST, J. 2008. Small CRISPR RNAs guide antiviral defense in prokaryotes. *Science,* 321**,** 960-964.

BRY, M., KIVELA, R., HOLOPAINEN, T., ANISIMOV, A., TAMMELA, T., SORONEN, J., SILVOLA, J., SARASTE, A., JELTSCH, M., KORPISALO, P., CARMELIET, P.,

LEMSTROM, K. B., SHIBUYA, M., YLA-HERTTUALA, S., ALHONEN, L., MERVAALA, E., ANDERSSON, L. C., KNUUTI, J. & ALITALO, K. 2010. Vascular Endothelial Growth Factor-B Acts as a Coronary Growth Factor in Transgenic Rats Without Inducing Angiogenesis, Vascular Leak, or Inflammation. *Circulation,* 122**,** 1725-1733.

BU, L., JIANG, X., MARTIN-PUIG, S., CARON, L., ZHU, S. J., SHAO, Y., ROBERTS, D. J., HUANG, P. L., DOMIAN, I. J. & CHIEN, K. R. 2009. Human ISL1 heart progenitors generate diverse multipotent cardiovascular cell lineages. *Nature,* 460**,** 113-U130.

BUCHHOLZ, D. E., HIKITA, S. T., ROWLAND, T. J., FRIEDRICH, A. M., HINMAN, C. R., JOHNSON, L. V. & CLEGG, D. O. 2009. Derivation of Functional Retinal Pigmented Epithelium from Induced Pluripotent Stem Cells. *Stem Cells,* 27**,** 2427-2434.

BURKHALTER, M. D., FRALISH, G. B., PREMONT, R. T., CARON, M. G. & PHILIPP, M. 2013. Grk5l Controls Heart Development by Limiting mTOR Signaling during Symmetry Breaking. *Cell Reports,* 4**,** 625-632.

BURRIDGE, P. W., ANDERSON, D., PRIDDLE, H., MUNOZ, M. D. B., CHAMBERLAIN, S., ALLEGRUCCI, C., YOUNG, L. E. & DENNING, C. 2007. Improved human embryonic stem cell embryoid body homogeneity and cardiomyocyte differentiation from a novel V-96 plate aggregation system highlights interline variability. *Stem Cells,* 25**,** 929-938.

BURRIDGE, P. W., KELLER, G., GOLD, J. D. & WU, J. C. 2012. Production of de novo cardiomyocytes: human pluripotent stem cell differentiation and direct reprogramming. *Cell Stem Cell,* 10**,** 16-28.

BURRIDGE, P. W., LI, Y. F., MATSA, E., WU, H., ONG, S. G., SHARMA, A., HOLMSTROM, A., CHANG, A. C., CORONADO, M. J., EBERT, A. D., KNOWLES, J. W., TELLI, M. L., WITTELES, R. M., BLAU, H. M., BERNSTEIN, D., ALTMAN, R. B. & WU, J. C. 2016. Human induced pluripotent stem cell-derived cardiomyocytes recapitulate the predilection of breast cancer patients to doxorubicin-induced cardiotoxicity. *Nat Med,* 22**,** 547-56.

BURRIDGE, P. W., MATSA, E., SHUKLA, P., LIN, Z. C., CHURKO, J. M., EBERT, A. D., LAN, F., DIECKE, S., HUBER, B., MORDWINKIN, N. M., PLEWS, J. R., ABILEZ, O. J., CUI, B., GOLD, J. D. & WU, J. C. 2014. Chemically defined generation of human cardiomyocytes. *Nat Methods,* 11**,** 855-60.

BURRIDGE, P. W., SHARMA, A. & WU, J. C. 2015. Genetic and Epigenetic Regulation of Human Cardiac Reprogramming and Differentiation in Regenerative Medicine. *Annual Review of Genetics, Vol 49,* 49**,** 461-484.

BURRIDGE, P. W., THOMPSON, S., MILLROD, M. A., WEINBERG, S., YUAN, X. A., PETERS, A., MAHAIRAKI, V., KOLIATSOS, V. E., TUNG, L. & ZAMBIDIS, E. T. 2011. A Universal System for Highly Efficient Cardiac Differentiation of Human Induced Pluripotent Stem Cells That Eliminates Interline Variability. *Plos One,* 6.

BYLUND, D. B., EIKENBERG, D. C., HIEBLE, J. P., LANGER, S. Z., LEFKOWITZ, R. J., MINNEMAN, K. P., MOLINOFF, P. B., RUFFOLO, R. R. & TRENDELENBURG, U. 1994. International Union of Pharmacology Nomenclature of Adrenoceptors. *Pharmacological Reviews,* 46**,** 121-136.

CAMILO, V., BARROS, R., MAGALHAES, A., DAVID, L. & ALMEIDA, R. 2010. SOX2 expression is repressed by the BMP pathway and H. pylori in AGS gastric cell line. *Ejc Supplements,* 8**,** 179-179.

CAMPBELL, S. G. & MCCULLOCH, A. D. 2011. Multi-scale computational models of familial hypertrophic cardiomyopathy: genotype to phenotype. *J R Soc Interface,* 8**,** 1550-61.

CAO, N., LIANG, H., HUANG, J., WANG, J., CHEN, Y., CHEN, Z. & YANG, H. T. 2013. Highly efficient induction and long-term maintenance of multipotent cardiovascular progenitors from human pluripotent stem cells under defined conditions. *Cell Res,* 23**,** 1119-32.

CAO, N., LIU, Z. M., CHEN, Z. Y., WANG, J., CHEN, T. T., ZHAO, X. Y., MA, Y., QIN, L. J., KANG, J. H., WEI, B., WANG, L., JIN, Y. & YANG, H. T. 2012. Ascorbic

acid enhances the cardiac differentiation of induced pluripotent stem cells through promoting the proliferation of cardiac progenitor cells. *Cell Research,* 22**,** 219-236.

CAPOTE, L. A., PEREZ, R. M. & LYMPEROPOULOS, A. 2015. GPCR signaling and cardiac function. *European Journal of Pharmacology,* 763**,** 143-148.

CARLSON, C., KOONCE, C., AOYAMA, N., EINHORN, S., FIENE, S., THOMPSON, A., SWANSON, B., ANSON, B. & KATTMAN, S. 2013. Phenotypic screening with human iPS cell-derived cardiomyocytes: HTS-compatible assays for interrogating cardiac hypertrophy. *J Biomol Screen,* 18**,** 1203-11.

CARROLL, D. 2011. Genome engineering with zinc-finger nucleases. *Genetics,* 188**,** 773-82.

CASSILL, J. A., WHITNEY, M., JOAZEIRO, C. A., BECKER, A. & ZUKER, C. S. 1991. Isolation of Drosophila genes encoding G protein-coupled receptor kinases. *Proc Natl Acad Sci U S A,* 88**,** 11067-70.

CHATTERJEE, K. & MASSIE, B. 2007. Systolic and diastolic heart failure: Differences and similarities. *Journal of Cardiac Failure,* 13**,** 569-576.

CHEN, B. H., GILBERT, L. A., CIMINI, B. A., SCHNITZBAUER, J., ZHANG, W., LI, G. W., PARK, J., BLACKBURN, E. H., WEISSMAN, J. S., QI, L. S. & HUANG, B. 2013. Dynamic Imaging of Genomic Loci in Living Human Cells by an Optimized CRISPR/Cas System. *Cell,* 155**,** 1479-1491.

CHEN, C. K., BURNS, M. E., SPENCER, M., NIEMI, G. A., CHEN, J., HURLEY, J. B., BAYLOR, D. A. & SIMON, M. I. 1999. Abnormal photoresponses and light-induced apoptosis in rods lacking rhodopsin kinase. *Proc Natl Acad Sci U S A,* 96**,** 3718-22.

CHEN, C. K., ZHANG, K., CHURCH-KOPISH, J., HUANG, W., ZHANG, H. B., CHEN, Y. J., FREDERICK, J. M. & BAEHR, W. 2001. Characterization of human GRK7 as a potential cone opsin kinase. *Molecular Vision,* 7**,** 305-313.

CHEN, G., GULBRANSON, D. R., HOU, Z., BOLIN, J. M., RUOTTI, V., PROBASCO, M. D., SMUGA-OTTO, K., HOWDEN, S. E., DIOL, N. R., PROPSON, N. E., WAGNER, R., LEE, G. O., ANTOSIEWICZ-BOURGET, J., TENG, J. M. & THOMSON, J. A. 2011. Chemically defined conditions for human iPSC derivation and culture. *Nat Methods,* 8**,** 424-9.

CHEN, K. G., MALLON, B. S., HAMILTON, R. S., KOZHICH, O. A., PARK, K., HOEPPNER, D. J., ROBEY, P. G. & MCKAY, R. D. G. 2012. Non-colony type monolayer culture of human embryonic stem cells. *Stem Cell Research,* 9**,** 237-248.

CHEN, K. G., MALLON, B. S., MCKAY, R. D. & ROBEY, P. G. 2014a. Human pluripotent stem cell culture: considerations for maintenance, expansion, and therapeutics. *Cell Stem Cell,* 14**,** 13-26.

CHEN, V. C., YE, J. J., HUA, G., LIU, F., CHEN, D. L., LIN, B., CHAI, J., SHUKLA, P., WU, J., HSU, D. & COUTURE, L. A. 2014b. Development of a Scalable Suspension Culture for Cardiac Differentiation From Human Pluripotent Stem Cells. *Molecular Therapy,* 22**,** S204-S205.

CHO, S. W., KIM, S., KIM, J. M. & KIM, J. S. 2013. Targeted genome engineering in human cells with the Cas9 RNA-guided endonuclease. *Nature Biotechnology,* 31**,** 230-232.

CHOI, S. M., LIU, H., CHAUDHARI, P., KIM, Y., CHENG, L. Z., FENG, J., SHARKIS, S., YE, Z. H. & JANG, Y. Y. 2011. Reprogramming of EBV-immortalized B-lymphocyte cell lines into induced pluripotent stem cells. *Blood,* 118**,** 1801-1805.

CHOULIKA, A., PERRIN, A., DUJON, B. & NICOLAS, J. F. 1995. Induction of Homologous Recombination in Mammalian Chromosomes by Using the I-Scei System of Saccharomyces-Cerevisiae. *Molecular and Cellular Biology,* 15**,** 1968-1973.

CHRISTOFFELS, V. M., HOOGAARS, W. M. H., TESSARI, A., CLOUT, D. E. W., MOORMAN, A. F. M. & CAMPIONE, M. 2004. T-box transcription factor Tbx2 represses differentiation and formation of the cardiac chambers. *Developmental Dynamics,* 229**,** 763-770.

CHUAI, G. H., WANG, Q. L. & LIU, Q. 2017. In Silico Meets In Vivo: Towards Computational CRISPR-Based sgRNA Design. *Trends Biotechnol,* 35**,** 12-21.

COLUCCI, W. S., WRIGHT, R. F. & BRAUNWALD, E. 1986. New Positive Inotropic Agents in the Treatment of Congestive-Heart-Failure - Mechanisms of Action and Recent Clinical Developments .2. *New England Journal of Medicine,* 314**,** 349-358.

CONG, L., RAN, F. A., COX, D., LIN, S. L., BARRETTO, R., HABIB, N., HSU, P. D., WU, X. B., JIANG, W. Y., MARRAFFINI, L. A. & ZHANG, F. 2013. Multiplex Genome Engineering Using CRISPR/Cas Systems. *Science,* 339**,** 819-823.

COOPER, D. M. F. 2005. Compartmentalization of adenylate cyclase and cAMP signalling. *Biochemical Society Transactions,* 33**,** 1319-1322.

COPIK, A. J., BALDYS, A., NGUYEN, K., SAHDEO, S., HO, H., KOSAKA, A., DIETRICH, P. J., FITCH, B., RAYMOND, J. R., FORD, A. P. D. W., BUTTON, D. & MILLA, M. E. 2015. Isoproterenol Acts as a Biased Agonist of the Alpha-1A-Adrenoceptor that Selectively Activates the MAPK/ERK Pathway. *Plos One,* 10.

COSTELLO, I., PIMEISL, I. M., DRAGER, S., BIKOFF, E. K., ROBERTSON, E. J. & ARNOLD, S. J. 2011. The T-box transcription factor Eomesodermin acts upstream of Mesp1 to specify cardiac mesoderm during mouse gastrulation. *Nature Cell Biology,* 13**,** 1084-U108.

COTECCHIA, S., DEL VESCOVO, C. D., COLELLA, M., CASO, S. & DIVIANI, D. 2015. The alpha1-adrenergic receptors in cardiac hypertrophy: Signaling mechanisms and functional implications. *Cellular Signalling,* 27**,** 1984-1993.

CRESCI, S., DORN, G. W., JONES, P. G., BEITELSHEES, A. L., LI, A. Y., LENZINI, P. A., PROVINCE, M. A., SPERTUS, J. A. & LANFEAR, D. E. 2012. Adrenergic-Pathway Gene Variants Influence Beta-Blocker-Related Outcomes After Acute Coronary Syndrome in a Race-Specific Manner. *Journal of the American College of Cardiology,* 60**,** 898-907.

DAAKA, Y., LUTTRELL, L. M. & LEFKOWITZ, R. J. 1997. Switching of the coupling of the beta2-adrenergic receptor to different G proteins by protein kinase A. *Nature,* 390**,** 88-91.

DANG, S. M., GERECHT-NIR, S., CHEN, J., ITSKOVITZ-ELDOR, J. & ZANDSTRA, P. W. 2004. Controlled, scalable embryonic stem cell differentiation culture. *Stem Cells,* 22**,** 275-82.

DAVID, R., BRENNER, C., STIEBER, J., SCHWARZ, F., BRUNNER, S., VOLLMER, M., MENTELE, E., MULLER-HOCKER, J., KITAJIMA, S., LICKERT, H., RUPP, R. & FRANZ, W. M. 2008. MesP1 drives vertebrate cardiovascular differentiation through Dkk-1-mediated blockade of Wnt-signalling. *Nature Cell Biology,* 10**,** 338-U75.

DEL MONTE, F., KAUMANN, A. J., POOLE-WILSON, P. A., WYNNE, D. G., PEPPER, J. & HARDING, S. E. 1993. Coexistence of functioning beta 1- and beta 2-adrenoceptors in single myocytes from human ventricle. *Circulation,* 88**,** 854-63.

DEN HARTOGH, S. C. & PASSIER, R. 2016. Concise Review: Fluorescent Reporters in Human Pluripotent Stem Cells: Contributions to Cardiac Differentiation and Their Applications in Cardiac Disease and Toxicity. *Stem Cells,* 34**,** 13-26.

DEN HARTOGH, S. C., WOLSTENCROFT, K., MUMMERY, C. L. & PASSIER, R. 2016. A comprehensive gene expression analysis at sequential stages of in vitro cardiac differentiation from isolated MESP1-expressing-mesoderm progenitors. *Scientific Reports,* 6.

DENHAM, M., BYE, C., LEUNG, J., CONLEY, B. J., THOMPSON, L. H. & DOTTORI, M. 2012. Glycogen Synthase Kinase 3 beta and Activin/Nodal Inhibition in Human Embryonic Stem Cells Induces a Pre-Neuroepithelial State That Is Required for Specification to a Floor Plate Cell Lineage. *Stem Cells,* 30**,** 2400-2411.

DENNING, C., ALLEGRUCCI, C., PRIDDLE, H., BARBADILLO-MUNOZ, M. D., ANDERSON, D., SELF, T., SMITH, N. M., PARKIN, C. T. & YOUNG, L. E. 2006. Common culture conditions for maintenance and cardiomyocyte differentiation of the human embryonic stem cell lines, BG01 and HUES-7. *International Journal of Developmental Biology,* 50**,** 27-37.

DENNING, C., BORGDORFF, V., CRUTCHLEY, J., FIRTH, K. S. A., GEORGE, V., KALRA, S., KONDRASHOV, A., HOANG, M. D., MOSQUEIRA, D., PATEL, A., PRODANOV, L., RAJAMOHAN, D., SKARNES, W. C., SMITH, J. G. W. & YOUNG, L. E. 2016. Cardiomyocytes from human pluripotent stem cells: From laboratory curiosity to industrial biomedical platform. *Biochimica Et Biophysica Acta-Molecular Cell Research,* 1863**,** 1728-1748.

DESPA, S., BOSSUYT, J., HAN, F., GINSBURG, K. S., JIA, L. G., KUTCHAI, H., TUCKER, A. L. & BERS, D. M. 2005. Phospholemman-phosphorylation mediates the beta-adrenergic effects on Na/K pump function in cardiac myocytes. *Circ Res,* 97**,** 252-9.

DING, Q. R., LEE, Y. K., SCHAEFER, E. A. K., PETERS, D. T., VERES, A., KIM, K., KUPERWASSER, N., MOTOLA, D. L., MEISSNER, T. B., HENDRIKS, W. T., TREVISAN, M., GUPTA, R. M., MOISAN, A., BANKS, E., FRIESEN, M., SCHINZEL, R. T., XIA, F., TANG, A., XIA, Y. L., FIGUEROA, E., WANN, A., AHFELDT, T., DAHERON, L., ZHANG, F., RUBIN, L. L., PENG, L. F., CHUNG, R. T., MUSUNURU, K. & COWAN, C. A. 2013. A TALEN Genome-Editing System for Generating Human Stem Cell-Based Disease Models. *Cell Stem Cell,* 12**,** 238-251.

DODOU, E., VERZI, M. P., ANDERSON, J. R., XU, S. M. & BLACK, B. L. 2004. Mef2c is a direct transcriptional target of ISL1 and GATA factors in the anterior heart field during mouse embryonic development. *Development,* 131**,** 3931-3942.

DOENCH, J. G., HARTENIAN, E., GRAHAM, D. B., TOTHOVA, Z., HEGDE, M., SMITH, I., SULLENDER, M., EBERT, B. L., XAVIER, R. J. & ROOT, D. E. 2014. Rational design of highly active sgRNAs for CRISPR-Cas9-mediated gene inactivation. *Nature Biotechnology,* 32**,** 1262-U130.

DOERR, L., THOMAS, U., GUINOT, D. R., BOT, C. T., STOELZLE-FEIX, S., BECKLER, M., GEORGE, M. & FERTIG, N. 2015. New Easy-to-Use Hybrid System for Extracellular Potential and Impedance Recordings. *Jala,* 20**,** 175-188.

DOETSCHMAN, T. C., EISTETTER, H., KATZ, M., SCHMIDT, W. & KEMLER, R. 1985. The in vitro development of blastocyst-derived embryonic stem cell lines: formation of visceral yolk sac, blood islands and myocardium. *J Embryol Exp Morphol,* 87**,** 27-45.

DOLATSHAD, N. F., HELLEN, N., JABBOUR, R. J., HARDING, S. E. & FOLDES, G. 2015. G-protein Coupled Receptor Signaling in Pluripotent Stem Cell-derived Cardiovascular Cells: Implications for Disease Modeling. *Front Cell Dev Biol,* 3**,** 76.

DORN, G. W. 2007. The fuzzy logic of physiological cardiac hypertrophy. *Hypertension,* 49**,** 962-970.

DORN, G. W. 2009. GRK mythology: G-protein receptor kinases in cardiovascular disease. *Journal of Molecular Medicine-Jmm,* 87**,** 455-463.

DOTTORI, M., LEUNG, J., TURNLEY, A. M. & PEBAY, A. 2008. Lysophosphatidic acid inhibits neuronal differentiation of neural stem/progenitor cells derived from human embryonic stem cells. *Stem Cells,* 26**,** 1146-1154.

DOUDNA, J. A. & CHARPENTIER, E. 2014. The new frontier of genome engineering with CRISPR-Cas9. *Science,* 346**,** 1077-+.

DREYER, A. K. & CATHOMEN, T. 2012. Zinc-finger nucleases-based genome engineering to generate isogenic human cell lines. *Methods Mol Biol,* 813**,** 145-56.

DU, X. J., AUTELITANO, D. J., DILLEY, R. J., WANG, B., DART, A. M. & WOODCOCK, E. A. 2000. beta(2)-adrenergic receptor overexpression exacerbates development of heart failure after aortic stenosis. *Circulation,* 101**,** 71-7.

DZIMIRI, N., MUIYA, P., ANDRES, E. & AL-HALEES, Z. 2004. Differential functional expression of human myocardial G protein receptor kinases in left ventricular cardiac diseases. *European Journal of Pharmacology,* 489**,** 167-177.

EBRAHIMI, B. 2015. Reprogramming barriers and enhancers: strategies to enhance the efficiency and kinetics of induced pluripotency. *Cell Regen (Lond),* 4**,** 10.

EDEL, M. J., MENCHON, C., MENENDEZ, S., CONSIGLIO, A., RAYA, A. & BELMONTE, J. C. I. 2010. Rem2 GTPase maintains survival of human embryonic stem cells as well as enhancing reprogramming by regulating p53 and cyclin D-1. *Genes & Development,* 24**,** 561-573.

EDER, A., VOLLERT, I., HANSEN, A. & ESCHENHAGEN, T. 2016. Human engineered heart tissue as a model system for drug testing. *Advanced Drug Delivery Reviews,* 96**,** 214-224.

EGGENSCHWILER, R., MOSLEM, M., FRAGUAS, M. S., GALLA, M., PAPP, O., NAUJOCK, M., FONFARA, I., GENSCH, I., WAHNER, A., BEH-PAJOOH, A., MUSSOLINO, C., TAUSCHER, M., STEINEMANN, D., WEGNER, F., PETRI, S., SCHAMBACH, A., CHARPENTIER, E., CATHOMEN, T. & CANTZ, T. 2016. Improved bi-allelic modification of a transcriptionally silent locus in patient-derived iPSC by Cas9 nickase. *Scientific Reports,* 6.

EL-ARMOUCHE, A. & ESCHENHAGEN, T. 2009. beta-Adrenergic stimulation and myocardial function in the failing heart. *Heart Failure Reviews,* 14**,** 225-241.

ELLIOTT, B., RICHARDSON, C., WINDERBAUM, J., NICKOLOFF, J. A. & JASIN, M. 1998. Gene conversion tracts from double-strand break repair in mammalian cells. *Molecular and Cellular Biology,* 18**,** 93-101.

ELLIOTT, D. A., BRAAM, S. R., KOUTSIS, K., NG, E. S., JENNY, R., LAGERQVIST, E. L., BIBEN, C., HATZISTAVROU, T., HIRST, C. E., YU, Q. C., SKELTON, R. J., WARD-VAN OOSTWAARD, D., LIM, S. M., KHAMMY, O., LI, X., HAWES, S. M., DAVIS, R. P., GOULBURN, A. L., PASSIER, R., PRALL, O. W., HAYNES, J. M., POUTON, C. W., KAYE, D. M., MUMMERY, C. L., ELEFANTY, A. G. & STANLEY, E. G. 2011. NKX2-5(eGFP/w) hESCs for isolation of human cardiac progenitors and cardiomyocytes. *Nat Methods,* 8**,** 1037-40.

EMBI, N., RYLATT, D. B. & COHEN, P. 1980. Glycogen-Synthase Kinase-3 from Rabbit Skeletal-Muscle - Separation from Cyclic-Amp-Dependent Protein-Kinase and Phosphorylase-Kinase. *European Journal of Biochemistry,* 107**,** 519-527.

EMORINE, L. J., MARULLO, S., BRIENDSUTREN, M. M., PATEY, G., TATE, K., DELAVIERKLUTCHKO, C. & STROSBERG, A. D. 1989. Molecular Characterization of the Human Beta-3-Adrenergic Receptor. *Science,* 245**,** 1118-1121.

ENGELHARDT, S., BOHM, M., ERDMANN, E. & LOHSE, M. J. 1996. Analysis of beta-adrenergic receptor mRNA levels in human ventricular biopsy specimens by quantitative polymerase chain reactions: progressive reduction of beta 1-adrenergic receptor mRNA in heart failure. *J Am Coll Cardiol,* 27**,** 146-54.

ERTAN, A. A., BERIAT, N. C., GURPINAR, A., ONUR, M. A. & CEHRELI, M. C. 2010. Vascular smooth muscle contraction/relaxation of rat carotid artery is not altered by bone grafting substitutes in vitro. *Oral Maxillofac Surg,* 14**,** 97-104.

ESCHENHAGEN, T., MUMMERY, C. & KNOLLMANN, B. C. 2015. Modelling sarcomeric cardiomyopathies in the dish: from human heart samples to iPSC cardiomyocytes. *Cardiovascular Research,* 105**,** 424-438.

ESPOSITO, G., RAPACCIUOLO, A., PRASAD, S. V. N., TAKAOKA, H., THOMAS, S. A., KOCH, W. J. & ROCKMAN, H. A. 2002. Genetic alterations that inhibit in vivo pressure-overload hypertrophy prevent cardiac dysfunction despite increased wall stress. *Circulation,* 105**,** 85-92.

FAIAL, T., BERNARDO, A. S., MENDJAN, S., DIAMANTI, E., ORTMANN, D., GENTSCH, G. E., MASCETTI, V. L., TROTTER, M. W. B., SMITH, J. C. & PEDERSEN, R. A. 2015. Brachyury and SMAD signalling collaboratively orchestrate distinct mesoderm and endoderm gene regulatory networks in differentiating human embryonic stem cells. *Development,* 142**,** 2121-+.

FISHER, G. W., FUHRMAN, M. H., ADLER, S. A., SZENT-GYORGYI, C., WAGGONER, A. S. & JARVIK, J. W. 2014. Self-Checking Cell-Based Assays for GPCR Desensitization and Resensitization. *Journal of Biomolecular Screening,* 19**,** 1220-1226.

FOLDES, G., MIOULANE, M., WRIGHT, J. S., LIU, A. Q., NOVAK, P., MERKELY, B., GORELIK, J., SCHNEIDER, M. D., ALI, N. N. & HARDING, S. E. 2011.

Modulation of human embryonic stem cell-derived cardiomyocyte growth: a testbed for studying human cardiac hypertrophy? *J Mol Cell Cardiol,* 50**,** 367-76.

FRANCO, D., LAMERS, W. H. & MOORMAN, A. F. M. 1998. Patterns of expression in the developing myocardium: towards a morphologically integrated transcriptional model. *Cardiovascular Research,* 38**,** 25-53.

FREUND, C., OOSTWAARD, D. W. V., MONSHOUWER-KLOOTS, J., VAN DEN BRINK, S., VAN ROOIJEN, M., XU, X. Q., ZWEIGERDT, R., MUMMERY, C. & PASSIER, R. 2008. Insulin redirects differentiation from cardiogenic mesoderm and endoderm to neuroectoderm in differentiating human embryonic stem cells. *Stem Cells,* 26**,** 724-733.

FUKUHARA, S., CHIKUMI, H. & GUTKIND, J. S. 2001. RGS-containing RhoGEFs: the missing link between transforming G proteins and Rho? *Oncogene,* 20**,** 1661-1668.

FURTADO, M. B., SOLLOWAY, M. J., JONES, V. J., COSTA, M. W., BIBEN, C., WOLSTEIN, O., PREIS, J. I., SPARROW, D. B., SAGA, Y., DUNWOODIE, S. L., ROBERTSON, E. J., TAM, P. P. L. & HARVEY, R. P. 2008. BMP/SMAD1 signaling sets a threshold for the left/right pathway in lateral plate mesoderm and limits availability of SMAD4. *Genes & Development,* 22**,** 3037-3049.

FUSAKI, N., BAN, H., NISHIYAMA, A., SAEKI, K. & HASEGAWA, M. 2009. Efficient induction of transgene-free human pluripotent stem cells using a vector based on Sendai virus, an RNA virus that does not integrate into the host genome. *Proc Jpn Acad Ser B Phys Biol Sci,* 85**,** 348-62.

FUSCO, A., SANTULLI, G., SORRIENTO, D., CIPOLLETTA, E., GARBI, C., DORN, G. W., 2ND, TRIMARCO, B., FELICIELLO, A. & IACCARINO, G. 2012. Mitochondrial localization unveils a novel role for GRK2 in organelle biogenesis. *Cell Signal,* 24**,** 468-75.

GALDOS, F. X., GUO, Y. X., PAIGE, S. L., VANDUSEN, N. J., WU, S. M. & PU, W. T. 2017. Cardiac Regeneration Lessons From Development. *Circulation Research,* 120**,** 941-959.

GARCIA-PRIETO, J., GARCIA-RUIZ, J. M., SANZ-ROSA, D., PUN, A., GARCIA-ALVAREZ, A., DAVIDSON, S. M., FERNANDEZ-FRIERA, L., NUNO-AYALA, M., FERNANDEZ-JIMENEZ, R., BERNAL, J. A., IZQUIERDO-GARCIA, J. L., JIMENEZ-BORREGUERO, J., PIZARRO, G., RUIZ-CABELLO, J., MACAYA, C., FUSTER, V., YELLON, D. M. & IBANEZ, B. 2014. beta3 adrenergic receptor selective stimulation during ischemia/reperfusion improves cardiac function in translational models through inhibition of mPTP opening in cardiomyocytes. *Basic Res Cardiol,* 109**,** 422.

GARCIAHIGUERA, I. & MAYOR, F. 1992. Rapid Agonist-Induced Beta-Adrenergic-Receptor Kinase Translocation in C6 Glioma-Cells. *Febs Letters,* 302**,** 61-64.

GARNEAU, J. E., DUPUIS, M. E., VILLION, M., ROMERO, D. A., BARRANGOU, R., BOYAVAL, P., FREMAUX, C., HORVATH, P., MAGADAN, A. H. & MOINEAU, S. 2010. The CRISPR/Cas bacterial immune system cleaves bacteriophage and plasmid DNA. *Nature,* 468**,** 67-+.

GASIUNAS, G., BARRANGOU, R., HORVATH, P. & SIKSNYS, V. 2012. Cas9-crRNA ribonucleoprotein complex mediates specific DNA cleavage for adaptive immunity in bacteria. *Proceedings of the National Academy of Sciences of the United States of America,* 109**,** E2579-E2586.

GASSER, S. & RAULET, D. 2006. The DNA damage response, immunity and cancer. *Seminars in Cancer Biology,* 16**,** 344-347.

GAUR, M., RITNER, C., SIEVERS, R., PEDERSEN, A., PRASAD, M., BERNSTEIN, H. S. & YEGHIAZARIANS, Y. 2010. Timed inhibition of p38MAPK directs accelerated differentiation of human embryonic stem cells into cardiomyocytes. *Cytotherapy,* 12**,** 807-817.

GAUTHIER, C., LEBLAIS, V., KOBZIK, L., TROCHU, J. N., KHANDOUDI, N., BRIL, A., BALLIGAND, J. L. & LE MAREC, H. 1998. The negative inotropic effect of beta(3)-adrenoceptor stimulation is mediated by activation of a nitric oxide

synthase pathway in human ventricle. *Journal of Clinical Investigation,* 102**,** 1377-1384.

GAUTHIER, C., ROZEC, B., MANOURY, B. & BALLIGAND, J. L. 2011. Beta-3 adrenoceptors as new therapeutic targets for cardiovascular pathologies. *Curr Heart Fail Rep,* 8**,** 184-92.

GE, D. X., LIU, X. J., LI, L., WU, J., TU, Q. F., SHI, Y. K. & CHEN, H. Q. 2009. Chemical and physical stimuli induce cardiomyocyte differentiation from stem cells. *Biochemical and Biophysical Research Communications,* 381**,** 317-321.

GENG, Y. J., ISHIKAWA, Y., VATNER, D. E., WAGNER, T. E., BISHOP, S. P., VATNER, S. F. & HOMCY, C. J. 1999. Apoptosis of cardiac myocytes in Gs alpha transgenic mice. *Circulation Research,* 84**,** 34-42.

GERDES, A. M., KELLERMAN, S. E., MOORE, J. A., MUFFLY, K. E., CLARK, L. C., REAVES, P. Y., MALEC, K. B., MCKEOWN, P. P. & SCHOCKEN, D. D. 1992. Structural Remodeling of Cardiac Myocytes in Patients with Ischemic Cardiomyopathy. *Circulation,* 86**,** 426-430.

GERECHT-NIR, S. & ITSKOVITZ-ELDOR, J. 2004. Human embryonic stem cells: a potential source for cellular therapy. *Am J Transplant,* 4 Suppl 6**,** 51-7.

GERHARDSTEIN, B. L., PURI, T. S., CHIEN, A. J. & HOSEY, M. M. 1999. Identification of the sites phosphorylated by cyclic AMP-dependent protein kinase on the beta(2) subunit of L-type voltage-dependent calcium channels. *Biochemistry,* 38**,** 10361-10370.

GERTOW, K., HIRST, C. E., YU, Q. C., NG, E. S., PEREIRA, L. A., DAVIS, R. P., STANLEY, E. G. & ELEFANTY, A. G. 2013. WNT3A Promotes Hematopoietic or Mesenchymal Differentiation from hESCs Depending on the Time of Exposure. *Stem Cell Reports,* 1**,** 53-65.

GHERGHICEANU, M., BARAD, L., NOVAK, A., REITER, I., ITSKOVITZ-ELDOR, J., BINAH, O. & POPESCU, L. M. 2011. Cardiomyocytes derived from human embryonic and induced pluripotent stem cells: comparative ultrastructure. *J Cell Mol Med,* 15**,** 2539-51.

GHOSH, Z., WILSON, K. D., WU, Y., HU, S. J., QUERTERMOUS, T. & WU, J. C. 2010. Persistent Donor Cell Gene Expression among Human Induced Pluripotent Stem Cells Contributes to Differences with Human Embryonic Stem Cells. *Plos One,* 5.

GOLD, J. I., GAO, E., SHANG, X., PREMONT, R. T. & KOCH, W. J. 2012. Determining the absolute requirement of G protein-coupled receptor kinase 5 for pathological cardiac hypertrophy: short communication. *Circ Res,* 111**,** 1048-53.

GONZALEZ, F., BARRAGAN MONASTERIO, M., TISCORNIA, G., MONTSERRAT PULIDO, N., VASSENA, R., BATLLE MORERA, L., RODRIGUEZ PIZA, I. & IZPISUA BELMONTE, J. C. 2009. Generation of mouse-induced pluripotent stem cells by transient expression of a single nonviral polycistronic vector. *Proc Natl Acad Sci U S A,* 106**,** 8918-22.

GONZALEZ, F., BOUE, S. & BELMONTE, J. C. I. 2011. Methods for making induced pluripotent stem cells: reprogramming a la carte. *Nature Reviews Genetics,* 12**,** 231-242.

GORSKI, S. A., VOGEL, J. & DOUDNA, J. A. 2017. RNA-based recognition and targeting: sowing the seeds of specificity. *Nat Rev Mol Cell Biol*.

GRATZ, S. J., UKKEN, F. P., RUBINSTEIN, C. D., THIEDE, G., DONOHUE, L. K., CUMMINGS, A. M. & O'CONNOR-GILES, K. M. 2014. Highly Specific and Efficient CRISPR/Cas9-Catalyzed Homology-Directed Repair in Drosophila. *Genetics,* 196**,** 961-+.

GROSSMAN, W., JONES, D. & MCLAURIN, L. P. 1975. Wall stress and patterns of hypertrophy in the human left ventricle. *J Clin Invest,* 56**,** 56-64.

GUY, C. P., MAJERNIK, A. I., CHONG, J. P. J. & BOLT, E. L. 2004. A novel nuclease-ATPase (Nar71) from archaea is part of a proposed thermophilic DNA repair system. *Nucleic Acids Research,* 32**,** 6176-6186.

HAFT, D. H., SELENGUT, J., MONGODIN, E. F. & NELSON, K. E. 2005. A guild of 45 CRISPR-associated (Cas) protein families and multiple CRISPR/Cas subtypes exist in prokaryotic genomes. *Plos Computational Biology,* 1**,** 474-483.

HALE, C. R., ZHAO, P., OLSON, S., DUFF, M. O., GRAVELEY, B. R., WELLS, L., TERNS, R. M. & TERNS, M. P. 2009. RNA-Guided RNA Cleavage by a CRISPR RNA-Cas Protein Complex. *Cell,* 139**,** 945-956.

HANNA, J., MARKOULAKI, S., SCHORDERET, P., CAREY, B. W., BEARD, C., WERNIG, M., CREYGHTON, M. P., STEINE, E. J., CASSADY, J. P., FOREMAN, R., LENGNER, C. J., DAUSMAN, J. A. & JAENISCH, R. 2008. Direct reprogramming of terminally differentiated mature B lymphocytes to pluripotency (vol 133, pg 250, 2008). *Cell,* 134**,** 365-365.

HARVEY, R. P. 2002. Patterning the vertebrate heart. *Nature Reviews Genetics,* 3**,** 544-556.

HASTY, P., RIVERAPEREZ, J. & BRADLEY, A. 1991. The Length of Homology Required for Gene Targeting in Embryonic Stem-Cells. *Molecular and Cellular Biology,* 11**,** 5586-5591.

HAUSDORFF, W. P., CARON, M. G. & LEFKOWITZ, R. J. 1990. Turning Off the Signal - Desensitization of Beta-Adrenergic-Receptor Function. *Faseb Journal,* 4**,** 2881-2889.

HEIN, L., ALTMAN, J. D. & KOBILKA, B. K. 1999. Two functionally distinct alpha(2)-adrenergic receptors regulate sympathetic neurotransmission. *Nature,* 402**,** 181-184.

HEINEKE, J. & MOLKENTIN, J. D. 2006. Regulation of cardiac hypertrophy by intracellular signalling pathways. *Nature Reviews Molecular Cell Biology,* 7**,** 589-600.

HENDRIKS, W. T., WARREN, C. R. & COWAN, C. A. 2016. Genome Editing in Human Pluripotent Stem Cells: Approaches, Pitfalls, and Solutions. *Cell Stem Cell,* 18**,** 53-65.

HERNANDEZ, D., MILLARD, R., SIVAKUMARAN, P., WONG, R. C. B., CROMBIE, D. E., HEWITT, A. W., LIANG, H., HUNG, S. S. C., PEBAY, A., SHEPHERD, R. K., DUSTING, G. J. & LIM, S. Y. 2016. Electrical Stimulation Promotes Cardiac Differentiation of Human Induced Pluripotent Stem Cells. *Stem Cells International*.

HERRMANN, F., GROSS, A., ZHOU, D., KESTLER, H. A. & KUHL, M. 2012. A Boolean Model of the Cardiac Gene Regulatory Network Determining First and Second Heart Field Identity. *Plos One,* 7.

HIEBLE, J. P., BYLUND, D. B., CLARKE, D. E., EIKENBURG, D. C., LANGER, S. Z., LEFKOWITZ, R. J., MINNEMAN, K. P. & RUFFOLO, R. R. 1995. International Union of Pharmacology .10. Recommendation for Nomenclature of Alpha(1)-Adrenoceptors - Consensus Update. *Pharmacological Reviews,* 47**,** 267-270.

HOCKEMEYER, D., SOLDNER, F., BEARD, C., GAO, Q., MITALIPOVA, M., DEKELVER, R. C., KATIBAH, G. E., AMORA, R., BOYDSTON, E. A., ZEITLER, B., MENG, X. D., MILLER, J. C., ZHANG, L., REBAR, E. J., GREGORY, P. D., URNOV, F. D. & JAENISCH, R. 2009. Efficient targeting of expressed and silent genes in human ESCs and iPSCs using zinc-finger nucleases. *Nature Biotechnology,* 27**,** 851-U110.

HODGKINS, A., FARNE, A., PERERA, S., GREGO, T., PARRY-SMITH, D. J., SKARNES, W. C. & IYER, V. 2015. WGE: a CRISPR database for genome engineering. *Bioinformatics,* 31**,** 3078-80.

HOLLENBERG, S. M. 2011. Vasoactive Drugs in Circulatory Shock. *American Journal of Respiratory and Critical Care Medicine,* 183**,** 847-855.

HOU, P., LI, Y., ZHANG, X., LIU, C., GUAN, J., LI, H., ZHAO, T., YE, J., YANG, W., LIU, K., GE, J., XU, J., ZHANG, Q., ZHAO, Y. & DENG, H. 2013. Pluripotent stem cells induced from mouse somatic cells by small-molecule compounds. *Science,* 341**,** 651-4.

HSU, P. D., LANDER, E. S. & ZHANG, F. 2014. Development and applications of CRISPR-Cas9 for genome engineering. *Cell,* 157**,** 1262-78.

HUANG, S. M. A., MISHINA, Y. M., LIU, S. M., CHEUNG, A., STEGMEIER, F., MICHAUD, G. A., CHARLAT, O., WIELLETTE, E., ZHANG, Y., WIESSNER, S., HILD, M., SHI, X. Y., WILSON, C. J., MICKANIN, C., MYER, V., FAZAL, A., TOMLINSON, R., SERLUCA, F., SHAO, W. L., CHENG, H., SHULTZ, M., RAU, C., SCHIRLE, M., SCHLEGL, J., GHIDELLI, S., FAWELL, S., LU, C., CURTIS, D., KIRSCHNER, M. W., LENGAUER, C., FINAN, P. M., TALLARICO, J. A., BOUWMEESTER, T., PORTER, J. A., BAUER, A. & CONG, F. 2009. Tankyrase inhibition stabilizes axin and antagonizes Wnt signalling. *Nature,* 461**,** 614-620.

HUDSON, J., TITMARSH, D., HIDALGO, A., WOLVETANG, E. & COOPER-WHITE, J. 2012. Primitive Cardiac Cells from Human Embryonic Stem Cells. *Stem Cells and Development,* 21**,** 1513-1523.

HULLMANN, J. E., GRISANTI, L. A., MAKAREWICH, C. A., GAO, E., GOLD, J. I., CHUPRUN, J. K., TILLEY, D. G., HOUSER, S. R. & KOCH, W. J. 2014. GRK5-Mediated Exacerbation of Pathological Cardiac Hypertrophy Involves Facilitation of Nuclear NFAT Activity. *Circulation Research,* 115**,** 976-U128.

HUNG, S. C., KANG, M. S. & KIEFF, E. 2001. Maintenance of Epstein-Barr virus (EBV) oriP-based episomes requires EBV-encoded nuclear antigen-1 chromosome-binding domains, which can be replaced by high-mobility group-I or histone H1. *Proc Natl Acad Sci U S A,* 98**,** 1865-70.

HUSSAIN, T. & MULHERKAR, R. 2012. Lymphoblastoid Cell lines: a Continuous in Vitro Source of Cells to Study Carcinogen Sensitivity and DNA Repair. *Int J Mol Cell Med,* 1**,** 75-87.

IEMITSU, M., MIYAUCHI, T., MAEDA, S., SAKAI, S., KOBAYASHI, T., FUJII, N., MIYAZAKI, H., MATSUDA, M. & YAMAGUCHI, I. 2001. Physiological and pathological cardiac hypertrophy induce different molecular phenotypes in the rat. *American Journal of Physiology-Regulatory Integrative and Comparative Physiology,* 281**,** R2029-R2036.

INUI, M., MIYADO, M., IGARASHI, M., TAMANO, M., KUBO, A., YAMASHITA, S., ASAHARA, H., FUKAMI, M. & TAKADA, S. 2014. Rapid generation of mouse models with defined point mutations by the CRISPR/Cas9 system. *Scientific Reports,* 4.

ISHINO, Y., SHINAGAWA, H., MAKINO, K., AMEMURA, M. & NAKATA, A. 1987. Nucleotide-Sequence of the Iap Gene, Responsible for Alkaline-Phosphatase Isozyme Conversion in Escherichia-Coli, and Identification of the Gene-Product. *Journal of Bacteriology,* 169**,** 5429-5433.

ITSKOVITZ-ELDOR, J., SCHULDINER, M., KARSENTI, D., EDEN, A., YANUKA, O., AMIT, M., SOREQ, H. & BENVENISTY, N. 2000. Differentiation of human embryonic stem cells into embryoid bodies comprising the three embryonic germ layers. *Molecular Medicine,* 6**,** 88-95.

JABER, M., KOCH, W. J., ROCKMAN, H., SMITH, B., BOND, R. A., SULIK, K. K., ROSS, J., LEFKOWITZ, R. J., CARON, M. G. & GIROS, B. 1996. Essential role of beta-adrenergic receptor kinase 1 in cardiac development and function. *Proceedings of the National Academy of Sciences of the United States of America,* 93**,** 12974-12979.

JAFFRE, F., BONNIN, P., MONASSIER, L. & MAROTEAUX, L. 2008. Dual critical role of angiotensin AT-1 and serotonin 5-HT(2B) receptors in non-cardiomyocytes for beta-adrenergic agonist induced pathological left-ventricular hypertrophy. *Fundamental & Clinical Pharmacology,* 22**,** 17-17.

JANSEN, R., VAN EMBDEN, J. D. A., GAASTRA, W. & SCHOULS, L. M. 2002. Identification of genes that are associated with DNA repeats in prokaryotes. *Molecular Microbiology,* 43**,** 1565-1575.

JASIN, M. & ROTHSTEIN, R. 2013. Repair of Strand Breaks by Homologous Recombination. *Cold Spring Harbor Perspectives in Biology,* 5.

JIA, F., WILSON, K. D., SUN, N., GUPTA, D. M., HUANG, M., LI, Z., PANETTA, N. J., CHEN, Z. Y., ROBBINS, R. C., KAY, M. A., LONGAKER, M. T. & WU, J. C. 2010. A nonviral minicircle vector for deriving human iPS cells. *Nat Methods,* 7**,** 197-9.

JIANG, S. X., FU, Y. G., WILLIAMS, J., WOOD, J., PANDARINATHAN, L., AVRAHAM, S., MAKRIYANNIS, A., AVRAHAM, S. & AVRAHAM, H. K. 2007. Expression and Function of Cannabinoid Receptors CB1 and CB2 and Their Cognate Cannabinoid Ligands in Murine Embryonic Stem Cells. *Plos One,* 2.

JINEK, M., CHYLINSKI, K., FONFARA, I., HAUER, M., DOUDNA, J. A. & CHARPENTIER, E. 2012. A programmable dual-RNA-guided DNA endonuclease in adaptive bacterial immunity. *Science,* 337**,** 816-21.

JOHN P. OVERINGTON, B. A.-L. A. A. L. H. 2006. How many drug targets are there? *Nat. Rev. Drug Discov.,* 5**,** 993-996.

JOHNSON, L. R., ROBINSON, J. D., LESTER, K. N. & PITCHER, J. A. 2013. Distinct Structural Features of G Protein-Coupled Receptor Kinase 5 (GRK5) Regulate Its Nuclear Localization and DNA-Binding Ability. *Plos One,* 8.

JONSSON, M. K. B., WANG, Q. D. & BECKER, B. 2011. Impedance-Based Detection of Beating Rhythm and Proarrhythmic Effects of Compounds on Stem Cell-Derived Cardiomyocytes. *Assay and Drug Development Technologies,* 9**,** 589-599.

JOPE, R. S. & JOHNSON, G. V. W. 2004. The glamour and gloom of glycogen synthase kinase-3. *Trends in Biochemical Sciences,* 29**,** 95-102.

JORDAN, B. A. & DEVI, L. A. 1999. G-protein-coupled receptor heterodimerization modulates receptor function. *Nature,* 399**,** 697-700.

KADARI, A., MEKALA, S., WAGNER, N., MALAN, D., KOTH, J., DOLL, K., STAPPERT, L., ECKERT, D., PEITZ, M., MATTHES, J., SASSE, P., HERZIG, S., BRUSTLE, O., ERGUN, S. & EDENHOFER, F. 2015. Robust Generation of Cardiomyocytes from Human iPS Cells Requires Precise Modulation of BMP and WNT Signaling. *Stem Cell Reviews and Reports,* 11**,** 560-569.

KAINUMA, S., MIYAGAWA, S., FUKUSHIMA, S., PEARSON, J., CHEN, Y. C., SAITO, A., HARADA, A., SHIOZAKI, M., ISEOKA, H., WATABE, T., WATABE, H., HORITSUGI, G., ISHIBASHI, M., IKEDA, H., TSUCHIMOCHI, H., SONOBE, T., FUJII, Y., NAITO, H., UMETANI, K., SHIMIZU, T., OKANO, T., KOBAYASHI, E., DAIMON, T., UENO, T., KURATANI, T., TODA, K., TAKAKURA, N., HATAZAWA, J., SHIRAI, M. & SAWA, Y. 2015. Cell-sheet therapy with omentopexy promotes arteriogenesis and improves coronary circulation physiology in failing heart. *Mol Ther,* 23**,** 374-86.

KAMAKURA, T., MAKIYAMA, T., SASAKI, K., YOSHIDA, Y., WURIYANGHAI, Y., CHEN, J. R., HATTORI, T., OHNO, S., KITA, T., HORIE, M., YAMANAKA, S. & KIMURA, T. 2013. Ultrastructural Maturation of Human-Induced Pluripotent Stem Cell-Derived Cardiomyocytes in a Long-Term Culture. *Circulation Journal,* 77**,** 1307-1314.

KAN, Y. N., RUIS, B., LIN, S. & HENDRICKSON, E. A. 2014. The Mechanism of Gene Targeting in Human Somatic Cells. *Plos Genetics,* 10.

KARPANEN, T., BRY, M., OLLILA, H. M., SEPPANEN-LAAKSO, T., LIIMATTA, E., LESKINEN, H., KIVELA, R., HELKAMAA, T., MERENTIE, M., JELTSCH, M., PAAVONEN, K., ANDERSSON, L. C., MERVAALA, E., HASSINEN, I. E., YLA-HERTTUALA, S., ORESIC, M. & ALITALO, K. 2008. Overexpression of Vascular Endothelial Growth Factor-B in Mouse Heart Alters Cardiac Lipid Metabolism and Induces Myocardial Hypertrophy. *Circulation Research,* 103**,** 1018-U247.

KATRITCH, V., CHEREZOV, V. & STEVENS, R. C. 2013. Structure-Function of the G Protein-Coupled Receptor Superfamily. *Annual Review of Pharmacology and Toxicology, Vol 53, 2013,* 53**,** 531-556.

KATTMAN, S. J., WITTY, A. D., GAGLIARDI, M., DUBOIS, N. C., NIAPOUR, M., HOTTA, A., ELLIS, J. & KELLER, G. 2011. Stage-Specific Optimization of Activin/Nodal and BMP Signaling Promotes Cardiac Differentiation of Mouse and Human Pluripotent Stem Cell Lines. *Cell Stem Cell,* 8**,** 228-240.

KAWAMURA, M., MIYAGAWA, S., MIKI, K., SAITO, A., FUKUSHIMA, S., HIGUCHI, T., KAWAMURA, T., KURATANI, T., DAIMON, T., SHIMIZU, T., OKANO, T. & SAWA, Y. 2012. Feasibility, Safety, and Therapeutic Efficacy of Human Induced

Pluripotent Stem Cell-Derived Cardiomyocyte Sheets in a Porcine Ischemic Cardiomyopathy Model. *Circulation,* 126**,** S29-+.

KAWAMURA, T., SUZUKI, J., WANG, Y. V., MENENDEZ, S., MORERA, L. B., RAYA, A., WAHL, G. M. & IZPISUA BELMONTE, J. C. 2009. Linking the p53 tumour suppressor pathway to somatic cell reprogramming. *Nature,* 460**,** 1140-4.

KEHAT, I., KENYAGIN-KARSENTI, D., SNIR, M., SEGEV, H., AMIT, M., GEPSTEIN, A., LIVNE, E., BINAH, O., ITSKOVITZ-ELDOR, J. & GEPSTEIN, L. 2001. Human embryonic stem cells can differentiate into myocytes with structural and functional properties of cardiomyocytes. *Journal of Clinical Investigation,* 108**,** 407-414.

KHAN, S. M., SLENO, R., GORA, S., ZYLBERGOLD, P., LAVERDURE, J. P., LABBE, J. C., MILLER, G. J. & HEBERT, T. E. 2013. The expanding roles of Gbetagamma subunits in G protein-coupled receptor signaling and drug action. *Pharmacol Rev,* 65**,** 545-77.

KIM, D., KIM, C. H., MOON, J. I., CHUNG, Y. G., CHANG, M. Y., HAN, B. S., KO, S., YANG, E., CHA, K. Y., LANZA, R. & KIM, K. S. 2009. Generation of human induced pluripotent stem cells by direct delivery of reprogramming proteins. *Cell Stem Cell,* 4**,** 472-6.

KIM, J., AHN, S., REN, X. R., WHALEN, E. J., REITER, E., WEI, H. J. & LEFKOWITZ, R. J. 2005. Functional antagonism of different G protein-coupled receptor kinases for beta-arrestin-mediated angiotensin II receptor signaling. *Proceedings of the National Academy of Sciences of the United States of America,* 102**,** 1442-1447.

KIM, S., KIM, D., CHO, S. W., KIM, J. & KIM, J. S. 2014. Highly efficient RNA-guided genome editing in human cells via delivery of purified Cas9 ribonucleoproteins. *Genome Research,* 24**,** 1012-1019.

KOCH, W. J., ROCKMAN, H. A., SAMAMA, P., HAMILTON, R. A., BOND, R. A., MILANO, C. A. & LEFKOWITZ, R. J. 1995. Cardiac-Function in Mice Overexpressing the Beta-Adrenergic-Receptor Kinase or a Beta-Ark Inhibitor. *Science,* 268**,** 1350-1353.

KOMOLOV, K. E., BHARDWAJ, A. & BENOVIC, J. L. 2015. Atomic Structure of GRK5 Reveals Distinct Structural Features Novel for G Protein-coupled Receptor Kinases. *Journal of Biological Chemistry,* 290**,** 20629-20647.

KONDRASHOV, A., MEIJER, H. A., BARTHET-BARATEIG, A., PARKER, H. N., KHURSHID, A., TESSIER, S., SICARD, M., KNOX, A. J., PANG, L. H. & DE MOOR, C. H. 2012. Inhibition of polyadenylation reduces inflammatory gene induction. *Rna-a Publication of the Rna Society,* 18**,** 2236-2250.

KOSS, K. L., PONNIAH, S., JONES, W. K., GRUPP, I. L. & KRANIAS, E. G. 1995. Differential Phospholamban Gene-Expression in Murine Cardiac Compartments - Molecular and Physiological Analyses. *Circulation Research,* 77**,** 342-353.

KUBALAK, S. W., MILLERHANCE, W. C., OBRIEN, T. X., DYSON, E. & CHIEN, K. R. 1994. Chamber Specification of Atrial Myosin Light Chain-2 Expression Precedes Septation during Murine Cardiogenesis. *Journal of Biological Chemistry,* 269**,** 16961-16970.

KUHN, R. & WEFERS, B. 2014. Editing and investigating genomes with TALE and CRISPR/Cas systems: genome engineering across species using TALENs. *Methods,* 69**,** 1.

KUMAR, S., CURRAN, J. E., GLAHN, D. C. & BLANGERO, J. 2016. Utility of Lymphoblastoid Cell Lines for Induced Pluripotent Stem Cell Generation. *Stem Cells Int,* 2016**,** 2349261.

KUNAPULI, P. & BENOVIC, J. L. 1993. Cloning and Expression of Grk5 - a Member of the G-Protein-Coupled Receptor Kinase Family. *Proceedings of the National Academy of Sciences of the United States of America,* 90**,** 5588-5592.

KURIAN, L., SANCHO-MARTINEZ, I., NIVET, E., AGUIRRE, A., MOON, K., PENDARIES, C., VOLLE-CHALLIER, C., BONO, F., HERBERT, J. M., PULECIO, J., XIA, Y., LI, M., MONTSERRAT, N., RUIZ, S., DUBOVA, I., RODRIGUEZ, C., DENLI, A. M., BOSCOLO, F. S., THIAGARAJAN, R. D., GAGE, F. H., LORING, J. F., LAURENT, L. C. & BELMONTE, J. C. I. 2013.

Conversion of human fibroblasts to angioblast-like progenitor cells. *Nature Methods,* 10**,** 77-U116.

KURNIK, D., CUNNINGHAM, A. J., SOFOWORA, G. G., KOHLI, U., LI, C., FRIEDMAN, E. A., MUSZKAT, M., MENON, U. B., WOOD, A. J. J. & STEIN, C. M. 2009. GRK5 Gln41Leu polymorphism is not associated with sensitivity to beta(1)-adrenergic blockade in humans. *Pharmacogenomics,* 10**,** 1581-1587.

LAFLAMME, M. A., CHEN, K. Y., NAUMOVA, A. V., MUSKHELI, V., FUGATE, J. A., DUPRAS, S. K., REINECKE, H., XU, C. H., HASSANIPOUR, M., POLICE, S., O'SULLIVAN, C., COLLINS, L., CHEN, Y. H., MINAMI, E., GILL, E. A., UENO, S., YUAN, C., GOLD, J. & MURRY, C. E. 2007. Cardiomyocytes derived from human embryonic stem cells in pro-survival factors enhance function of infarcted rat hearts. *Nature Biotechnology,* 25**,** 1015-1024.

LALEFAR, N. R., WITKOWSKI, A., SIMONSEN, J. B. & RYAN, R. O. 2016. Wnt3a nanodisks promote ex vivo expansion of hematopoietic stem and progenitor cells. *Journal of Nanobiotechnology,* 14.

LAVERTY, H. G., BENSON, C., CARTWRIGHT, E. J., CROSS, M. J., GARLAND, C., HAMMOND, T., HOLLOWAY, C., MCMAHON, N., MILLIGAN, J., PARK, B. K., PIRMOHAMED, M., POLLARD, C., RADFORD, J., ROOME, N., SAGER, P., SINGH, S., SUTER, T., SUTER, W., TRAFFORD, A., VOLDERS, P. G. A., WALLIS, R., WEAVER, R., YORK, M. & VALENTIN, J. P. 2011. How can we improve our understanding of cardiovascular safety liabilities to develop safer medicines? *British Journal of Pharmacology,* 163**,** 675-693.

LEE, A. S., TANG, C., RAO, M. S., WEISSMAN, I. L. & WU, J. C. 2013. Tumorigenicity as a clinical hurdle for pluripotent stem cell therapies. *Nature Medicine,* 19**,** 998-1004.

LEFKOWITZ, R. J. 2007. Seven transmembrane receptors: something old, something new. *Acta Physiologica,* 190**,** 9-19.

LEFKOWITZ, R. J., INGLESE, J., KOCH, W. J., PITCHER, J., ATTRAMADAL, H. & CARON, M. G. 1992. G-Protein-Coupled Receptors - Regulatory Role of Receptor Kinases and Arrestin Proteins. *Cold Spring Harbor Symposia on Quantitative Biology,* 57**,** 127-133.

LEHNART, S. E. 2013. Understanding the physiology of heart failure through cellular and in vivo models-towards targeting of complex mechanisms. *Experimental Physiology,* 98**,** 622-628.

LI, J., NING, Y., HEDLEY, W., SAUNDERS, B., CHEN, Y., TINDILL, N., HANNAY, T. & SUBRAMANIAM, S. 2002. The Molecule Pages database. *Nature,* 420**,** 716-7.

LI, W. L. & DING, S. 2010. Small molecules that modulate embryonic stem cell fate and somatic cell reprogramming. *Trends in Pharmacological Sciences,* 31**,** 36-45.

LI, W. L., WEI, W., ZHU, S., ZHU, J., SHI, Y., LIN, T., HAO, E., HAYEK, A., DENG, H. & DING, S. 2009. Generation of Rat and Human Induced Pluripotent Stem Cells by Combining Genetic Reprogramming and Chemical Inhibitors (vol 4, pg 16, 2009). *Cell Stem Cell,* 4**,** 370-370.

LI, X., BURNIGHT, E. R., COONEY, A. L., MALANI, N., BRADY, T., SANDER, J. D., STABER, J., WHEELAN, S. J., JOUNG, J. K., MCCRAY, P. B., JR., BUSHMAN, F. D., SINN, P. L. & CRAIG, N. L. 2013. piggyBac transposase tools for genome engineering. *Proc Natl Acad Sci U S A,* 110**,** E2279-87.

LIAN, X., HSIAO, C., WILSON, G., ZHU, K., HAZELTINE, L. B., AZARIN, S. M., RAVAL, K. K., ZHANG, J., KAMP, T. J. & PALECEK, S. P. 2012. Robust cardiomyocyte differentiation from human pluripotent stem cells via temporal modulation of canonical Wnt signaling. *Proc Natl Acad Sci U S A,* 109**,** E1848-57.

LIAN, X. J., ZHANG, J. H., AZARIN, S. M., ZHU, K. X., HAZELTINE, L. B., BAO, X. P., HSIAO, C., KAMP, T. J. & PALECEK, S. P. 2013a. Directed cardiomyocyte differentiation from human pluripotent stem cells by modulating Wnt/beta-catenin signaling under fully defined conditions. *Nature Protocols,* 8**,** 162-175.

LIAN, X. J., ZHANG, J. H., ZHU, K. X., KAMP, T. J. & PALECEK, S. P. 2013b. Insulin Inhibits Cardiac Mesoderm, Not Mesendoderm, Formation During Cardiac

Differentiation of Human Pluripotent Stem Cells and Modulation of Canonical Wnt Signaling Can Rescue This Inhibition. *Stem Cells,* 31**,** 447-457.

LIANG, P., SALLAM, K., WU, H. D., LI, Y. X., ITZHAKI, I., GARG, P., ZHANG, Y., VERMGLINCHAN, V., LAN, F., GU, M. X., GONG, T. Y., YAN, Z. G., HE, C. J., EBERT, A. D., SANCHEZ-FREIRE, V., CHURKO, J., HU, S. J., SHARMA, A., LAM, C. K., SCHEINMAN, M. M., BERS, D. M. & WU, J. C. 2016. Patient-Specific and Genome-Edited Induced Pluripotent Stem Cell-Derived Cardiomyocytes Elucidate Single-Cell Phenotype of Brugada Syndrome. *Journal of the American College of Cardiology,* 68**,** 2086-2096.

LIEU, D. K., LIU, J., SIU, C. W., MCNERNEY, G. P., TSE, H. F., ABU-KHALIL, A., HUSER, T. & LI, R. A. 2009. Absence of transverse tubules contributes to non-uniform Ca(2+) wavefronts in mouse and human embryonic stem cell-derived cardiomyocytes. *Stem Cells Dev,* 18**,** 1493-500.

LIGGETT, S. B., CRESCI, S., KELLY, R. J., SYED, F. M., MATKOVICH, S. J., HAHN, H. S., DIWAN, A., MARTINI, J. S., SPARKS, L., PAREKH, R. R., SPERTUS, J. A., KOCH, W. J., KARDIA, S. L. R. & DORN, G. W. 2008. A GRK5 polymorphism that inhibits beta-adrenergic receptor signaling is protective in heart failure. *Nature Medicine,* 14**,** 510-517.

LIN, Y., LINASK, K. L., MALLON, B., JOHNSON, K., KLEIN, M., BEERS, J., XIE, W., DU, Y., LIU, C., LAI, Y., ZOU, J., HAIGNEY, M., YANG, H., RAO, M. & CHEN, G. 2017. Heparin Promotes Cardiac Differentiation of Human Pluripotent Stem Cells in Chemically Defined Albumin-Free Medium, Enabling Consistent Manufacture of Cardiomyocytes. *Stem Cells Transl Med,* 6**,** 527-538.

LOBMEYER, M. T., WANG, L. W., ZINEH, I., TURNER, S. T., GUMS, J. G., CHAPMAN, A. B., COOPER-DEHOFF, R. M., BEITELSHEES, A. L., BAILEY, K. R., BOERWINKLE, E., PEPINE, C. J. & JOHNSON, J. A. 2011. Polymorphisms in genes coding for GRK2 and GRK5 and response differences in antihypertensive-treated patients. *Pharmacogenetics and Genomics,* 21**,** 42-49.

LOGAN, C. Y. & NUSSE, R. 2004. The Wnt signaling pathway in development and disease. *Annual Review of Cell and Developmental Biology,* 20**,** 781-810.

LOH, K. M., ANG, L. T., ZHANG, J. Y., KUMAR, V., ANG, J., AUYEONG, J. Q., LEE, K. L., CHOO, S. H., LIM, C. Y. Y., NICHANE, M., TAN, J. R., NOGHABI, M. S., AZZOLA, L., NG, E. S., DURRUTHY-DURRUTHY, J., SEBASTIANO, V., POELLINGER, L., ELEFANTY, A. G., STANLEY, E. G., CHEN, Q. F., PRABHAKAR, S., WEISSMAN, I. L. & LIM, B. 2014. Efficient Endoderm Induction from Human Pluripotent Stem Cells by Logically Directing Signals Controlling Lineage Bifurcations. *Cell Stem Cell,* 14**,** 237-252.

LOH, Y. H., AGARWAL, S., PARK, I. H., URBACH, A., HUO, H. G., HEFFNER, G. C., KIM, K. T., MILLER, J. D., NG, K. W. & DALEY, G. Q. 2009. Generation of induced pluripotent stem cells from human blood. *Blood,* 113**,** 5476-5479.

LOHSE, M. J., ENGELHARDT, S. & ESCHENHAGEN, T. 2003. What is the role of beta-adrenergic signaling in heart failure? *Circ Res,* 93**,** 896-906.

LORENZ, W., INGLESE, J., PALCZEWSKI, K., ONORATO, J. J., CARON, M. G. & LEFKOWITZ, R. J. 1991. The Receptor Kinase Family - Primary Structure of Rhodopsin Kinase Reveals Similarities to the Beta-Adrenergic-Receptor Kinase. *Proceedings of the National Academy of Sciences of the United States of America,* 88**,** 8715-8719.

LUDWIG, A., ZONG, X., JEGLITSCH, M., HOFMANN, F. & BIEL, M. 1998. A family of hyperpolarization-activated mammalian cation channels. *Nature,* 393**,** 587-91.

LUDWIG, T. E., BERGENDAHL, V., LEVENSTEIN, M. E., YU, J. Y., PROBASCO, M. D. & THOMSON, J. A. 2006. Feeder-independent culture of human embryonic stem cells. *Nature Methods,* 3**,** 637-646.

LYMPEROPOULOS, A. & BATHGATE, A. 2013. Arrestins in the Cardiovascular System. *Molecular Biology of Arrestins,* 118**,** 297-334.

LYMPEROPOULOS, A. & NEGUSSIE, S. 2013. beta Arrestins in Cardiac G Protein-Coupled Receptor Signaling and Function: Partners in Crime or "Good Cop, Bad Cop"? *International Journal of Molecular Sciences,* 14**,** 24726-24741.

LYMPEROPOULOS, A., RENGO, G. & KOCH, W. J. 2012. GRK2 Inhibition in Heart Failure: Something Old, Something New. *Current Pharmaceutical Design,* 18**,** 186-191.

LYMPEROPOULOS, A., RENGO, G. & KOCH, W. J. 2013. Adrenergic Nervous System in Heart Failure Pathophysiology and Therapy. *Circulation Research,* 113**,** 739-753.

MA, J. Y., GUO, L., FIENE, S. J., ANSON, B. D., THOMSON, J. A., KAMP, T. J., KOLAJA, K. L., SWANSON, B. J. & JANUARY, C. T. 2011. High purity human-induced pluripotent stem cell-derived cardiomyocytes: electrophysiological properties of action potentials and ionic currents. *American Journal of Physiology-Heart and Circulatory Physiology,* 301**,** H2006-H2017.

MAEHR, R., CHEN, S. B., SNITOW, M., LUDWIG, T., YAGASAKI, L., GOLAND, R., LEIBEL, R. L. & MELTON, D. A. 2009. Generation of pluripotent stem cells from patients with type 1 diabetes. *Proceedings of the National Academy of Sciences of the United States of America,* 106**,** 15768-15773.

MAHFOUZ, M. M., PIATEK, A. & STEWART, C. N., JR. 2014. Genome engineering via TALENs and CRISPR/Cas9 systems: challenges and perspectives. *Plant Biotechnol J,* 12**,** 1006-14.

MAILLET, M., VAN BERLO, J. H. & MOLKENTIN, J. D. 2013. Molecular basis of physiological heart growth: fundamental concepts and new players. *Nature Reviews Molecular Cell Biology,* 14**,** 38-48.

MAKAROVA, K. S., ARAVIND, L., GRISHIN, N. V., ROGOZIN, I. B. & KOONIN, E. V. 2002. A DNA repair system specific for thermophilic Archaea and bacteria predicted by genomic context analysis. *Nucleic Acids Research,* 30**,** 482-496.

MAKAROVA, K. S., ARAVIND, L., WOLF, Y. I. & KOONIN, E. V. 2011a. Unification of Cas protein families and a simple scenario for the origin and evolution of CRISPR-Cas systems. *Biology Direct,* 6.

MAKAROVA, K. S., GRISHIN, N. V., SHABALINA, S. A., WOLF, Y. I. & KOONIN, E. V. 2006. A putative RNA-interference-based immune system in prokaryotes: computational analysis of the predicted enzymatic machinery, functional analogies with eukaryotic RNAi, and hypothetical mechanisms of action. *Biology Direct,* 1.

MAKAROVA, K. S., HAFT, D. H., BARRANGOU, R., BROUNS, S. J. J., CHARPENTIER, E., HORVATH, P., MOINEAU, S., MOJICA, F. J. M., WOLF, Y. I., YAKUNIN, A. F., VAN DER OOST, J. & KOONIN, E. V. 2011b. Evolution and classification of the CRISPR-Cas systems. *Nature Reviews Microbiology,* 9**,** 467-477.

MAKAROVA, K. S., WOLF, Y. I., ALKHNBASHI, O. S., COSTA, F., SHAH, S. A., SAUNDERS, S. J., BARRANGOU, R., BROUNS, S. J. J., CHARPENTIER, E., HAFT, D. H., HORVATH, P., MOINEAU, S., MOJICA, F. J. M., TERNS, R. M., TERNS, M. P., WHITE, M. F., YAKUNIN, A. F., GARRETT, R. A., VAN DER OOST, J., BACKOFEN, R. & KOONIN, E. V. 2015. An updated evolutionary classification of CRISPR-Cas systems. *Nature Reviews Microbiology,* 13**,** 722-736.

MAKAROVA, K. S., WOLF, Y. I. & KOONIN, E. V. 2013. The basic building blocks and evolution of CRISPR-Cas systems. *Biochemical Society Transactions,* 41**,** 1392-+.

MALI, P., YANG, L. H., ESVELT, K. M., AACH, J., GUELL, M., DICARLO, J. E., NORVILLE, J. E. & CHURCH, G. M. 2013. RNA-Guided Human Genome Engineering via Cas9. *Science,* 339**,** 823-826.

MANDAI, M., WATANABE, A., KURIMOTO, Y., HIRAMI, Y., MORINAGA, C., DAIMON, T., FUJIHARA, M., AKIMARU, H., SAKAI, N., SHIBATA, Y., TERADA, M., NOMIYA, Y., TANISHIMA, S., NAKAMURA, M., KAMAO, H., SUGITA, S., ONISHI, A., ITO, T., FUJITA, K., KAWAMATA, S., GO, M. J., SHINOHARA, C., HATA, K., SAWADA, M., YAMAMOTO, M., OHTA, S., OHARA, Y., YOSHIDA, K., KUWAHARA, J., KITANO, Y., AMANO, N., UMEKAGE, M., KITAOKA, F., TANAKA, A., OKADA, C., TAKASU, N., OGAWA, S., YAMANAKA, S. &

TAKAHASHI, M. 2017. Autologous Induced Stem-Cell-Derived Retinal Cells for Macular Degeneration. *New England Journal of Medicine,* 376**,** 1038-1046.

MANDERS, E., BOGAARD, H. J., HANDOKO, M. L., VAN DE VEERDONK, M. C., KEOGH, A., WESTERHOF, N., STIENEN, G. J., DOS REMEDIOS, C. G., HUMBERT, M., DORFMULLER, P., FADEL, E., GUIGNABERT, C., VAN DER VELDEN, J., VONK-NOORDEGRAAF, A., DE MAN, F. S. & OTTENHEIJM, C. A. 2014. Contractile dysfunction of left ventricular cardiomyocytes in patients with pulmonary arterial hypertension. *J Am Coll Cardiol,* 64**,** 28-37.

MARION, R. M., STRATI, K., LI, H., MURGA, M., BLANCO, R., ORTEGA, S., FERNANDEZ-CAPETILLO, O., SERRANO, M. & BLASCO, M. A. 2009. A p53-mediated DNA damage response limits reprogramming to ensure iPS cell genomic integrity. *Nature,* 460**,** 1149-53.

MARRAFFINI, L. A. & SONTHEIMER, E. J. 2008. CRISPR Interference Limits Horizontal Gene Transfer in Staphylococci by Targeting DNA. *Science,* 322**,** 1843-1845.

MARTINI, J. S., RAAKE, P., VINGE, L. E., DEGEORGE, B. R., CHUPRUN, J. K., HARRIS, D. M., GAO, E., ECKHART, A. D., PITCHER, J. A. & KOCH, W. J. 2008. Uncovering G protein-coupled receptor kinase-5 as a histone deacetylase kinase in the nucleus of cardiomyocytes (vol 105, pg 12457, 2008). *Proceedings of the National Academy of Sciences of the United States of America,* 105**,** 17206-17206.

MARTINS, S. A. M., TRABUCO, J. R. C., MONTEIRO, G. A., CHU, V., CONDE, J. P. & PRAZERES, D. M. F. 2012. Towards the miniaturization of GPCR-based live-cell screening assays. *Trends in Biotechnology,* 30**,** 566-574.

MATKOVICH, S. J., DIWAN, A., KLANKE, J. L., HAMMER, D. J., MARREEZ, Y., ODLEY, A. M., BRUNSKILL, E. W., KOCH, W. J., SCHWARTZ, R. J. & DORN, G. W. 2006. Cardiac-specific ablation of G-protein receptor kinase 2 redefines its roles in heart development and beta-adrenergic signaling. *Circulation Research,* 99**,** 996-1003.

MAYTIN, M. & COLUCCI, W. S. 2002. Molecular and cellular mechanisms of myocardial remodeling. *J Nucl Cardiol,* 9**,** 319-27.

MCDEVITT, T. C., LAFLAMME, M. A. & MURRY, C. E. 2005. Proliferation of cardiomyocytes derived from human embryonic stem cells is mediated via the IGF/PI 3-kinase/Akt signaling pathway. *Journal of Molecular and Cellular Cardiology,* 39**,** 865-873.

MEHTA, A., RAMACHANDRA, C. J. A., SEQUIERA, G. L., SUDIBYO, Y., NANDIHALLI, M., YONG, P. J. A., KOH, C. H. & SHIM, W. 2014. Phasic modulation of Wnt signaling enhances cardiac differentiation in human pluripotent stem cells by recapitulating developmental ontogeny. *Biochimica Et Biophysica Acta-Molecular Cell Research,* 1843**,** 2394-2402.

MELKOUMIAN, Z., WEBER, J. L., WEBER, D. M., FADEEV, A. G., ZHOU, Y. E., DOLLEY-SONNEVILLE, P., YANG, J. W., QIU, L. Q., PRIEST, C. A., SHOGBON, C., MARTIN, A. W., NELSON, J., WEST, P., BELTZER, J. P., PAL, S. & BRANDENBERGER, R. 2010. Synthetic peptide-acrylate surfaces for long-term self-renewal and cardiomyocyte differentiation of human embryonic stem cells. *Nature Biotechnology,* 28**,** 606-U95.

MERKLE, F. T., NEUHAUSSER, W. M., SANTOS, D., VALEN, E., GAGNON, J. A., MAAS, K., SANDOE, J., SCHIER, A. F. & EGGAN, K. 2015. Efficient CRISPR-Cas9-Mediated Generation of Knockin Human Pluripotent Stem Cells Lacking Undesired Mutations at the Targeted Locus. *Cell Reports,* 11**,** 875-883.

MERKLE, J. A. & SCHUPBACH, G. M. 2015. Identification of genes involved in oocyte specification and differentiation. *Molecular Biology of the Cell,* 26.

MIKAMI, M., TOKI, S. & ENDO, M. 2016. Precision Targeted Mutagenesis via Cas9 Paired Nickases in Rice. *Plant and Cell Physiology,* 57**,** 1058-1068.

MILLER, J. C., HOLMES, M. C., WANG, J. B., GUSCHIN, D. Y., LEE, Y. L., RUPNIEWSKI, I., BEAUSEJOUR, C. M., WAITE, A. J., WANG, N. S., KIM, K. A., GREGORY, P. D., PABO, C. O. & REBAR, E. J. 2007. An improved zinc-finger

nuclease architecture for highly specific genome editing. *Nature Biotechnology,* 25**,** 778-785.

MILLER, R. J., BANISADR, G. & BHATTACHARYYA, B. J. 2008. CXCR4 signaling in the regulation of stem cell migration and development. *Journal of Neuroimmunology,* 198**,** 31-38.

MIN, K. D., ASAKURA, M., LIAO, Y. L., NAKAMARU, K., OKAZAKI, H., TAKAHASHI, T., FUJIMOTO, K., ITO, S., TAKAHASHI, A., ASANUMA, H., YAMAZAKI, S., MINAMINO, T., SANADA, S., SEGUCHI, O., NAKANO, A., ANDO, Y., OTSUKA, T., FURUKAWA, H., ISOMURA, T., TAKASHIMA, S., MOCHIZUKI, N. & KITAKAZE, M. 2010. Identification of genes related to heart failure using global gene expression profiling of human failing myocardium. *Biochemical and Biophysical Research Communications,* 393**,** 55-60.

MINAMI, I., YAMADA, K., OTSUJI, T. G., YAMAMOTO, T., SHEN, Y., OTSUKA, S., KADOTA, S., MORONE, N., BARVE, M., ASAI, Y., TENKOVA-HEUSER, T., HEUSER, J. E., UESUGI, M., AIBA, K. & NAKATSUJI, N. 2012. A Small Molecule that Promotes Cardiac Differentiation of Human Pluripotent Stem Cells under Defined, Cytokine- and Xeno-free Conditions. *Cell Reports,* 2**,** 1448-1460.

MINAMISAWA, S., WANG, Y. B., CHEN, J., ISHIKAWA, Y., CHIEN, K. R. & MATSUOKA, R. 2003. Atrial chamber-specific expression of sarcolipin is regulated during development and hypertrophic remodeling. *Journal of Biological Chemistry,* 278**,** 9570-9575.

MITALIPOVA, M. M., RAO, R. R., HOYER, D. M., JOHNSON, J. A., MEISNER, L. F., JONES, K. L., DALTON, S. & STICE, S. L. 2005. Preserving the genetic integrity of human embryonic stem cells. *Nature Biotechnology,* 23**,** 19-20.

MITCHESON, J. S., CHEN, J., LIN, M., CULBERSON, C. & SANGUINETTI, M. C. 2000. A structural basis for drug-induced long QT syndrome. *Proceedings of the National Academy of Sciences of the United States of America,* 97**,** 12329-12333.

MOHANRAJU, P., MAKAROVA, K. S., ZETSCHE, B., ZHANG, F., KOONIN, E. V. & VAN DER OOST, J. 2016. Diverse evolutionary roots and mechanistic variations of the CRISPR-Cas systems. *Science,* 353**,** 556-+.

MOJICA, F. J. M., DIEZ-VILLASENOR, C., GARCIA-MARTINEZ, J. & SORIA, E. 2005. Intervening sequences of regularly spaced prokaryotic repeats derive from foreign genetic elements. *Journal of Molecular Evolution,* 60**,** 174-182.

MOJICA, F. J. M., DIEZ-VILLASENOR, C., SORIA, E. & JUEZ, G. 2000. Biological significance of a family of regularly spaced repeats in the genomes of Archaea, bacteria and mitochondria. *Molecular Microbiology,* 36**,** 244-246.

MONTO, F., OLIVER, E., VICENTE, D., RUEDA, J., AGUERO, J., ALMENAR, L., IVORRA, M. D., BARETTINO, D. & D'OCON, P. 2012. Different expression of adrenoceptors and GRKs in the human myocardium depends on heart failure etiology and correlates to clinical variables. *Am J Physiol Heart Circ Physiol,* 303**,** H368-76.

MONZEN, K., HIROI, Y., KUDOH, S., AKAZAWA, H., OKA, T., TAKIMOTO, E., HAYASHI, D., HOSODA, T., KAWABATA, M., MIYAZONO, K., ISHII, S., YAZAKI, Y., NAGAI, R. & KOMURO, I. 2001. Smads, TAK1, and their common target ATF-2 play a critical role in cardiomyocyte differentiation. *Journal of Cell Biology,* 153**,** 687-698.

MOORE, C. A., MILANO, S. K. & BENOVIC, J. L. 2007. Regulation of receptor trafficking by GRKs and arrestins. *Annu Rev Physiol,* 69**,** 451-82.

MOORMAN, A. F. M. & CHRISTOFFELS, V. M. 2003. Cardiac chamber formation: Development, genes, and evolution. *Physiological Reviews,* 83**,** 1223-1267.

MORETTI, A., BELLIN, M., WELLING, A., JUNG, C. B., LAM, J. T., BOTT-FLUGEL, L., DORN, T., GOEDEL, A., HOHNKE, C., HOFMANN, F., SEYFARTH, M., SINNECKER, D., SCHOMIG, A. & LAUGWITZ, K. L. 2010. Patient-Specific Induced Pluripotent Stem-Cell Models for Long-QT Syndrome. *New England Journal of Medicine,* 363**,** 1397-1409.

MORRELL, N. W., BLOCH, D. B., TEN DIJKE, P., GOUMANS, M. J. T. H., HATA, A., SMITH, J., YU, P. B. & BLOCH, K. D. 2016. Targeting BMP signalling in cardiovascular disease and anaemia. *Nature Reviews Cardiology,* 13**,** 106-120.

MUELLENER, D., RUDIN, O., PAULI, U. & ZINK, P. 1989. [Sex determination of human blood micro-stains and single hairs using specific DNA amplification with polymerase chain reaction]. *Arch Kriminol,* 184**,** 175-85.

MULEPATI, S. & BAILEY, S. 2011. Structural and biochemical analysis of nuclease domain of clustered regularly interspaced short palindromic repeat (CRISPR)-associated protein 3 (Cas3). *J Biol Chem,* 286**,** 31896-903.

MUMMERY, C., WARD-VAN OOSTWAARD, D., DOEVENDANS, P., SPIJKER, R., VAN DEN BRINK, S., HASSINK, R., VAN DER HEYDEN, M., OPTHOF, T., PERA, M., DE LA RIVIERE, A. B., PASSIER, R. & TERTOOLEN, L. 2003. Differentiation of human embryonic stem cells to cardiomyocytes - Role of coculture with visceral endoderm-like cells. *Circulation,* 107**,** 2733-2740.

MUMMERY, C. L., ZHANG, J., NG, E. S., ELLIOTT, D. A., ELEFANTY, A. G. & KAMP, T. J. 2012. Differentiation of human embryonic stem cells and induced pluripotent stem cells to cardiomyocytes: a methods overview. *Circ Res,* 111**,** 344-58.

MURRY, C. E. & KELLER, G. 2008. Differentiation of embryonic stem cells to clinically relevant populations: Lessons from embryonic development. *Cell,* 132**,** 661-680.

NAJAFI, A., SEQUEIRA, V., KUSTER, D. W. D. & VAN DER VELDEN, J. 2016. beta-adrenergic receptor signalling and its functional consequences in the diseased heart. *European Journal of Clinical Investigation,* 46**,** 362-374.

NAKAGAWA, M., KOYANAGI, M., TANABE, K., TAKAHASHI, K., ICHISAKA, T., AOI, T., OKITA, K., MOCHIDUKI, Y., TAKIZAWA, N. & YAMANAKA, S. 2008. Generation of induced pluripotent stem cells without Myc from mouse and human fibroblasts. *Nat Biotechnol,* 26**,** 101-6.

NARAZAKI, G., UOSAKI, H., TERANISHI, M., OKITA, K., KIM, B., MATSUOKA, S., YAMANAKA, S. & YAMASHITA, J. K. 2008. Directed and systematic differentiation of cardiovascular cells from mouse induced pluripotent stem cells. *Circulation,* 118**,** 498-506.

NAYAK, A. S., CUTIE, A. J., JOCHSBERGER, T. & KAY, A. I. 1986. The Effect of Various Additives on the Stability of Isoproterenol Hydrochloride Solutions. *Drug Development and Industrial Pharmacy,* 12**,** 589-601.

NEITZEL, H. 1986. A routine method for the establishment of permanent growing lymphoblastoid cell lines. *Hum Genet,* 73**,** 320-6.

NESBIT, C. E., GROVE, L. E., YIN, X. & PROCHOWNIK, E. V. 1998. Differential apoptotic behaviors of c-myc, N-myc, and L-myc oncoproteins. *Cell Growth Differ,* 9**,** 731-41.

NGUYEN, P. K., NEOFYTOU, E., RHEE, J. W. & WU, J. C. 2016. Potential Strategies to Address the Major Clinical Barriers Facing Stem Cell Regenerative Therapy for Cardiovascular Disease: A Review. *JAMA Cardiol,* 1**,** 953-962.

NIE, Y., BERGENDAHL, V., HEI, D. J., JONES, J. M. & PALECEK, S. P. 2009. Scalable culture and cryopreservation of human embryonic stem cells on microcarriers. *Biotechnol Prog,* 25**,** 20-31.

NIE, Z., HU, G., WEI, G., CUI, K., YAMANE, A., RESCH, W., WANG, R., GREEN, D. R., TESSAROLLO, L., CASELLAS, R., ZHAO, K. & LEVENS, D. 2012. c-Myc is a universal amplifier of expressed genes in lymphocytes and embryonic stem cells. *Cell,* 151**,** 68-79.

NISHIMURA, T., YAMADA, Y. & KAWAI, C. 1980. Echocardiographic Evaluation of Long-Term Effects of Exercise on Left-Ventricular Hypertrophy and Function in Professional Bicyclists. *Circulation,* 61**,** 832-840.

NISHISHITA, N., MURAMATSU, M. & KAWAMATA, S. 2015. An effective freezing/thawing method for human pluripotent stem cells cultured in chemically-defined and feeder-free conditions. *American Journal of Stem Cells,* 4**,** 38-+.

NORRIS, A. D., KIM, H. M., COLAIACOVO, M. P. & CALARCO, J. A. 2015. Efficient Genome Editing in Caenorhabditis elegans with a Toolkit of Dual-Marker Selection Cassettes. *Genetics,* 201**,** 449-+.

NOSEDA, M., PETERKIN, T., SIMOES, F. C., PATIENT, R. & SCHNEIDER, M. D. 2011. Cardiopoietic Factors Extracellular Signals for Cardiac Lineage Commitment. *Circulation Research,* 108**,** 129-152.

OBERGRUSSBERGER, A., JUHASZ, K., THOMAS, U., STOLZLE-FEIX, S., BECKER, N., DORR, L., BECKLER, M., BOT, C., GEORGE, M. & FERTIG, N. 2016. Safety pharmacology studies using EFP and impedance. *Journal of Pharmacological and Toxicological Methods,* 81**,** 223-232.

OKADA, H. & MAK, T. W. 2004. Pathways of apoptotic and non-apoptotic death in tumour cells. *Nat Rev Cancer,* 4**,** 592-603.

OKITA, K., MATSUMURA, Y., SATO, Y., OKADA, A., MORIZANE, A., OKAMOTO, S., HONG, H., NAKAGAWA, M., TANABE, K., TEZUKA, K., SHIBATA, T., KUNISADA, T., TAKAHASHI, M., TAKAHASHI, J., SAJI, H. & YAMANAKA, S. 2011. A more efficient method to generate integration-free human iPS cells. *Nature Methods,* 8**,** 409-U52.

OKITA, K., YAMAKAWA, T., MATSUMURA, Y., SATO, Y., AMANO, N., WATANABE, A., GOSHIMA, N. & YAMANAKA, S. 2013. An Efficient Nonviral Method to Generate Integration-Free Human-Induced Pluripotent Stem Cells from Cord Blood and Peripheral Blood Cells. *Stem Cells,* 31**,** 458-466.

OPPERMANN, M., KIRCHHOFF, S. & LEFKOWITZ, R. J. 1996. Monoclonal antibodies reveal receptor specificity among G protein-coupled receptor kinases. *Journal of Leukocyte Biology***,** 205-205.

OU, D. B., ZENG, D., JIN, Y., LIU, X. T., TENG, J. W., GUO, W. G., WANG, H. T., SU, F. F., HE, Y. & ZHENG, Q. S. 2013. The Long-Term Differentiation of Embryonic Stem Cells into Cardiomyocytes: An Indirect Co-Culture Model. *Plos One,* 8.

PAIGE, S. L., OSUGI, T., AFANASIEV, O. K., PABON, L., REINECKE, H. & MURRY, C. E. 2010. Endogenous Wnt/beta-Catenin Signaling Is Required for Cardiac Differentiation in Human Embryonic Stem Cells. *Plos One,* 5.

PAIGE, S. L., PLONOWSKA, K., XU, A. & WU, S. M. 2015. Molecular Regulation of Cardiomyocyte Differentiation. *Circulation Research,* 116**,** 341-353.

PAQUET, D., KWART, D., CHEN, A., SPROUL, A., JACOB, S., TEO, S., OLSEN, K. M., GREGG, A., NOGGLE, S. & TESSIER-LAVIGNE, M. 2016. Efficient introduction of specific homozygous and heterozygous mutations using CRISPR/Cas9. *Nature,* 533**,** 125-+.

PARIKH, A., WU, J. C., BLANTON, R. M. & TZANAKAKIS, E. S. 2015. Signaling Pathways and Gene Regulatory Networks in Cardiomyocyte Differentiation. *Tissue Engineering Part B-Reviews,* 21**,** 377-392.

PARK, E. J., OGDEN, L. A., TALBOT, A., EVANS, S., CAI, C. L., BLACK, B. L., FRANK, D. U. & MOON, A. M. 2006. Required, tissue-specific roles for Fgf8 in outflow tract formation and remodeling. *Development,* 133**,** 2419-2433.

PARSONS, X. H. 2016. Direct Conversion of Pluripotent Human Embryonic Stem Cells Under Defined Culture Conditions into Human Neuronal or Cardiomyocyte Cell Therapy Derivatives. *Methods Mol Biol,* 1307**,** 299-318.

PASSIER, R., OOSTWAARD, D. W. V., SNAPPER, J., KLOOTS, J., HASSINK, R. J., KUIJK, E., ROELEN, B., DE LA RIVIERE, A. B. & MUMMERY, C. 2005. Increased cardiomyocyte differentiation from human embryonic stem cells in serum-free cultures. *Stem Cells,* 23**,** 772-780.

PATTANAYAK, V., LIN, S., GUILINGER, J. P., MA, E. B., DOUDNA, J. A. & LIU, D. R. 2013. High-throughput profiling of off-target DNA cleavage reveals RNA-programmed Cas9 nuclease specificity. *Nature Biotechnology,* 31**,** 839-+.

PENELA, P., MURGA, C., RIBAS, C., TUTOR, A. S., PEREGRIN, S. & MAYOR, F. 2006. Mechanisms of regulation of G protein-coupled receptor kinases (GRKs) and cardiovascular disease. *Cardiovascular Research,* 69**,** 46-56.

PENG, W. F., FENG, M. X., FENG, X., LIANG, Y. X. & SHE, Q. X. 2015. An archaeal CRISPR type III-B system exhibiting distinctive RNA targeting features and mediating dual RNA and DNA interference. *Nucleic Acids Research,* 43**,** 406-417.

PEREIRA, P. N. G., DOBREVA, M. P., MAAS, E., CORNELIS, F. M., MOYA, I. M., UMANS, L., VERFAILLIE, C. M., CAMUS, A., LOPES, S. M. C. D., HUYLEBROECK, D. & ZWIJSEN, A. 2012. Antagonism of Nodal signaling by BMP/Smad5 prevents ectopic primitive streak formation in the mouse amnion. *Development,* 139**,** 3343-3354.

PHILIPP, M., BERGER, I. M., JUST, S. & CARON, M. G. 2014. Overlapping and Opposing Functions of G Protein-coupled Receptor Kinase 2 (GRK2) and GRK5 during Heart Development. *Journal of Biological Chemistry,* 289**,** 26119-26130.

PHILIPP, M., BREDE, M. & HEIN, L. 2002. Physiological significance of alpha(2)-adrenergic receptor subtype diversity: one receptor is not enough. *American Journal of Physiology-Regulatory Integrative and Comparative Physiology,* 283**,** R287-R295.

PIERCE, K. L., PREMONT, R. T. & LEFKOWITZ, R. J. 2002. Seven-transmembrane receptors. *Nature Reviews Molecular Cell Biology,* 3**,** 639-650.

PITCHER, J., LOHSE, M. J., CODINA, J., CARON, M. G. & LEFKOWITZ, R. J. 1992. Desensitization of the Isolated Beta-2-Adrenergic Receptor by Beta-Adrenergic-Receptor Kinase, Camp-Dependent Protein-Kinase, and Protein-Kinase-C Occurs Via Distinct Molecular Mechanisms. *Biochemistry,* 31**,** 3193-3197.

PITCHER, J. A., FREEDMAN, N. J. & LEFKOWITZ, R. J. 1998. G protein-coupled receptor kinases. *Annual Review of Biochemistry,* 67**,** 653-692.

POPPLEWELL, L., KOO, T., LECLERC, X., DUCLERT, A., MAMCHAOUI, K., GOUBLE, A., MOULY, V., VOIT, T., PAQUES, F., CEDRONE, F., ISMAN, O., YANEZ-MUNOZ, R. J. & DICKSON, G. 2013. Gene Correction of a Duchenne Muscular Dystrophy Mutation by Meganuclease-Enhanced Exon Knock-In. *Human Gene Therapy,* 24**,** 692-701.

POURCEL, C., SALVIGNOL, G. & VERGNAUD, G. 2005. CRISPR elements in Yersinia pestis acquire new repeats by preferential uptake of bacteriophage DNA, and provide additional tools for evolutionary studies. *Microbiology-Sgm,* 151**,** 653-663.

PUIG-SANVICENS, V. A. C., SEMINO, C. E. & ZUR NIEDEN, N. I. 2015. Cardiac differentiation potential of human induced pluripotent stem cells in a 3D self-assembling peptide scaffold. *Differentiation,* 90**,** 101-110.

RAJESH, D., DICKERSON, S. J., YU, J. Y., BROWN, M. E., THOMSON, J. A. & SEAY, N. J. 2011. Human lymphoblastoid B-cell lines reprogrammed to EBV-free induced pluripotent stem cells. *Blood,* 118**,** 1797-1800.

RAMIREZ, M. T., ZHAO, X. L., SCHULMAN, H. & BROWN, J. H. 1997. The nuclear deltaB isoform of Ca2+/calmodulin-dependent protein kinase II regulates atrial natriuretic factor gene expression in ventricular myocytes. *J Biol Chem,* 272**,** 31203-8.

RAN, F. A., HSU, P. D., LIN, C. Y., GOOTENBERG, J. S., KONERMANN, S., TREVINO, A. E., SCOTT, D. A., INOUE, A., MATOBA, S., ZHANG, Y. & ZHANG, F. 2013a. Double Nicking by RNA-Guided CRISPR Cas9 for Enhanced Genome Editing Specificity. *Cell,* 154**,** 1380-1389.

RAN, F. A., HSU, P. D., WRIGHT, J., AGARWALA, V., SCOTT, D. A. & ZHANG, F. 2013b. Genome engineering using the CRISPR-Cas9 system. *Nature Protocols,* 8**,** 2281-2308.

RANA, M. S., CHRISTOFFELS, V. M. & MOORMAN, A. F. M. 2013. A molecular and genetic outline of cardiac morphogenesis. *Acta Physiologica,* 207**,** 588-615.

RAO, J., PFEIFFER, M. J., FRANK, S., ADACHI, K., PICCINI, I., QUARANTA, R., ARAUZO-BRAVO, M., SCHWARZ, J., SCHADE, D., LEIDEL, S., SCHOLER, H. R., SEEBOHM, G. & GREBER, B. 2016. Stepwise Clearance of Repressive Roadblocks Drives Cardiac Induction in Human ESCs. *Cell Stem Cell,* 18**,** 341-353.

RASMUSSEN, M. A., HOLST, B., TUMER, Z., JOHNSEN, M. G., ZHOU, S. L., STUMMANN, T. C., HYTTEL, P. & CLAUSEN, C. 2014. Transient p53 Suppression Increases Reprogramming of Human Fibroblasts without Affecting Apoptosis and DNA Damage. *Stem Cell Reports,* 3**,** 404-413.

REDFERN, W. S., CARLSSON, L., DAVIS, A. S., LYNCH, W. G., MACKENZIE, I., PALETHORPE, S., SIEGL, P. K. S., STRANG, I., SULLIVAN, A. T., WALLIS, R., CAMM, A. J. & HAMMOND, T. G. 2004. Relationships between preclinical cardiac electrophysiology, clinical QT interval prolongation and torsade de pointes for a broad range of drugs: evidence for a provisional safety margin in drug development (vol 58, pg 32, 2003). *Cardiovascular Research,* 63**,** 186-187.

REN, Y. M., LEE, M. Y., SCHLIFFKE, S., PAAVOLA, J., AMOS, P. J., GE, X., YE, M. Y., ZHU, S. J., SENYEI, G., LUM, L., EHRLICH, B. E. & QYANG, Y. B. 2011. Small molecule Wnt inhibitors enhance the efficiency of BMP-4-directed cardiac differentiation of human pluripotent stem cells. *Journal of Molecular and Cellular Cardiology,* 51**,** 280-287.

REUBINOFF, B. E., PERA, M. F., FONG, C. Y., TROUNSON, A. & BONGSO, A. 2000. Embryonic stem cell lines from human blastocysts: somatic differentiation in vitro. *Nature Biotechnology,* 18**,** 399-404.

RICHARDS, M., FONG, C. Y., CHAN, W. K., WONG, P. C. & BONGSO, A. 2002. Human feeders support prolonged undifferentiated growth of human inner cell masses and embryonic stem cells. *Nature Biotechnology,* 20**,** 933-936.

ROBERTSON, C., TRAN, D. D. & GEORGE, S. C. 2013. Concise Review: Maturation Phases of Human Pluripotent Stem Cell-Derived Cardiomyocytes. *Stem Cells,* 31**,** 829-837.

ROBINSON, J. D. & PITCHER, J. A. 2013. G protein-coupled receptor kinase 2 (GRK2) is a Rho-activated scaffold protein for the ERK MAP kinase cascade. *Cellular Signalling,* 25**,** 2831-2839.

ROBINTON, D. A. & DALEY, G. Q. 2012. The promise of induced pluripotent stem cells in research and therapy. *Nature,* 481**,** 295-305.

ROCKMAN, H. A., CHOI, D. J., RAHMAN, N. U., AKHTER, S. A., LEFKOWITZ, R. J. & KOCH, W. J. 1996a. Receptor-specific in vivo desensitization by the G protein-coupled receptor kinase-5 in transgenic mice. *Proceedings of the National Academy of Sciences of the United States of America,* 93**,** 9954-9959.

ROCKMAN, H. A., CHOI, D. J., RAHMAN, N. U., AKHTER, S. A., LEFKOWITZ, R. J. & KOCH, W. J. 1996b. Receptor-specific in vivo desensitization by the G protein-coupled receptor kinase-5 in transgenic mice. *Proc Natl Acad Sci U S A,* 93**,** 9954-9.

ROCKMAN, H. A., KOCH, W. J. & LEFKOWITZ, R. J. 2002. Seven-transmembrane-spanning receptors and heart function. *Nature,* 415**,** 206-212.

ROHRER, D. K. 1998. Physiological consequences of beta-adrenergic receptor disruption. *Journal of Molecular Medicine-Jmm,* 76**,** 764-772.

RONA, G., CHAPPEL, C. I., BALAZS, T. & GAUDRY, R. 1959. An Infarct-Like Myocardial Lesion and Other Toxic Manifestations Produced by Isoproterenol in the Rat. *Archives of Pathology,* 67**,** 443-455.

ROSKAMS, J., BAKIN, R., DAWSON, T., LEFKOWITZ, R. & RONNETT, G. 1993. Beta-Adrenergic-Receptor Kinase-2 and Beta-Arrestin-2 as Mediators of Odorant-Induced Desensitization. *Journal of Cellular Biochemistry***,** 267-267.

ROUET, P., SMIH, F. & JASIN, M. 1994. Expression of a Site-Specific Endonuclease Stimulates Homologous Recombination in Mammalian-Cells. *Proceedings of the National Academy of Sciences of the United States of America,* 91**,** 6064-6068.

SAGA, Y., KITAJIMA, S. & MIYAGAWA-TOMITA, S. 2000. Mesp1 expression is the earliest sign of cardiovascular development. *Trends in Cardiovascular Medicine,* 10**,** 345-352.

SANCHEZ-FREIRE, V., LEE, A. S., HU, S. J., ABILEZ, O. J., LIANG, P., LAN, F., HUBER, B. C., ONG, S. G., HONG, W. X., HUANG, M. & WU, J. C. 2014. Effect of Human Donor Cell Source on Differentiation and Function of Cardiac Induced Pluripotent Stem Cells. *Journal of the American College of Cardiology,* 64**,** 436-448.

SAPRANAUSKAS, R., GASIUNAS, G., FREMAUX, C., BARRANGOU, R., HORVATH, P. & SIKSNYS, V. 2011. The Streptococcus thermophilus CRISPR/Cas system provides immunity in Escherichia coli. *Nucleic Acids Res,* 39**,** 9275-82.

SARA S. NUNES, N. F., ARIC PAHNKE, JASON W. MIKLAS, MARK LI, JOHN COLES, MARK GAGLIARDI, GORDON KELLER, AND MILICA RADISIC 2016. Human Stem Cell-Derived Cardiac Model of Chronic Drug Exposure. *ACS Biomater. Sci. Eng.*

SATO, P. Y., CHUPRUN, J. K., SCHWARTZ, M. & KOCH, W. J. 2015. The Evolving Impact of G Protein-Coupled Receptor Kinases in Cardiac Health and Disease. *Physiological Reviews,* 95**,** 377-404.

SCHAAF, S., SHIBAMIYA, A., MEWE, M., EDER, A., STOHR, A., HIRT, M. N., RAU, T., ZIMMERMANN, W. H., CONRADI, L., ESCHENHAGEN, T. & HANSEN, A. 2011. Human Engineered Heart Tissue as a Versatile Tool in Basic Research and Preclinical Toxicology. *Plos One,* 6.

SCHLUTER, K. D. 2001. Beta2-adrenergic receptor overexpression exacerbates development of heart failure after aortic stenosis. *Circulation,* 103**,** e11; author reply e11.

SCHUNDER, E., RYDZEWSKI, K., GRUNOW, R. & HEUNER, K. 2013. First indication for a functional CRISPR/Cas system in Francisella tularensis. *International Journal of Medical Microbiology,* 303**,** 51-60.

SEFTON, M., BLANCO, M. J., PENELA, P., MAYOR, F. & NIETO, M. A. 2000. Expression of the G protein-coupled receptor kinase 2 during early mouse embryogenesis. *Mechanisms of Development,* 98**,** 127-131.

SHALEM, O., SANJANA, N. E., HARTENIAN, E., SHI, X., SCOTT, D. A., MIKKELSEN, T. S., HECKL, D., EBERT, B. L., ROOT, D. E., DOENCH, J. G. & ZHANG, F. 2014. Genome-Scale CRISPR-Cas9 Knockout Screening in Human Cells. *Science,* 343**,** 84-87.

SHAO, Y., GUAN, Y., WANG, L., QIU, Z., LIU, M., CHEN, Y., WU, L., LI, Y., MA, X., LIU, M. & LI, D. 2014. CRISPR/Cas-mediated genome editing in the rat via direct injection of one-cell embryos. *Nat Protoc,* 9**,** 2493-512.

SHARMA, A., BURRIDGE, P. W., MCKEITHAN, W. L., SERRANO, R., SHUKLA, P., SAYED, N., CHURKO, J. M., KITANI, T., WU, H. D., HOLMSTROM, A., MATSA, E., ZHANG, Y., KUMAR, A., FAN, A. C., DEL ALAMO, J. C., WU, S. M., MOSLEHI, J. J., MERCOLA, M. & WU, J. C. 2017. High-throughput screening of tyrosine kinase inhibitor cardiotoxicity with human induced pluripotent stem cells. *Science Translational Medicine,* 9.

SHARMA, A., LI, G., RAJARAJAN, K., HAMAGUCHI, R., BURRIDGE, P. W. & WU, S. M. 2015. Derivation of Highly Purified Cardiomyocytes from Human Induced Pluripotent Stem Cells Using Small Molecule-modulated Differentiation and Subsequent Glucose Starvation. *Jove-Journal of Visualized Experiments*.

SHEN, B., ZHANG, W. S., ZHANG, J., ZHOU, J. K., WANG, J. Y., CHEN, L., WANG, L., HODGKINS, A., IYER, V., HUANG, X. X. & SKARNES, W. C. 2014. Efficient genome modification by CRISPR-Cas9 nickase with minimal off-target effects. *Nature Methods,* 11**,** 399-+.

SHICHI, H. & SOMERS, R. L. 1978. Light-dependent phosphorylation of rhodopsin. Purification and properties of rhodopsin kinase. *J Biol Chem,* 253**,** 7040-6.

SHIMIZU, I. & MINAMINO, T. 2016. Physiological and pathological cardiac hypertrophy. *Journal of Molecular and Cellular Cardiology,* 97**,** 245-262.

SHIMOJI, K., YUASA, S., ONIZUKA, T., HATTORI, F., TANAKA, T., HARA, M., OHNO, Y., CHEN, H., EGASGIRA, T., SEKI, T., YAE, K., KOSHIMIZU, U., OGAWA, S. & FUKUDA, K. 2010. G-CSF Promotes the Proliferation of Developing Cardiomyocytes In Vivo and in Derivation from ESCs and iPSCs. *Cell Stem Cell,* 6**,** 227-237.

SHMAKOV, S., ABUDAYYEH, O. O., MAKAROVA, K. S., WOLF, Y. I., GOOTENBERG, J. S., SEMENOVA, E., MINAKHIN, L., JOUNG, J., KONERMANN, S., SEVERINOV, K., ZHANG, F. & KOONIN, E. V. 2015. Discovery and Functional Characterization of Diverse Class 2 CRISPR-Cas Systems. *Molecular Cell,* 60**,** 385-397.

SIE, L., LOONG, S. & TAN, E. K. 2009. Utility of lymphoblastoid cell lines. *J Neurosci Res,* 87**,** 1953-9.

SIEHLER, S. 2009. Regulation of RhoGEF proteins by G12/13-coupled receptors. *British Journal of Pharmacology,* 158**,** 41-49.

SIMMERMAN, H. K. B. & JONES, L. R. 1998. Phospholamban: Protein structure, mechanism of action, and role in cardiac function. *Physiological Reviews,* 78**,** 921-947.

SKELTON, R. J. P., COSTA, M., ANDERSON, D. J., BRUVERIS, F., FINNIN, B. W., KOUTSIS, K., ARASARATNAM, D., WHITE, A. J., RAFII, A., NG, E. S., ELEFANTY, A. G., STANLEY, E. G., POUTON, C. W., HAYNES, J. M., ARDEHALI, R., DAVIS, R. P., MUMMERY, C. L. & ELLIOTT, D. A. 2014. SIRPA, VCAM1 and CD34 identify discrete lineages during early human cardiovascular development. *Stem Cell Research,* 13**,** 172-179.

SMALL, E. M. & KRIEG, P. A. 2004. Molecular regulation of cardiac chamber-specific gene expression. *Trends in Cardiovascular Medicine,* 14**,** 13-18.

SNIR, M., KEHAT, I., GEPSTEIN, A., COLEMAN, R., ITSKOVITZ-ELDOR, J., LIVNE, E. & GEPSTEIN, L. 2003. Assessment of the ultrastructural and proliferative properties of human embryonic stem cell-derived cardiomyocytes. *American Journal of Physiology-Heart and Circulatory Physiology,* 285**,** H2355-H2363.

SOARES, F. A. C., SHELDON, M., RAO, M., MUMMERY, C. & VALLIER, L. 2014. International Coordination of Large-Scale Human Induced Pluripotent Stem Cell Initiatives: Wellcome Trust and ISSCR Workshops White Paper. *Stem Cell Reports,* 3**,** 931-939.

SPINELLI, L., TRIMARCO, V., DI MARINO, S., MARINO, M., IACCARINO, G. & TRIMARCO, B. 2010. L41Q polymorphism of the G protein coupled receptor kinase 5 is associated with left ventricular apical ballooning syndrome. *European Journal of Heart Failure,* 12**,** 13-16.

SRIVASTAVA, D., THOMAS, T., LIN, Q., KIRBY, M. L., BROWN, D. & OLSON, E. N. 1997. Regulation of cardiac mesodermal and neural crest development by the bHLH transcription factor, dHAND. *Nature Genetics,* 16**,** 154-160.

STADTFELD, M., NAGAYA, M., UTIKAL, J., WEIR, G. & HOCHEDLINGER, K. 2008. Induced Pluripotent Stem Cells Generated Without Viral Integration. *Science,* 322**,** 945-949.

STANTON, H. C., BRENNER, G. & MAYFIELD, E. D. 1969. Studies on Isoproterenol-Induced Cardiomegaly in Rats. *American Heart Journal,* 77**,** 72-&.

STEFANOVIC, S. & ZAFFRAN, S. 2017. Mechanisms of retinoic acid signaling during cardiogenesis. *Mech Dev,* 143**,** 9-19.

STEINER, D., KHANER, H., COHEN, M., EVEN-RAM, S., GIL, Y., ITSYKSON, P., TURETSKY, T., IDELSON, M., AIZENMAN, E., RAM, R., BERMAN-ZAKEN, Y. & REUBINOFF, B. 2010. Derivation, propagation and controlled differentiation of human embryonic stem cells in suspension. *Nat Biotechnol,* 28**,** 361-4.

STRASSER, A., HARRIS, A. W., JACKS, T. & CORY, S. 1994. DNA-Damage Can Induce Apoptosis in Proliferating Lymphoid-Cells Via P53-Independent Mechanisms Inhibitable by Bcl-2. *Cell,* 79**,** 329-339.

STRASSER, R. H., BENOVIC, J. L., CARON, M. G. & LEFKOWITZ, R. J. 1986. Beta-Agonist and Prostaglandin-E1-Induced Translocation of the Beta-Adrenergic-Receptor Kinase - Evidence That the Kinase May Act on Multiple Adenylate Cyclase-Coupled Receptors. *Proceedings of the National Academy of Sciences of the United States of America,* 83**,** 6362-6366.

SUGISHITA, Y., KOSEKI, S., MATSUDA, M., YAMAGUCHI, T. & ITO, I. 1983. Myocardial Mechanics of Athletic Hearts in Comparison with Diseased Hearts. *American Heart Journal,* 105**,** 273-280.

SULAKHE, P. V. & VO, X. T. 1995. Regulation of phospholamban and troponin-I phosphorylation in the intact rat cardiomyocytes by adrenergic and cholinergic stimuli: roles of cyclic nucleotides, calcium, protein kinases and phosphatases and depolarization. *Mol Cell Biochem,* 149-150**,** 103-26.

SUN, N., PANETTA, N. J., GUPTA, D. M., WILSON, K. D., LEE, A., JIA, F., HU, S., CHERRY, A. M., ROBBINS, R. C., LONGAKER, M. T. & WU, J. C. 2009. Feeder-free derivation of induced pluripotent stem cells from adult human adipose stem

cells. *Proceedings of the National Academy of Sciences of the United States of America,* 106**,** 15720-15725.

SUN, N. & ZHAO, H. M. 2014. Seamless Correction of the Sickle Cell Disease Mutation of the HBB Gene in Human Induced Pluripotent Stem Cells Using TALENs. *Biotechnology and Bioengineering,* 111**,** 1048-1053.

SWYNGHEDAUW, B. 1999. Molecular mechanisms of myocardial remodeling. *Physiol Rev,* 79**,** 215-62.

TAKAHASHI, K. & YAMANAKA, S. 2006. Induction of pluripotent stem cells from mouse embryonic and adult fibroblast cultures by defined factors. *Cell,* 126**,** 663-76.

TAKAHASHI, K. & YAMANAKA, S. 2016. A decade of transcription factor-mediated reprogramming to pluripotency. *Nature Reviews Molecular Cell Biology,* 17**,** 183-193.

TAKASHIMA, S., SUGIMOTO, N., TAKUWA, N., OKAMOTO, Y., YOSHIOKA, K., TAKAMURA, M., TAKATA, S., KANEKO, S. & TAKUWA, Y. 2008. G12/13 and Gq mediate S1P2-induced inhibition of Rac and migration in vascular smooth muscle in a manner dependent on Rho but not Rho kinase. *Cardiovasc Res,* 79**,** 689-97.

TAKEBE, T. 2013. Generation of human liver tissue from an induced pluripotent stem cell-derived organ bud transplant. *Journal of Physiological Sciences,* 63**,** S86-S86.

TAKEI, S., ICHIKAWA, H., JOHKURA, K., MOGI, A., NO, H., YOSHIE, S., TOMOTSUNE, D. & SASAKI, K. 2009. Bone morphogenetic protein-4 promotes induction of cardiomyocytes from human embryonic stem cells in serum-based embryoid body development. *American Journal of Physiology-Heart and Circulatory Physiology,* 296**,** H1793-H1803.

TANAKA, A., YUASA, S., MEARINI, G., EGASHIRA, T., SEKI, T., KODAIRA, M., KUSUMOTO, D., KURODA, Y., OKATA, S., SUZUKI, T., INOHARA, T., ARIMURA, T., MAKINO, S., KIMURA, K., KIMURA, A., FURUKAWA, T., CARRIER, L., NODE, K. & FUKUDA, K. 2014. Endothelin-1 Induces Myofibrillar Disarray and Contractile Vector Variability in Hypertrophic Cardiomyopathy-Induced Pluripotent Stem Cell-Derived Cardiomyocytes. *Journal of the American Heart Association,* 3.

TANAKA, T., TOHYAMA, S., MURATA, M., NOMURA, F., KANEKO, T., CHEN, H., HATTORI, F., EGASHIRA, T., SEKI, T., OHNO, Y., KOSHIMIZU, U., YUASA, S., OGAWA, S., YAMANAKA, S., YASUDA, K. & FUKUDA, K. 2009. In vitro pharmacologic testing using human induced pluripotent stem cell-derived cardiomyocytes. *Biochemical and Biophysical Research Communications,* 385**,** 497-502.

TANG, T. H., BACHELLERIE, J. P., ROZHDESTVENSKY, T., BORTOLIN, M. L., HUBER, H., DRUNGOWSKI, M., ELGE, T., BROSIUS, J. & HUTTENHOFER, A. 2002. Identification of 86 candidates for small non-messenger RNAs from the archaeon Archaeoglobus fulgidus. *Proceedings of the National Academy of Sciences of the United States of America,* 99**,** 7536-7541.

TASHIRO, A., MASUDA, T. & SEGAWA, I. 1990. Morphometric Comparison of Mitochondria and Myofibrils of Cardiomyocytes between Hypertrophic and Dilated Cardiomyopathies. *Virchows Archiv a-Pathological Anatomy and Histopathology,* 416**,** 473-478.

THOMAS, D., KIEHN, J., KATUS, H. A. & KARLE, C. A. 2004. Adrenergic regulation of the rapid component of the cardiac delayed rectifier potassium current, I-Kr, and the underlying hERG ion channel. *Basic Research in Cardiology,* 99**,** 279-287.

THOMSON, J. A., ITSKOVITZ-ELDOR, J., SHAPIRO, S. S., WAKNITZ, M. A., SWIERGIEL, J. J., MARSHALL, V. S. & JONES, J. M. 1998. Embryonic stem cell lines derived from human blastocysts. *Science,* 282**,** 1145-7.

TOWBIN, J. A. & BOWLES, N. E. 2002. The failing heart. *Nature,* 415**,** 227-233.

TRAN, T. H., WANG, X. R., BROWNE, C., ZHANG, Y., SCHINKE, M., IZUMO, S. & BURCIN, M. 2009. Wnt3a-Induced Mesoderm Formation and Cardiomyogenesis in Human Embryonic Stem Cells. *Stem Cells,* 27**,** 1869-1878.

TRAYNHAM, C. J., HULLMANN, J. & KOCH, W. J. 2016. Canonical and non-canonical actions of GRK5 in the heart. *Journal of Molecular and Cellular Cardiology,* 92**,** 196-202.

TSAI, S. Q. & JOUNG, J. K. 2016. Defining and improving the genome-wide specificities of CRISPR-Cas9 nucleases. *Nature Reviews Genetics,* 17**,** 300-312.

TSAI, S. Q., ZHENG, Z., NGUYEN, N. T., LIEBERS, M., TOPKAR, V. V., THAPAR, V., WYVEKENS, N., KHAYTER, C., IAFRATE, A. J., LE, L. P., ARYEE, M. J. & JOUNG, J. K. 2015. GUIDE-seq enables genome-wide profiling of off-target cleavage by CRISPR-Cas nucleases. *Nature Biotechnology,* 33**,** 187-197.

TULLOCH, N. L., MUSKHELI, V., RAZUMOVA, M. V., KORTE, F. S., REGNIER, M., HAUCH, K. D., PABON, L., REINECKE, H. & MURRY, C. E. 2011. Growth of Engineered Human Myocardium With Mechanical Loading and Vascular Coculture. *Circulation Research,* 109**,** 47-U195.

TURAN, S., GALLA, M., ERNST, E., QIAO, J. H., VOELKEL, C., SCHIEDLMEIER, B., ZEHE, C. & BODE, J. 2011. Recombinase-Mediated Cassette Exchange (RMCE): Traditional Concepts and Current Challenges. *Journal of Molecular Biology,* 407**,** 193-221.

UCHIDA, E. 1975. Contraction and relaxation of vascular smooth muscle and calcium, strontium, barium. *Jpn Circ J,* 39**,** 565-70.

UNGERER, M., BOHM, M., ELCE, J. S., ERDMANN, E. & LOHSE, M. J. 1993. Altered Expression of Beta-Adrenergic-Receptor Kinase and Beta-1-Adrenergic Receptors in the Failing Human Heart. *Circulation,* 87**,** 454-463.

UOSAKI, H., FUKUSHIMA, H., TAKEUCHI, A., MATSUOKA, S., NAKATSUJI, N., YAMANAKA, S. & YAMASHITA, J. K. 2011. Efficient and scalable purification of cardiomyocytes from human embryonic and induced pluripotent stem cells by VCAM1 surface expression. *PLoS One,* 6**,** e23657.

URNOV, F. D., MILLER, J. C., LEE, Y. L., BEAUSEJOUR, C. M., ROCK, J. M., AUGUSTUS, S., JAMIESON, A. C., PORTEUS, M. H., GREGORY, P. D. & HOLMES, M. C. 2005. Highly efficient endogenous human gene correction using designed zinc-finger nucleases. *Nature,* 435**,** 646-651.

URNOV, F. D., REBAR, E. J., HOLMES, M. C., ZHANG, H. S. & GREGORY, P. D. 2010. Genome editing with engineered zinc finger nucleases. *Nat Rev Genet,* 11**,** 636-46.

VALLIER, L., ALEXANDER, M. & PEDERSEN, R. A. 2005. Activin/Nodal and FGF pathways cooperate to maintain pluripotency of human embryonic stem cells. *J Cell Sci,* 118**,** 4495-509.

VAN DEN AMEELE, J., TIBERI, L., BONDUE, A., PAULISSEN, C., HERPOEL, A., IACOVINO, M., KYBA, M., BLANPAIN, C. & VANDERHAEGHEN, P. 2012. Eomesodermin induces Mesp1 expression and cardiac differentiation from embryonic stem cells in the absence of Activin. *Embo Reports,* 13**,** 355-362.

VAN DEN BERG, C. W., ELLIOTT, D. A., BRAAM, S. R., MUMMERY, C. L. & DAVIS, R. P. 2015. Differentiation of Human Pluripotent Stem Cells to Cardiomyocytes Under Defined Conditions. *Methods Mol Biol*.

VAN DER OOST, J., JORE, M. M., WESTRA, E. R., LUNDGREN, M. & BROUNS, S. J. J. 2009. CRISPR-based adaptive and heritable immunity in prokaryotes. *Trends in Biochemical Sciences,* 34**,** 401-407.

VAN HOUTE, S., EKROTH, A. K. E., BRONIEWSKI, J. M., CHABAS, H., ASHBY, B., BONDY-DENOMY, J., GANDON, S., BOOTS, M., PATERSON, S., BUCKLING, A. & WESTRA, E. R. 2016. The diversity-generating benefits of a prokaryotic adaptive immune system. *Nature,* 532**,** 385-+.

VAN MEER, B. J., TERTOOLEN, L. G. J. & MUMMERY, C. L. 2016. Concise Review: Measuring Physiological Responses of Human Pluripotent Stem Cell Derived Cardiomyocytes to Drugs and Disease. *Stem Cells,* 34**,** 2008-2015.

VATTER, P., STOESSER, C., SAMEL, I., GIERSCHIK, P. & MOEPPS, B. 2005. The variable C-terminal extension of G-protein-coupled receptor kinase 6 constitutes an accessorial autoregulatory domain. *Febs Journal,* 272**,** 6039-6051.

VESTERGAARD, G., GARRETT, R. A. & SHAH, S. A. 2014. CRISPR adaptive immune systems of Archaea. *Rna Biology,* 11**,** 156-167.

VOIT, R. A., HENDEL, A., PRUETT-MILLER, S. M. & PORTEUS, M. H. 2014. Nuclease-mediated gene editing by homologous recombination of the human globin locus. *Nucleic Acids Research,* 42**,** 1365-1378.

WAKEFIELD, I. D., POLLARD, C., REDFERN, W. S., HAMMOND, T. G. & VALENTIN, J. P. 2002. The application of in vitro methods to safety pharmacology. *Fundam Clin Pharmacol,* 16**,** 209-18.

WANG, G., YANG, L., GRISHIN, D., RIOS, X., YE, L. Y., HU, Y., LI, K., ZHANG, D., CHURCH, G. M. & PU, W. T. 2017. Efficient, footprint-free human iPSC genome editing by consolidation of Cas9/CRISPR and piggyBac technologies. *Nat Protoc,* 12**,** 88-103.

WANG, G. F., NIKOVITS, W., SCHLEINITZ, M. & STOCKDALE, F. E. 1998. A positive GATA element and a negative vitamin D receptor-like element control atrial chamber-specific expression of a slow myosin heavy-chain gene during cardiac morphogenesis. *Molecular and Cellular Biology,* 18**,** 6023-6034.

WANG, L., SCHULZ, T. C., SHERRER, E. S., DAUPHIN, D. S., SHIN, S., NELSON, A. M., WARE, C. B., ZHAN, M., SONG, C. Z., CHEN, X., BRIMBLE, S. N., MCLEAN, A., GALEANO, M. J., UHL, E. W., D'AMOUR, K. A., CHESNUT, J. D., RAO, M. S., BLAU, C. A. & ROBINS, A. J. 2007. Self-renewal of human embryonic stem cells requires insulin-like growth factor-1 receptor and ERBB2 receptor signaling. *Blood,* 110**,** 4111-9.

WANG, W. C. H., MIHLBACHLER, K. A., BLEECKER, E. R., WEISS, S. T. & LIGGETT, S. B. 2008. A polymorphism of G-protein coupled receptor kinase5 alters agonist-promoted desensitization of beta(2)-adrenergic receptors. *Pharmacogenetics and Genomics,* 18**,** 729-732.

WANG, Z., ORON, E., NELSON, B., RAZIS, S. & IVANOVA, N. 2012. Distinct Lineage Specification Roles for NANOG, OCT4, and SOX2 in Human Embryonic Stem Cells. *Cell Stem Cell,* 10**,** 440-454.

WARREN, L., MANOS, P. D., AHFELDT, T., LOH, Y. H., LI, H., LAU, F., EBINA, W., MANDAL, P. K., SMITH, Z. D., MEISSNER, A., DALEY, G. Q., BRACK, A. S., COLLINS, J. J., COWAN, C., SCHLAEGER, T. M. & ROSSI, D. J. 2010. Highly efficient reprogramming to pluripotency and directed differentiation of human cells with synthetic modified mRNA. *Cell Stem Cell,* 7**,** 618-30.

WEIL, J., ZOLK, O., GRIEPENTROG, J., WENZEL, U., ZIMMERMANN, W. H. & ESCHENHAGEN, T. 2006. Alterations of the preproenkephalin system in cardiac hypertrophy and its role in atrioventricular conduction. *Cardiovasc Res,* 69**,** 412-22.

WHITE, M. F. 2009. Structure, function and evolution of the XPD family of iron-sulfur-containing 5 '-> 3 ' DNA helicases. *Biochemical Society Transactions,* 37**,** 547-551.

WIEDENHEFT, B., STERNBERG, S. H. & DOUDNA, J. A. 2012. RNA-guided genetic silencing systems in bacteria and archaea. *Nature,* 482**,** 331-338.

WILSON, R., AINSCOUGH, R., ANDERSON, K., BAYNES, C., BERKS, M., BONFIELD, J., BURTON, J., CONNELL, M., COPSEY, T., COOPER, J. & ET AL. 1994. 2.2 Mb of contiguous nucleotide sequence from chromosome III of C. elegans. *Nature,* 368**,** 32-8.

WOLTJEN, K., MICHAEL, I. P., MOHSENI, P., DESAI, R., MILEIKOVSKY, M., HAMALAINEN, R., COWLING, R., WANG, W., LIU, P. T., GERTSENSTEIN, M., KAJI, K., SUNG, H. K. & NAGY, A. 2009. piggyBac transposition reprograms fibroblasts to induced pluripotent stem cells. *Nature,* 458**,** 766-U106.

WONG, R. C. B., TELLIS, I., JAMSHIDI, P., PERA, M. & PEBAY, A. 2007. Anti-apoptotic effect of sphingosine-1-phosphate and platelet-derived growth factor in human embryonic stem cells. *Stem Cells and Development,* 16**,** 989-1001.

WOO, A. Y., SONG, Y., XIAO, R. P. & ZHU, W. 2015. Biased beta2-adrenoceptor signalling in heart failure: pathophysiology and drug discovery. *Br J Pharmacol,* 172**,** 5444-56.

WOOD, A. J., LO, T. W., ZEITLER, B., PICKLE, C. S., RALSTON, E. J., LEE, A. H., AMORA, R., MILLER, J. C., LEUNG, E., MENG, X. D., ZHANG, L., REBAR, E. J., GREGORY, P. D., URNOV, F. D. & MEYER, B. J. 2011. Targeted Genome Editing Across Species Using ZFNs and TALENs. *Science,* 333**,** 307-307.

WOODCOCK, E. A., DU, X. J., REICHELT, M. E. & GRAHAM, R. M. 2008. Cardiac alpha(1)-adrenergic drive in pathological remodelling. *Cardiovascular Research,* 77**,** 452-462.

WOODGETT, J. R. 1994. Regulation and Functions of the Glycogen-Synthase Kinase-3 Subfamily. *Seminars in Cancer Biology,* 5**,** 269-275.

WORZFELD, T., WETTSCHURECK, N. & OFFERMANNS, S. 2008. G(12)/G(13)-mediated signalling in mammalian physiology and disease. *Trends in Pharmacological Sciences,* 29**,** 582-589.

WU, H., LEE, J., VINCENT, L. G., WANG, Q., GU, M., LAN, F., CHURKO, J. M., SALLAM, K. I., MATSA, E., SHARMA, A., GOLD, J. D., ENGLER, A. J., XIANG, Y. K., BERS, D. M. & WU, J. C. 2015. Epigenetic Regulation of Phosphodiesterases 2A and 3A Underlies Compromised beta-Adrenergic Signaling in an iPSC Model of Dilated Cardiomyopathy. *Cell Stem Cell,* 17**,** 89-100.

WU, J. B., HUNT, S. D., XUE, H. P., LIU, Y. & DARABI, R. 2016. Generation and Characterization of a MYF5 Reporter Human iPS Cell Line Using CRISPR/Cas9 Mediated Homologous Recombination. *Scientific Reports,* 6.

WU, L. Y., JIA, Z. Q., YAN, L. H., WANG, W. P., WANG, J. J., ZHANG, Y. Z. & ZHOU, C. Y. 2013. Angiotensin II promotes cardiac differentiation of embryonic stem cells via angiotensin type 1 receptor. *Differentiation,* 86**,** 23-29.

XIA, G. B., GAO, Y. Z., TERADA, N., JIN, S. G., RANUM, L., SWANSON, M. S. & ASHIZAWA, T. 2014. TALEN-Mediated Gene Editing Leads to Complete Loss of Intranuclear Foci in DM1 Neural Stem Cells Derived from Human DM1 iPS Cells. *Annals of Neurology,* 76**,** S56-S56.

XIANG, Y. & KOBILKA, B. K. 2003. Myocyte adrenoceptor signaling pathways. *Science,* 300**,** 1530-2.

XIAO, R. P., TOMHAVE, E. D., WANG, D. J., JI, X. W., BOLUYT, M. O., CHENG, H. P., LAKATTA, E. G. & KOCH, W. J. 1998. Age-associated reductions in cardiac beta(1)- and beta(2)-adrenergic responses without changes in inhibitory G proteins or receptor kinases. *Journal of Clinical Investigation,* 101**,** 1273-1282.

XIE, F., YE, L., CHANG, J. C., BEYER, A. I., WANG, J. M., MUENCH, M. O. & KAN, Y. W. 2014. Seamless gene correction of beta-thalassemia mutations in patient-specific iPSCs using CRISPR/Cas9 and piggyBac. *Genome Research,* 24**,** 1526-1533.

XU, C. H., INOKUMA, M. S., DENHAM, J., GOLDS, K., KUNDU, P., GOLD, J. D. & CARPENTER, M. K. 2001. Feeder-free growth of undifferentiated human embryonic stem cells. *Nature Biotechnology,* 19**,** 971-974.

XU, X. Q., GRAICHEN, R., SOO, S. Y., BALAKRISHNAN, T., RAHMAT, S. N. B., SIEH, S., THAM, S. C., FREUND, C., MOORE, J., MUMMERY, C., COLMAN, A., ZWEIGERDT, R. & DAVIDSON, B. P. 2008. Chemically defined medium supporting cardiomyocyte differentiation of human embryonic stem cells. *Differentiation,* 76**,** 958-970.

YAMAUCHI, K., SUMI, T., MINAMI, I., OTSUJI, T. G., KAWASE, E., NAKATSUJI, N. & SUEMORI, H. 2010. Cardiomyocytes develop from anterior primitive streak cells induced by beta-catenin activation and the blockage of BMP signaling in hESCs. *Genes Cells,* 15**,** 1216-27.

YANG, C. F., CHOU, K. Y., WENG, Z. C., HUNG, S. C., LAI, S. T., HSU, C. P. & WANG, J. S. 2008. Cardiac myocyte progenitors from adult hearts for myocardial regenerative therapy. *Journal of the Chinese Medical Association,* 71**,** 79-85.

YANG, H., WANG, H. Y., SHIVALILA, C. S., CHENG, A. W., SHI, L. Y. & JAENISCH, R. 2013. One-Step Generation of Mice Carrying Reporter and Conditional Alleles by CRISPR/Cas-Mediated Genome Engineering. *Cell,* 154**,** 1370-1379.

YANG, X., RODRIGUEZ, M., PABON, L., FISCHER, K. A., REINECKE, H., REGNIER, M., SNIADECKI, N. J., RUOHOLA-BAKER, H. & MURRY, C. E. 2014. Tri-iodo-l-thyronine promotes the maturation of human cardiomyocytes-derived from induced pluripotent stem cells. *J Mol Cell Cardiol,* 72**,** 296-304.

YARFITZ, S. & HURLEY, J. B. 1994. Transduction Mechanisms of Vertebrate and Invertebrate Photoreceptors. *Journal of Biological Chemistry,* 269**,** 14329-14332.

YESTER, J. W. & KUHN, B. 2017. Mechanisms of Cardiomyocyte Proliferation and Differentiation in Development and Regeneration. *Curr Cardiol Rep,* 19**,** 13.

YING, Q. L., WRAY, J., NICHOLS, J., BATLLE-MORERA, L., DOBLE, B., WOODGETT, J., COHEN, P. & SMITH, A. 2008. The ground state of embryonic stem cell self-renewal. *Nature,* 453**,** 519-U5.

YOSHIMITSU, R., HATTORI, K., SUGIURA, S., KONDO, Y., YAMADA, R., TACHIKAWA, S., SATOH, T., KURISAKI, A., OHNUMA, K., ASASHIMA, M. & KANAMORI, T. 2014. Microfluidic Perfusion Culture of Human Induced Pluripotent Stem Cells Under Fully Defined Culture Conditions. *Biotechnology and Bioengineering,* 111**,** 937-947.

YOUNG, C. S., HICKS, M. R., ERMOLOVA, N. V., NAKANO, H., JAN, M., YOUNESI, S., NAKANO, A., NELSON, S. F., MICELI, M. C., SPENCER, M. J. & PYLE, A. D. 2016. Functional Restoration of Dystrophin Protein in HiPSC-Derived Skeletal Myotubes and Cardiomyocytes After CRISPR/Cas9-Mediated Deletion of 530-725kb of DMD. *Molecular Therapy,* 24**,** S290-S290.

YU, J. Y., CHAU, K. F., VODYANIK, M. A., JIANG, J. L. & JIANG, Y. 2011. Efficient Feeder-Free Episomal Reprogramming with Small Molecules. *Plos One,* 6.

YU, J. Y., HU, K. J., SMUGA-OTTO, K., TIAN, S. L., STEWART, R., SLUKVIN, I. I. & THOMSON, J. A. 2009. Human Induced Pluripotent Stem Cells Free of Vector and Transgene Sequences. *Science,* 324**,** 797-801.

YU, J. Y., VODYANIK, M. A., SMUGA-OTTO, K., ANTOSIEWICZ-BOURGET, J., FRANE, J. L., TIAN, S., NIE, J., JONSDOTTIR, G. A., RUOTTI, V., STEWART, R., SLUKVIN, I. I. & THOMSON, J. A. 2007. Induced pluripotent stem cell lines derived from human somatic cells. *Science,* 318**,** 1917-1920.

YUSA, K. 2013. Seamless genome editing in human pluripotent stem cells using custom endonuclease-based gene targeting and the piggyBac transposon. *Nature Protocols,* 8**,** 2061-2078.

YUSA, K. 2015. piggyBac Transposon. *Microbiology Spectrum,* 3.

YUSA, K., RAD, R., TAKEDA, J. & BRADLEY, A. 2009. Generation of transgene-free induced pluripotent mouse stem cells by the piggyBac transposon. *Nature Methods,* 6**,** 363-U69.

ZALEWSKA, M., SIARA, M. & SAJEWICZ, W. 2014. G protein-coupled receptors: abnormalities in signal transmission, disease states and pharmacotherapy. *Acta Pol Pharm,* 71**,** 229-43.

ZEE, R. Y., COOK, N. R., REYNOLDS, R., CHENG, S. & RIDKER, P. M. 2005. Haplotype analysis of the beta2 adrenergic receptor gene and risk of myocardial infarction in humans. *Genetics,* 169**,** 1583-7.

ZETSCHE, B., GOOTENBERG, J. S., ABUDAYYEH, O. O., SLAYMAKER, I. M., MAKAROVA, K. S., ESSLETZBICHLER, P., VOLZ, S. E., JOUNG, J., VAN DER OOST, J., REGEV, A., KOONIN, E. V. & ZHANG, F. 2015. Cpf1 Is a Single RNA-Guided Endonuclease of a Class 2 CRISPR-Cas System. *Cell,* 163**,** 759-771.

ZHANG, J. H., KLOS, M., WILSON, G. F., HERMAN, A. M., LIAN, X. J., RAVAL, K. K., BARRON, M. R., HOU, L. Q., SOERENS, A. G., YU, J. Y., PALECEK, S. P., LYONS, G. E., THOMSON, J. A., HERRON, T. J., JALIFE, J. & KAMP, T. J. 2012. Extracellular Matrix Promotes Highly Efficient Cardiac Differentiation of Human Pluripotent Stem Cells The Matrix Sandwich Method. *Circulation Research,* 111**,** 1125-1136.

ZHANG, J. H., WILSON, G. F., SOERENS, A. G., KOONCE, C. H., YU, J. Y., PALECEK, S. P., THOMSON, J. A. & KAMP, T. J. 2009. Functional Cardiomyocytes Derived From Human Induced Pluripotent Stem Cells. *Circulation Research,* 104**,** E30-E41.

ZHANG, L., GUO, J., ZHANG, P., XIONG, Q., WU, S. C., XIA, L., ROY, S. S., TOLAR, J., O'CONNELL, T. D., KYBA, M., LIAO, K. & ZHANG, J. 2015. Derivation and high engraftment of patient-specific cardiomyocyte sheet using induced pluripotent stem cells generated from adult cardiac fibroblast. *Circ Heart Fail,* 8**,** 156-66.

ZHANG, Q., JIANG, J., HAN, P., YUAN, Q., ZHANG, J., ZHANG, X., XU, Y., CAO, H., MENG, Q., CHEN, L., TIAN, T., WANG, X., LI, P., HESCHELER, J., JI, G. & MA, Y. 2011. Direct differentiation of atrial and ventricular myocytes from human embryonic stem cells by alternating retinoid signals. *Cell Res,* 21**,** 579-87.

ZHANG, Z. Y., ZHOU, B. & XIE, L. P. 2002. Modulation of protein kinase signaling by protein phosphatases and inhibitors. *Pharmacology & Therapeutics,* 93**,** 307-317.

ZHAO, X. L., GUTIERREZ, L. M., CHANG, C. F. & HOSEY, M. M. 1994. The Alpha(1)-Subunit of Skeletal-Muscle L-Type Ca Channels Is the Key Target for Regulation by a-Kinase and Protein Phosphatase-1c. *Biochemical and Biophysical Research Communications,* 198**,** 166-173.

ZHOU, T., BENDA, C., DUNZINGER, S., HUANG, Y. H., HO, J. C., YANG, J. Y., WANG, Y., ZHANG, Y., ZHUANG, Q., LI, Y. H., BAO, X. C., TSE, H. F., GRILLARI, J., GRILLARI-VOGLAUER, R., PEI, D. Q. & ESTEBAN, M. A. 2012. Generation of human induced pluripotent stem cells from urine samples. *Nature Protocols,* 7**,** 2080-2089.

ZHU, W. Z., ZHENG, M., KOCH, W. J., LEFKOWITZ, R. J., KOBILKA, B. K. & XIAO, R. P. 2001. Dual modulation of cell survival and cell death by beta(2)-adrenergic signaling in adult mouse cardiac myocytes. *Proceedings of the National Academy of Sciences of the United States of America,* 98**,** 1607-1612.

ZOU, J. Z., MAEDER, M. L., MALI, P., PRUETT-MILLER, S. M., THIBODEAU-BEGANNY, S., CHOU, B. K., CHEN, G. B., YE, Z. H., PARK, I. H., DALEY, G. Q., PORTEUS, M. H., JOUNG, J. K. & CHENG, L. 2009. Gene Targeting of a Disease-Related Gene in Human Induced Pluripotent Stem and Embryonic Stem Cells. *Cell Stem Cell,* 5**,** 97-110.

ZUCKER, I. H. 2017. Guidelines in Cardiovascular Research; a First for the American Journal of Physiology: Heart and Circulatory Physiology. *Am J Physiol Heart Circ Physiol***,** ajpheart 00151 2017.

ZWI, L., CASPI, O., ARBEL, G., HUBER, I., GEPSTEIN, A., PARK, I. H. & GEPSTEIN, L. 2009. Cardiomyocyte Differentiation of Human Induced Pluripotent Stem Cells. *Circulation,* 120**,** 1513-1523.

Appendix 1

Product Name	Supplier	Catalogue Number
1-thioglycerol	Sigma-Aldrich	M6145
100 pre-paid sequencing vouchers	Source Bioscience	GSL 1601
A-83-01	R&D Systems	2939
Accutase	Sigma-Aldrich	A6964
ADRB1 Tagman Assay	Applied Biosystems (Thermal Fisher)	Hs02330048_s1
ADRB2 Taqman Assay	Applied Biosystems (Thermal Fisher)	Hs00240532_s1
Agarose	Life Technologies	15510-027
Amersham ECL Prime Western Blotting detection reagent	GE Healthcare Life Science	RPN2232
Ampicillin	Fisher Scientific	BP1760
Angiotensin II	Sigma Aldrich	A9525-5Mg
Angiotensin II (AGTR1) Taqman assay	Applied Biosystems (Thermal Fisher)	Hs00258938_m1
Anti-human GRK5 antibody	Santa Cruz Biotechnology	Sc-11396
Anti-human GRK5 antibody	Abcam	Ab64943
Anti-human TRA-1-81 PE	eBioscience	12-8883-82
B27 supplement	Life Technologies	0080085-SA
Beta-tubulin (9F3) Rabbit mAb	New England Biolabs	2128P
bFGF	R&D Systems	233-FB-01M
BMP4	Peprotech EC	314-BP-010
Cell Dissociation Buffer (CDB)	Life Technologies	13150-016
CGP-20712A methanesulfonate	Sigma-Aldrich	I127-5MG
Chemically defined lipids	Fisher Scientific	11548846
CHIR99021	R&D systems	4423
DAPI	Sigma-Aldrich	D9542
DMEM	Sigma-Aldrich	D5030
DMEM-F12	Life Technologies	1152039
DMSO Hydri-Max	Sigma-Aldrich	D2650
DMSO, Reagent Plus	Sigma-Aldrich	D5879
DNeasy Blood and Tissue Kit	Qiagen	69504
dNTPs	Promega	U1511
Dorsomorphin	R&D	3093/10
EDTA	Sigma-Aldrich	E9884
EGTA	Sigma-Aldrich	E0396
Endothelin 1	Sigma-Aldrich	E7764
Endothelin 1 receptor (EDNRA) Taqman assay	Applied Biosystems (Thermal Fisher)	Hs03988672_m1
Essential 8 medium	Thermo Fisher	A1517001
EthBr	Sigma-Aldrich	E1510
FBS	BIOCHROM	S0115
Fibronectin	Sigma-Aldrich	F0895
Fibronectin from human plasma	BioReagent	F0895 5MG
First strand cDNA synthesis kit	GE healthcare	27-9361-01
Foskolin	R&D system	1099
Gibson Assembly Master Mix	New England Biolabs	E2611L

Product Name	Supplier	Catalogue Number
Glutamax	Life Technologies	35050038
GRK2 Taqman Assay	Applied Biosystems (Thermal Fisher)	Hs00176395_m1
GRK5 Taqman Assay	Applied Biosystems (Thermal Fisher)	Hs00992173_m1
H_2O, molecular graded	Sigma-Aldrich	W4502
HA-100	Insight Biotechnology UK	64393
Hank's Balanced Salt solution	Life Technologies	13180-046
HEPES	Sigma-Aldrich	H3784
Human serum	Sigma-Aldrich	H4522
Hyclone FBS	GE Hyclone	SH30070.03E
ICI 118,551 hydrochloride	Sigma-Aldrich	C231-10MG
Isoprenaline	R&D Systems	1747
KaryoMax Colcemid	Life Technologies	15212012
KCl	Sigma-Aldrich	P5405
KSR	Life Technologies	10828028
KY02111	R&D	4731
L-glutamine	Life Technologies	25030024
Lamin A/C (4C11) mouse mAb	New England Biolabs	4777T
Matrigel™	BD Biosciences	354234
MMC	Acros organics	226940020
Mouse Anti-human MLC-2a	Synaptic systems	311-011
mTeSR	Stemcell Technologies	5851
N2 supplement	Thermal Fisher	17502001
NaCl	Sigma-Aldrich	S5886
NEAA	Life Technologies	11140035
One Shot® Top10 competent cells	Invitrogen	C5050-03
PBS	Life Technologies	14190
PCR Purification kit	Qiagen	28104
PD0325901	R&D system	4192
PE beads	Miltenyi Biotec.	130-048-801
Phusion® High-Fidelity DNA polymerase	New England Biolabs	M0530L
Propranolol hydrochloride	Sigma-Aldrich	P0884-1G
Puromycin	Sigma-Aldrich	P8833
PVA	Sigma-Aldrich	P8136
QIAquick Gel extraction kit	Qiagen	28704
QIAquick PCR purification kit	Qiagen	28104
Rabbit Anti-human MLC2v	ProteinTech Europe	10906-1-AP
Recombinant human Activin-A	Life Technologies	PHC9564
Reverse Transcriptase: SuperScript III	Invitrogen	18080-044
RNA isolation NucleoSpin RNA	Macherey-Nagel	740955.50
RNase ZAP	Applied Biosystems	AM9780
RNeasy kit	Qiagen	74101
RPMI 1640	Life Technologies	21875034
Sodium citrate	Fisher Scientific	S/3320
Sodium Pyruvate	Sigma-Aldrich	S8636
StemPro® 34 SFM media	Life Technologies	10639-011
Streptavidin Paramagnetic beads	Promega	Z5481

Product Name	**Supplier**	**Catalogue Number**
TaqMan Fast Advanced Master Mix	Applied Biosystems (Thermal Fisher)	4444963
Tris-Acetate	Fisher Scientific	BP152-1
Triton X100	Sigma-Aldrich	T8532
Tween 20	Fisher Scientific	BP337-100
Vitronectin	Life Technologies	A14700
XAV939	R&D	3748
β-mecaptoethanol	Sigma-Aldrich	63689